



**Studying Arrhythmogenic Right Ventricular Cardiomyopathy /
Dysplasia Using Induced Pluripotent Stem Cells**

**David Lee
Doctor of Philosophy**

Institute of Genetic Medicine
Faculty of Medical Sciences
Newcastle University
November 2018

Abstract

Arrhythmogenic right ventricular cardiomyopathy / dysplasia (ARVC/D) is a cause of ventricular arrhythmia and heart failure in adults. Fifty percent of subjects with ARVC/D carry pathogenic variants in the genes encoding desmosomal proteins. ARVC/D is associated with changes in cardiac desmosomal ultrastructure and the cellular distribution of desmosomal proteins in cardiomyocytes. These changes may be part of a common pathway of pathogenesis for the disease.

Induced pluripotent stem cell derived cardiomyocytes (iPSC-CMs) carrying ARVC/D associated variants have been reported to recapitulate features of the disease. Five iPSC-CM models of ARVC/D have been reported, all of which carry mutations in the gene encoding the desmosomal protein plakophilin 2.

In this study iPSC-CMs were generated from the peripheral blood mononuclear cells of a control subject and three subjects with ARVC/D. The ARVC/D iPSC-CMs carried pathogenic variants three different desmosomal genes: plakophilin 2 (*PKP2*), desmoglein 2 (*DSG2*), and desmoplakin (*DSP*) that have not been studied previously using cellular or animal models.

No differences were found in either the cellular distribution of desmosomal proteins or the ultrastructure of desmosomes when ARVC/D and control iPSC-CMs were compared. It was concluded that iPSC-CMs are not as robust a platform for modelling ARVC/D as had been previously reported.

The expression of desmosomal genes in iPSCs were at levels similar to those seen in iPSC-CMs. The differentiation of iPSCs to iPSC-CMs was associated with a decrease in the expression of genes encoding desmosomal cadherins and an increase in those encoding arm-repeat proteins. There was also evidence of desmosomal protein expression and the presence of desmosomes in iPSC cultures. It is suggested that intercellular adhesion junctions containing desmosomal proteins have a role in the maintenance of pluripotency in iPSCs *in vitro* and changes in desmosomal gene and protein expression are important in defining the cardiac differentiation of iPSCs.

Acknowledgements

Although the work in this thesis is my own it would not have been possible without the help and support of others.

I'd like to thank my supervisors Prof Lyle Armstrong, Prof Majlinda Lako and Dr Andrew Owens for their support and advice. I'd like to thank Prof Armstrong in particular for support in securing the funding and ethical approval for the project, in developing my skills in cell culture and molecular analysis and for his patience and checking this manuscript. I'm grateful to both Prof Armstrong and Prof Lako for providing me with opportunities to contribute to other projects within the group. I'm grateful to Dr Owens for arranging access of myocardial tissue samples via his own research projects.

I'd like to thank other members of the stem cell group for their support in developing my laboratory skills and providing constructive suggestions regarding experimental design and data interpretation. In particular I'd like to thank: Dr Dario Melguizo-Sanchis, Dr Valeria Chichagova, Dr Carla Mellough, Dr Joseph Collin, Dr Chunbo Yang, Dr Dean Hallam and Dr Aurora Gomez-Duran. I'm grateful to Dr Georgios Anyfantis for the preparation of inactivated MEF feeder layers for pluripotent culture and for conducting the teratoma assay.

I'd like to thank other researchers at Newcastle University for the donation of cell lines used as controls. In particular Dr Mustafa Al-Musawi and Dr Ruth Valentine for the donation of the HaCaT cell line.

I'd like to thank Prof Stefan Przyborski and his colleagues at Durham University for the processing and histological examination of samples from the teratoma assay.

I'm grateful to Dr Hussein Sheikh Ali Mohamoud (Princess Al Jawhara Al-Brahim Centre of Excellence in Research of Hereditary Disorders, King Abdulaziz University, KSA) for performing SNP array analysis, to Dr Ian Wilson for help with the analysis of genetic identify using these data and to Dr Simon Zwolinski (Northern Genetics Service) for training and support in the interpretation of cytogenetic abnormalities indicated by the SNP array data.

I'd like to give special thanks to all the staff at the Newcastle University Electron Microscopy Service for their work in the processing of samples for TEM analysis and their patience in supporting the many hours needed to acquire the TEM images in this study. I'm particularly grateful to Dr Kathryn White for providing training to operate the electron microscope and for answering my many questions. I'd like to

thank Islam al Shamleh for his time in participation in quantitative TEM image analysis.

I'm grateful to the staff of the flow cytometry facility and particularly to Ian Dimmick for training in flow cytometry and support in designing flow cytometry experiments.

I'd like to thank Prof Sian Harding's group (Imperial College London) for providing the facilities for the collection of calcium transient imaging and particularly Dr Nicola Hellen training and support in these experiments.

I'd like to thank Dr Mauro Santibáñez-Koref and Dr Kim Pearce for advice on statistical analyses.

I'm grateful to Dr Stephen Lord (The Newcastle upon Tyne Hospitals NHS Foundation Trust) for the initial discussions of research ideas from which this study originated and his consistent and generous support for the project and me. I'd like to thank both Dr Lord and Dr Paul Brennan (Northern Genetics Service) for their help in identifying participants for recruitment and participation in the assessment of clinical data.

I'd like to thank the Newcastle upon Tyne Hospitals NHS Charity for funding this work and The Newcastle upon Tyne Hospitals NHS Foundation Trust for acting as sponsor and host for the recruitment of participants.

Finally I'd like to thank all the family and friends that have supported and encouraged me through this project.

Table of contents

Abstract	iii
Acknowledgements	v
Table of contents	viii
List of figures	xvi
List of tables	xx
List of abbreviations.....	xxiv
Chapter 1. Introduction	1
1.1 Overview of induced pluripotent stem cells and iPSC derived cardiomyocytes	
2	
1.1.1 Pluripotency <i>in vivo</i>	2
1.1.1 Pluripotency <i>in vitro</i>	4
1.1.2 Cellular reprogramming and blood derived iPSCs.....	5
1.1.3 The maintenance of human PSCs <i>in vitro</i>	7
1.1.4 PSC-CM generation.....	8
1.1.5 PSC-CM maturation.....	11
1.1.6 PSC-CMs and disease modelling	12
1.2 Overview of the desmosome	14
1.2.1 Desmosomal ultrastructure	14
1.2.2 Desmosomal cadherins	18
1.2.3 Desmosomal arm-repeat proteins.....	22
1.2.4 Desmoplakin	23
1.2.5 The composition and organization of proteins within the cardiac	
desmosome and their correlation with ultrastructural features	24
1.2.6 Desmosomal proteins and intercellular adhesion	26
1.2.7 Desmosomal proteins and intracellular signalling pathways.....	27
1.3 Overview of arrhythmogenic right ventricular cardiomyopathy / dysplasia	31
1.3.1 Clinical features	31
1.3.2 The pathogenesis of ARVC/D	38
1.4 Hypotheses, aims and objectives	53
Chapter 2 Methods	54
2.1 Recruitment of study participants and the origin of cells lines and tissues...	54

2.1.1	Recruitment of subjects from which peripheral blood samples were collected.....	54
2.1.2	Recruitment of subjects from which myocardial samples were collected.....	54
2.1.3	Control fibroblasts and fibroblast derived iPSCs	54
2.1.4	Immortalised human keratinocytes.....	54
2.1.5	Human embryonic stem cells	55
2.2	The collection and processing of samples of right atrial appendage.....	55
2.3	The collection and processing of blood samples.....	55
2.3.1	Blood sampling.....	55
2.3.2	Density gradient centrifugation	55
2.3.3	Estimation of the concentration of cells within a single cell suspension using a haemocytometer.....	56
2.3.4	FACS sorting of CD3+ cells.....	56
2.4	Cellular reprogramming.....	57
2.4.1	Pre-transduction culture	57
2.4.2	Transduction.....	58
2.4.3	Post transduction culture	58
2.5	Clonal expansion and maintenance culture of iPSCs on MEF feeder layers.....	59
2.5.1	Preparation of plates containing a MEF feeder layer	59
2.5.2	Preparation of MEF conditioned pluripotent cell culture medium.....	60
2.5.3	Clonal expansion on inactivated MEF feeder layers	60
2.6	Clonal expansion and maintenance culture in feeder-free conditions.....	61
2.6.1	Preparation of Matrigel coated cultureware.....	61
2.6.2	Transfer of pluripotent cells from culture on MEF feeder layers to feeder-free conditions.....	61
2.6.3	Culture and passaging of pluripotent cells in feeder-free conditions.....	62
2.7	Spontaneous differentiation of iPSCs.....	62
2.7.1	Embryoid body differentiation.....	62
2.7.2	Teratoma assay.....	62
2.8	Directed cardiac differentiation of iPSCs after embryoid body formation	63
2.8.1	Enzymatic EB formation	63
2.8.2	Aggrewell EB formation.....	64
2.8.3	Directed cardiac differentiation	64
2.9	Directed cardiac differentiation of iPSCs as a monolayer	65
2.10	Purification of iPSC-CMs following directed differentiation.....	66

2.10.1	Purification based on SIRPA expression	66
2.10.2	Metabolic purification	66
2.11	Culture of immortalized keratinocytes	67
2.12	Cryopreservation of culture cells	67
2.12.1	Cryopreservation of cells following directed cardiac differentiation	68
2.12.2	Cryopreservation of MEFs and immortalised keratinocytes.....	68
2.13	Collection of samples for molecular analysis	70
2.13.1	Collection of a cell pellet from adherent cultures of iPSCs for DNA and RNA extraction.	70
2.13.2	Collection of human right atrial appendage tissue samples for RNA extraction.....	70
2.13.3	Collection of samples from contracting cultures for RNA extraction	70
2.14	Genomic DNA analysis	71
2.14.1	Extraction of genomic DNA from PBMCs and cultured cells.	71
2.14.2	SNP array analysis	71
2.14.3	Mutation sequencing.....	74
2.14.4	TCR re-arrangement assay	75
2.15	RNA analysis.....	76
2.15.1	Extraction of RNA	76
2.15.2	Assessment of RNA quality	76
2.15.3	Synthesis of cDNA from RNA	77
2.15.4	PCR to assess persistence of reprogramming vectors.....	77
2.15.5	qPCR	79
2.15.6	Selection of reference genes for RT-qPCR data	84
2.15.7	Processing qPCR data.....	85
2.16	Flow cytometry and FACS	86
2.16.1	Assessment of pluripotency associated protein expression in expandable clones.....	86
2.16.2	Assessment of iPSC-CM markers in contracting cultures	88
2.16.3	FACS of cells from contracting cultures based on SIRPA expression and the assessment of cTnI expression in the resulting populations.	90
2.17	Phase contrast Microscopy	92
2.18	Immunofluorescence microscopy.....	92
2.18.1	Pluripotency associated proteins	92
2.18.2	Germ cell layer marker proteins.....	93

2.18.3	Cardiac sarcomeric, gap junction and desmosomal protein.....	93
2.19	Imaging of calcium and voltage transients	97
2.19.1	Preparation of cultures for imaging.	97
2.19.2	Loading cells with Fluo-4-AM and imaging of transients	98
2.20	TEM analysis	99
2.20.1	Collection of samples from adherent cell cultures	99
2.20.2	Collection of right atrial appendage samples	99
2.20.3	Sample processing	99
2.20.4	TEM Image acquisition	100
2.20.5	TEM image analysis	102
2.21	Statistical analysis	104
Chapter 3. Clinical Characteristics Of Study Participants		105
3.1	Introduction.....	105
3.2	Aims	105
3.3	Results	105
3.3.1	Subject 0101	106
3.3.2	Subject 0202	111
3.3.3	Subject 0203	116
3.3.4	Control subjects from which blood samples were collected	120
3.3.5	Control subjects from which right atrial appendage myocardium was collected.....	120
3.4	Discussion and conclusion	121
Chapter 4. The Derivation And Characterisation Of Patient Specific iPSCs From The Peripheral Blood Of Subjects With And Without ARVC/D		122
4.1	Introduction.....	122
4.2	Aims and hypotheses	122
4.3	Results	123
4.3.1	The selection of PBMC reprogramming protocols for testing.....	123
4.3.2	Non-T-cell derived iPSC protocol testing	124
4.3.3	T-cell derived iPSC protocol testing	125
4.3.4	Choice of protocol for iPSC lines derived from ARVC/D subjects.....	126
4.3.5	Overview of iPSC characterisation	126
4.3.6	Genetic identity of clonal cell lines with respect to parent PBMCs.....	129
4.3.7	Mutation sequencing	129

4.3.8	T-cell receptor gene re-arrangement	131
4.3.9	Genomic copy number variations	132
4.3.10	Sendai vector elimination.....	135
4.3.11	Colony and cell morphology.....	137
4.3.12	Pluripotency marker gene expression.....	137
4.3.13	Pluripotency marker protein expression.....	141
4.3.14	Assessments of differentiation potential	144
4.3.15	Assessment of expression of the proteins indicating differentiation to the three primitive germ cell layers after spontaneous embryoid body differentiation. 144	
4.3.16	Teratoma assay	146
4.4	Discussion.....	146
4.5	Conclusions	148

Chapter 5. The Derivation Of Cardiomyocytes From Blood Derived iPSCs And Their Characterisation..... 150

5.1	Introduction	150
5.2	Aims and hypotheses.....	151
5.3	Results	151
5.3.1	Embryoid body differentiation	152
5.3.2	Monolayer differentiation.....	152
5.3.3	The selection of a protocol for further work.....	152
5.3.4	Characterisation of contracting cultures generated by monolayer differentiation	154
5.3.5	Spontaneous contractions	154
5.3.6	Calcium transient imaging.....	155
5.3.7	Sarcomeric and pluripotency related gene expression	156
5.3.8	Expression of sarcomeric proteins.....	158
5.3.9	Ultrastructural features of iPSC-CMs.....	159
5.3.10	Purification of iPSC-CMs by FACS based on SIRPA expression	160
5.3.11	Purification of iPSC-CMs by metabolic selection	162
5.3.12	The selection of a purification method and its application in further work 163	
5.4	Discussion.....	165
5.4.1	The testing of two cardiac differentiation protocols.....	165
5.4.2	Characterisation of contracting cultures.....	165

5.4.3	Purification.....	168
5.5	Conclusions.....	171
Chapter 6. Desmosomes, Desmosomal Genes And Desmosomal Proteins In		
hESCs, iPSCs, iPSC-CMs And Myocardium..... 173		
6.1	Introduction.....	173
6.2	Aims and hypotheses.....	173
6.3	Results.....	173
6.3.1	The identification of desmosomes in iPSCs, iPSC-CMs, RAA and hESCs 173	
6.3.2	Frequency of desmosomes within TEM images.....	175
6.3.3	IDP morphology.....	175
6.3.4	Desmosomal gene expression, experimental design and sample details. 176	
6.3.5	Comparison of desmosomal gene expression in PBMCs, iPSCs, iPSC- CMs and RAA.....	177
6.3.6	Comparison of desmosomal gene expression between individual cell lines in PSCs and iPSC-CMs.....	181
6.3.7	Cellular localisation of desmosomal proteins in iPSCs.....	184
6.3.8	Cellular localisation of desmosomal proteins in iPSC-CMs.....	185
6.4	Discussion.....	191
6.4.1	Desmosomal ultrastructure and quantitative assessments of morphology 191	
6.4.2	Desmosomes in iPSCs and hESCs.....	191
6.4.3	The effect of ARVC/D associated mutations on desmosomal gene expression.....	194
6.4.4	Desmosomal gene expression in iPSC-CMs relative to iPSCs and RAA 196	
6.4.5	Desmosomal protein localisation in control an ARVC/D iPSCs and iPSC- CMs 197	
6.5	Limitations.....	198
6.6	Conclusions.....	199
Chapter 7. A Comparison Of Desmosomal Ultrastructure In Control And		
ARVC/D iPSC-CMs. 201		
7.1	Introduction.....	201

7.2	Aims and hypotheses.....	201
7.3	Results.....	202
7.3.1	Sampling and data structure.....	202
7.3.2	Hazy desmosomes.....	202
7.3.3	Desmosomal asymmetry.....	203
7.3.4	Desmosomal length.....	207
7.3.5	Desmosomal width.....	209
7.4	Discussion.....	210
7.4.1	Hazy desmosomes.....	211
7.4.2	Asymmetrical desmosomes.....	215
7.4.3	Desmosomal length.....	215
7.4.4	Desmosomal gap width.....	216
7.4.5	Desmosomal plaque width.....	217
7.4.6	Limitations.....	219
7.5	Conclusions.....	219
	Chapter 8. Conclusion And Future Perspectives.....	221
8.1	Major findings.....	221
8.2	Limitations.....	222
8.3	Suggestions for future work.....	223
8.4	Significance of the findings.....	226
	References.....	228
	Appendix.....	275
	Summary of pre-transduction culture media from reports of the reprogramming of PBMCs to iPSCs.....	275
	Summary of directed cardiac differentiation protocols.....	279
	SNP array quality control indices.....	283
	Copy number variations in iPSCs.....	284
	Genetic identity.....	289
	T-cell receptor gene rearrangements.....	289
	Selection of reference genes for RT-qPCR experiments.....	291
	Flow cytometry for pluripotency markers.....	293
	Immunofluorescence microscopy for pluripotency associated proteins.....	294
	Expression of proteins indicating differentiation to the three primitive germ cell layers.....	297

The testing of primer sets using in RT-qPCR experiments to assess desmosomal gene expression..... 300

List of figures

Figure 1 Summary of the early stages of embryonic development.....	3
Figure 2 Pathway of differentiation from pluripotent cell to cardiomyocytes.....	10
Figure 3 Ultrastructural features of the cardiac sarcomere.....	11
Figure 4 Schematic illustration of desmosomal ultrastructure.....	15
Figure 5 Representative TEM image of typical desmosome ultrastructure.	16
Figure 6 Schematic illustrations of the ultrastructural features of desmosomes reported by different authors and using different methods of sample preparation.	17
Figure 7 Schematic of the structure of desmosomal cadherins.....	19
Figure 8 Classification of arm-repeat proteins	22
Figure 9 Structure of desmosomal arm repeat proteins.	23
Figure 10 Desmoplakin structure.....	24
Figure 11 A proposed organisation of desmosomal proteins within a cardiac desmosome and their correlation with features seen by TEM.....	26
Figure 12 Canonical Wnt signalling	29
Figure 13 Generation of iPSCs from nucleated peripheral blood cells.	57
Figure 14 Monolayer directed cardiac differentiation protocol.....	66
Figure 15 Organisation of Sendai virus and vectors and predicted binding sites primer set used in their detection.	79
Figure 16 Classification of flow cytometry events as cells and single cells.	87
Figure 17 Analysis of flow cytometry data	88
Figure 18 A TEM image of a section of desmosome at different magnifications.....	101
Figure 19 Criteria used to define a desmosome and cardiac desmosome.....	102
Figure 20 A region of a desmosome illustrating the definitions of the three desmosomal width parameters.	103
Figure 21 An example of the measurement of desmosomal length parameters.	104
Figure 22 12-lead ECG recording of ventricular tachycardia recorded at age 46 in subject 0101.....	108
Figure 23 Pedigree chart for subject 0101.....	108
Figure 24 Illustration of PKP2 c.2146-1G>C.	109
Figure 25 Histology of myocardium from explanted heart of 0101-C41	109
Figure 26 12-lead ECG recording from subject 0101 showing sinus bradycardia at a rate of 56bpm.	110
Figure 27 12-lead ECG of ventricular tachycardia recorded from subject 0202.....	112

Figure 28 Illustration of <i>DSG2</i> c.691-5T>A.	112
Figure 29 Pedigree chart for subject 0202.	113
Figure 30 12-lead ECG recording from subject 0202 showing sinus bradycardia at a rate of 55bpm.	114
Figure 31 12-lead ECG recording from subject 0202 showing sinus bradycardia at a rate of 59bpm.	115
Figure 32 Signal averaged ECG (SAECG) recording from 0202.	116
Figure 33 12-lead ECG of a ventricular tachycardia recorded in subject 0203.	117
Figure 34 Illustration of <i>DSP</i> c.3195C>G.	118
Figure 35 Pedigree chart for subject 0203.	118
Figure 36 12-lead ECG from subject 0203 showing sinus rhythm.	119
Figure 37 Example of a colony observed by phase contrast microscopy with “stem-cell-like” features arising from primary culture of transduced PBMC on an inactivated MEF feeder layer.	125
Figure 38 Examples of comparison of SNP array fluorescence data.	129
Figure 39 A representative chromatograph from Sanger sequencing experiments.	130
Figure 40 Representative example of a CNV detected by analysis of SNP microarray.	135
Figure 41 Screening for the persistence of Sendai reprogramming vectors in iPSC clones by RT-PCR.	136
Figure 42 Phase contrast microscopy images of expandable clones and reference cell lines.	137
Figure 43 Comparison of expression of pluripotency associated genes between clonal cell lines (iPSCs) and an hESC line (H9) by qPCR.	139
Figure 44 Expression of pluripotency associated genes in PBMCs and clonal lines (iPSCs)	140
Figure 45 Immunofluorescence microscopy for OCT4 and TRA-1-60.	143
Figure 46 Immunofluorescence microscopy for germ-layer markers	145
Figure 47 Phase contrast microscopy images of EBs in suspension culture during cardiac differentiation protocol.	153
Figure 48 Proportion of experiments yielding contracting cultures, per cell line and in total.	155
Figure 49 Calcium transients recorded from differentiated cultures.	156

Figure 50 RT-qPCR data illustrating the expression of genes encoding pluripotency markers and sarcomeric proteins in iPSCs and contracting cultures generated from these lines by directed cardiac differentiation.	157
Figure 51 Proportion of cells in contracting cultures expressing cTnI as determined by flow cytometry.....	158
Figure 52 Immunofluorescence microscopy for sarcomeric proteins in cells differentiated from iPSCs.	159
Figure 53 Sarcomeric ultrastructure in RAA cardiomyocytes and cells produced by directed differentiation	160
Figure 54 Co-expression of cTnI and SIRPA in cells from contracting cultures	161
Figure 55 Bar chart showing the proportion of cells expressing cTnI in samples before and after SIRPA based FACS, as assessed by flow cytometry	162
Figure 56 The effect of exposure of contracting cultures to metabolic purification medium on the proportion of iPSC-CMs in culture, as quantified by flow cytometry.....	163
Figure 57 Comparison of the proportion of iPSC-CMs in samples from experiments with and without metabolic purification.....	164
Figure 58 TEM images of desmosomes in iPSCs, iPSC-CMs and RAA	174
Figure 59 Desmosomes in iPSCs and hESCs.....	175
Figure 60 Assessment of the IDP-intermediate filament junction in desmosomes from iPSC-CMs and RAA.	176
Figure 61 Comparison of the expression of desmosomal genes in PBMCs iPSCs, iPSC-CMs and RAA	179
Figure 62 Expression of DSC1 and its isoforms in HaCaT, iPSC-CMs and RAA ...	181
Figure 63 Expression of major desmosomal genes in PSCs.....	182
Figure 64 Expression of major desmosomal genes in iPSC-CMs	183
Figure 65 Immunofluorescence microscopy images of desmosomal protein signal in immortalised keratinocytes (HaCaT) and pluripotent cell lines.	186
Figure 66 Immunofluorescence microscopy images of desmosomal protein signal in ARVC/D iPSCs.....	187
Figure 67 Representative immunofluorescence microscopy image of desmosomal protein localisation in iPSC-CMs	188
Figure 68 Nuclear localisation of punctate JUP and PKP2 signal in iPSC-CMs.....	190
Figure 69 The effect of tilting a sample within the electron beam upon the appearance of desmosomes images by TEM.....	203

Figure 70 Examples of asymmetrical desmosomes.....	205
Figure 71 Total length of asymmetrical segments of desmosomes in control and ARVC/D iPSC-CMs	205
Figure 72 The length and frequency of asymmetrical desmosomes in iPSC-CMs from control and ARVC/D lines.	206
Figure 73 Histogram of individual desmosomal length measurements.....	208
Figure 74 Total desmosomal length and interquartile range of total lengths in control and ARVC/D iPSC-CMs	208
Figure 75 Desmosomal width in control and ARVC/D lines	210
Figure 76 Schematic representing a simplified desmosome; its possible orientations within a TEM level; and the effect of tilting a level within the electron beam of a TEM on the resultant image.....	212
Figure 77 Images provided in Caspi <i>et al.</i> of hazy and abnormal desmosomes.....	214
Figure 78 Image from Caspi <i>et al.</i> illustrating the desmosomal width parameters measured in that study.	219
Figure 79 Characterisation of CNV predicted to be at 20p11.1-20q11.21 in the iPSC line 2-C4.	285
Figure 80 Characterisation of CNV predicted to be at 4q34.3 - 4q35.1 in the iPSC line 2-C1.	285
Figure 81 Characterisation of CNV predicted to be at 7q36.1 in the iPSC line 2-C1.	286
Figure 82 Characterisation of CNV predicted to be at 22q11.1 - 22q11.21 in the iPSC line 2-C1.	286
Figure 83 Characterisation of CNVs predicted to be at 14q11.2 in the multiple iPSC lines.	287
Figure 84 Data plots of the T-cell receptor rearrangement assays which yielded positive results.	290
Figure 85 Immunofluorescent microscopy for pluripotency markers.....	294
Figure 86 Immunofluorescence microscopy assessment of TUJ1, SMA and AFP expression in cultures generated from iPSCs that underwent differentiation in the presence of serum	296
Figure 87 Expression of desmosomal genes in HaCaT cells.....	301

List of tables

Table 1 Reference ranges for the concentrations of mononuclear cells found in the peripheral blood of healthy Caucasian adults and their characteristic surface markers.	6
Table 2. Reports of reprogramming PBMCs to iPSCs and the vectors used.	7
Table 3 Features of hPSC-CM maturation	13
Table 4 Techniques proposed for the quantification of PSC-CM maturity.....	13
Table 5 Comparison to the ultrastructural features of different adhesion junction, adapted from Muir 1965	14
Table 6 Publications providing typical values for desmosomal width parameters	18
Table 7 Summary of the molecular interactions reported between the intracellular regions of desmosomal plaque proteins.....	21
Table 8 Diagnostic criteria for ARVC/D	32
Table 9 Diagnostic categories of ARVC/D	34
Table 10. Symptoms, clinical features and prognosis of clinical defined ARVC/D for published cohorts.	35
Table 11. ARVC/D associated genes, their functions and reports of inheritance patterns associated with mutations in these genes.....	36
Table 12. Prevalence of ARVC/D associated mutations in published cases series ..	37
Table 13 Pathogenic mutations listed in the ARVD/C Genetic Variants Database. ..	39
Table 14 Protein domains associated with of pathogenic variants of all types in the major desmosomal genes	39
Table 15 Protein domains associated with of pathogenic missense variants in the major desmosomal genes	40
Table 16 Comparison of the results of studies of ARVC/D in which quantitative assessments of desmosomal morphology were performed.	42
Table 17 Summary of studies describing the desmosomal immunohistology of cardiac tissue from cases of ARVC	46
Table 18 Studies assessing plakoglobin expression by immunohistology in genotyped cases of ,ARVC/D.....	47
Table 19. Animal models of desmosomal gene abnormalities and ARVC/D associated desmosomal mutations	48
Table 20 Cellular models of desmosomal gene abnormalities and ARVC/D associated desmosomal mutations	50
Table 21 Summary of ultrastructural features of ARVC/D myocardium.	52

Table 22 Composition of major culture media and reagents.....	69
Table 23 Definitions of CNV type used by BlueFuse Multi algorithm.....	73
Table 24 Thermocycler program for amplification of genomic DNA prior to sequencing	74
Table 25 Primers used for the amplification of genomic DNA prior to sequencing. ..	75
Table 26 Primers used to initiate Sanger sequencing reaction.....	75
Table 27 Expected size ranges of PCR products in T-cell receptor re-arrangement assay	76
Table 28 Thermocycler program for reverse transcription	77
Table 29 Thermocycler program for amplification of genomic DNA prior to sequencing and of cDNA in non-quantitative PCR experiments	78
Table 30 Primers used for the amplification of cDNA in RT-PCR experiments.....	78
Table 31 Thermocycler program for qPCR reactions.....	80
Table 32 Primers targeting reference genes used in RT-qPCR experiments	81
Table 33 Primers targeting pluripotency associated genes used in RT-qPCR experiments	82
Table 34 Primers targeting genes encoding cardiac sarcomeric proteins used in RT- qPCR experiments.....	82
Table 35 Primers targeting genes encoding desmosomal plaque proteins used in RT- qPCR experiments.....	83
Table 36 Antibodies used in flow cytometry experiments.	91
Table 37 Antibodies used in preparation of samples from immunofluorescence microscopy for cell from the three germ cell layers.	95
Table 38 Primary antibodies used in immunofluorescence microscopy experiments	95
Table 39 Secondary antibodies used in immunofluorescence microscopy experiments	96
Table 40 Axiovert200M Filters.....	97
Table 41 Axioimager Filters.....	97
Table 42 The criteria used to identify a desmosome and cardiac desmosome within a TEM image.	102
Table 43 Definitions of desmosomal width and length parameters.....	103
Table 44 Diagnosis of ARVC/D in subjects recruited to the study as defined in the current task force criteria.	106
Table 45 Characteristics of control subjects from which blood samples were obtained.	120

Table 46 Baseline characteristics of subjects from which right atrial appendage myocardium was collected.	121
Table 47 Results of initial reprogramming experiments aimed at generating non-T-cell derived iPSCs.	124
Table 48 Results of initial reprogramming experiments aimed at generating T-cell derived iPSCs.....	125
Table 49 Summary of iPSC characterisation.....	128
Table 50 Correlation co-efficient values for generated by comparison of “red” fluorescence intensity values in iPSC lines with those of the PBMCs used in the reprogramming experiments from which they were generated.	129
Table 51 Pathogenic CNVs acquired by iPSC clones during reprogramming.....	134
Table 52 Unadjusted Ct values from the assessment of pluripotency associated genes in clonal cell lines (iPSCs) and an hESC line (H9) by qPCR	140
Table 53 Unadjusted Ct values from the assessment of pluripotency associated genes in PBMCs and clonal lines (iPSCs)	141
Table 54 Summary of immunofluorescence microscopy for the three primitive germ cell layers	145
Table 55 Summary of the characterisation of contracting cultures performed in different cell lines.....	154
Table 56 Unadjusted Ct values from the assessment of expression of genes encoding pluripotency markers and sarcomeric proteins in iPSCs and iPSC-CMs.....	158
Table 57 Unadjusted Ct values from the assessment of expression of desmosomal gene in PBMCs, iPSCs, iPSC-CMs and RAA samples.....	180
Table 58 Unadjusted Ct values from the assessment of <i>DSC1</i> isoform expression in iPSC-CMs, HaCaT cell and RAA.	181
Table 59 Unadjusted Ct values from the assessment of the expression of desmosomal genes in pluripotent cell lines.....	183
Table 60 Unadjusted Ct values from the assessment of desmosomal gene expression in iPSC-CMs.	184
Table 61 Pre-transduction culture conditions used for the reprogramming of CD34+ populations isolated from PBMCs	274
Table 62 Pre-transduction culture medium compositions used in publications describing the generation of T-cell derived iPSCs	276

Table 63 Pre-transduction culture medium composition used in publications describing the generation of iPSCs from mixed PBMC samples	277
Table 64 Protocols for directed embryoid body differentiation of hPSCs to cardiomyocytes	279
Table 65 Protocols for directed monolayer differentiation of hPSCs to cardiomyocytes	281
Table 66 SNP microarray quality control indices for PBMC and iPSC lines	282
Table 67 Summary of CNVs detected by SNP microarray in all samples tested	284
Table 68 Summary of genes affected by those CNVs classified as pathogenic	288
Table 69 Results of T-cell receptor rearrangement assay	288
Table 70 Reference genes ranked by M value	290
Table 71 Reference genes ranked by the GeNorm algorithm.....	292
Table 72 Expression of pluripotency associated proteins assessed by flow cytometry, fluorescence of labelled sample relative to unlabelled sample	292
Table 73 Expression of pluripotency associated proteins by iPSCs assessed by flow cytometry, proportion of labelled sample classified as positive.	293
Table 74 Reduction in percentage of single cell events in labelled sample classified as positive when FMO isotype control sample was used to define threshold rather than the unlabelled sample	293

List of abbreviations

6FAM	6-carboxyfluorescein
A-band	Anisotropic band
AFP	Alpha-fetoprotein
ANOVA	Analysis of variance
APC	Adenomatosis polyposis coli
ARVC/D	Arrhythmogenic right ventricular cardiomyopathy / dysplasia
BAF	B allele frequency
bFGF	Basic fibroblast growth factor
BLAST	Basic local alignment search tool
BMP	Bone morphogenetic protein
BSA	Body surface area
CD	Cluster of differentiation
cDNA	Complementary DNA
CHIR	CHIR99021
CK1 α	Casein kinase 1 α
CNV	Copy number variation
CMRI	Cardiac magnetic resonance imaging
cTnI	Cardiac troponin I
cTnT	Cardiac troponin T
CMOS	Complementary metal–oxide–semiconductor
CXR	carboxy-X-rhodamine
DAPI	4',6-diamidino-2-phenylindole
dH ₂ O	Distilled water
DL	Desmosomal length
DMEM	Dulbecco's modified Eagles medium
DNA	Deoxyribonucleic acid
dNTP	Deoxynucleoside triphosphate
DES	Desmin
DGV	Database of genomic variants
DKK1	Dickkopf related protein 1
DPBS	Dulbeccos phosphate buffered saline
DSC1	Desmocollin 1
DSC2	Desmocollin 2
DSC3	Desmocollin 3

dsDNA	Double stranded DNA
DSG1	Desmoglein 1
DSG2	Desmoglein 2
DSG3	Desmoglein 3
DSG4	Desmoglein 4
DSM	Dorsomorphin
DSP	Desmoplakin
ECG	Electrocardiogram
EB	Embryoid body
ECB	Extra-cellular calcium binding domain
ECIM	Embryoid body cardiac induction medium
EDTA	Ethylenediaminetetraacetic acid
EF	Ejection fraction
EMB	Endomyocardial biopsy
ESC	Embryonic stem cell
FACS	Fluorescence activated cell sorting
FBS	Fetal bovine serum
FGF	Fibroblast growth factor
FLT3L	FMS related tyrosine kinase 3 ligand
FMO	Fluorescence minus one
F protein	Fusion protein
fps	Frames per second
Frz	Frizzled transmembrane receptor
FSC-A	Forward scatter area
FSC-H	Forward scatter height
GAPDH	Glyceraldehyde-3-phosphate dehydrogenase
GFR	Growth factor reduced
GSK	Glycogen synthase kinase
GTEx	Genotype-tissue expression project
HCM	Hypertrophic cardiomyopathy
HDF	Human dermal fibroblasts
HEPES	4-(2-hydroxyethyl)-1-piperazineethanesulfonic acid
hESC	Human embryonic stem cell
HEX	Hexachlorofluorescein
hiPSC	Human induced pluripotent stem cell

HPA	Human protein atlas
HPC	Haemopoetic progenitor cell
hPSC	Human pluripotent stem cell
hPSC-CM	Human pluripotent stem cell derived cardiomyocyte
H-zones	Heller zones
IA	Intracellular anchor
I-bands	Isotropic bands
ICD	Intercalated disc
ICM	Inner cell mass
ICS	Intracellular cadherin sequence
IDCM	Idiopathic dilated cardiomyopathy
IDP	Inner dense plaque
IF	Intermediate filaments
IgG	Immunoglobulin G
IgM	Immunoglobulin M
IHC	Immunohistochemistry
IIW	Inter-inner dense plaque width
IL2	Interleukin-2
IL3	Interleukin-3
IL6	Interleukin-6
IMW	Intermembrane width
IOW	Inter-ODP width
iPSC	Induced pluripotent stem cell
iPSC-CM	Induced pluripotent stem cell derived cardiomyocyte
iPSC-SkM	Induced pluripotent stem cell derived skeletal myocytes
ISCA	International standards for cytogenetic arrays
ITS-G	Insulin-Transferrin-Selenium
JUP	Plakoglobin
KLF4	Kruppel like factor 4
KO-DMEM	Knock-out DMEM
KSR	Knock-out serum replacement
LBBB	Left bundle branch block
LED	Light emitting diode
LEF1	Lymphoid enhancer binding factor 1
LMNA	Lamin A/C

LP	Long pass
LRP	Lipoprotein receptor related protein 5/6
LV	Left ventricle
LVEF	Left ventricular ejection fraction
MAP kinase	Mitogen-activated protein kinase
MCIM	Monolayer cardiac induction medium
MCMM	Monolayer cardiac maintenance medium
mCPC	Mouse cardiac progenitor cell
MCPM	Monolayer cardiac purification medium
MEF	Mouse embryonic fibroblast
M-lines	Mittelscheibes
MOI	Multiplicity of infection
MRI	Magnetic resonance imaging
mTeSR1-RI	mTeSR1 containing 10uM RI
MWU	Mann-Whitney U test
MYC	MYC proto-oncogene
NCBI	National Centre for Biotechnology Information
NEAA	Non-essential amino acids
NF2	Neurofibromin 2 / Merlin
NFW	Nuclease free water
NK cell	Natural killer cell
NOD/SCID	Non-obese diabetic / Severe combined immune deficiency
NRVM	Neonatal rat ventricular myocytes
NTCEM	Non-T-cell expansion medium
NTS	Normal Tyrode's solution
OCT3/4	Octamer binding protein 3/4 / POU class 5 homeobox 1
OCT4	Octamer binding protein 4 / POU class 5 homeobox 1
ODP	Outer dense plaque
OMIM	Online Mendelian inheritance in man
ORO	Oil red O
OsO4	Osmium tetroxide
PBMC	Peripheral blood mononuclear cell
PCR	Polymerase chain reaction
PKC α	Phosphokinase C α
PKP1	Plakophilin 1

PKP2	Plakophilin 2
PKP3	Plakophilin 3
PKP4	Plakophilin 4
PL	Plaque length
PLAX	Parasternal long axis
PLN	Phospholambin
PM(i)	Intracellular surface of the plasma membrane
PM(e)	Extracellular surface of the plasma membrane
PP2A	Protein phosphatase 2A
pPKC α	Phosphorylated protein kinase C α
PRD	Plakin repeat domain
PRL	Proline rich linker
PSAX	Parasternal short axis
PSC	Pluripotent stem cell
PSC-CM	Pluripotent stem cell derived cardiomyocytes
qPCR	Quantitative polymerase chain reaction
RAA	Right atrial appendage
RBBB	Right bundle branch block
RI	Rock inhibitor, Y27632
RNA	Ribonucleic acid
RPMI	Roswell Park Memorial Institute 1640 medium
RPMI-20	Roswell Park Memorial Institute 1640 medium supplemented with 20% fetal bovine serum
RT	Reverse transcriptase
RT-qPCR	Reverse transcription quantitative polymerase chain reaction
RUD	Repeat unit domain
RV	Right ventricle
RVOT	Right ventricular outflow tract
RYR2	Cardiac ryanodine receptor
SAECG	Signal averaged ECG
SCD	Sudden cardiac death
SCF	Stem cell factor
SD	Standard deviation
SEM	Standard error of the mean

SeV	Sendai vector
SIRPA	Signal regulatory protein α / Tyrosine-protein phosphatase non-receptor type substrate 1
SMA	Smooth muscle actin
SNP	Single nucleotide polymorphism
SOX2	SRY-box 2
SSC-A	Side scatter area
SSEA4	Stage specific embryonic antigen 4
TCEM	T-cell expansion medium
TEM	Transmission electron microscopy
TCEM	T-cell expansion medium
TCF/LEF	Transcription factor / lymphoid enhancer binding factor
TCF4	Transcription factor 4
TDW	Total desmosomal width
TGF3B	Transforming growth factor 3 β
TM	Transmembrane sequence
TMEM43	Transmembrane protein 43
TNNI3	Cardiac troponin I
TPM	Transcripts per million
TPO	Thrombopoietin
TRA	T-cell receptor α
TRB	T-cell receptor β
TRD	T-cell receptor δ
TRG	T-cell receptor γ
TRITC	Tetramethylrhodamine isothiocyanate
TTN	Titin
TUJ1	Beta-III tubulin
TUNEL	Terminal deoxynucleotidyl transferase dUTP nick end labelling
UCSC	University of California Santa Cruz
VEGF	Vascular endothelial growth factor
VT	Ventricular tachycardia
WMA	Wall motion abnormalities
Wnt	Wingless-related integration site
Z-lines	Zwischenscheibes

Chapter 1. Introduction

Arrhythmogenic right ventricular cardiomyopathy / dysplasia (ARVC/D) is an adult onset cardiomyopathy presenting with ventricular arrhythmias and heart failure (Pilichou *et al.*, 2016) (Corrado *et al.*, 2017). Mutations in genes encoding desmosomal proteins are identified in approximately 50% of probands (Ackerman *et al.*, 2011). Studies of the myocardium of ARVC/D patients have found abnormalities in desmosomal ultrastructure, desmosomal protein localisation and the expression of desmosomal and non-desmosomal genes (Pilichou *et al.*, 2016). These changes will be referred to collectively as desmosomal dysfunction in this manuscript and have been hypothesised to be part of a common pathway in the pathogenesis of ARVC/D (van Tintelen *et al.*, 2007).

Animal and cellular models have been used to study the pathogenesis of ARVC/D (Table 19, Table 20). Patient specific induced pluripotent stem cell derived cardiomyocytes (iPSC-CMs) are one type of cellular model that has been used for this purpose. iPSC-CMs carrying ARVC/D associated desmosomal mutations manifest similar abnormalities in desmosomal structure and function that have been observed in the myocardium of subjects with the disease (Caspi *et al.*, 2013) (Ma *et al.*, 2012) (Kim *et al.*, 2013) (Basso, 2006) (Asimaki *et al.*, 2009). These studies have modelled five different mutations, all of which affected that same gene, plakophilin 2 (*PKP2*). The aim of this study is to generate patient specific iPSC-CM models of ARVC/D caused by mutations that have not been modelled previously, particularly those in genes other than *PKP2*.

The first part of the chapter will discuss the generation of induced pluripotent stem cells (iPSCs) and of iPSC-CMs. The second part of the chapter will discuss the desmosome, and desmosomal proteins. The third part of the chapter will discuss the clinical features of ARVC/D and their recapitulation in animal and cellular models. The chapter will conclude with an outline of the aims of this study and the hypotheses to be investigated.

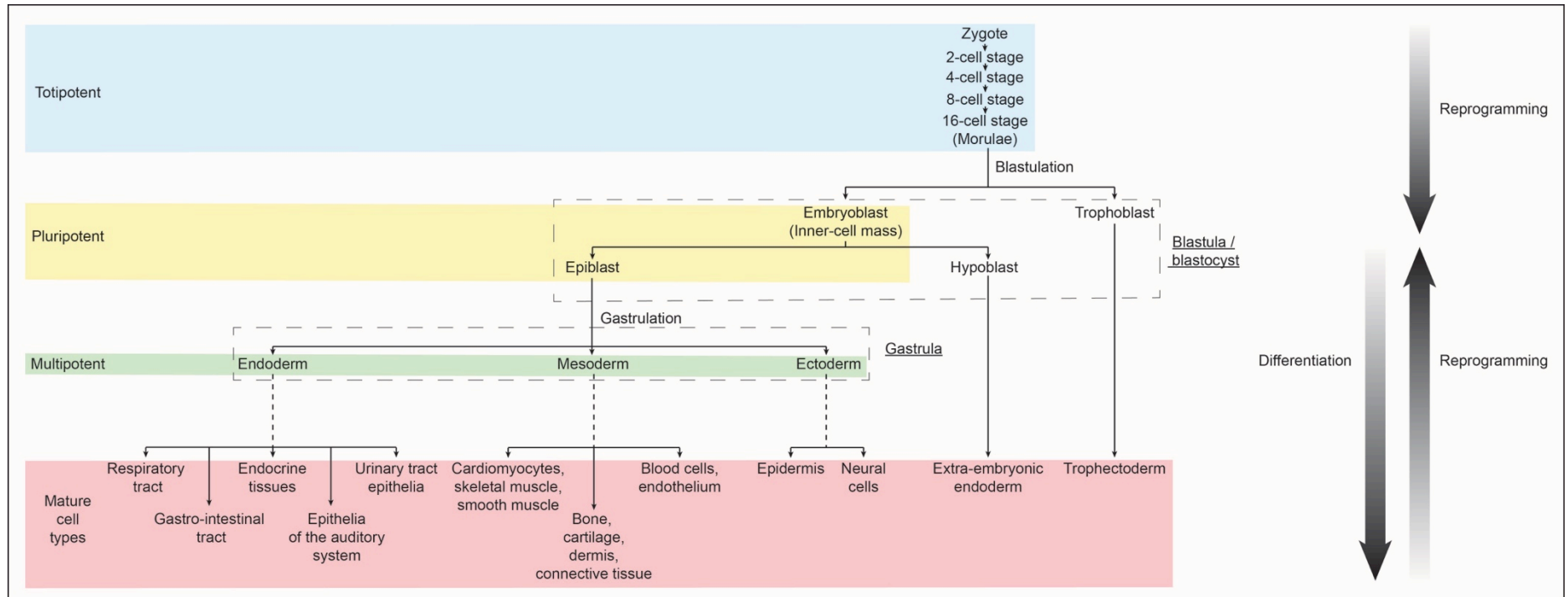
1.1 Overview of induced pluripotent stem cells and iPSC derived cardiomyocytes

1.1.1 Pluripotency *in vivo*

In the embryo the first cells that may be considered pluripotent are the embryoblasts^a that constitute the inner cell mass (ICM) of the blastocyst (Figure 1) (Hanna *et al.*, 2010). Pluripotent cells have the ability to give rise to any cell type (and therefore any tissue) of the mature organism, including gametes, thereby allowing the reproduction of their genetic code to subsequent generations. Pluripotency is distinguished from totipotency in that pluripotent cells are unable to give rise to the trophoctoderm. *In vivo*, cells of the embryo, from the point of the fertilised ovum to the late morula stage are considered totipotent. At the onset of blastulation, cells of the morula undergo specification to either pluripotent cells of the ICM, or non-pluripotent cells of the trophoctoderm (Figure 1)

The process by which pluripotent cells develop into the multiple cell types found in mature tissues is called differentiation. Each transition from a progenitor to a more differentiated cell type defines and limits the cellular identities or fates at which a cell may ultimately arrive *in vivo*.

^a Embryoblasts are also referred to as epiblasts, and are defined in distinction from hypoblasts that form the trophoctoderm.



3

Figure 1 Summary of the early stages of embryonic development.

Cells fulfilling the definition of toti-, pluri-, and multi-potent are indicated.

Multi-potent cells differentiate to mature cell type via multiple intermediate progenitor cell types (not shown).

1.1.1 Pluripotency *in vitro*

Embryonic stem cells (ESCs) and induced pluripotent stem cells (iPSC) are types of pluripotent cell lines that can be maintained in culture. ESCs and iPSCs will be referred to collectively as pluripotent stem cells (PSCs) in this work. Embryonic stem cell lines are derived from the embryoblasts of the inner cell mass (ICM) (Thomson *et al.*, 1998). Induced pluripotent stem cells (iPSC) are pluripotent lines that are generated from non-pluripotent cell types (Takahashi *et al.*, 2007).

Pluripotent cells *in vitro* have a number of characteristics. They avoid senescence and are therefore theoretically capable of undergoing mitosis indefinitely (Singh *et al.*, 2016). They have a characteristic pattern of gene and protein expression, including a number of pluripotency markers, which are expressed at high levels when the cells are in maintenance culture and whose expression levels decrease during differentiation. A large number of such markers have been described (see Zhao *et al.*, 2012 for a review). Details of the pluripotency markers assessed in this study are discussed in Chapter 4. Gene expression is regulated by epigenetic mechanisms such as DNA methylation and histone modification (Chen and Riggs, 2011) (Kouzarides, 2007). Despite similarities in the expression of pluripotency markers between ICM embryoblasts and PSCs there are differences in epigenetic marker patterns in the two cell types. ICM embryoblasts have a globally hypomethylated genome, whereas the genome of ESCs and iPSCs is highly methylated (Santos *et al.*, 2002) (Meissner *et al.*, 2008). This has been interpreted to indicate that widespread genomic de-methylation is not a necessary condition for pluripotency and is consistent with the idea that pluripotency is mediated by the expression of a key pluripotency associated genes.

The ultimate test of pluripotency for cells *in vitro* is their ability to recapitulate the cells of the ICM by giving rise to all cells within a mature organism. This can be demonstrated by a successful tetraploid complementation assay followed by evidence of the production of gametes in the resulting organism (thereby demonstrating germ-line transmission to subsequent generations) (Nagy *et al.*, 1990) (Nagy *et al.*, 1993) (Boland *et al.*, 2009) (Okita *et al.*, 2007) (Zhao *et al.*, 2009). The differentiation potential of human pluripotent cell lines cannot be tested in this way for ethical and practical reasons. The challenge of defining and demonstrating pluripotency in human cell pluripotent cell lines is discussed in more details in Chapter 4.

1.1.2 Cellular reprogramming and blood derived iPSCs

iPSCs are generated from differentiated cell types by a process called reprogramming (Jaenisch and Young, 2008). Reprogramming involves changing the epigenetic profile of mature cells such that the resulting gene expression patterns resemble those of pluripotent cells (Reik *et al.*, 2001) (Papp and Plath, 2013).

Cellular reprogramming may be achieved by the overexpression of four pluripotency associated genes: *KLF4*, *OCT3/4*, *SOX2* and *MYC* (Takahashi *et al.*, 2007). A vector based on Sendai virus may be used to introduce and drive expression of these genes (Fusaki *et al.*, 2009) (Nishimura *et al.*, 2011). Sendai virus is an enveloped single negative strand ribonucleic acid (RNA) non-integrating member of the *Paramyxoviridae* family (Li *et al.*, 2000). The infectivity of the Sendai virus is dependent on the presence of F protein within the viral envelope that mediates its fusion with a host cell's plasma membrane. The envelope of a Sendai vector contains F protein but the gene encoding the protein is absent from the genome it transmits to the cell it invades (Inoue *et al.*, 2003). F deficient Sendai vectors are therefore capable of transferring genetic material into cells, and will lead to the production of virus-like particles which are released into the extracellular space, but these particles are incapable of fusing with other cells due to the lack of F-protein in their envelopes. This characteristic, in combination with the non-integrating nature of the vector contribute to the eventual elimination of the vector within cells over successive passages (Fusaki *et al.*, 2009). This technology has been developed into a widely used commercial reprogramming system (Life Technologies, 2013).

Regardless of the method of transfection the epigenetic changes induced by transgenes trigger the upregulation of endogenous pluripotency factors that perpetuate the pluripotent state after the decline of transgene expression.

Nucleated peripheral blood cells are an attractive target for the generation of patient specific iPSCs for several reasons. Peripheral blood sampling is a low risk and common procedure in clinical practice and is therefore more likely to be acceptable to potential donors than more invasive and infrequently performed procedures such as skin biopsy (from which fibroblasts are obtained for reprogramming). A typical 10ml blood sample contains $>10 \times 10^6$ nucleated cells, of which $60 \pm 20\%$ may typically be isolated by techniques such as density gradient centrifugation (Amersham Biosciences, 2001). Since most reprogramming protocols involve the transduction of between 0.1 to 0.5×10^6 cells, blood samples represent an abundant source of cells for reprogramming.

Peripheral blood contains a mixture of different types of nucleated cells (Table 1) iPSCs have been generated from several PBMC types with varying degrees of efficiency (Table 2). Different cell types are characterised morphologically and by the cluster of differentiation (CD) molecules expressed at their plasma membranes .

PBMC type		Surface markers	Reference ranges (x10 ⁶ /ml)	
Lymphocytes	Mature T-cell	CD3+	1.1 - 3.4	0.67 – 2.89
	Mature B-cell	CD19+		0.08 – 0.78
	NK T-cells	CD3-, CD16+, CD56+		0.07 – 0.99
Monocytes		CD14+	0.16 - 0.62	
Multi-potent progenitor cells (HPCs)		CD34+	0.0006 – 0.0049	

Table 1 Reference ranges for the concentrations of mononuclear cells found in the peripheral blood of healthy Caucasian adults and their characteristic surface markers.

(Bain, 1996) (Reichert *et al.*, 1991) (Sekhsaria *et al.*, 1996)

The expansion of a target cell type during pre-transduction culture appears to be an important factor in determining its susceptibility to reprogramming (Egli *et al.*, 2008). The protocols used to generate iPSCs from PBMCs have sought to optimise reprogramming efficiency by identifying cytokines and growth factors that promote proliferation of the target cell type in pre-transduction culture. Summaries of the pre-transduction culture conditions used in these protocols are given in the appendix (Table 61 to Table 63).

Paper	Target cell type.		Vector	MOI	Efficiency
(Seki <i>et al.</i> , 2012)	T-cells		Sendai	20	0.1-0.2%
(Brown <i>et al.</i> , 2010)			Gamma-retrovirus	NA	0.01%
(Merling <i>et al.</i> , 2013)	Non-T-cells	Purified CD34+ cells	Sendai	6	>0.024% *
(Mack <i>et al.</i> , 2011)		Purified CD34+ cells	Episome	NA	0.0007-0.07% ∞
(Lin Ye <i>et al.</i> , 2013)		Un-purified, but high proportion of myelo-erythroid progenitors	Sendai	10	0.02-0.27% *
(Chou <i>et al.</i> , 2011)			Episome	NA	0.0007%
(Su <i>et al.</i> , 2013)		Mixed PBMCs	Lentivirus	4	0.2%
(Kunisato <i>et al.</i> , 2011)			Gamma-retrovirus	NA	0.004-0.006%
(Loh <i>et al.</i> , 2010)			Lentivirus	5	0.0008-0.001%
(Ohmine <i>et al.</i> , 2011)		PBMCs purified according to adhesion to culture plates	Lentivirus	5	0.002-0.01%

Table 2. Reports of reprogramming PBMCs to iPSCs and the vectors used.

Efficiency is defined as the number of colonies with a stem cell like morphology per input cell with the exception of the studies indicated by * which assessed TRA-1-81 positive colonies and the study indicate by ∞ which assessed TRA-1-60 positive colonies per input cell.

1.1.3 The maintenance of human PSCs *in vitro*

Culture conditions stimulate the expansion of iPSCs and ESCs *in vitro* whilst maintaining their pluripotency through a combination of soluble factors within the culture medium and insoluble factors of the culture surface to which they are attached (Xu *et al.*, 2001). Pluripotency culture systems for human PSC can be divided into two groups: (1) those employing co-culture with another cell type – referred to as a feeder layer and (2) feeder-free conditions without such cells. Mouse embryonic fibroblasts (MEFs) are widely used as a feeder layer (Thomson *et al.*, 1998) (Reubinoff *et al.*, 2000). MEFs are thought to support pluripotency by the excretion of factors into the culture medium. Feeder-free culture systems were developed to improve the consistency of culture conditions and to avoid the potential for feeder cells to contaminate PSC samples used in subsequent applications (Xu *et al.*, 2001). One such culture system involves mTeSR1 medium (StemCell Technologies) with cells adherent to cultureware coated in Matrigel (Corning)^a (Ludwig *et al.*, 2006).

^a Matrigel is a solution of solubilized basement membrane proteins including laminin, collagen IV, and heparin sulphate proteoglycans derived from cultures of Engelbreth-Holm-Swarm mouse sarcoma (Kleinman *et al.*, 1982). It also contains TGF-β, epidermal growth factor, fibroblast growth factor and tissue plasminogen activator (Kleinman *et al.*, 1986).

1.1.4 PSC-CM generation

Cardiac differentiation involves a transition of cell identity from pluripotency to cardiomyocytes via a series of intermediate cell types, each of which is associated with a characteristic pattern of gene and protein expression (Figure 2) (Cao *et al.*, 2008) (Beqqali *et al.*, 2006) (Germanguz *et al.*, 2011) (He *et al.*, 2003).

The differentiation of pluripotent cells *in vitro* can be triggered by the withdrawal of factors known to maintain pluripotency, combined with exposure to growth factors that encourage differentiation to specific lineages. Differentiation triggered by the withdrawal (or failure) of pluripotency maintenance conditions is referred to as spontaneous differentiation. This may be achieved by both changing the compositions of culture medium and by the culture of cells in suspension, thereby detaching them from their supportive protein matrix and encouraging the formation of clusters of cells called embryoid bodies (EBs). Cardiomyocytes may be generated by spontaneous differentiation of PSCs, but the efficiency of this technique is low with <1% of the output cells expressing cardiac troponin proteins (Kehat *et al.*, 2001) (Boheler *et al.*, 2002) (Xu *et al.*, 2002).

Differentiation in which the culture conditions are manipulated with the intention of differentiating cells to a specific fate is referred to as directed differentiation. Directed differentiation protocols have taken advantage of an increasing knowledge of temporal interplay of signalling pathways that mediate cardiac differentiation. In directed cardiac differentiation protocols, mesodermal specification is promoted by the upregulation of one or more of the canonical Wnt, BMP or Activin pathways (Ueno *et al.*, 2007) (Paige *et al.*, 2010) (Zhang *et al.*, 2008) (Kitamura *et al.*, 2007) (Kubo *et al.*, 2004) (Gadue *et al.*, 2006). Cardiac mesodermal specification is promoted by upregulation of BMP, Activin and FGF signalling and downregulation of canonical Wnt signalling (Kattman *et al.*, 2011) (Yang *et al.*, 2008) (Yang *et al.*, 2008). The development of cardiac progenitors from cardiac mesoderm is promoted by upregulation of FGF signalling and downregulation of Wnt, Activin and BMP signalling (Kattman *et al.*, 2011) (Zhang *et al.*, 2008). Other factors that have been found to influence cardiac differentiation and maturation include: ascorbic acid, insulin, p38 MAP kinase inhibition and VEGF and hypoxic culture conditions (Cao *et al.*, 2012) (Freund *et al.*, 2008) (Lei Ye *et al.*, 2013) (Burrige *et al.*, 2011) (Graichen *et al.*, 2008).

Directed cardiac differentiation protocols can be divided into two broad categories, those involving the formation of EBs and those involving cells grown in a monolayer.

Tables summarising and comparing selected protocols are provided in the appendix (Table 64 and Table 65). The efficiencies of these protocols have been reported to be >70%, though in some cases achieving this requires modification of the protocol to account for the characteristics of the hPSC line (Burrige *et al.*, 2011).

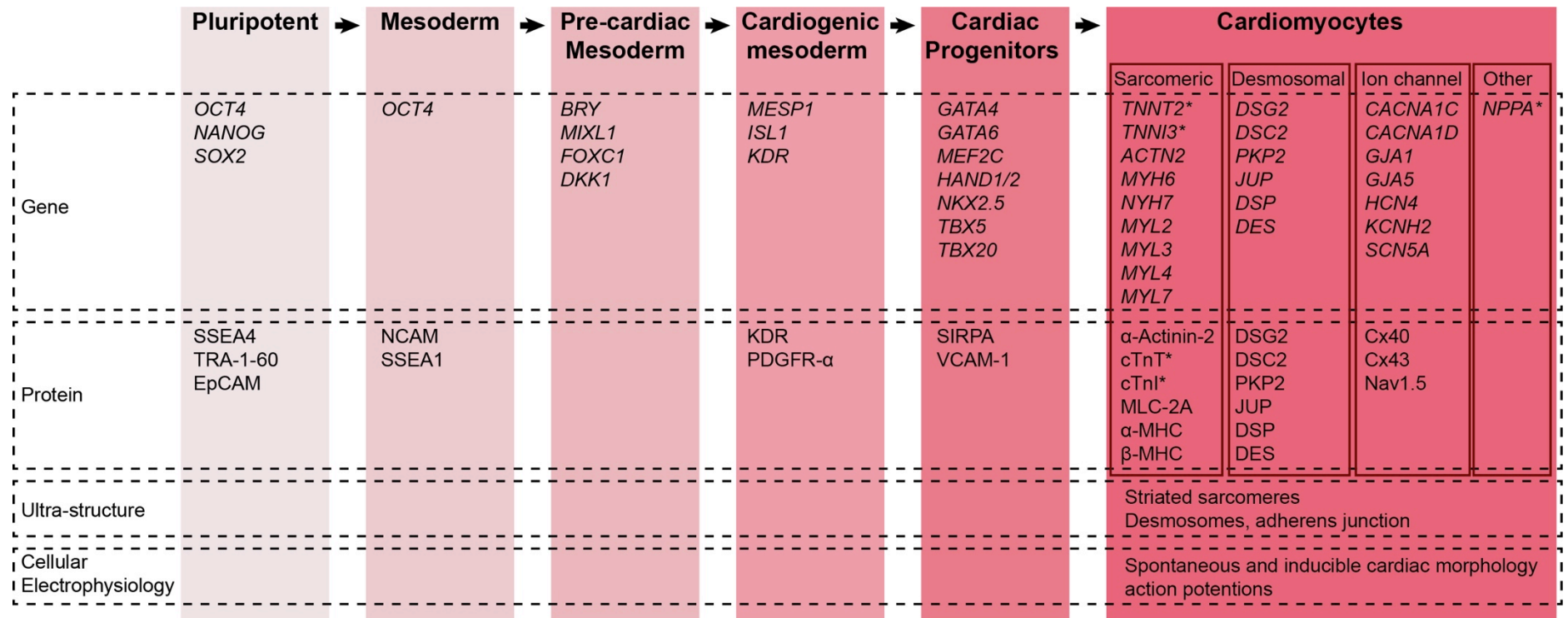


Figure 2 Pathway of differentiation from pluripotent cell to cardiomyocytes.

The genes and proteins listed are a selection of those cited in publications describing cardiac differentiation markers. Genes and proteins whose expression is limited to cardiomyocytes are indicated (*)

1.1.5 PSC-CM maturation

Features that have been used as evidence of successful cardiac differentiation are listed in Figure 2. The presence of spontaneous contractions within differentiated culture indicates that there are cells containing the myofibrils necessary for both repetitive contraction and the fluctuating calcium transients needed to mediate them. The presence of spontaneous contractions increases the probability that these cultures contain cardiomyocytes. Striated myofibrils may be identified by immunofluorescence microscopy and transmission electron microscopy (TEM). The ultrastructural features of striated myofibrils are summarised in Figure 3.

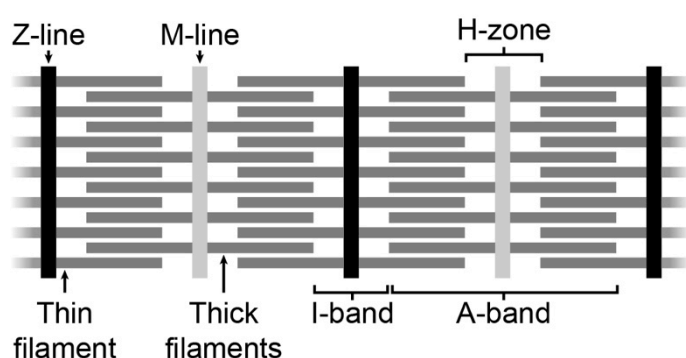


Figure 3 Ultrastructural features of the cardiac sarcomere.

A simplified illustration of the molecular organisation of a cardiac sarcomere and its ultrastructural features. Myofibrils are traversed at regular intervals along their length by electron dense *Zwischenscheibes* (Z-lines), mid way between Z lines are the less dense *Mittelscheibes* (M-lines). M-lines sit in the middle of regions of lower electron density called Heller (H) zones. Z-lines also sit in the middle of regions of lower electron density called isotropic (I) bands. The regions between adjacent I-bands are called A-bands. This appearance is produced by two groups of partially overlapping fibres. Thin filaments consisting mainly of actin are anchored at the Z-lines. Thick filaments consisting mainly of myosin are anchored at the M-lines. A-bands correspond to the whole region of a sarcomere in which thick filaments are present. I-bands correspond to regions in which there are thin filaments alone (without overlapping thick filaments). H-zones correspond to regions in which there are thick filaments alone (without overlapping thin filaments) (Sonnenblick, 1968).

Other cell types also express of the genes and proteins expressed by cardiomyocytes e.g. skeletal myocytes. For this reason, cardio-specific markers such as the cardiac isoforms of troponins T and I are typically used to assess the efficiency of cardiac differentiation protocols (Figure 2).

PSC-CMs are similar to fetal cardiomyocytes in terms of gene expression, protein expression, ultrastructure, electrophysiology and cellular metabolism (Table 3). The characteristics of PSC-CMs change during maintenance culture (Lundy *et al.*, 2013).

Several reports have described using these changes to generate an index of cardiomyocyte maturity (Table 4). These indices have several potential uses including: (1) providing a tool for assessing techniques to accelerate maturation and (2) allowing investigators to assess and control for cardiomyocyte maturity when comparing PSC-CM populations e.g. in disease modelling studies.

A range of strategies have been reported to augment the maturation of PSC-CMs. Media additives found to influence maturation include ascorbic acid and tri-iodothyronine (Cao *et al.*, 2012) (Yang *et al.*, 2014). Other investigators have reported that maturation can be facilitated by manipulating mechanical aspects of the culture environment such as the matrix to which they adhere to cultureware, culture in micro-patterned cultureware or on biological scaffolds to which loading conditions can be controlled (Salick *et al.*, 2014) (Ruan *et al.*, 2016) (Guyette *et al.*, 2016) (Fong *et al.*, 2016) (Chun *et al.*, 2015). Regulation of the rate of contraction by pacing has also been found to influence maturation (Lieu *et al.*, 2013) (Ruan *et al.*, 2016).

1.1.6 PSC-CMs and disease modelling

Prior to the development of PSC-CMs the techniques for studying cardiomyocytes *in vitro* were limited to fetal and neonatal rodent myocytes or the immortalised mouse cardiomyocytes line (HL-1) (Claycomb *et al.*, 1998). When studying human cardiac disease, human PSC-CMs have an obvious attraction of being derived from the same species. The development of patient specific hiPSCs presented the opportunity to develop disease models without the need for genetic modification of cell lines and to develop models where the causative mutations were unknown. hPSC-CMs have been used to study a range of inherited human cardiac diseases and have been reported to successfully recapitulate aspects of their phenotypes (Sallam *et al.*, 2014). Many of the diseases studied have an onset of clinical features in adulthood and consequently the issue of iPSC-CM maturity is important in interpreting the findings of these studies. For example iPSC-CMs express both fetal and adult isoforms of cardiac troponin I (cTnI) (Bedada *et al.*, 2014). When using these cells to model hypertrophic cardiomyopathy due to mutations in *TNNI3* the expression of the fetal isoform of cTnI (encoded by *TNNI1*) must be taken into account.

Characteristics			hPSC-CMs and fetal cardiomyocytes	Adult ventricular cardiomyocytes
Morphology			Small, circular Abundant cytoplasm	Large rectangular Scant cytoplasm, abundant contractile apparatus
Contractile apparatus	Protein expression	Myosin light chains	Majority of cells “double positive” for MLC-2V and MLC-2A	Majority of cells contain only MLC-2V
		Myosin heavy chains	β -MHC more abundant than α -MHC	No change
	Ultrastructure	Myofibrils	Sparse and disorganised	Abundant and organised into sarcomeres
		I, H and M bands	Absence initially May develop with prolonged culture.	Present
		T-tubules	Absent	Present
Mitochondria and metabolism			Energy source	High glucose, low fatty acid metabolism
			Ultrastructure	Low number and low density of mitochondrial cristae.
Electro-physiology	AP morphology and component currents	Spontaneous contraction	Spontaneous depolarisation, Large I_f (funny current) associated with spontaneous phase 4 depolarisation	Absent or infrequent spontaneous depolarisations Reduced or absent I_f (funny current)
		Depolarisation (phase 0)	Slow upstroke (5-50 V/S) Low amplitude 70-90mV	Rapid upstroke (150 – 300V/s) High amplitude (110 – 120 mV)
		Repolarisation (phase 4)	Elevated diastolic resting potential (approx. -40mV) Weak “rapid delayed rectifier current” (I_{kr} , Kv11.1) Absent I_{kt} (inward rectifier, Kir2.1, Kir2.2)	Low diastolic resting potential (approx. -85mV) Strong “rapid delayed rectifier current “ (I_{kr} , Kv11.1) Presence of an inward rectifier (I_{kt} , Kir2.1, Kir2.2)

Table 3 Features of hPSC-CM maturation

Adapted from Mummery *et al.* (Mummery *et al.*, 2012)

Modality	Details	Reference
Gene expression	Whole transcriptome data of PSC-CMs compared with gene expression of cardiomyocytes in <i>in vivo</i> from subjects of varying ages.	(Uosaki <i>et al.</i> , 2015) (van den Berg <i>et al.</i> , 2015) (Uosaki and Taguchi, 2016)
	Ratio of ventricular myosin light chain (encoded by <i>MYL2</i>) relative to atrial myosin light chain (encoded by <i>MYL7</i>) is indicative chamber specification of PSC-CMs and therefore maturation	(Bedada <i>et al.</i> , 2016) (Kamakura <i>et al.</i> , 2013)
Immunofluorescence microscopy	Automated digital image analysis to assess the organisation of myofibrils within PSC-CMs, greater degrees of parallel orientation indicated greater maturity.	(Pasqualini <i>et al.</i> , 2015)
Western blotting	The ratio of fetal troponin I (ssTnI) (encoded by <i>TNNI1</i>) to cardiac troponin I (cTnI) (encoded by <i>TNNI3</i>)	(Bedada <i>et al.</i> , 2014)
TEM	I-bands, H-zones and M-lines appear in a characteristic temporal pattern during maturation over 12 months.	(Kamakura <i>et al.</i> , 2013)

Table 4 Techniques proposed for the quantification of PSC-CM maturity.

1.2 Overview of the desmosome

The term desmosome is reported to have been coined in the 1920s to refer to nodular bodies at points of cell to cell contact observed by light microscopy that were hypothesised to mediate intercellular adhesion (Holthöfer *et al.*, 2007) ^a.

From the 1950s onwards the junctions mediating intercellular interactions were studied by electron microscopy. Junctions were observed to consist of protein dense regions of adjacent sections of plasma membranes separated by a region of extra-cellular space. In cardiac tissue three main types of junction were differentiated on morphological grounds: desmosomes, adherens junctions and gap junctions (Muir, 1965). Desmosomes were distinguished from other junction types by the laminated appearance of their protein dense regions, which were referred to as desmosomal plaques (Table 5).

The following discussion will first summarise desmosomal ultrastructure, then outline the three major types of proteins from which desmosomes are assembled (desmosomal cadherins, arm-repeat proteins ^b and plakins) and finally discuss the aspects of desmosomal function which are relevant to ARVC/D.

	Type of intercellular junction		
	Desmosome	Adherens junction	Gap junction
Membrane associated plaques and their appearance	Yes, laminated	Yes, non-laminated	No
Association with cytoskeletal filaments	Intermediate filaments	Thin filaments of myofibrils	No
Midline within the intermembranous gap	Yes	No	No
Size of intermembranous gap	Approx. 20-30nm	Approx. 20nm	<2nm

Table 5 Comparison to the ultrastructural features of different adhesion junction, adapted from Muir 1965
(Muir, 1965)

1.2.1 Desmosomal ultrastructure

Desmosomal plaques in mammals have been reported to range from 0.1µm to >2µm in diameter, with variations between tissue types and species (Holthöfer *et al.*, 2007). When studied in cross section, by transmission electron microscopy (TEM) desmosomal plaques may be divided into five regions (Figure 4) (Figure 5) (Holthöfer

^a These structures were first observed in the late 1800's in the spinous layer of epidermis (Schultze, 1864) (Bizzozero, 1864) (Schrön, 1863).

^b Also referred to as armadillo proteins.

et al., 2007): (1) an extracellular domain between adjacent plasma membranes, containing fibrillar proteins oriented perpendicular to the membranes, with a more dense linear structure parallel to and midway between them referred to as the dense midline, (2) a section of the plasma membrane containing the transmembrane domains of desmosomal plaque proteins, (3) a cytoplasmic region adjacent to the plasma membrane containing a high density of protein referred to as the outer dense plaque (ODP), (4) a cytoplasmic region adjacent to the ODP with a slightly lower density of proteins referred to as the inner dense plaque (IDP) and (5) intermediate filaments (IF) passing through or adjacent to the IDP.

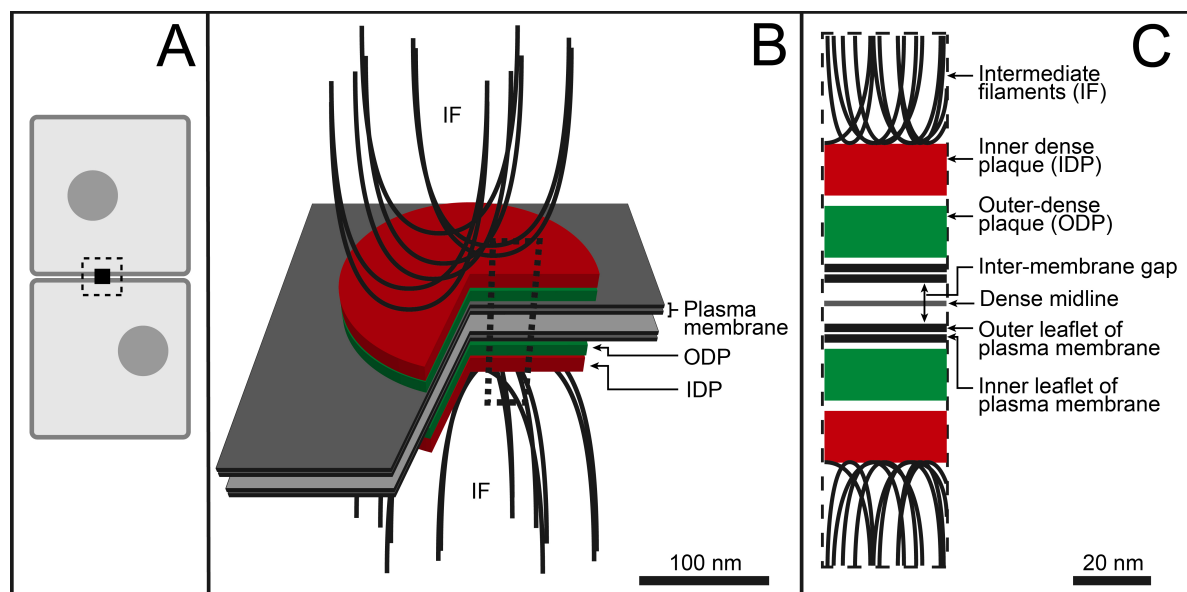


Figure 4 Schematic illustration of desmosomal ultrastructure

Desmosomes are typically found where plasma membranes of two cells are adjacent (Panel A). A schematic representation of the three dimensional structure of a desmosome is presented in Panel B, illustrating the laminated plaques. The boxed region in panel B is shown in detail in panel C. This type of cross sectional view may be seen in TEM images of desmosomes and the key feature in such an image are illustrated in Panel C.

The appearance of a desmosome when imaged by transmission electron microscopy (TEM) depends on the fixation and staining technique employed (Figure 5) (Figure 6). Sample preparation involves labelling proteins with heavy metal ions. Heavy metal ions absorb electrons from a TEM imaging beam and therefore regions of higher protein density absorb a greater proportion of the TEM beam. The extent to which a region absorbs electrons is commonly referred to as its electron density.

The typical appearance of a desmosome fixed with osmium tetroxide (OsO₄) and stained with aqueous uranyl acetate and alkaline lead citrate is presented in Figure 5.

Some investigators have reported that the cytoplasmic side of the ODP is more dense than that adjacent to the plasma membrane (Figure 6, panels A, C) (Kelly, 1966) (North *et al.*, 1999). Investigators using cryo-electron microscopy have reported that within this less dense ODP region there is a sub-region of higher density which they attributed to the localisation of plakophilin molecules (Figure 6, Panel D) (Al-Amoudi *et al.*, 2011). The IDP has been reported to be separated from the ODP in a similar manner by a region of lower protein density.

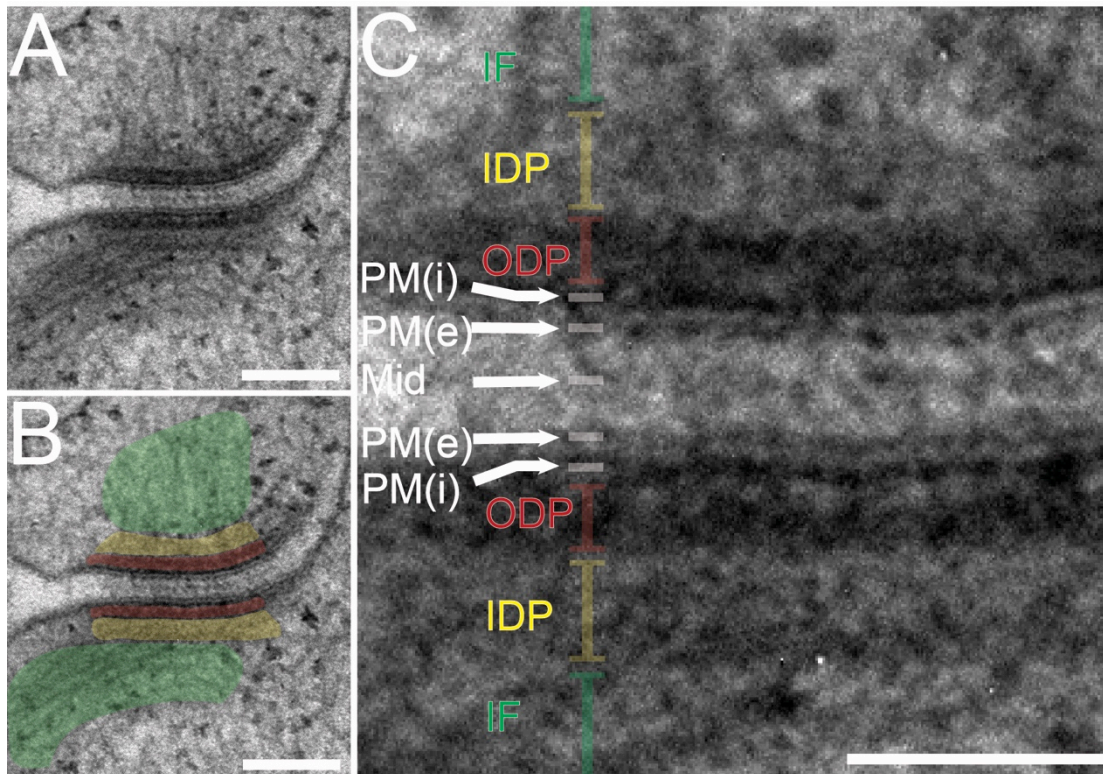


Figure 5 Representative TEM image of typical desmosome ultrastructure.

Panel A presents a TEM image of a desmosome from a sample of HaCaT cells (passage 72), taken at 130,000x magnification. Panel B presents the same image as panel A with shading to indicate the regions occupied by the intermediate filaments (green), inner dense plaque (yellow) and outer dense plaque (red). Panel C shows a selected region of panel A with annotations to indicate the regions occupied by intermediate filaments (IF), inner dense plaque (IDP), outer dense plaque (ODP), intracellular surface of the plasma membrane (PM(i)), extracellular surface of the plasma membrane (PM(e)), midline (Mid). The scale bars represent 100nm in panels A and B, and 50nm in panel C.

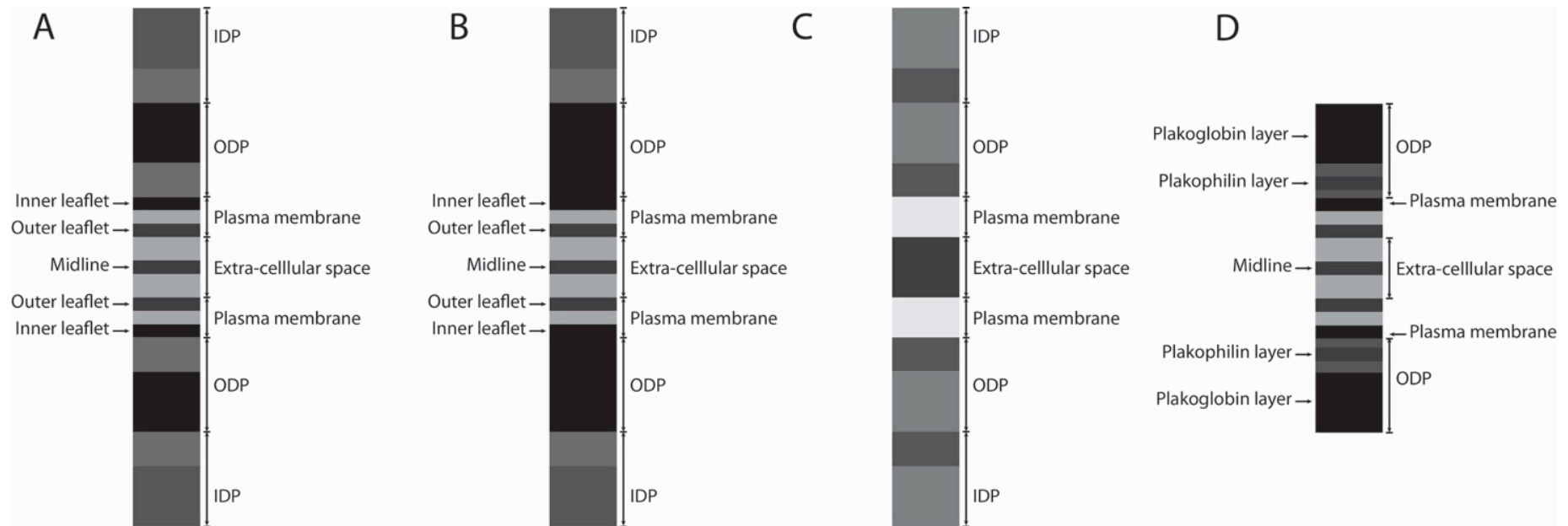


Figure 6 Schematic illustrations of the ultrastructural features of desmosomes reported by different authors and using different methods of sample preparation.

Panel A illustrates the findings of Kelly in samples that were fixed with OsO_4 , embedded in resin and stained with aqueous uranyl acetate and alkaline lead citrate solutions (Kelly, 1966). The ODP was reported to contain an electron lucent region separating its more electron dense cytoplasmic region from the plasma membrane (Kelly, 1966). Panel B and C illustrate the findings of North et al (North et al., 1999). Panel B shows the findings in samples that were fixed with 2% formaldehyde / 2% glutaraldehyde, then OsO_4 , then embedded in resin and stained with aqueous uranyl acetate and alkaline lead citrate solutions. Although the electro-lucent region reported by Kelly was not apparent the investigator did identify a region of lower protein density at this location using negative staining (Panel C). Panel D shows the findings of Al-Amoudi et al. in samples prepared using cryo-electron tomography (Al-Amoudi et al., 2011). Two regions of increased density distinct from the plasma membrane were identified within the ODP region and term the plakoglobin and plakophilin layers.

Many investigators have reported typical ranges for the dimensions of desmosomal components. Only a small number of these publications describe data sets from which these ranges were derived (Table 6) and few studies provide a detailed description of the locations within a desmosome between which these width parameters are measured e.g. several publications report typical values for the desmosomal gap (Table 6) but do not indicate whether these measurements are made between the inner leaflet, outer leaflet, or the electro-lucent line separating them. As a result it is difficult to know whether differences in the dimensions of desmosomes in these studies results from biological variation or differing methodology.

Publication	Sample size (n)	Intermembrane width (nm)	ODP width (nm)	Less dense region within IDP (nm)	Tono-filaments
(North <i>et al.</i> , 1999)	Not specified	20-50	Entire region: 15-20nm from plasma membrane	<10nm region separating ODP and IDP 15-20nm	-
(McNutt, 1970)	Not specified	25-35	-	-	-
(Karrer, 1960)	Not specified	22	Dense region: 16nm	-	-
(Kelly, 1966)	Not specified		Dense region: 15-20		40-70nm from plasma membrane
(Garrod <i>et al.</i> , 2005)	50	23.9±0.5nm	-	-	-

Table 6 Publications providing typical values for desmosomal width parameters

1.2.2 Desmosomal cadherins

The desmosomal cadherins are type 1 trans-membrane proteins belonging to the cadherin superfamily. They have been divided into two groups: desmocollins and desmogleins on the basis of structural differences at their C-termini (outlined below) (Figure 7).

At the time of this study, three genes had been identified in humans encoding desmocollins and four encoding desmogleins. Each desmocollin gene may be transcribed into two isoforms referred to as a or b, with the a isoform being the longer of the two. To date only one transcript has been identified from each of the *DSG1*, *DSG2* and *DSG3* genes. Two transcript variants of *DSG4* have been described, the shorter (variant 1) lacks a sequence in the intracellular anchor domain encoded by exon 14 (Whittock and Bower, 2003).

The structure of desmosomal cadherins are summarised in Figure 7. All desmosomal cadherins contain a similar extra-cellular component consisting of four

extra-cellular calcium-binding domains (ECB). Each ECB consists of a seven stranded β -barrel, adjacent domains are connected by flexible linker regions within which calcium ions can be accommodated (Overduin *et al.*, 1995) (Shapiro *et al.*, 1995) (Boggon *et al.*, 2002). Both the desmogleins and the desmocollin a isoforms contain a 72 amino acids long intracellular cadherin sequence (ICS) at its C-terminus. Desmogleins contain three additional domains at their C terminus that are not present in desmocollins, namely: a proline rich linker (PRL), a repeat unit domain (RUD) and a terminal domain. The RUD consist of a variable number repeating 29 amino acid motif desmogleins 1, 2, 3 and 4 contain 5, 6, 2, and 3 repeating units respectively (Garrod and Chidgey, 2008).

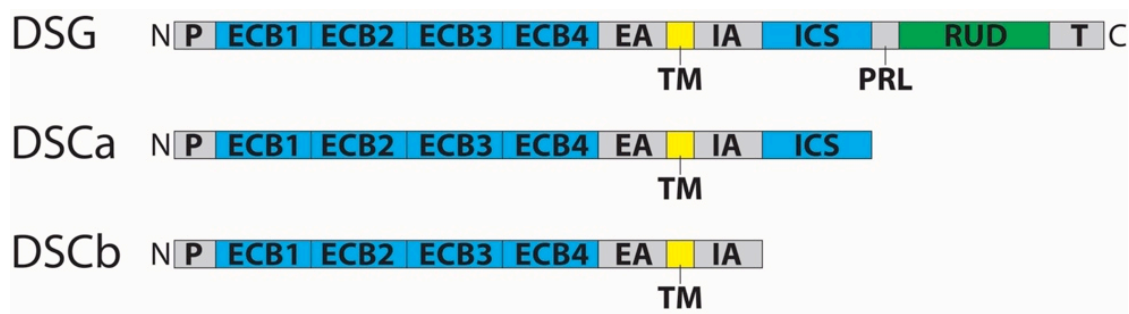


Figure 7 Schematic of the structure of desmosomal cadherins.

Non-folded pre-pro-proteins are represented with the regions responsible for different functions labelled. Annotations indicate: the precursor sequence (P), extra-cellular calcium binding sequence (ECB), extra-cellular anchor (EA), transmembrane sequence (TM), intracellular anchor (IA), intracellular cadherin-like sequence (ICS), proline-rich linker (PRL), repeat unit domain (RUD) and carboxy-terminal domain (T).

The ECB1 domain has been identified as the principle site of binding between desmosomal cadherins from adjacent cells, this binding has been referred to as trans-dimerisation (Boggon *et al.*, 2002). All desmosomal cadherins contain a tryptophan residue at position two in the ECB1 domain that is essential for trans-dimerisation. During trans-dimerization the hydrophobic tryptophan residues are associated with hydrophobic pockets in the ECB1 domains of the opposing molecules (Boggon *et al.*, 2002). Desmosomal cadherins can also interact in cis with each other through their ECB domains, producing parallel oriented clusters of cadherins described as “adhesion zippers” (Brieher *et al.*, 1996) (Garrod *et al.*, 2005). The ECB domains are separated by linker regions containing calcium binding domains which are thought to regulate cadherin shape and thence then changes in desmosomal structure and adhesion associated with calcium dependent and independent binding (Trojanovsky *et al.*, 1999) (Garrod *et al.*, 2005).

The intracellular cadherin-like sequence (ICS) mediates binding of desmosomal cadherins with JUP (Trojanovsky *et al.*, 1994b) (Trojanovsky *et al.*, 1994a) (Roh and Stanley, 1995). The intracellular anchor (IA) sequence is thought to mediate the binding of desmosomal cadherins with plakophilins and desmoplakin (Bonné *et al.*, 2003) (Chen, 2002).

			Arm repeat protein				DSP
			JUP	PKP1	PKP2	PKP3	
Desmosomal cadherin	DSC1	a	(Witcher <i>et al.</i> , 1996) (Smith and Fuchs, 1998)	(Smith and Fuchs, 1998)	(Chen, 2002)	(Bonné <i>et al.</i> , 2003)	(Trojanovsky <i>et al.</i> , 1994b)
		b	-	-	-	-	-
	DSC2	a	(Bornslaeger <i>et al.</i> , 2001)	-	(Chen, 2002)	(Bonné <i>et al.</i> , 2003)	
		b	-	-	-	-	-
	DSC3	a	-	-	-	(Bonné <i>et al.</i> , 2003)	
		b	-	-	-	(Bonné <i>et al.</i> , 2003)	-
	DSG1		(Mathur <i>et al.</i> , 1994) (Witcher <i>et al.</i> , 1996) (Chitaev <i>et al.</i> , 1998) (Smith and Fuchs, 1998) (Bornslaeger <i>et al.</i> , 2001)	(Smith and Fuchs, 1998) (Hatzfeld <i>et al.</i> , 2000)	(Chen, 2002)	(Bonné <i>et al.</i> , 2003)	(Bornslaeger <i>et al.</i> , 2001)
		DSG2	-	-	(Chen, 2002)	(Bonné <i>et al.</i> , 2003)	
		DSG3	(Roh and Stanley, 1995)	-	-	(Bonné <i>et al.</i> , 2003)	
		DSG4	-	-	-	-	
DSP			(Kowalczyk <i>et al.</i> , 1997), (Smith and Fuchs, 1998) (Bornslaeger <i>et al.</i> , 2001)	(Smith and Fuchs, 1998), (Kowalczyk <i>et al.</i> , 1999) (Hatzfeld <i>et al.</i> , 2000), (Bornslaeger <i>et al.</i> , 2001)	(Chen, 2002)	(Bonné <i>et al.</i> , 2003)	-

Table 7 Summary of the molecular interactions reported between the intracellular regions of desmosomal plaque proteins.

1.2.3 Desmosomal arm-repeat proteins

Plakoglobin and the plakophilins are members of the armadillo (or arm-repeat) group of proteins (Figure 8) (Hatzfeld *et al.*, 2003). Three major desmosomal plakophilins have been identified named PKP 1 to 3.

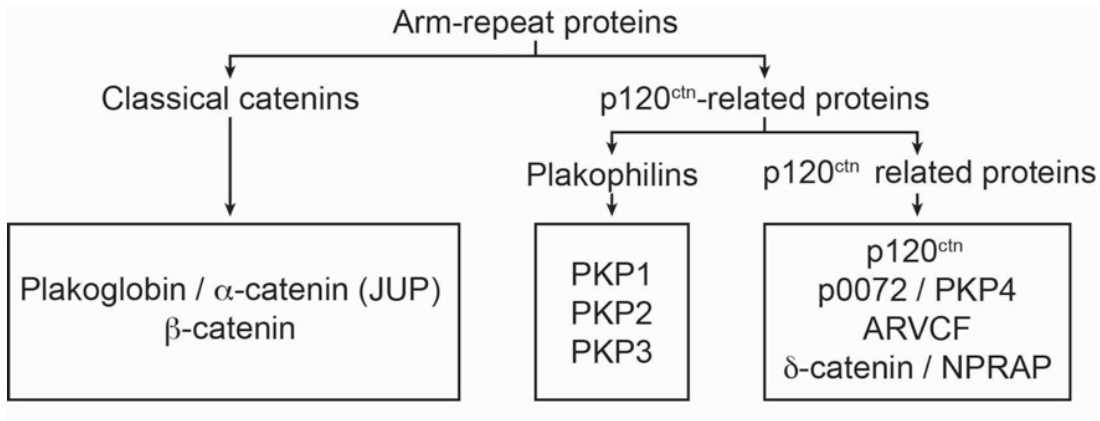


Figure 8 Classification of arm-repeat proteins

Adapted from (Hatzfeld, 2007).

The structure of arm-repeat proteins is summarised in Figure 9. Arm-repeat proteins have a central domain in containing repeats of a 45 amino acid long arm-repeat sequence bracketed at either end by head and tail domains (Hatzfeld, 2007). Each central domain repeat forms a cluster of three α -helices, these repeat units are then packed to form a superhelix. Plakoglobin contains 12 arm repeats whilst members of the plakophilin group contain nine arm repeats with an sequence between the 5th and 6th repeats that introduces a bend in the domain (Choi and Weis, 2005). Although splice variants of the plakoglobin gene exist they are thought to encode the same full-length protein. Each plakophilin gene may be transcribed as two isoforms referred to as a and b; the b isoform is longer of the two.

Interactions between desmosomal arm-repeat proteins and other desmosomal components are summarised in Table 7.

Plakoglobin binds to the ICS domain of desmogleins and desmocollin a isoforms via the first three units of its arm-repeat domain (Chitaev *et al.*, 1998) (Chitaev *et al.*, 1996). The site of within the plakoglobin molecule which interacts with desmoplakin has yet to be characterised (Holthöfer *et al.*, 2007). Plakoglobin can also bind to proteins in the canonical Wnt signalling pathway (see 1.2.7). Binding to TCF/LEF transcription factors is mediated via a domain at its C-terminus (Simcha *et al.*, 1998).

Plakophilins bind to the plakin domain of DSP via their N-terminus / head domain (Kowalczyk *et al.*, 1999). There is also evidence that the N-terminus / head domain of plakophilins interacts with desmogleins (Hatzfeld *et al.*, 2000). The functions of the C-terminus tail of plakophilins are less well characterised, but have been implicated in the localisation of plakophilins to the plasma membrane (Sobolik-Delmaire *et al.*, 2006).

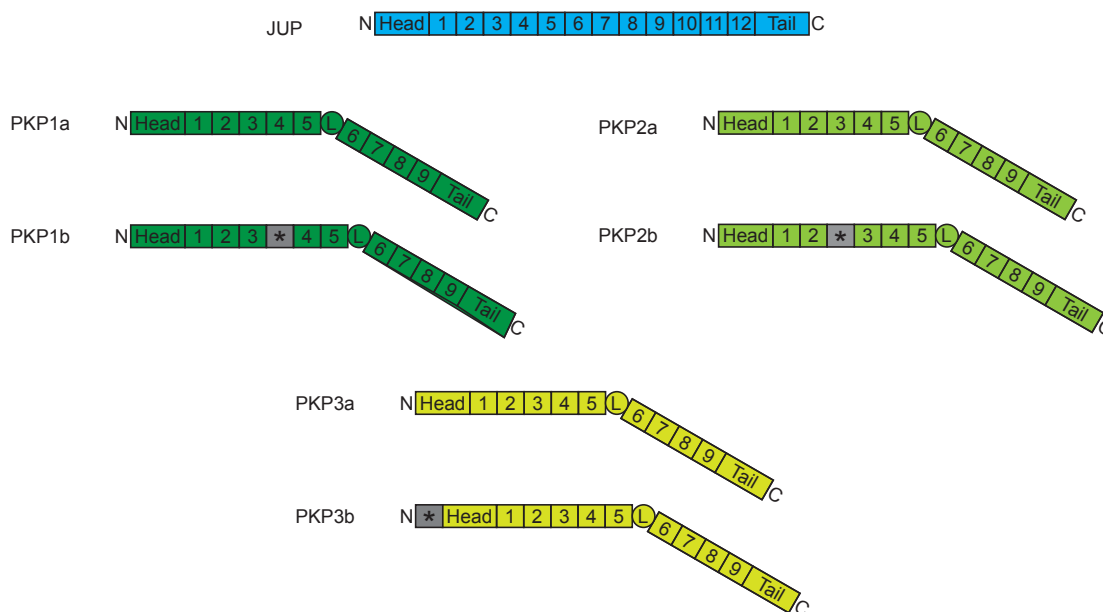


Figure 9 Structure of desmosomal arm repeat proteins.

Arm-repeat domains are numbered. For the plakophilins the sequence which introduced a bend in the arm-repeat domain (L) is indicated as are the additional sequences which render the b isoforms longer than the a isoforms (*).

1.2.4 Desmoplakin

Desmoplakin is thought to be obligatory component of mature desmosomes. It links the desmosomal plaques to intermediate filaments (IF). In epithelial cells the main IF protein is keratin, in cardiomyocytes it is desmin (Garrod and Chidgey, 2008). The structure of desmoplakin is summarised in Figure 10. Desmoplakin is a member of the plakin family of proteins that are defined by containing plakin domains. The plakin domain of desmoplakin consists of a pair of spectrin repeats, linked by an Src-homology 3 domain (Jefferson *et al.*, 2007). Each repeat is organised into a cluster of three α -helices (Jefferson *et al.*, 2007). The plakin domain is located at the N-terminus of desmoplakin. The C-terminus of desmoplakin contains a series of three plakin repeat domains (PRD) (designated A, B and C) and a glycine-serine-arginine rich domain. The plakin domain and PRD are separated by central rod domain,

organised into a coiled-coil α -helix. Desmoplakin exists in two isoforms, DSP I and DSP II, which differ in the length of their rod domain, the later of these being the shorter.

Desmoplakin binds to plakoglobin and plakophilins via its N-terminus plakin domain (Kowalczyk *et al.*, 1997) (Kowalczyk *et al.*, 1999). Within the desmosome, desmoplakin molecules are thought to form homo-dimers through their rod domains (Green *et al.*, 1990). Intermediate filaments bind to the C-terminus plakin repeat domains (PRDs) located at the carboxy terminus of desmoplakin (Stappenbeck and Green, 1992) (Fontao *et al.*, 2003).

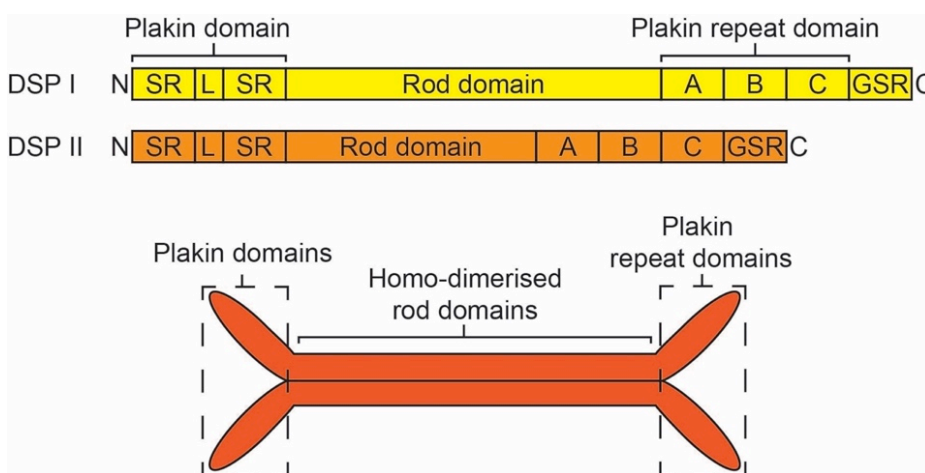


Figure 10 Desmoplakin structure.

Spectrin repeat (SR), Src-homology 3 linker region (L), glycine-serine-arginine rich domain (GSR).

1.2.5 The composition and organization of proteins within the cardiac desmosome and their correlation with ultrastructural features.

The repertoire of desmosomal proteins expressed in the heart is more limited than in other desmosome bearing tissues such as the skin. The major desmosomal cadherins are DSC2 and DSG2, with both isoforms of DSC2 being expressed (De Bortoli *et al.*, 2010). The major arm-repeat proteins are JUP and PKP2, with only the shorter PKP2a isoform being expressed at a protein level (Gandjbakhch *et al.*, 2011). The shorter isoform of desmoplakin (DSP I) has been reported to be absent from cardiac tissue (Angst *et al.*, 1990). The longer isoform of desmoplakin DSP II has been identified in all desmosome-bearing tissues, and is therefore thought to be the only isoform present in the heart.

A model of the molecular organisation of proteins within cardiac desmosomal plaques (based on the organisation of epithelial desmosomes) is presented in Figure 11.

The intermembrane gap is bridged by the extra-cellular domains of desmosomal cadherins that link at their terminal ECB1 domains. The overlap of these proteins is thought to be responsible for the dense midline seen in some desmosomes ^a.

Desmocollins and desmogleins are capable of forming heterophilic and homophilic trans-dimers (Chitaev and Troyanovsky, 1997) (Marcozzi *et al.*, 1998) (Runswick *et al.*, 2001) (Syed *et al.*, 2002). There is evidence that the majority of trans-dimerization in desmosomes is homophilic and isoform specific (Nie *et al.*, 2011).

The cytoplasmic domains of desmosomal cadherins interact with desmoplakin via arm repeat proteins (PKP2 and JUP). The concentration of proteins mediating these interactions is responsible for the ODP seen by TEM. The homodimers of DSP then extend from the cytoplasmic surface of the ODP to interact with the intermediate filaments composed of desmin in the region corresponding to the IDP.

Adhesion junctions with a typical desmosomal morphology have been identified in the heart (Muir, 1965) however it has not yet been demonstrated that these junctions have the same molecular organisation as the epidermal desmosomes described by North *et al.*. Desmosomal proteins have also been demonstrated to participate in cardiac adhesion junctions other than those with a typical desmosomal morphology (see below) the molecular architecture of these junctions has also not been fully characterised (Borrmann *et al.*, 2006) (Franke *et al.*, 2006) (Pieperhoff and Franke, 2007).

^a Associated with a calcium independent binding state (Garrod *et al.*, 2005).

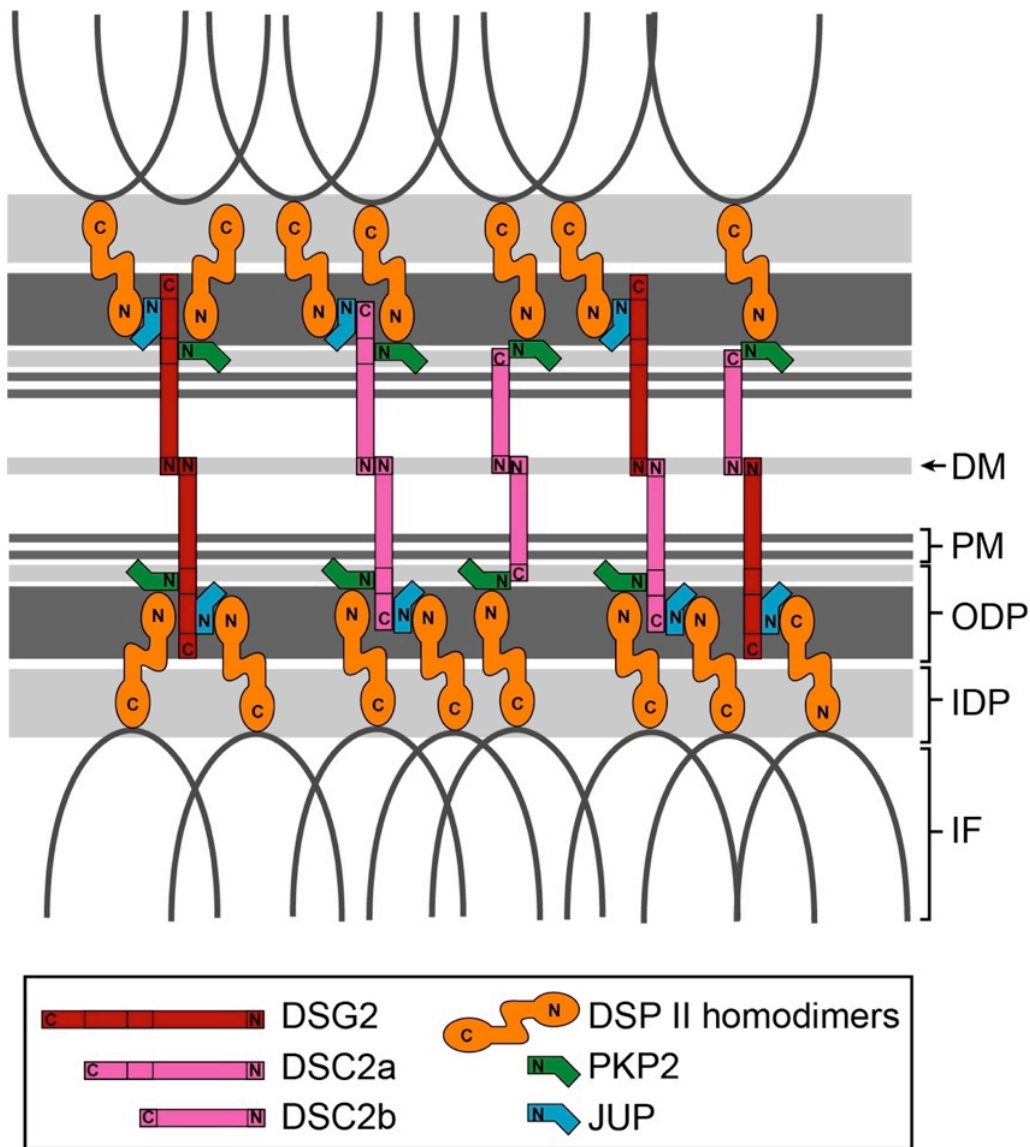


Figure 11 A proposed organisation of desmosomal proteins within a cardiac desmosome and their correlation with features seen by TEM.

This model assumes that the organisation of cardiac desmosomes is similar to that described by North *et al.* in epidermal desmosomes. It shows a possible molecular architecture for cardiac desmosomes using the more limited repertoire of desmosomal proteins described in the reports outlined in 1.2.5 .

1.2.6 Desmosomal proteins and intercellular adhesion

Desmosomes provide a mechanism by which the cytoskeleton of adjacent cells may be linked. They are abundant in tissues exposed to high levels of mechanical stress e.g. the epidermis. In circumstances where desmosomal adhesion is disrupted then tissue damage is more readily induced (Delva *et al.*, 2009). For these reasons the maintenance of tissue integrity is regarded as a major function of desmosomes.

In adult mammalian hearts desmosomes have been reported to constitute between 8-15% of the adhesion junctions (Forbes and Sperelakis, 1985). Immunoelectron and immunofluorescence microscopy data has suggested that desmoplakin, plakoglobin, PKP2, DSC2 and DSG2 are components of long adhesion junctions found at the intercalated discs which lack the typical ultrastructural characteristics of desmosomes (Franke *et al.*, 2006) (Borrmann *et al.*, 2006). These investigators have proposed that during cardiac development desmosomes and adherens junctions become concentrated and coalesce at the intercalated discs to form junctions referred to as area composita (Pieperhoff and Franke, 2007). At the level of molecular architecture, these area composita may be composed of a mosaic of regions arranged as desmosomal and fascia adherens plaques. Alternatively they may have an entirely novel molecular architecture composed of desmosomal and fascia adherens proteins. In support of the later possibility plakoglobin has been shown to be interchangeable with β -catenin in binding to α -catenin and the cytoplasmic domain of E-cadherin (the major transmembrane cadherin in adherens junctions) (Cowin *et al.*, 1986) (Chitaev *et al.*, 1996). Plakoglobin has a lower binding affinity for E-cadherin than desmosomal cadherins and this is thought to account for its lower abundance at adhesion junctions than at desmosomes in tissue with these distinct junction types (Chitaev *et al.*, 1996).

In addition to the role of desmosomal proteins in facilitating the mechanical connections between cells they have been shown to regulate the localisation of structures mediating their electrical activity. Abnormalities in desmosomal protein abundance and function have been associated with reduction in the abundance of gap junctions, gap junction proteins and the voltage gated sodium channel Nav1.5 at the intercalated discs with (Kaplan *et al.*, 2004) (Tandri *et al.*, 2008) (Gehmlich *et al.*, 2011) (Swope *et al.*, 2012) (Noorman *et al.*, 2013) (Sato *et al.*, 2011). The mechanisms responsible for this have yet to be fully elucidated but there is evidence that DSP can regulate gap junction localisation via the regulation of microtubules (Patel *et al.*, 2014).

1.2.7 Desmosomal proteins and intracellular signalling pathways

In addition to their roles in desmosomal adhesion, plakoglobin and the plakophilins have roles in intracellular signalling pathways. Non-membrane bound, cytoplasmic and nuclear pools of plakoglobin and the plakophilins have been reported in many

cell types (Heid *et al.*, 1994) (Mertens *et al.*, 1996) (Bonné *et al.*, 1999) (Schmidt *et al.*, 1997).

Plakoglobin has structural and functional similarities to β -catenin, which in addition to its role as a component of adhesion junctions is a key regulator of canonical Wnt signalling (Figure 12). β -catenin and plakoglobin are capable of binding to TCF/LEF transcription factors^a and modifying the activity of these molecules (Simcha *et al.*, 1998) (Miravet, 2001) (Maeda *et al.*, 2004). Despite the similarities between plakoglobin and β -catenin, they have different binding sites to TCF/LEF transcription factors and differing effects on gene transcription. TCF4 binds to the first 50 amino acids in plakoglobin, and to residues 51-80 in β -catenin (Miravet, 2001). Plakoglobin binding to TCF4 inhibits gene transcription, whereas binding to β -catenin increases transcriptional activity (Miravet, 2001). β -catenin and plakoglobin can bind to LEF1, but plakoglobin does so with much lower efficiency and results in a lesser degree of transcription factor activation (Simcha *et al.*, 1998).

The abundance of cytoplasmic and nuclear β -catenin and plakoglobin is regulated by a cytoplasmic multi-protein complex of adenomatosis polyposis coli (APC), axin, glycogen synthase kinase 3 β (GSK), casein kinase 1 α (CK1 α) and protein phosphatase 2A (PP2A). After binding to this complex, β -catenin and plakoglobin are phosphorylated by GSK^b leading to their degradation by ubiquitin dependent proteolysis (Kodama *et al.*, 1999) (Ben-Ze'ev and Geiger, 1998).

Experimentally induced changes in plakoglobin abundance have been shown to influence canonical Wnt signalling. Homozygous knock-out of plakoglobin results in an increase in β -catenin binding to TCF4 (which normally binds preferentially to plakoglobin), resulting in increased transcriptional activation of Wnt signalling targets (J. Li *et al.*, 2011).^c

Over expression of plakoglobin causes the displacement of β -catenin from adhesion junctions (Salomon *et al.*, 1997), the inhibition of β -catenin degradation by the destruction complex (Miller and Moon, 1997) and the accumulation of both β -catenin and plakoglobin within the nucleus (Simcha *et al.*, 1998). Since plakoglobin and β -catenin bind to different site on TCF/LEF transcription factors, the net effect on Wnt

^a The N-terminus of TCF/LEF transcription factor binds to the arm-repeat region of β -catenin. The C-terminus of β -catenin then interacts with TCF/LEF to increase its activity.

^b The N-terminus serine residue (S28) is a critical site of phosphorylation in this process.

^c Knock-out models lacking plakoglobin develop normally during the earliest stages of development, then develop lethal cardiac and epidermal abnormalities (Haegel *et al.*, 1995) (Bierkamp *et al.*, 1996) (Ruiz *et al.*, 1996).

signalling is not simply determined by their relative concentrations as might occur if there was competition for the same site.

It has also been suggested that over-expression of plakoglobin may increase Wnt signalling independently of its effects on β -catenin by binding to inhibitors of TCF/LEF transcription (Merriam *et al.*, 1997).

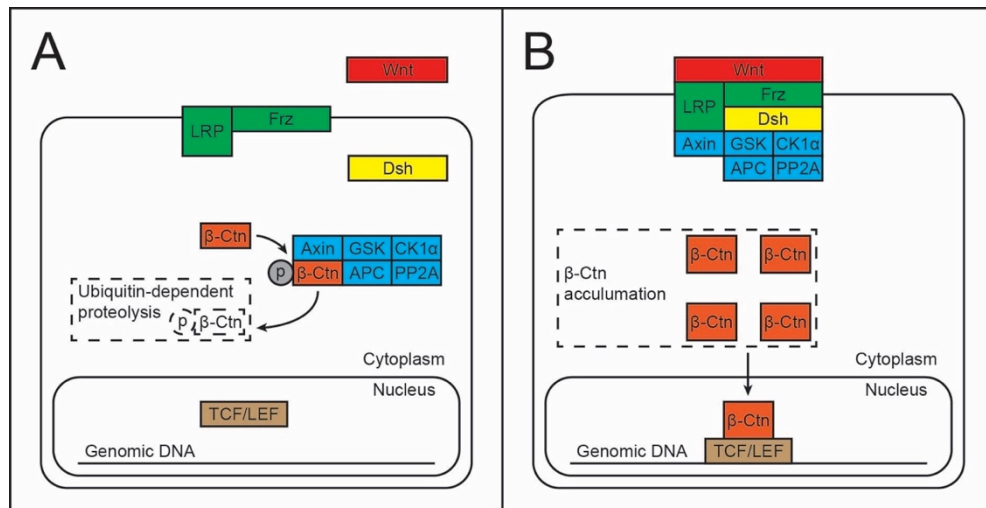


Figure 12 Canonical Wnt signalling

In the absence of activation (A) a destruction complex of adenomatosis polyposis coli (APC), axin, glycogen synthase kinase 3 β (GSK), casein kinase 1 α (CK1 α) and protein phosphatase 2A (PP2A) bind to and phosphorylates serine residues in β -catenin (β -Ctn). Phosphoserine residues in the N-terminus are recognised by ubiquitin ligase β -TrCP, which catalyses ubiquitination and thereby directing it to degradation. (B) Binding of a Wnt ligand to the transmembrane receptors frizzled (Frz) and lipoprotein receptor related protein 5/6 (LRP) triggers the binding of axin and dishevelled (Dsh) to their cytoplasmic domains. Dsh inhibits GSK resulting in a reduction in activity of the destruction complex. B-catenin levels increase in both the cytoplasm and nucleus. Nuclear β -catenin binds to TCF/LEF transcription factors that then change the expression of downstream targets of Wnt signalling. In some cases binding of β -catenin results in transcription factor binding to enhancer sites and promotion of gene expression. In other cases binding of β -catenin releases constitutive inhibition of gene expression by transcription factors (Akiyama, 2000).

Several mechanisms by which PKP2 may influence gene expression have been reported. It may have a role in regulating ribosomal an tRNA through binding to RNA polymerase III within the nucleus (Mertens *et al.*, 2001). It can interact directly with β -catenin-TCF/LEF Wnt activation (Chen, 2002). It may also influence Wnt signalling via phosphorylated protein kinase C α (pPKC α) and the Hippo pathway. Phosphorylated protein kinase C α (pPKC α) associates with the plasma membrane and adhesion junctions through its interaction with PKP2. Reduced membrane

localisation of pPKC α leads to a reduction in neurofibromin 2 (NF2) phosphorylation, a subsequent increase in Hippo pathway activity and thence the inhibition of Wnt signalling (Heallen *et al.*, 2011) (Bass-Zubek *et al.*, 2009) (S. N. Chen *et al.*, 2013).

1.3 Overview of arrhythmogenic right ventricular cardiomyopathy / dysplasia

1.3.1 Clinical features

The diagnosis ARVC/D is made using criteria that collate aspects of clinical presentation with the results diagnostic tests (Table 8) (Table 9) (Marcus *et al.*, 2010). Cases of ARVC/D most commonly present between the ages of 20 and 50 with symptoms of ventricular arrhythmias and may go on to develop heart failure due ventricular dysfunction. The clinical features of ARVC/D in published case series' are summarised in Table 10.

ARVC/D has a prevalence of between 1:000 to 1:5000 (Thiene *et al.*, 2007) (Gemayel *et al.*, 2001) (Rampazzo *et al.*, 1994) (Peters *et al.*, 2004). The risk of sudden cardiac death (SCD) in ARVC/D is between 0.08 and 4.5% per year (Corrado *et al.*, 2017).

The therapeutic options in ARVC/D are limited to: (1) the control of arrhythmias with drugs and catheter ablation, (2) the prevention of sudden death by implantation of a implantable cardioverter-defibrillator and (3) cardiac transplant in severe cases (Corrado *et al.*, 2017) (Pilichou *et al.*, 2016).

ARVC/D is familial in 20-30% of cases and it follows an autosomal dominant pattern of inheritance in most familial cases (Hulot, 2004) (Dalal, 2005) (Quarta *et al.*, 2011a).

The first ARVC/D associated mutation to be identified was in the gene encoding the desmosomal plaque protein plakoglobin (*JUP*). Subsequent investigators identified ARVC/D associated mutations in four other genes encoding desmosomal plaque proteins (Table 11). Overall, mutations in desmosomal genes are identified in around 50% of ARVC/D probands (Table 12) (Ackerman *et al.*, 2011). This led to suggestions that desmosomal dysfunction was central to the pathogenesis of ARVC/D (van Tintelen *et al.*, 2007). Fewer studies are available to estimate the prevalence of non-desmosomal mutations in ARVC/D populations but were found in only 5% of a recent series of 502 cases (Bhonsale *et al.*, 2017). In some cases the function of these proteins has been linked to the pathogenic mechanisms proposed for desmosomal mutations, others are thought to have different modes of pathogenesis and produce a phenocopy of ARVC/D (Corrado *et al.*, 2017).

Category of clinical feature		Test modality	Major criteria	Minor criteria
I	Global or regional dysfunction and structural alterations	Echocardiography	<ul style="list-style-type: none"> Regional RV akinesia, dyskinesia or aneurysm and ≥ 1 of the following (measured at end diastole) <ul style="list-style-type: none"> RVOT diameter measured in PLAX: <ul style="list-style-type: none"> $\geq 32\text{mm}$ $\geq 19\text{mm/m}^2$ if corrected for BSA RVOT diameter measured in PSAX: <ul style="list-style-type: none"> $\geq 36\text{mm}$ $\geq 21\text{mm/m}^2$ if corrected for - Fractional area change $\leq 33\%$ 	<ul style="list-style-type: none"> Regional RV akinesia, dyskinesia and ≥ 1 of the following (measured at end diastole) <ul style="list-style-type: none"> RVOT diameter measured in PLAX: <ul style="list-style-type: none"> ≥ 29 to $< 32\text{mm}$ ≥ 16 to $< 19\text{mm/m}^2$ if corrected for BSA RVOT diameter measured in PSAX: <ul style="list-style-type: none"> ≥ 32 to $< 36\text{mm}$ ≥ 18 to $< 21\text{mm/m}^2$ if corrected for BSA Fractional area change $> 33\%$ to $\leq 40\%$
		Cardiac MRI	<ul style="list-style-type: none"> Regional RV akinesia, dyskinesia or dyssynchronous RV contraction and ≥ 1 of the following: <ul style="list-style-type: none"> Ratio of RV end-diastolic volume to BSA <ul style="list-style-type: none"> $\geq 110\text{ml/m}^2$ (male) $\geq 100\text{ml/m}^2$ (female) RV ejection fraction $\leq 40\%$ 	<ul style="list-style-type: none"> Regional RV akinesia, dyskinesia or dyssynchronous RV contraction and ≥ 1 of the following: <ul style="list-style-type: none"> Ratio of RV end-diastolic volume to BSA <ul style="list-style-type: none"> ≥ 100 to $< 110\text{ml/m}^2$ (male) ≥ 90 to $< 100\text{ml/m}^2$ (female) RV ejection fraction $> 40\%$ to $\leq 45\%$
		RV Angiography	Regional RV akinesia, dyskinesia or aneurysm	
II	Tissue characterization	Endomyocardial Biopsy	<ul style="list-style-type: none"> Residual myocytes: <ul style="list-style-type: none"> $< 60\%$ by morphometric analysis $< 50\%$ if estimated and fibrous replacement of the RV free wall myocardium in ≥ 1 sample (with or without fatty replacement of tissue) 	<ul style="list-style-type: none"> Residual myocytes <ul style="list-style-type: none"> 60% to 75% by morphometric analysis 50% to 65% if estimated and fibrous replacement of the RV free wall myocardium in > 1 sample (with or without fatty replacement of tissue)
III	Repolarisation abnormalities	ECG	<ul style="list-style-type: none"> Inverted T waves: <ul style="list-style-type: none"> in the absence of complete RBBB, <ul style="list-style-type: none"> in V1, V2, and V3 or beyond. (in individuals > 14 years of age) 	<ul style="list-style-type: none"> Inverted T waves: <ul style="list-style-type: none"> In the absence of complete RBBB <ul style="list-style-type: none"> in V1 and V2 in V4, V5, or V6 In the presence of complete RBBB <ul style="list-style-type: none"> in V1, V2, V3, and V4 (in individuals > 14 years of age)

Table 8 Diagnostic criteria for ARVC/D
(continued overleaf) (Marcus *et al.*, 2010)

(continued from previous page)

IV	Depolarization/conduction abnormalities	ECG	<ul style="list-style-type: none"> Epsilon wave (a reproducible low-amplitude signals between end of QRS complex to onset of the T wave in V1 to V3) 	<ul style="list-style-type: none"> Terminal activation duration of QRS ≥ 55 ms (measured from the nadir of the S wave to the end of the QRS, including R' in V1, V2 or V3, in the absence of complete RBBB)
		SAECG		<ul style="list-style-type: none"> ≥ 1 of the following: <ul style="list-style-type: none"> Filtered QRS duration ≥ 114 ms Duration of terminal QRS $< 40 \mu V$, ≥ 38 ms Root-mean-square voltage of terminal 40 ms ≤ 20 mV (in the absence of a QRS duration of ≥ 110 ms on the standard ECG)
V	Arrhythmias	ECG	<ul style="list-style-type: none"> Nonsustained or sustained ventricular tachycardia of left bundle-branch morphology: <ul style="list-style-type: none"> with a superior axis (negative or indeterminate QRS in leads II, III, and aVF and positive in lead aVL) 	<ul style="list-style-type: none"> Nonsustained or sustained ventricular tachycardia of left bundle-branch block morphology: <ul style="list-style-type: none"> with an inferior axis (positive QRS in leads II, III and aVF and negative in lead aVL) or of unknown axis
		Ambulatory ECG		<ul style="list-style-type: none"> 500 ventricular extra-systoles per 24 hours
VI	Family history	Family history	<ul style="list-style-type: none"> First degree relative: <ul style="list-style-type: none"> With a diagnosis ARVC/D based on the current diagnostic criteria. With a diagnosis of ARVC/D based on the pathological diagnostic standard (from tissue obtained at autopsy or surgery) 	<ul style="list-style-type: none"> First degree relative: <ul style="list-style-type: none"> With a diagnosis of ARVC/D but in whom it is not possible or practical to determine whether the family member meets current diagnostic criteria. Suffering premature sudden death (< 35 years of age) due to suspected ARVC/D . Second degree relative: <ul style="list-style-type: none"> With a diagnosis ARVC/D based on the current diagnostic criteria. With a diagnosis of ARVC/D based on the pathological diagnostic standard (from tissue obtained at autopsy or surgery).
		Genetic testing	<ul style="list-style-type: none"> Identification of a pathogenic ARVC/D mutation in the patient under evaluation. * 	

RV = right ventricle, RVOT = right ventricular outflow tract, PLAX = parasternal long axis, PSAX = parasternal short axis, BSA = body surface area, ECG = electrocardiogram, SAECG = signal averaged electrocardiogram, RBBB = right bundle branch block.

* A pathogenic mutation is a DNA alteration associated with ARVC/D that alters or is expected to alter the encoded protein, is unobserved or rare in a large non-ARVC/D control population, and either alters or is predicted to alter the structure or function of the protein or has demonstrated linkage to the disease phenotype in a conclusive pedigree.

Diagnostic category	Number of criteria	Diagnostic points
Definite	<ul style="list-style-type: none"> • Major criteria in ≥ 2 different categories • Major criterion, and ≥ 2 minor criteria, all in different categories • Minor criteria in ≥ 4 different categories 	≥ 4
Borderline	<ul style="list-style-type: none"> • Major criterion and minor criterion in different categories • Minor criteria in 3 different categories 	3
Possible	<ul style="list-style-type: none"> • 1 Major criterion. • Minor criteria in 2 different categories 	2

Table 9 Diagnostic categories of ARVC/D

The latest diagnostic schema for ARVC/D classifies the clinical features of the disease a major or minor criteria (as described in Table 8). These criteria are then grouped into 6 categories. An individual is given two “diagnostic points” for each category in which ≥ 1 major criterion have been identified and one “diagnostic point” for each category in which no major but ≥ 1 minor criterion have been identified. The individual is then given a diagnostic category based on the total number of diagnostic points given (Marcus *et al.*, 2010).

Publication		(Peters et al., 2004)	(Hulot, 2004)	(Dalal, 2005)	(Cho et al., 2007)	(Sen-Chowdhry et al., 2007)	(Marcus et al., 2009)	(Watkins et al., 2009)	(Pinamonti et al., 2011)	(Quarta et al., 2011a)	(Cox et al., 2011)			
Country		Germany	France	US	Korea	UK	US	South Africa	Italy	UK	Netherlands			
Size of population studied		80	130	69	37	200	108	50	96	46	147			
Diagnostic criteria used to define cases		1994	1994	1994	1994	1994	1994	1994	1994	2010	2010			
Diagnostic categorization of study population		100% definite	100% definite	100% definite	100% definite	100% definite	68% definite, 26% borderline, 6% unaffected	100% definite	100% definite	100% definite	100% definite			
Gender (% Male)		56%	77%	52%	51%	49%	57%	66%	68%	58.7%	75%			
Age (years)	Presentation	NR	Mean: 32±14 Range 10 to 73	Mean: 30±12	Mean: 41±15	37±16 Range 12-76 (at unspecified time point)	Mean: 36±15	Mean: 33±14	NR	NR	Mean: 37±14			
	Diagnosis	Mean: 45.6 Range: 22-91	NR	NR	NR		Mean: 38±13 Range 12 to 63	NR	Mean 34±15	38±13	NR			
Symptoms	Time point	Unspecified	Unspecified	Presentation	Presentation	Unspecified	Presentation	Presentation	Presentation	Presentation	Presentation			
	Palpitations	60%	67%	36%	30%	42%	56%	72%	41%	46%	NR			
	Dizziness or pre-syncope	NR	NR	12%	30%	29%	27%	42%	NR		NR			
	Syncope	30%	32%	30%	12%	21%	32%	15%	1%		1%			
	Cardiac arrest	1%	13%	1.5%	3%	NR	1%	4%	3%		8%			
	Chest pain	80%	27%	3%	8%	13.5%	14%	36%	4%		NR			
	Symptoms of right heart failure	4%	17%	4%	NR	NR	5%	12%	17%		NR			
Asymptomatic	NR	6%	22%	27%	42.5%	NR	2%	27	54%					
Ventricular arrhythmia	Non-sustained VT	20%	79%	77%	16%	20.5%	NR	82%	23%	22%	NR			
	Sustained VT	NR	6%	NR	19%	1%	35%	82%	34%	41%	81%			
	VF	NR	6%	NR	5%	NR	NR	NR	NR	11%	8%			
Ventricular dysfunction	RV dysfunction	Global	100%	54%	82%	NR	NR	NR	88%	100%	26%	76%		
		Regional	NR	48%	NR	92%								
	LV dysfunction	LV dilation	NR	NR	NR	14%	40%	NR	NR	14%	28%	NR		
		Reduced LVEF		10%		5%				18%			26%	
	LV WMAs:	NR	NR	41%	33%	45%								
Prognosis	Duration of follow-up (years)	Mean	2.4	8.1±7.8	NR	2.3±2.2	NR	NR	NR	10.7±7.7	NR	12±9		
		Median	NR	6	6 (IQR: 2 to 13)	1.4			4.6	10	NR	NR		
	Annual mortality	SCD	0.3%	0.7%	0.5%	0	NR	NR	1.9%	0.6%	NR	0.2%		
		Death due to heart failure	NR	1.3%	0.3%				NR	NR		0.9%	0.6%	0.1%
		All cause	NR	2.3%	NR				NR	NR		NR	2.8%	1.9%
Age of death (years)	NR	NR	NR	NR	NR	NR	NR	Mean: 36.9±14.7	NR	NR	NR			

Table 10. Symptoms, clinical features and prognosis of clinical defined ARVC/D for published cohorts.

NR = not reported, WMA = ventricular wall motion abnormalities, LVEF = left ventricular ejection fraction, SCD = sudden cardiac death . RV dysfunction is defined as any abnormalities on echo, MRI or RV angiography constituting a major or minor criteria for the diagnosis of ARVC/D. Unless otherwise stated, LV dysfunction is defined as any degree of regional or global LV dysfunction identified by echo or MRI.

Type of protein encoded	Gene		Localisation (and function) of protein	Reports describing autosomal dominant inheritance of ARVC/D due to mutations in this gene	Reports describing autosomal dominant recessive of ARVC/D due to mutations in this gene
Desmosomal	DSC2	Desmocollin 2	Desmosomal plaques (intercellular adhesion)	(Syrris <i>et al.</i> , 2006), (Heuser <i>et al.</i> , 2006)	(Simpson <i>et al.</i> , 2009)
	DSG2	Desmoglein 2	Desmosomal plaques (intercellular adhesion)	(Pilichou, 2006)	(Torsten B Rasmussen <i>et al.</i> , 2013)
	JUP	Plakoglobin	Desmosomal plaques, Adherens junction (intercellular adhesion)	(Asimaki <i>et al.</i> , 2007)	(McKoy <i>et al.</i> , 2000)
	PKP2	Plakophilin 2	Desmosomal plaque protein	(Gerull <i>et al.</i> , 2004)	(Awad <i>et al.</i> , 2006)
	DSP	Desmoplakin	Desmosomal plaque protein	(Rampazzo <i>et al.</i> , 2002)	(Alcalai <i>et al.</i> , 2003)
	CTNNA3 *	α T-catenin	Desmosomal plaque and adherens junction protein	(van Hengel <i>et al.</i> , 2013)	-
	p0072 / PKP4 *	Plakophilin 4	Desmosomal plaques (intercellular adhesion)	(Gandjbakhch <i>et al.</i> , 2013)	
	PERP *	p53 effector related to PMP22	Desmosomal plaques (intercellular adhesion)	(Gandjbakhch <i>et al.</i> , 2013)	
Non-desmosomal	TMEM43	Transmembrane protein 43	Nuclear envelope (unknown), Intercalated discs (unknown), Sarcolemma (unknown)	(Merner <i>et al.</i> , 2008)	-
	RYR2	Ryanodine receptor 2	Sarcoplasmic reticulum (Receptor for calcium triggered calcium release from sarcoplasmic reticulum in cardiomyocytes)	(Tiso <i>et al.</i> , 2001)	-
	TGFB3	Transforming growth factor beta 3	Cytokine (cellular adhesion and extra-cellular matrix formation)	(Beffagna <i>et al.</i> , 2005)	-
	LMNA	Lamin A/C	Nuclear envelope	(Quarta <i>et al.</i> , 2011b)	-
	TTN	Titin	Sarcomeric protein connects the Z discs to the M line of a sarcomere	(Taylor <i>et al.</i> , 2011)	-
	DES	Desmin	Intermediate filament of the cytoskeleton	(van Tintelen <i>et al.</i> , 2009), (Klauke <i>et al.</i> , 2010)	-
	PLN	Phospholamban	Sarcoplasmic reticulum (regulates SERCA2 / Calcium ATPase pump)	(van der Zwaag <i>et al.</i> , 2012)	-
	CDH2	N-cadherin	Transmembrane protein in adherens junctions	(Mayosi <i>et al.</i> , 2017)	-

Table 11. ARVC/D associated genes, their functions and reports of inheritance patterns associated with mutations in these genes.

* Pathogenicity not well established, rare variants identified in one to two cases.

Publication	Un-selected probands												Desmosomal mutation negative probands				
	(den Haan <i>et al.</i> , 2009)	(Bauce <i>et al.</i> , 2010)	(Fressart <i>et al.</i> , 2010)	(Klauke <i>et al.</i> , 2010)	(Cox <i>et al.</i> , 2011)	(Xu <i>et al.</i> , 2010)	(Quarta <i>et al.</i> , 2011a)	(Quarta <i>et al.</i> , 2011b)	(Groeneweg <i>et al.</i> , 2013)	(Baskin <i>et al.</i> , 2013)	(Lorenzon <i>et al.</i> , 2013)	Summary / Range	(Taylor <i>et al.</i> , 2011)	(Haywood <i>et al.</i> , 2013)	(Gandjbakhch <i>et al.</i> , 2013)	(van Hengel <i>et al.</i> , 2013)	
Total number of probands †	82	42	135	12	149	195	44	108	142	195	91	12 - 195	38	143	64	74	
Number of probands with ≥1 ARVC/D associated mutation (per gene)	DSC2	0 (0%)	2 (5%)	2 (2%)	1 (8%)	4 (3%)	4 (2%)	3 (8%)	9 (12%)	3 (2%)	2 (1%)	NR	0 - 12%	Negative	Negative	Negative	Negative
	DSG2	7 (9%)	5 (12%)	14 (10%)	2 (16%)	5 (3%)	10 (5%)	13 (33%)	22 (30%)	6 (4%)	2 (1%)	NR	1 - 33%		Negative	Negative	Negative
	JUP	1 (1%)	0 (0%)	0 (0%)	0 (0%)	0 (0%)	2 (1%)	0 (0%)	0 (0%)	0 (0%)	NR	NR	0 - 1%	NT	Negative	Negative	Negative
	PKP2	37 (45%)	9 (21%)	42 (31%)	4 (33%)	78 (52%)	38 (19%)	13 (33%)	25 (34%)	74 (52%)	20 (10%)	NR	10 - 52%	Negative	Negative	Negative	Negative
	DSP	1 (1%)	7 (12%)	6 (5%)	0 (0%)	2 (1%)	10 (5%)	10 (26%)	17 (23%)	1 (1%)	4 (2%)	NR	0 - 26%		Negative	Negative	Negative
	≥1 desmosomal gene (any)	43 (52%)	23 (55%)	62 (46%)	8 (67%)	87 (58%)	52 (27%)	32 (73%)	61 (56%)	102 (71%)	28 (14%)	NR	14 - 73%	Negative	Negative	Negative	Negative
	TMEM43										6 (3%)*		3%		1 (1%)		
	RYR2	NT	NT	NT	NT	NT	NT	NT	NT	NT	NT	NR	Unknown	NT	NT	NT	NT
	TGFB3		2 (5%)										5%				
	LMNA	NT	NT	NT	NT	NT	NT	NT	4 (4%)	NT	NT	NR	4%	NT	NT	NT	NT
	TTN													7 (18%)			
	DES	NT	NT	NT	1 (8%)	NT	0 (0%)	NT	NT	NT	NT	2 (2%)	0 - 8%	NT	NT	NT	NT
	PLN									19 (13%)*			13%				0 (0%)
	CTNNA3	NT	NT	NT	NT	NT	NT	NT	NT	NT	NT	NT	Unknown	NT	NT	0 (0%)	2 (2%)
PERP															1 (1%)		
PKP4	NT	NT	NT	NT	NT	NT	NT	NT	NT	NT	NT	Unknown	NT	NT	1 (1%)	NT	
Homozygous	0 (0%)	0 (0%)	1 (1%)	0 (0%)	1 (1%)	0 (0%)	NR	NR	NR	0 (0%)	0 (0%)	0 - 1%	NT	NR	0 (0%)	0 (0%)	
Compound heterozygous	3 (4%)	1 (2%)	2 (2%)	0 (0%)	0 (0%)	7 (4%)	NR	NR	NR	0 (0%)	0 (0%)	0 - 4%	NT		0 (0%)	0 (0%)	
Double heterozygous	3 (4%)	2 (5%)	2 (2%)	0 (0%)	2 (1%)	14 (7%)	NR	NR	NR	0 (0%)	1 (1%)	NR	NT		1 (1%)	NT	

Table 12. Prevalence of ARVC/D associated mutations in published cases series

NT= not tested, NR = not reported, NA = not applicable

† All probands included have a definite diagnosis of ARVC/D by the 1995 or 2010 criteria.

* Only 1 proven pathogenic non-desmosomal

1.3.2 The pathogenesis of ARVC/D

Our understanding of the pathogenesis of ARVC/D has developed through (1) an examination of its pathological features in myocardial tissue (2) the identification of pathogenic genetic variants associated with the disease and (3) the use of animal and cellular models with which the mechanisms of pathogenesis can be examined.

When compared with myocardium from healthy controls, the myocardium of ARVC/D subjects has been reported to have: (1) an increase in the proportion of fibroblasts and extra-cellular matrix relative to cardiomyocytes, (2) infiltration of fatty tissue between myocardial fibres, (3) evidence of cardiomyocyte death, including by apoptosis, (4) cardiomyocyte steatosis and (5) the presence of inflammatory infiltrates (Marcus *et al.*, 1982) (Thiene *et al.*, 1988) (Fontaliran *et al.*, 1991) (Basso *et al.*, 1996) (Burke *et al.*, 1998) (Tabib, 2003) (Basso and Thiene, 2005) (Basso *et al.*, 2008) (Young *et al.*, 2009) (Lobo *et al.*, 1992) (Fornes *et al.*, 1998) (Corrado *et al.*, 1997) (Chimenti *et al.*, 2004).

At the time of writing, more than 400 pathogenic variants, spread across 13 different genes have been reported to be associated with ARVC/D. Of 412 variants in a large online database, 364 (88%) were in the five main desmosomal genes (van der Zwaag *et al.*, 2018). The number and type of pathogenic variants in these major desmosomal genes are summarised in Table 13. The locations of pathogenic mutations with respect to the domains of the transcribed desmosomal proteins are summarised in Table 14. The majority (63% in the ARVD/C Genetic Variants Database) of pathogenic desmosomal mutations are radical i.e. they are nonsense mutations (23%), frameshift insertions or deletions (26%) or splice site mutations (14%). Such mutations may be predicted to generate transcripts which are either not translated or generate a truncated peptide. By contrast missense are predicted to be translated to mutant proteins containing a single amino acid change and be pathogenic by modifying their binding properties. For each desmosomal protein some domains are more common sites for pathogenic variants than others (e.g. the ECB for DSC2 and DSG2; the arm-repeat domain for PKP2 and JUP; the spectrin repeat domains for DSP). Despite these patterns ARVC/D may result from a variant affecting almost any domain of the desmosomal proteins (see Table 14 and Table 15).

Pathogenic variants		<i>DSC2</i>	<i>DSG2</i>	<i>PKP2</i>	<i>JUP</i>	<i>DSP</i>
Total (364)		42	50	171	15	86
Missense		23 (55%)	29 (58%)	38 (22%)	10 (67%)	33 (38%)
Radical	Total	19 (45%)	21 (42%)	133 (78%)	5 (33%)	53 (62%)
	Nonsense	4 (10%)	6 (12%)	39 (23%)	1 (7%)	(34%)
	Insertion / deletion, in-frame or frameshift	9 (21%)	9 (18%)	67 (39%)	3 (20%)	19 (22%)
	Splice site	6 (14%)	6 (12%)	27 (16%)	1 (7%)	5 (6%)

Table 13 Pathogenic mutations listed in the ARVD/C Genetic Variants Database.

The ARVD/C Genetic Variants Database is maintained by the University Medical Centre Groningen Department of Genetic, Cardiogenetics Research Group and is a open access resource which collates published data on ARVC/D associated variants (van der Zwaag *et al.*, 2018).

Gene	Total	Most frequently affected domains (≥30% variants)		Less frequently affected domains (<30% variants)	
<i>DSC2</i>	42	Extracellular cadherin binding domain	29 (69%)	Intracellular cadherin sequence	4 (10%)
				Propeptide	8 (19%)
				Other	1 (2%)
<i>DSG2</i>	50	Extracellular cadherin binding domain	28 (56%)	Extracellular anchor	4 (8%)
				Intracellular anchor	1 (2%)
				Intracellular cadherin sequence	4 (8%)
				Repeat unit domain	5 (10%)
				Propeptide	4 (8%)
				Other	4 (8%)
<i>PKP2</i>	171	Arm-repeat domain	116 (68%)	C-terminus	1 (<1%)
		N-terminus	52 (30%)	Other	2 (2%)
<i>JUP</i>	15	Arm-repeat domain	8 (53%)	C-terminus	2 (14%)
		N-terminus	5 (33%)		
<i>DSP</i>	86	Spectrin repeat domain	36 (42%)	C-terminus	2 (2%)
				Plakin repeat domain	17 (20%)
				Central rod domain	23 (27%)
				Other	8 (9%)

Table 14 Protein domains associated with of pathogenic variants of all types in the major desmosomal genes

This table summarises the same dataset presented in Table 13 and originates from the ARVD/C Genetic Variants Database (van der Zwaag *et al.*, 2018).

Gene	Total	Most frequently affected domains		Less frequently affected domains	
<i>DSC2</i>	23	Extracellular cadherin binding domain	16 (70%)	Intracellular cadherin sequence	2 (9%)
				Propeptide	4 (17%)
				Other	1 (4%)
<i>DSG2</i>	29	Extracellular cadherin binding domain	16 (55%)	Extracellular anchor	2 (7%)
				Intracellular anchor	0
				Intracellular cadherin sequence	3 (10%)
				Repeat unit domain	2 (7%)
				Propeptide	4
				Other	2 (7%)
<i>PKP2</i>	38	Arm-repeat domain	29 (76%)	C-terminus	0
		N-terminus	9 (24%)	Other	0
<i>JUP</i>	10	Arm-repeat domain	7 (70%)	C-terminus	1 (10%)
		N-terminus	2 (20%)		
<i>DSP</i>	33	Spectrin repeat domain	15 (45%)	C-terminus	2 (6%)
				Plakin repeat domain	7 (21%)
				Central rod domain	7 (21%)
				Other	2 (6%)

Table 15 Protein domains associated with of pathogenic missense variants in the major desmosomal genes

This table summarises the same dataset presented in Table 13 and originates from the ARVD/C Genetic Variants Database (van der Zwaag *et al.*, 2018).

Several studies have studied the effects of ARVC/D variants on other desmosomal plaque proteins by immunoblotting (to assess overall tissue content) and immunofluorescence microscopy (to assess cellular distribution) in either myocardial tissue or cellular or animal models. These studies are summarised in Table 18, Table 19 and Table 20.

Instead, investigations have focussed on identifying common pathways by which these diverse variants induce the same clinical phenotype. To this end studies have examined: (1) on inter-cellular adhesion (by examination of desmosomal ultrastructure and the mechanical properties of tissue expressing mutant proteins) and (2) on the intracellular signalling pathways (both in the myocardium of ARVC/D subjects and in disease models).

Studies of desmosomal ultrastructure support the idea that ARVC/D is associated with changes in desmosomal organisation, irrespective of the details of associated mutations. Abnormal ultrastructural features have been reported in cardiac tissue from subjects with ARVC/D since the 1980s (Table 21). A reduction in the abundance

of desmosomes and increase in desmosomal gap width in ARVC/D subjects has been one of the most consistently reported features of these reports.

The most methodologically robust of these studies was from Basso *et al.* (Basso, 2006). They examined myocardium obtained by endomyocardial biopsy and compared 21 cases of ARVC/D (of which 10 were carriers of a pathogenic variant in *DSP*, *PKP2* or *DGS2*), 10 cases of idiopathic dilated cardiomyopathy (IDCM) and 10 samples from donor transplant hearts. They conducted morphometric analysis of the major intercalated disc (ICD) structures i.e. desmosomes, adherens junctions and gap junctions. When compared to controls, ARVC/D samples had a smaller number of desmosomes per unit length of ICD but an overall increase in the amount of desmosomal plaque at the ICDs due to an increase in desmosomal length. In addition the average intermembrane gap width of desmosomes was greater in ARVC/D compared with controls. The IDCM cases had trends in these parameters in the same directions as the ARVC/D cases but the differences between them and controls did not reach statistical significance. Similarly the difference between ARVC/D and IDCM cases in these parameters did not reach statistical significance. Overall this study supports the proposal that changes in cardiomyocytes desmosomal ultrastructure are a feature of ARVC/D irrespective of genotype but that they are also present in other forms of cardiomyopathy.

Desmosomal ultrastructure has been assessed in animal models of reduced or deficient *DSC2*, *JUP*, *PKP2* and *DSP*, and those of over-expression of mutant *DSG2* and *DSP* (Table 19). Whilst all of these studies describe some form of abnormality at the intercalated discs (ICDs) there was no single characteristic that was reported consistently. Abnormalities included: a complete disruption of the ICD including desmosomes, a loss of the desmosomal midline, a reduction in the abundance of desmosomes and desmosomal pallor. None of these studies performed quantitative analysis of desmosomal ultrastructure.

The only cellular models of ARVC/D in which desmosomal ultrastructure was assessed have been iPSC-CMs described by Caspi *et al.* Both Caspi *et al.* and Basso *et al.* reported desmosomal pallor and Caspi *et al.* reported the presence of blurred and asymmetrical desmosomes in ARVC/D lines but not in control iPSC-CMs. Caspi *et al.* also performed quantitative analysis of desmosomal width and reported the same increase in the width of the desmosomal gap as had been described studies of desmosomes in the myocardium of ARVC/D cases (Table 16). Caspi *et al.*

reported an increase in desmosomal widths relative to a control iPSC-CM, but did not study desmosomal length or abundance.

	Caspi et al iPSC-CM	Basso et al Cardiac tissue	Lahtinen et al Cardiac tissue
Subjects Control vs ARVC/D	1 vs 1	10 vs 21	10 vs 3
Gap width (nm) Control vs ARVC/D	24±1 vs 32±2 33% greater p<0.05	22±3 vs 29±9 32% greater p=0.004	22±3 vs 32±18 45% greater p not given
Total desmosomal width (nm) Control vs ARVC/D	101±5 vs 171±12 69% greater p<0.001	-	-
Length (nm) Control vs ARVC/D	-	160±80 vs 310±80 94% greater p<0.001	-
Abundance (desmosomes per 10µm) Control vs ARVC/D	-	5.6±2 vs 3.3±1 41% less p=0.01	5.5±3 vs 3.1±0.4 45% less p not given

Table 16 Comparison of the results of studies of ARVC/D in which quantitative assessments of desmosomal morphology were performed.

Measurements presented are the mean±SEM for a given study group

The changes in molecular structure and organisation associated with these changes in desmosomal morphology are produced has not been elucidated. In the discussion of their findings, Basso *et al.* 2006 propose only that the increase in desmosomal gap width could be due “abnormal expression of transmembrane proteins” and that the pallor of plaques could be due to an “abnormal composition” of desmosomal plaque proteins. In other tissues desmosomal gap width has been demonstrated to be a dynamic feature. Conformational changes in desmosomal cadherins may be triggered by intracellular regulators acting via protein kinase C α (PKC α) to phosphorylate the intracellular component of the desmosomal plaque (Wallis *et al.*, 2000) (Garrod *et al.*, 2005). It is unlikely that the differences reported in ARVC/D represent occur by this mechanism. The mean difference in desmosomal gap induced by PKC α was reported to be 9% (24±0.5 nm vs 22±0.5 nm) (Garrod *et al.*, 2005), much smaller than the 32-45% differences reported in studies of ARVC/D. Evidence of the dynamic nature of desmosome morphology does make the idea that mutations affecting proteins constituting the desmosome affect the structure of extracellular domains of desmosomal cadherins more plausible.

The effects of ARVC/D an mutation on the mechanical properties of a cellular model of ARVC/D have been studied by Huang *et al.* . They generating a desmosome

producing cell line (HEK cells) which stably expressed a mutant JUP protein associated with ARVC/D which lacked its N-terminal domain (Huang *et al.*, 2008). Intercellular adhesion (assessed by both drag-deform and dispase fragmentation assays) was reduced compared with controls. These techniques have not been used to study other ARVC/D associated mutations to date.

The role of desmosomal proteins (particularly JUP and PKP2) in intracellular signalling was outlined in 1.2.7. The suggestion that changes to these pathways had a role in ARVC/D pathogenesis arose from the following observations. Firstly that the plakoglobin signal at the intercalated discs of myocardial samples appeared to be reduced in ARVC/D subjects regardless of the gene in which an ARVC/D associated variant was located. Secondly that there was evidence of changes in these pathways in animal and cellular models of ARVC/D, the effects of which were known to regulate the processes of fibrosis, adogenesis and apoptosis that were noted in pathological studies of the disease. These observations are discussed in more detail below.

Studies using immunofluorescence and immunohistochemistry to assess the abundance and localisation of desmosomal proteins in ARVC/D myocardium are summarised in Table 17. Plakoglobin signal intensity has been described as reduced in 75-91% of patients across cohorts of between 17 and 34 cases (Table 18). A reduction in the intensity of plakoglobin signal at the intercalated discs was noted in ARVC/D subjects with and without ARVC/D associated mutations and appeared to be independent of the gene in which mutations were located (Table 18).

The loss of plakoglobin from intercalated discs has also been reported in animal and cellular models of ARVC/D, summarised in Table 19 and Table 20. In particular a mouse model of DSP deficiency has been shown to produce an increase in the cytoplasmic and nuclear abundance of plakoglobin associated with a downregulation of canonical Wnt signalling (Garcia-Gras, 2006) (Lombardi *et al.*, 2011). DSP deficiency also disturbs upstream regulators of the Hippo signalling pathway (protein kinase C- α and neurofibromin-2), the resultant activation of the Hippo pathway also down-regulates canonical Wnt signalling (S. N. Chen *et al.*, 2013) (Heallen *et al.*, 2011). Downregulation of Wnt signalling is associated with adipogenesis, fibrosis and apoptosis and is therefore an appealing candidate for a part of a common-pathway of ARVC/D pathogenesis (Ross, 2000) (Longo, 2002) (Pećina-Slaus, 2010) (Rao and Kuhl, 2010). Downregulation of Wnt signalling has also been reported in iPSC-CM

models of ARVC/D caused by *PKP2* mutations. In both iPSC-CM models *PKP2* expression was reduced by the mutation. A similar reduction in *PKP2* expression in HL-1 cells has been shown to suppress Wnt signalling via upregulation of the Hippo pathway (S. N. Chen *et al.*, 2013).

Additional evidence for the role of Wnt signalling suppression in ARVC/D has come from studies demonstrating that GSK3 β inhibitors (which increase Wnt signalling) can rescue animal and cellular models of ARVC/D caused by variants in *JUP*, *DSG2* and *PKP2* from the disease phenotype (Asimaki *et al.*, 2014) (Chelko *et al.*, 2016) (Hariharan *et al.*, 2014). The work of Chelko *et al.* is of particular interest as they studied human myocardium of ARVC/D patients with a range of and desmosomal mutations and those with no identified mutations and found that GSK3 β was localised to the intercalated discs in ARVC/D patients but to the nucleus in both controls and patients with other forms of cardiomyopathy (Chelko *et al.*, 2016). This is consistent with the idea that changes in Wnt signalling are part of a common pathway of disease pathogenesis and that they are specific to ARVC/D.

The downregulation of Wnt signal has not been reported universally in ARVC/D or ARVC/D models. Down-stream targets of Wnt have been reported to be up regulated in a whole transcriptome analysis of ARVC/D myocardium and in a mouse model of ARVC/D caused by *DSG2* deficiency (Kant *et al.*, 2016).

In addition the theory that the downregulation of Wnt signalling in ARVC/D is mediated by nuclear redistribution of plakoglobin from the plasma membrane has been challenged by studies which found no reduction in plakoglobin signal in ARVC/D myocardium (Tavora *et al.*, 2013) (Vite *et al.*, 2013) (Kant *et al.*, 2016). The origin of these apparent conflicting findings was investigated by Kant *et al.* who conducted a rigorous and well controlled quantitative analysis of immunofluorescence intensity from four anti-plakoglobin antibodies targeting different epitopes, including the antibody (15F11) used in all the studies reporting a reduced plakoglobin signal (Kant *et al.*, 2016). This study indicated that plakoglobin was not reduced in abundance at the intercalated discs and that the reduced signal detected with 15F11 labelling was due to epitope masking possibly due to changes in the organisation of proteins within the desmosomal plaques (Kant *et al.*, 2016). This idea is consistent with the hypothesis from TEM studies that ARVC/D is associated with organisational changes in the desmosomal plaques.

In summary, electron and immunofluorescence microscopy studies suggest that changes in desmosomal structure are a common feature of the disease and there is good evidence that ARVC/D is mediated by the suppression of Wnt signalling. However the molecular mechanisms by which ARVC/D associated mutations lead to these changes has yet to be clearly elucidated.

Publication	Mutation	Protein assessed by immunohistology												Number of cases	Cases in which signal of ≥ 1 desmosomal protein is reduced
		DSC2	DSG2	JUP	PKP2	DSP	β -Catenin	α -Catenin	TMEM43	DES	N-Cad	Cx43	Nav1.5		
(Ermakov <i>et al.</i> , 2014)	Various	NA	NA	\leftrightarrow / \downarrow	NA	NA	NA	NA	NA	NA	NA	NA	NA	5	3/5 (60%)
(Vite <i>et al.</i> , 2013)	DSG2	\leftrightarrow	\leftrightarrow / \downarrow	\leftrightarrow	\leftrightarrow	NA	\leftrightarrow	NA	NA	NA	\leftrightarrow	NA	NA	7	3/7 (42%)
(Tavora <i>et al.</i> , 2013)	Unknown	NA	NA	\leftrightarrow	\leftrightarrow	\leftrightarrow	NA	NA	NA	NA	\leftrightarrow	\leftrightarrow	NA	23	0/23 (0%)
(T B Rasmussen <i>et al.</i> , 2013)	DSP	NA	NA	NA	NA	\leftrightarrow / \downarrow	NA	NA	NA	NA	NA	NA	NA	3	2/3 (66%)
(Torsten B Rasmussen <i>et al.</i> , 2013)	DSG2	NA	\leftrightarrow	\leftrightarrow	NA	\leftrightarrow	NA	NA	NA	NA	\leftrightarrow	\leftrightarrow	NA	9	0/9 (0%)
(Noorman <i>et al.</i> , 2013)	Various	NA	NA	\leftrightarrow / \downarrow	\leftrightarrow / \downarrow	NA	NA	NA	NA	NA	\leftrightarrow	\leftrightarrow / \downarrow	\leftrightarrow / \downarrow	19	14/19 (74%) (JUP)
(Kwon <i>et al.</i> , 2013)	Unknown	NA	NA	\leftrightarrow / \downarrow	NA	NA	NA	NA	NA	NA	\leftrightarrow	\leftrightarrow	NA	17	13/17 (76%)
(van der Zwaag <i>et al.</i> , 2012)	PLN	NA	NA	\leftrightarrow / \downarrow	NA	NA	NA	NA	NA	NA	\leftrightarrow	NA	NA	7	5/7 (71%)
(Munkholm <i>et al.</i> , 2012)	Various	NA	NA	\leftrightarrow / \downarrow	NA	NA	NA	NA	NA	NA	NA	NA	NA	34	29/34 (85%)
(Kirchner <i>et al.</i> , 2012)	PKP2	NA	NA	\leftrightarrow / \downarrow	NA	NA	NA	NA	NA	NA	\leftrightarrow	NA	NA	2	1/2 (50%)
(Gehmlich <i>et al.</i> , 2012)	DSG2	NA	NA	\downarrow	NA	NA	NA	NA	NA	NA	\leftrightarrow	NA	NA	1	1/1 (100%)
(Gehmlich <i>et al.</i> , 2011)	DSC2, DSG2	NA	NA	\downarrow	NA	NA	NA	NA	NA	NA	\leftrightarrow	\leftrightarrow	NA	1	
(Quarta <i>et al.</i> , 2011b)	LMNA	NA	NA	\leftrightarrow / \downarrow / \blacklozenge	NA	NA	NA	NA	NA	NA	NA	NA	NA	1	1/1 (100%)
(Lahtinen <i>et al.</i> , 2011)	DSG2	NA	\downarrow	\downarrow	\downarrow	\downarrow	NA	NA	NA	NA	\leftrightarrow	\leftrightarrow	NA	1	1/1 (100%)
(Christensen <i>et al.</i> , 2011)	TMEM43	NA	NA	\downarrow	\leftrightarrow	NA	NA	NA	\downarrow	NA	NA	\leftrightarrow	NA	2	2/2 (100%)
(Otten <i>et al.</i> , 2010)	DES	NA	NA	\leftrightarrow	\downarrow	\downarrow	NA	NA	NA	\leftrightarrow (Abn)	\leftrightarrow	\leftrightarrow	NA	2	2/2 (100%)
(Katja Gehmlich <i>et al.</i> , 2010)	DSG2	NA	NA	\downarrow	\downarrow	\downarrow	NA	NA	NA	NA	\leftrightarrow	\downarrow	NA	1	1/1 (100%)
(Fidler <i>et al.</i> , 2009)	PKP2	NA	NA	NA	\leftrightarrow	\leftrightarrow	NA	NA	NA	NA	\leftrightarrow	\downarrow	NA	1	0/1 (0%)
(Asimaki <i>et al.</i> , 2009)	Various	NA	NA	\downarrow	\downarrow	\downarrow	NA	NA	NA	NA	\leftrightarrow	\downarrow	NA	22	21/22 (95%)
(Lahtinen <i>et al.</i> , 2008)	PKP2	NA	NA	NA	\leftrightarrow	NA	NA	NA	NA	NA	NA	NA	NA	1	0/1 (0%)
(Kaplan <i>et al.</i> , 2004)	JUP	\leftrightarrow *	NA	\downarrow	\leftrightarrow	\leftrightarrow	\leftrightarrow	\leftrightarrow	NA	NA	\leftrightarrow	\downarrow	NA	4	4/4 (100%)

Table 17. Summary of studies describing the desmosomal immunohistology of cardiac tissue from cases of ARVC

\leftrightarrow = Protein abundance unchanged, \downarrow = Protein abundance reduced, NA = Not assessed, * DSC2/3, \blacklozenge a reduced number for ICDs were detected by plakoglobin IHC, the intensity of the signal was not described as reduced.

Results of genetic screening	Type of protein encoded	Gene	Publications	Proportion of cases in which a reduction in JUP identified	
ARVC/D associated mutation identified	Desmosomal	DSC2	(Munkholm <i>et al.</i> , 2012) (3 cases)*	3/3 (100%)	25/28 (89%)
		DSG2	(Asimaki <i>et al.</i> , 2009) (2 cases) (Munkholm <i>et al.</i> , 2012) (1 case)* (Lahtinen <i>et al.</i> , 2011) (1 case)	4/4 (100%)	
		JUP	(Asimaki <i>et al.</i> , 2009) (1 case) (Munkholm <i>et al.</i> , 2012) (1 case)*	2/2 (100%)	
		PKP2	(Asimaki <i>et al.</i> , 2009) (2 cases) (Munkholm <i>et al.</i> , 2012) (3 cases)* (Noorman <i>et al.</i> , 2013) (11 cases)	13/16 (81%)	
		DSP	(Asimaki <i>et al.</i> , 2009) (3 cases)	3/3 (100%)	
	Non-desmosomal	TMEM43	(Christensen <i>et al.</i> , 2011) (2 cases)	2/2 (100%)	18/22 (81%)
		RYR2	-		
		TGF	-		
		LMNA	(Quarta <i>et al.</i> , 2011b) (1 case)	1/1 (100%)	
		TTN	-		
		DES	(Otten <i>et al.</i> , 2010) (2 cases)	2/2 (100%)	
No ARVC/D associated mutation identified			(Noorman <i>et al.</i> , 2013) (2 cases) (van der Zwaag <i>et al.</i> , 2012) (7 cases)	7/9 (78%)	
			(Asimaki <i>et al.</i> , 2009) (3 cases) (Noorman <i>et al.</i> , 2013) (5 cases)	6/8 (75%)	

Table 18 Studies assessing plakoglobin expression by immunohistology in genotyped cases of ,ARVC/D.

Studies were selected on the basis of similar staining protocol, in particular the choice of anti-JUP dilution. * The series reported by Munkholm et al at 2012 consisted of 6 cases with ARVC/D associated mutations, they reported 3 cases to be digenic carriers but did not describe which mutations were co-existent.

Gene	Publication	Animal	Model				Abnormalities						
			Over expression of wild type protein	Knock-out / knock-down	Mutated gene expression	Mutation, Protein modification	Gross histology and clinical findings	Localisation and content of desmosomal proteins.	Desmosomal ultrastructure	Adipogenesis and Fibrosis	Wnt signalling	Apoptosis	Details
DSC2	(Heuser <i>et al.</i> , 2006)	Zebra-fish		●		Knock-down <i>DSC2</i>	✓	NA	✓	NA	NA	NA	<ul style="list-style-type: none"> • Cardiomegaly • Bradycardia • Reduced myocardial contractility • Loss of midline / desmoglea at cardiac desmosomes (TEM)
					●	c.631-2A>G Splice acceptor site mutation p. M211fsX221 Expressed in context of knock down <i>DSC2</i>	✓	NA	NA	NA	NA	NA	<ul style="list-style-type: none"> • Reported as not rescuing cardiac phenotype, details not given.
DSG2	(Krusche <i>et al.</i> , 2011)	Mouse			●	Homozygous knock-out exons 4-6 (EC1/EC2) (no human analog)	✓	NA	NA	✓	NA	NA	<ul style="list-style-type: none"> • Cardiomegaly • Reduced myocardial contractility • Cardiac fibrosis (TC)
	(Pilichou <i>et al.</i> , 2009)	Mouse			●	c.797A>G p.N266S Overexpression	✓	X	X	✓	NA	✓	<ul style="list-style-type: none"> • Cardiomegaly, myocardial thinning., electrical conduction delay • No change in desmosomal protein localisation. (IM) • No change in desmosomal appearance or gap width (TEM) • Fibrosis (TC), no marked increase in adipogenesis • Increased apoptosis (TUNEL), and necrosis
JUP	(Swope <i>et al.</i> , 2012)	Mouse		●		Cardiac restricted, inducible homozygous <i>JUP</i> and <i>CTNNB1</i> knock-out.	✓	✓	✓	✓	NA	✓	<ul style="list-style-type: none"> • Cardiomegaly, and thickening of ventricular walls • Reduced PKP2, DSG2, DSP, N-cad, Cx43 localisation to membrane (IM). • Reduced total, PKP2, DSP, DSG2, N-cad. (WB) • Complete loss of normal ICD architecture (TEM). • Fibrosis (TC), but no adiposis (ORO) • Increased apoptosis (TUNEL)
	(Lombardi <i>et al.</i> , 2011)	Mouse	●			Overexpression.	✓	✓	NA	NA	NA	NA	<ul style="list-style-type: none"> • Cardiomegaly • Overexpressed WT protein at membrane, and in cytoplasm and nucleus (WB, IM)
					●	c.2157_2158delTG, p.G680fsX690 expressed on background of heterozygous <i>JUP</i> knock-out.	✓	✓	NA	NA	NA	NA	<ul style="list-style-type: none"> • Cardiomegaly • Reduced mutant <i>JUP</i> at the membrane, accumulation in nucleus and cytoplasm (WB, IM)
	(D. Li <i>et al.</i> , 2011)	Mouse		●		Cardiac restricted, inducible homozygous <i>JUP</i> knock-out.	✓	✓	✓	✓ / X	✓	✓	<ul style="list-style-type: none"> • Cardiomegaly, thinning of ventricular walls • Reduced PKP2, DSG2, DSP, Cx43 localisation to membrane (IM). • Reduced total, PKP2, no change in DSP or DSG2. (WB) • Number and length of desmosomes reduced. Number and length of fascia adherens increased • Fibrosis (TC), but no adiposis (ORO) • Increase in β-catenin and unphosphorylated β-catenin. Upregulation of gene targets of canonical Wnt signalling. • Increased apoptosis (TUNEL)
(Bierkamp <i>et al.</i> , 1996)	Mouse		●		Homozygous knock-out	✓	NA	✓	NA	NA	NA	<ul style="list-style-type: none"> • Embryonic lethality, myocardial wall thinning. • Desmosomes, pale, reduced density, reduced number (TEM). 	

Table 19. Animal models of desmosomal gene abnormalities and ARVC/D associated desmosomal mutations

✓ = Abnormality found on testing, X = No abnormality found on testing, NA = Not assessed

TF = TOPFlash assay, IM = immunofluorescence microscopy, WB = Western immunoblot, FC = Flow cytometry, PC = single cell patch clamping, ORO = oil red O staining and light microscopy, TEM = transmission electron microscopy, TUNEL = terminal deoxynucleotidyl transferase dUTP nick end labelling, qPCR = quantitative reverse transcriptase polymerase chain reaction. (continued below)

(Table 16 continued)

Gene	Publication	Animal	Model				Abnormalities						
			Over expression of wild type protein	Knock-out / knock-down	Mutated gene expression	Mutation, Protein modification	Gross histology and clinical findings	Localisation and content of desmosomal proteins.	Desmosomal ultrastructure	Adipo-genesis and Fibrosis	Wnt signalling	Apoptosis	Details
PKP2	(Grossmann <i>et al.</i> , 2004)	Mouse	-	●	-	Homozygous knock-out	✓	✓	✓	NA	NA	X	<ul style="list-style-type: none"> Embryonic lethality, myocardial wall thinning. Loss of co-localisation of DSP with PKP2, JUP, DSG2, N-Cad (IM). Reduction in DSG2 signal (IM) (WB) Redistribution of JUP and DSP to cytoplasm (IM) (WB) Desmosomes indistinct. (TEM) No increase in apoptosis (TUNEL)
DSP	(Gomes <i>et al.</i> , 2012)	Mouse		●		Heterozygous cardiac restricted knockout	✓	✓	NA	✓	NA	NA	<ul style="list-style-type: none"> Higher incidence of inducible VT No change in I_{Na} (PC) or SCN5A expression (qPCR) Cytoplasmic localisation of Cx43. (IM) Reduction in JUP and DSP signal (IM) Fibrofatty infiltration. (TC) (ORO)
	(Yang, 2006)	Mouse	●			Cardiac restricted, overexpression.	X	X	✓	X	NA	X	<ul style="list-style-type: none"> Normal cardiac morphology and function Increase electron density of fascia adherens (TEM)
					●	c.8501G>A p. R2834H Cardiac restricted, overexpression.	✓	✓ / X	✓	✓	NA	✓	<ul style="list-style-type: none"> Cardiomegaly and impaired ventricular function. Reduced colocalisation of DES with DSP, no change in colocalisation of JUP, PKP2, Cx43 with DSP (IM) Redistribution of JUP, PKP2 and Cx43 from cytoskeleton to cytoplasm. (WB) Widening intercellular gap throughout ID length (TEM) Spontaneous adipogenesis (ORO), and fibrosis (TC) Increased apoptosis (TUNEL)
					●	c.88G>A p.V30M Cardiac restricted, overexpression.	✓	NA	NA	NA	NA	NA	<ul style="list-style-type: none"> Embryonic lethality Myocardial thinning
					●	c.269A>G p.Q90R Cardiac restricted, overexpression.	✓	NA	NA	NA	NA	NA	<ul style="list-style-type: none"> Embryonic lethality Myocardial thinning
	(Garcia-Gras, 2006)	Mouse		●		Homozygous, cardiac restricted knock-out	✓	NA	NA	✓	✓	X	<ul style="list-style-type: none"> High rate of embryonic lethality Cardiomegaly, myocardial thinning Fibrosis (TC) and adiposis (ORO) Reduced expression of canonical Wnt signalling target genes, suggesting suppression of signalling (qPCR)
				●		Heterozygous, cardiac restricted knock-out	✓	✓	NA	✓	✓	X	<ul style="list-style-type: none"> Cardiomegaly Increased nuclear JUP (WB), no change in cytosolic content. Fibrosis (TC) and adiposis (ORO), upregulation of proadipogenic gene expression (qPCR). Reduced expression of canonical Wnt signalling target genes, suggesting suppression of signalling (qPCR) No increase in apoptosis (TUNEL)
	(Gallicano <i>et al.</i> , 2001)	Mouse			●	Homozygous knock-out	✓	✓	NA	NA	NA	NA	<ul style="list-style-type: none"> Embryonic lethality Myocardial thinning Reduction in DSG2 signal, no change in PG, (IH)

✓ = Abnormality found on testing, X = No abnormality found on testing, NA = Not assessed

TF = TOPFlash assay, IM = immunofluorescence microscopy, IH = immunohistochemistry, WB = Western immunoblot, FC = Flow cytometry, PC = single cell patch clamping, ORO = oil red O staining and light microscopy, TC = Trichrome staining for fibrosis e.g. Masson's, TEM = transmission electron microscopy, TUNEL = terminal deoxynucleotidyl transferase dUTP nick end labelling, qPCR = quantitative reverse transcriptase polymerase chain reaction

Gene	Publication	Cell type	Over expression of wild type protein	Knock-out / Knock-down	Mutated gene expression	Mutation, Protein modification	Abnormalities					Details
							Localisation and content of desmosomal proteins.	Desmosomal ultrastructure	Adipo-genesis and Fibrosis	Wnt signalling	Apoptosis	
DSC2	(K. Gehmlich <i>et al.</i> , 2010)	HL-1 and NRVM			●	c.2687_2688insGA, p.A897fsX900	✓	NA	NA	NA	NA	<ul style="list-style-type: none"> • Mutant protein localisation to cell border (IM) • Some accumulation of mutant protein in golgi apparatus (IM)
					●	c.607 C>T p.R203C	✓	NA	NA	NA	NA	<ul style="list-style-type: none"> • Failure of mutant protein to localise to cell border (IM) • Accumulation of mutant protein in cytoplasmic vesicles (IM)
					●	c.824 C>T p.T275M	✓	NA	NA	NA	NA	<ul style="list-style-type: none"> • Mutant protein localised to cell border, (IM) • Accumulation of mutant protein in cytoplasmic vesicles and golgi apparatus. (IM)
	(Beffagna <i>et al.</i> , 2007)	HL-1 and NRVM			●	c.304G>A p.E102K	✓	NA	NA	NA	NA	<ul style="list-style-type: none"> • Mutant protein localised to cell border (IM) • Accumulation of mutant protein in cytoplasm. (IM)
					●	c.1034T>C p.E134T	✓	NA	NA	NA	NA	<ul style="list-style-type: none"> • Reduced localisation of mutant protein to cell border, (IM) • Accumulation of mutant protein in cytoplasm. (IM)
DSG2	No published cardiac cellular models											
JUP	(Lombardi <i>et al.</i> , 2011)	mCPC	●				NA	NA	✓	✓	NA	<ul style="list-style-type: none"> • Spontaneous adipogenesis (ORO) • Suppressed canonical Wnt signalling. (qPCR) • Upregulated non-canonical Wnt signalling (qPCR)
				●			NA	NA	✓	✓	NA	<ul style="list-style-type: none"> • Resistant to adipogenesis despite proadipogenic culture.(ORO) • Upregulation of canonical Wnt signalling. (qPCR)
					●	Mutant transgene c.2157_2158delTG, p.G680fsX690 expressed on background of heterozygous JUP knock-out.	NA	NA	✓	✓	NA	<ul style="list-style-type: none"> • Spontaneous adipogenesis (ORO) • Suppressed canonical Wnt signalling. (qPCR) • Upregulated non-canonical Wnt signalling (qPCR)
PKP2	(Caspi <i>et al.</i> , 2013)	iPSC-CM			●	c.972insT/N p.A324fsX335	✓	✓	✓	NR	NR	<ul style="list-style-type: none"> • Reduced total PKP2, JUP, Cx43 signal (IM). • Pale, indistinct, dissymmetrical desmosomes, increased desmosomal gap width, increased total external desmosomal width (TEM) • Spontaneous adipogenesis (TEM)
					●	c.148_151delACAG/ N p.T50SfsX110	✓	NR	✓	✓	✓	<ul style="list-style-type: none"> • Reduced PKP2, JUP, Cx 43 signal (IM), (localisation not assessed) • Spontaneous adipogenesis and accelerated adipogenesis with proadipogenic medium (TEM) • Suppressed canonical Wnt signalling (IM) • Increase apoptosis (TUNEL)
	(Kim <i>et al.</i> , 2013)	iPSC-CM			●	c.2484C>T Cryptic splicing exon 12: r.2483_2489del frameshift.mutation	✓	NR	✓	✓	✓	<ul style="list-style-type: none"> • Nuclear localisation of JUP (IM) • Accelerated adipogenesis ith proadipogenic medium (ORO), upregulation of proadipogenic gene expression (qPCR) • Suppressed canonical Wnt signalling (IM) (TF) • Increase apoptosis with proadipogenic culture (TUNEL)
					●	c.2013delC R672fsX683	✓	NR	✓	✓	✓	<ul style="list-style-type: none"> • Nuclear localisation of JUP (IM) • Accelerated adipogenesis ith proadipogenic medium (ORO), upregulation of proadipogenic gen expression (qPCR) • Suppressed canonical Wnt signalling (IM) • Increase apoptosis with proadipogenic culture (TUNEL)
	(Ma <i>et al.</i> , 2012)	iPSC-CM			●	c.1841T>C p.L614P	✓	✓	✓	NA	NA	<ul style="list-style-type: none"> • Reduced total PKP2, JUP, no change in DSP, Cx43, N-cad signal (IM). • Desmosomes "less dense" unquantified (TEM) • Greater spontaneous adipogenesis (ORO)

Table 20 Cellular models of desmosomal gene abnormalities and ARVC/D associated desmosomal mutations

✓ = Abnormality found on testing, ✗ = No abnormality found on testing, NA = Not assessed

NRVM= neonatal rat ventricular myocytes, mCPC = mouse cardiac progenitor cells, iPSC-CM = induced pluripotent stem cell derived cardiomyocytes, TF = TOPFlash assay, IM = immunofluorescence microscopy, WB = Western immunoblot, FC = Flow cytometry, PC = single cell patch clamping, ORO = oil red O staining and light microscopy, TEM = transmission electron microscopy, TUNEL = terminal deoxynucleotidyl transferase dUTP nick end labelling, qPCR = quantitative reverse transcriptase polymerase chain reaction. (continued below)

(Table 17 continued)

Gene	Publication	Cell type	Over expression of wild type protein	Knock-out / Knock-down	Mutated gene expression	Mutation, Protein modification	Abnormalities					Details	
							Localisation and content of desmosomal proteins.	Desmosomal ultrastructure	Adipo-genesis and Fibrosis	Wnt signalling	Apoptosis		
PKP2 (cont')	(Kirchner <i>et al.</i> , 2012)	HL-1			●	c.2386T>C p.C796R	✓	NA	NA	NA	NA	<ul style="list-style-type: none"> Reduced mutant PKP2 protein content (WB) Accumulation of mutant protein in cytoplasm and nucleus (IM) No effect on JUP distribution (IM) 	
	(Fidler <i>et al.</i> , 2009)	HL-1		●			NA	NA	NA	NA	NA	<ul style="list-style-type: none"> Possible reduction in Cx43 content 	
	(Joshi-Mukherjee <i>et al.</i> , 2008)	NRVM				●	c.235C>T p.R79X	✓	NA	NA	NA	NA	<ul style="list-style-type: none"> Reduced localisation of mutant to membrane, increase cytoplasmic signal (IM) (WB) No change in DSP localisation and signal (IM) (WB) Reduced Cx43 signal (IM) (WB)
					●	c.534_535insCT p.C179fsX190	✓	NA	NA	NA	NA	<ul style="list-style-type: none"> Reduced localisation of mutant to membrane, increase cytoplasmic signal (IM) (WB) No change in DSP or Cx43 localisation. 	
DSP	(Zhang <i>et al.</i> , 2013)	HL-1		●			NA	NA	NA	NA	NA	<ul style="list-style-type: none"> Redistribution of Cx43 to cytoplasm, reduction in total content, reduced rate of intercellular dye transfer. (IM) (WB) (FC) Redistribution of Nav1.5 to cytoplasm, reduction in total content, changes in cellular action potential (IM) (WB) (FC) (PC) 	
	(Garcia-Gras, 2006)	HL-1		●			✓	NA	✓	✓	X	<ul style="list-style-type: none"> Redistribution of JUP from cytoplasmic to nuclear distribution.(IM) (WB) No change in β-catenin content by 2-fold reduction in canonical Wnt signalling activity (TF). Accelerated adipogenesis in proadipogenic medium (ORO), upregulation of proadipogenic gene expression. (qPCR) Upregulation of profibrotic gene expression (qPCR) No change in apoptosis (TUNEL) 	

✓ = Abnormality found on testing, X = No abnormality found on testing, NA = Not assessed

NRVM= neonatal rat ventricular myocytes, mCPC = mouse cardiac progenitor cells, iPSC-CM = induced pluripotent stem cell derived cardiomyocytes, TF = TOPFlash assay, IM = immunofluorescence microscopy, WB = Western immunoblot, FC = Flow cytometry, PC = single cell patch clamping, ORO = oil red O staining and light microscopy, TEM = transmission electron microscopy, TUNEL = terminal deoxynucleotidyl transferase dUTP nick end labelling, qPCR = quantitative reverse transcriptase polymerase chain reaction.

		Guiraudon et al. 1989	Roncall et al. 1989	Kaplan et al. 2004	Lahtinen et al. 2008	Pilichou et al. 2006	Basso et al. 2006
Sample	Source	EMB	EMB	EMB	EMB	EMB	EMB
	Handling	Not reported	Fixed from fresh	Frozen before fixative	Recovered from paraffin	Fixed from fresh	Fixed from fresh
Desmosomes	Abundance	Reduced	-	-	Reduced	Reduced*	Reduced*
	Length	Reduced	-	-	(Reduced §)	(Reduced §)	Increased*
	Electron density	-	Reduced	-	-	(Reduced ¶)	(Reduced ¶)
	Plaque width	-	Reduced	-	-	-	-
	Gap width	-	-	-	-	Increased*	Increased*
	General appearance	-	Hazy or ill-defined	-	-	-	-
Adherens junctions	Abundance	Reduced	-	-	-	-	-
	Length	-	-	-	-	-	-
	Electron density	Reduced	Reduced	-	-	-	-
	Plaque width	-	Reduced	-	-	-	-
	Gap width	-	-	-	Increased	-	No change
Gap junctions	General appearance	-	No change	-	-	-	-
	Abundance	-	-	Reduced*	-	-	No change
	Length	-	-	Reduced*	-	-	No change
ICD	General appearance	-	-	-	Vacuolated	-	-
	Tortuosity / convolutions	Reduced	Reduced	-	-	Measured but not reported*	No change
Myofibrils	General appearance	-	No change	-	-	-	No change
T-tubules	General appearance	-	Contain fibrillar material	-	-	-	No change
Lipid droplets	Abundance	-	No change	-	-	-	Increased
Data from non-ARVC/D control myocardium provided for comparison		No	No	Yes	Yes	Yes	Yes

Table 21 Summary of ultrastructural features of ARVC/D myocardium.

* quantitative analysis

§ small abnormally located desmosomes noted, length of desmosomes at the intercalated discs not described

¶ Pallor of the “internal plaques” reported, thought to refer to the IDPs

1.4 Hypotheses, aims and objectives

The main aim of this project was to determine whether patient specific iPSC-CMs carrying ARVC/D associated genetic variants showed abnormalities in desmosomal protein expression, localisation and ultrastructure.

More specifically this project aimed to generate patient specific iPSC-CM disease models of genetic variants that had not previously been investigated using this technique, including those in genes other than *PKP2*.

The main hypotheses investigated in this project were that patient specific iPSC-CMs from subjects with ARVC/D caused by desmosomal mutations differ from control iPSC-CMs in that:

- Mutation specific disturbances in the abundance of desmosomal gene transcripts and the abundance and cellular localisation of desmosomal proteins will be seen in ARVC/D iPSC-CMs.
- All ARVC/D iPSC-CMs will have a reduction in the intensity of immunofluorescence signal of plakoglobin at their intercellular junctions relative to control iPSC-CMs.
- ARVC/D iPSC-CMs have desmosomes with abnormal ultrastructural characteristics such as asymmetry and indistinct plaque morphology, and such features are absent in control iPSC-CMs.
- The desmosomes of ARVC/D iPSC-CMs have an increase in the width of their intermembrane gap and in the width of their desmosomal plaques relative to control iPSC-CMs.

Chapter 2 Methods

2.1 Recruitment of study participants and the origin of cells lines and tissues.

2.1.1 Recruitment of subjects from which peripheral blood samples were collected

Control blood derived iPSCs were generated from healthy volunteers that were recruited via the “Collection of blood, plasma and urine samples from healthy volunteers“ programme based at the Newcastle University, Northern Institute of Cancer Research (ethics committee reference 00216).

iPSCs derived from subjects with ARVC/D were generated from participants in the Arrhythmogenic Cardiomyopathy Induced Pluripotent Stem-cell Study (ACIS), (NHS research ethics committee reference 14/EM/1147).

2.1.2 Recruitment of subjects from which myocardial samples were collected

Sample of right atrial appendage were collected from subjects recruited via “The isolation and characterisation of cell lines, including adult human stem cells, from tissue discarded following cardiothoracic surgery” study (NHS research ethics committee reference 10/H0908/56)

2.1.3 Control fibroblasts and fibroblast derived iPSCs

Some experiments included the human dermal fibroblasts (HDFs), AD3-C1 iPSCs and iPSC-CMs. HDFs purchase from Lonza (Product CC-2511, LOT0000264781) and originated from a 31 year old female who was not known to have a history or family history of hereditary cardiac disease or sudden cardiac death. AD3-C1 was generated as from these HDFs under ethical approvals secured by the Lonza. The line was generated outside the present study but using the same Sendai based reprogramming system and was kindly donated by Prof Lyle Armstrong.

2.1.4 Immortalised human keratinocytes

Some experiments included an immortalised human keratinocyte line (HaCaT) as a control. This is a commercially available cell line (ThermoFisher) that was kindly donated by Dr Mustafa Al-Musawi (Newcastle University).

2.1.5 Human embryonic stem cells

Some experiments used commercially obtained H9 (WA09) human embryonic stem cells (WiCell Research Institute) (NIHhESC-10-0062) as controls.

2.2 The collection and processing of samples of right atrial appendage

Sample of right atrial appendage (RAA) were collected from subjects undergoing routine cardiac surgery performed by Dr Andrew Owens. It was standard clinical practice in this surgery to excise and discard a portion of the RAA to allow the subject to receive cardiopulmonary bypass. This was performed as follows, after accessing the heart via a sternotomy under general anaesthesia, a purse string suture was placed around the base of the RAA. An incision was then made into the RAA through which a cannula was passed into the right atrium. The suture was tightened to allow haemostasis and the remainder of the RAA proximal to the suture was excised and discarded. As part of the study protocol (see above) an investigator was present in the operating theatre at the time of the surgery and collected the RAA immediately after excision. The tissue was then divided into samples to be used for RNA extraction or TEM analysis and handled as described in 2.13.2 and 2.20.2.

2.3 The collection and processing of blood samples

2.3.1 Blood sampling

A tourniquet was applied to the upper arm of subjects, a site selected for venepuncture, the skin over the was swabbed with an alcohol and 10-30ml of blood drawn into sterile blood collection tubes pre-treated with ethylenediaminetetraacetic acid (EDTA) to achieve a concentration of 5mM in the final sample. Samples were kept at room temperature and processed within 6 hours of collection.

2.3.2 Density gradient centrifugation

The mononuclear cell fraction of whole blood was isolated by density gradient centrifugation by a standard technique (GE Healthcare Life Sciences, 2005). Blood samples of 10-30ml volume were diluted 1:1 with Dulbecco's phosphate buffered saline (DPBS), layered over Ficoll-Paque Premium 1.077g/ml (GE) and centrifuged for at 400 g, 20°C for 40min, beginning with a slow acceleration and no break applied to the deceleration. The buffy coat at the interface between ficoll and plasma was collected with a Pasteur pipette, diluted in 50ml of DPBS and centrifuged at 400 g, 20°C for 10 minutes. The supernatant was discarded, the pellet resuspended in

DPBS and centrifuged again at 200g, 20°C for 10 minutes. The supernatant was discarded, the pellet resuspended in DPBS and centrifuged again at 200g, 20°C for 10 minutes. The supernatant was discarded, the pellet resuspended in culture medium, flow buffer or sort buffer as appropriate. The total population of viable mononuclear cells obtained estimated using a haemocytometer and trypan blue as described below.

2.3.3 Estimation of the concentration of cells within a single cell suspension using a haemocytometer

Single cell suspensions were prepared in a known volume such that their concentration was in the range of 0.2 to 2.0 x10⁶ cells/ml. Sample were gently triturated to ensure uniform suspension. A 10µl sample was removed, diluted 1:1 with trypan blue 0.05% and incubated at room temperature for 2 minutes. Samples were loaded into a Neubauer haemocytometer and visualised using Nikon TS100 inverted microscope. The average number of viable cells across four 1mm² (1x10⁻⁴ml) counting areas was calculated, from which the concentration of cells in the original suspension could be estimated.

2.3.4 FACS sorting of CD3+ cells

In some experiments CD3+ cells were purified from PBMCs by FACS. 1x10⁸ freshly isolated PBMCs were suspended in 100µl of sterile sort buffer (DPBS, 0.2% fetal bovine serum (FBS), 2mM EDTA) and incubated with anti-CD3-V500 (BD) in the dark at 4°C for 30minutes before being washed in flow buffer, centrifuged at 400g for 5 minutes, the supernatant aspirated, then resuspended in 500µl of flow buffer. DAPI was added at 0.25mg/ml immediately prior to analysis. Samples were processed using a BD FACSFusion sorter. Live singlet cells expressing CD3 were sorted into PBMC base medium. Purified samples were centrifuged, resuspended in culture medium without cytokines and the concentrations of cells estimated as described above cells ready for pre-transduction culture.

2.4 Cellular reprogramming

The process of reprogramming is summarised in Figure 13.

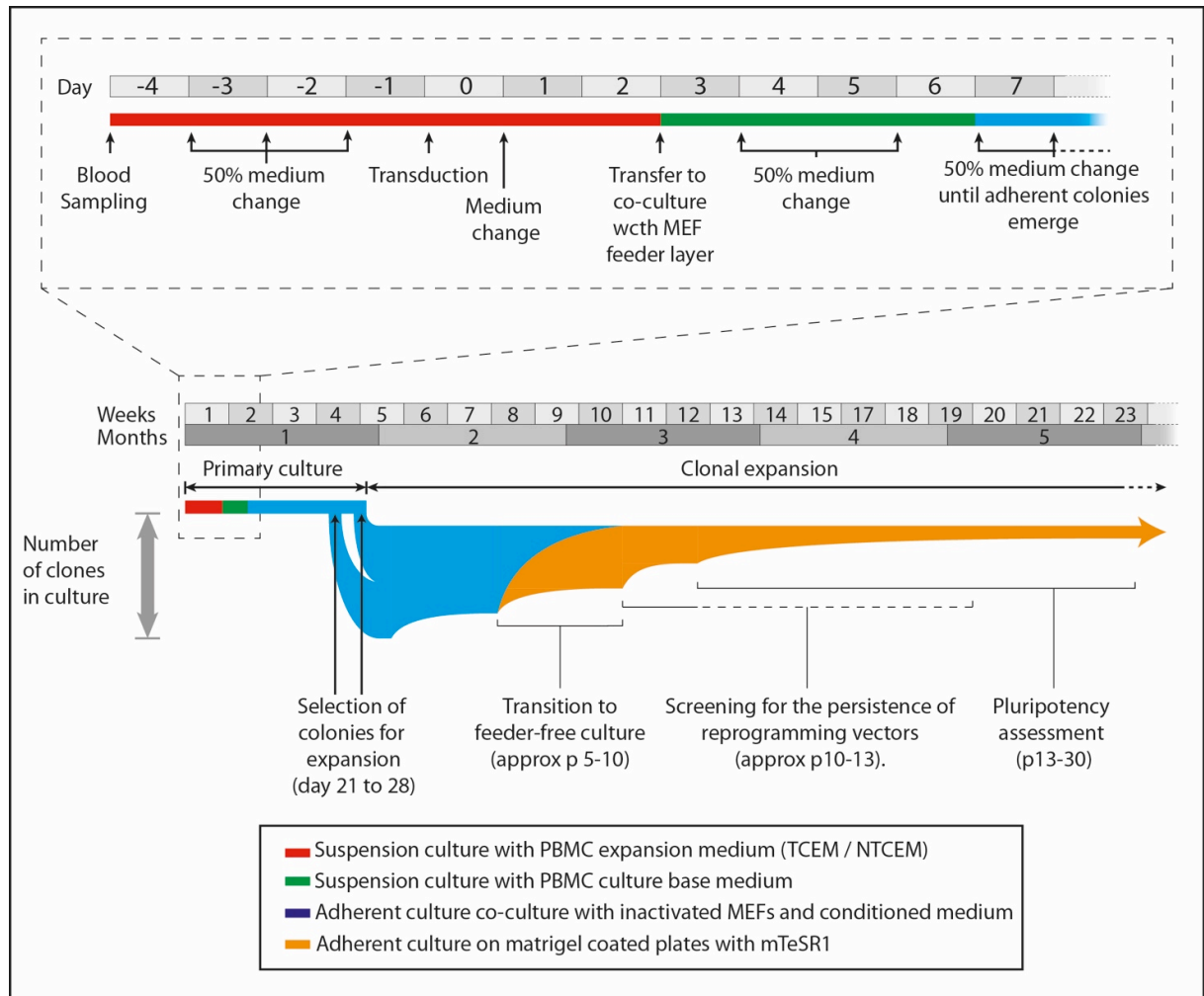


Figure 13 Generation of iPSCs from nucleated peripheral blood cells.

2.4.1 Pre-transduction culture

PBMCs were cultured in either T-cell expansion medium (TCEM) or non-T-cell expansion medium (NTCEM). The base PBMC media for both media consisted of Stemline II medium (Sigma) with 1% penicillin/streptomycin.

TCEM consisted of base media supplemented with IL2 100ng/ml (R&D). In addition, beads coated with anti-CD3 and anti-CD28 (Life technologies) with a bead to cell ratio of 1:1 were included in TCEM on the first day of pre-transduction culture.

NTCEM consisted of base medium supplemented with SCF 100ng/ml, FLT3L 100ng/ml, TPO 100ng/ml, IL6 100ng/ml and IL3 100ng/ml (all from R&D).

All blood cells were seeded at a density of 1.0×10^6 cells/ml and 1.0×10^6 cells/well in a 24 well ultra low attachment plates (Costar). Cultures were incubated at 37°C in

a humidified atmosphere with 5% CO₂ (referred to hereafter as standard conditions). Each day the cultures were removed from the incubator taking care not to disturb the cells at the bottom of the well. The upper 50% of the medium was aspirated from each well, and replaced with an equal volume of fresh expansion medium (TCEM or NTCEM as appropriate).

2.4.2 Transduction

After 4 days of pre-transduction culture the total population of cultured cells was estimated using a haemocytometer and between 30 and 100 x10³ cells collected for transduction. The cell suspension was centrifuged and resuspended in fresh pre-transduction culture media to which hexadimethrine bromide (Sigma) 4 µg/ml and Cytotune 2.0 reprogramming vectors (Life Technologies) were then added. The final volumes of cell suspension and reagents were calculated to ensure that the final volume of the cell suspension was 300µl, which was then transferred to a single well of a ultra-low attachment 96 well plate (Costar) and incubated overnight in standard conditions.

Cytotune 2.0 consists of 3 types of vector: a polycistronic vector encoding *SOX2*, *OCT4* and *KLF4*, a vector encoding *MYC* and a vector encoding *KLF4*.

Transductions were performed with a multiplicity of infection (MOI) of 5, 5 and 3 for each vector respectively.

2.4.3 Post transduction culture

On day 1 after transduction the cells were collected and centrifuged at 200g, 20°C for 10 minutes, the supernatant aspirated, and the cells resuspended in 1ml of fresh expansion medium and re-plated in a 24 well ultra low attachment plates (Costar).

On day 3 after transduction cells were collected, centrifuged at 200g, 20°C for 10 minutes, the supernatant aspirated, resuspended in base medium alone (without cytokines) and the total viable cell count was estimated using a haemocytometer. The cells were transferred to pre-prepared plates containing inactivated MEFs. Transduced cells were plated at a density ranging from 500 to 5000 cells per cm² cultured area.

On days 4 and 6 the upper 50% of the medium was removed from each well, and replaced with fresh base PBMC medium. From day 7 the upper 50% of the medium was removed from each well (as previously described), and replaced with conditioned PSC medium (see 2.5.2 for composition) daily until the appearance of

adherent colonies. Thereafter the whole volume of medium was changed daily. Cultures were observed for the appearance of colonies with an “embryonic stem cell like” morphology i.e. small cells with a high nuclear to cytoplasmic ratio. Whole colonies were transferred manually to fresh MEF feeders for further expansion.

2.5 Clonal expansion and maintenance culture of iPSCs on MEF feeder layers

2.5.1 Preparation of plates containing a MEF feeder layer

Pregnant Swiss MF1 mice containing 12.5 to 14 day embryos were sacrificed by a method compliant with university regulations. Following abdominal dissection the uterine horns were identified, dissected and placed in a petri dish containing DPBS, 10% FBS and 1% pen/strep (all from Life Technologies). The embryos were released from the amniotic sacs and the limbs, heads, tails and visible organs removed using fine dissection scissors and forceps. The remaining torsos were transferred to a petri dish containing 1% trypsin/EDTA (Life Technologies) in a sterile tissue culture hood. The tissues were minced for 1 minute with fine scissors, incubated for 5 minutes at 37°C and triturated with a 1ml pipette to facilitate dissociation. Twice the volume of fibroblast medium (Dulbecco’s modified Eagle medium (DMEM) - high glucose, 10% FBS, 1% pen/strep, 1% Glutamax, 1% Minimal essential medium non-essential amino acids (NEAA) (all from Life Technologies)) was added to inactivate the trypsin. The cell suspension was triturated through a 19G needle 1-2 times then centrifuged at 300g for 5 minutes, the supernatant aspirated and the pellet resuspended in fibroblast medium. Cell suspension was plated in T75cm² tissue culture flasks in a total volume of 10mls with approximately 3 embryos per flask. The cells were incubated in standard conditions. The medium was replaced with fresh fibroblast medium daily until they were 90% confluent, where upon they were either cryo-preserved or passaged for further expansion.

MEFs were passaged by aspirating the spent medium, washing the flask with DPBS, incubating 0.05% trypsin/EDTA for 5 minutes at 37°C and inactivating the trypsin by adding double the volume of fibroblast medium. The cell suspension was collected, centrifuged at 800g for 5 minutes, the supernatant aspirated, the cells resuspended in fibroblast medium and transferred to new flask with a split ratio of 1:3.

Tissue culture plates of the format intended for pluripotent cell culture were treated with the addition of 0.1% gelatin (Sigma) sufficient to cover the culture surface

followed by incubation at room temperature for 2 hours. Gelatin was aspirated from the plates immediately before use. Confluent flasks of MEFs between passages 3 and 5 were inactivated by irradiation (67.2Gy). A single cell suspension was prepared using 0.05% trypsin/EDTA as described above for passaging and transferred to the gelatin coated wells to provide a density of 15-20 x10³ cells per cm² of culture area. Plates were incubated in standard conditions for a minimum of 1 and a maximum of 4 days. On the day of use the fibroblast medium was aspirated, the plate washed with DPBS, sufficient conditioned pluripotent cell medium added to cover the well and the plate incubated until needed.

2.5.2 Preparation of MEF conditioned pluripotent cell culture medium.

Suspensions of inactivated MEFs were prepared as described above and plated in a tissue culture flask at a density of 56x10³ cells/cm². The following day the flask was washed with DPBS, replaced with 0.4ml/cm² growth area of stem cell medium and incubated. Stem cell medium consists of Knock-out DMEM (KO-DMEM), 20% knockout serum replacement (KSR), 1% pen/step, 1% NEAA, 1% Glutamax-I, 10ng/ml basic fibroblast growth factor (bFGF) (all from Life Technologies). The medium was collected and replaced every 24hrs for 10 days. During the period of collection, medium was stored at 4°C. At the end of the collection period medium was passed through a 0.2µm filter, aliquoted, frozen and stored at -20°C until use of for up to 3 months. On the day of use the medium was supplemented with 1% insulin-transferrin-selenium (ITS-G) (Life Technologies) and a further 10µg/ml bFGF.

2.5.3 Clonal expansion on inactivated MEF feeder layers

Pluripotent cells were cultured in standard conditions on with inactivated MEFs and conditioned pluripotent cell medium. The medium was changed daily and the size and morphology of the colonies observed to determine the optimal timing of passaging. In preparation for passaging differentiated areas were released from the colony with a 19-gauge needle or a 10µl pipette tip, the differentiated fragments aspirated and fresh conditioned PSC medium added to the well. Conditioned PSC medium was added to new MEF plates as described earlier.

Very early passage iPSCs (p1-4) were passaged manually. Colonies were cut into fragments with a needle or 10µl pipette tip, the fragments released manually from the culture surface, collected in a 1ml pipette and transferring them to new MEF feeder plates.

Clones that had expanded to fill a well of a 12 well plate or more were passaged enzymatically. After cleaning, the medium was aspirated, the culture washed with DPBS and then incubated with 1mg/ml collagenase IV (Gibco) in KO-DMEM for 4-7 minutes in standard conditions until the edges of colonies appear to be lifting from the culture surface. The collagenase solution was then aspirated and replaced with conditioned PSC medium. Colony fragments were released from the culture surface by the hydraulic action of medium gently expelled from a P1000 pipette. If necessary, fragments were gently triturated with a serological pipette to reduce their size. The suspension of colony fragments was then transferred to a new MEF feeder plate (prepared as described above). Split ratios (in terms of growth area) ranged from 1:1 to 1:6 depending on the growth characteristics of the cells. Cells were passaged every 4-7 days. Clones that were slow growing or showing high levels of differentiation in repeated passages were discarded.

2.6 Clonal expansion and maintenance culture in feeder-free conditions

2.6.1 Preparation of Matrigel coated cultureware

Tissue culture plates coated with hES qualified Matrigel (Corning) were prepared as per the manufacturer's instructions. The manufacturer provides a recommended volume of Matrigel necessary to coat a culture area of 215-235cm² – referred to as an aliquot. Aliquots of Matrigel were thawed on ice, diluted with 25ml of ice-cold DMEM/F12 1:1 (Life Technologies) per aliquot and plated onto pre-chilled cultureware at a density of approximately 0.12ml/cm² of growth area i.e. 1ml per well of a 6 well plate. Plates could be stored for up to 1 week at 4°C, in all cases were incubated at room temperature for 1 hour before use and the Matrigel solution aspirated from the plate immediately before use.

2.6.2 Transfer of pluripotent cells from culture on MEF feeder layers to feeder-free conditions

For each clone, colonies, co-cultured with or without inactivated MEFs, in a single well were selected for an attempted adaptation to feeder-free conditions. Cultures were passaged using the same techniques as for enzymatic except that care was taken not to disrupt the colonies into fragments. Where possible whole colonies including surrounding inactivated MEFs were lifted from the culture surface. The suspension of colonies was then collected using a serological pipette (being careful to avoid

disruption to the colonies) and transferred to a single well of a Matrigel coated plate. After 24 hours and daily thereafter the medium was changed to mTeSR1 and cultures were cleaned and passaged as described in 2.6.1.

2.6.3 Culture and passaging of pluripotent cells in feeder-free conditions

Pluripotent cells adapted to growth on Matrigel with mTeSR1 medium (StemCell Technologies) were incubated in standard conditions with daily medium changes. Cultures were passaged when they reached 80% confluence or showing signs of differentiation or reached 4 days since the previous passage. Differentiated areas were removed with a 10µl pipette tip immediately before passaging. Pluripotent cells were released from adherent culture using Versene (Lonza), which is a solution containing calcium and magnesium ion chelating agents including 0.05% EDTA. The plates were washed with DPBS, incubated with Versene for 4-8 minutes at room temperature, the Versene was aspirated and a suspension of aggregated colony fragments produced by flushing the well with mTeSR1 using a 1ml pipette. The suspension was distributed to Matrigel coated plate in a ratio from 1:2 to 1:6.

2.7 Spontaneous differentiation of iPSCs

2.7.1 Embryoid body differentiation

Pluripotent cells were cultured in feeder-free conditions such that they formed large (2-3mm diameter) colonies at 3-5 days after passaging. Cultured cells were washed in DPBS and then incubated with Dispase-Collagenase medium (DMEM-F12, 0.5mg/ml Dispase, 1mg/ml Collagenase IV (both from Gibco)) for 30-60 minutes at 37°C, until the colonies were released completely by tapping the plate. Fragments were collected with a serological pipette, allowed to settle in a centrifuge tube, resuspended in mTeSR1, transferred to an ultra-low attachment plates and incubated in standard conditions. On day 1, 3, and 5, 50% of the medium was removed and replaced with spontaneous differentiation medium (DMEM-F12 with 20% FBS). On day 7 EBs were transferred to plates coated with 0.2% gelatin and cultured for a further 7 days (14 days total), when they were prepared for immunofluorescence microscopy for markers of differentiation to the three germ layers.

2.7.2 Teratoma assay

Teratoma assay was performed at Newcastle University as part of an existing project (*In vivo* behaviour of progenitor cells, Home Office Project licence 6004508)

in accordance with the UK CCCR Guidelines for the Welfare of Animals in Experimental Neoplasia (Workman *et al.*, 1998) (Workman *et al.*, 2010).

iPSCs were cultured in feeder-free conditions to approximately 70% confluence, the medium was aspirated, the culture washed with DPBS and incubated with Versene for 7 minutes at 20°C. The Versene was aspirated and the colonies detached from the plate by washing with cell buffer (DPBS with 2% FBS). The cell suspension was centrifuged at 200g, for 3 minutes at 20°C, the supernatant aspirated and the pellet resuspended in sufficient cell buffer to give an approximate concentration of 5×10^6 cells/ml. The cell suspension was chilled to 4°C and mixed with an equal volume of Matrigel that had been thawed from frozen and held at 4°C to avoid gelling.

Subcutaneous injections of the iPSC-Matrigel suspension were performed on 8 week old male ICRF-Foxn1^{nu} mice (Harlan Laboratories) according to an existing departmental protocol. Each animal received a single 200µl injection of 0.5×10^6 cells to a flank. Each clone was tested in two mice.

From 3 weeks after the injections mice were examined weekly for the appearance of tumours. Tumours were harvested when one of 3 end-points were reached, either a tumour reached 1cm³, the animal showed signs of distress or 3 months had elapsed since injection. Mice were euthanased using CO₂ chamber and checked for the absence of vital signs. The skin over each tumour was incised with a scalpel and the tumour dissected, severing any vascular connection. Tumours were fixed in 4% formaldehyde at 4°C for 12-16 hours then washed with dH₂O 3 times. Tumours were then incubated in graded solution of ethanol (70%, 80%, 90%, 95%) for 2 hours each and then stored in 95% ethanol until ready for further processing.

Samples were processed and underwent either Masson's Trichrome staining, Weigherts haematoxylin staining or Mayer's haematoxylin and eosin staining as per an established protocol.

2.8 Directed cardiac differentiation of iPSCs after embryoid body formation

Three different methods of embryoid bodies (EB) formation were studied. All techniques used pluripotent cells cultured in feeder-free conditions to a point estimated to be 24hrs before the time at which they would normally be passaged.

2.8.1 Enzymatic EB formation

In some experiments EBs were formed enzymatically. Cultured cells were washed in DPBS and then incubated with Dispase-Collagenase medium for 5-20 minutes at

37°C, until the edges of colonies started to detach. mTeSR1 was added and colonies were dispersed into large aggregates mechanically by a serological pipette and gentle trituration. Fragments were plated in ultra-low attachment plates in mTeSR1 and incubated in standard conditions for a further 24hrs before starting directed cardiac differentiation.

2.8.2 Aggrewell EB formation

Aggrewell 400Ex plates (StemCell Technologies) were prepared as per the manufacturers instructions to ensure all wells were prefilled with mTeSR1-RI (mTeSR1, 10µM Y27632 (Chemdea)). Cultured pluripotent cells were washed with DPBS and then incubated with Accutase (Life Technologies) for 7-9 minutes at 37°C until the cells were visibly detached from the plate. mTeSR1-RI was then added to each plate and the suspension gently triturated with a 5ml serological pipette to produce a single cells suspension. Cells were centrifuged at 200g, for 5 minutes, at 20°C, the supernatant aspirated and the pellet resuspended in mTeSR1-RI. The density of cells in suspension was estimated using a haemocytometer and the appropriate number of cells transferred to each well of the Aggrewell plate necessary to generate EBs of 300 cells each. The plate was then centrifuged at 100g, for 3 minutes, 20°C and incubated in standard conditions. After 24hours the EBs were loosened from the wells into suspension by gentle pipetting with a 1ml pipette and collection with a 5ml serological pipette and transferred to an ultra-low attachment plates. EBs were incubate in mTeSR1 for a further 24 hours before starting directed cardiac differentiation.

2.8.3 Directed cardiac differentiation

The first day of exposure to the cardiac differentiation medium was referred to as day 0 of the protocol. On day 0 EBs were collected in a serological pipette and allowed to settle in a centrifuge tube for 10 minutes. The supernatant was aspirated and the EBs resuspended in embryoid body cardiac induction medium (ECIM) consisting of StemPro34, 1% Pen/Strep, 1% GlutaMax (all from Life Technologies), 1mM ascorbic acid and 0.4mM monothioglycerol (both from Sigma) .On day 0 this was supplemented with 1ng/ml BMP4 (R&D). On day 1 the medium was changed, using the same method, to ECIM supplemented with 10ng/ml BMP4, 6ng/ml Activin A (R&D) and 5ng/ml bFGF. On day 3 the medium was changed, using the same method, to ECIM supplemented with 150ng/ml Dickkopf related protein 1 (DKK1)

(R&D). On day 5 the medium was changed, using the same method, to ECIM supplemented with 10ng/ml vascular endothelial growth factor (VEGF) (R&D), 2µg/ml SB431542 (Tocris) and 118ng/ml dorsomorphin (DSM) (R&D). On day 7 the medium was changed, using the same method, to ECIM supplemented with 150ng/ml DKK1, 10ng/ml VEGF. EBs were then plated at a density of approximately 5 EBs/cm² on tissue culture plates coated with 0.1% gelatin. On day 10 and every 3 days thereafter the medium was replaced with ECIM supplemented with 10ng/ml VEGF and 5ng/ml bFGF EBs were observed daily for evidence of attachment and spontaneous contraction.

2.9 Directed cardiac differentiation of iPSCs as a monolayer

iPSCs were differentiated to iPSC-CMs using a modified version of an published protocol and is summarised in Figure 14 (Lian *et al.*, 2013a). iPSCs were cultured as described in 2.6 with the exception that were adapted to culture on growth factor reduced (GFR) rather than hESC qualified Matrigel. The manufacturer provides an estimate of the protein content of each batch of GFR Matrigel. Matrigel plates were prepared as described in 2.6.1 with the exception that the dilution of Matrigel was performed to achieve a protein content of 0.13mg/ml in the solution used to coat cultureware giving 15µg of Matrigel per cm² of culture area.

iPSCs were passaged into 12 well plates at a density such that they reached confluence 3-4 days after passaging. The differentiation protocol was initiated when the cultures were estimated visually to be between 80-100% confluent. On day 0 of differentiation, mTeSR1 was replaced with monolayer cardiac induction medium (MCIM) (RPMI 1640, 2% B27 without insulin (both from Life Technologies)) supplemented with CHIR99021 trihydrochloride (Tocris) at either 6, 9 or 12µM concentrations depending on the cell line and passage. On day 1 the medium was changed to MCIM alone. On day 3 the medium was changed to a mixture of fresh MCIM and the medium from the culture in a 1:1 ratio, this was supplemented with 5µM IWP2 (Tocris). On day 5 the medium was changes to MCIM alone. On day 7 the medium was changed to monolayer cardiac maintenance medium (MCMM) (RPMI 1640 with 2% B27 (both from Life Technologies)). Thereafter the medium was replaced with fresh MCMM medium every 2-3 days until cultures were collected for analysis, with the exception of those cultures that underwent metabolic purification (see below).

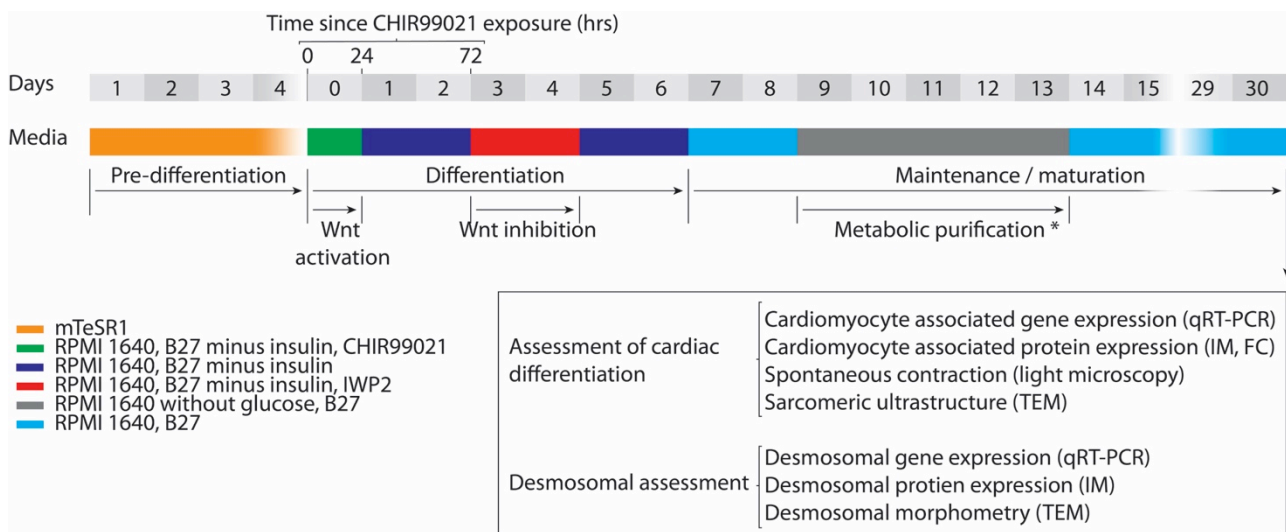


Figure 14 Monolayer directed cardiac differentiation protocol.

(*) Metabolic purification was not performed in all experiments.

2.10 Purification of iPSC-CMs following directed differentiation

2.10.1 Purification based on SIRPA expression

See 2.16.3.

2.10.2 Metabolic purification

In monolayer cardiac differentiation experiments that underwent metabolic purification the medium was changed to metabolic purification medium consisting of monolayer cardiac purification medium (MCP) medium (RPMI 1640 without glucose supplemented with 2% B27). During the initial testing of this protocol this change occurred on day 12 of differentiation, in subsequent experiments it was on day 9. Purification medium was the changed every other day. During the initial testing of the protocol the medium was changed back to cardiomyocytes MCMM after 7 days, in subsequent experiments this occurred after 5 days. The day after change back to MCMM cultures were either analysed by flow cytometry or replated. Culture were replated by changing the medium to maintenance medium supplemented with 10 μ M Y27632 and incubated for 2 hours in standard conditions. The cultures were then washed with DPBS and incubated 0.25% trypsin/EDTA in standard conditions for 5-20minutes until the fragments detached from the culture surface. Fragments were gently triturated to produce clusters of cells and equal volume of RPMI-20 (RPMI 1640 with 20% FBC) added to inactivate the trypsin. The cell suspension was

centrifuged at 200g for 4 minutes at 20°C, the supernatant aspirated and the pellet resuspended in RPMI-20 supplemented with 10µM Y27632. The concentration of cells in suspension was estimated using a haemocytometer and the cells were transferred to Matrigel coated cultureware (prepared as described earlier) at a density of 0.125 – 0.25 x10⁶ cells per cm² and incubated overnight in standard conditions. The follow day the medium was changed to maintenance medium and changed every 2-3 days thereafter.

2.11 Culture of immortalized keratinocytes

Immortalised keratinocytes (HaCaT) were cultured on tissue culture plastic-ware coated in MEF medium (Advanced DMEM (Life Technologies), 10% FBS, 1% Glutamax). The medium was changes every 48 hours. When cultures reached 90-100% confluence they were washed with DPBS and incubated with 0.05% trypsin/EDTA, at 37°C for 5-20 minutes until they were released from the culture surface gentle agitation. An equal volume of MEF medium was added to the suspension which was then collected, centrifuged at 200g for 4 minutes, 20°C. The supernatant was aspirated and the pellet resuspended with MEF medium. The cell suspension was then passaged to fresh culture vessels with a split ratio of 1:4. Cultures typically reached confluence 2-5 days after passaging depending on the starting density.

2.12 Cryopreservation of culture cells

Cells in feeder-free culture conditions were collected for cryopreservation once the cultures had reached 60-80% confluence. This typically occurred 3-4 days after passaging.

Cells were collected from adherent culture in feeder-free conditions as follows. Culture medium was aspirated and the adherent culture washed with DPBS. Adherent cultures were then incubated with Accutase, approximately 150ul per cm² of culture area, for 3 minutes at 37°C. Cultures were then gently agitated and observed under the microscope to determine whether cells had begun to detach from the culture surface. If not then they were incubated further until this occurred. Once detachment of the cells from the culture surface had been observed, all cells were detached from the culture surface by gentle flushing with mTeSR1-RI using a P1000 pipette. The total volume of mTeSR1-RI added was at least equal to that of the Accutase to terminate its activity. The cell suspension was collected with a

serological pipette, transferred to a 15ml centrifuge tube and centrifuged at 200g for 3 minutes, at room temperature. The supernatant was then aspirated leaving a cell pellet. The cell pellet was then resuspended in freezing medium, that had been pre-chilled to 4°C. The volume of freezing medium used to re-suspend the cells was determined by the area of the culture surface from which they were collected. Cells from each square centimetre of culture surface were resuspended in 50-100ul of freezing medium i.e. cells from a single well of a 6 well plate, having a culture area of 9cm², were resuspended in 0.5 – 1ml of freezing medium. The cell suspension was then transferred to cryotubes within an isopropanol filled freezing container (Mr Frosty, Nalgene) that had been pre-chilled to 4°C. 0.5 to 1ml of suspension was placed in each cryotube. Freezing containers were then transferred to a -80 freezer for at least 24 hours. Samples were then stored at either -80°C or in liquid nitrogen (-180°C).

2.12.1 Cryopreservation of cells following directed cardiac differentiation

Cells were incubated with maintenance medium supplemented with 10µM Y27632 for 2 hours. The medium was then aspirated, the cells were washed with DPBS and then incubated with cardiac dissociation medium for 15-30 minutes until the cells detached from the culture surface with gentle agitation and hydraulic action by flushing with a P1000 pipette. If possible the size of fragments was reduced to small clusters by trituration with a serological pipette. An equal volume of RPMI-20 was added, the suspension transferred to a 15ml centrifuge tube and centrifuged at 200g for 3 minutes, at room temperature. The supernatant was then aspirated leaving a cell pellet. The cell pellet was then resuspended in freezing medium, that had been pre-chilled to 4°C. The cell suspension was then transferred to cryotubes and frozen as described for pluripotent cells.

2.12.2 Cryopreservation of MEFs and immortalised keratinocytes

Culture medium was aspirated and the adherent culture washed with DPBS. Adherent cultures were then incubated with 0.05% trypsin/EDTA for 3-5 minutes in the case of MEFs and 5-20 minutes in the case of HaCaT cells, at 37°C, until they were released from the culture surface gentle agitation. An equal volume of MEF medium was added to the suspension which was then collected, centrifuged at 200g for 4 minutes, 20°C. The supernatant was aspirated and the pellet resuspended in freezing medium – without Y27632 at a concentration of 2-10 x10⁶ cells per ml. The

cell suspension was then transferred to cryotubes and frozen as described for pluripotent cells.

	Component	Concentration / molarity
Freezing medium	FBS	80% (v/v)
	DMSO	20% (v/v)
	Y27632	10uM
PSC medium	KO-DMEM	-
	KSR	20%
	Glutamax	1%
	Pen/Strep	1%
	NEAA	1%
	bFGF	10ng/ml
Conditioned PSC medium	PSC medium (co-cultured with inactivated MEFs, filtered)	-
	ITS	1%
	bFGF	10ng/ml
MEF medium	Advanced DMEM	
	FBS	10%
	Glutamax	1%
	Pen/Strep	1%
mTeSR1-RI	mTeSR1	
	Y27632	10µM
Collagenase IV medium	KO-DMEM	
	Collagenase IV	1mg/ml
Dispase-Collagenase medium	DMEM:F12	
	Dispase	0.5mg/ml
	Collagenase IV	1mg/ml
Embryoid body cardiac induction medium (ECIM)	StemPro34	-
	Glutamax	1%
	Pen/Strep	1%
	L-ascorbic acid	1mM
	1-thioglycerol	0.4mM
	Pen/Strep	1%
Monolayer cardiac induction medium (MCIM)	RPMI 1640	
	B27 supplement minus insulin	2%
	Pen/Strep	1%
Monolayer cardiac maintenance medium (MCMM)	RPMI 1640	
	B27 supplement	2%
	Pen/Strep	1%
Monolayer cardiac purification medium (MCPM)	RPMI 1640 without glucose	
	B27 supplement	2%
	Pen/Strep	1%
Flow cytometry cell buffer	DPBS	
	PBS	2%
RPMI-20	RPMI 1640	
	FBS	20%
Cardiomyocyte dissociation medium	Cell dissociation buffer	50%
	Trypsin/EDTA 0.25%	50%

Table 22 Composition of major culture media and reagents

2.13 Collection of samples for molecular analysis

2.13.1 Collection of a cell pellet from adherent cultures of iPSCs for DNA and RNA extraction.

All samples were obtained from cells grown in feeder-free conditions. Samples of iPSCs were collected for assessment of transgene expression from passage 10 onwards. If transgene expression was identified in the initial samples further samples were taken every 2-4 passages until it became absent or the clone was abandoned. Assessments of pluripotency gene expression were collected at passage numbers greater than that at which transgene expression was first undetectable.

Cells were collected from adherent cultures in feeder-free conditions as follows. Culture medium was aspirated and the adherent culture washed with DPBS. Adherent cultures were then incubated with Accutase, approximately 150ul per cm² of culture area, for 5 minutes at 37°C. Cultures were then gently agitated and observed under the microscope to determine whether cells had begun to detach from the culture surface. If not then they were incubated further until this occurred. Once detachment was observed, all cells were detached from the culture surface by gentle flushing with DPBS using a P1000 pipette. The total volume of DPBS added was at least equal to that of the Accutase to terminate its activity. The cell suspension was collected with a serological pipette, transferred to a 15ml centrifuge tube and centrifuged at 400g for 4 minutes, at room temperature. The supernatant was then aspirated leaving a cell pellet. If not processed immediately cell pellets were stored at -80oC for a maximum of 1 week.

2.13.2 Collection of human right atrial appendage tissue samples for RNA extraction.

Immediately following excision during surgery myocardial tissue was finely minced and placed in RNAlater (Sigma) and stored at 4°C for a maximum of 7 days until RNA extraction was performed.

2.13.3 Collection of samples from contracting cultures for RNA extraction

Single cell suspensions were prepared from contracting cultures as described in 2.16.2. These samples were then divided into two aliquots. One aliquot was analysed by flow cytometry to assess the proportion of iPSC-CMs within the sample. The

second aliquot was centrifuged at 400g for 4 minutes, at room temperature. The supernatant was then aspirated leaving a cell pellet. If not processed immediately cell pellets were stored at -80°C for a maximum of 1 week.

2.14 Genomic DNA analysis

2.14.1 Extraction of genomic DNA from PBMCs and cultured cells.

Genomic DNA was extracted from pelleted cells using the QIAamp DNA Micro kit (QIAGEN) as per the manufacturers protocol for the “isolation of genomic DNA from small volumes of blood”.

The yield of dsDNA from each extraction estimated by photo-absorbance spectrometry using the Qubit BR assay (Life Technologies) as per the manufacturers instruction. The Qubit assay utilises a dsDNA binding dye to aid the accuracy of quantification.

The levels of contamination with proteins and salts were assessed by photo-absorbance spectrometry using a Nanodrop 2000 (Thermo). Samples with 260:280 ratios >1.8 were considered to have minimal levels of proteins contamination and those with 260:230 ratios >1.8 considered to have minimal levels of salt contamination. Samples with either ratio below these levels were discarded.

2.14.2 SNP array analysis

Genomic DNA was assessed for evidence of copy number variations (CNV) using a SNP microarray. The HumanCytoSNP-12v2.1 kit (Illumina) was used and experiments were conducted using the protocols recommended by the manufacturer (Illumina, 2009). The HumanCytoSNP-12v2.1 array contains probes for 299,140 SNPs at loci throughout the genome (Illumina, 2016). Each position on the array tests a single SNP by hybridisation of genomic DNA to probes specific to the SNP locus. Each SNP is bi-allelic and each position on the array contains a two probes (one specific to each allele) distinguished by conjugation to either dinitrophenol or biotin, referred to as the red and green fluorophores respectively. Fluorescence output is quantified with an imaging system, and the resulting data consist of paired data sets of red and green signal intensity for each location in the array.

Fluorescence data were then processed using Beeline 2.0 and Genomestudio 2011.1 software (Illumina) to determine the genotype of each sample tested. The two

parameters used to describe genotype are B allele frequency (BAF) and Log R ratio (Peiffer *et al.*, 2006).

BAF values are derived from the ratio of green and red signal intensities after polar normalisation and comparison to values from reference data sets from normal subjects (Peiffer *et al.*, 2006). Homozygosity at a locus (with or without the presence of a CNV) would result in signal that is either exclusively red or exclusively green this would be represented by a BAF of 0 or 1 respectively. Heterozygosity and balanced duplications (where there are an equal number of copies of each allele) would be represented by a BAF of 0.5. CNVs resulting in an unequal number of copies of each allele would be represented by a BAF of approximately 0.33 or 0.66, depending on which allele was more abundant.

Log R ratio values are derived from the total fluorescence intensity for each array position (i.e. the sum of intensities in the red and green data sets) after polar normalization and comparison to values from reference data sets from normal subjects. In the absence of CNV the log R ratio of a SNP should approximate 0 (Peiffer *et al.*, 2006). A hemizygous deletion (loss of one of the two alleles) reduces the log R ratio to approximately -0.5. A duplication (giving three copies of an allele) increases the log R ratio to approximately 0.4. A triplication (giving four copies of the allele) increases the log R ratio to approximately 0.5.

Assessment of the BAF and Log R ratio values of multiple loci within a genomic region allow the identification and characterisation of CNVs.

The quality of data sets were assessed before looking for evidence of CNVs by consideration of the median log R deviation and the median call rate. Both parameters are calculated by arranging all autosomal SNPs in ascending genomic order, dividing them into non-overlapping bins of 1000 SNPs per bin. The call rate and standard deviation of Log R ratios are calculated for each bin, followed by the median of these values across all bins ("BlueFuse Multi v4.3 Software Guide," 2016). Data sets with either or both a median call rate of <0.95 and a median Log R deviation >0.23 were rejected.

Data sets that passed the quality control assessment were analysed with BlueFuse Multi v4.4 software (Illumina). BlueFuse Multi contains an algorithm which identifies CNVs on the basis of regional changes in BAF and Log R ratios and classifies CNVs as "benign?", "unknown?" or "pathogenic?" by cross referencing them with the locations of normal and pathogenic CNVs that have been reported previously in large

online databases (Table 23). Log R ratio and BAF charts were also examined by the author in the BlueFuse Multi interface to identify CNVs not detected by the BlueFuse algorithm.

Possible abnormalities were then assessed manually by the author with help from Dr Simon Zwolinski. Possible CNV were firstly accepted as genuine or rejected as artefact by manual inspection of the Log R ratio and BAF charts and by comparison to reference data run on the same array. In the case of CNVs in iPSC lines interpretation was aided by comparison to the originating PBMC sample.

CNVs that were accepted as genuine were then assessed using the UCSC Genome Browser which allow the identification of case reports describing the clinical phenotypes associated with CNVs.

Classification	Definition
Benign?	Region must be fully covered by either: <ul style="list-style-type: none"> • significant CNVs from the DGV database • benign CNVs from the ISCA database and not overlapping a known disease region, and not overlapping an ISCA pathogenic CNV region
Unknown?	Regions not meeting the criteria for benign? or pathogenic?
Pathogenic?	Less than 80% of the region is covered by a DGV region of the same type, and the region must be either: <ul style="list-style-type: none"> • ≥ 1Mb in size • overlapping a known disease region • fully covered by an ISCA pathogenic region of the same type.

Table 23 Definitions of CNV type used by BlueFuse Multi algorithm

The Database of Genomic Variants (DGV) collates reports of cytogenetic variants found in healthy subjects from affiliated laboratories (MacDonald *et al.*, 2014). The International Standards for Cytogenomic Arrays (ISCA) consortium database collates cytogenetic abnormalities reported by affiliated laboratories (Kaminsky *et al.*, 2011). An ISCA review committee may categorise a variant as pathogenic after consideration of clinical data from the submitting laboratory, previous submission to the NCBI/ISCA database and data from the UCSC and OMIM databases (Illumina, 2017).

An assessment of the genetic identity of an iPSC line relative to the PBMCs used in the reprogramming experiment from which it was derived can be made using the ~300,000 SNP genotypes characterised by the microarray. Genotype information is

expressed as the fluorescence intensity at a location on the array. Samples with the same genotype should have a similar fluorescence of a given fluorochrome at the comparable positions on the array. If the red fluorescence of all positions on the array for two genetically similar samples are plotted against each other the data points would be expected to cluster around a single line described by $x=y$. If genetically dissimilar samples are plotted against each other the data would be expected to cluster around five lines reflecting the possible genotype mismatches (including option of a failed call in one of the samples). Pearson's correlation co-efficient (r) may be used to describe this relationship, with values close to 1 implying a similar genetic identity and values closer to 0.5 implying differing identities.

2.14.3 Mutation sequencing

PCR reactions were prepared with Immomix Red (Bioline) master-mix. Target regions were amplified by PCR using the primers listed in Table 25. Each 20 μ l PCR reactions contained 3mM MgCl₂, 1 μ M primers and 0.25ng/ μ l DNA. The concentration of other components within the reaction such as the heat activated *taq* polymerase is proprietary information. Reactions were run on Eppendorf Mastercycler gradient thermocycler. Details of the thermocycler program are given in Table 24.

Name of stage		Details of stage
Taq activation		95°C, 10mins
Cycle	Denaturing	95°C, 1min
	Annealing	60°C, 1min
	Extension	72°C, 2min
	Number of cycles	35
Final extension		72°C, 10min
Holding		4°C, indefinite

Table 24 Thermocycler program for amplification of genomic DNA prior to sequencing

The products of the amplification reaction were purified using the QIAquick PCR purification kit (QIAGEN) using the manufacturers recommended protocol. Sanger sequencing of a single strand of the purified cDNA was performed according to the protocol of a commercial provider (GATC Biotech Ltd).

Reported sequences were compared to genomic DNA using an online platform (BLAST) to confirm amplification of the region of interest ("Basic Local Alignment Search Tool (BLAST)," n.d.).

Target	Fw/Rv	Sequence*	Size of product from target (bp)
DSP c.3195C>G	Fw	gtagcgcgacggccagtGATCGAAGTTTTGGAAGAGGAGC	223
	Rv	cagggcgcagcgatgacTTTTGCTTAGCCGACTTCCC	
PKP2 c.2146-1G>C	Fw	gtagcgcgacggccagtTCGTGAAATCAAATACAATAGCACT	217
	Rv	cagggcgcagcgatgacAGATTCCGGGACAGATTCT	
DSG2 c.691-5T>A	Fw	gtagcgcgacggccagtGGACTAAAACCAGAAAGCCAGATG	148
	Rv	cagggcgcagcgatgacGCCATCTCTTGCTTCTACTGTC	
DSC2 c.2686_2687dupGA	Fw	gtagcgcgacggccagtATGAAGGAAGAGGATCGGTGG	197
	Rv	cagggcgcagcgatgacCCACTGGCTTTCAGAGACTTATTA	

Table 25 Primers used for the amplification of genomic DNA prior to sequencing.

*Primers directed to target a genomic sequence consist of a “tag” sequence (shown in lowercase) followed by sequence designed to target

Target	Sequence
Amplicon forward strand	GTAGCGCGACGGCCAGT
Amplicon reverse strand	CAGGGCGCAGCGATGAC

Table 26 Primers used to initiate Sanger sequencing reaction

2.14.4 TCR re-arrangement assay

Re-arrangements of *TRG* and *TRB* may be detected by multiplex PCR. Standards for the design of assays used in clinical practice have been established (Sandberg *et al.*, 2005). A commercial multiplex PCR kit meeting these standards was used in this work (IdentiClone TCRB + TCRG T-cell clonality assay, Invivoscribe) and performed according to the manufacturers protocol by Northgene Ltd, Newcastle upon Tyne. The PCR reactions in this assay employed multiple primers targeted to conserved variable (V) joining (J) and diversity (D) regions of two T-cell receptor genes (*TRB* or *TRG*). A PCR product will only be generated from genes that have undergone rearrangement. These primers will amplify the region when V(D)J recombination has occurred. Reverse primers are labelled with either 6-carboxyfluorescein (6FAM) or hexachlorofluorescein (HEX) fluorophores allowing detection using the ABI fluorescence detection platform. Reactions yielding a PCR product with a size within one of the pre-specified ranges is considered positive (Table 27).

Reaction	Expected size of products (fluorochrome)	Gene	Target
TRB reaction A	240-285 (6FAM)	TRB	V β - J β 2
	240-285 (HEX)		V β - J β 1
TRB reaction B	240-285 (6FAM)		V β - J β 2
TRB reaction C	170-210 (6FAM)		D β - J β 2
	285-325 (HEX)		D β - J β 1
TRG reaction A	175-195 (6FAM)		TRG
	230-255 (6FAM)	V γ 1-8 - J γ 1.1/2.1	
	145-175 (HEX)	V γ 10 - J γ 1.3/2.3	
	195-230 (HEX)	V γ 1-8 - J γ 1.3/2.3	
TRG reaction B	110-140 (6FAM)	V γ 11 - J γ 1.1/2.1	
	195-220 (6FAM)	V γ 9 - J γ 1.1/2.1	
	80-110 (HEX)	V γ 11 - J γ 1.3/2.3	
	160-195 (HEX)	V γ 9 - J γ 1.3/2.3	

Table 27 Expected size ranges of PCR products in T-cell receptor re-arrangement assay

2.15 RNA analysis

2.15.1 Extraction of RNA

RNA was extracted from PBMCs and cultured cells using the ReliaPrep RNA cell miniprep system (Promega) according to the manufacturers protocol, which includes DNase I treatment. Between 0.1 and 2 x10⁶ cells were used in each extraction with the resulting RNA eluted into a minimum of 10 μ l of NFW. Typical yields of RNA were between 1 – 100 μ g per sample.

RNA was extracted from myocardial tissue using the ReliaPrep RNA tissue miniprep system (Promega) according to the manufacturers protocol including DNase I treatment. Between 5-10 mg of tissue were used in each extraction with the resulting RNA eluted into a minimum of 10 μ l of NFW. Typical yields of RNA were between 1 – 10 μ g per sample.

2.15.2 Assessment of RNA quality

RNA yield and the levels of contamination with proteins and salts were assessed by photo-absorbance spectrometry using a Nanodrop 2000 (Thermo). Samples with 260:280 ratios >1.8 were considered to have minimal levels of proteins contamination and those with 260:230 ratios >1.8 considered to have minimal levels of salt contamination. Samples with either ratio below these levels were discarded.

2.15.3 Synthesis of cDNA from RNA

cDNA was synthesised using the GoScript Reverse Transcription System (Promega) as per the manufacturers protocol. Each 10µl annealing reaction contained 100ng/µl RNA and 100ng/ul primer. cDNA prepared for assessment of transgenes was synthesised using random primers provided in the kit. cDNA prepared for the assessment of endogenous gene expression was synthesised using oligo(dt)15 primers provided in the kit. Annealing reactions were run on an Eppendorf Mastercycler gradient thermocycler. Additional reagents were then added to each annealing reaction, the resulting 40µl reverse transcription reactions contained 25ng/µl RNA, 25ng/µl primer, 4mM MgCl₂, 0.5mM dNTPs and 8 U/µl GoScript reverse transcriptase (RT), Reverse transcription reactions were run on the same thermocycler as the annealing reaction. Details of thermocycler program are provided in Table 28. cDNA was stored at -20°C until used for PCR experiments.

Reaction	Name of stage	Details of stage
Annealing	Annealing	70°C, 5 mins
	Holding	4°C, indefinite
Reverse transcription	Priming	25°C, 5 mins
	Reverse transcription	42°C, 1 hour
	RT inactivation	70°C, 15mins
	Holding	4°C, indefinite

Table 28 Thermocycler program for reverse transcription

2.15.4 PCR to assess persistence of reprogramming vectors

PCR reactions to determine if reprogramming vectors were detectable within cultured cells were prepared using the GoTaq G2 DNA PCR system (Promega) as per the manufacturers protocol. The sequences of the primers used are given in Table 30 and the locations they amplify within the Sendai RNA are illustrated in Figure 15. Each 10µl reaction volume reactions contained 0.25ng/µl cDNA, 1µM primers, 0.2mM dNTPs, 0.025 U/µl G2 *Taq* polymerase and 1.5mM MgCl₂. Reactions were run on an Eppendorf Mastercycler gradient thermocycler. Details of thermocycler program are provided in Table 29.

PCR products were separated by electrophoresis in 2% agarose gels containing 0.01% Gel Red (Biotium) and imaged using a GelDoc-It 310 Imaging System (UVP).

Name of stage		Details of stage
Initial denaturing / Taq activation		95°C, 2mins
Cycle	Denaturing	95°C, 30s
	Annealing	X °C , 1min *
	Extension	72°C, 2min
	Number of cycles	35
Final extension		72°C, 10min
Holding		4°C, indefinite

Table 29 Thermocycler program for amplification of genomic DNA prior to sequencing and of cDNA in non-quantitative PCR experiments

* annealing temperatures varied between primer sets depending on the results of optimisation experiments.

Target	Fw /Rv	Sequence	Binding site	Annealing temperature (°C)	Size of product from target (bp)
SeV	Fw	GGATCACTAGGTGATATCGAGC	<i>L</i>	61	181
	Rv	ACCAGACAAGAGTTTAAGAGATATGTATC	Non-coding region 3' to <i>L</i>		
SeV-KLF4	Fw	CCTACACAAAGAGTTCCCAT	Exon 4 of <i>KLF4</i>	64	309
	Rv	AATGTATCGAAGGTGCTCAA	<i>N</i>		
SeV-KOS	Fw	ATGCACCGCTACGACGTGAGCGC	Exon 1 of <i>SOX2</i>	64	528
	Rv	ACCAGACAAGAGTTTAAGAGATATGTATC	Non-coding region 3' to <i>L</i>		
SeV-MYC	Fw	TAACTGACTAGCAGGCTTGTCG	Non-coding region 3' to <i>HN</i>	58	532
	Rv	TCCACATACAGTCCTGGATGATGATG	Exon 2 of <i>MYC</i>		

Table 30 Primers used for the amplification of cDNA in RT-PCR experiments.

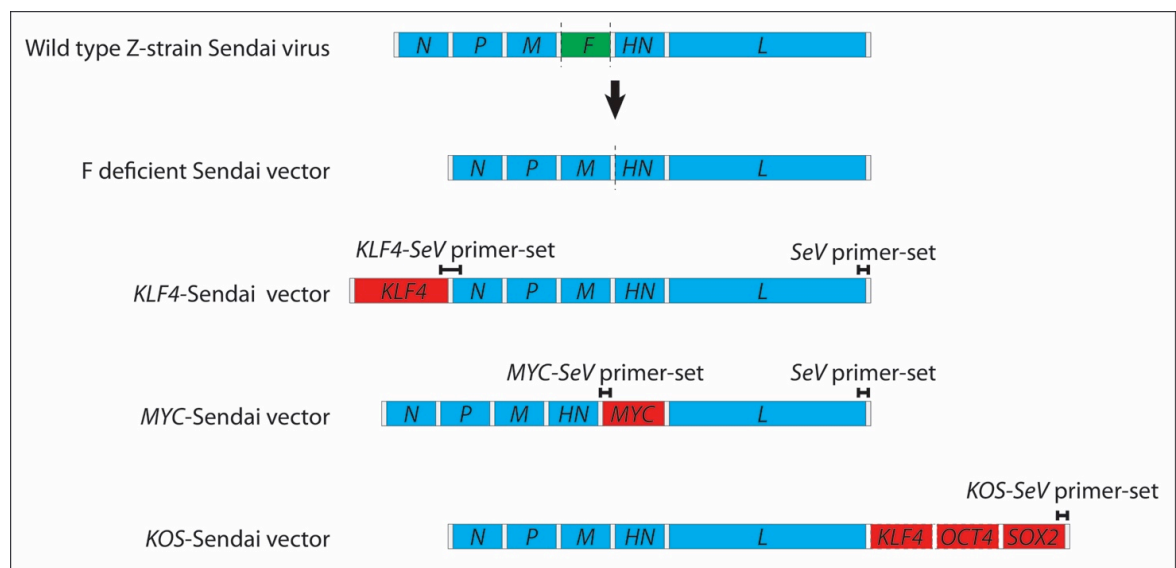


Figure 15 Organisation of Sendai virus and vectors and predicted binding sites primer set used in their detection.

The wild type Z strain Sendai virus is an enveloped single strand RNA virus consisting of 6 single exon genes separated by non-coding regions. The genes encode nucleocapsid protein (N), phosphoprotein (P), matric protein (M), fusion protein (F), Haemagglutinin-Neuraminidase (HN) and large protein (L). The structure of the Cytotune 2.0 vectors is proprietary information but may be inferred from the binding sites of the primer sets recommended by the manufacturer to detect the vectors. The predicted binding sites of primer sets were identified using Primer-BLAST (Ye *et al.*, 2012) to searching against all RNA and DNA reference sequences.

2.15.5 qPCR

qPCR reactions were prepared using GoTaq qPCR Master Mix (Promega) as per the manufacturers instructions. Each 10µl qPCR reaction contained 0.25ng/µl cDNA, 1µM primers, 0.3µM carboxy-X-rhodamine (CXR) reference dye. The master mix also contained a heat activated *Taq* polymerase, the BRYT Green dsDNA indicator dye the concentrations of which are proprietary information.

Reactions were run in 384 well plates (Applied Biosciences) on a QuantStudio 7 Flex (Applied Biosciences) qPCR machine, using QuantStudio 6 and 7 Flex Real Time PCR system software v1.0. A melt curve was performed in all experiments. Details of the PCR and melt curve program as given in (Table 31).

Name of stage		Details of stage
Initial holding		50°C, 2mins
Taq activation		95°C, 10mins
Cycle	Denaturing	95°C, 15s
	Annealing and extension	60 °C, 1min
	Number of cycles	40
Melt Curve	Denaturing	95oC, 15s
	Annealing and extension	60 °C, 1min
	Melt curve	0.05°C/s to 95°C

Table 31 Thermocycler program for qPCR reactions

The rate of change between stages of the program was 1.6°C/s, with the exception of the melt curve

The efficiencies of all primers were assessed from a standard curve generated from 4 fold serial dilutions of cDNA pooled from PSCs, iPSC-CMs, HaCaT cells and right atrial appendage (RAA). Efficiency were calculated by QuantStudio 6 and 7 Flex Real Time PCR system software v1.0 from standard curves containing 3-5 data points. Satisfactory primers had an estimated efficiency of 90-100% estimated from standard curves with an R^2 of >0.990.

Target	Strand targeted by Primer	Sequence	Location of primer binding	Efficiency / R2 / points on 4-fold dilution standard curve	Size of product from target (bp)
<i>ACTB</i>	Fw	GCACAGAGCCTCGCCTT	Exon 1	91% / 0.995 / 5	77
	Rev	GTTGTCGACGACGAGCG	Exon 2		
<i>ENOX2</i>	Fw	*		-	*
	Rev	*			
<i>ERCC6</i>	Fw	*		-	*
	Rev	*			
<i>GAPDH</i>	Fw	TGCACCACCAACTGCTTAGC	Exon 7	112% / 0.998 / 4	87
	Rev	GGCATGGACTGTGGTCATGAG	Exon 7-8 junction		
<i>PRDM4</i>	Fw	*	Accession sequence: NM_012406 Anchor nucleotide: 2346 Intron spanning	-	Context length: 174bp
	Rev	*			
<i>RPL7</i>	Fw	GGCTTCGATTAACATGCTGAGG	Exon 4	-	177
	Rev	CAGATGATGCCGTATTTACCAAGAG	Exon 5-6 junction		
<i>RNF20</i>	Fw	*		-	*
	Rev	*			
<i>SCLY</i>	Fw	*		-	*
	Rev	*			
<i>SDHA</i>	Fw	TGGGAACAAGAGGGCATCTG	Exon 2	92% / 0.994 / 5	86
	Rev	CCACCACTGCATCAAATTCATG	Exon 3		
<i>UBE4A</i>	Fw	*		-	*
	Rev	*			
<i>VIPAS39</i>	Fw	*	Accession sequence: NM_022067 Anchor nucleotide: 448 Intron spanning	-	Context length: 166bp
	Rev	*			

Table 32 Primers targeting reference genes used in RT-qPCR experiments

Target	Strand targeted by Primer	Sequence	Location of primer binding	Efficiency / R2 / points on 4-fold dilution standard curve	Size of product from target (bp)
KLF4	Fw	TTACCAAGAGCTCATGCCACC	Exon 3-4 junction	98% / 0.999 / 3	222
	Rev	GCGAATTTCCATCCACAGCC	Exon 5		
MYC	Fw	CACCAGCAGCGACTCTGA	Exon 2	105% / 0.996 / 5	138
	Rev	CTGTGAGGAGGTTTGCTGTG	Exon 3		
OCT4A	Fw	AGCTGGAGAAGGAGAAGCTG	Exon 1	98% / 0.996 / 3	183
	Rev	TGGTCGTTTGGCTGAATACCT	Exon 3		
SOX2	Fw	TTGTTTCGATCCCAACTTTCC	Exon 1	-	198
	Rev	ACATGGATTCTCGGCAGACT	Exon 1		

Table 33 Primers targeting pluripotency associated genes used in RT-qPCR experiments

Target	Strand targeted by Primer	Sequence	Location of primer binding	Efficiency / R2 / points on 4-fold dilution standard curve	Size of product from target (bp)
ACTN2	Fw	ACAGCATTGAGGAGATCCAGAGT	Exon 14-15 junction	97% / 0.992 / 5	211
	Rev	TGCTTCACCTTGTCCTCACTTG	Exon 15-16 junction		
MYH6	Fw	TCTCCGACAACGCCTATCAGTAC	Exon 5	94% / 0.997 / 3	140
	Rev	GTCACCTATGGCTGCAATGCT	Exon 7		
MYH7	Fw	GGCAAGACAGTGACCGTGAAG	Exon 3-4 junction	96% / 0.996 / 3	133
	Rev	CGTAGCGATCCTTGAGGTTGTA	Exon 4		
MYL2	Fw	CCTTGGGCGAGTGAACGT	Exon 3-5 junction	97% / 0.991 / 5	120
	Rev	GGGTCCGCTCCCTTAAGTTT	Exon 4-5 junction		
TNNI3	Fw	CCAACTACCGCGCTTATGC	Exon 3	90% / 0.997 / 3	120
	Rev	CTCGCTCCAGCTCTTGCTTT	Exon 5		
TNNT2	Fw	ACTTGGAGGCAGAGAAGTTCG	Exon 14	99% / 0.993 / 4	108
	Rev	GGGTCTTGGAGACTTTCTGGTTATC	Exon 15-16 junction		

Table 34 Primers targeting genes encoding cardiac sarcomeric proteins used in RT-qPCR experiments

Target	Strand targeted by Primer	Sequence	Location of primer binding	Efficiency / R2 / points on 4-fold dilution standard curve	Size of product from target (bp)
DSC1 a+b	Fw	GCTGTGTGTTGTCAAGCCATTG	Exon 9-10 junction	98% / 0.993 / 4	110
	Rev	TAGGAGTTTGTGAGCTCGCTG	Exon 10		
DSC1 a	Fw	CTCGGCTTGGCGAAAAGGTG	Exon 15-17 junction (specific to the "a" splice variant)	95% / 0.996 / 5	156
	Rev	GAAACTCCAGTCCCTCTTCTTCC	Exon 17		
DSC1 b	Fw	ATATGCGTACACGGACTGGC	Exon 15	93% / 0.997 / 5	74
	Rev	TCAGAGTGTGCCTCTAATGGATTC	Exon 16 (specific to the "b" splice variant)		
DSC2 a+b	Fw	GCATCCTGTTTACGCTGGTC	Exon 14	-	180
	Rev	AAACTCCCTGAGCAGAAGCG	Exon 15		
DSC3 a+b	Fw	ACTTGGAAAATGGGCAATCCTTG	Exon 13	106% / 0.981 / 5	186
	Rev	TTGGCAGAGCACACTCTATCG	Exon 14-15 junction		
DSG1	Fw	CAACGACTGTTAGGTATGTAATGGG	Exon 10	-	144
	Rev	AGAGAATCGTTCCTTGGTATTTTCC	Exon 10-11 junction		
DSG2	Fw	ACCTGAAGACAAGGTGGTGC	Exon 13-14 junction	98% / 0.999 / 3	166
	Rev	CCACCTTCCATCCATCTCGG	Exon 14		
DSG3	Fw	TGTTGACCTGTGACTGTGGG	Exon 13	102% / 0.998 / 3	138
	Rev	TATTTGTGATTTCTTGTCTTCAGG	Exon 13-14 junction		
DSG4	Fw	GATCAACAAATGCTACCTCGGC	Exon 11-12	-	87
	Rev	TGTCCTTCACCAGGATTGGG	Exon 12		
DSP I+II	Fw	CAGGATGTAATTTCTCGGCG	Exon 1	94% / 0.998 / 3	135
	Rev	ATCAAGCAGTCGGAGCAGTT	Exon 2		
JUP	Fw	CTCAACAAGAACAACCCCAAG	Exon 5	98% / 0.991 / 5	141
	Rev	ACTGTAGTTACGCATGATCTGC	Exon 6		
PKP1 a+b	Fw	GACATGTGGTCCAGCAAGGAAC	Exon 12	96% / 0.998 / 3	170
	Rev	TCTCAGCTGGGTCAATCTTCTG	Exon 13-14 junction		
PKP2 a+b	Fw	GCACGCGACCTTCTAAACAC	Exon 12	94% / 0.997 / 3	168
	Rev	TGTCTTCTTAAACTGAGCCTTCTTG	Exon 13-14 junction		
PKP3 a+b	Fw	CAAATGCGAGGACAAGAGCGT	Exon 7-8 junction	95% / 0.997 / 3	75
	Rev	ATCTCGTCGTAGAGGCGGTAG	Exon 8		

Table 35 Primers targeting genes encoding desmosomal plaque proteins used in RT-qPCR experiments

2.15.6 Selection of reference genes for RT-qPCR data

The stability of reference gene expression varies between tissue and cell types (Vandesompele *et al.*, 2002). The geNorm algorithm (accessed via QBase+) was used to select the combination of reference genes that had the greatest stability for the combination of tissue and cell types compared by RT-qPCR in this study from a pre-defined list of candidates. The first stage of the algorithm was to conduct a GeNorm pilot experiment to assess the gene expression in multiple samples from each of the tissue or cell types to be assessed. Fifteen 15 cDNA samples were assessed of which 3 were from PBMCs of different individuals, 3 from iPSC lines, 3 from iPSC-CMs, one was from a hESC line and 3 were from RAA samples. Eleven potential reference genes candidates were evaluated (see Table 32), seven of these genes were pre-selected by a commercial provider (Primer Design), the other four genes were those used in previous ARVC/D iPSC-CM studies and commonly used in our laboratory. The RT-qPCR reactions as a single experiment as described above.

Ct values from this experiment were processed by the geNorm algorithm which is a component of the QBase+ software package. The geNorm algorithm uses the Ct values to calculate an M-value and coefficient of variance (CV) for each reference. M-values are an index of the variability of gene expression relative to other genes across the sample set. Genes with a high stability will have similar variations expression levels across the sample types and therefore lower M and CV values (Vandesompele *et al.*, 2002). When tested in groups of samples from a similar cell type, reference genes with M values of <0.5 and a CV values of $<25\%$ are considered to be stably expressed (Hellemans *et al.*, 2007). In groups of samples from a range of cell types stable reference genes are indicated by M values of <1.0 and a CV values of $<50\%$ (Hellemans *et al.*, 2007).

The geNorm algorithm then assesses the mean M-value of the candidate genes and determines the gene which, if excluded, would reduce the mean M-value of the remaining group by the greatest amount. This process was repeated iteratively and the genes are ranked in the order that they were excluded. Then, starting with the two most stable reference genes, the improvement in stability resulting from inclusion of the third most stable gene was calculated and expressed by a GeNormV value. GeNormV values of >0.15 are considered to indicate that the additional gene should be used, this process was repeated iteratively until the additional of a further

reference gene was associated with a GeNormV value of ≤ 0.15 at which point the group of reference genes recommended by the algorithm was identified (Vandesompele *et al.*, 2002).

2.15.7 Processing qPCR data

qPCR data were analysed using QuantStudio software (Life Technologies). Each primer set was assessed in three technical repeats for each cDNA sample. Technical repeats differing by >0.5 Ct were considered for exclusion as outliers. The mean Ct (mCt) value of technical repeats was calculated for each sample. A mean of mCt (RefCt) values of the two reference genes (*VIPAS39* and *PRDM4*) was calculated for each sample. Target gene expression normalised to reference gene expression (Δ Ct) was calculated as:

$$\Delta Ct = mCt - RefCt$$

In some cases this gene expression in cell line was expressed with respect to that in a control cell line or tissue in these cases the $\Delta\Delta$ Ct value was calculated as follows:

$$\Delta\Delta Ct = \Delta Ct (\text{sample of interest}) - \Delta Ct (\text{control sample})$$

Fold expression was then calculated as $2^{-\Delta Ct}$ or $2^{-\Delta\Delta Ct}$ as appropriate.

The expression levels of pluripotency marker genes in hESCs in maintenance culture were considered to be indicative of those associated with the state of pluripotency in general. Therefore the expression of these genes in specific cell lines or types was expressed relative to the mean expression across the 3 passages of H9 hESCs.

The expression levels of cardiomyocyte marker genes in RAA was considered to be indicative of cardiomyocytes in general. Therefore the expression of these genes in specific cell lines or types was expressed relative to the mean expression across the 3 samples of RAA.

Calibration to a reference cell type was not used in the assessment of desmosomal gene expression in order that these data could provide an indication of the absolute levels of gene expression of the different genes in a particular cell or tissue type e.g. to assess whether the expression of one or more of the three desmocollin genes is dominant in a particular cell or tissue type.

2.16 Flow cytometry and FACS

2.16.1 Assessment of pluripotency associated protein expression in expandable clones

Cultures of adherent cells were prepared as follows, maintenance medium was removed, cultures were washed once with DPBS and then incubated at room temperature with Accutase for 5-10 minutes until cells could be detached from the culture surface and fragmented by gentle trituration. Accutase was inactivated by adding an equal volume of DPBS and the cell suspension filtered through a 40µM nylon mesh (BD) to remove any clumps. Samples were centrifuged at 400g, at room temperature for 4 minutes the supernatant aspirated. The pellets were resuspended by in DPBS and an equal volume of 4% formaldehyde added (giving a final concentration of 2% formaldehyde) and incubated for 15 minute at room temperature. Samples were centrifuged at 400g, 20°C for 4 minutes the supernatant aspirated. Cells were permeabilised by resuspension of the pellet with ice cold 90% methanol at -20°C for at least 4 hours. The methanol was diluted with DPBS and the samples centrifuged at 400g, 20°C for 4 minutes the supernatant aspirated.

The cellular debris used in experimental set-up of the these experiments was generated by the incubation of unfixed iPSCs exposed to 0.1% triton X-100 before fixation as described above.

Samples undergoing labelling were first blocked by resuspension in 10% FBS and incubation for 30 minutes. Aliquots of 1×10^5 cells were incubated with antibodies to the proteins of interest in a volume of 100ul, in the dark, at room temperature for 45 minutes. The antibodies and dilutions used are detailed in Table 36.

. Pluripotency marker protein signals were assessed using a single colour experimental design for the control iPSC clones from subject 2 i.e. each sample was divided into multiple aliquots with each aliquot labelled for a different target protein. iPSC clones derived from ARVC/D subjects were assessed using a multi-colour experimental design i.e. an aliquot of sample was co-labelled with multiple antibodies. The same antibodies were used for all experiments. Samples were washed twice using a BD FACS lyse wash assistant machine prior to analysis.

Samples were analysed using an LSR II (BD). The fluorochromes of the antibodies used were selected to avoid overlap in their absorption spectra where possible such that each was maximally excited by a different wavelength laser in the LSR-II. In

addition the filter-sets associated with each laser were selected to ensure that the fluorescence quantified was limited to a range of wavelengths in which the overlap in emission spectra of fluorochromes was minimal. The combination of laser and filter-set used to measure fluorescence from a specific fluorochrome will be referred to as its channel. For multi-colour experiments preliminary experiments defined the colour compensation parameters to be used in these experiments and these parameters were kept constant across experiments at different time points.

Events likely to be derived from cells were distinguished from those from debris by having forward scatter area (FSC-A) and side scatter area (SSC-A) values within specified ranges (Figure 16). The gate used to exclude debris was validated experimentally using samples of cellular debris (generated as described above). Events likely to be derived from single rather than clusters of cells were defined by a similar gate defining a range of FSC-A and forward scatter height (FSC-H) values clustered around the line described by $x=y$ (Figure 16), this gate could not be validated experimentally.

A target of 10,000 single cell events was set per sample. Samples in which <5,000 single cell events could be collected were repeated.

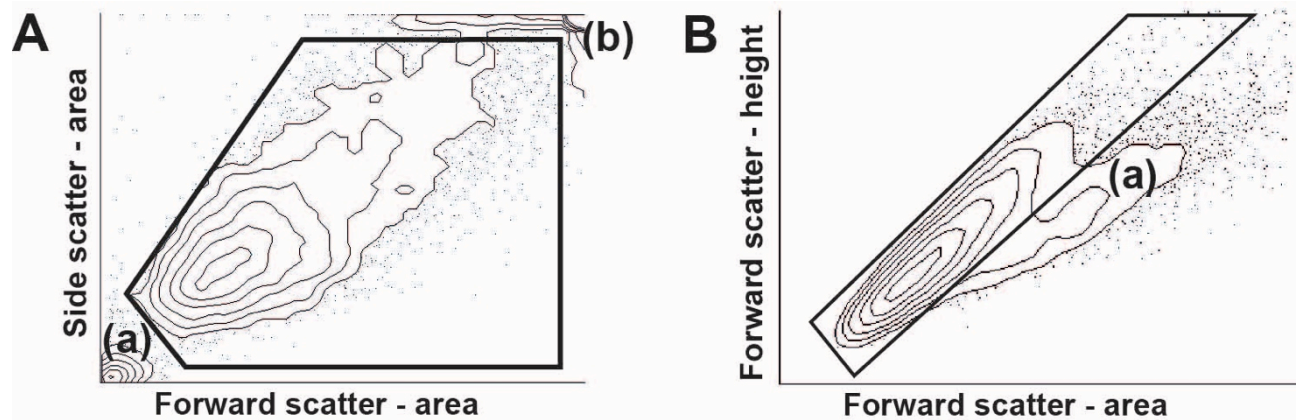


Figure 16 Classification of flow cytometry events as cells and single cells.

Panel A shows a contour plot of forward scatter – area (FSC-A) against side scatter – area (SSC-A) for all flow cytometry events. The criterion defining the subset of all events that was classified as “cell” events is described by the polygonal gate. This gate excludes small (a) and large (b) events that are likely to be debris. Panel B shows a contour plot of forward scatter – area (FSC-A) against forward scatter – height (FSC-H) for all the “cell” events defined in panel A. The criteria defining “cell” events as “single cell” events are described by the polygonal gate which approximates the line $x=y$. This gate excludes events with higher area to height ratios (a) that are likely to be clusters of cells.

Flow cytometry data were analysed with FACSDiva 8.0.1 software (BD). For each channel (pluripotency marker), single cell events from a labelled sample were classified as positive if the fluorescence value exceeded a specific threshold. This threshold was the 99th centile of fluorescence values of single cell events in an unlabelled aliquot of the same sample (Figure 17).

The difference between the median fluorescence of labelled and unlabelled single cell events was also assessed (Figure 17).

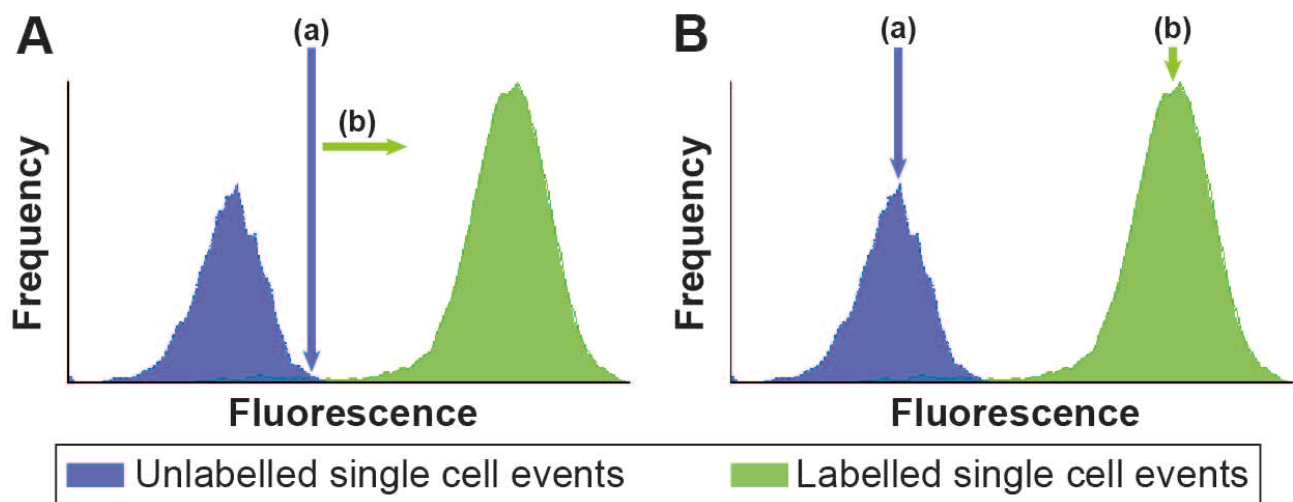


Figure 17 Analysis of flow cytometry data

Panel A illustrates the classification of labelled cells as positive for the expression of a target protein. The 99th centile fluorescence value of unlabelled single cell event was identified (a). All single cell events in the labelled sample with a fluorescence value greater than this threshold were classified as positive for the marker protein (b). Panel B illustrated the assessment of relative fluorescence. The median fluorescence of unlabelled single cell event (a) was subtracted from the median fluorescence of labelled single cell events (b).

2.16.2 Assessment of iPSC-CM markers in contracting cultures

After aspiration of culture medium contracting cultures were washed with DPBS and a single cell suspension was prepared by incubation with either 0.25% Trypsin/EDTA or Accutase (both from Gibco).

Samples for experiments in which signal regulatory protein α (SIRPA) expression was assessed were incubated with Accutase for up to 45 minutes in standard conditions and triturated to produce a single cell suspension. Enzyme activity was stopped by the addition of a volume of DPBS equal to that of the Accutase.

Samples in all other experiments were incubated with 0.25% Trypsin/EDTA (Gibco) for 10-20 minutes in standard conditions and triturated to produce a single cell

suspension. Enzyme activity was stopped by the addition of a volume of RPMI-20 equal to that of the trypsin.

Cell suspensions produced by either method were filtered through a 100 μ M nylon mesh, centrifuged at 400g for 4 minutes, room temperature, the supernatant aspirated.

The pellet was resuspended in DPBS, the number of cells in the sample estimated by haemocytometer and aliquoted into two samples. One sample was used for analysis by flow cytometry and the second for the analysis of RNA (see 2.13.3). The flow cytometry aliquot was centrifuged at 400g for 4 minutes, room temperature, the supernatant aspirated.

In experiments in which cell viability was assessed and the pellet resuspended in 100 μ l of DPBS containing 1:100 Zombie aqua and incubated at room temperature in the dark, for 15 minutes. DPBS was added, samples were centrifuged at 400g for 4 minutes, room temperature, the supernatant aspirated, the pellet was resuspended in DPBS and the sequence repeated to wash the cells. In all other experiments this stage was omitted.

After centrifugation the pellet was loosened in 50 μ l of DPBS and resuspended in \geq 2ml of 4% formaldehyde. The suspension was incubated for 20 minutes at room temperature. Samples were centrifuged at 400g for 4 minutes, room temperature, the supernatant aspirated, then resuspended in 0.1% Triton X-100 in DPBS for 10 minutes. Samples were centrifuged at 400g for 4 minutes, room temperature, the supernatant aspirated, then resuspended 10% FBS in DPBS and incubated for 30 minutes at room temperature. The number of cell was assessed by haemocytometer during this time. Samples were centrifuged at 400g for 4 minutes, room temperature, the supernatant aspirated, and the pellet resuspended in flow buffer (2% FBS in DPBS) to give a concentration of 1×10^5 cells/ml. Aliquots of 1×10^5 cells were incubated with antibodies to the proteins of interest in a volume of 100 μ l, in the dark, at room temperature for 45 minutes. The antibodies used were: anti-cTnI-Alexa647 (1:20), anti-cTnT-PE (1:20) anti-SIRPA-PE (1:100) and isotype controls from the same manufacturer and matched for protein concentration. Samples were washed once using a BD wash/lyse machine prior to analysis.

The flow cytometry set-up and analysis of data were performed using the same protocol as described in 2.16.1.

2.16.3 FACS of cells from contracting cultures based on SIRPA expression and the assessment of cTnI expression in the resulting populations.

After aspiration of culture medium contracting cultures were washed with DPBS and a single cell suspension was prepared by incubation with Accutase for up to 45 minutes in standard conditions. A single cell suspension was produced by gentle trituration and an equal volume of DPBS added to the suspension to stop enzyme activity. The cell suspension was filtered through a 100µM nylon mesh, centrifuged at 200g for 4 minutes, room temperature, the supernatant aspirated and the pellet resuspended in 10% FBS in DPBS. The number of cells was estimated by haemocytometer and the sample concentration adjusted to achieve 20×10^6 cells/ml. Aliquots of this suspension were incubated with antibodies for 20 minutes at room temperature in the dark. The antibodies used were anti-SIRPA-PE (1:100) and an isotype control from the same manufacturer and matched for protein concentration. Further details of the antibodies are given in Table 36. Samples were centrifuged at 200g for 4 minutes, room temperature, the supernatant aspirated and the pellet resuspended in 2% FBS in DPBS.

Samples were sorted using a FACSAria flow cytometer (BD), fitted with a 100µm nozzle in the flow cell. Cells were distinguished from debris, and single cell events distinguished from clusters of cells using the same as approach as describe in 2.16.1. Single cell events from the sample labelled with the SIRPA antibody were classified as being SIRPA positive if their fluorescence exceeded that of the 97th centile of cells from the same sample labelled with the corresponding isotype control (Table 36). Both the SIRPA positive and SIRPA negative fractions were collected for analysis.

SIRPA positive, SIRPA negative and non-sorted cells were fixed, permeabilised, labelled with anti-cTnI-Alexa647, and analysed as described in 2.16.2.

	Name	Manufacturer	Product identification code	Host species	Immunogen	Clonality	Reported inter-species reactivity	Isotype	Conjugated fluorochrome
Pluripotency markers	Anti-OCT4-488	BD Pharmingen	611202	Mouse	Synthetic peptide, aa 252-372 of mouse Oct3 [∞]	Monoclonal (40/Oct-3)	Humans, mouse	IgG1k	Alexa Fluor 488 (Alexa488)
	Anti-TRA-1-60-PE	BD Pharmingen	560071	Mouse	Human Embryonal Carcinoma Cell Line	Monoclonal (TRA-1-60)	Human	IgMk	Phycoerythrin (PE)
	Anti-SSEA4-PerCP-Cy5.5	BD Pharmingen	561565	Mouse	Human Teratocarcinoma Cell Line	Monoclonal (MC813-70)	Human, Mouse	IgG3k	Peridinin-chlorophyll protein - cyanine 5.5 (PerCP-Cy5.5)
	Anti-NANOG-647	Cell Signalling Technologies	5448	Rabbit	Synthetic peptide, n-terminus of human NANOG	Monoclonal (D73G4)	Human	IgG	Alexa Fluor 647 (Alexa647)
Cardiac sarcomeric proteins	Anti-Tnl-647	BD Pharmingen	564409	Mouse	Human tissue	Monoclonal (C5)	Human, mouse	IgG2bk	Alexa Fluor 647 (Alexa647)
	Anti-TnT-PE	BD Pharmingen	564767	Mouse	Rabbit cardiac troponin T	Monoclonal (13-11)	Human, mouse, rabbit, pig,	IgG1k	Phycoerythrin (PE)
Cardiomyocyte surface markers	Anti-SIRPA	BD Pharmingen	563441	Mouse	Human SIRPA extracellular domain recombinant protein	Monoclonal (SE5A5)	None	IgG1k	Phycoerythrin (PE)
Isotype controls	Isotype control-488	BD Phosflow	557782	Mouse	None*	Monoclonal (MOPC-21)	None	IgG1k	Alexa Fluor 488 (Alexa488)
	Isotype control IgM - PE	BD Pharmingen	555584	Mouse	Trinitrophenol (TNP) - Keyhole Limpet Hemocyanin	Monoclonal (G155-228)	None	IgMk	Phycoerythrin (PE)
	Isotype control IgG1-PE	BD Pharmingen	554680	Mouse	None*	Monoclonal (MOPC-21)	None	IgG1k	Phycoerythrin (PE)
	Isotype control-mouse 647	BD Phosflow	558713	Mouse	dansyl (5-[dimethylamino] naphthalene-1-sulfonyl)	Monoclonal (27-35)	None	IgG2bk	Alexa Fluor 647 (Alexa647)
	Isotype control-rabbit 647	Cell Signalling Technologies	2985	Rabbit	Unknown	Monoclonal (DA1E)	None	IgG	Alexa Fluor 647 (Alexa647)

Table 36 Antibodies used in flow cytometry experiments.

*Mouse myeloma immunoglobulin identified as having low human reactivity by screening.

[∞]Maximum homology in humans is with OCT4 (90%), Mouse Oct3 sequence compared with human reference proteome using protein blast tool.

2.17 Phase contrast Microscopy

Live cell imaging was performed using an Zeiss Axiovert200M microscope fitted with a Zeiss Axiocam HRc 1.4 Megapixel CCD camera and operated using Axiovision 4.8.2 imaging software. 14bit, 1300x1030 pixel, monochrome images of iPSC colony morphology were acquired with a 10x objective.

Video recordings of spontaneously contracting cultures were acquired with Zeiss 1.25x Plan-Neofluar air objective and whilst the microscope stage was heated to 37°C.

2.18 Immunofluorescence microscopy

2.18.1 Pluripotency associated proteins

iPSC colonies in feeder-free culture were fixed with 4% formaldehyde for 15 minutes at room temperature. Samples to be labelled with an anti-OCT4 antibody were permeabilised with 0.1% Triton X-100 for 15 minutes. All samples were blocked with 10% FBS in DPBS for 30 minutes. Samples were incubated overnight, with primary antibodies diluted in labelling solution (DPBS with 1% bovine serum albumin) at 4°C. The primary antibodies and dilutions used were: mouse anti-OCT4 (1:100) and mouse anti-TRA-1-60 (1:100). More details of the primary antibodies are given in Table 38. Samples were washed three times in DPBS, three minutes per wash and then incubated with a rabbit anti-mouse TRITC secondary antibody (1:200), in the dark for one hour at room temperature. More details of the secondary antibody are given in Table 39.

Samples then incubated with DPBS containing DAPI 1µg/ml for 15 minutes before 2 further washes with DPBS. DBPS was then added to all sample and they imaged immediately.

Images were acquired with a Zeiss Axiovert200M inverted microscope fitted with an HBO100 mercury arc lamp, Zeiss filter set numbers 02, 13 and 15 (Table 40), a Zeiss Axiocam HRc 1.4 Megapixel CCD camera and operated using Axiovision 4.8.2 imaging software. 14bit, 1300x1030 pixel, monochrome images of fluorescence signal were acquired with a Zeiss Plan-Apochromat 10x air objective. In some cases Z-stack images were acquired. Samples labelled with secondary antibodies only, were imaged with the same exposure times as the corresponding sample labelled with both primary and secondary antibodies.

2.18.2 Germ cell layer marker proteins

Cultures of adherent differentiated cells were prepared for imaging using the 3 germ cell layer immunocytochemistry (Life Technologies) as per the manufacturers instructions. Samples were fixed with “fixative solution” containing 4% formaldehyde for 15 minutes at 20°C. At this point some samples were stored at 4°C in DPBS for up to 2 weeks until further processing. Samples were permeabilised with “permeabilisation solution” containing 1% saponin for 15 minutes at 20°C, then blocked with “blocking solution” containing 3% bovine serum albumin for 30 minutes, at 20°C. Samples were single labelled with primary antibodies diluted in blocking solution by incubation overnight at 4°C. The following day samples were washed three times in DPBS, three minutes per wash, and then incubated with the appropriate secondary antibody diluted in blocking solution for 1 hour at room temperature. Samples were then washed 3 times with DPBS, 3 minutes per wash with the final wash containing NucBlue fixed cell stain (DAPI). DPBS was then added to all samples and they were imaged immediately. Details of the antibodies and the concentrations used are given in Table 37.

Images were acquired using the same equipment and protocol as described in 2.18.1.

2.18.3 Cardiac sarcomeric, gap junction and desmosomal protein

After the aspiration of culture medium dishes were washed with DPBS and incubated with 0.25% trypsin/EDTA for 15-30minutes and triturated with a serological pipette to aid the dissociation of clumps. A volume of RPMI-20 equal to that of the trypsin was added to each well to stop the enzymatic activity. The cell suspension was filtered through a 100um nylon sieve and the filtrate centrifuged 400g 4mins 20°C. After aspiration of the supernatant the pellet was re-suspend in RPMI 1640 supplemented with 20% FBS (Life Technologies) and 10µm Y27632 (Chemicon). Concentrations of cells in suspension were estimated by haemocytometer. Cells were then plated onto 13mm diameter coverslips within 4 well plates (Nunc) that had been previously coated with 0.01% gelatin. Approximately 50×10^3 cells were plated to each well and incubated for 48 hours in standard conditions. After the aspiration of culture medium dishes were washed with DPBS and fixed with 4% formaldehyde for 30 minutes at room temperature. After a further wash with DPBS they were

permeabilised with 0.1% Triton X-100 for 15 minutes at room temperature, blocked with 5% donkey serum for 30 minutes at room temperature and then incubated overnight with primary antibodies at 4°C. The primary antibodies were: goat anti cTnT (1:400), mouse anti-PKP2 (1:100), mouse anti-DSP (1:200), mouse anti-JUP (1:100), mouse anti-DSC2 (1:100), mouse anti-DSG2 (1:100), mouse anti-sarcomeric alpha actinin (1:400). More details of the primary antibodies are given in Table 38. Samples were washed three times with DPBS and then incubated with secondary antibodies for one hour, in the dark, at room temperature. The secondary antibodies were: donkey anti-mouse alexa 488, donkey anti-goat alexa 488, donkey anti-goat alexa 555 and donkey anti-mouse alexa 647 (all used at 1:400). Samples then incubated with DPBS containing DAPI 1µg/ml for 15 minutes before 2 further washes with DPBS. Coverslips were inverted and mounted on glass slides with Vectashield and sealed with nail varnish.

Images were acquired with a Zeiss Axioimager Z1 fitted with an Apotome 2.0, an HBO100 mercury arc lamp, Zeiss filter set numbers 49, 38HE, 20HE and 50 (Table 41), a Zeiss AxioCam HRm 1.4 Megapixel CCD camera and operated using Axiovision 4.8.2 imaging software. 14bit, 1300x1030 pixel, monochrome images of fluorescence signal were acquired with a Zeiss Plan-Apochromat 63x oil immersion objective. Z-stacks of optical sections were acquired. Images used to compare fluorescence of a given labelling combination between samples were acquired with the same exposure time. Secondary only labelled samples were imaged with the same exposure times as their primary labelled counterpart.

Target germ-cell layer	Primary antibody	Secondary antibody
Neuro-ectoderm	Rabbit anti-TUJ1, 1:500	Donkey anti-rabbit AF488, 1:250
Mesoderm	Mouse anti-SMA, IgG2a, 1:100	Goat anti-mouse IgG2a AF555, 1:250
Endoderm	Mouse anti-AFP, IgG1, 1:500	Goat anti-mouse IgG1 AF488, 1:250

Table 37 Antibodies used in preparation of samples from immunofluorescence microscopy for cell from the three germ cell layers.

All antibodies were included in the kit produced by Life Technologies.

	Name	Manufacturer	Product identification code	Host species	Immunogen	Clonality	Reported inter-species reactivity	Isotype	Secondary Abs used with this primary
Pluripotency markers	Anti-OCT3/4	BD Transduction laboratories	611202	Mouse	Recombinant protein, aa 252-372 of mouse Oct3 [∞]	Monoclonal (40/Oct-3)	Humans, mouse	IgG1k	TRITC rabbit anti-mouse
	Anti-TRA-1-60	BD Pharmingen	560071	Mouse	Human Embryonal Carcinoma Cell Line	Monoclonal (TRA-1-60)	Human	IgMk	TRITC rabbit anti-mouse
Sarcomeric proteins	Anti- α SA	ThermoFisher (Thermo)	MA122863	Mouse	Purified rabbit skeletal α -actinin	Monoclonal (EA-53)	Human, Mouse, extensive cross-reactivity other species	IgG1k	647-donkey-anti-mouse
	Anti-TnT	Abcam	ab64623	Goat	Human cardiac troponin T	Polyclonal	Human	IgG	488-donkey-anti-goat 555-donkey-anti-goat
Desmosomal proteins	Anti-DSC2/3	ThermoFisher (Invitrogen)	32-6200	Mouse	Extracellular domain, human DSC2, N-terminus *	Monoclonal (7G6)	Human,	IgG1k	488-donkey-anti-mouse
	Anti-DSG2	ThermoFisher (Invitrogen)	32-6100	Mouse	Human DSG2	Monoclonal (6D8)	Human	IgG1k	488-donkey-anti-mouse
	Anti-PKP2	Abcam	ab151402	Mouse	Recombinant protein, aa 1-350 of human PKP2, N-terminus.	Monoclonal (8H6)	Human, Mouse	IgG1k	488-donkey-anti-mouse
	Anti-JUP	Sigma	P8087	Mouse	Recombinant chicken JUP [★]	Monoclonal (15F11)	Human, dog, cow	IgG1k	488-donkey-anti-mouse
	Anti-DSP	Abcam	ab16434	Mouse	Full length cow desmoplakin	Monoclonal (2Q400)	Human, Mouse, Rat, Chicken, Cow	IgG1k	488-donkey-anti-mouse

Table 38 Primary antibodies used in immunofluorescence microscopy experiments

[∞]Maximum homology in humans is with OCT4 (90%), Mouse Oct3 sequence compared with human reference proteome using protein blast tool.

* Cross reacts with identical sequences on DSC3

★ Does not cross react with β -catenin

Name	Manufacturer	Product identification code	Host species	Immunogen	Clonality	Reported interspecies reactivity	Isotype	Conjugated fluorochrome
TRITC rabbit anti-mouse	Sigma	T2402	Rabbit	Mouse IgG	Polyclonal	None	IgG	Tetramethylrhodamine isothiocyanate (TRITC)
Donkey-anti-goat-488	ThermoFisher (Molecular probes)	A-11055	Donkey	Mouse IgG	Polyclonal	None	IgG	Alexa Fluor 488 (Alexa 488)
Donkey-anti-goat-555	ThermoFisher (Molecular probes)	A-21432	Donkey	Mouse IgG	Polyclonal	None	IgG	Alexa Fluor 555 (Alexa 555)
Donkey-anti-mouse-647	ThermoFisher (Molecular probes)	A-31571	Donkey	Mouse IgG	Polyclonal	None	IgG	Alexa Fluor 647 (Alexa 555)
Donkey-anti-mouse-488	ThermoFisher (Molecular probes)	A-21202	Donkey	Mouse IgG	Polyclonal	None	IgG	Alexa Fluor 488 (Alexa 488)

Table 39 Secondary antibodies used in immunofluorescence microscopy experiments

Zeiss filter set number	Excitation filter wavelength (nm)	Emission filter wavelength (nm)	Fluorochrome (peak excitation wavelength (nm), peak emission wavelength (nm))
02	300-400	>420	DAPI (358, 463)
13	450-490	505-530	Alex488 (493, 520)
15	540-552	>590	TRITC (555, 580)
			Alexa555 (555, 565)

Table 40 Axiovert200M Filters

Zeiss filter set number	Excitation filter wavelength (nm)	Emission filter wavelength (nm)	Fluorochrome (peak excitation wavelength (nm), peak emission wavelength (nm))
49	300-400	420-470	DAPI (358, 463)
38HE	450-490	500-550	Alex488 (493, 520)
20HE	540-552	568-647	Alexa555 (555, 565)
50	625-655	665-715	Alexa647 (653, 669)

Table 41 Axioimager Filters

2.19 Imaging of calcium and voltage transients

2.19.1 Preparation of cultures for imaging.

On day 25-30 of differentiation contracting cultures were re-plated into culture dishes that were 35mm in diameter and contained a central 7mm diameter glass bottomed depression (MatTek). Before plating the cells the glass bottomed depression was coated in Matrigel using the same technique previously described for plastic cultureware. Dishes were coated immediately before use. Dishes were incubated for at least 30 minutes at room temperature before use.

iPSC-CM monolayers were re-plated onto glass bottomed dishes (MatTek) as follows. MCM was replaced with RPMI-20-R1 and incubated for 2 hours. Dishes were washed with DPBS and incubated with 0.25% trypsin/EDTA for 15-30minutes and triturated with a serological pipette to aid the dissociation of clumps. A volume of RPMI-20 equal to that of the trypsin was added to each well to stop the enzymatic activity. The cell suspension was filtered through a 100um nylon sieve and the filtrate centrifuged 400g 4mins 20°C. The cell pellet was resuspended in RPMI-20-R1 and the concentration of the cell suspension estimated with a haemocytometer. The volume of RPMI with which the cell pellet was resuspended was decided based on the culture area of iPSC-CMs trypsinised. The Matrigel coating solution was aspirated from the dishes and the depressed region of the dishes filled with a bleb of

cell suspension containing the desired number of cells. Dishes were incubated in standard conditions for 8 hours before replacing the solution with MCMM, 2ml of solution per well. Re-plated cells were cultured for 5-7 days with medium changes every 2-3 days.

A fraction of the cell solution was not plated and prepared were prepared for flow cytometry assessment of cTnT expression as previously described.

2.19.2 Loading cells with Fluo-4-AM and imaging of transients

For each differentiation experiment 3 different dishes of re-plated cells were prepared for imaging. Every dish contained spontaneously contracting regions identified by phase contrast microscopy before loading with Fluo-4-AM.

Cultures were incubated for 20 minutes in standard culture conditions with MCMM containing 4ug/ml Fluo-4-AM and that had been pre-warmed to 37°C. During imaging the culture medium was replaced with normal Tyrode's solution (NTS) consisting of an aqueous solution of 140mM NaCl, 6mM KCl, 1mM MgCl₂, 5mM HEPES, 2mM CaCl₂, 10mM D-glucose, adjusted to a pH of 7.4. The labelling medium in each dish was changed for 2ml of NTS, that had been pre-warmed to 37°C, and the dishes were then incubated in the dark, on the microscope stage, heated to 37°C, in room air, for 20 minutes.

Imaging was performed with a Nikon Ellipse TE2000-U fitted with a Redshirt-CMOS camera. Calcium imaging was performed with a 470nm LED and 475nm LP filter. All images were acquired using a Nikon x40 Plan Fluor oil emersion objective. Calcium transients were imaged at a 250 frames per second (fps) for between 5 and 15s seconds.

If spontaneous transients were present they were recorded in 3 different locations. Field pacing using a pulse of 20V and 10ms duration was then delivered and the resultant transients recorded. The frequency of pacing was 1Hz except for the following circumstances. If the rate of spontaneous transients exceeded 1 Hz, then the lowest pacing rate that exceeded the spontaneous rate was used. If pacing at 1Hz failed to result in a transient for every pacing pulse then the rate was lowered to achieve the fastest rate at which this was present.

Images were acquired using Neuroplex v9.6.0 software. The same software was used to manually define an area within the images in which fluorescence was judged to vary through time and to calculate the mean fluorescence signal intensity of this

area in each frame of the recording. Graphical representations of these data were constructed using GraphPad Prism 7.

2.20 TEM analysis

2.20.1 Collection of samples from adherent cell cultures

Culture medium was aspirated from tissue culture plates containing adherent cultures and washed with RPMI. Cultures were incubated with TEM dissociation solution (Dispase 2.4U/ml in RPMI), for 30-45minutes at 37°C, 5% CO₂. Cultures either detached spontaneously from the culture surface or were released by gentle flushing using a P1000 pipette. Detached cultures were transferred to a 1.5ml microcentrifuge tube using a Pasteur pipette that had been modified to have a wide tip aperture to reduce shear stress during pipetting. The sample was allowed to settle by gravity over 5 minutes and the dissociation solution aspirated with a P1000 pipette. TEM fixative buffer (2% glutaraldehyde in 0.1M sodium cacodylate buffer) was added to each tube and the samples stored at 4°C until the next stage of processing. Samples were stored for a maximum of 1 month in these conditions.

2.20.2 Collection of right atrial appendage samples

Immediately after excision from the subject, cardiac tissue was manually dissected with a scalpel into fragments no larger than 3mm diameter and placed into TEM fixative buffer. Samples stored at 4°C until the next stage of processing. Samples were stored for a maximum of 1 month in these conditions.

2.20.3 Sample processing

TEM samples were processed in batches of 5-10 samples. Samples were washed in cacodylate buffer 3 times, for a minimum of 30 minutes per wash before being incubated overnight in cacodylate buffer. The following day the samples were washed twice in dH₂O, for 15 minutes per wash, then incubated with the secondary fixative (1% osmium tetroxide in dH₂O) for 1 hour. Samples were then washed twice with dH₂O, for 15 minutes per wash.

Dehydration using acetone was performed as follows. Samples were incubated with 25% acetone for 30 minutes, 50% acetone for 30 minutes, 75% acetone for 30 minutes and then twice with 100% acetone for 60 minutes each time.

Impregnation with epoxy resin (Epoxy pre mix, TAAB, T028H) was performed as follows. Samples were incubated with 25% resin in acetone for 60 minutes, 50% resin in acetone for 60 minutes, 75% resin in acetone for 60 minutes, twice times in 100%

resin for 1 hour each time and finally in 100% resin for at least 3hrs. Samples were then incubated at 60°C for 24 hours to solidify the resin.

Semi-thin sections of approximately 0.5µm were cut and stained with 1% toluidine blue in 1% borax to identify the location of samples within the resin. Ultrathin sections of approximately 70 nm were then cut using a diamond knife on a RMC MT-XL ultramicrotome. The sections were stretched with chloroform to eliminate compression and mounted on Pioloform-filmed copper grids.

2.20.4 TEM Image acquisition

Images were acquired by a single investigator who was blinded to the sample identity. Sections were examined using a Philips CM 100 Compustage (FEI) Transmission Electron Microscope operating at 100kV/. Digital images were collected using an Optronics 1824x1824 pixel CD camera with the AMT image capture software - AMT40 version 5.42 (Deben).

The scaling factor necessary to calculate spatial data from TEM images was estimated using a shadow cast carbon diffraction grating replica with 2160 lines per millimetre. The grid was imaged at 19,000X magnification, three measurements of a ten line distance within the grid were made by a single observer in both of the two perpendicular axes within the grid (i.e. a total of six measurements) and the mean distance in pixels was equated to 4.6296296µm. The scaling factor was re-calculated once a month.

Grids were first examined at approximately 500X magnification and the locations of levels within a grid recorded. Random locations within a level were then searched at 13,500X magnification for putative desmosomes i.e. electron dense adhesion junctions associated with the plasma membranes. When viewing iPSC-CM and RAA samples only those locations in which striated myofibrils could be identified were searched for adhesion junctions.

Image magnification is a determinant of image resolution and resolution affects the precision of spatial measurements made from the image. An increase in magnification will be accompanied by a reduction in dynamic range of pixel values within the image unless it is accompanied by an increase in electron beam density. Images with a high dynamic range will describe the regions of the desmosome with a greater range of pixel values, rendering them more easily distinguishable. There is an upper limit to the density of electron beam that may be generated by a microscope

and this determines the maximum magnification at which the dynamic range of an image can be maintained.

In order to determine the optimal magnification at which to acquire images for morphometric analysis the same desmosome was imaged at a range of magnifications with the electron beam density adjusted to maximise the dynamic range of the image in each case (Figure 18). Identification of the intra and extra-cellular surfaces of the plasma membrane was taken as a useful indicator of image quality. These structures are sensitive to being obscured by either pixelation or a loss of dynamic range.

At magnifications up to 92,000x the plasma membrane appeared pixelated and difficult to localise. A loss of dynamic range was apparent at 340,000x. Image quality was optimal at magnifications between 130,000x and 245,000x. The maximum density of a microscope's electron beam may vary due to operational factors e.g. microscope filament performance. Variations in the thickness of TEM sections may require increased electron beam density to obtain an adequate image at a given magnification. In order to minimise the potential of these factors to affect image quality it was decided that all images used for quantitative desmosomal analysis would be acquired at 130,000x.

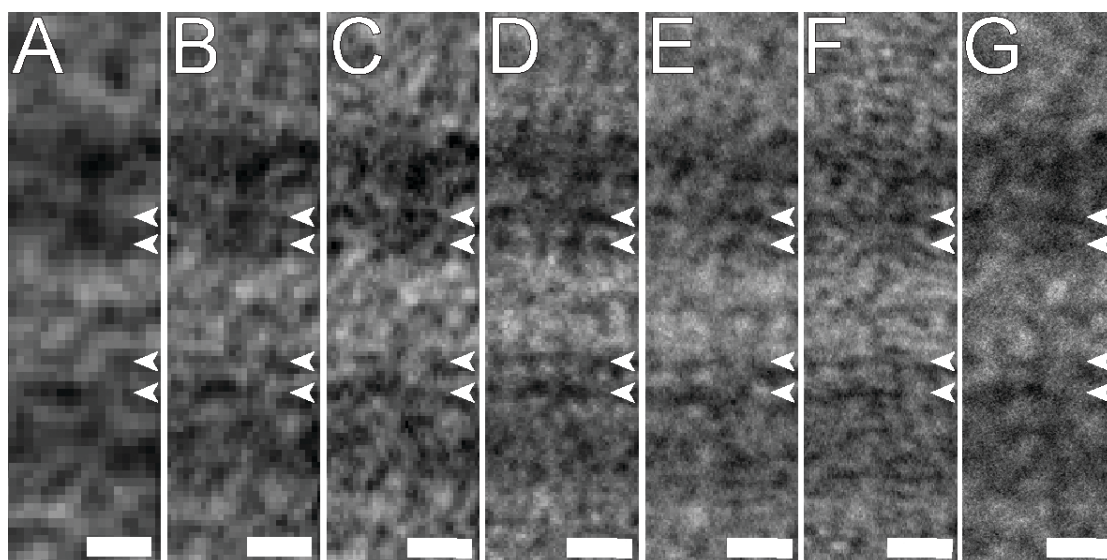


Figure 18 A TEM image of a section of desmosome at different magnifications
The magnifications illustrated are 46,000x (Panel A), 64,000x (Panel B), 92,000x (Panel C), 130,000x (Panel D), 180,000x (Panel E), 245,000x (Panel F), 340,000x (Panel G). The locations intra and extracellular surfaces of the plasma membrane are indicated (arrow-heads). Scale bars represent 10nm.

Junctions viewed at 130,000X magnification were then assessed to determine whether they met the criteria for classification as a desmosome (Table 42) (Figure 19) and thereby inclusion in the study.

Term	Definition
Desmosome	Two bi-laminated, electron dense plaques, oriented in parallel, localised to a plasma membrane and separated by a region of extra-cellular space.
Cardiac desmosome	A desmosome localised to the plasma membrane of a cell containing striated myofibrils.

Table 42 The criteria used to identify a desmosome and cardiac desmosome within a TEM image.

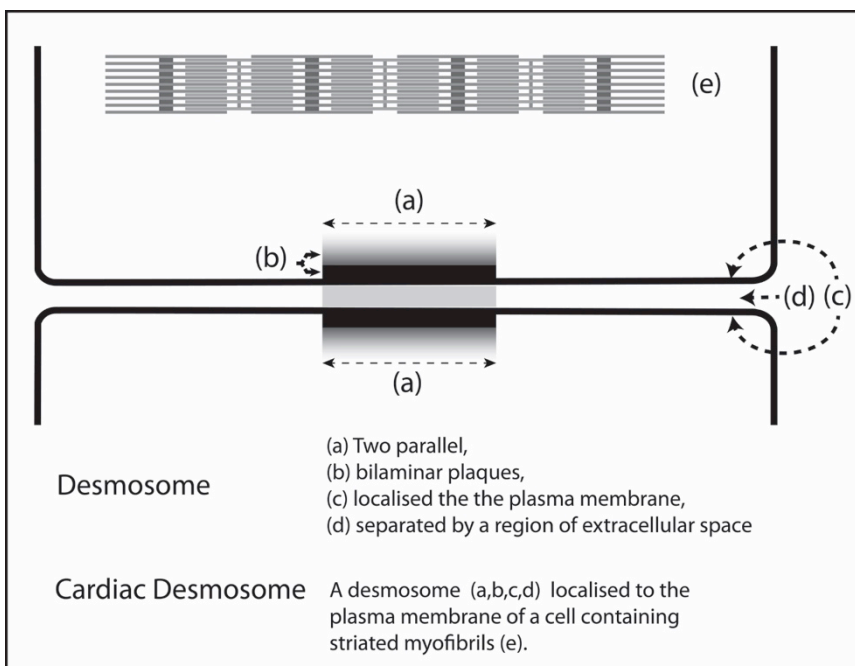


Figure 19 Criteria used to define a desmosome and cardiac desmosome.

Samples were tilted to a position between -50° and $+50^{\circ}$ from horizontal to the angle at which the investigator estimated the intermembranous gap and clarity of the junction plaques to be greatest. Optimised images were then acquired for analysis.

2.20.5 TEM image analysis

TEM images were analysed using digital image analysis software (FIJI).

Definitions of the desmosomal width parameters measured are described in Table 43 and illustrated in Figure 20.

Desmosomal Parameter	Definition
Intermembrane width 1 (IMW1)	The length of a straight line, that is perpendicular the midline of the desmosome, which begins at the pixel judged to be closest to the centre of the linear structure representing the extra-cellular surface of the plasma membrane, and ending at the pixel judged to be closest to the centre of the same structure on the opposite side of the intermembrane gap.
Intermembrane width 2 (IMW2)	The length of a straight line, that is perpendicular the midline of the desmosome, which begins at the pixel judged to be closest to the centre of the linear structure representing the cytoplasmic surface of the plasma membrane, and ending at the pixel judged to be closest to the centre of the same structure on the opposite side of the intermembrane gap.
Inter-ODP width (IOW)	The length of a straight line, that is perpendicular the midline of the desmosome, which begins at the pixel judged to represent the cytoplasmic surface of the ODP, and ends at the pixel judged to represent the cytoplasmic surface of the ODP on the opposite plaque.
Desmosomal length (DL)	The length of a curved line that traces the midline of the intermembrane gap over the distance that is judged to be formed by two parallel ODPs.
Desmosomal plaque length (PL)	The length of a curved line that traces the mid point of an ODP over its length.

Table 43 Definitions of desmosomal width and length parameters

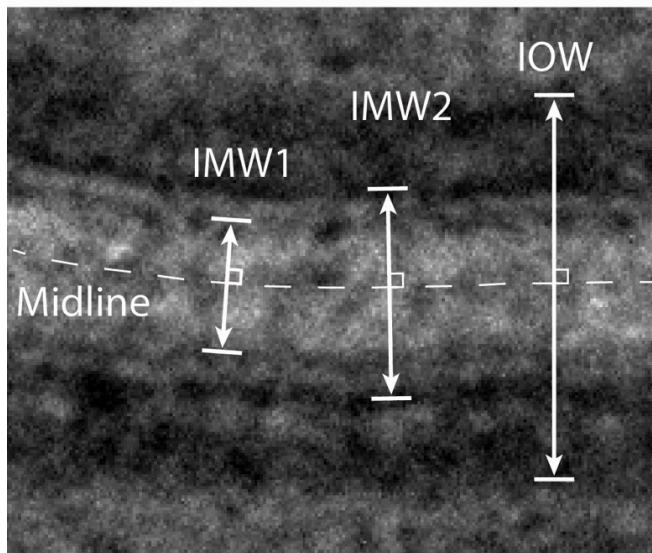


Figure 20 A region of a desmosome illustrating the definitions of the three desmosomal width parameters.

Examples of locations at which the three width parameters: intermembrane width 1 (IMW1), intermembrane width 2 (IMW2) and inter-ODP width (IOW) may be measured are indicated. The midline is indicated by a dashed line and each desmosome width parameter measurement is perpendicular to this line at the point of their intersection.

Images were assessed as having adequate quality for assessment if any region of a desmosome had two parallel regions of ODP and plasma membrane that were sufficiently distinct to measure at least one of the desmosomal width parameters. Images not meeting this criterion were excluded. Each parameter was measured at three different locations on each image.

Definitions of desmosomal length parameters are given in Table 43 and illustrates in Figure 21.

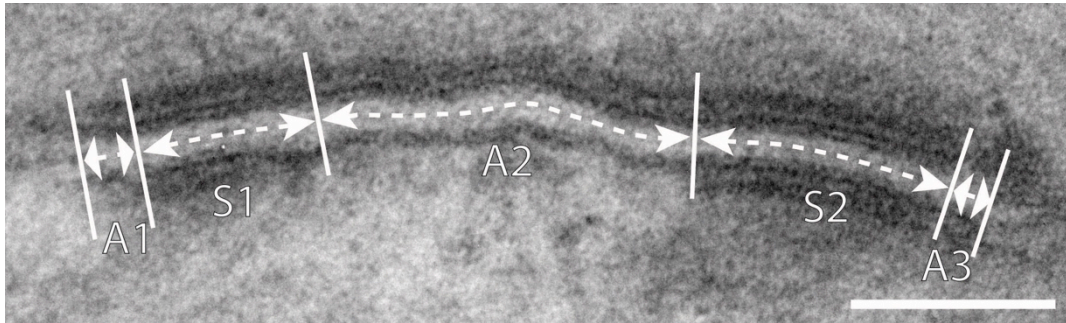


Figure 21 An example of the measurement of desmosomal length parameters. Segments in which there are symmetrical desmosomal plaques i.e. parallel plaques on both sides of the intermembrane gap, are indicated (S1 and S2). Segments in which the desmosome is asymmetrical i.e. a plaque on only one side of the intermembrane gap are also indicated (A1, A2 and A3). All length measurements are made along the midline of the intermembrane gap. The scale bar represents 100nm.

2.21 Statistical analysis

Data from continuous variables are summarised as either mean (standard deviation) unless otherwise stated. For data sets with ≥ 8 values the similarity of distribution of sample data to a Gaussian distribution was assessed with the D'Agostino and Pearson omnibus K2 normality test. Comparisons of pairs of datasets were made using either a two tailed unpaired T-test or a two tailed Mann-Whitney U test as appropriate. Comparisons of groups of more than two datasets were made using either a one way ANOVA followed by a post hoc Tukey's multiple comparisons test, or a Kruskal-Wallis test followed by a post hoc Dunn's multiple comparisons test. P values < 0.05 were considered statistically significant. Statistical analysis was performed using GraphPad Prism 7c Software Inc. (San Diego, CA, USA).

Chapter 3. Clinical Characteristics Of Study Participants

3.1 Introduction

This chapter will discuss the recruitment of subjects from which blood and myocardial samples were obtained.

3.2 Aims

The aim of this part of the project were:

- To recruit three subjects with a clinical diagnosis of ARVC/D from which iPSCs would be generated to the study.
- To confirm that these subjects met the 2010 task force criteria for having a definite diagnosis of ARVC/D through the collation of data from their clinical records.
- To recruit control subjects without inherited cardiac disease or a family history of inherited cardiac disease to the study from which control iPSC lines would be generated.
- To collect samples of myocardium from adult subjects without inherited cardiac disease or a family history of inherited cardiac disease to act as a positive control for assessments of cardiac gene expression and ultrastructure.

3.3 Results

Three subjects (0101, 0202 and 0203) with a clinical diagnosis of ARVC/D were recruited to the study. In all three cases data from their clinical records was such that they were categorised as having a definite diagnosis of ARVC/D according to the 2010 task force criteria (Marcus *et al.*, 2010). The major and minor criteria identified in these clinical data that resulted in the classification of ARVC/D as definite is summarised in Table 44.

A detailed description of these clinical data are given in subsequent sections.

			Subject					
			0101		0202		0203	
			Major	Minor	Major	Minor	Major	Minor
Category	I	Global or regional dysfunction and structural alterations (Echocardiography, CMRI)					✓	
	II	Tissue characterization	✓					
	III	Repolarisation abnormalities (12-lead ECG)	✓		✓		✓	
	IV	Depolarization / conduction abnormalities (12-lead ECG, SAECG)		✓	✓	✓		✓
	V	Arrhythmias (12-lead ECG)	✓		✓			✓
	VI	Family history / Genetic testing	✓	✓	✓		✓	
Diagnosis of ARVC/D			Definite		Definite		Definite	

Table 44 Diagnosis of ARVC/D in subjects recruited to the study as defined in the current task force criteria.

The table indicates (✓) if a subject's clinical features met one or more of the major or minor criteria for diagnosis for a given category.

3.3.1 Subject 0101

Subject 0101 was a male of 57 years of age at the point of recruitment. He presented with chest pains, palpitations and dyspnoea as an emergency to a hospital at age 46. He was found to have a broad complex tachycardia on admission that was considered to be ventricular tachycardia (VT) (Figure 22). He underwent coronary angiography which found no obstructive coronary disease. An echocardiogram showed a dilated right ventricle with severely impaired systolic function. He subsequently underwent the implantation of an implantable cardioverter defibrillator. During follow-up his 12-lead ECG developed features typical of ARVC/D (Figure 26). At age 56 he developed symptomatic right heart failure. Shortly after recruitment to this study (and after providing a blood sample for reprogramming) he underwent cardiac transplantation. Gross pathological and histological examination of the explanted heart was consistent with the diagnosis of ARVC/D (Figure 25).

Subject 0101 underwent sequencing of *PKP2*, *DSG2*, *DSC2* and *DSP* as part of his clinical management to facilitate screening of his family for ARVC/D. Sequencing identified the mutation *PKP2* c.2146-1G>C (Figure 24). The mutation disrupts the G of the invariant AG nucleotides of the splice acceptor site of intron 10. Splice site mutations may produce exon skipping, cryptic splicing or intron retention. Possible cryptic splice acceptor site have been reported in intron 12 or exon 13 (Svensson et

et al., 2016). Exons 11 to 12 encode arm-repeats 6 to 7 and most of arm repeat 8. Exon 11 also encodes part of the linker sequence preceding arm-repeat 6 which introduces a bend into PKP2. Aberrant splicing commonly results in the introduction of a premature stop codon leading to nonsense mediated decay of the mRNA and a reduction in gene expression. However if a viable transcript were generated then this variant may produce a truncated PKP2 molecule lacking multiple arm repeats. As discussed in the function of these arm repeats in PKP2 is uncertain since most interactions with DSP and desmosomal cadherins appears to be at the N-terminus domain. This mutation has been associated with ARVC/D in previously published cases however it has not been studied with animal or cellular models (Gerull *et al.*, 2004) (Syrris, 2006) (Dalal, 2006) (Watkins *et al.*, 2009) (Asimaki *et al.*, 2009) (Philips *et al.*, 2014) (Svensson *et al.*, 2016). Asimaki *et al.* reported a reduction in the immunofluorescence microscopy signal of both PKP2 and JUP at the intercalated discs of myocardial tissue for a subject with this variant (Asimaki *et al.*, 2009). However there have been no studies verifying whether the variant results in a mutant protein and therefore whether this reduction in myocardial immunofluorescence signal represents an absolute reduction in PKP2 or intracellular redistribution.

Several members of his family carry the same mutation but one of these relatives (his nephew) had the clinical features of ARVC/D. Other carriers were asymptomatic and had normal cardiac investigations including his father who was 94 years old at the time of the study. There was no history of ARVC/D or inherited cardiac disease in the maternal side of 0101's pedigree, i.e no family history suggesting inheritance of a predisposition to ARVC/D from both parents.

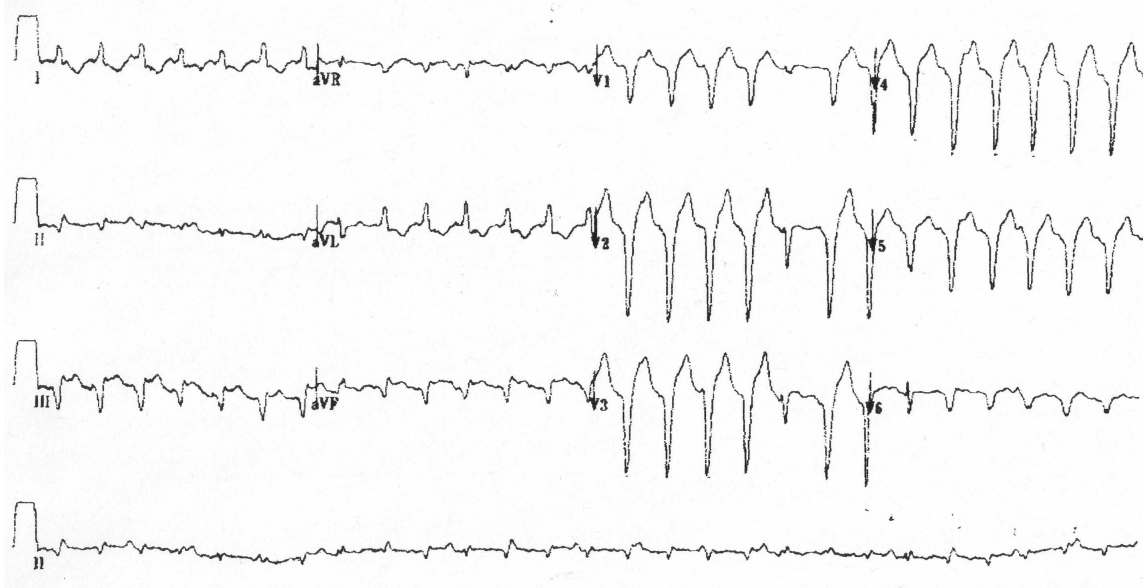


Figure 22 12-lead ECG recording of ventricular tachycardia recorded at age 46 in subject 0101.

The ventricular rate is approximately 160bpm, the QRS duration is >120ms, the QRS complexes have a left bundle branch block (LBBB) morphology (QS in V1 and an absence of q waves in I) and a superior axis (overall negative QRS in aVF). This arrhythmia would constitute a major criterion for ARVC/D within the current diagnostic guidelines.

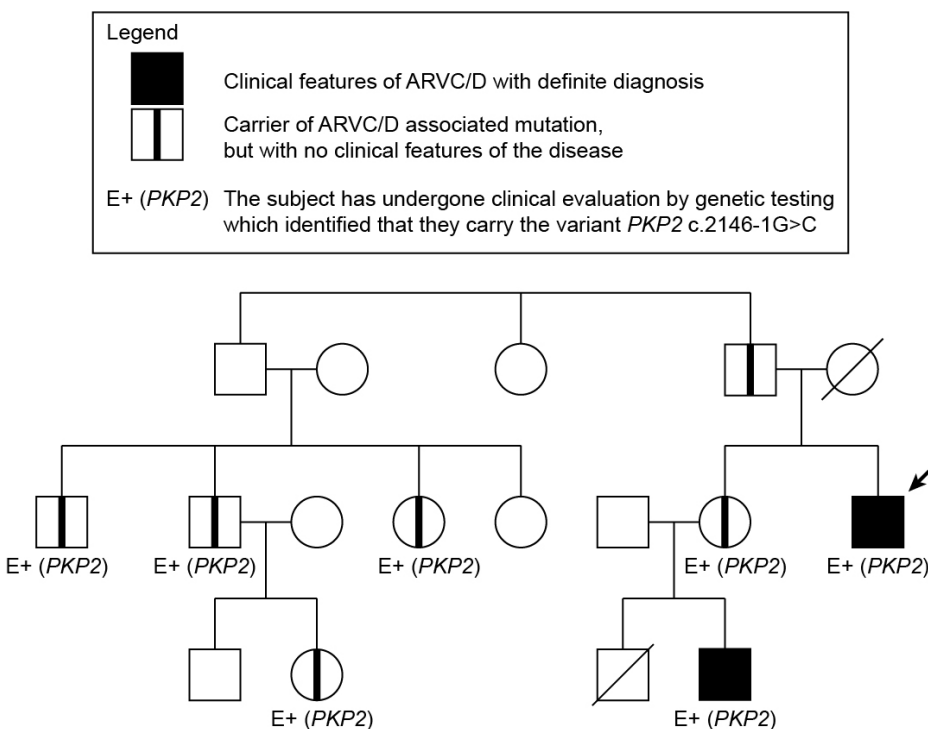


Figure 23 Pedigree chart for subject 0101.

The chart was constructed using standardised nomenclature and symbols (Bennett *et al.*, 2008). Only branches of the family with either clinically affected individuals or mutation carriers are shown.

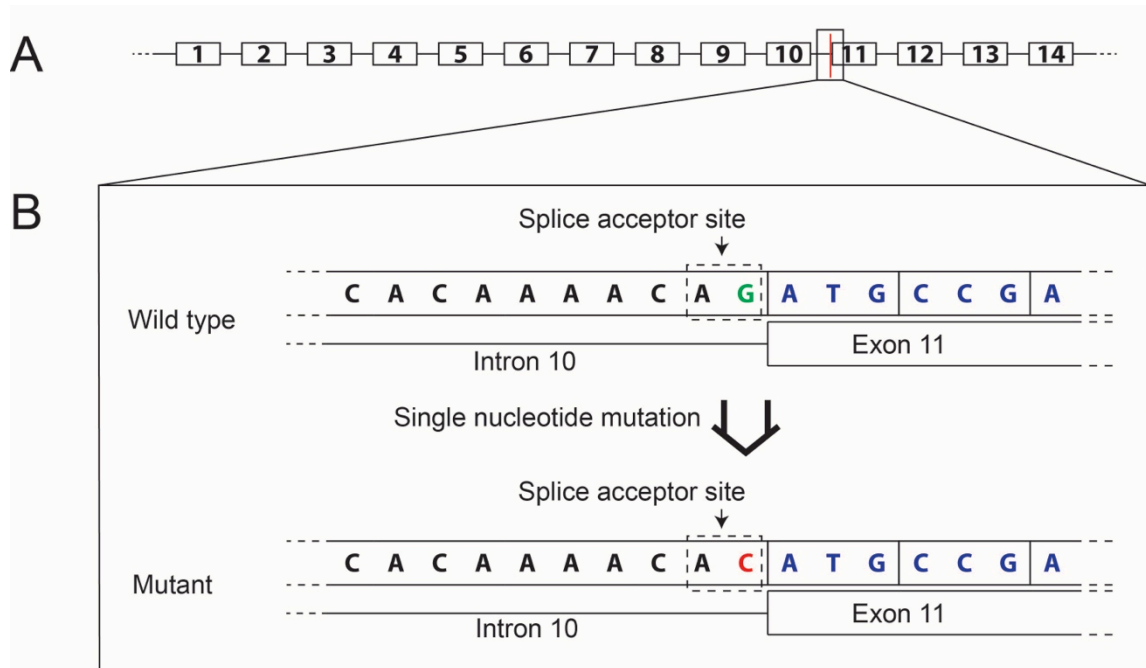


Figure 24 Illustration of *PKP2* c.2146-1G>C.

The location of the mutation within the gene is illustrated (A). The mutation disrupts the G of the invariant AG nucleotides of the splice acceptor site of intron 10 (B). The mutation is predicted to result in aberrant splicing of exon 11 (Alamut v1.5).

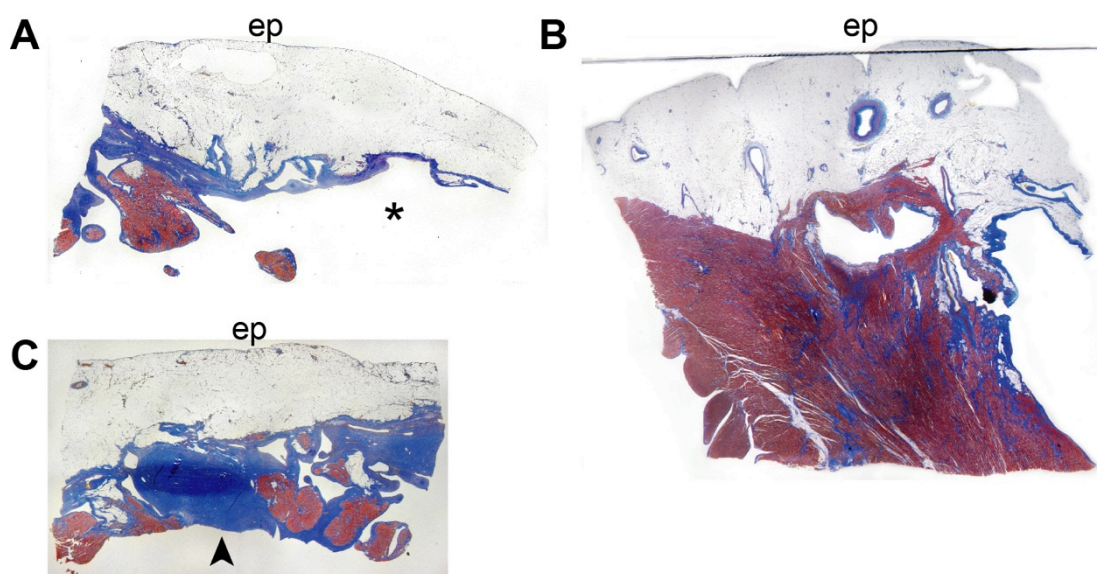


Figure 25 Histology of myocardium from explanted heart of 0101-C41

Light microscopy images of myocardial tissue from the explanted heart of subject 0101-C41. All panels show tissue prepared with a Martius, scarlet and blue (MSB) stain in which connective tissue is labelled blue and fibrin stains red. Panels A and C shows samples from the anterior right ventricle in which part of the ventricular wall is seen to consist of only connective tissue and epicardial fat with no myocardium. In panel A the ventricular wall is thinned (*), in panel C the connective tissue makes up a layer of similar depth to the remaining myocardium (arrowhead). Panel B shows a sample from the anterior septum showing the presence of connective tissue within the myocardium. The epicardial surface of samples is indicated (ep).

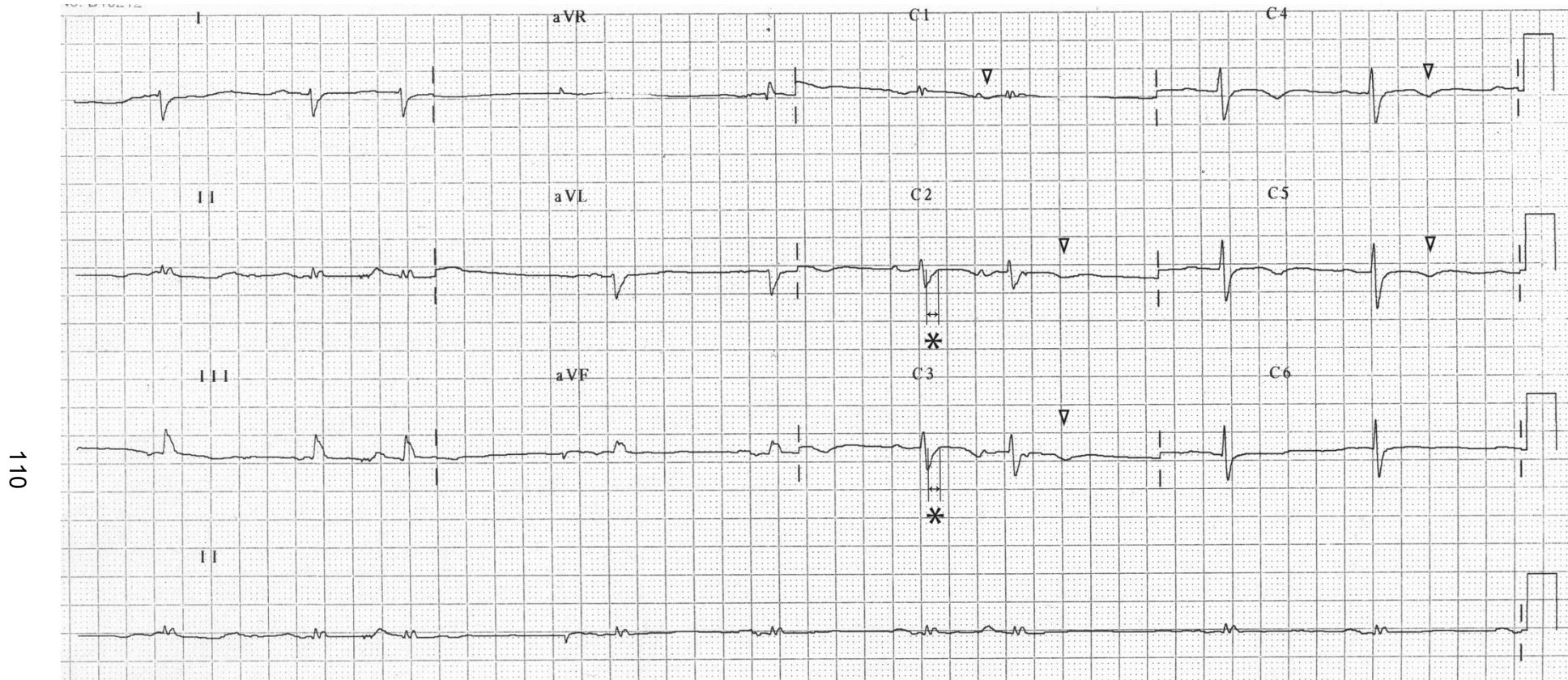


Figure 26 12-lead ECG recording from subject 0101 showing sinus bradycardia at a rate of 56bpm.

The QRS duration is 104ms. The duration of the terminal phase of the S-wave in leads V2 and V3 (labelled C2 and C3 in the image) measures approximately 80ms (*) and there are inverted T-waves in leads V1 to V5 (hollow arrowheads). These findings constitute a minor criterion from the depolarisation abnormalities category (VI) and a major criterion from the repolarisation category (III) within the current diagnostic guidelines. Horizontal scale 40ms/mm. Vertical Scale 1mV/mm.

3.3.2 Subject 0202

Subject 0202 was a male of 44 years of age at the point of recruitment. He presented with palpitations to a hospital at age 40. He was found to be in a broad complex tachycardia that was considered to be VT (Figure 27). He underwent coronary angiography which found no obstructive coronary artery disease. A cardiac MRI identified mild right ventricular dilation and systolic impairment but no regional wall motion abnormalities. An electrophysiology study induced VT of an identical morphology to the clinical VT and an implantable cardioverter-defibrillator was implanted. During follow up his 12-lead ECG developed features typical of ARVC/D including T-wave inversion in the pre-cordial leads (Figure 30). The T-wave inversion was not permanent and appeared to resolve in subsequent recordings (Figure 31). A signal averaged ECG provided additional evidence of depolarisation / conduction abnormalities (Figure 32).

Subject 0202 underwent sequencing of *PKP2*, *DSG2*, *DSC2* and *DSP* as part of his clinical management to facilitate screening of his family for ARVC/D. Sequencing identified the mutation *DSG2* c.691-5T>A (Figure 28). *In silico* analysis predicted this to disrupt the polypyrimidine tract upstream of the splice acceptor site of intron 6 and thereby lead to skipping of exon 7 and the creation of an alternative acceptor splice site (Alamut v2.2). As part of the patient's clinical assessment, RNA was extracted from a peripheral blood sample and the region between exons 6 to 8 was sequenced. This identified transcripts lacking exon 7 and an in-frame CAG insertion between exons 6 and 8 that was predicted to result in the insertion of a glutamine residue. On this basis the mutation was classified as pathogenic. Exon 7 encodes part of the second extra-cellular binding domain (ECB2). As described in 1.2.2 the ECBs mediate the trans and cis dimerisation of desmosomal cadherins. Therefore mutant proteins resulting from this variant (if integrated into the desmosomal plaques) would be predicted to disrupt the organisation of proteins within the desmosomal gap. This variant has not been reported previously in association with ARVC/D therefore there have been no studies of the myocardium of patients with this variant. Similarly there are no animal or cellular models of this variant.

Several other members of his family were found to be carriers of the variant, but none of them had clinical features of ARVC/D Figure 29.

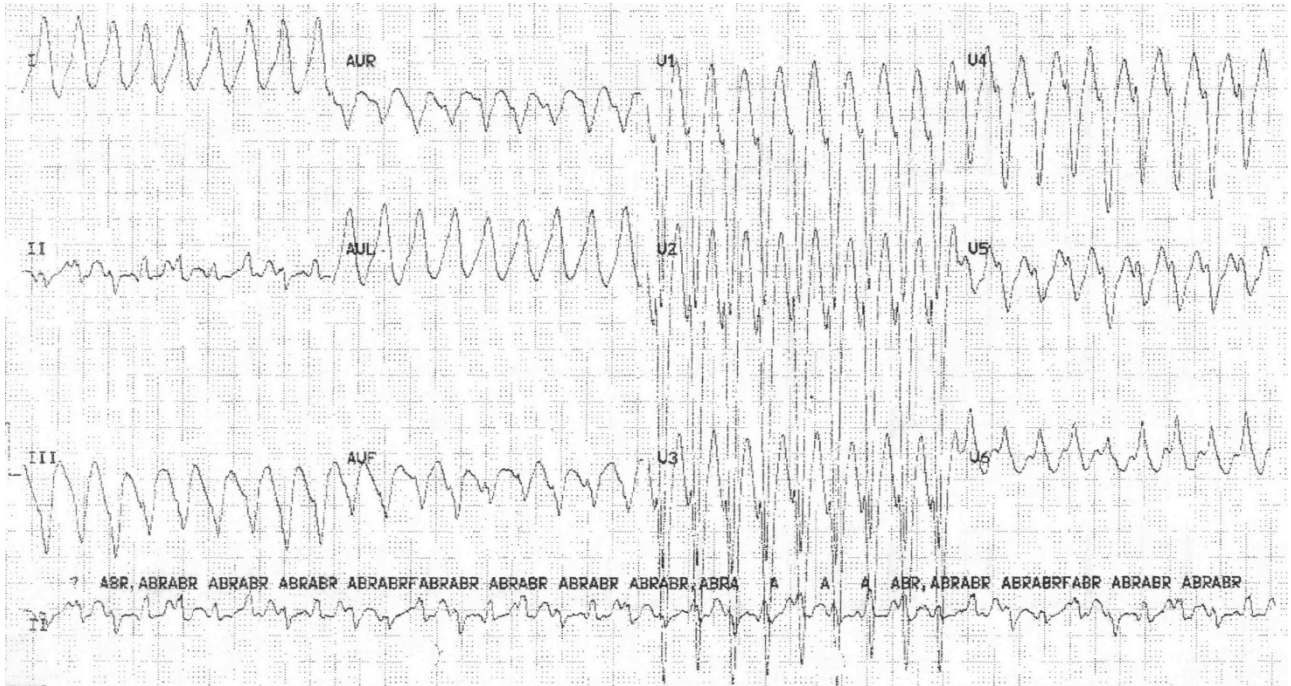


Figure 27 12-lead ECG of ventricular tachycardia recorded from subject 0202. The ventricular rate is 210bpm. The QRS duration is >120ms, the QRS complexes have a LBBB morphology (rS or QS in V1 and an absence of q waves in I, V5 and V6), and a superior axis (indicated by the overall negative QRS in aVF). This arrhythmia would constitute a major criterion for ARVC/D within the current diagnostic guidelines. Horizontal scale 40ms/mm. Vertical Scale 1mV/mm.

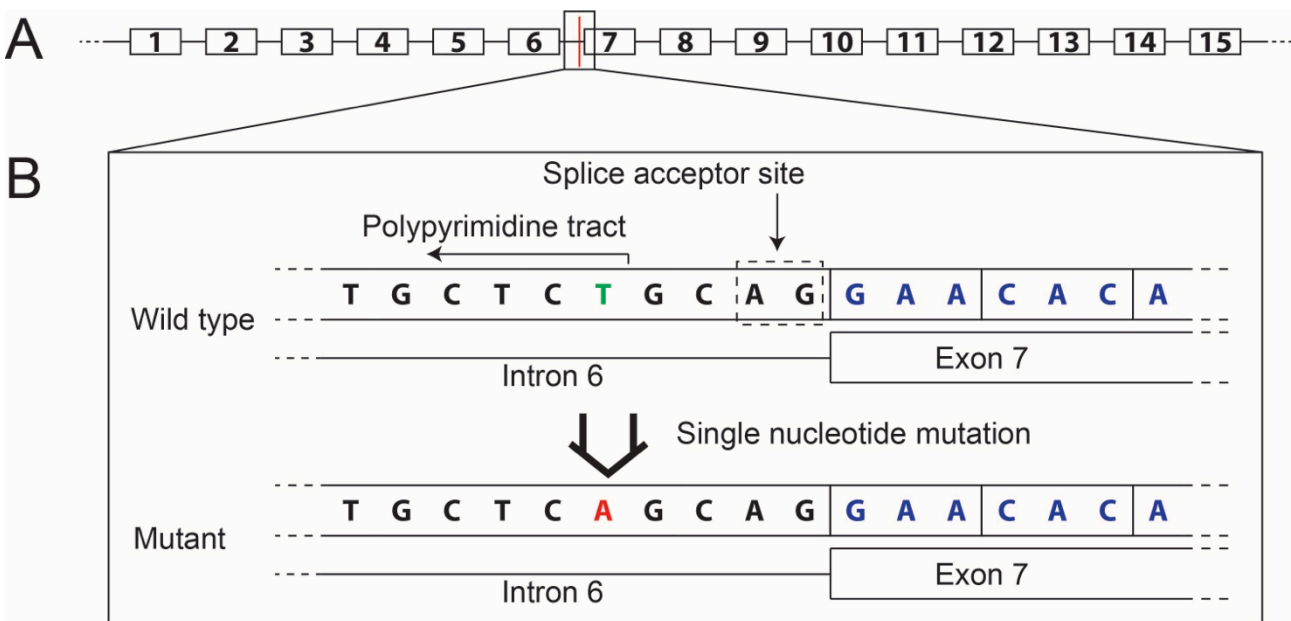


Figure 28 Illustration of *DSG2* c.691-5T>A. The location of the mutation within the gene is illustrated (A). The mutation disrupts the polypyrimidine tract upstream of the splice acceptor site of intron 6 (B). The mutation is predicted to result in aberrant splicing of exon 7 (Alamut v2.2).

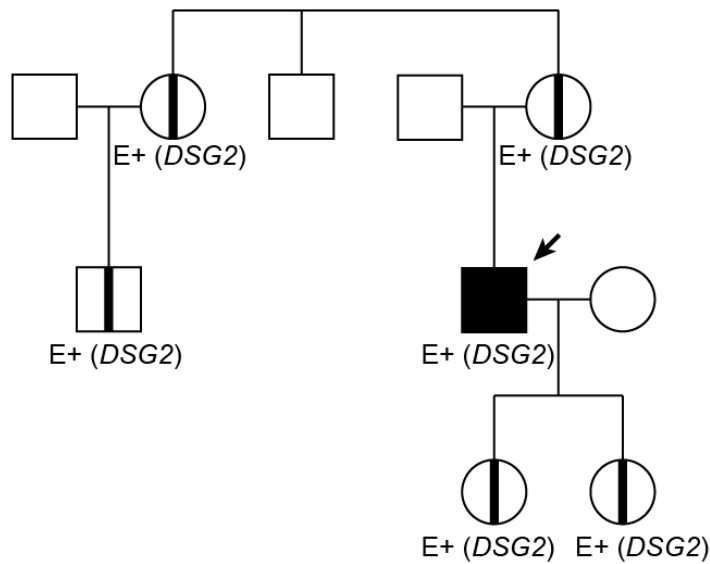
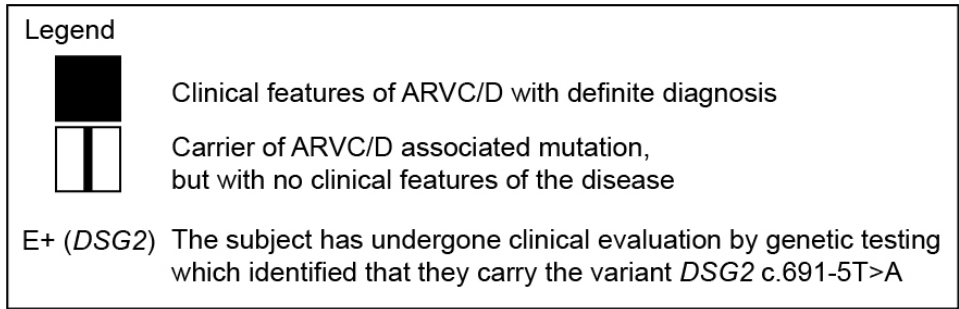


Figure 29 Pedigree chart for subject 0202.

The chart was constructed using standardised nomenclature and symbols (Bennett *et al.*, 2008). Only branches of the family with either clinically affected individuals or mutation carriers are shown.

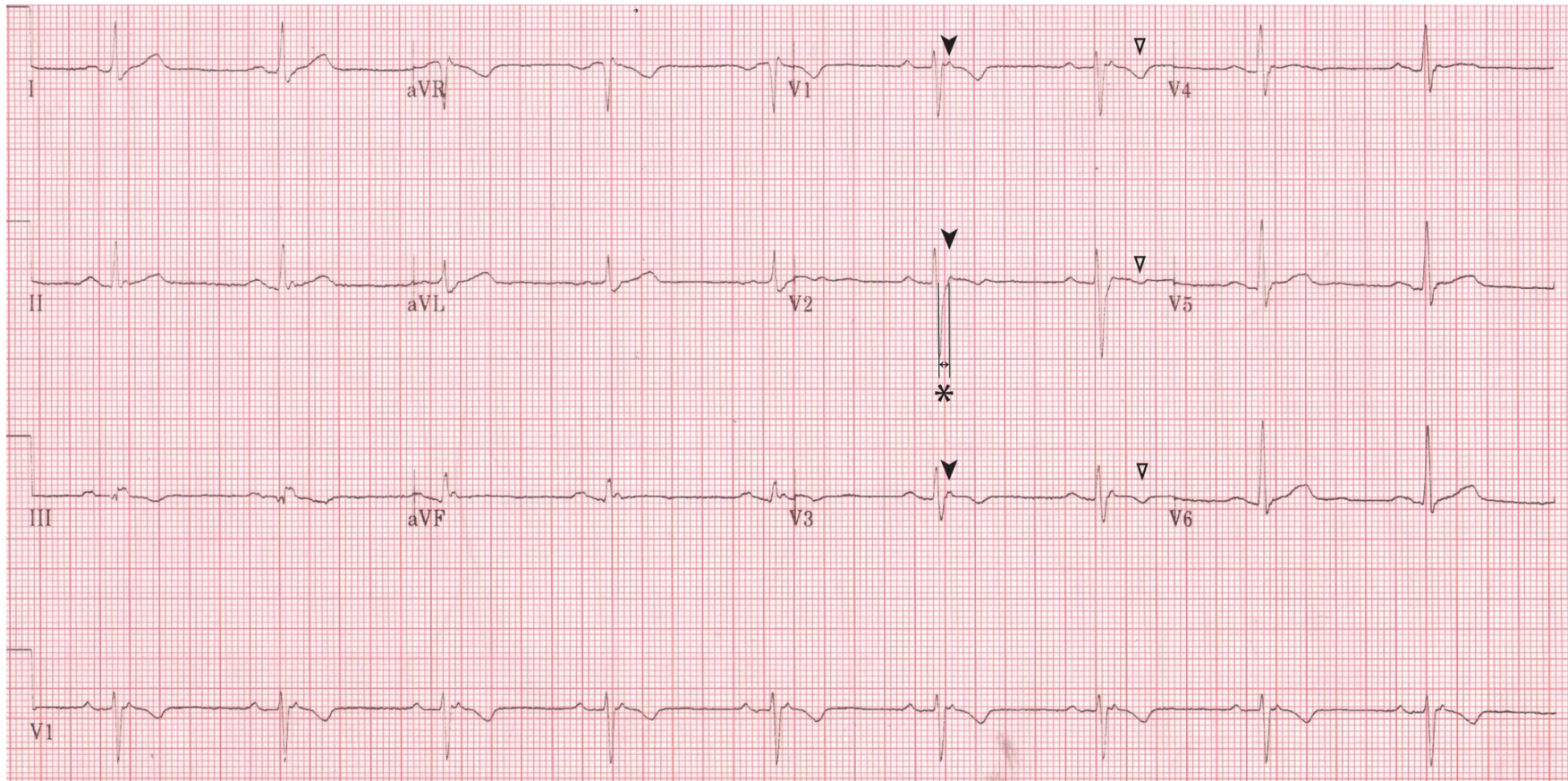


Figure 30 12-lead ECG recording from subject 0202 showing sinus bradycardia at a rate of 55bpm.

The QRS duration is 106ms. An Epsilon wave is present in leads V1 - V3 (solid arrowheads), the terminal phase of the S-wave in lead V2 is approximately 60ms in duration (asterisk) and there are inverted T-waves in leads V1 to V3 (hollow arrowheads). These findings constitute a major and a minor criterion from the depolarisation abnormalities category (VI) and a major criterion from the repolarisation category (III) within the current diagnostic guidelines. Horizontal scale 40ms/mm. Vertical Scale 1mV/mm.

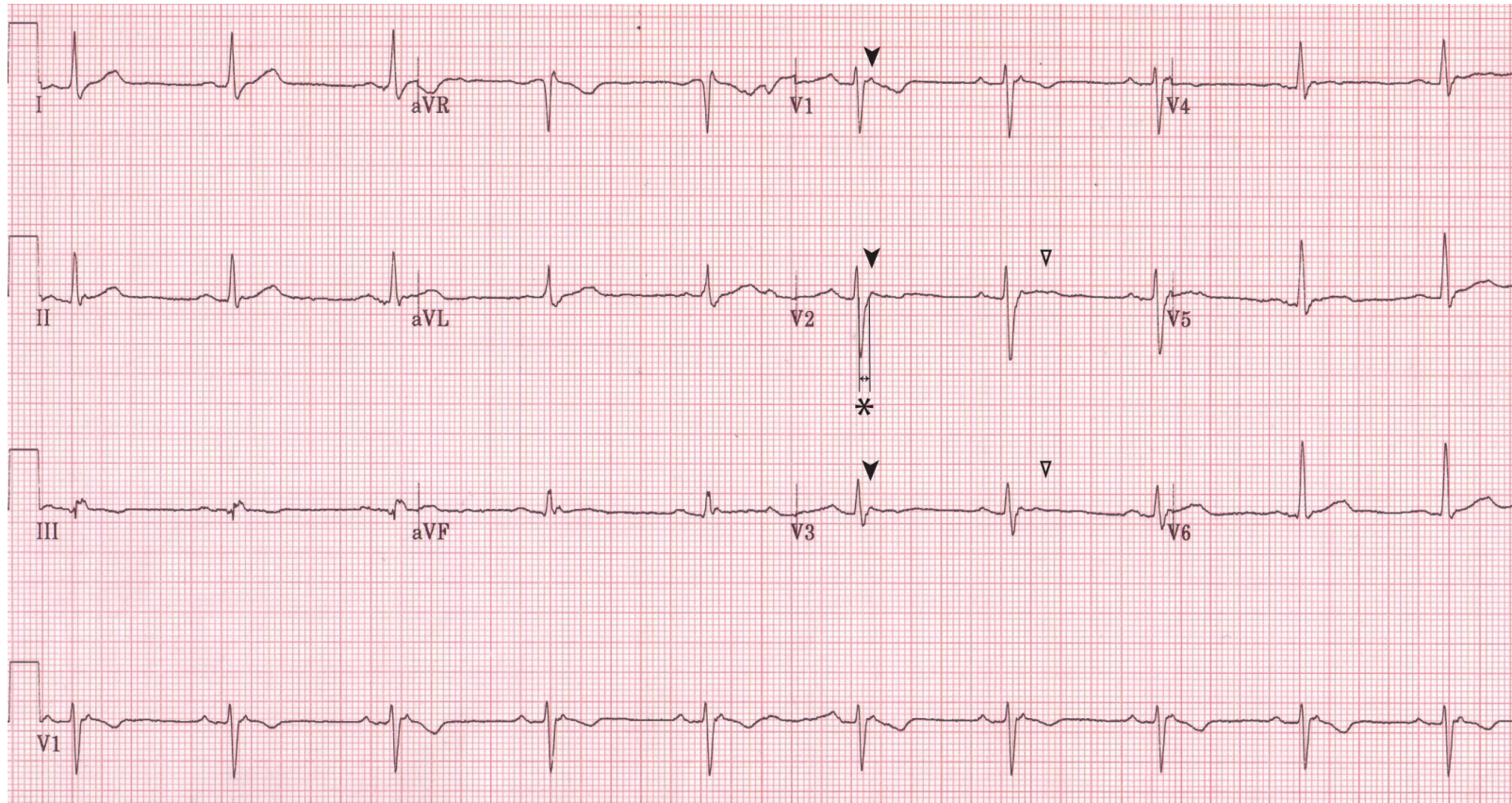


Figure 31 12-lead ECG recording from subject 0202 showing sinus bradycardia at a rate of 59bpm.

The QRS duration is 110ms. An Epsilon wave is still present in leads V1 - V3 (solid arrowheads), the terminal phase of the S-wave in lead V2 is remains approximately 60ms in duration (asterisk). The T-waves in leads V2 to V3 (hollow arrowheads) are now flattened rather than inverted and therefore do not constitute a criterion for the diagnosis of ARVC/D within the current diagnostic guidelines. Horizontal scale 40ms/mm. Vertical Scale 1mV/mm.

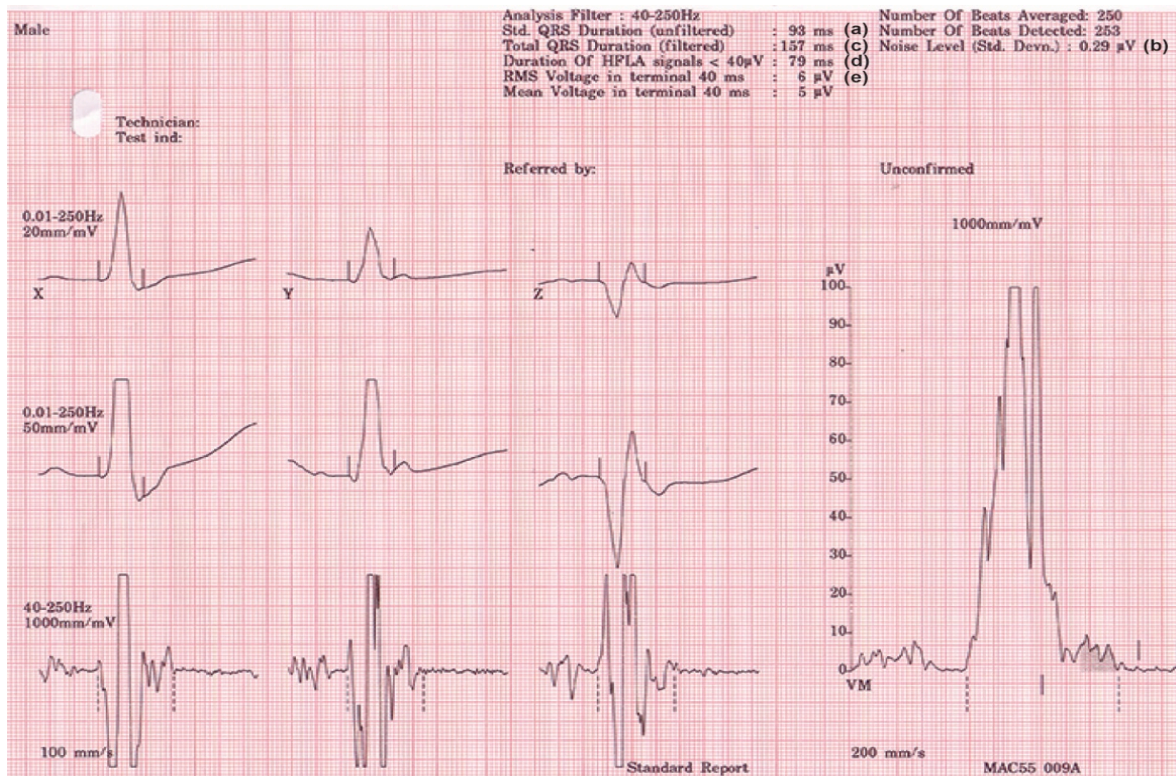


Figure 32 Signal averaged ECG (SAECG) recording from 0202.

The unfiltered QRS duration is 93ms excluding the presence of complete RBBB. The recording is of acceptable quality, averaging over 250 beats and with a noise level (b) of 0.29 μ V. The filtered QRS duration (c) is >114ms (153ms) and the duration of the terminal part of the QRS that is <40 μ V (d) is >38ms (79ms). The root mean square of the voltage in the terminal 40ms of the QRS complex (e) is <40 μ V (6 μ V). Each of these features constitutes a minor criterion in the depolarisation abnormalities category within the current diagnostic guidelines.

3.3.3 Subject 0203

Subject 0203 was a female of 70 years of age at the point of recruitment. She presented to hospital at age 67 with acute breathlessness and found to be in a broad complex tachycardia that was considered to be VT (Figure 33). A cardiac MRI scan identified a severely dilated RV with focal thinning and dyskinesia consistent with ARVC/D. She underwent ICD implantation during this admission. During subsequent follow up her 12-lead ECG (Figure 36) showed features typical of ARVC/D. Structural and functional abnormalities of the right ventricle continued to be noted by echocardiography including a dyskinetic RV free wall and an RVOT diameter of 44mm (or 23.4mm/m² when indexed to body surface area).

Subject 0203 underwent sequencing of *PKP2*, *DSG2*, *DSC2* and *DSP* as part of her clinical management to facilitate screening of her family for ARVC/D. Sequencing identified the mutation *DSP* c.3195C>G which results in a premature stop codon at

amino acid position 1065 (p.Tyr1065X) (Figure 34). The variant lies within exon 23 which encodes the central rod domain and is included in both isoforms of DSP (DSP I and DSP II). If translated it is predicted to result in a truncated protein lacking the C-terminal plakin repeat domain that is responsible for binding to intermediate filaments.

This mutation has not been previously reported in association with ARVC/D, but similar heterozygous nonsense mutations in this region have been (“ARVC database,” n.d.). There are no cellular or animal models of ARVC/D resulting from DSP truncated in the central rod domain. It could be speculated that since the resulting mutant protein would contain the N-terminal spectrin repeat domains, it would be capable of interacting with arm repeat proteins within the desmosomal plaque. In this circumstance it might be expected that changes in the morphology of the inner dense plaque region (where DSP interacts with intermediate filaments) are more likely than changes to the outer dense plaque morphology and desmosomal gap with and the redistribution of arm repeat proteins.

Several other members of her family were found to be carriers of the variant. One of the subject’s sons was a carrier and suffered from VT, but no formal diagnosis of ARVC/D was made before he died from an unrelated condition. Other mutation carriers did not have clinical features of ARVC/D.

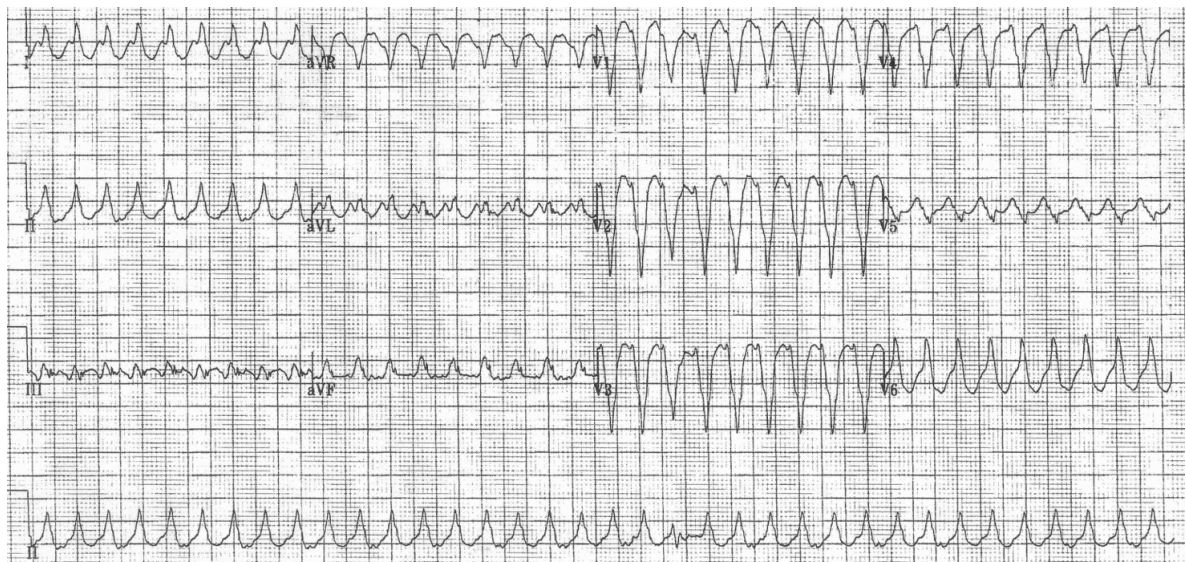


Figure 33 12-lead ECG of a ventricular tachycardia recorded in subject 0203. The ventricular rate is 216bpm, the QRS duration is >120ms, the QRS complexes have a LBBB morphology (QS in V1 and an absence of q waves in I and V6) and an inferior axis (overall positive QRS morphology in aVF). This arrhythmia would constitute a minor criterion for ARVC/D within the current diagnostic guidelines.

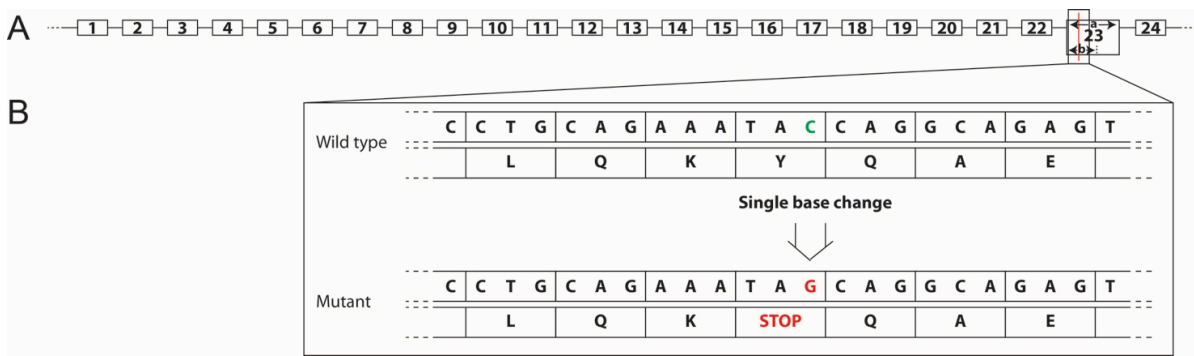


Figure 34 Illustration of *DSP* c.3195C>G.

The location of the mutation within the gene is illustrated (A). Exon 23 undergoes alternative splicing producing a transcript encoding the DSP I isoform, which contains the entire coding sequence (a) and a transcript encoding the DSP II isoform which contains the only first part of the exon (b). The mutation lies within the section of exon 23 that is included in both transcripts and results in a premature stop codon that, if translated, would result in a truncated protein lacking the carboxy-terminus that is responsible for binding to intermediate filaments.

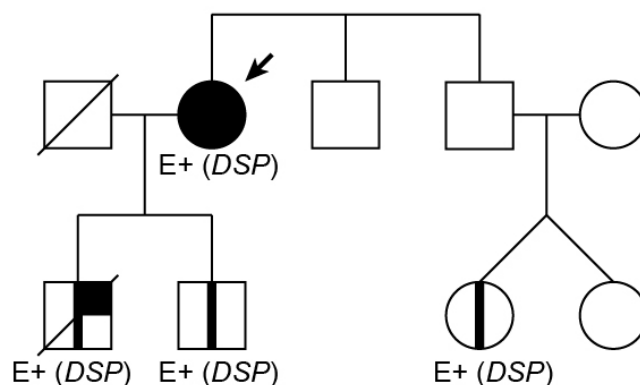
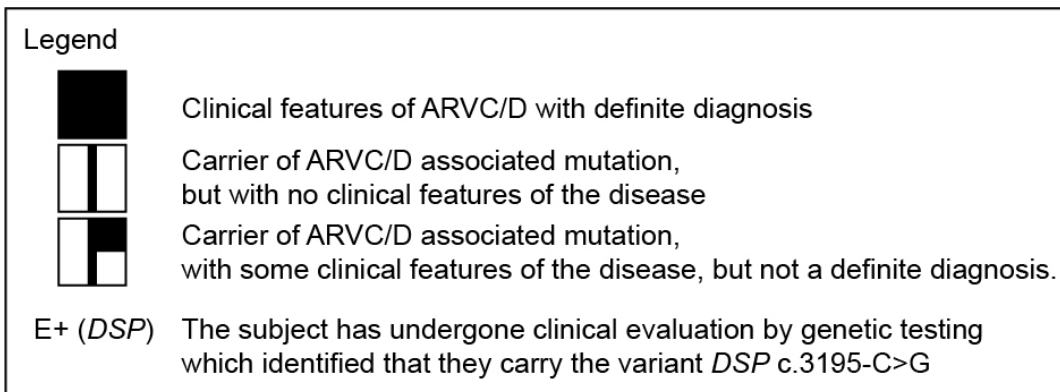


Figure 35 Pedigree chart for subject 0203.

The chart was constructed using standardised nomenclature and symbols (Bennett *et al.*, 2008). Only branches of the family with either clinically affected individuals or mutation carriers are shown.

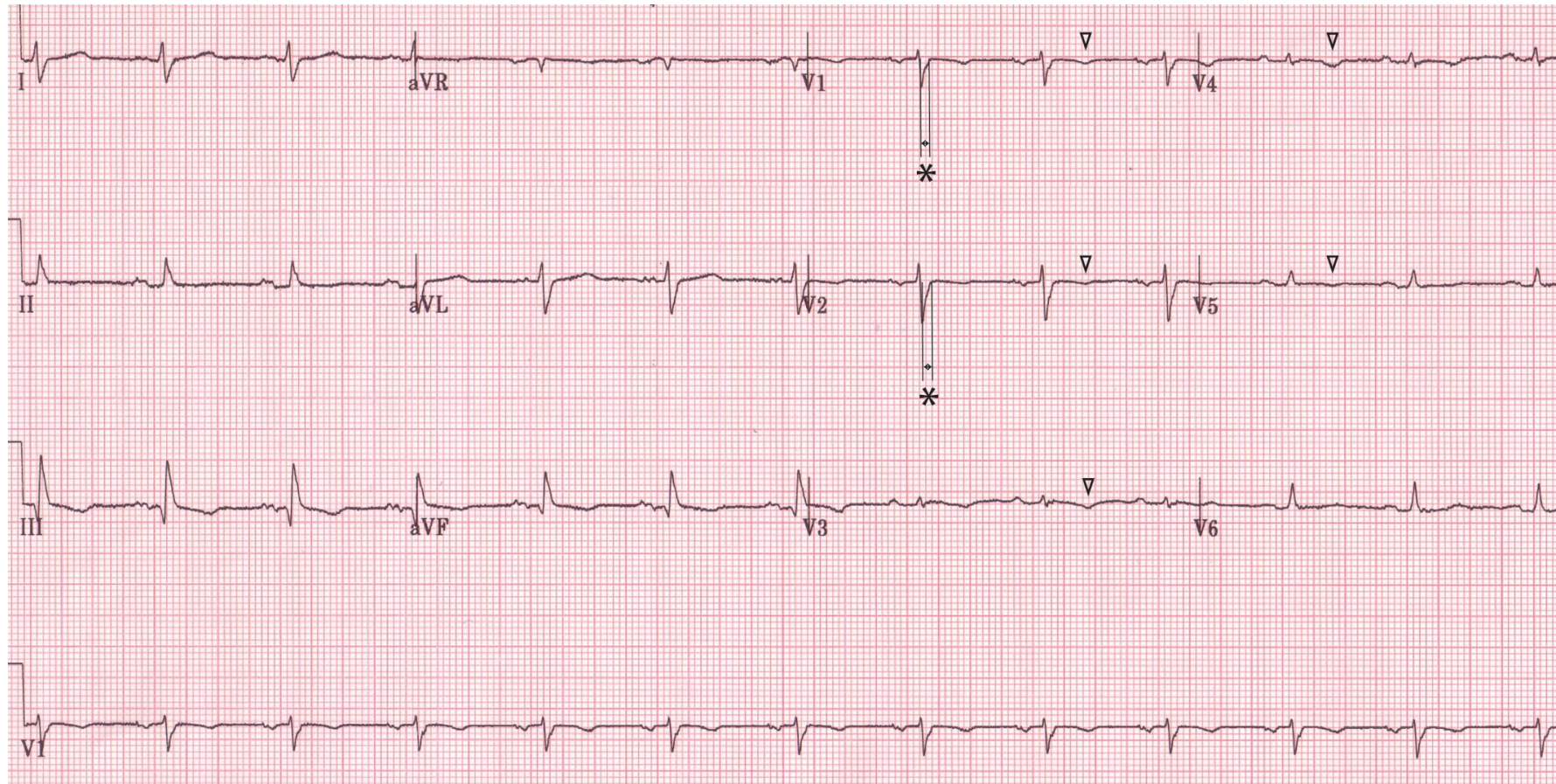


Figure 36 12-lead ECG from subject 0203 showing sinus rhythm.

The QRS duration is 96ms, excluding complete RBBB. The terminal phase of the S-wave in lead V1 and V2 is approximately 60ms in duration and the T-waves are inverted in leads V1 to V5 (hollow arrowhead). These findings constitute a minor criterion from the depolarisation abnormalities category (VI) and a major criterion from the repolarisation category (III) within the current diagnostic guidelines. Horizontal scale 40ms/mm. Vertical Scale 1mV/mm.

3.3.4 Control subjects from which blood samples were collected

A total of four control subjects were recruited to provide peripheral blood samples. All subjects had no history or family history of hereditary cardiac disease or sudden cardiac death. The sequencing of desmosomal genes was not performed in control subjects. Their baseline demographics are summarised in Table 45.

The initial experimental design was to generate the same number of control iPSC lines as ARVC/D lines. However, due to resource constraints this was modified to the generate clones from a single control subject. At the point in time that this decision was made iPSC clones had been successfully generated from subject 2 but not from the other control subjects. It was decided to use iPSCs from subject 2 as controls for the ARVC/D lines to avoid using the additional resources necessary to generate control lines from the male controls. Samples from the three male control subjects were used in the comparison of gene expression in peripheral blood mononuclear cells (PBMCs) with other tissue types.

Subject	Sex	Age at sample point of collection (years)
2	Female	34
6	Male	36
7	Male	33
8	Male	32

Table 45 Characteristics of control subjects from which blood samples were obtained.

3.3.5 Control subjects from which right atrial appendage myocardium was collected

Samples of right atrial appendage (RAA) myocardium were used in some analyses of cardiac and desmosomal gene expression and in transmission electron microscopy (TEM) experiments. These samples were collected as part of a different study and were kindly donated by Dr Andrew Owens.

All subjects from which RAA tissue was collected were undergoing elective cardiac surgery involving cardiopulmonary bypass for valvular or ischaemic heart disease. Part of the right atrial appendage is routinely resected during this procedure. Tissue that would otherwise be discarded was collected for analysis. Subjects had no history or family history of ARVC/D or inherited cardiac disease. All subjects had normal right ventricular size and function documented as by cardiac imaging

(echocardiography or cardiac MRI) as part of their clinical care. Their baseline characteristics are summarised in Table 46.

Subject	Sex	Age at sample point of collection (years)	Indication for surgery
RAA1	Male	72	Aortic valve disease
RAA2	Female	85	Aortic valve disease
RAA3	Female	67	Aortic valve disease and coronary artery disease
RAA4	Female	66	Aortic valve disease

Table 46 Baseline characteristics of subjects from which right atrial appendage myocardium was collected.

3.4 Discussion and conclusion

Three subjects with a definite ARVC/D phenotype and desmosomal mutations classified as pathogenic were successfully recruited to give blood for the generation of iPSCs. None of the mutations carried by these subjects have been studied in cellular or animal models previously. Furthermore two of the ARVC/D mutations in this study are in genes for which (as the time of writing) iPSC-CM models have yet to be reported. The present study therefore has the potential to expand our understanding of the potential of iPSC-CMs to model ARVC/D.

It is accepted that the use of iPSCs from a single female subject as a control for comparison to multiple ARVC/D iPSC lines, two of which are from male subjects is a limitation to the study design. Specifically it weakens the argument that any conclusions from a comparison of individual cell lines in this study indicate a more general pattern of difference between control and ARVC/D iPSCs. Further work will be needed with a larger number of control iPSC lines to establish the generalizability of this study's conclusions.

Chapter 4. The Derivation And Characterisation Of Patient Specific iPSCs From The Peripheral Blood Of Subjects With And Without ARVC/D

4.1 Introduction

This chapter will describe the generation of induced pluripotent stem cells (iPSCs) from nucleated peripheral blood cells. The principles of generating iPSCs from peripheral blood cells are outlined in Chapter 1. The reprogramming protocols used in this study are described in Chapter 2.

The first part of this chapter will describe the results of two different reprogramming protocols and the rationale for choosing one over the other in subsequent work.

The second part of the chapter will describe the assessment of pluripotency in the clonal lines produced from both the initial and subsequent reprogramming experiments.

The cell lines assessed in this chapter will be referred to as expandable clones. At the end of the chapter and thereafter cell lines which were classified as pluripotent will be referred to as iPSCs.

4.2 Aims and hypotheses

It was hypothesised that the transduction of PBMCs with reprogramming vectors followed by their maintenance in appropriate culture conditions would induce persistent changes in cellular behaviour, gene expression and protein expression consistent with pluripotency. These changes were expected to consist of the following characteristics.

- Cells would change from being non-adherent and non-clustered, i.e. cultured as a suspension, to forming adherent expanding colonies.
- Pluripotency marker gene and protein expression would be up-regulated with respect to PBMCs.
- The expression of pluripotency marker genes and proteins would be at a level comparable to that of established pluripotent cell lines.
- When allowed to differentiate there would be evidence from patterns of protein expression and tissue histology that the cells are capable of forming tissues from each of the three germ cell layers.

It was hypothesised that the change in characteristics from PBMCs to pluripotent cells would not be attributable to changes in genomic DNA acquired during reprogramming.

4.3 Results

4.3.1 The selection of PBMC reprogramming protocols for testing

At the time this work was begun the reprogramming PBMCs to iPSCs had not (to the best of our knowledge) been attempted previously at Newcastle University. In the initial phase of this study it was decided to adapt two protocols from published work and test their efficacy in generating iPSCs from a control subject.

When choosing the protocols to adapt we excluded those using vectors that integrated transgenes into the iPSC genome (e.g. lentivirus) in order to avoid the possibility of mutation and transgene re-activation that might undermine evidence of pluripotency in resultant cell lines. Within Newcastle University there was already experience of using a commercial, non-integrating, Sendai based reprogramming system (Cytotune 2.0, Thermo-Fisher) in reprogramming fibroblasts to iPSCs. Protocols using Sendai vectors were therefore considered in preference to other techniques.

PBMC samples consist of a mixture of cell types (Table 1) and reprogramming protocols differ depending on the cell type at which they are directed. Protocols have been published describing iPSC generation from peripheral blood haematopoietic progenitor cells, erythroblasts and T-cells (see appendix Tables 60 to 62). At the time of writing the feasibility of reprogramming certain human PBMC types (e.g. monocytes) has yet to be established. The culture conditions used prior to transduction differ depending on the type of cell that is the target of reprogramming e.g. protocols to reprogram T-cells typically employed the cytokine IL2 and anti-CD3 antibodies whereas protocols to reprogram CD34+ progenitor cells typically used a combination of SCF, FLT3L, IL6, IL3 and TPO (see appendix Tables 49 to 51 for references and comparison of media compositions in different published protocols). Some of these protocols used mechanical selection of the target cell type before pre-transduction culture e.g. FACS. Others relied on the pre-transduction culture conditions to favour the proliferation one type of PBMC over others.

The two protocols chosen were each designed to target different PBMC types: T-cells and non-T-cells. The non-T-cell protocol was adapted from two recommended

by the manufacturer of the reprogramming vector for the generation of iPSCs from a mixed PBMC sample (Life Technologies, 2012) (Life Technologies, 2013). The cell type at which this protocol is targeted was not specified by the manufacturer, but the composition of this medium is similar to those used for the reprogramming of CD34+ cells. The T-cell protocol tested was adapted from two publications describing the generation of T-cell derived iPSCs from a starting population of mixed PBMCs (Seki *et al.*, 2011) (Brown *et al.*, 2010). These adapted protocols were referred to as the non-T-cell and T-cell protocols respectively.

4.3.2 Non-T-cell derived iPSC protocol testing

PBMCs samples from three control subjects were cultured and transduced using the non-T-cell protocol. Co-culture of transduced PBMCs from the same subject with inactivated MEF feeders resulted in adherent colonies with ESC-like characteristics by phase contrast microscopy in all experiments (Figure 37). For each reprogramming experiment a sample of un-transduced cells were cultured in parallel to the transduced cells from the same subject. No colonies resulted from the culture of un-transduced PBMCs. Despite the formation of adherent colonies, expandable clones could only be established in one experiment and therefore one subject (subject 2) (Table 47).

Subject	Cell type	Pre-transduction culture		Number of cells transduced ($\times 10^3$)	Number of colonies with and ES-like morphology from initial plating of transduced PBMCs	Results of expansion culture
		Duration (days)	PBMC population size after pre-transduction culture (percentage of starting population)			
1	Unselected / mixed PBMCs	5	50%	100	5	No expandable clones
2		5	110%	100	11	3 expandable clones
4		4	100%	200	1	No expandable clones

Table 47 Results of initial reprogramming experiments aimed at generating non-T-cell derived iPSCs.

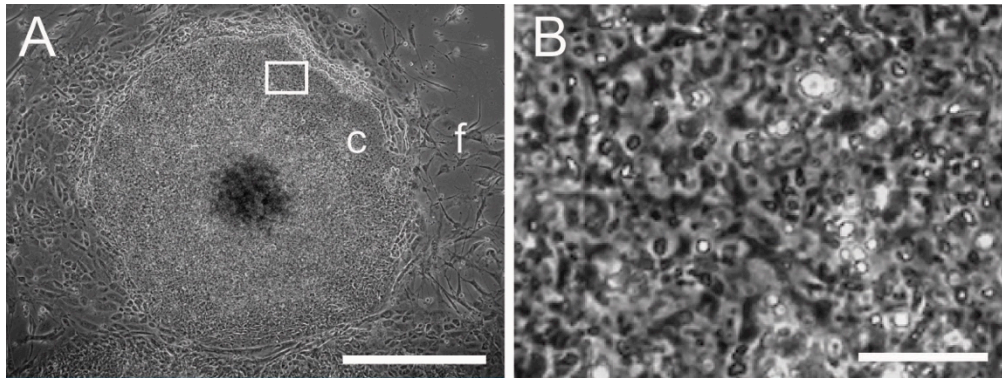


Figure 37 Example of a colony observed by phase contrast microscopy with “stem-cell-like” features arising from primary culture of transduced PBMC on an inactivated MEF feeder layer.

Panel A shows the colony (c) as compact, circular and flat, surrounded by more sparsely distributed fusiform cells (f). Panel B shows the boxed area from panel A in detail. The cells within the colony are $\leq 10\mu\text{M}$ in diameter with a high nuclear to cytoplasmic ratio. Scale bars indicate $500\mu\text{M}$ and $50\mu\text{M}$ respectively.

4.3.3 T-cell derived iPSC protocol testing

PBMCs samples from three control subjects were cultured and transduced using the T-cell protocol. Transduced PBMCs from the first subject using the T-cell protocol failed to generate any adherent colonies. In order to maximise the number of T-cells exposed to reprogramming vectors the two subsequent experiments used a population of CD3+ cells purified from the initial blood sample by FACS. Adherent colonies with an ESC-like morphology developed in the initial MEF co-culture of transduced cells. No colonies developed in parallel cultures of un-transduced cells. Expandable clones could only be established in the experiment using cells from subject 2 (Table 48). No expandable clones could be established from subject 3.

Subject	Cell type	Pre-transduction culture		Number of cells transduced ($\times 10^3$)	Number of colonies with and ES-like morphology from initial plating of transduced PBMCs	Results of expansion culture
		Duration (days)	PBMC population size after pre-transduction culture (percentage of starting population)			
1	Unselected / mixed PBMCs	4	160%	50	0	NA
2	FACS sorted CD3+ cells	11	910%	50	8	3 expandable clones
3	FACS sorted CD3+ cells	8	330%	326	>100	No expandable clones

Table 48 Results of initial reprogramming experiments aimed at generating T-cell derived iPSCs.

4.3.4 Choice of protocol for iPSC lines derived from ARVC/D subjects

The experimental assessments of the pluripotency of the clonal lines generated is described later in this chapter and confirmed that both protocols had generated iPSCs from subject 2. Further work demonstrated and that these iPSCs could differentiate to cardiomyocytes and generate desmosomes (see chapters 3, 4 and 5).

It was therefore concluded that either the non-T-cell protocol or the T-cell protocol (when applied to FACS sorted CD3⁺ cells) could be considered for the generation of iPSCs from subjects with ARVC/D. The non-T-cell protocol was chosen for further work due to the additional cost and labour associated with FACS sorting CD3⁺ cells for the T-cell protocol.

PBMCs from three subjects with ARVC/D (0101, 0202 and 0203) were transduced as part of the non-T-cell protocol. In all experiments adherent colonies with an ESC-like morphology developed in cultures of transduced cells and no such colonies were observed in cultures of un-transduced cells. Multiple expandable clones were obtained from all experiments.

4.3.5 Overview of iPSC characterisation

An overview of the characterisation of all the iPSC clones generated is given in Table 49. Characterisation assessments can fall into two broad groups: (1) assessments of cellular identity and (2) assessments of pluripotency.

The assessments of cellular identity had the following aims:

- To determine whether the clones generated originated from the subject sampled and that the clones derived from ARVC/D subjects carried the ARVC/D associated pathogenic mutations reported during clinical testing.
- To determine whether the clones originated from T-cells or non-T-cells.

Assessments of pluripotency were of three types:

- Those to identify characteristics which preclude pluripotency, such as the persistence of transgene expression and the presence of acquired pathogenic cytogenetic abnormalities.
- Those that identify markers of pluripotency in un-differentiated cells, this includes cellular morphology and the expression of pluripotency associated genes and proteins.
- Those that identify the tissues generated when a cell line is allowed to differentiate.

Not all clones underwent all forms of characterisation assessment. The rationale for selection of some clones over others for full characterisation is given in subsequent sections.

Subject / Line	Clone	Sendai and transgene expression	SNP microarray		Mutation sequencing	TRB and TRG rearrangement	Colony morphology (phase contrast microscopy)	Pluripotency associated gene expression (RT-qPCR)	Pluripotency associated protein expression		Spontaneous differentiation to 3 germ cell layers	Teratoma assay
			CNV	Genetic identity					Flow cytometry	Immuno-fluorescence microscopy		
2	C2	✓					✓					
	C3	✓	✓	✓		✓	✓	✓	✓	✓	✓	✓
	C7	✓	✓	✓		✓	✓	✓	✓	✓	✓	
	C1	✓					✓					
	C4	✓	✓	✓		✓	✓	✓	✓	✓	✓	
	C6	✓	✓	✓	✓	✓	✓	✓	✓	✓	✓	✓
0101	C4	✓					✓		✓	✓	✓	
	C12	✓					✓		✓	✓	✓	
	C41	✓	✓	✓	✓		✓	✓	✓	✓	✓	
0202	C7	✓					✓		✓	✓	✓	
	C10	✓					✓		✓	✓	✓	
	C13	✓	✓	✓	✓		✓	✓	✓	✓	✓	
0203	C8	✓					✓		✓	✓	✓	
	C12	✓					✓		✓	✓	✓	
	C13	✓	✓	✓	✓		✓	✓	✓	✓	✓	

Table 49 Summary of iPSC characterisation

✓ Indicates that an assessment of this clone was performed with this modality

4.3.6 Genetic identity of clonal cell lines with respect to parent PBMCs

Data from genomic DNA analysed by single nucleotide polymorphism (SNP) microarray was used to assess the genetic identity of clonal cell lines with respect to PBMCs. This was performed by the comparison of fluorescence values encoding SNP genotypes from clonal cell lines with those from PBMCs (Figure 38) (see methods for full description). All analyses indicated that clonal lines were derived from the PBMCs that were transduced (Table 50).

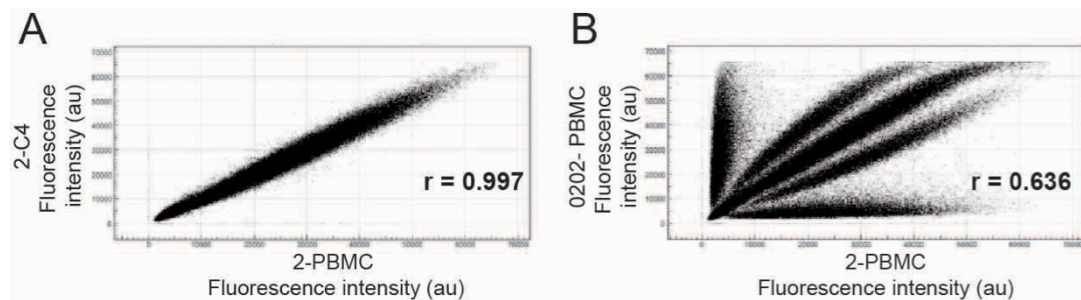


Figure 38 Examples of comparison of SNP array fluorescence data.

Panel A shows comparison of two samples with a similar genetic identity indicated by a clustering of points on the $x=y$ axis and quantified by the correlation co-efficient (r) which approaches 1. Panel B shows comparison between two samples with dissimilar genetic identities and a correlation co-efficient approaching 0.5. Abbreviations: arbitrary units (au).

Comparison	Correlation co-efficient
2-PBMC vs 2-C1(NT)	0.996
2-PBMC vs 2-C4(NT)	0.997
2-PBMC vs 2-C6(NT)	0.996
2-PBMC vs 2-C3(T)	0.997
2-PBMC vs 2-C3(T)	0.996
2-PBMC vs 2-C7(T)	0.995
0101-PBMC vs 0101-C41	0.993
0202-PBMC vs 0202-C13	0.993
0203-PBMC vs 0203-C8	0.992
Negative control (2-PBMC vs 0202-PBMC)	0.636

Table 50 Correlation co-efficient values for generated by comparison of “red” fluorescence intensity values in iPSC lines with those of the PBMCs used in the reprogramming experiments from which they were generated.

4.3.7 Mutation sequencing

ARVC/D associated mutations had been identified in the ARVC/D subjects by clinical screening prior to enrolment. The presence of these mutations in the corresponding clonal lines was confirmed by Sanger sequencing. The sequencing of 2-C6 confirmed that subject 2 did not carry any of these mutations and was therefore appropriate to use as a control for these lines (Figure 39).

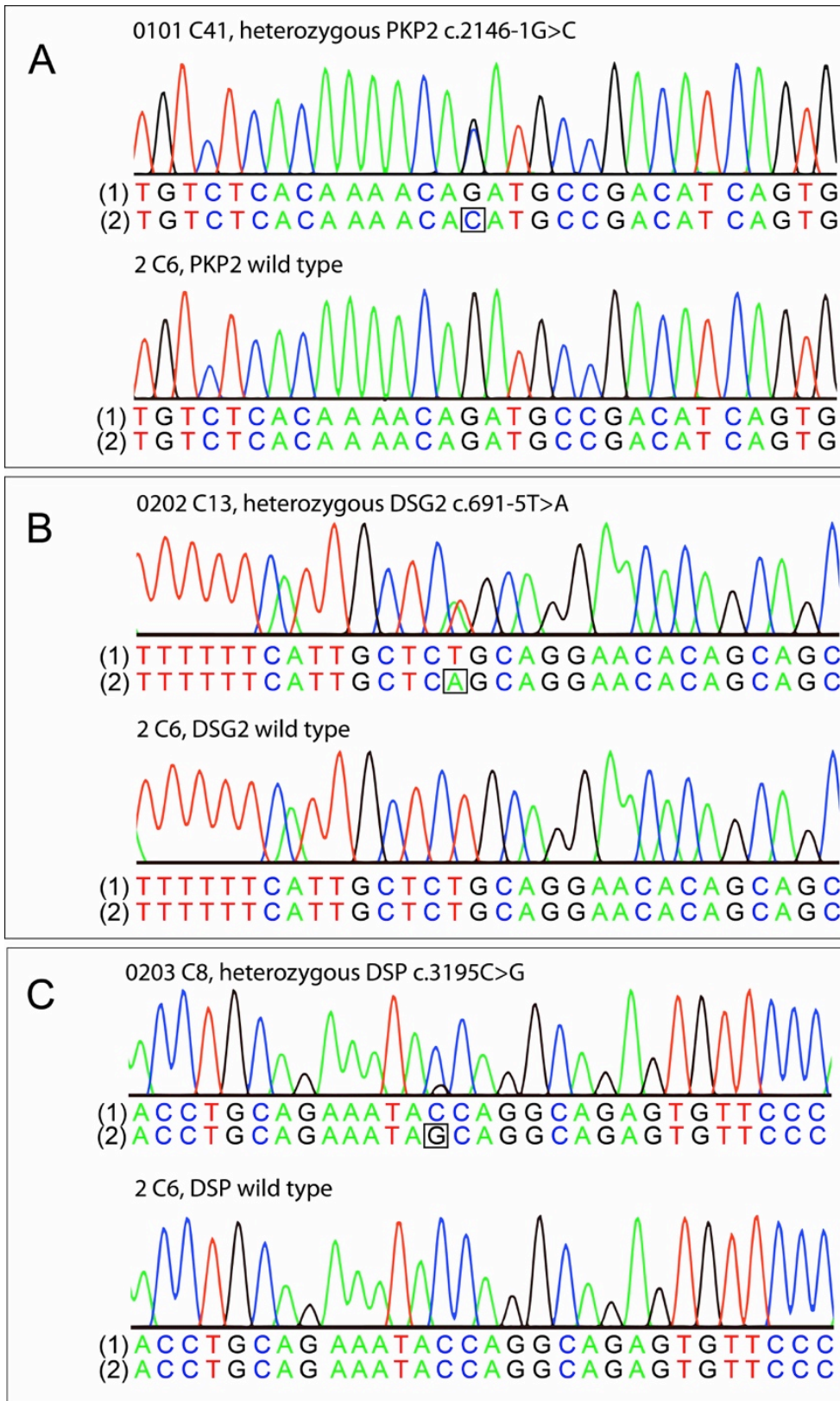


Figure 39 Chromatographs from Sanger sequencing experiments. Panels A-C demonstrate that in each ARVC/D iPSC clone carried the same ARVC/D associated mutation as the subject from which it was derived and that these mutations were absent in a control iPSC line (2-C6).

4.3.8 T-cell receptor gene re-arrangement

T-cell receptors may consist of either α and β chains or γ and δ chains. Each T-cell expresses a single T-cell receptor type and is thereby classified as a $\alpha\beta$ T-cell or a $\gamma\delta$ T-cell. In the peripheral blood 85-99% of T-cells are of the $\alpha\beta$ type (Eberl *et al.*, 2003). The α , β , γ and δ chains are encoded by the T-cell receptor α (*TRA*) T-cell receptor β (*TRB*), T-cell receptor δ (*TRD*) and T-cell receptor γ (*TRG*) genes respectively. These genes contain multiple exons that may encode the variable (V), diversity (D) and joining (J) regions of the chains. During the maturation of a T-cell these genes undergo rearrangement in which segments of genomic DNA are spliced out and three VDJ regions are made contiguous. The multiple possible combinations of VDJ exons and in splice sites within them produce the highly variable protein sequences encoding the antigen-binding site of the T-cell receptor.

In developing T-cells the re-arrangement events leading to T-cell receptor expression follow an ordered sequence. Re-arrangement of *TRB*, *TRD* and *TRG* occur first and almost simultaneously. Re-arrangement of *TRA* is thought to occur after a T-cell has committed to the $\alpha\beta$ lineage, and should therefore be absent in $\gamma\delta$ T-cells (Mahe *et al.*, 2017).

The identity of T-cells can be inferred from the presence or absence of gene re-arrangements. An absence of *TRA* or *TRB* re-arrangement is indicative of $\gamma\delta$ T-cells and conversely the absence of *TRG* re-arrangement indicates $\alpha\beta$ T-cells⁹. Both $\alpha\beta$ and $\gamma\delta$ T-cells may contain rearrangements in *TRB* and *TRG*. In this situation only one of the rearrangements will be productive in terms of a translatable protein. The multiplex PCR assay used in this study does not assess the productivity of rearrangements. However, unsuccessful *TRB* re-arrangements are reported to be rare and therefore cells with both *TRG* and *TRB* rearrangements are most likely to be $\alpha\beta$ T-cells (Joachims *et al.*, 2006).

All six clones from subject 2 were assessed for rearrangements in the T-cell receptor β gene (*TRB*) and the T-cell receptor γ gene (*TRG*). Rearrangements were detected in all three clones derived using the T-cell protocol (2-C2, 2-C3 and 2-C7). No rearrangements were identified in the clones derived using the non-T-cell protocol (2-C1, 2-C4 and 2-C6) (see appendix Table 69 and Figure 84 for full details of results).

⁹ *TRD* is always absent in $\alpha\beta$ T-cells, since it lies within *TRA* and is therefore spliced out during *TRA* rearrangement.

The SNP microarray identified a complete loss of SNPs in a region predicted to be 400kb long on 14q11.2 in all three clones derived using the T-cell protocol (2-C2, 2-C3 and 2-C7). This region includes the variable regions of *TRA* and the entirety of *TRD* (Appendix Figure 83). The finding indicates that *TRA* re-arrangement was present and that these cell lines originated from $\alpha\beta$ T-cells, since they could not be from $\gamma\delta$ T-cells if the *TRD* genes had been completely deleted. No such deletions were detected in any clones derived using the non-T-cell protocol (2-C1, 2-C4 and 2-C6). No copy number variations (CNVs) were detected in this region in the three ARVC/D clones assessed by SNP microarray (0101-C41, 0202-C13 and 0203-C8). It is therefore reasonable to conclude that these clones did not originate from $\alpha\beta$ T-cells. The probability that these cells originated from $\gamma\delta$ T-cells is low since $\gamma\delta$ T-cells are infrequent in the peripheral blood (~ 7% of all lymphocytes in peripheral blood and therefore <7% of PBMCs) and the pre-transduction culture conditions used in ARVC/D lines did not favour T-cell reprogramming (Mitogawa *et al.*, 1992)¹⁰. Analysis of these clones by multiplex PCR would be necessary for confirmation.

Overall the results of the T-cell receptor gene rearrangement assay and the microarray data support two hypotheses. Firstly that use of the T-cell reprogramming protocol with a population of CD3+ PBMCs is effective in generating iPSC lines from $\alpha\beta$ T-cells. Secondly that use of the non-T-cell reprogramming protocol in an unselected PBMC population is effective in generating iPSCs from non-T-cells and has a low (less than one in six) probability of generating iPSCs from T-cells.

4.3.9 Genomic copy number variations

All PBMC samples, the six clones from subject 2 and one clone each from the three ARVC/D subjects were screened for copy number variations (CNVs) using a single nucleotide polymorphism (SNP) microarray (see methods). Summaries of the quality control indices from the analysis of each sample, of all the CNVs detected and of the genes affected by the pathogenic CNVs are given in the appendix (Tables 65 to 66 and Figures 79 to 82).

No pathogenic CNVs, or CNVs of unknown significance were detected in any of the PBMC samples. Two of the non-T cell derived clones from subject 2 (2-C4 and 2-C1) were found to have acquired regions in which there was a gain in copy number suggestive of a duplication (appendix Figures 79 to 82, Table 66) (Table 51) (Figure

¹⁰ The absence of CNVs in the regions of TRD, TRB or TRG in these clones does not exclude the possibility of there being re-arrangements in these genes since the microarray was not sufficiently sensitive to detect the rearrangements of *TRB* in 2-C3 and 2-C7, or of *TRG* in 2-C2 and 2-C7 detected by multiplex PCR. Similarly there is no information regarding its sensitivity in detecting re-arrangements in *TRD*.

40). For the single CNV identified in 2-C4 and one of the CNVs in 2-C1 there were clinical reports of subjects with duplications of the same region who manifested multiple congenital abnormalities (Sharma *et al.*, 2014) (Schinzel *et al.*, 1981) (Avila *et al.*, 2013). This provides evidence that although these CNVs are associated with developmental abnormalities they do not compromise pluripotency since this would be expected to result in embryonic lethality. No inference of this type could be made with respect to the other two duplications identified in 2-C1.

The gain in copy number at 20q11 found in 2-C4 has been reported in >20% of hESC lines and 18% of hiPSC lines (International Stem Cell Initiative *et al.*, 2011) (Martins-Taylor *et al.*, 2011). Its prevalence has been attributed to the presence of *BCL2L1* in this region. *BCL2L1* down regulates apoptosis and its upregulation by a gain in copy number is reported to increase cell survival (Avery *et al.*, 2013). After the initial mutation it is hypothesised that this provides cells carrying the CNV with a selective advantage in maintenance culture resulting in them becoming the most abundant cell type within a culture (Lefort *et al.*, 2008).

The reported incidence of cytogenetic abnormalities varies depending on the method of analysis. When screened by karyotyping a prevalence of 12% has been reported (Taapken *et al.*, 2011). By contrast studies using high resolution SNP arrays have detected at least one CNV the majority of iPSC lines with a increase incidence at higher passage numbers (Laurent *et al.*, 2011). In this context the prevalence of CNVs detected in this study is relatively low. This may be explained by the lower resolution of array used in this study. In addition although the quality control indices for the array data were within acceptable limits they were not optimal, indicating some noise in the data (Appendix Table 66). Both of these factors could have reduced the sensitivity of the assay to detect small CNVs and those present at low levels of mosaicism.

The use of multiple non-T-cell clones was to be important in the assessment of cardiac differentiation protocols in subsequent work, particularly in determining whether there was any difference in the differentiation potential of T-cell and non-T-cell derived iPSCs. Since there were no other non-T-cell clones available it was decided to complete the characterisation of either 2-C1 or 2-C4 despite the CNVs. If the selected clone was found to be pluripotent it would be considered for use in cardiac differentiation experiments.

The CNVs in 2-C1 and 2-C4 did not include any pluripotency marker genes, desmosomal genes or genes associated with intercellular adhesion in cardiomyocytes. Clinical reports of the 20q11 duplication found in 2-C4 described subjects as having a normal cardiac phenotype suggesting no effect on cardiac differentiation potential (Avila *et al.*, 2013). By contrast cardiac malformations were reported in subjects with a 22q11 duplication similar to that found in 2-C1. On this basis 2-C4 was selected for further characterisation.

Since only two non-T-cell derived clones from subject 2 were fully characterised (2-C4 and 2-C6), statistical comparisons between T-cell derived and non-T-cell derived clones were not possible. Given this limitation and the resource intensive nature of iPSC characterisation it was decided that the value of characterisation of all three T-cell clones was limited. Two T-cell derived iPSC clones (2-C3 and 2-C7) were selected at random for full characterisation.

Sample	Predicted location of CNV		Size of CNV (bp)	Copy number gain or loss	Related clinical phenotype
	Cytogenetic	GRCh37/h19			
2-C1	4q34.3 - 4q35.1	4:181,008,167-183,628,586	2,620,420	Gain	None
	7q36.1	7:150,327,024-151,893,675	1,566,652	Gain	None
	22q11.1 - 22q11.21	22:16,079,545-18,908,641	2,829,097	Gain	Cat eye syndrome (Schinzel <i>et al.</i> , 1981) (OMIM 115470)
2-C4	20p11.1 - 20q11.21	20:26,158,741-31,042,348	4,883,608	Gain	20q11 duplication syndrome (Avila <i>et al.</i> , 2013)

Table 51 Pathogenic CNVs acquired by iPSC clones during reprogramming.

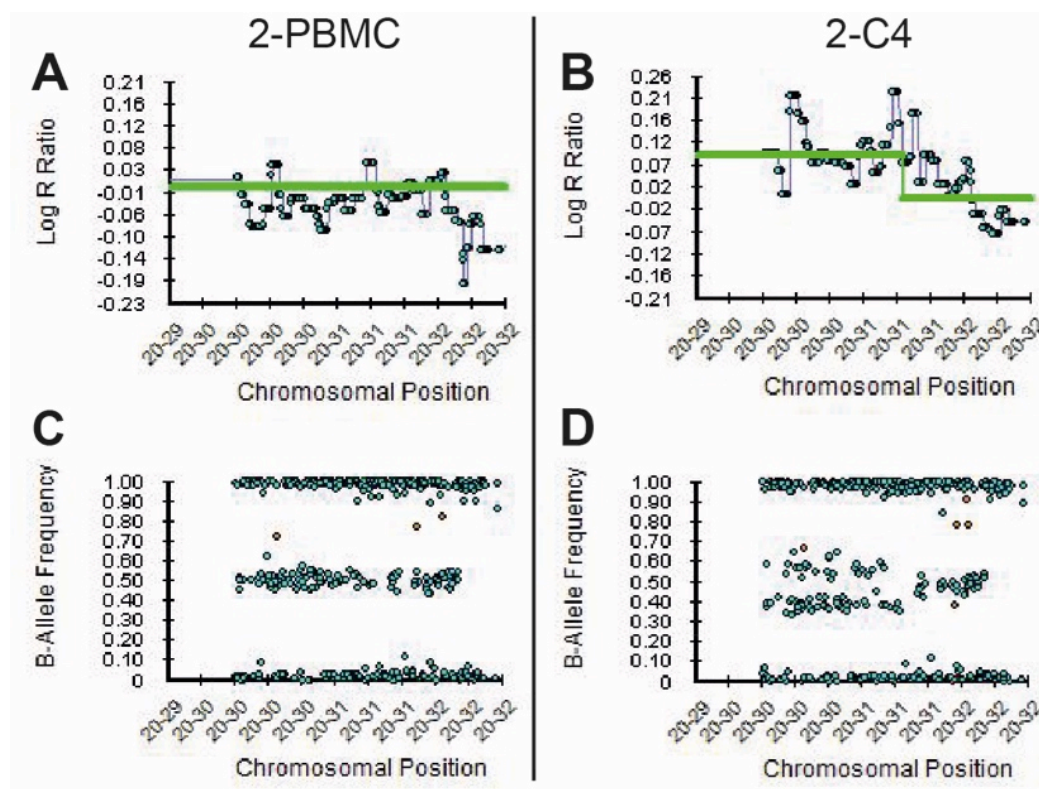


Figure 40 Representative example of a CNV detected by analysis of SNP microarray.

Panels B and D illustrate a pathogenic CNV predicted to be at 20p11.1-20q11.21 in the iPSC line 2-C4. Panels A and C illustrate the corresponding data from PBMCs from subject 2. X-axis ticks indicate approximate positions within GRCh37/h19 e.g. “20-30” indicates the approximate position 30,000,000 in chromosome 20. Data from valid SNP calls are displayed as blue dots, no-calls are displayed as orange dots. The average Log R ratio is indicated by a green line, this is at zero in regions the BlueFuse Multi algorithm considers structurally normal. CNVs are indicated by a step change in this line, with the degree of deviation indicating the median Log R ratio across the CNV. The localised increase in log R ratio (B) and pattern of B-allele frequency (BAF) values (D) in the same region suggest an increase in copy number of this region in 2-C4. The absence of these patterns in the PBMCs (A)(C) support the hypothesis that this CNV was acquired during generation of the clonal line.

4.3.10 Sendai vector elimination

All clones were tested for the persistence of Sendai vector RNA by RT-PCR (see methods). Any adherent colonies that remained in the initial MEF plate after picking clones for expansion were tested for the presence of Sendai vector by RT-PCR in samples. All samples were collected within 30 days of transduction. Evidence of Sendai vector was found in all samples (Figure 41). There was no evidence of Sendai vector in any clones at the passage numbers used for pluripotency assessments (Figure 41). These experiments provided evidence that the formation of

adherent expandable clones was associated with successful transduction with the reprogramming vectors.

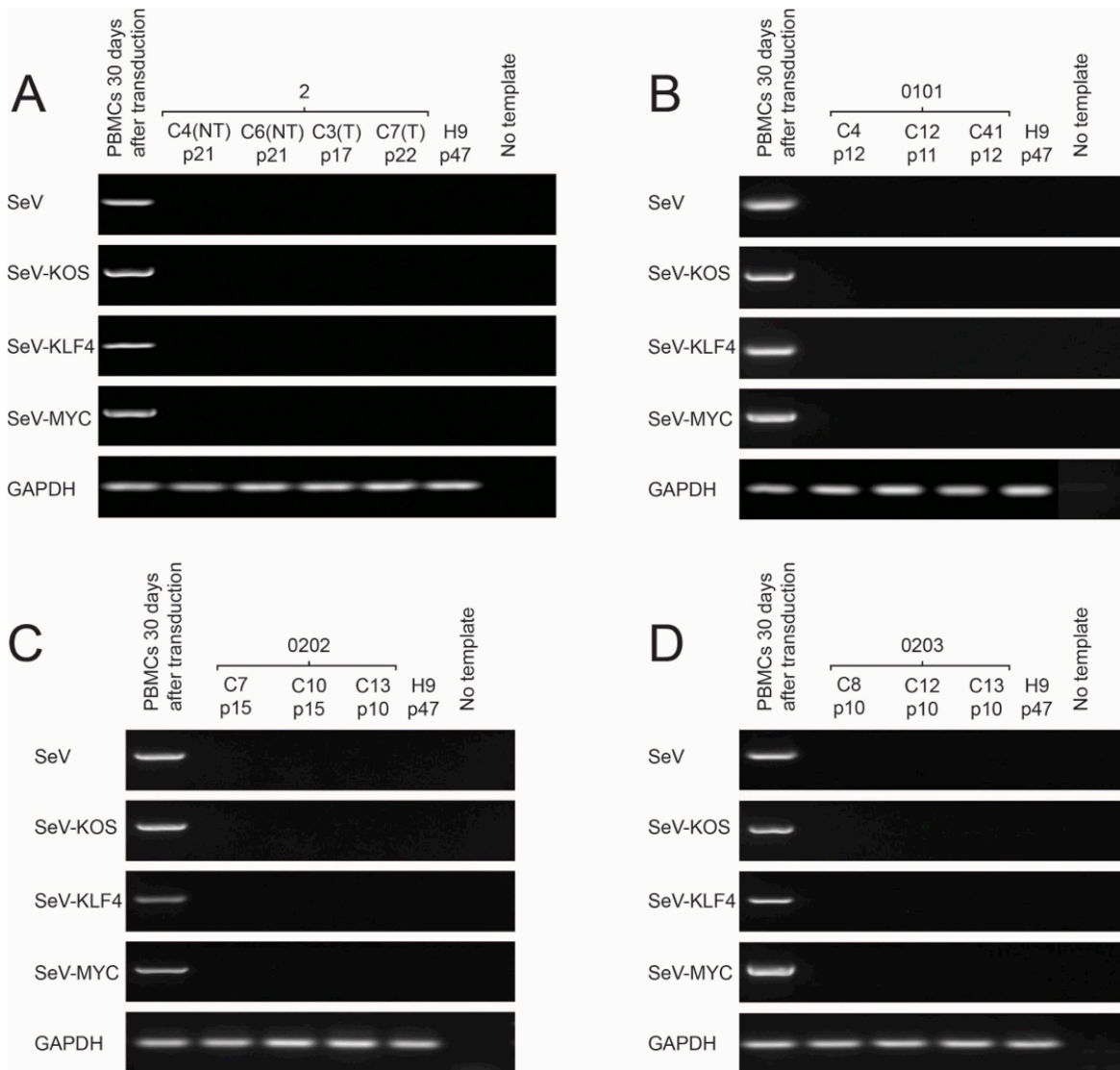


Figure 41 Screening for the persistence of Sendai reprogramming vectors in iPSC clones by RT-PCR.

Cropped images of gels showing the regions in which PCR product of the expected size would be expected (ladder not shown). False positive results due to reagent contamination with cDNA are excluded by the absence of signal in the no template sample. *GAPDH* serves as a positive control for the presence of template cDNA within the other samples tested. The absence of signal in the H9 samples indicates that the primers do not amplify components of a pluripotent cell's endogenous transcriptome. The signal from all three Sendai vectors (SeV) in the cells collected within 30 days of transduction indicate that transduction was successful. The absence of these signals in the iPSC clones indicates that the SeVs have been eliminated during the subsequent culture.

4.3.11 Colony and cell morphology

When viewed with phase contrast microscopy all expandable clones had morphological features that were similar to those of the reference pluripotent cell lines (H9 hESCs) and dissimilar to non-pluripotent fibroblasts (Figure 42).

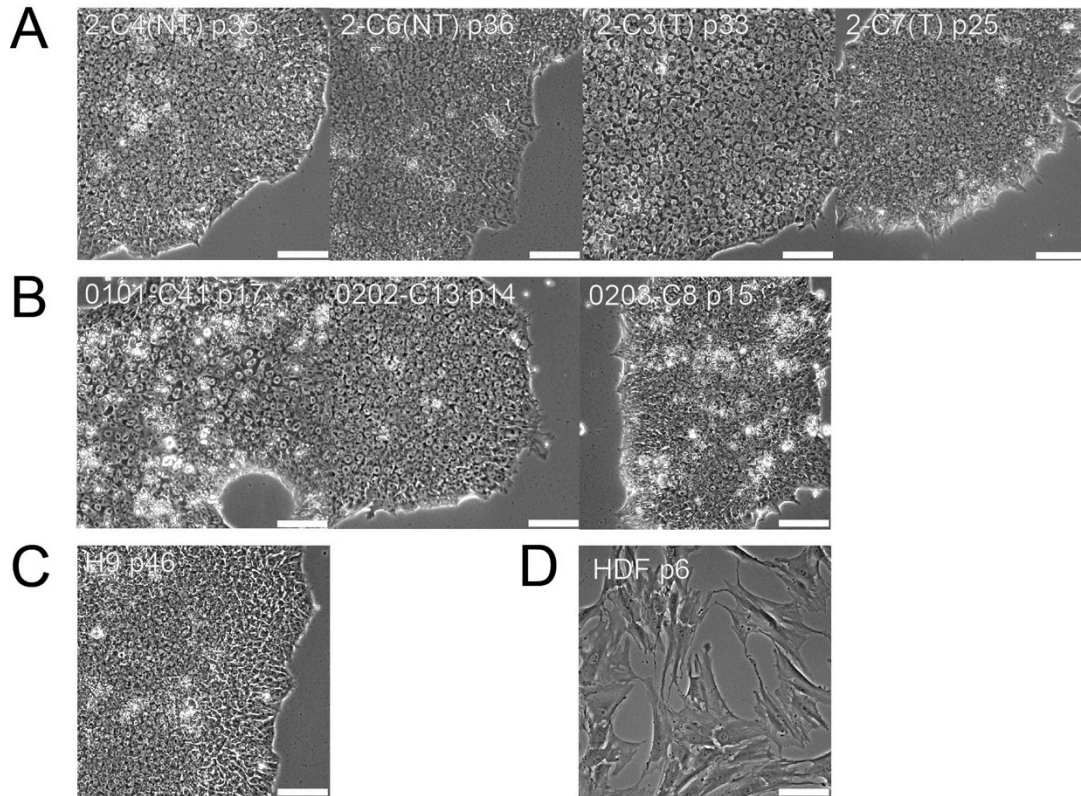


Figure 42 Phase contrast microscopy images of expandable clones and reference cell lines.

Expandable clones (panels A and B) and hESCs (panel C) formed similar flat, compact colonies, which expanded radially until becoming confluent and consisted of cells of approximately $10\mu\text{M}$ diameter with a high nuclear to cytoplasmic ratio (Figure 42). These were distinct from fibroblasts which formed sparse stellate cells with a large area of cytoplasmic (panel D). Scale bars illustrate $100\mu\text{m}$.

4.3.12 Pluripotency marker gene expression

Up-regulated *OCT4A* (Nichols *et al.*, 1998) (Matin *et al.*, 2004), *NANOG* (Chambers *et al.*, 2003) (Mitsui *et al.*, 2003) (Loh *et al.*, 2006) and *SOX2* (Avilion *et al.*, 2003) (Fong *et al.*, 2008) expression have been established as critically important in the maintenance of pluripotency *in vitro*. Both the *KLF* and *MYC* families of transcription factors are up-regulated and essential to the maintenance of pluripotency in ESCs (Jiang *et al.*, 2008) (Varlakhanova *et al.*, 2010). *KLF4* and *MYC* are included in these families but are not independently critical due to functional redundancy within these groups (Nakatate *et al.*, 2006) (Jiang *et al.*, 2008) (Varlakhanova *et al.*, 2010) (Malynn *et al.*, 2000) (Davis *et al.*, 1993).

The expression of these genes was assessed by RT-qPCR in all clonal lines, an hESC line (H9) and in PBMC samples.

No significant differences were detected between the hESC line (H9) and individual clones for any of the genes assessed (Figure 43) (Table 52). This is consistent with the hypothesis that the clones were pluripotent. Since only one hESC line was tested it cannot be determined whether there is any difference in expression between clonal lines generated by our methodology and hESCs in general.

When comparing clonal lines to the non-pluripotent PBMCs there was evidence of higher levels of *NANOG*, *OCT4A* and *SOX2* expression in the clonal lines (Figure 44) (Table 53). This is consistent also with the hypothesis that the clonal lines are pluripotent.

KLF4 expression was higher in PBMCs relative to the clonal lines and no significant difference was detected in the level of *MYC* expression between the two cell types (Figure 44) (Table 53). These findings are consistent with previous reports describing the upregulation of *KLF4* and *MYC* expression in the most abundant PBMCs cell types relative to pluripotent cells. A meta-analysis of publicly available gene expression array data found *KLF4* expression was higher in monocytes and CD34+ progenitors cells than hESCs and found *MYC* expression to be similar between PBMCs and hESC lines (Mabbott *et al.*, 2013). Similar patterns have been described in reports of the generation of iPSCs from PBMCs (Brown *et al.*, 2010) (Loh *et al.*, 2009) (Seki *et al.*, 2010) (Chou *et al.*, 2011) (Kunisato *et al.*, 2011). The relative expression of *KLF4* and *MYC* in clonal lines and PBMCs identified in this study is consistent with the pluripotency of the clonal lines, but also illustrates that these genes have functions in addition to mediating pluripotency.

PBMC expression data represent the average expression across a population of mixed cell types. Therefore these expression levels reflect those in the most abundant PBMC types. There may have been populations of PBMCs within that sample in which all these genes were up-regulated but which were too scarce to influence the overall expression levels. Since each clone may be derived from any single cell within the PBMC sample these data cannot prove that the reprogramming process up-regulated these genes in a clone relative to its originating cell type.

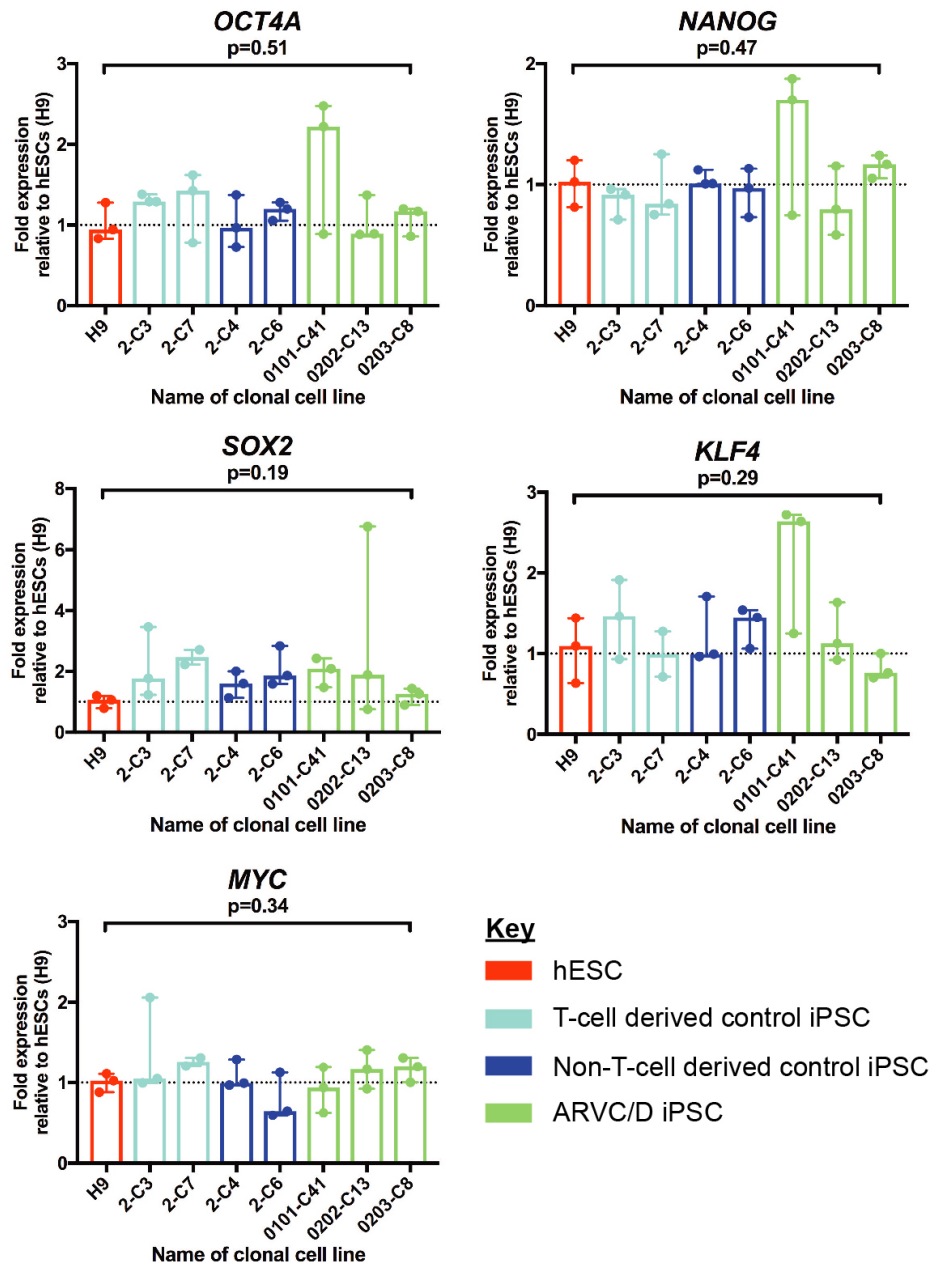


Figure 43 Comparison of expression of pluripotency associated genes between clonal cell lines (iPSCs) and an hESC line (H9) by qPCR.

Bar charts indicate the median and range of expression levels. The expression levels of these marker genes in hESCs in maintenance culture were considered to be indicative of those associated with pluripotency in general. Therefore expression in the clonal cell lines (iPSCs) and H9 hESCs is presented relative to the mean expression across the three passages of H9 hESCs assessed. For each clonal line gene expression was assessed in three samples each from a different passage. (Kruskal-Wallis) tests were used to look for significant ($p > 0.05$) differences between clones.

Cell type	Cell line	OCT4A	NANOG	SOX2	KLF4	MYC
hESC	H9	14.9±0.2	20.0±0.1	17.8±0.1	25.5±0.4	21.9±0.1
T-cell derived control iPSCs	2-C3	15.7±0.3	21.4±0.3	17.6±0.2	25.9±0.8	22.3±0.7
	2-C7	15.5±0.2	21.0±0.2	18.1±0.3	27.2±0.5	23.1±0.3
Non-T-cell derived control iPSCs	2-C4	15.3±0.2	20.3±0.2	17.5±0.3	25.6±0.5	22.1±0.4
	2-C6	15.6±0.1	21.0±0.2	17.7±0.1	26.1±0.1	23.2±0.2
ARVC/D iPSCs	0101-C41	15.5±0.4	20.9±0.4	17.8±0.0	25.4±0.5	23.0±0.0
	0202-C13	16.2±0.5	21.6±0.6	17.1±0.3	25.7±0.3	22.1±0.3
	0203-C8	15.3±0.0	20.2±0.1	17.9±0.0	26.1±0.3	22.0±0.1

Table 52 Unadjusted Ct values from the assessment of pluripotency associated genes in clonal cell lines (iPSCs) and an hESC line (H9) by qPCR
For each cell line the mean±SEM gene expression assessed in three samples each from a different passage are given.

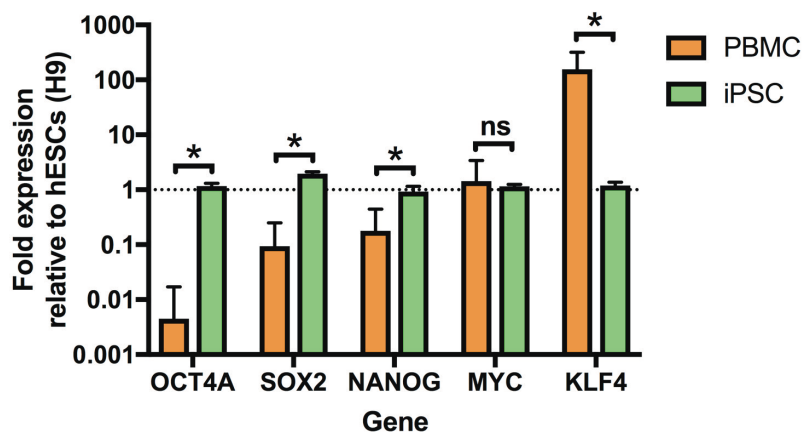


Figure 44 Expression of pluripotency associated genes in PBMCs and clonal lines (iPSCs)

Bar charts indicate median values, whiskers indicate 75th centile values. The expression levels of these marker genes in hESCs in maintenance culture were considered to be indicative of those associated with pluripotency in general. Therefore expression in the clonal cell lines (iPSCs) and H9 hESCs is presented relative to the mean expression across three passages of H9 hESCs. PBMC data were derived from six samples from unrelated subjects including the three ARVC/D subjects. Clonal line data were derived from seven lines, the three clones from different ARVC/D subjects and four clones from the control subject 2 (2-C3, 2-C7, 2-C4 and 2-C6). Gene expression for each clone was the mean of the expression in samples from three different passages. For each gene, a Mann-Whitney U test was used to look for differences between cell types. Exact significance p values < 0.05 are indicated by *.

Cell type	<i>OCT4A</i>	<i>SOX2</i>	<i>NANOG</i>	<i>MYC</i>	<i>KLF4</i>
PBMC	23.1±0.2	23.2±0.3	23.2±0.3	22.9±0.2	20.2±0.4
iPSC	15.6±0.3	17.6±0.2	21.0±0.4	22.6±0.2	26.0±0.3

Table 53 Unadjusted Ct values from the assessment of pluripotency associated genes in PBMCs and clonal lines (iPSCs)

The mean±SEM un adjusted Ct values are presented. PBMC data were derived from six samples from unrelated subjects including the three ARVC/D subjects. Clonal line data were derived from seven lines, the three clones from different ARVC/D subjects and four clones from the control subject 2 (2-C3, 2C7, 2-C4 and 2-C6).

4.3.13 Pluripotency marker protein expression

Evidence of the expression of *NANOG* and *OCT4* provided by RT-qPCR analysis is described in the previous section. The detection the proteins encoded by these genes was sought by flow cytometry and immunofluorescence microscopy.

In addition to the nuclear transcription factors, the expressions of two surface markers of pluripotency (SSEA4 and TRA-1-60) were sought by these modalities. Stage specific embryonic antigen 4 (SSEA4) is a carbohydrate epitope on a globo-series ganglioside found in the plasma-membrane (Kannagi *et al.*, 1983). TRA-1-60 is the carbohydrate epitope for a monoclonal antibody of the same name located on podocalyxin (Schopperle and DeWolf, 2007). Both molecules are expressed at high levels in ESCs, have decreased expression during differentiation and are considered pluripotency markers (Henderson *et al.*, 2002) (Draper *et al.*, 2002).

All expandable clones, an hESC line (H9) and fibroblasts (HDF) were assessed for the expression of *NANOG*, *OCT4*, TRA-1-60 and SSEA4 using flow cytometry. The average number of single cell events assessed per sample was 7993±1535 (mean±SD).

hESC samples were chosen as positive controls for the assay on the basis that they were a pluripotent cell line that would be expected to express the target proteins at high levels. For every pluripotency marker, the difference between the median fluorescence of labelled and unlabelled hESCs $>1.5 \times 10^3$ au (Appendix Table 72).

Fibroblasts were chosen as a negative control for the assay on the basis that they were a non-pluripotent cell line which would be expected to express the target proteins at low levels or not at all. For every pluripotency marker, the differences between the median fluorescence of labelled and unlabelled fibroblasts was $<0.5 \times 10^3$ au (Appendix Table 72).

In all clones and for every pluripotency marker, the difference between the median fluorescence of labelled and unlabelled samples was $>2.0 \times 10^3$ (Appendix Table 72). This supports the hypothesis that the iPSC clones express the four pluripotency markers and do so at a high level similar to that seen in hESCs.

In every iPSC clone assessed and for all four pluripotency makers, the proportion of single cell events classified as positive for the expression of a given protein was $\geq 93\%$ (Appendix Table 73). This suggests that the majority of cells the maintenance cultures were in an undifferentiated state.

The use of unlabelled cells rather than those labelled with an isotype antibody to define the threshold for classifying events as positive or negative for a given protein is a methodological limitation in this work. Non-specific binding by a pluripotency marker antibody could increase the fluorescence of an event above the threshold despite the absence of the target protein.

An estimate of the contribution of non-specific binding was made using isotype controls in a small number of samples ($n=3$). Because these samples were examined in a multicolour experiment, each isotype control sample was also labelled with the three pluripotency marker antibodies not under investigation. This is referred to as a fluorescence-minus-one (FMO) with an isotype control sample. The effect of using this FMO with an isotype control to classifying events as positive rather than unlabelled cells on the percentage of positive events was assessed. In the case of OCT4, TRA1-60 and SSEA4 the use of an FMO with an isotype control reduced the percentage of event classed as positive by $<2\%$. The reduction in the percentage of NANOG positive events was variable ranging from 2-13% (Appendix Table 74). These data suggest that the percentage of clonal cells expressing pluripotency markers is likely to have been over estimated in experiments without an FMO isotype control. Despite this overestimate the majority of clonal cells would be expected to be classified as expressing the pluripotency marker protein.

OCT4 and TRA-1-60 expression in iPSC lines was also assessed by immunofluorescence microscopy. The primary antibodies used in these experiments were identical to those used to assess these proteins in the flow cytometry experiments except for the lack of a conjugated fluorochrome. Signal was compared with an hESC line (H9) and human dermal fibroblasts (HDF) that acted as positive (pluripotent) and negative (non-pluripotent) controls respectively.

The highest intensity OCT4 signal in the hESCs (H9) positive control co-localised with DAPI (Appendix Figure 85). This suggests nuclear localisation and is consistent with its known function as a transcription factor.

The TRA-1-60 signal in the hESCs (H9) appeared as a cluster of adjacent polygons with the highest intensity signal at their borders and a lower intensity, diffuse signal internally (Appendix Figure 85). This is consistent with descriptions of TRA-1-60 as being located on the extracellular surface of the plasma membrane.

The fluorescence signals from the fibroblast (HDF) and secondary only negative controls were close to that of auto-fluorescence and showed no characteristic localisation (Appendix Figure 85).

In all clonal lines assessed the OCT4 and TRA-1-60 signal resembled that of the hESCs (H9) positive controls rather than the HDF negative controls (Figure 45) (Appendix Figure 85). This supports the hypothesis that the clonal lines express pluripotency associated proteins.

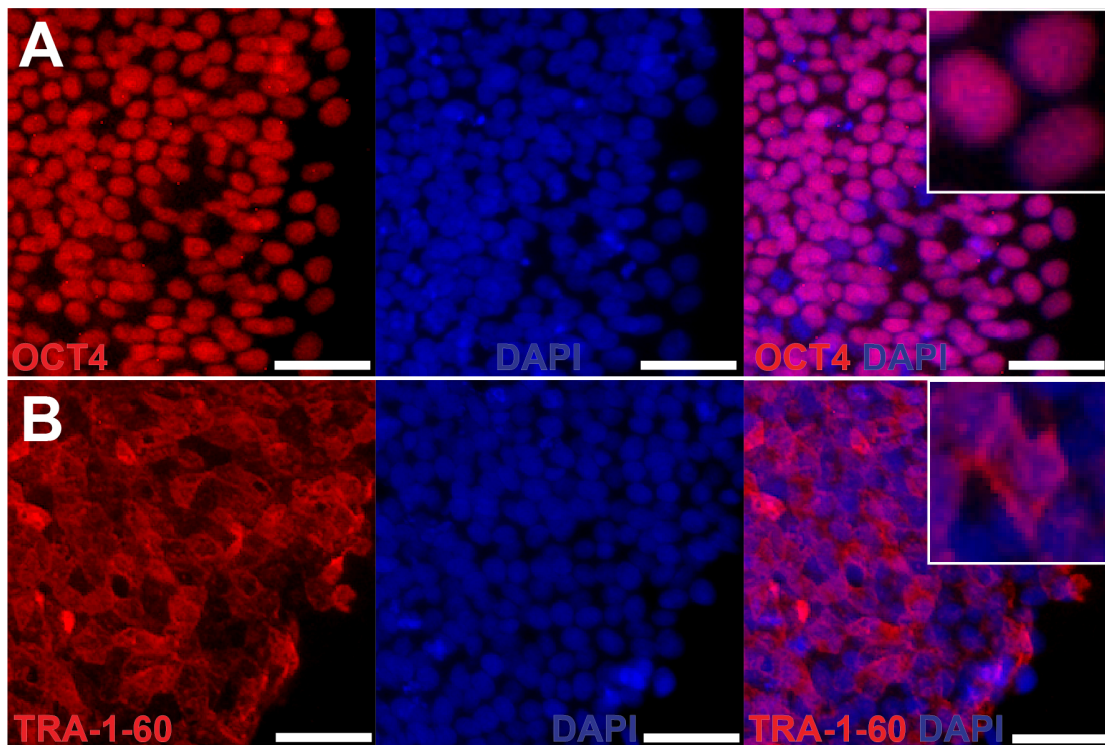


Figure 45 Immunofluorescence microscopy for OCT4 and TRA-1-60.

The panels show signal obtained from 2-C7(T) p27 and are representative of the signal seen in all other pluripotent cell lines assessed. Panel A shows OCT4 signal and its co-localisation with DAPI (see inset), consistent with a nuclear distribution. Panel B shows TRA-1-60 signal which is diffuse but with linear higher intensity regions (see inset), consistent with localisation to the plasma membrane. Scale bars illustrate 50 μ M.

4.3.14 Assessments of differentiation potential

The expression of pluripotency markers is not unique to pluripotent cells. The embryonal carcinoma cell line 2102Ep has been described as nullipotent despite expressing high levels of pluripotency markers (Josephson *et al.*, 2007). hESCs cultured to high passage numbers have reduced differentiation potential despite high levels of expression of pluripotency markers (Park *et al.*, 2008). Therefore although the expression of these markers is consistent with pluripotency, evidence of an expandable clone's capacity to differentiate to all three germ layers must be obtained before it may be considered pluripotent.

The differentiation potential of clonal lines were assessed using two methods. All clones were differentiated *in vitro* by embryoid body formation (Wobus *et al.*, 1984). The resultant tissues were assessed for protein markers of the three germ cell layers by immunofluorescence microscopy. A limited number of clones were assessed using *in vivo* differentiation by the teratoma formation assay (Wobus *et al.*, 1984) (Wesselschmidt, 2011). The resultant tissues were then assessed histologically for tissue architecture typical of tissues from the three germ cell layers.

4.3.15 Assessment of expression of the proteins indicating differentiation to the three primitive germ cell layers after spontaneous embryoid body differentiation.

Expandable clones were induced to differentiate by the formation of embryoid bodies and then cultured as adherent tissues in the presence of serum (see methods). Immunofluorescence microscopy of the resulting cultures was performed to identify expression of proteins specific to each of the three germ cell layers. The expression of β III tubulin (TUJ1) in neuron-like filamentous structures was considered a marker of neuro-ectoderm. The expression of smooth muscle actin (SMA) in a diffuse fibrillar pattern within polygonal and stellate structures was considered a marker of mesoderm. The expression of α -fetoprotein (AFP) in compact cuboidal cells was considered a marker of endoderm.

A characteristic pattern of expression of all three proteins was found in all of the seven clones that underwent full characterisation and use in cardiac differentiation experiments i.e. 2-C3, 2-C7, 2-C4, 2-C6, 0101-C41, 0202-C13 and 0203-C8 (Figure 46) (Table 54) (Appendix Figure 86).

Evidence of differentiation to all three germ cell layers was not obtained for some clones. Specifically no evidence of differentiation of 0202-C7, 0202-C10 and 0203-

C12 to neuro-ectoderm was obtained. There was also no evidence of the differentiation of 0203-C12 and 0203-C13 to endoderm.

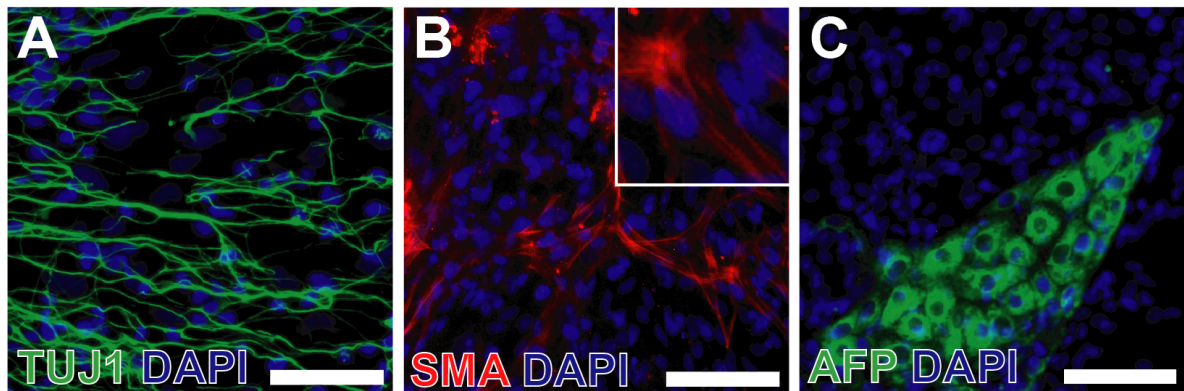


Figure 46 Immunofluorescence microscopy for germ-layer markers

The panels show signal obtained from 2-C3(T) and are representative of the positive signals seen in all other pluripotent cell lines. Panel A shows beta III tubulin (TUJ1) signal in a linear branching pattern consistent with the localisation of the protein to branching filamentous processes associated with neural (neuro-ectodermal) cells. Panel B shows a diffuse fibrillar (see inset) smooth muscle actin (SMA) signal suggesting stellate and polygonal cells typical of mesodermal smooth muscle cells. Panel C shows α -fetoprotein (AFP) signal in compact cells typical of endodermal hepatic progenitors. Scale bars indicate 100 μ m.

Subject	Clones	Neuro-ectoderm (TUJ1)	Mesoderm (SMA)	Endoderm (AFP)
2	C1	✓	✓	✓
	C4	✓	✓	✓
	C6	✓	✓	✓
	C2	✓	✓	✓
	C3	✓	✓	✓
	C7	✓	✓	✓
0101	C4	✓	✓	✓
	C12	✓	✓	✓
	C41	✓	✓	✓
0202	C7	✗	✓	✓
	C10	✗	✓	✓
	C13	✓	✓	✓
0203	C8	✓	✓	✓
	C12	✗	✓	✗
	C13	✓	✓	✗

Table 54 Summary of immunofluorescence microscopy for the three primitive germ cell layers

iPSCs were allowed to differentiate in the presence of serum and were assessed for the expression of proteins indicative of each of the three germ cell layers by immunofluorescence microscopy. Target protein signal identified (✓). No evidence of target protein (✗).

4.3.16 Teratoma assay

The differentiation potential of 2-C6 and 2-C3 were assessed by teratoma assay. 2-C6 produced tumours with a typical teratoma histology. 2-C3 produced cystic tumours with some differentiated tissues but no typical teratoma histology.

The generation of teratomas by 2-C6 is consistent with the line being pluripotent. The protocol used in this work has been reported to yield teratomas in 80-100% of mice injected with hESC lines (Gropp *et al.*, 2012) (Prokhorova *et al.*, 2009) (Hentze *et al.*, 2009). In this context the absence of teratoma in the tumours generate from 2-C3 suggests that this line is not pluripotent. This is inconsistent with the results of *in vitro* differentiation experiments in which there was evidence that 2-C3 could differentiate to all three germ layers.

There are several possible explanations for these apparently conflicting results. There is evidence that cultures of pluripotent cell lines have sub-populations with methodology specific differentiation capacities. It has been reported that for a single culture the subpopulations responsible for teratoma generation are distinct from those that generate the three germ layers by *in vitro* differentiation (Stewart *et al.*, 2010). It may be that 2-C3 contains a sub-population capable of *in vitro* differentiation but lacks a sub-population able to form teratomas.

Alternatively teratoma tissue could have been present but undetected if it was localised and not sampled in the sections examined. It is possible that an error could have occurred in the handling of the 2-C3 sample leading to the injection of non-pluripotent cells. Due to the high cost of the assay in labour and materials it was decided not to investigate these possibilities by repeating the assay for 2-C3. Instead it must be concluded that evidence for the pluripotency of 2-C3 is not as strong as for other clonal lines.

4.4 Discussion

In its strictest sense pluripotency is defined as the ability of a cell to give rise to any cell within a mature organism (Daley *et al.*, 2009). A less demanding and more widely used definition requires only the capacity to differentiate to cell types from each of the three germ layers. Cells classified as pluripotent by the second definition may lack the capacity to differentiate to the cell types found in mature organisms and may be restricted in their potential cell fates.

The most stringent experimental tests of pluripotency for a cultured cell line are the tetraploid complementation assay and to a lesser degree, chimera formation (Nagy *et*

al., 1990) (Boland *et al.*, 2009) (Kang *et al.*, 2009). Human cell lines cannot be tested in these ways due to both legal and practical constraints. This essentially precludes the classification of human cell lines as pluripotent according to the strictest definition of the term.

Experimental evidence of pluripotency according the second definition may be obtained by the identification of cells from the three germ layers in tissue generated by the differentiation of cells *in vitro* or as part of a teratoma assay (Singh *et al.*, 2016).

Only two clonal lines were assessed by teratoma assay in this study due to the time and resource intensive nature of the test. The assay provided evidence of pluripotency in only one of these clones, the non-T-cell derived 2-C6. This provided evidence that the non-T-cell protocol was capable of generating iPSCs meeting the most stringent criteria available for the assessment of human cell lines.

In vitro differentiation followed by immunofluorescence microscopy to identify expression of a single protein markers per germ layer was the principle method of assessing differentiation capacity in this study. All the clonal lines selected for cardiac differentiation showed evidence of pluripotency using this assay. The combination of these results with the expression of pluripotency markers in an undifferentiated state was the basis upon which they were classified as pluripotent and therefore iPSCs. Pluripotent cells exhibit considerable heterogeneity in their differentiation potential. Cell lines may exhibit a greater or lesser resistance to leave the pluripotent state and have a tendency to differentiate towards some cell fates over others (Osafune *et al.*, 2008) (Park *et al.*, 2008) (Hu *et al.*, 2010). The mechanisms regulating this phenomenon are not well understood.

The assessment and manipulation of heterogeneity in differentiation potential is important to the study of embryonic development and for studies using pluripotent cells as a substrate for tissue generation i.e. for disease modelling or regenerative medicine. One approach to this issue has been to examine global gene expression patterns of pluripotent cells in maintenance culture. The Pluri-test assay uses this approach and quantifies the predicted pluripotency of a cell line relative to a pluripotent reference as a pluripotency score and a novelty score indicating the degree of pluripotency associated gene expression and the degree of divergence in the pattern of expression from reference pluripotent lines respectively (Müller *et al.*,

2011). Pluripotent lines are defined as having a high pluripotency score and a low novelty score.

An alternative approach is the quantitative assessment of tissues generated when PSCs differentiate. Attempts to quantify the abundance of tissue and cell type by microscopy are labour intensive and difficult to scale to the high throughput applications. Multi-gene assays allow a quantitative assessment of a large number of germ layer markers from a relatively small amount of tissue, within a relatively short time frame and are easily scalable. The TeratoScore and hPSC ScoreCard are examples of this type of assay (Avior *et al.*, 2015) (Tsankov *et al.*, 2015). The TeratoScore summarises gene expression within tumours produced by the teratoma assay protocol, into a single value that reflects the probability that a histological analysis would find all three germ layers to be present within that tissue. The hPSC ScoreCard assesses the products of *in vitro* differentiation experiments produces values reflecting the abundance of each of the three germ layers relative to undifferentiated tissues.

All of these gene expression based techniques would have enhanced the characterisation of iPSCs generated in this study. The PluriTest assay would allow the comparison of gene expression in the iPSC lines with the 223 hESC and 41 iPSC lines making up the pluripotent reference for the assay as opposed to the single hESC line used in the RT-qPCR analyses in this study. The TeratoScore could have helped to determine whether the absence of teratoma histology in 2-C3 derived tumours reflected a lack of the tissue in the tumour or an error in sampling and analysis of the tissue. The hPSC ScoreCard would have provided more robust evidence of differentiation to the 3 germ cell layers than the single markers assessed by immunofluorescence microscopy. It may also have allowed the screening of clones for those with the greatest tendency to mesodermal differentiation and therefore a higher probability of efficient cardiac differentiation.

4.5 Conclusions

This study has demonstrated the generation of clonal cell lines from the PBMCs of a control subject and three subjects with ARVC/D. These clonal line have been shown to meet the criteria established by the study to be defined as pluripotent and therefore as iPSCs.

Both of the reprogramming protocols tested by this study have been demonstrated to be effective in generating iPSCs. The T-cell reprogramming protocol was shown to

be effective in generating iPSC lines from $\alpha\beta$ T-cells when applied to CD3+ PBMCs. Use of the non-T-cell reprogramming protocol was shown to be effective in generating iPSCs from an un-selected PBMC population and there is evidence that it is successful in promoting the reprogramming of non-T-cells in preference to T-cells.

Further assessments of these clones by techniques such as the PluriTest, hPSC ScoreCard and TeratoScore would be valuable in further characterising their pluripotency and should be considered in the assessment of any further cell lines generated using the protocols described in this study.

Chapter 5. The Derivation Of Cardiomyocytes From Blood Derived iPSCs And Their Characterisation.

5.1 Introduction

This chapter will discuss the generation of cardiomyocytes from iPSCs. The principles of generating iPSC derived cardiomyocytes (iPSC-CMs) are outlined in Chapter 1 and details of the differentiation protocols are given in Chapter 2.

The first part of this chapter will describe the testing of two types of cardiac differentiation protocols. The first type of protocol involved embryoid body formation (EB) and the differentiation of iPSCs in suspension culture. The second type of protocol differentiated iPSCs as an adherent monolayer. All the protocols tested were based on those described in previous reports (Kattman *et al.*, 2011) (Lian *et al.*, 2013a). The two EB protocols tested in this study were based on the methodology described by Kattman *et al.*, but differed in several respects (Kattman *et al.*, 2011). Kattman *et al.* used iPSCs co-cultured with mouse embryonic fibroblasts (MEFs) from which EBs were formed by enzymatic digestion of adherent colonies into multi-cellular fragments. Both the EB protocols in the present study used iPSCs cultured with mTeSR1 and Matrigel. One of the EB protocols used in this study used the same approach to EB formation as Kattman *et al.*, the other involved the formation of EBs by forced aggregation of a single cell suspension. The monolayer protocol used in this work was unchanged from the methodology described by Lian *et al.* (Lian *et al.*, 2013a). The goal of the work described in the first part of this chapter was to determine if these protocols could generate contracting cultures and to select one protocol for subsequent experiments.

The second part of the chapter will describe the characterisation of contracting cultures from multiple iPSC lines using the protocol selected in the first part of the chapter. The goal of these experiments was to determine if these cultures contained functional iPSC-CMs as defined by patterns of gene and protein expression, ultrastructural features and electrophysiological characteristics that are analogous to *in vivo* cardiomyocytes.

The third part of the chapter will describe attempts to generate contracting cultures that contain $\geq 75\%$ iPSC-CMs and to obtain RNA samples that are suitable for analysis by RT-qPCR from samples of this type¹¹. Two protocols for generating

¹¹ The hypotheses regarding desmosomal gene expression investigated in subsequent chapters were specific to iPSC-CMs therefore a consistent and high proportion of iPSC-CMs was necessary in samples to be used for these analyses. The target of

samples of this type were tested, both of which have been reported previously (Dubois *et al.*, 2011) (Tohyama *et al.*, 2013). The first protocol used fluorescence activated cell sorting (FACS) to select iPSC-CMs from a cell suspension on the basis of the expression of the cell surface protein, signal regulatory protein α (SIRPA) (Dubois *et al.*, 2011). The second protocol involved the exposure of contracting cultures to medium containing no glucose with the intention of inducing the death of non-cardiomyocytes and leaving viable iPSC-CMs (Tohyama *et al.*, 2013). The goal of the work described in this part of the chapter was to select one of these protocols and to generate samples suitable for later analysis from multiple cell lines.

5.2 Aims and hypotheses

It was hypothesised that iPSC-CM could be generated from iPSCs using a protocol based on previously published methodologies. Successful differentiation was expected to result in:

- Spontaneously contracting cultures in which intracellular calcium transients could be detected in association with these contractions.
- The downregulation of pluripotency associated gene expression in contracting cultures relative to iPSCs.
- The upregulation of genes encoding cardiac sarcomeric proteins in contracting culture relative to iPSCs.
- The expression of cardiac sarcomeric proteins in contracting cultures and the organisation of these proteins into striated myofibrils that have ultrastructural features similar to those observed in myocardial tissue.

It was also hypothesised that the cell populations containing $\geq 75\%$ iPSC-CMs could be obtained consistently using a combination of this protocol and a protocol for the purification of iPSC-CMs from contracting cultures.

5.3 Results

The first differentiation experiments performed were to test the EB cardiac differentiation protocol. This work was conducted before PBMC derived iPSCs had been fully characterised. An hESC line (H9) and an iPSC line (SBNeo1-C3) that was generated outside this study were used in these experiments.

$\geq 75\%$ cardiomyocytes was chosen as it was predicted to be achievable in the majority of experiments using a combination of differentiation and purification protocols.

5.3.1 Embryoid body differentiation

Two of the EB protocols (referred to as EB protocol A and EB protocol B) were tested. These protocols differed in the technique used for form EBs.

EB protocol A involved the enzymatic digestion of iPSC cultures to form fragments of approximately 500µm diameter. Fragments were then cultured in suspension culture for seven days to encourage EB formation. Duplicate experiments, each using approximately 2×10^6 cells were conducted with SBNeo1-C3. The majority of EBs generated with these experiments disintegrated into debris during the initial seven days of suspension culture and those that survived did not generate adherent cultures (Figure 47 A).

EB protocol B involved the enzymatic digestion of iPSC cultures to produce a single cell suspension from which EBs were formed by forced aggregation in a micro-well plate (Aggrewell 400Ex, Stem cell technologies). EBs were cultured in suspension in the same manner as in EB protocol A. Duplicate experiments, each using 1.4×10^6 cells, aggregated in 4,700 microwells to produce EBs of approximately 300 cells each, were conducted with SBNeo1-C3 and H9. Once again the SBNeo3-C3 iPSC derived EBs fragmented and did not survive suspension culture (Figure 47 B). H9 hESC EB survived suspension culture in both experiments and successfully adhered to gelatin coated plates (Figure 47 C). In one of these two experiments spontaneous contractions were identified.

5.3.2 Monolayer differentiation

The monolayer protocol was tested in both SBNeo1-C3 and H9. Each line was tested in five independent experiments with each experiment using cells from a different passage. Each experiment was conducted in one or two 12 well plates that were estimated to contain $12-24 \times 10^6$ iPSCs at the start of differentiation. Contracting cultures were observed in multiple wells in one (20%) of the five experiments using SBNeo1-C3 and in two (40%) of the five experiments using H9.

5.3.3 The selection of a protocol for further work

The monolayer protocol was selected for subsequent experiments since it resulted in contracting cultures from both cell lines tested, whereas the EB protocols had only yielded contracting cultures from H9 hESCs.

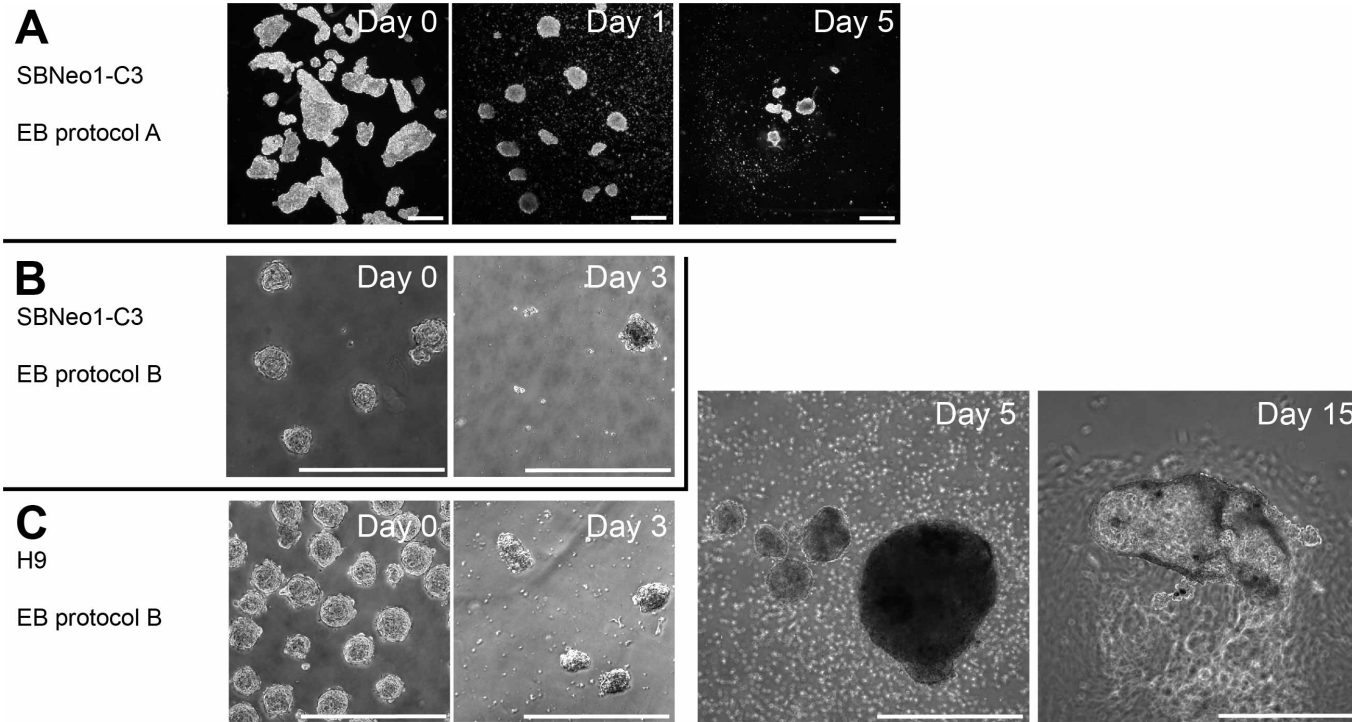


Figure 47 Phase contrast microscopy images of EBs in suspension culture during cardiac differentiation protocol

Panels in row A are representative of the appearance of EBs during differentiation of SBNeo1-C3. Fragments generated by enzymatic digestion of adherent cultures are shown on the day 0 image. The formation of EBs that decrease in size over the duration of suspension culture and the accompanying cellular debris resulting from the degeneration of EB are shown in the images from days 1 and 5. Panels in row B and C are representative of the appearance of EBs during the AggreWell differentiation protocol. EBs of similar size were seen on days 0 and 3. On day 5 larger EBs were observed in the H9 experiment, which subsequently yielded adherent contracting cultures by day 15. Scale bars illustrate 500 μ m.

5.3.4 Characterisation of contracting cultures generated by monolayer differentiation

The extent to which contracting cultures were characterised varied between cell lines (Table 55).

		Spontaneous contraction		Sarcomeric and pluripotency related gene expression	Sarcomeric protein expression		Sarcomeric ultrastructure
Subject / Line	Clone	Phase contrast microscopy	Calcium transient imaging	RT-qPCR	Flow cytometry	Immuno-fluorescence microscopy	TEM
2	C3	✓		✓	✓	✓	✓
	C7	✓		✓	✓	✓	✓
	C4	✓		✓	✓	✓	✓
	C6	✓	✓	✓	✓	✓	✓
0101	C41	✓			✓	✓	✓
0202	C12	✓		✓	✓	✓	✓
0203	C8	✓	✓	✓	✓	✓	✓

Table 55 Summary of the characterisation of contracting cultures performed in different cell lines.

Cell lines assessed by a specific modality are indicated (✓), the results of these assessments are described in subsequent sections.

5.3.5 Spontaneous contractions

Spontaneous contractions were identified and recorded by bright-field microscopy. Regions of spontaneously contracting cells were detected within 15 days of the start of differentiation in cultures from all cell lines.

The frequency with which individual experiments resulted in spontaneously contracting cultures is an indication of the efficacy of the protocol. Over the entire duration of the study, and across all cell lines, 97 monolayer differentiation experiments were initiated. Spontaneously contracting cultures were generated by 61 (63%) of these experiments. The proportion of experiments using 0101-C41 that yielded contracting cultures was significantly lower than other cell lines (Fishers exact test $p < 0.05$). The mean proportion of experiments yielding contracting cultures for per cell line was 67% (SD 6) (Figure 48).

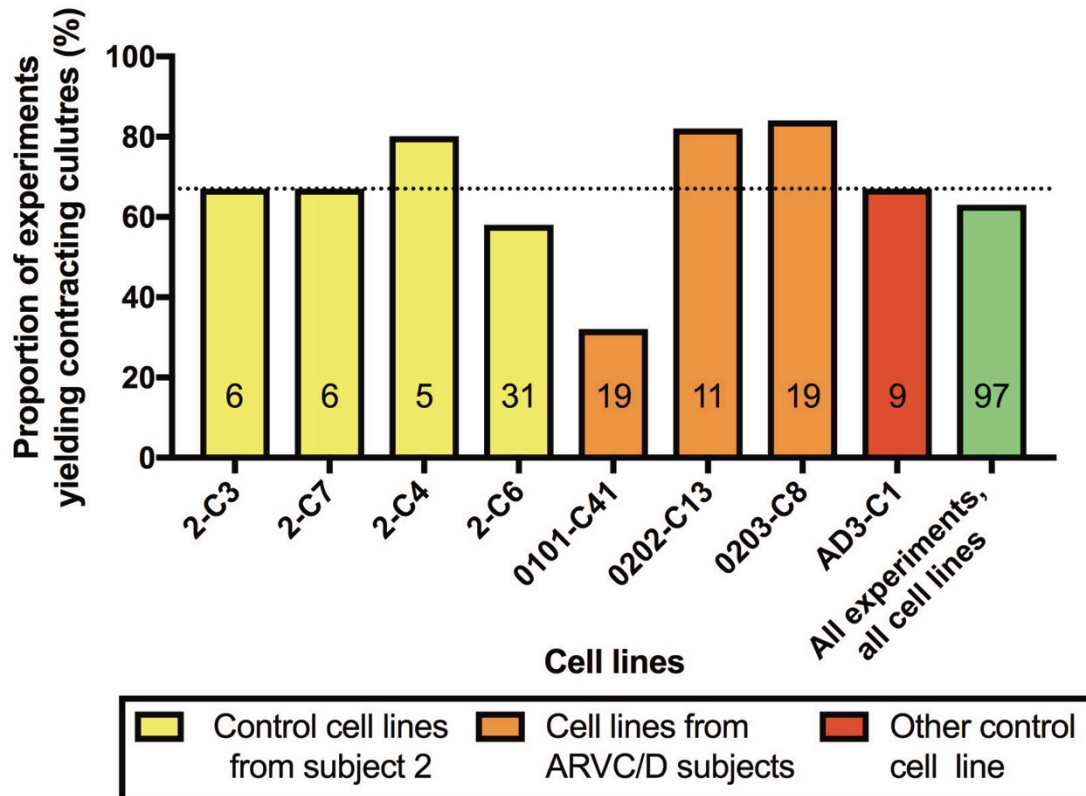


Figure 48 Proportion of experiments yielding contracting cultures, per cell line and in total.

The number of experiments performed with each line is indicated by the figure within each bar. The mean proportion of experiments yielding contracting cultures across all cell lines is indicated by the dotted line. Pairwise comparisons using Fishers exact test found the proportion of experiments in which contracting cultures were observed were significantly lower in 0101-C41 than for 0202-C13 and 0203-C8 ($p < 0.05$). All other differences were non-significant.

5.3.6 Calcium transient imaging

Two cell lines were assessed for the presence of spontaneous calcium transients by fluorescence microscopy (2-C6 and 0203-C8). Each line was assessed in two independent differentiation experiments. Cells from each differentiation experiment were re-plated into multiple glass bottomed culture dishes and three dishes containing spontaneously contracting cells were imaged from each experiment. Spontaneous calcium transients were identified in iPSC-CMs from both lines (Figure 49). Spontaneous transients were recorded in four (67%) of the six dishes across both the experiments that used 2-C6. Spontaneous transients were recorded in two (33%) of the six dishes containing differentiated 0203-C8, with both dishes originating from the same differentiation experiment. Field pacing was applied to all dishes and resulted in induced calcium transients in all cases.

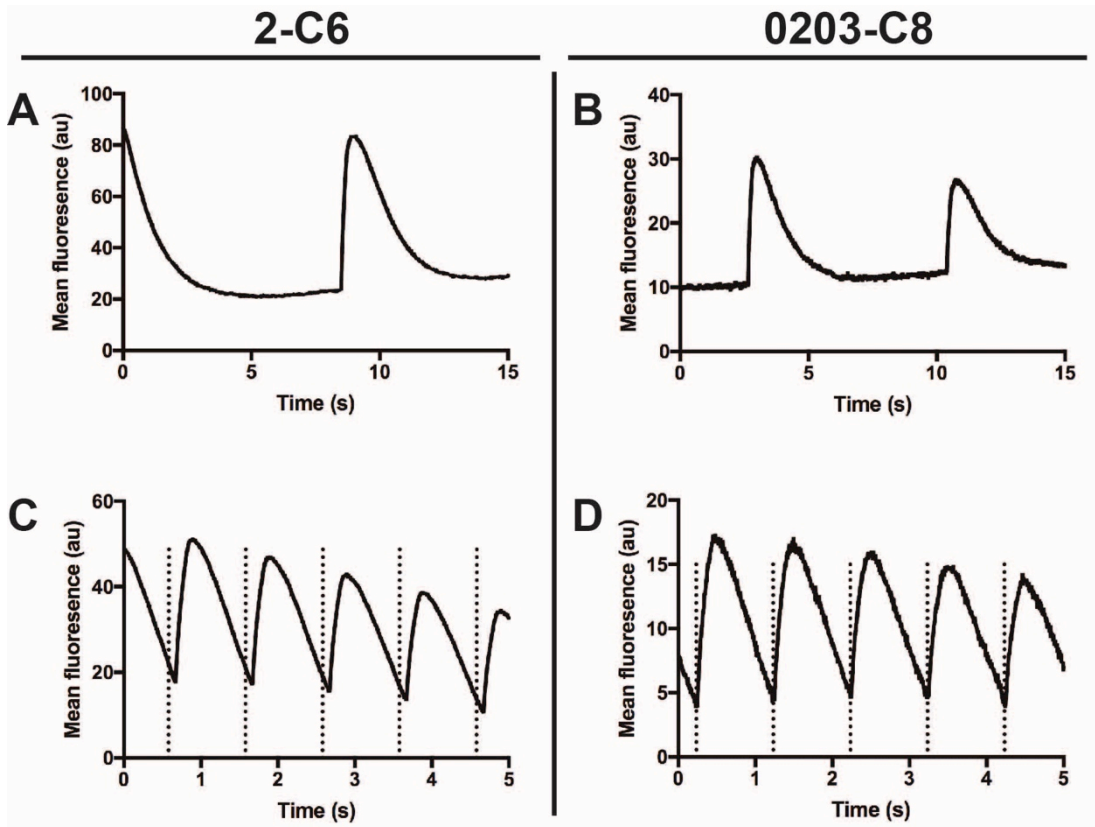


Figure 49 Calcium transients recorded from differentiated cultures.

Representative data from contracting cultures derived from 2-C6 (Panels A and C) and 0203-C8 (Panels B and D) are shown. Panels A and B illustrate spontaneous transients recorded from each cell line. Panels C and D illustrate calcium transients triggered by field pacing at 1Hz.

5.3.7 Sarcomeric and pluripotency related gene expression

The expression of pluripotency marker genes (*NANOG*, *OCT4*) and genes encoding sarcomeric proteins (*ACTN2*, *TNNT2*, *TNNI3*, *MYH6*, *MYH7*) were assessed by RT-qPCR. For each iPSC clone the mean expression was estimated from three different passages. For differentiated cells the mean expression was estimated from three different differentiation experiments.

NANOG, *OCT4* and *TNNT2* expression levels were assessed in all clones that underwent cardiac differentiation except 0101-C41¹². The median expression of *NANOG* in iPSCs was 4.9 times that of the contracting cultures and the median expression of *OCT4A* in iPSCs was 209 times that of the contracting cultures (Figure 50, panel A) (Table 56). The median expression of *TNNT2* was 265 fold greater in the contracting cultures than in the iPSCs (Figure 50, panel B) (Table 56). These

¹² Due to the low number of differentiations using 0101-C41 that yielded contracting cultures a limited quantity of RNA was available for RT-qPCR. It was decided that these samples would be used for assessments of desmosomal rather than sarcomeric gene expression.

differences were statistically significant (exact p values from 2 tailed Mann-Whitney U (MWU) test were <0.05).

The expression of the other sarcomeric genes was only assessed in the four clones from subject 2. The median expressions of *ACTN2*, *TNNI3*, *MYH6*, *MYH7* in contracting cultures were 318, 40, 7700 and 8100 times that of the expression in iPSCs (Figure 50, Panel B) (Table 56). These differences were statistically significant (exact p values from 2 tailed MWU test were <0.05).

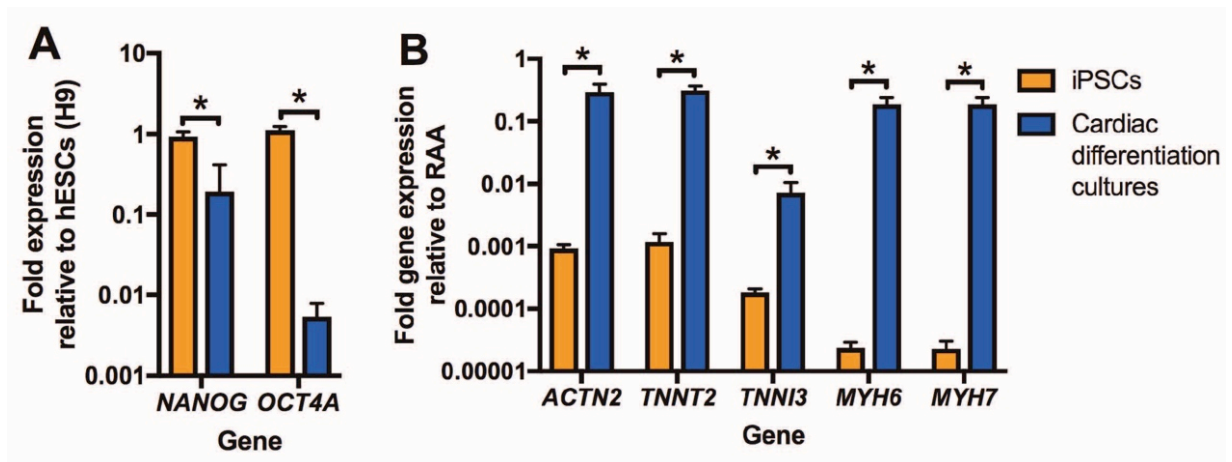


Figure 50 RT-qPCR data illustrating the expression of genes encoding pluripotency markers and sarcomeric proteins in iPSCs and contracting cultures generated from these lines by directed cardiac differentiation.

Pluripotency gene expression is presented in panel A, sarcomeric gene expression is presented in panel B. The expression levels of pluripotency marker genes in hESCs in maintenance culture were considered to be indicative of those associated with pluripotency in general. The qPCR experiment summarised in panel A was performed to provide evidence of a loss of pluripotency during differentiation therefore expression iPSCs and iPSC-CMs is presented relative to the mean expression of these genes across the three passages of H9 hESCs. The expression levels of sarcomeric genes in RAA tissue is considered to be reflective of those found in cardiomyocytes in general. The qPCR experiment summarised in panel B was performed to provide evidence of differentiation of iPSCs towards a cardiomyocyte phenotype therefore expression iPSCs and iPSC-CMs is presented relative to the mean expression of these genes from RAA samples from three different subjects. Figures represent the median and 75th centile for each population. The number of clones assessed was considered too small for statistical estimates of data normality to be reliable. Assessments of the differences between iPSCs and the differentiated cells using a 2 tailed Mann-Whitney U test that produced exact p values <0.05 are indicated (*).

Gene	Cell type	
	iPSC	iPSC-CM
<i>NANOG</i>	21.1±0.4	22.9±0.3
<i>OCT4A</i>	15.7±0.3	23.3±0.2
<i>ACTN2</i>	25.8±0.1	17.8±0.1
<i>TNNT2</i>	26.6±0.3	15.4±0.1
<i>TNNI3</i>	28.2±0.0	23.4±0.3
<i>MYH6</i>	31.1±0.1	18.7±0.3
<i>MYH7</i>	31.2±0.1	18.7±0.3

Table 56 Unadjusted Ct values from the assessment of expression of genes encoding pluripotency markers and sarcomeric proteins in iPSCs and iPSC-CMs.

5.3.8 Expression of sarcomeric proteins

The expression of cardiac troponin I (cTnI) by differentiated cells in spontaneously contracting cultures was assessed by flow cytometry. TnI positive cells were detected in all contracting cultures. The mean proportion of cells that were classified as positive for cTnI across all experiments was 37% (SD 26, n=32, median 41%, Q1-Q3 11-56%, range 1 to 86%). There was no significant difference in the proportion of cTnI positive cells between different clones (Figure 51).

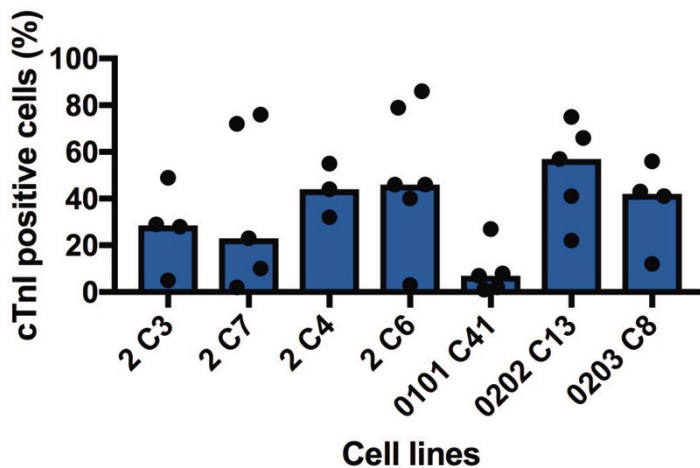


Figure 51 Proportion of cells in contracting cultures expressing cTnI as determined by flow cytometry.

Bars indicate median values. The results of individual experiments are indicated by data points.

Cells labelled with antibodies to alpha actinin (α Act2) and the cardiac troponin T (cTnT) were identified by immunofluorescence microscopy in all contracting cultures. In all cases the signals from these proteins were spatially distinct and combined to

formed linear structures traversed by alternating bands of cTnT and α Act2 signal (Figure 52).

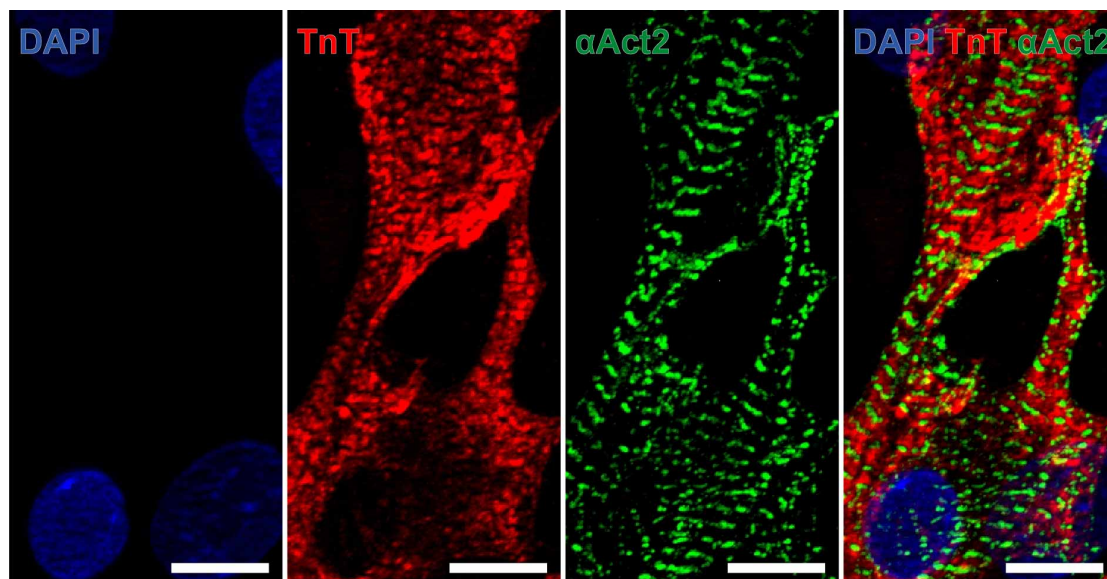


Figure 52 Immunofluorescence microscopy for sarcomeric proteins in cells differentiated from iPSCs.

Maximum intensity projections from Z-stacks of immunofluorescence microscopy images of cTnT and α Act2 signals from cells differentiated from 2-C6 iPSCs. The pattern of signals is representative of those seen in all contracting cultures. No signal was observed in cells labelled with secondary antibodies only (data not shown). The scale bar indicates 10 μ m.

5.3.9 Ultrastructural features of iPSC-CMs

The ultrastructural features of cardiac sarcomeres are described and defined in Chapter 1. Samples of adult human right atrial appendage (RAA) acted as a positive control for the TEM assessment. Striated myofibrils with M lines and H zones were identified in RAA samples (Figure 53 A). A bands and I were not clearly seen in the RAA samples.

Contracting cultures generated from iPSCs were examined at 30 days from the start of differentiation (see methods). Striated myofibrils were identified in all samples from contracting cultures. M lines were not identified in any sarcomeres assessed. H zones and I bands were present in some sarcomeres (Figure 53 B).

Some cultured cells contained contractile apparatus in which the fibres were not oriented in parallel, some of these structures contained both Z-lines and structures similar to the dense bodies described in smooth muscle (Figure 53 C).

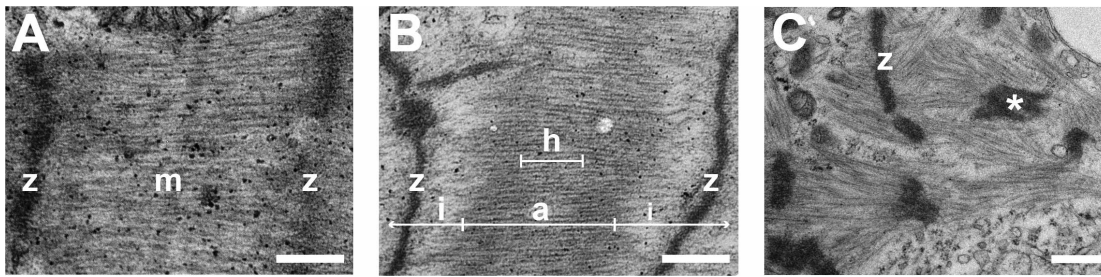


Figure 53 Sarcomeric ultrastructure in RAA cardiomyocytes and cells produced by directed differentiation

Representative TEM images of sarcomeres in RAA (Panel A) and cells generated by directed differentiation from 2-C6 and 2-C7 (Panels B and C respectively). The Z-lines defining sarcomeres are indicated (z). M lines (m) were identifiable in the sarcomeres of RAA cardiomyocytes (A) but not in differentiated cells (B). I bands (i), A bands (a) and H zones (h) were identified in the sarcomeres of cultured cells (B) but not in RAA cardiomyocytes (A). Some cultured cells (C) contained fibres that were not organised in parallel running between Z-lines and dense bodies similar to smooth muscle (*). Scale bars indicate 500nm

5.3.10 Purification of iPSC-CMs by FACS based on SIRPA expression

Despite optimisation of the differentiation protocol to maximise efficiency only 4/32 (13%) of un-purified monolayer differentiation experiments assessed by flow cytometry contained cultures containing $\geq 75\%$ cTnI positive cells.

Protocols for the purification of iPSC-CM were investigated to obtain samples of the purity necessary for assessment of iPSC-CM desmosomal gene expression. The first protocol tested was based on the expression of SIRPA, a cell surface molecule reported to be a marker of PSC derived cardiomyocytes (Dubois *et al.*, 2011).

The co-expression of cTnI and SIRPA by cells from contracting cultures was assessed in samples from two independent differentiation experiments. The samples from these experiments contained 55% and 72% cTnI positive cells overall. Of those cells classed as positive for SIRPA, 77% and 98% co-expressed cTnI, suggesting that collection of SIRPA positive cells would produce samples of the required quality (Figure 54).

Samples from a further three independent differentiation experiments were then sorted by FACS on the basis of SIRPA expression and the proportion of cells expressing cTnI subsequently analysed. In two samples the SIRPA positive fractions contained $\geq 75\%$ cTnI positive cells and one sample (2-C6-WB2) failed to reach this standard (Figure 55). 2-C6-WB2 contained 13% cTnI positive cells prior to sorting, this is lower than that contained in the other two samples (41% and 82%).

Attempts were made to extract RNA from the two SIRPA positive samples containing $\geq 75\%$ cTnI positive cells. Samples were analysed using the Nanodrop spectrophotometer (see methods). The yields from these samples were $0.22\mu\text{g}/\times 10^6$ cells and $0.44\mu\text{g}/\times 10^6$ cells, which are less than a twentieth of the expected yields from cultured cells described by the manufacturer of the kit used for RNA extraction (Promega, 2012). An additional result of the low yield was that the 260/230 ratios for these samples were 0.24 and 1.23, suggesting a high concentration of salts and making the samples unsuitable for analysis in this study.

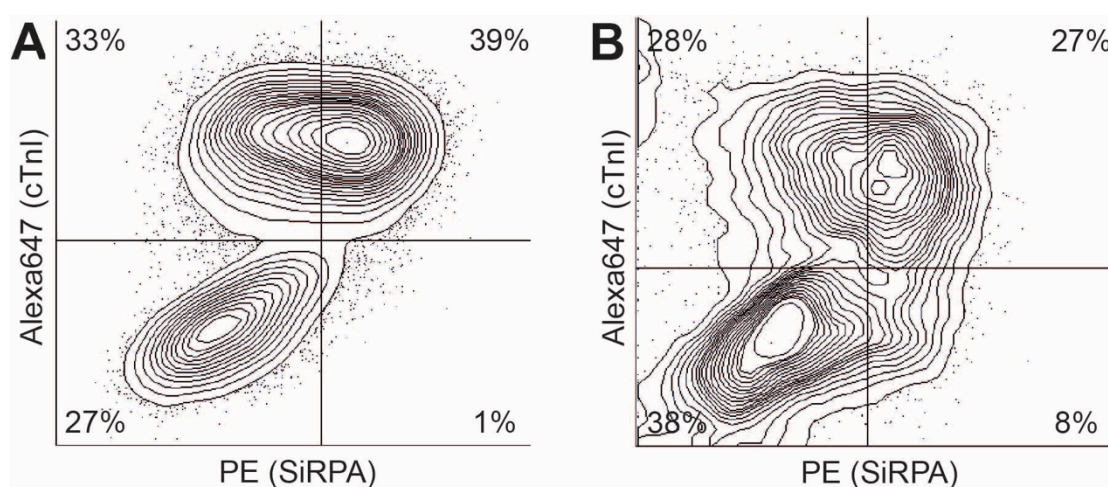


Figure 54 Co-expression of cTnI and SIRPA in cells from contracting cultures
 Contour plots of single cell events co-labelled with antibodies to cTnT and SIRPA showing the fluorescence intensities of corresponding fluorophores when excited during flow cytometry. Panels A and B show data from the analysis of cells from two independent experiments (2-C4-WB2 and 2-C7-WB5). The protocol for defining the position of gates is described in Methods. The proportion of all single cell events falling in each quadrant is illustrated.

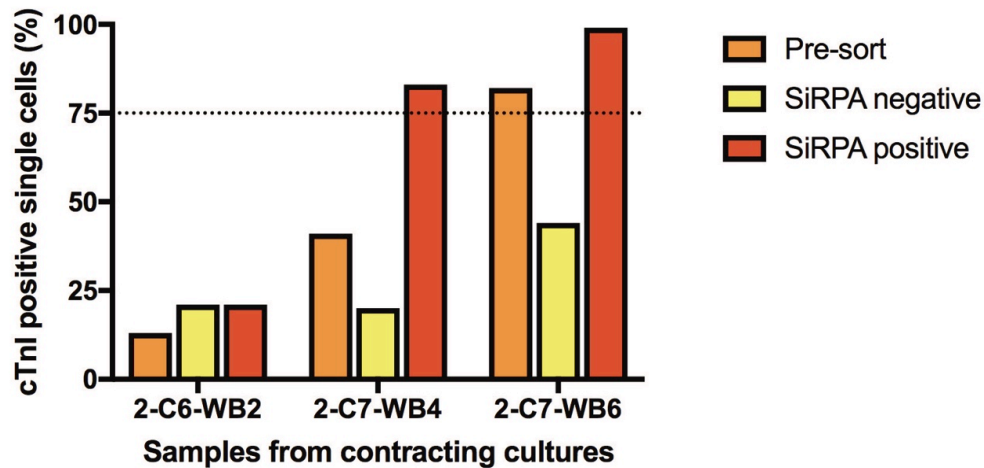


Figure 55 Bar chart showing the proportion of cells expressing cTnI in samples before and after SiRPA based FACS, as assessed by flow cytometry
 The method of identifying single cell events and classifying events as positive for a marker are described in the methods section. The target of $\geq 75\%$ cTnI positive cells is illustrated by the dotted line. Each bar represents the results of a single experiment.

5.3.11 Purification of iPSC-CMs by metabolic selection

Metabolic purification by the exposure of contracting cultures to medium lacking glucose was initially tested in contracting cultures from a single differentiation experiment (2-C4-WB4) (Figure 56). The experiment was conducted using contracting cultures in a single 12 well plate, with the proportion of cTnI positive cells in each well being assessed by flow cytometry. Pre-purification iPSC-CM content was estimated from a single well. The other wells were cultured with either purification medium for 7 days from day 12 followed by return to normal cardiomyocytes maintenance medium (MCMM) (n=4) or in MCMM throughout (n=7). The proportion of cells expressing cTnT were analysed on day 21 by flow cytometry. The median (Q1-Q2) percentages of cTnT positive cells in the purified and unpurified wells were 71% (61-82) and 50% (47-70), with no significant difference between the two groups, assessed by the Mann-Whitney U test (Figure 56).

RNA of the quality required for further analysis was successfully extracted from samples exposed to metabolic purification.

The proportion of cells and iPSC-CMs within purified cultures that were viable after purification was also investigated in this experiment. After preparation of the single cell suspension, but before fixation, samples were incubated with Zombie aqua dye (BioLegend), which will only stain cells with a compromised plasma membrane. Once

exposed to a fixative Zombie dyes do not redistribute to label other cells and therefore it was inferred that Zombie positive cells were dead before fixation. The median (Q1-Q2) proportion of single cells (i.e. including non-cardiomyocytes) that were dead before fixation was 7.6% (2.4-12.0) in the metabolic purification samples and 1.9% (1.7-3.4) in the control samples. The proportions of iPSC-CMs (i.e. troponin positive cells) that were dead before fixation were 4.6% (2.3-7.4) in the metabolic purification samples and 2.1% (1.7-3.8) in the control samples. There was no significant difference in proportion of dead cells between purified and non-purified samples in either parameter.

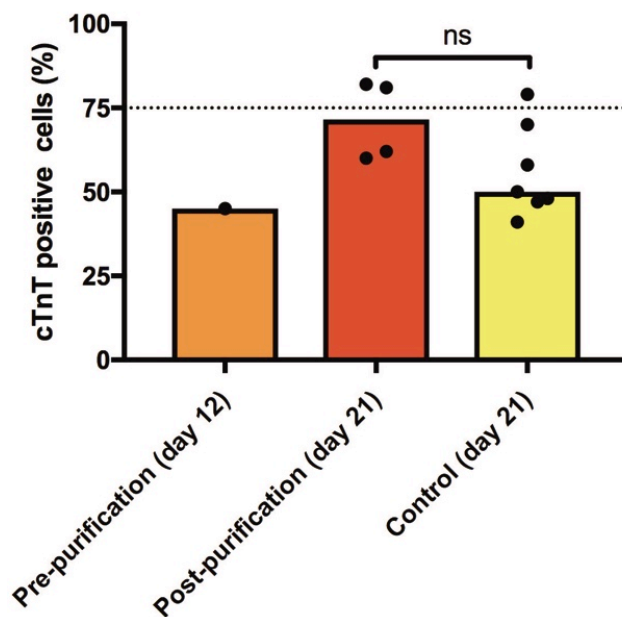


Figure 56 The effect of exposure of contracting cultures to metabolic purification medium on the proportion of iPSC-CMs in culture, as quantified by flow cytometry.

Each point represents the result of a flow cytometry analysis from cells contained within a single well of a 12 well plate. Samples were compared using a 2-tailed Mann-Whitney U test, exact p values $p > 0.05$ were considered non-significant (ns).

5.3.12 The selection of a purification method and its application in further work

The data from initial testing did not demonstrate the efficacy of metabolic purification. Samples of cells containing $\geq 75\%$ iPSC-CMs were collected from cultures exposed to this protocol and RNA was successfully extracted from these cells. Therefore the metabolic purification protocol was used in subsequent attempts to obtain high purity iPSC-CM samples.

The metabolic purification protocol was modified such that purification medium was introduced at an earlier point in differentiation (day 9) and for a shorter period (5 days). This modified protocol was used in differentiation and purification experiments with five different cell lines. Of the 19 experiments yielding spontaneously contracting cultures that were assessed by flow cytometry, samples consisting of $\geq 75\%$ iPSC-CMs were obtained from 18 experiments (95%) (Figure 57). All cultures in these experiments were exposed to purification medium i.e. there were no control cultures that had MCMM throughout.

At least three RNA samples suitable for use in desmosomal gene expression analysis were obtained for each of 0202-C13, 0203-C8, 2-C6 and AD3-C1 but not for 0101-C41. Despite 19 independent differentiation experiments using 0101-C41, including eight which used the metabolic purification protocol, samples containing $\geq 75\%$ iPSC-CMs could only be produced in one experiment.

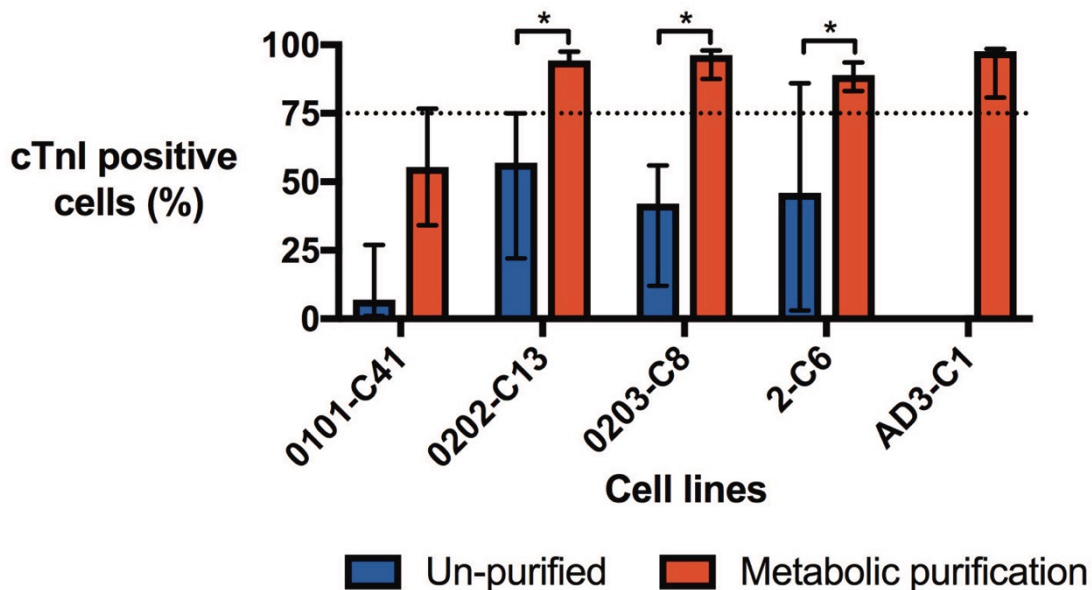


Figure 57 Comparison of the proportion of iPSC-CMs in samples from experiments with and without metabolic purification.

Bars indicate the median proportion of cTnI positive cells across multiple experiments. Whiskers indicate the range. The data from experiments in which metabolic purification was not performed are the same as presented in Figure 51. Experiments conducted with and without purification were compared with a 2-tailed MWU test, exact p values < 0.05 are indicated (*).

5.4 Discussion

5.4.1 The testing of two cardiac differentiation protocols

The monolayer differentiation protocol was selected in preference to the EB protocols on the basis that it generated contracting cultures from the iPSC line tested (SBNeo1-C3).

EB protocol A was used to generate iPSC-CMs from multiple cell lines in a subsequent study in our lab thereby validating the protocol (Yang *et al.*, 2017). The generation of iPSC-CMs using EB protocol B has not been reported. The generation of iPSC-CMs from iPSCs cultured on Matrigel with MEF conditioned medium using the Aggrewell plate system has been reported (Pesi *et al.*, 2014).

The reasons for the failure of the EB protocols to generate contracting cultures in this study are unclear but the following hypotheses could be investigated. (1) Failure of the EB protocol was due to chance. Since not all experiments generated contracting cultures the probability of this outcome is related to the number of experimental repeats performed and the number of EBs undergoing differentiation. The EB protocols in this study were tested in only two experimental repeats per cell line and with a relatively small starting population of EBs. (2) Failure of the EB protocol reflects an incompatibility between it and the SBNeo1-C3 cultures. The potential of SBNeo1-C3 to produce iPSC-CMs was confirmed using the monolayer differentiation protocol. The efficiency of differentiation of this line may vary between protocols. Yang *et al.* did not use SBNeo1-C3 in their study and to date there have been no reports iPSC-CMs being generate from this line using this protocol (Yang *et al.*, 2017). (3) Failure of EB protocol B are due to differences between it and the protocol used by Pesi *et al.*, namely that iPSCs were cultured in in MEF conditioned medium (rather than mTeSR1) before EB formation (Pesi *et al.*, 2014).

Further experiments and protocol optimisation would be necessary to investigate these hypotheses further.

5.4.2 Characterisation of contracting cultures

The upregulation of cardio-specific genes (*TNNT2*, *TNNI3*) and the expression of their proteins (detected by immunofluorescence microscopy and flow cytometry) provided evidence that a proportion of iPSCs differentiated to a cardiomyocyte lineage. Subsequent analyses provided evidence that the cells expressing these genes and proteins also had the functional characteristics of cardiomyocytes.

Immunofluorescence microscopy provided evidence that the cTnT expressed was organised into striated myofibrils in association with α Act2. The cTnT and α Act2 signals were spatially distinct, consistent with the localisation of α Act2 to the Z-discs and cTnT to the sarcomeres.

Myofibrils are composed of a large number of proteins, the expression of genes encoding three of these (*MYH6*, *MYH7* and *ACTN2*) was assessed in this study and were expressed at higher levels in contracting cultures than in iPSCs. Myofibril contraction is a calcium dependent process and therefore the presence of spontaneous contractions would be consistent with the presence and functionality of the apparatus necessary to mediate rapid cycling changes in intracellular calcium concentration. The presence of these calcium transients was confirmed by fluorescence microscopy. The ability of field pacing to trigger these calcium transients is also consistent with the presence of the voltage gated trans-membrane ion channels that mediate the cardiac action potential. The synchronisation of contractions within cultures is consistent with presence of intercellular junctions forming an electrical syncytium by which action potentials are transmitted through cultures.

Skeletal myocytes also contain striated myofibrils and express *MYH6*, *MYH7* and *ACTN2*. The generation of iPSC derived skeletal myocytes (iPSC-SkM) within 35 days of the start of differentiation has been reported using a protocol that has similarities to the cardiac differentiation protocol used in this study (Shelton *et al.*, 2016). Both protocols involve the direction of iPSCs to mesodermal specification by the upregulation of Wnt signalling using with the GSK3 inhibitor CHIR99021 (Lian *et al.*, 2013a) (Shelton *et al.*, 2014). Thereafter the protocols differ in that the cardiac differentiation protocol involves a subsequent inhibition of Wnt signalling and an absence of insulin in the culture medium to promote cardiomyocyte specification from cardiac mesoderm, whereas this is not a component of skeletal muscle protocols (Kattman *et al.*, 2011) (Lian *et al.*, 2013a) (Willems *et al.*, 2011) (Lian *et al.*, 2013b) (Shelton *et al.*, 2016). The expression of cardiac lineage markers *Nkx2-5* and *MYH6* was reported in cultures of iPSC-SkMs derived using the CHIR based protocol (Shelton *et al.*, 2014). This supports the idea that these cell types may co-exist in cultures of differentiated iPSCs generated by protocols with these similar characteristics.

The assessment of sarcomeric protein expression by immunofluorescence microscopy provided an opportunity to screen for the presence of skeletal myocytes within differentiated cultures. α Act2 is expressed at the Z-discs of both skeletal and cardiac myocytes whereas cTnT is cardio-specific. No cells were observed that contained striated α Act2 signal in the absence of cTnT. Although this cannot exclude the presence of iPSC-SkMs it suggest that, if they are present, it is at a low frequency. The presence of skeletal myocytes in differentiated cultures could be investigated in further work by screening for a larger range of protein markers that distinguish skeletal from cardiac myocytes markers such as Pax7, aortic smooth muscle actin and myosin light chain kinase 2 .

In adult cardiomyocytes studied by TEM, striated myofibrils have the following typical features. They consist of bundles of fibres traversed at regular intervals by electron-dense Z-lines. The region between two adjacent Z lines on the same myofibril is referred to as a sarcomere. A range of proteins are localised to the sarcomeres including actin, myosins, troponins and titin. The organisation of proteins within the sarcomere gives rise to regions of greater and lesser protein density which appear as regions of differing electron density in TEM images. Regions in which actin and myosins overlap are more electron dense than non-overlapping regions and define features referred to as A bands, I bands and H-zones. The identification of these A and I bands in the cells of iPSC derived contracting cultures in this study is further evidence of the expression of the multiple sarcomeric proteins and their organisation into myofibrils. The reasons for the lack of identifiable I band and A bands in the RAA samples studies by TEM are unclear. It was hypothesised that this was because the samples were fixed whilst the sarcomeres were in a contracted state.

The identification of striated myofibrils allows myocytes to be distinguished from other cell types within TEM samples. There are no ultrastructural features by which cardiac myofibrils can be distinguished from those found in skeletal muscle. Therefore, strictly speaking, the identification of striated myofibrils by TEM is consistent with, rather than proof of cardiac differentiation. The immunofluorescence data discussed above did not support the idea that iPSC-SkMs were present in contracting cultures and therefore supported the assumption that cells containing striated myofibrils by TEM were iPSC-CMs.

5.4.3 Purification

A goal of this study is to compare the levels of expression of genes encoding desmosomal proteins in iPSC-CMs with and without ARVC/D associated mutations. The presence of non-cardiomyocytes within samples of differentiated cells collected for analyses such as RT-qPCR and western blotting have the potential to influence the level of gene expression detected within those samples. For example the presence of a high proportion of non-cardiomyocytes in which a low level of desmosomal gene expression is normal would result in the average expression level in that sample to be lower than if it contained only cardiomyocytes. Without controlling for this variable it cannot be determined whether differences in gene expression between cell lines are due to differences in their expression in iPSC-CMs or due to the influence of non-cardiomyocyte populations within the samples. The potential for non-cardiomyocytes to influence the result can be minimised by obtaining samples with a uniformly high percentage of iPSC-CMs. A target of $\geq 75\%$ of cells expressing cTnI was chosen for samples to be used in assessments of desmosomal gene expression.

Strategies to achieve high purity samples can be divided into those directed at optimising the efficiency of differentiation and those directed at purifying iPSC-CMs from a mixed population.

The monolayer differentiation protocol used in this study was adapted from that published by Lian *et al.* who reported the production of cultures containing 80-98% iPSC-CMs across multiple cell lines (Lian *et al.*, 2013a). The protocol modifications recommended by the authors to optimise differentiation efficiency were pursued in all cell lines. Despite these attempts, cultures with a consistent high proportion of iPSC-CMs could not be generated consistently.

The decrease in *OCT4A* and *NANOG* expression in contracting cultures relative to iPSCs suggests that the reduced efficiency was not due to a failure of the protocol to induce the differentiation of iPSCs. The cell types constituting the non-cardiomyocyte fraction of contracting cultures were not characterised in greater detail in this study.

Two strategies for purifying iPSC-CMs from mixed populations were investigated. The first strategy assessed was the purification of live cells by FACS according to expression of the surface protein SIRPA (Dubois *et al.*, 2011). The second strategy was purification by culture in the absence of glucose thereby causing the death of

non-cardiomyocytes which have less resistance to this type of metabolic stress than iPSC-CMs (Tohyama *et al.*, 2013).

The ability of SIRPA based selection to purify iPSC-CMs from a sample is based on the principle that a high proportion of SIRPA positive cells are iPSC-CMs. The finding that 77-98% of SIRPA positive cells expressed cTnI in this study are broadly in agreement with those of Dubois *et al.* for whom 67-90% of SIRPA positive cells expressed cTnT (Dubois *et al.*, 2011).

We found the sensitivity of SIRPA based selection to be lower than that reported by Dubois *et al.* In our sample 42-55% of SIRPA negative cells expressed cardiac troponin compared with 5-16% in the experiments reported by Dubois (Dubois *et al.*, 2011). Differences in study protocols may account for this apparent discrepancy. Dubois *et al.* employed the EB based cardiac differentiation protocol described by Kattman *et al.* . This may result in iPSC-CMs with higher levels of SIRPA expression than the monolayer protocol used in this study. The most mature cultures sorted by Dubois *et al.* were 20 days into differentiation compared with the 30 day old cultures used in this study the proportion of cells. This may indicate that the proportion of iPSC-CMs expressing SIRPA decreases over time. Finally, Dubois *et al.* identified iPSC-CMs on the basis of cTnT expression, whereas in this study antibodies to cTnI were used. Different antibody specificities may account for these different results.

Overall selection on the basis of SIRPA identified 49-54% of cTnI positive cells in culture in our study suggesting that a large proportion of iPSC-CMs cannot be purified using the protocol employed in this study. Alternative strategies for FACS based purification other than SIRPA have been proposed. The combination of CD90 (THY1), CD31 (PECAM1), CD140B (PDGFRB) and CD49A (ITGA1) has been reported to identify the majority of non-cardiomyocytes in differentiated cultures at day 20 (Dubois *et al.*, 2011). Purification based on negative selection using these markers may allow the collection of a greater proportion of the iPSC-CM population than with SIRPA.

Results of the attempt to purify 2-C6-WB2 (in which only 13% of the initial sample were cardiomyocytes) by FACS also merit further discussion. Dubois *et al.* reported that samples containing approximately 10% iPSC-CMs could be purified to contain 60-70% iPSC-CMs (Dubois *et al.*, 2011). Samples containing 40% hESC-CMs could be purified to 90±4% iPSC-CMs (Dubois *et al.*, 2011). It was hypothesised that SIRPA sorting may be unable to adequately purify samples containing a low

percentage of iPSC-CMs and this may account for the failure to purify 2-C6-WB2. It was also notable that the proportion of cTnI positive cells was higher in the SIRPA negative fractions of 2-C6-WB2 than in the unsorted sample. It was therefore hypothesised that the process of FACS itself acts to remove non-cardiomyocytes. Further experiments would be necessary to investigate both these hypotheses.

The low yield of RNA from sorted SIRPA positive cells coupled with the high salt to nucleic acid ratio in these samples made them unsuitable for use in RT-qPCR experiments. It was hypothesised that the process of FACS resulted in cell injury that reduced the RNA yield in these samples. Further experiments would be necessary to investigate this hypothesis and optimise the FACS protocol to allow RNA samples of the required quantity and quality to be obtained from sorted iPSC-CMs.

Taken together it was concluded that the feasibility of obtaining RNA samples for FACS purified samples containing $\geq 75\%$ iPSC-CM has not been established in this study.

The purification of iPSC-CMs by modifying culture conditions to cause the death of non-cardiomyocytes was first described by Tohyama *et al.* (Tohyama *et al.*, 2013). The technique is based on the observation that cardiomyocytes can survive culture with medium that does not contain glucose whereas non-cardiomyocytes die rapidly in these condition (Tohyama *et al.*, 2013). Purification by glucose free culture has been reported to be able to generate cultures in which $>95\%$ of cells are reported to be iPSC-CMs from initial cultures with as little as 8% of this cell type present (Tohyama *et al.*, 2013) (Burrige *et al.*, 2014).

Tests of the purification protocol in this study found that within a single experiment (2-C4-WB4) only produced cultures containing $\geq 75\%$ iPSC-CMs in 50% of wells tested. A modified version of the protocol generated cultures containing $\geq 75\%$ iPSC-CMs in all experiments across three cell lines but only in 50% of experiments involving 0101-C41. When considering the effect of purification on individual cell lines, the proportion of iPSC-CMs was significantly greater in the experiments where the purification protocol was used, than in earlier experiments when it was not, in three of the four cell lines assessed. This would be consistent with the purification protocol being effective. There were no control cultures that were not exposed to the purification medium in these experiments. Therefore, the possibility that these results occurred due to the efficiency of differentiation and not the effect of purification cannot be excluded.

If it is accepted that metabolic purification did increase the proportion of iPSC-CMs in some cultures then reasons for the success of the modified purification protocol and failure of the protocol tested with 2-C4-WB4 may be considered. The protocols differed from the initial purification protocol in two respects: (1) the purification began at an earlier stage of differentiation (day 9 vs day 12) and (2) the duration of exposure to the purification medium was less (5 vs 7 days)¹³. Both purification start points (day 9 and day 12) are close to that reported by Burrige *et al.* (day 10) whose protocol produced cultures containing >90% iPSC-CMs. There is no evidence from published reports to support the idea that the earlier start point resulted in improved efficiency. Tohyama *et al.* reported that the duration of purification influenced the resulting proportion of iPSC-CMs in a culture (Tohyama *et al.*, 2013). They reported that a culture starting with 4% iPSC-CMs was enriched to 33% iPSC-CMs after 4 days of purification and to >90% after 6 days. This suggests that high purity samples obtained in the later experiments were generated in spite of, rather than as a result of, shortening the purification duration from 7 to 5 days.

The proportion of dead cells (identified by the Zombie dye) contained within the 2C4-WB4 cultures after exposure to the purification medium was relatively low (median 8%) and not significantly different from control cultures. This suggests that if cells died during purification, they were released into the culture medium rather than remaining within cultures. The proportion of dead iPSC-CMs was also low in the purified sample (median 5%) and consequently, in subsequent experiments, where Zombie was not used, it was assumed that the proportion of single cell events expressing a cardiac troponin was indicative of the proportion of viable iPSC-CMs from which RNA could be extracted.

5.5 Conclusions

Directed cardiac differentiation of iPSCs in adherent feeder-free culture conditions is feasible using the monolayer differentiation protocol. The feasibility iPSC differentiation by the EB differentiation protocols tested was not established in this study.

The resultant contracting cultures contained iPSC-CMs expressing a typical array of sarcomeric proteins that are arranged into myofibrils with many of the ultrastructural characteristics of adult cardiomyocytes. The iPSC-CMs in these cultures have the

¹³ These modifications followed discussions with Dr Nicola Hellen, Imperial College London, who used a similar protocol.

functional characteristics of cardiomyocytes including spontaneous and voltage inducible contractions associated with calcium transients.

RNA samples from samples containing $\geq 75\%$ live iPSC-CMs may be obtained in experiments in which cultures have been exposed to the metabolic purification protocol. The data from this study are consistent with the efficacy of this purification protocol. The feasibility of iPSC-CM purification by FACS for SIRPA using the protocol testing in this study was not established.

Chapter 6. Desmosomes, Desmosomal Genes And Desmosomal Proteins In hESCs, iPSCs, iPSC-CMs And Myocardium

6.1 Introduction

This chapter will discuss the identification of desmosomes in pluripotent cell cultures and iPSC-CMs. It will also discuss the patterns of expression of desmosomal genes and the localisation of desmosomal plaque proteins in these tissues. A summary of normal desmosomal morphology and the localisation of desmosomal proteins has been described in chapter 1, along with a discussion of the changes to these parameters in ARVC/D myocardium and iPSC-CM models of ARVC/D.

6.2 Aims and hypotheses

It was hypothesised that:

- hESCs and iPSCs contain inter-cellular adhesions that have the characteristic ultrastructural features of desmosomes.
- hESCs and iPSCs express a range of desmosomal plaque proteins and the cellular distribution of these proteins is consistent with their incorporation in the focal intercellular adhesion junctions.
- iPSCs, iPSC-CMs and RAA myocardium have different patterns of desmosomal gene expression.
- The ARVC/D mutations investigated in this study will result in a reduction in the abundance of transcripts from the affected genes.
- ARVC/D iPSC-CMs exhibit a redistribution of desmosomal plaque proteins to the cytoplasm or nucleus that is identifiable by immunofluorescence microscopy.

6.3 Results

6.3.1 The identification of desmosomes in iPSCs, iPSC-CMs, RAA and hESCs

Desmosomes were identified in iPSCs, iPSC-CMs and RAA myocardium (Figure 58) and in hESCs (Figure 59). Desmosomes in all tissue types had a typical appearance. Bi-laminar structures defining the intercellular gap were attributed to the plasma membrane. Electron-dense ODPs were observed on the cytoplasmic side of this laminated structure, often separated by a region of reduced electron density. The cytoplasmic side of the ODPs abutted with less dense IDPs which were, in-turn

associated with intermediate filaments within the cytoplasm (Figure 58 D to F). In some desmosomes a dense midline was also visible (Figure 58 D and F).

Desmosomes were identified in two different iPSC lines and H9 hESCs, but were very sparse and only seen at the edges of these samples (Figure 59). The cytoplasm adjacent to the IDPs in these PSC desmosomes had a less granular appearance than in iPSC-CMs and RAA suggesting less abundant intermediate filaments. In RAA, desmosomes were exclusively co-localised with adherens junctions and myofibrils to the regions of highly convoluted plasma membrane between adjacent cells i.e forming the expected area composita of the intercalated discs (ICDs) (Figure 58 C). Desmosomes were found in regions similar to ICDs in iPSC-CMs (Figure 58 B), but were also seen in isolation.

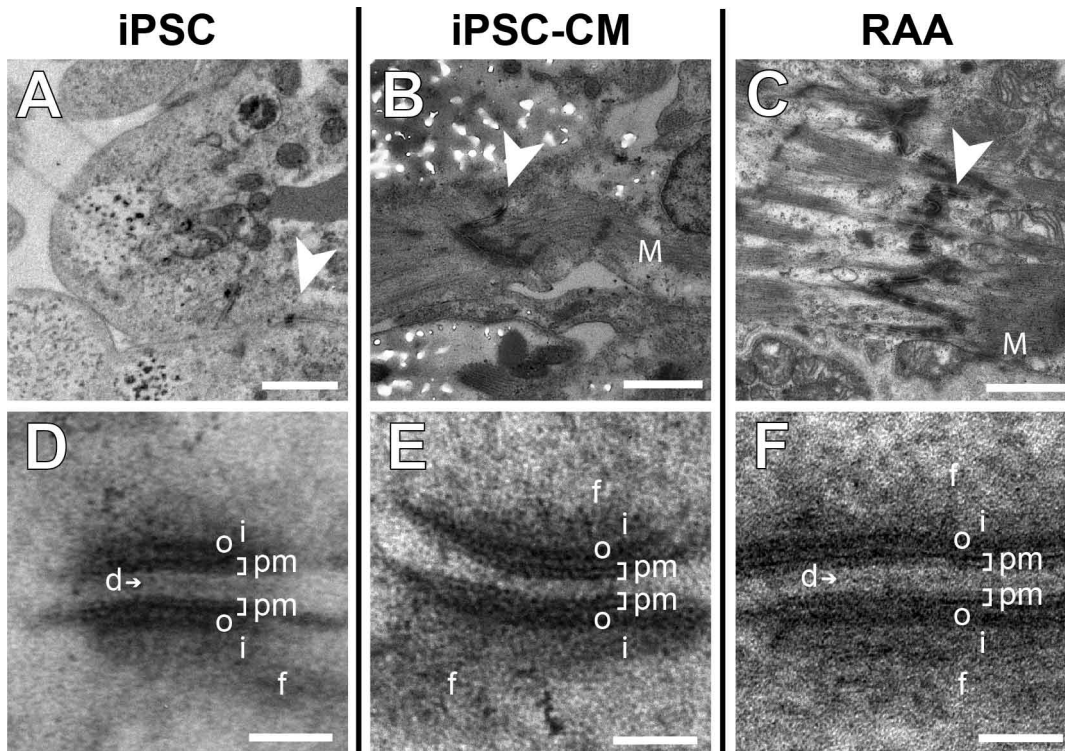


Figure 58 TEM images of desmosomes in iPSCs, iPSC-CMs and RAA

Panels A and D show areas images from samples of 2-C6 iPSCs collected from feeder-free maintenance culture. Panels A to C are low magnification images in which the locations of desmosomes are indicated by arrowheads. In panels B and C the locations of striated myofibrils are indicated (M). Panels D to F are high magnification images of desmosomes illustrating the typical laminated appearance of their plaques. The region of the plasma membrane (pm), ODP (o), IDP (i) and intermediate filaments (f) that converge on the plaque are indicated. A dense midline (d) is also visible in D and F. Scale bars in images A to C indicate 1 μ m, and in images D to F indicate 50nm.

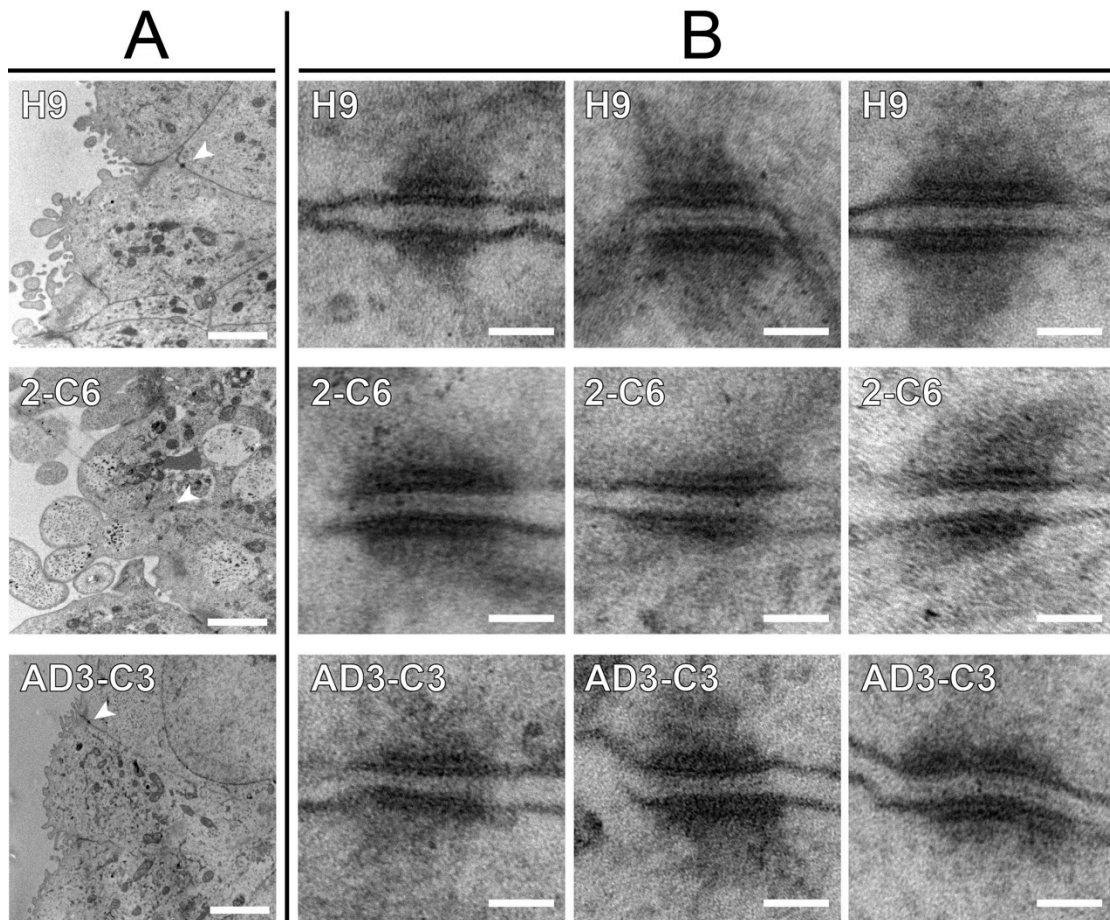


Figure 59 Desmosomes in iPSCs and hESCs

Scale bars in section A indicate 1 μm. Scale bars in section B indicate 50 nm.

6.3.2 Frequency of desmosomes within TEM images

Regions of a sample containing 2-C6 iPSC-CMs were selected at random and imaged at 13,500X (each image covering 59nm² of sample). 64% of the images contained no desmosomes. Additionally only a subset those images containing desmosomes were of sufficient quality for morphometric analysis, this proportion was not quantified. Approximately 6 hours of TEM imaging time were needed to obtain the 30 fully optimised high magnification images necessary for morphometric evaluation, for each cell line assessed. A similar finding was observed in the RAA sample (no desmosomes were seen in 77% of images). Although theoretically this technique could have been used to assess the abundance of desmosomes within samples this approach was not performed due to the resource constraints.

6.3.3 IDP morphology

In the majority of desmosomes imaged in both iPSC-CMs and cardiomyocytes the edge of the IDP on the cytoplasmic side of the plaque did not appear as a continuous

boundary running parallel to the ODP. In some desmosomes the IDP appeared as a region of heterogeneous electron density that became gradually less dense with increasing distance from the plaque until it merged with the region of the intermediate filaments. In other desmosomes a distinct boundary was present, but it followed a broken or tortuous path that was not a consistent distance from, or parallel to, the ODP (Figure 60).

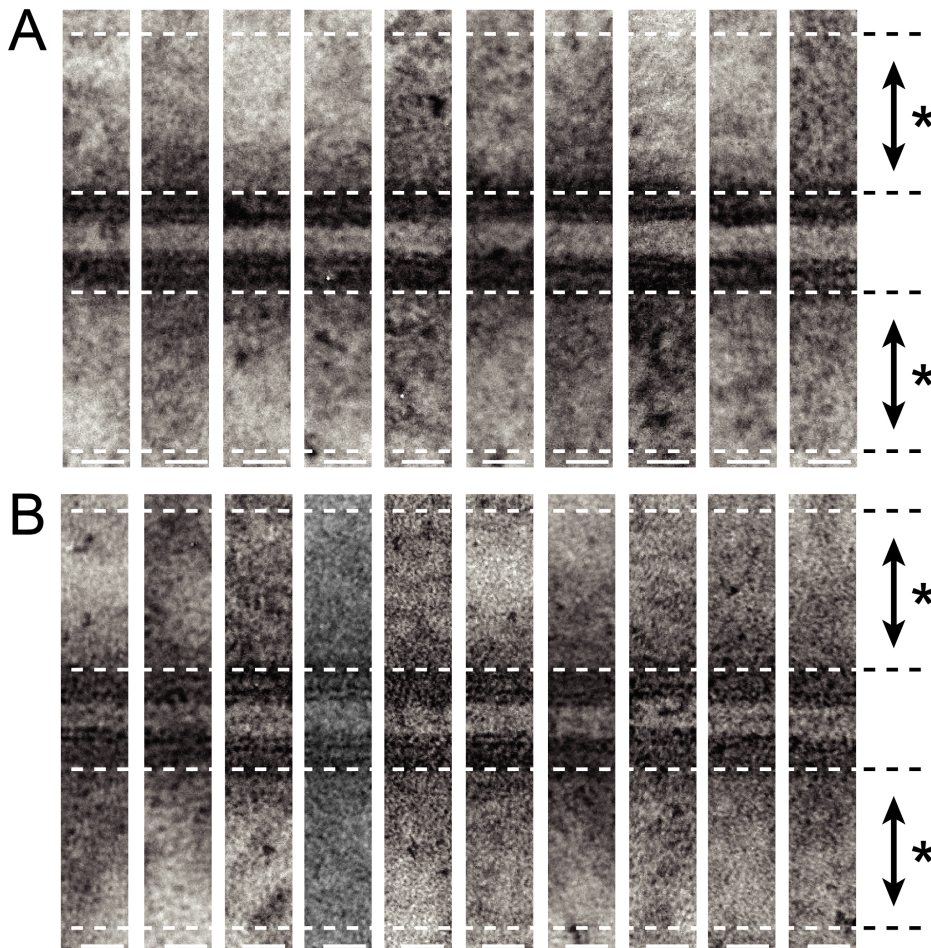


Figure 60 Assessment of the IDP-intermediate filament junction in desmosomes from iPSC-CMs and RAA.

Representative regions of desmosomes from control iPSC-CMs (2-C6) (Panel A) and RAA myocardium (Panel B). Structure representing the IDP and the IDP-IF junction were sought in the indicated region between the dashed lines (*). Scale bars indicate 20nm.

6.3.4 Desmosomal gene expression, experimental design and sample details.

The expression of genes encoding desmosomal proteins was assessed in PBMCs, iPSCs, iPSC-CMs and RAA tissue. Samples from HaCaT cells and RAA were used as positive controls for the primers. Primer sets were validated in for all genes except that for *DSG1*. This primer set generated the product of the expected size from HaCaT samples by RT-PCR, but in RT-qPCR experiments the expression levels

were very low, with the mean Ct being 32 (SD 1.2). Desmosomal gene expression was normalised to a combination of reference genes selected to be most stable across the four cell types from preliminary experiments analysed using the geNorm algorithm. The mean Ct for reference genes in these experiments was 24 (SD 0.8). A more detailed description of the results of these experiments is given in the appendix.

Expression in PBMCs was assessed in samples from seven subjects including the three from which ARVC/D lines were derived. iPSC samples consisted of RNA from eight iPSC lines (2-C3, 2-C7, 2-C4, 2-C6, AD3-C1, 0101-C41, 0202-C13 and 0203-C8). Each line was assessed with RNA from three different passages. iPSC-CM samples consisted of RNA from the four lines in which samples containing $\geq 75\%$ cTnI positive cells could be obtained (2-C6, AD3-C1, 0202-C13 and 0203-C8). Each line assessed with RNA from three independent cardiac differentiation experiments. Expression in RAA was assessed in four samples from different individuals.

6.3.5 Comparison of desmosomal gene expression in PBMCs, iPSCs, iPSC-CMs and RAA

In the analysis of these data, expression data from AD3-C1 iPSCs (a fibroblast derived cell line) were excluded to allow the comparison of PBMCs with blood derived iPSCs.

DSC1 expression was very low or effectively absent in iPSCs and iPSC-CMs (mean expression $< 10\%$ of the mean expression of reference genes) but expressed at a high level in RAA (mean 6.0, SEM 2.1) (mean unadjusted Ct 22.6, SEM 2.6) (Figure 61) (Table 57). The expression of *DSC1* by RAA and its absence in iPSC-CMs and HaCaT cells was confirmed by assessment with two additional primer sets to *DSC1a* and *DSC1b* (Figure 62) (Table 58). These experiments suggested that both isoforms of the protein may be present in the myocardium.

DSC2 was expressed in iPSCs, iPSC-CMs and RAA (Figure 61) (Table 57). The expression in PBMCs was approximately 10 fold lower than in the desmosome bearing tissues. The differences in mean expression between tissue types were statistically significant (one way ANOVA $p < 0.001$). The mean expression of *DSC2* in iPSCs (1.80, SEM 0.20) (unadjusted Ct 23.2, SEM 0.2) was higher than in PBMCs (0.18, SEM 0.12) (unadjusted Ct 25.6, SEM 0.8) (Tukey's test $p < 0.0001$) and iPSC-CMs (1.05, SEM 0.15) (unadjusted Ct 23.9, SEM 0.2) (Tukey's test $p = 0.01$).

DSC3 was also expressed in iPSCs, iPSC-CMs and RAA, but not in PBMCs (Figure 61) (Table 57). The differences in mean expression between tissue types were

statistically significant (one way ANOVA $p < 0.001$). Mean expression in iPSCs (0.66, SEM 0.05) (unadjusted Ct 24.6, SEM 0.2) and iPSC-CMs (1.2, SEM 0.5) (unadjusted Ct 24.4, SEM 0.5) were similar (Tukey's test $p > 0.05$), but the mean expression in RAA (0.17, SEM 0.11) (unadjusted Ct 28.3, SEM 0.8) was lower than iPSC-CMs (Tukey's test $p = 0.03$).

DSG2 was the most abundantly expressed of the four desmogleins in all three desmosome bearing tissues (Figure 61) (Table 57). The mean expression of DSG2 in iPSC-CMs (1.20, SEM 0.09) (unadjusted Ct 23.5, SEM 0.2) was similar to that of RAA (1.5, SEM 0.39) (unadjusted Ct 24.5, SEM 0.6) (Tukey's test $p > 0.05$), but lower than the mean of iPSCs (3.93, SEM 0.28) (unadjusted Ct 22.1, SEM 0.2) (Tukey's test $p < 0.0001$). The expression of *DSG1*, *DSG3* and *DSG4* was low or absent in all desmosome bearing tissues (all mean expression levels $< 10\%$ of reference genes).

PKP2 was the most abundantly expressed plakophilin in all three desmosome bearing tissues, and was also expressed at low levels in PBMCs (Figure 61) (Table 57). The differences in mean expression between tissue types were statistically significant (one way ANOVA $p < 0.001$). The mean expression in iPSC-CMs (76.2, SEM 1.3) (unadjusted Ct 17.5, SEM 0.1) was higher than the mean expression in both iPSCs (4.0, SEM 0.3) (unadjusted Ct 22.0, SEM 0.2) and RAA (42.1, SEM 4.5) (unadjusted Ct 19.6, SEM 0.4) (Tukey's test $p < 0.0001$ for both). The difference between the mean expression of *PKP2* in PBMCs (0.11, SEM 0.03) (unadjusted Ct 28.1, SEM 0.3) and iPSCs did not reach statistical significance in the post hoc analysis.

JUP was expressed in the three desmosome bearing cell types and in PBMCs (Figure 61) (Table 57). The differences in mean expression between tissue types were statistically significant (one way ANOVA $p < 0.001$). The mean expression in iPSC-CMs (9.52, SEM 0.56) (unadjusted Ct 20.7, SEM 0.3) was similar to that of RAA (8.88, SEM 1.45) (unadjusted Ct 21.9, SEM 0.4) (Tukey's test $p > 0.05$), and greater than that of iPSCs (5.14, SEM 0.45) (unadjusted Ct 22.0, SEM 0.3) (Tukey's test $p = 0.0004$). The mean expression in PBMCs (0.64, SEM 0.08) (unadjusted Ct 25.5, SEM 0.5) was less than that of the iPSCs (Tukey's test $p < 0.0001$).

DSP expression was noted in iPSCs (mean 1.80, SEM 0.19) (unadjusted Ct 23.2, SEM 0.2), iPSC-CMs (mean 3.87, SEM 0.59) (unadjusted Ct 21.8, SEM 0.2) and RAA (mean 3.64, SEM 1.16) (unadjusted Ct 23.3, SEM 0.7), but not in PBMCs (Figure 61) (Table 57). Although the differences in mean expression between tissue

types were statistically significant (one way ANOVA $p < 0.001$), post hoc analysis did not identify significant pairwise differences.

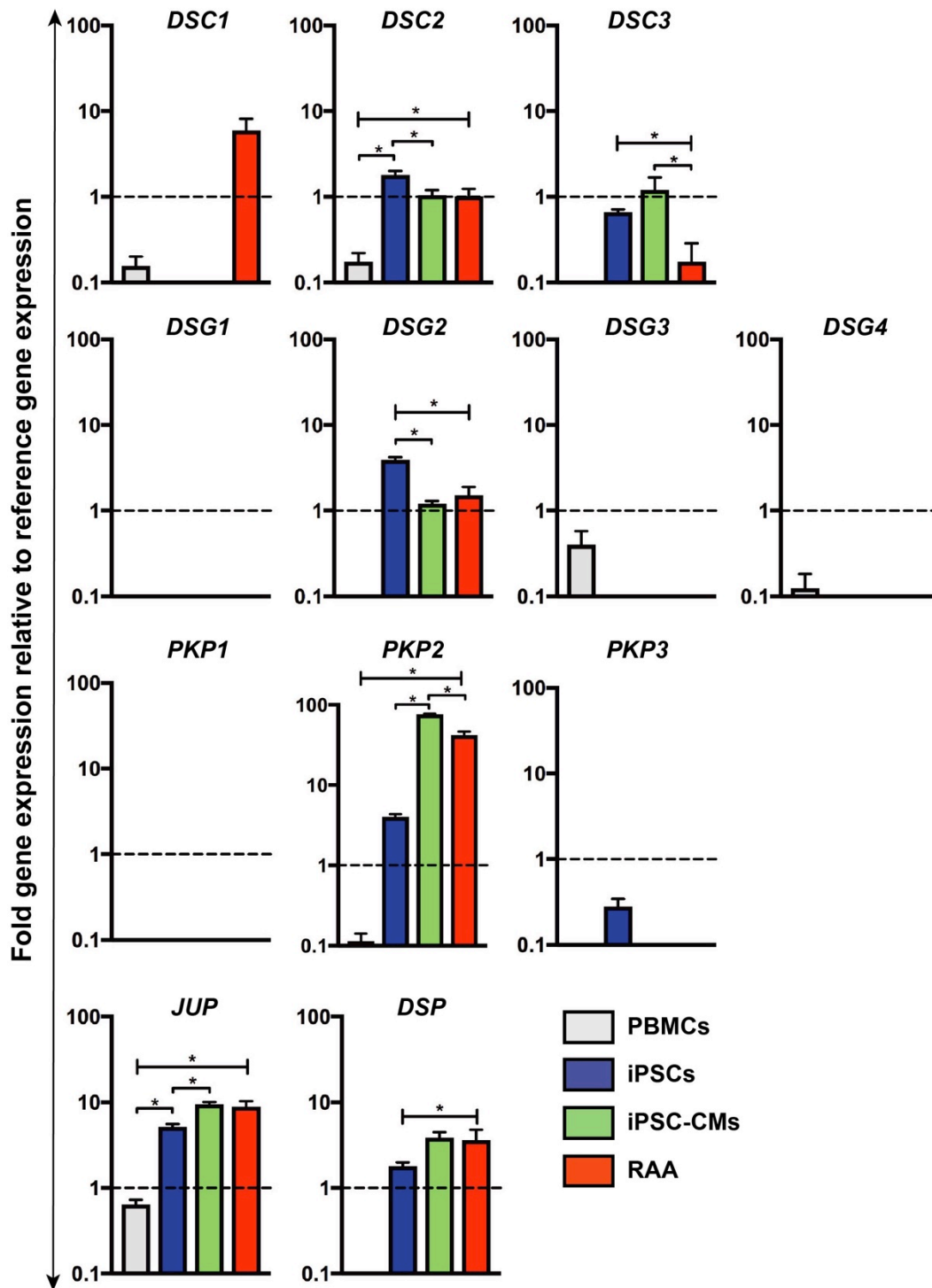


Figure 61 Comparison of the expression of desmosomal genes in PBMCs iPSCs, iPSC-CMs and RAA

The expression of genes of interest relative to mean reference gene expression is presented. (Continued over)

Bars illustrate the mean expression for each cell/tissue type. Data are presented without calibration to a reference cell type in order that the figure provides an indication of the relative expression of different genes within a given cell type (e.g. it illustrates the relative expression of DSC2 and DSC3 in PBMCs) in addition to the comparison of a gene between cell types. Whiskers illustrate the SEM. The data were generated from seven PBMC samples, seven PBMC derived iPSC lines (each tested in three different passages), four iPSC-CM lines (each tested with samples from at least three different differentiation experiments in which >75% of the cells expressed cTnI by flow cytometry) and four RAA samples. Genes with mean expression levels <0.1 were considered effectively absent and these data are not displayed. Raw Ct values associated with these data are presented in Table 57. Means were compared by one way ANOVA and post hoc pairwise comparisons made by Tukey's test. P values <0.05 are indicated (*)

Gene	PBMC	iPSC	iPSC-CM	RAA
<i>DSC1</i>	27.8±0.8	>30	>30	22.6±0.6
<i>DSC2</i>	25.6±0.8	23.2±0.2	23.9±0.2	25.0±0.6
<i>DSC3</i>	>30	24.6±0.2	24.4±0.5	28.3±0.8
<i>DSG1</i>	>30	>30	>30	28.6±0.8
<i>DSG2</i>	>30	22.1±0.2	23.5±0.2	24.5±0.6
<i>DSG3</i>	27.0±0.4	29.9±0.2	28.9±0.5	>30
<i>DSG4</i>	29.1±0.6	>30	29.9±0.3	>30
<i>PKP1</i>	>30	>30	>30	>30
<i>PKP2</i>	28.1±0.3	22.0±0.2	17.5±0.1	19.6±0.4
<i>PKP3</i>	>30	25.6±0.4	>30	>30
<i>JUP</i>	25.5±0.5	22.0±0.3	20.7±0.3	21.9±0.4
<i>DSP</i>	>30	23.2±0.2	21.8±0.2	23.3±0.7

Table 57 Unadjusted Ct values from the assessment of expression of desmosomal gene in PBMCs, iPSCs, iPSC-CMs and RAA samples.
The values presented are the means samples ± SEM.

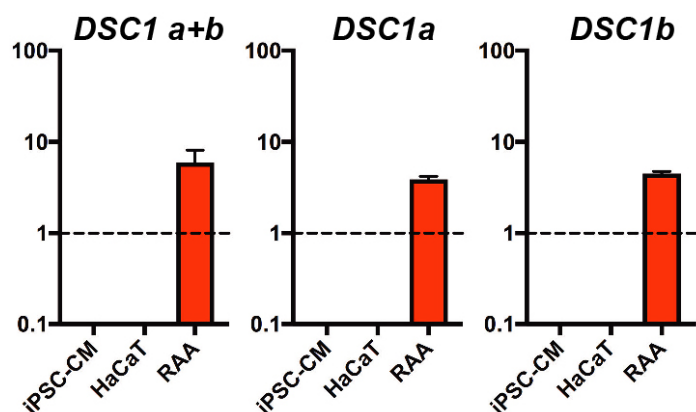


Figure 62. Expression of DSC1 and its isoforms in HaCaT, iPSC-CMs and RAA

The expression of genes of interest relative to mean reference gene expression is presented. Bars illustrate the mean expression for each cell/tissue type. Whiskers illustrate the SEM. Data are presented without calibration to a reference cell type in order that the figure provides an indication of the relative expression of the isoforms in the same cell type. Genes with mean expression levels <0.1 were considered effectively absent and these data are not displayed. The data were generated from four iPSC-CM lines (each tested with samples from at least three different differentiation experiments in which >75% of the cells expressed cTnI by flow cytometry), three passages of HaCaT cells and four RAA samples.

Gene	Cell type		
	iPSC-CM	HaCaT	RAA
<i>DSC1 a+b</i>	>30	28.5±0.4	22.6±0.6
<i>DSC1a</i>	>30	29.8±0.3	22.8±0.4
<i>DSC1b</i>	>30	29.8±0.5	22.6±0.4

Table 58 Unadjusted Ct values from the assessment of DSC1 isoform expression in iPSC-CMs, HaCaT cell and RAA.

The values presented are the means samples ± SEM.

6.3.6 Comparison of desmosomal gene expression between individual cell lines in PSCs and iPSC-CMs

Differences in genes expression between the nine pluripotent cell lines assessed were noted for *DSC2*, *DSC3*, *DSG2* and *PKP2* in the (one way ANOVA, $p < 0.05$) (Figure 63) (Table 58).

Amongst the four iPSC-CM lines a significant difference between cell lines was only noted for *DSP* (one way ANOVA, $p < 0.05$) (Figure 64) (Table 60).

Post hoc analysis of iPSCs suggested that the expression of *DSC3*, *DSG2* and *PKP2* was greater in AD3-C1 than other lines in multiple pairwise comparisons (Tukey's test $p < 0.05$) (Figure 63). This trend was not reproduced in iPSC-CMs (Figure 64). Similarly although *DSC2* expression was greater in 0202-C13 than other

iPSCs but there was no difference in expression of *DSC2* by 0202-C13 iPSC-CMs compared to other iPSC-CMs (Figure 64).

Post hoc analysis suggested that the mean expression of *DSP* in 0203-C8 iPSC-CMs (2.4, SEM 0.1) (unadjusted Ct 22.3, SEM 0.2) was significantly less than 0202-C13 (5.2, SEM 0.1) (unadjusted Ct 21.1, SEM 0.3) (Tukey's test $p=0.001$) (Figure 64) (Table 60), other pairwise comparisons were non-significant. The pattern of expression of *DSP* in iPSCs also suggested a trend towards lower *DSP* expression in 0203-C8 compared with other cell lines but this did not reach statistical significance.

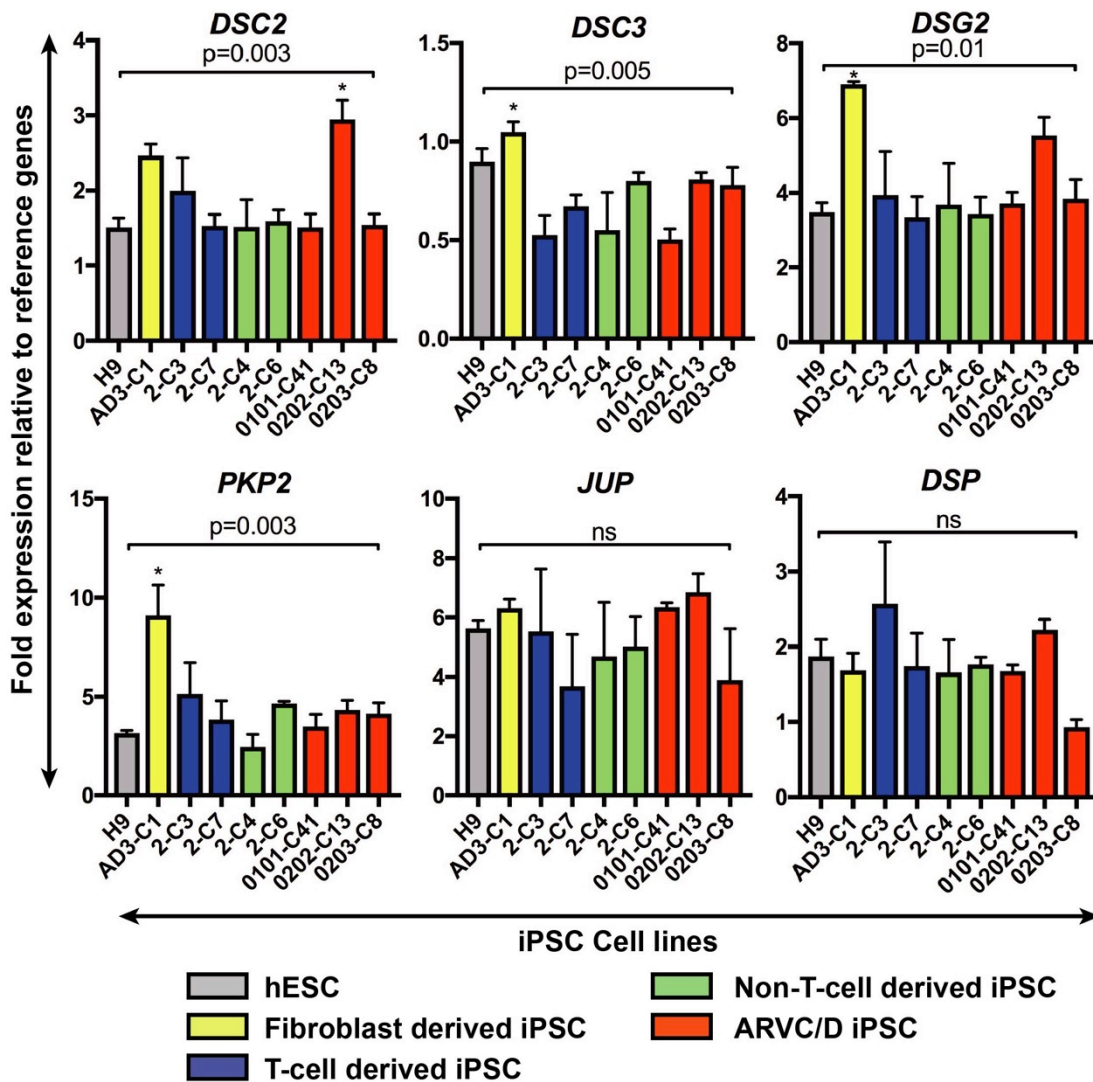


Figure 63 Expression of major desmosomal genes in PSCs

Bars indicate mean expression levels across three different passages. Expression levels of desmosomal genes are expressed relative to mean reference gene expression in the sample sample. Whiskers indicate SEM. Differences between cell lines were investigated with a one way ANOVA test, $\alpha=0.05$. Post hoc pairwise comparisons were made using Tukey's test, samples with one or more comparisons with a $p<0.05$ are indicated (*).

iPSC	Genes					
	<i>DSC2</i>	<i>DSC3</i>	<i>DSG2</i>	<i>PKP2</i>	<i>JUP</i>	<i>DSP</i>
H9	22.9±0.2	23.6±0.2	21.6±0.2	21.8±0.1	21.4±0.5	22.5±0.2
AD3-C1	22.1±0.1	23.3±0.0	20.6±0.2	20.2±0.2	20.7±0.1	22.7±0.1
2-C3	23.6±0.9	25.5±0.8	22.7±1.1	22.3±1.0	22.5±1.3	23.4±1.0
2-C7	23.8±0.6	25.0±0.6	22.7±0.7	22.5±0.3	23.5±1.8	23.7±0.9
2-C4	23.2±0.6	24.9±0.8	22.0±0.7	22.6±0.6	21.9±1.0	23.1±0.6
2-C6	23.2±0.1	24.2±0.1	22.1±0.1	21.7±0.0	21.6±0.2	23.1±0.1
0101-C41	23.4±0.2	25.0±0.2	22.1±0.2	22.2±0.3	21.3±0.1	23.2±0.1
0202-C13	21.8±0.0	23.7±0.1	20.9±0.0	21.3±0.0	20.6±0.1	22.2±0.1
0203-C8	23.1±0.3	24.1±0.3	21.8±0.3	21.7±0.3	22.4±1.1	23.9±0.3

Table 59 Unadjusted Ct values from the assessment of the expression of desmosomal genes in pluripotent cell lines.

The values presented are the means samples ± SEM.

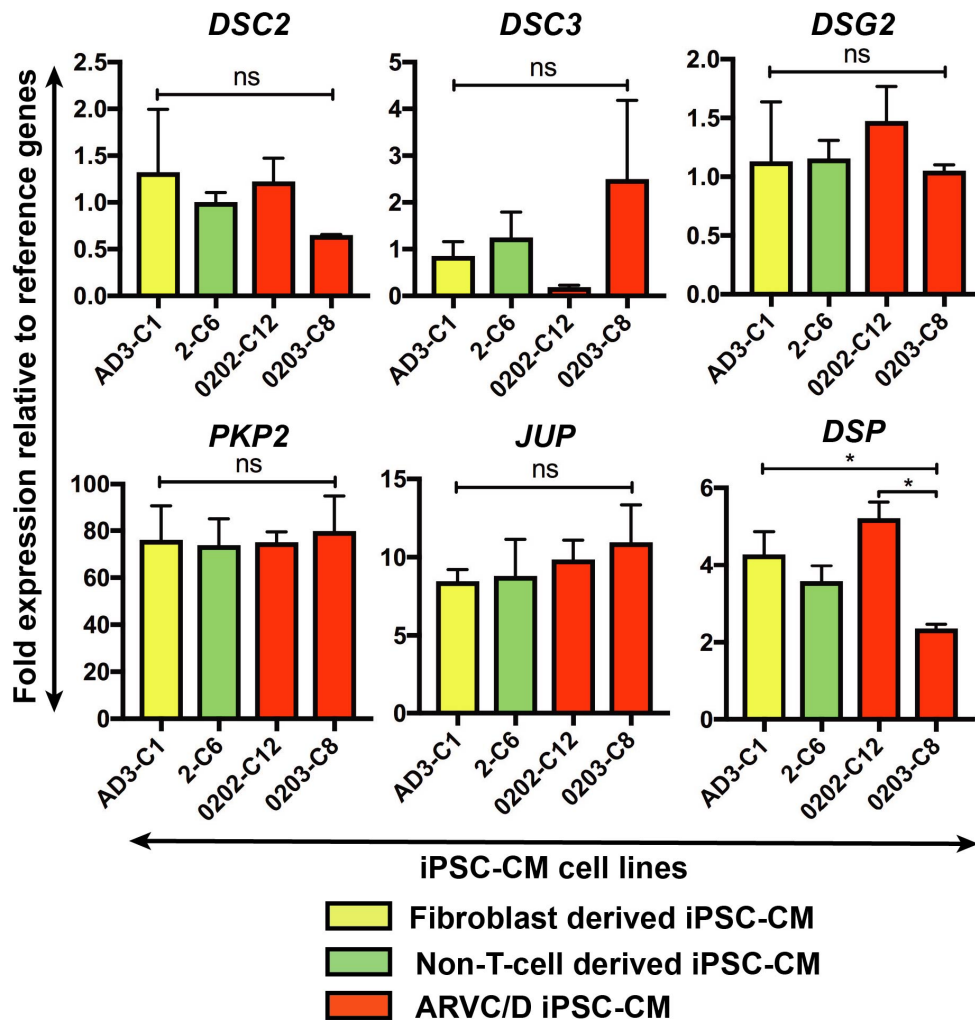


Figure 64 Expression of major desmosomal genes in iPSC-CMs

Bars indicate mean expression levels for each cell line across samples from three independent differentiation experiments, with the exception of 2-C6 which was across 5 experiments. Whiskers indicate SEM. Differences between cell lines were investigated with the one-way ANOVA, post hoc pairwise comparisons were made with Tukey's test p values <0.05 are indicated (*).

iPSC-CM	Genes					
	<i>DSC2</i>	<i>DSC3</i>	<i>DSG2</i>	<i>PKP2</i>	<i>JUP</i>	<i>DSP</i>
AD3-C1	23.7±0.6	24.3±0.7	23.9±0.5	17.6±0.3	20.7±0.2	21.7±0.2
2-C6	23.9±0.2	24.4±0.7	23.8±0.2	17.8±0.3	21.6±1.0	22.2±0.3
0202-C13	23.3±0.5	26.0±0.2	23.0±0.4	17.3±0.2	20.2±0.3	21.1±0.3
0203-C8	24.2±0.2	23.0±0.9	23.5±0.2	17.3±0.3	20.2±0.3	22.3±0.2

Table 60 Unadjusted Ct values from the assessment of desmosomal gene expression in iPSC-CMs.

The values presented are the means samples ± SEM.

6.3.7 Cellular localisation of desmosomal proteins in iPSCs

Immunofluorescence microscopy was used to assess the cellular localisation of DSP, JUP, PKP2, DSG2 and DSC2. The antibody to DSC2 was also known to cross react with DSC3. HaCaT cells were used as a positive control for these studies. This cell line has been reported to form desmosomes and express a wide range of desmosomal plaque proteins in previous publications (Kimura *et al.*, 2007) (Nie *et al.*, 2011). The presence of desmosomes in HaCaT cell cultures by TEM analysis was also confirmed in the study (data not shown).

In the HaCaT cell line an abundant punctate signal forming linear patterns distinct from the DAPI signal was seen with all antibodies (Figure 65). In addition to the linear patterns a more diffuse signal punctate was seen in some cells. Desmosomal protein signal was not observed to co-localise with DAPI.

Desmosomal protein localisation was assessed in five pluripotent cell lines: 2-C6 iPSCs and H9 hESCs (Figure 65) and the three ARVC/D iPSCs (Figure 66). Each line was assessed in a single passage.

The DSC2/3, DSG2 and DSP signal in all iPSCs (control and ARVC/D) formed a clear puncti-linear pattern that often enclosed nuclei. The DSG2 signal in 0203-C8 iPSCs appeared less abundant such that it formed a more scattered punctate signal rather than lines suggesting a boundary between cells. Manual analysis of individual slices of Z-stack images found that the DSC2/3, DSG2 and DSP signals did not co-localise with the DAPI signal of the nucleus.

Punctate signals were also observed with labelling of PKP2 and JUP signal in iPSCs but not in H9 hESCs in which it appeared diffuse and cytoplasmic. In some areas the punctate JUP signal was organised into linear patterns, but for both JUP and PKP2 the signal was mostly not organised into a pattern. Punctate PKP2 signal that co-

localised with nuclear DAPI signal was seen in all iPSC lines (control and ARVC/D) and in the HaCaT cells (Figure 65) (Figure 66).

6.3.8 Cellular localisation of desmosomal proteins in iPSC-CMs

iPSC-CMs were studied from 2-C6, 0101-C41, 0202-C13 and 0203-C8. For each cell line, samples from three independent differentiation experiments were studied, with all five desmosomal antibodies assessed in each experiment. Signal associated with iPSC-CMs was identified by co-labelling with an antibody to cTnT.

Signal for all desmosomal proteins was seen in all cell lines (Figure 67). All the antibodies produced a punctate signal. This signal was frequently organised into puncti-linear patterns or regions of continuous linear signal consistent with the presence of adjacent intercellular adhesion junctions at the plasma membrane.

In some cells the punctate signal was not clearly organised into linear patterns. This was particularly noticeable in the assessment of DSG2 signal in 0202-C13 and 0203-C8. The DSG2 signal in 0203-C8 also appeared less abundant than in the control cell line (Figure 67), echoing the pattern seen in undifferentiated iPSCs. Occasional punctate JUP and PKP2 signal that co-localised with the nucleus was noted in both the control and ARVC/D iPSC-CMs (Figure 68).

The signal intensity for all antibodies was highly variable both within samples and between experimental repeats. Samples from both control and ARVC/D clones contained clusters of iPSC-CMs in which no desmosomal signal was apparent and other regions in which there was a strong signal.

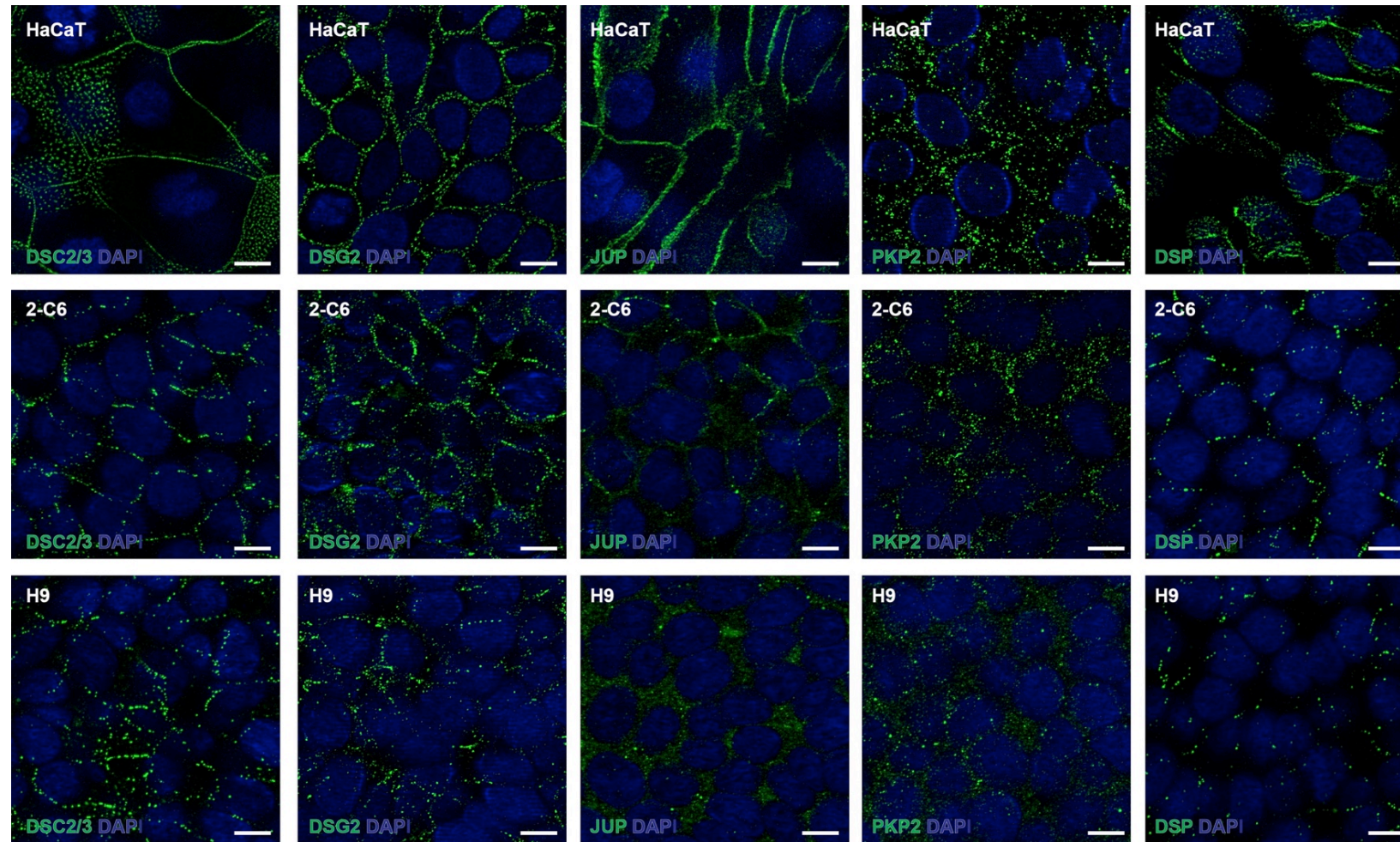


Figure 65 Immunofluorescence microscopy images of desmosomal protein signal in immortalised keratinocytes (HaCaT) and pluripotent cell lines. Scale bars indicate 10 μ m.

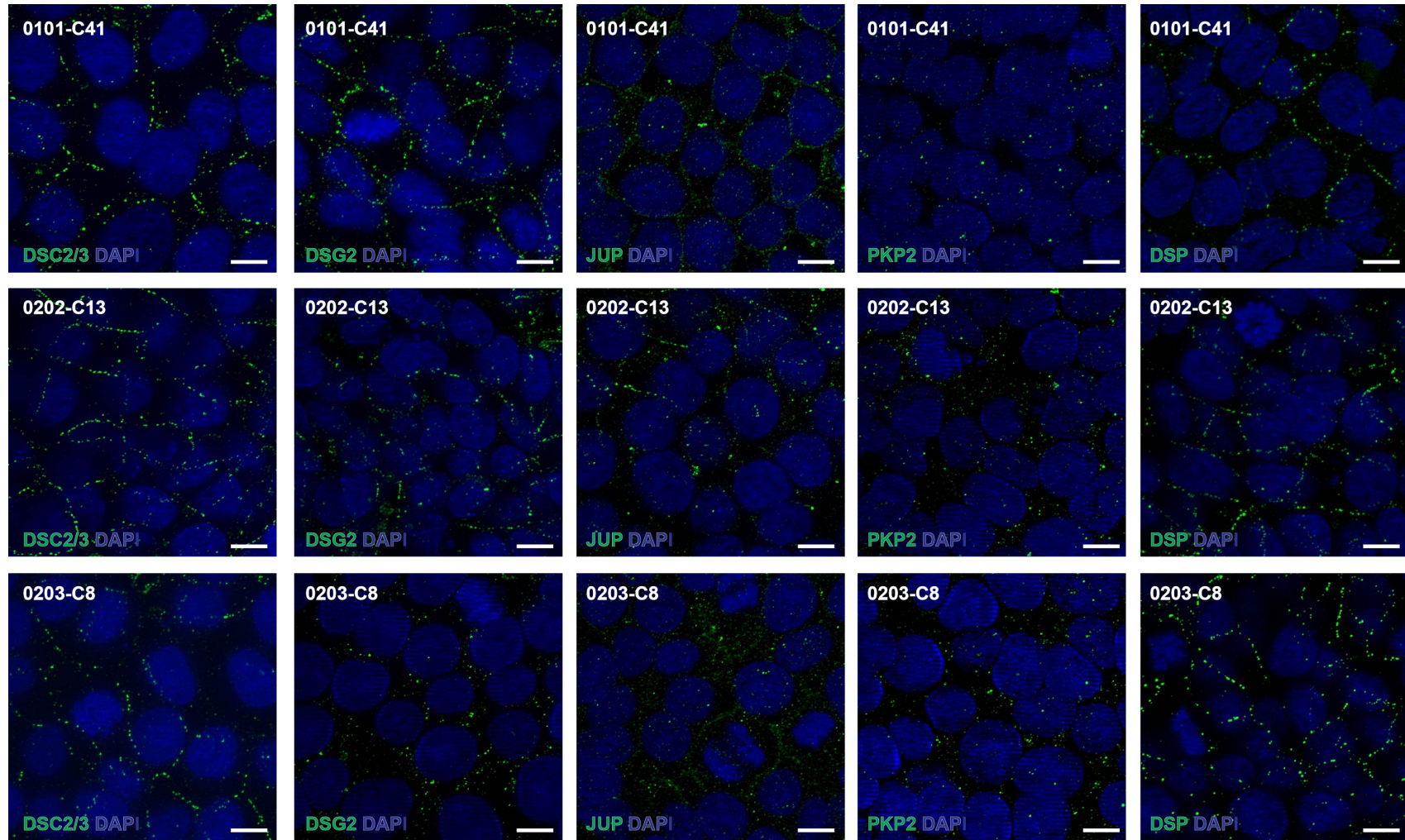


Figure 66 Immunofluorescence microscopy images of desmosomal protein signal in ARVC/D iPSCs. Scale bars indicate 10 μ m.

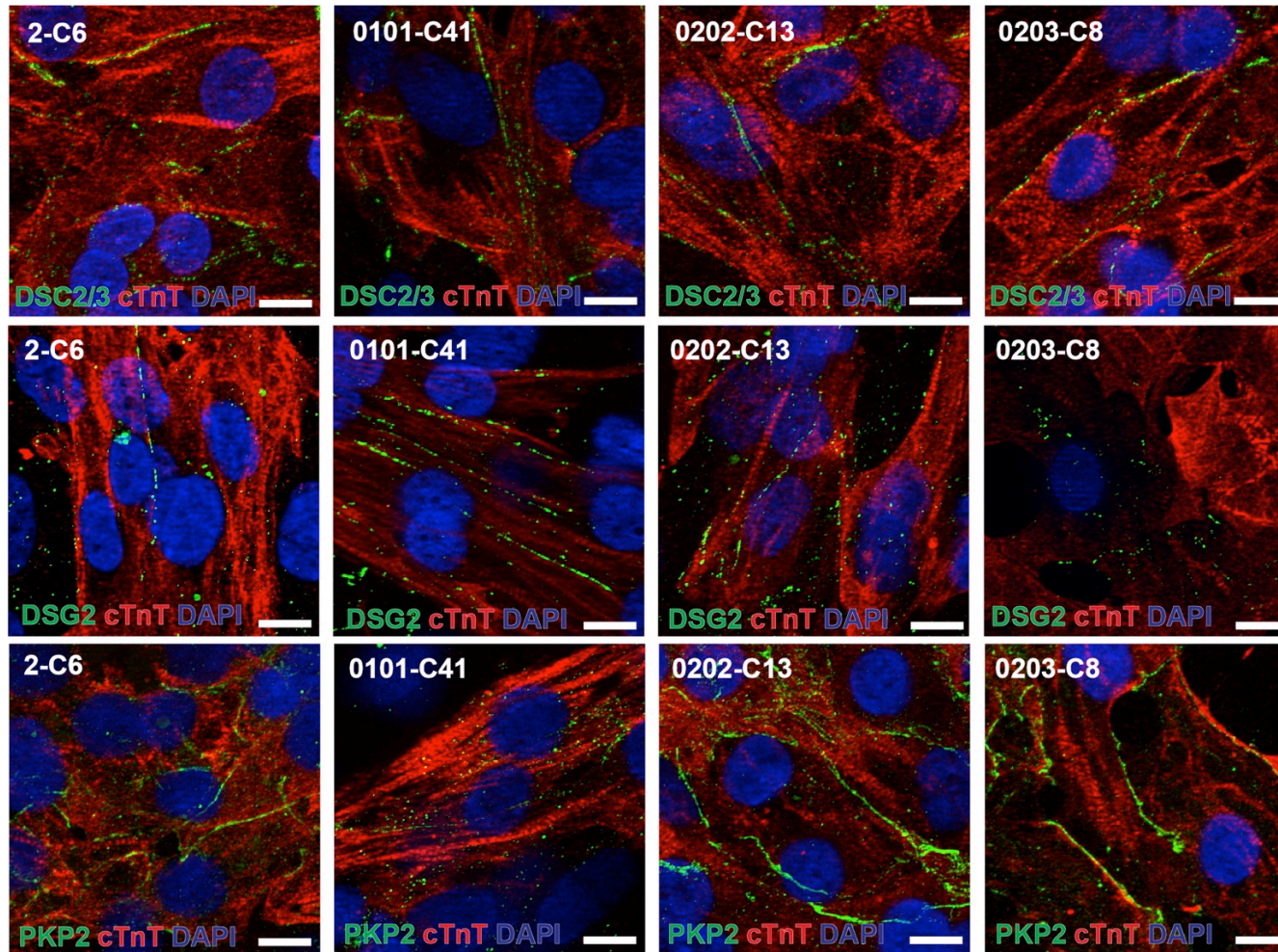
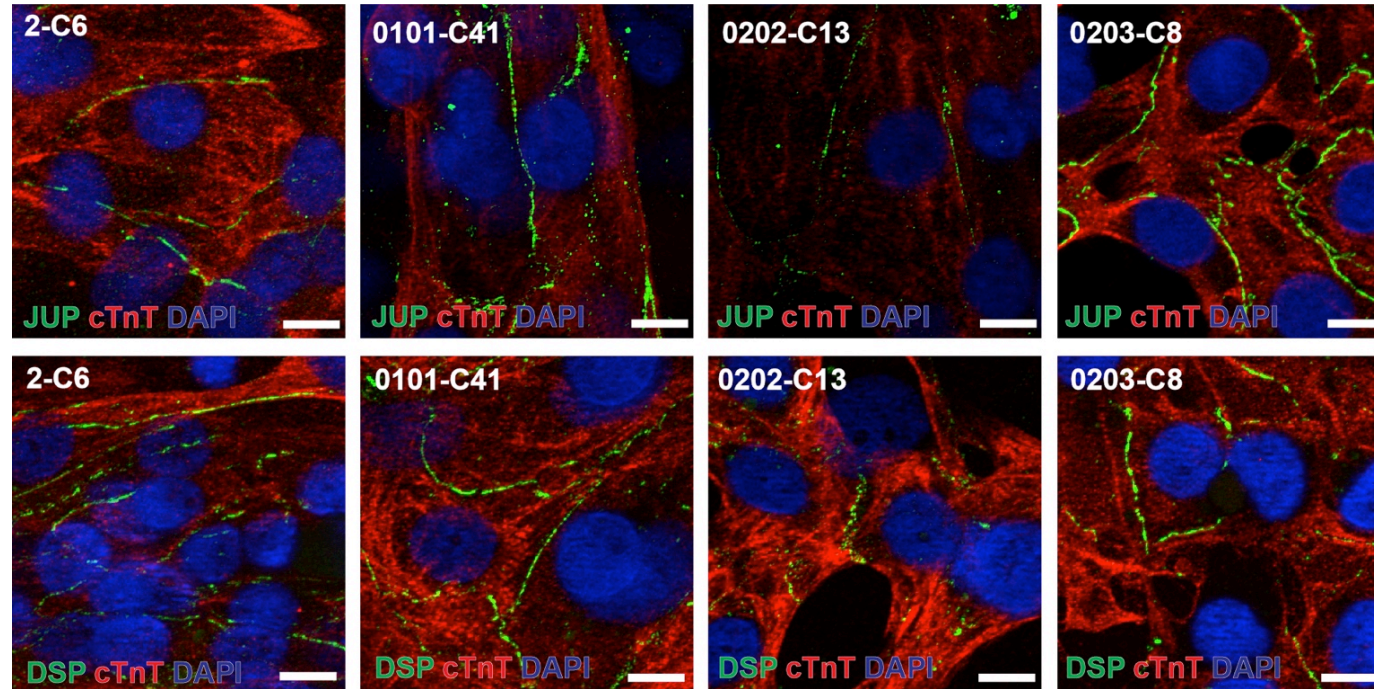


Figure 67 Representative immunofluorescence microscopy image of desmosomal protein localisation in iPSC-CMs

(continued)



Scale bars indicate 10 μ m

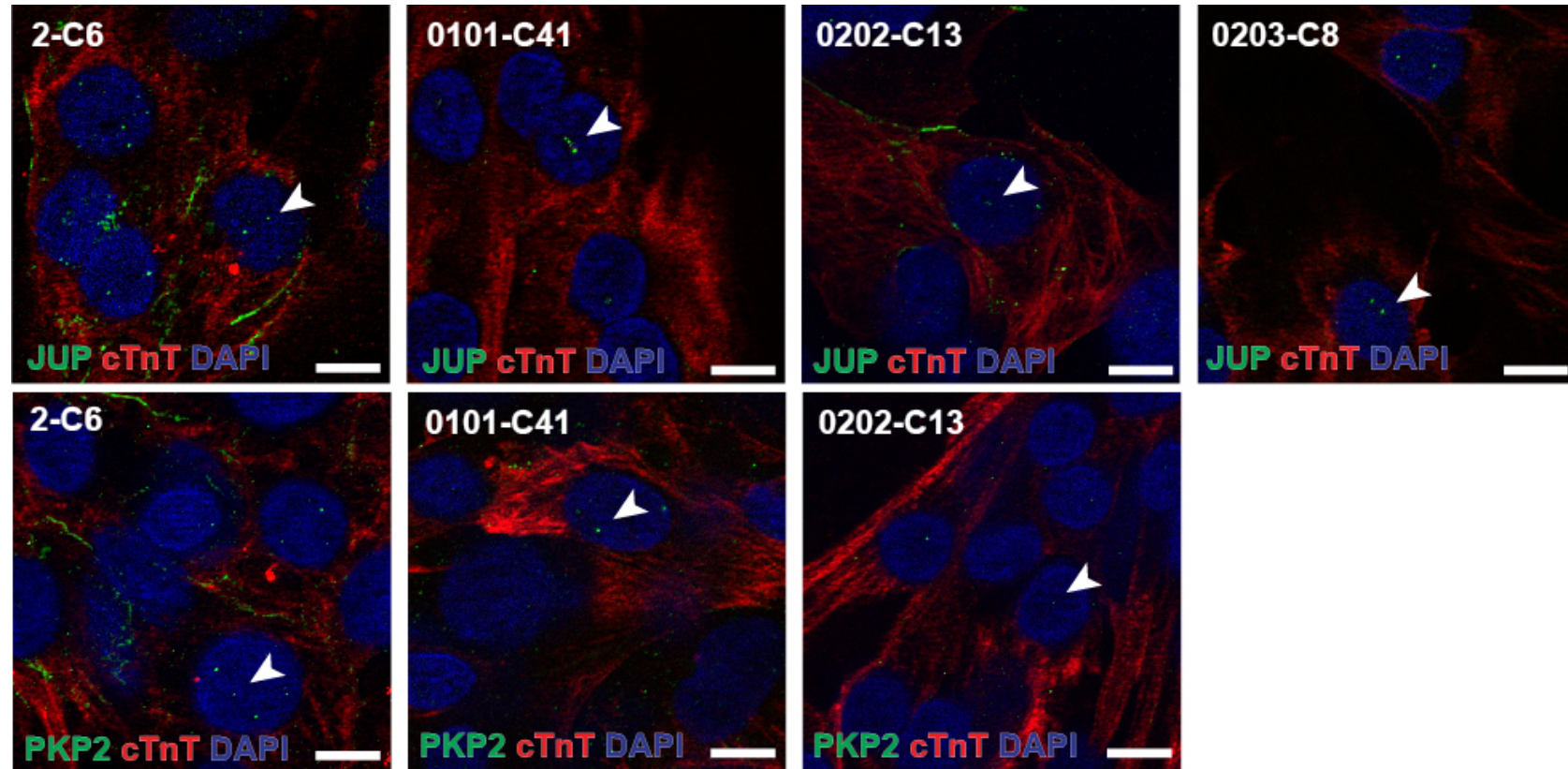


Figure 68 Nuclear localisation of punctate JUP and PKP2 signal in iPSC-CMs
Single slice images from Z-stack suggesting co-localisation of punctate JUP and PKP2 signal with nuclear DAPI signal (arrow heads).
Scale bars indicate 10 μ m

6.4 Discussion

6.4.1 Desmosomal ultrastructure and quantitative assessments of morphology

The data in this chapter demonstrate that the study methodology was capable of generating images of desmosomes of sufficient quality for quantitative analyses of desmosomal morphology. The bi-laminar appearance attributed to the plasma membrane and the ODP separated from this by the less electron dense region are similar to those reported in the studies discussed in chapter 1 (Kelly, 1966) (North *et al.*, 1999). These structures were a sufficiently consistent feature of the desmosome images that they were considered suitable to define the parameters used for morphometric analysis.

The IDP is thought to consist of rod domains and plakin repeat domains (PRD) of DSP along with points of interaction with intermediate filaments (IF) (Holthöfer *et al.*, 2007). The initial plan for this study was to use this junction to define a parameter referred to as the inter-IDP width (IIW). IIW was to be the distance between the IDP-IF junctions of adjacent plaques of a desmosome, thereby encompassing both the ODP and intermembranous gap. This parameter was chosen because it was comparable to a parameter measured by Caspi *et al.* called total desmosomal width, which was reported to be significantly increased in ARVC/D iPSC-CMs compared with controls (Caspi *et al.*, 2013). In this study the junction of the IDP and the intermediate filaments was not consistent in being either identifiable or a consistent distance from the edge of the ODP. Consequently it was decided that the IIW could not be measured. Difficulty in defining the IDP-IF junction as a line that is parallel to the ODP has been reported in previous publications that have attempted to quantify desmosomal widths (Al-Amoudi *et al.*, 2011). There are several possible explanations for this finding. Since definition of the IDP-IF junction requires a step change in the protein density between the IDP and IFs it could be obscured by the density associated with converging IFs. Alternatively it may suggest that the organisation of DSP within the plaque is such that the IF binding PRD is not located at a single distance from the ODP edge.

6.4.2 Desmosomes in iPSCs and hESCs

The data from this study suggest that pluripotent cells *in vitro* (iPSCs and hESCs) express desmosomal genes at levels that are comparable to that found in

desmosome bearing tissues (myocardium) and are greater than in non-desmosome bearing tissues (PBMCs). TEM analysis confirmed the presence of desmosomes in cultures of both iPSCs and hESCs. The puncti-linear signal seen by immunofluorescence microscopy in these cultures is consistent with both the expression of desmosomal proteins and with their localisation to focal inter-cellular adhesion junctions.

Previous reports have suggested that desmosomes are absent from the inner cell mass (ICM) (the archetypal pluripotent cell type) *in vivo* (Ducibella *et al.*, 1975). In these studies of mouse embryos desmosomes were detected by TEM in the late morulae stage. Following compaction and blastulation they are localised to the trophectoderm. Desmosomes appear to be absent from the inner cell mass (ICM) until it begins to differentiate into epithelia of the primitive germ cell layers (Jackson *et al.*, 1981). The expression of some desmosomal genes (*DSC3*, *DSG2*, *JUP*, *DSP*) have been reported to be expressed throughout embryonic development (Den *et al.*, 2006). Homozygous knock-out mouse models of *DSC3*, *DSG2*, *JUP*, *PKP2* or *DSP* have been found to result in embryonic lethality. In *DSC3* and *DSG2* knock-out models this occurs before or around the time of implantation and is thought to represent abnormalities in the trophectoderm (Den *et al.*, 2006) (Eshkind *et al.*, 2002). In *DSP* knock-out embryos, implantation occurs as normal but abnormalities in tissue architecture develop in the blastocoel (Gallicano *et al.*, 1998). *PKP2* and *JUP* knock-out does not appear to affect early embryonic development but does result in death in mid-gestation from cardiovascular abnormalities (Bierkamp *et al.*, 1996) (Grossmann *et al.*, 2004). Taken together these studies do not suggest that desmosomal proteins are important to the function of pluripotent cells of the ICM *in vivo*.

Despite their absence in the ICM, desmosomes have been reported in cultures of ESCs *in vitro* (Sathananthan *et al.*, 2002). In addition the expression of a range of desmosomal genes has been reported in cultures of pluripotent cell lines in a meta-analysis of publically available RNA expression data (Mabbott *et al.*, 2013). Other investigators have described intercellular junctions between ESCs that lack the laminated plaque and connections to the cytoskeleton that are typical of desmosomes but contain at least one desmosomal plaque protein (*DSG2*) (Eshkind

et al., 2002)ⁿ. This study was specifically focused on identifying structures with the typical ultrastructural features of desmosomes in PSCs. The frequency of junctions without this morphology, such as the immature junctions described by Eshkind *et al.* was not systematically assessed.

Collectively, previous reports and the data from this study support the idea that the expression of desmosomal genes and the organisation of their proteins into intercellular junctions is a characteristic of PSCs *in vitro*.

The function of these proteins in PSCs remains unclear. It has been reported that the knock-out of *JUP* in ESCs had no effect on the maintenance of pluripotency (Sun *et al.*, 2017). Similar knock-out experiments in PSCs for the other desmosomal genes have not been reported and may be a useful focus for future work.

Since desmosomes are most commonly found in differentiated epithelia, it could be argued that the identification of desmosomes at the edges of PSC colonies indicates a loss of pluripotency in these regions. It is a limitation of the study methodology that co-labelling of pluripotency markers and desmosomal proteins was not performed in order to investigate this possibility. There is evidence that the organisation of the cytoskeleton (and associated adhesions junctions) in cells at the peripheries of ESC colonies represents a mechanism for the maintenance of pluripotency. Bundles of actin and myosin filaments have been identified in peripheral cells forming a band circumscribing the colony centre (Närvä *et al.*, 2017) (Rosowski *et al.*, 2015). It has been suggested these fibres generate mechanical forces within PSC via focal adhesions of the cells to the culture substrate and that these forces act to maintain pluripotency within the colony and regulate colony expansion. If mechanical forces do have a role in maintaining pluripotency and regulating colony growth it is also possible that intercellular adhesion has a role in this process. In this context the ability of ESCs to form intercellular adhesion junctions (such as desmosomes) in peripheral cells of colonies may have a role in maintaining pluripotency *in vitro*. The intermediate filament protein vimentin has been reported to be expressed in ESCs at a level comparable to that of fibroblasts, although its organisation in cells in colonies has not been characterised (Boraas *et al.*, 2016). The hypothesis that intercellular adhesion mediated by desmosomes (or junctions containing desmosomal proteins)

ⁿ The cells in which Eshkind *et al.* reported these immature junctions did not express the DSP protein which is known to both regulate desmosome formation and mediate interactions with intermediate filaments. Therefore it may be that the immature junctions in this report are secondary to an abnormality in the cell line studied and are not representative of ESCs in general.

has a role in maintaining pluripotency regulating colony growth and could be a focus for future work.

6.4.3 The effect of ARVC/D associated mutations on desmosomal gene expression

The ARVC/D cell lines in this study carried mutations in *PKP2*, *DSG2* and *DSP*.

The *PKP2* mutation carried by 0101-C41 was predicted to result in aberrant splicing of exon 11, a region that is included in transcripts encoding PKP2b and the dominant shorter cardiac isoform PKP2a^o (Gandjbakhch *et al.*, 2011). The primer set used to assess *PKP2* expression was designed such that it would amplified transcripts containing exon 12 and a correctly spliced exon 13-14 junction. This primer set therefore assessed the total quantity of transcripts encoding both PKP2a and PKP2b including any in which exon 11 might be missing due to mutation induced exon skipping. Since it was not possible to generate samples containing >75% iPSC-CMs from 0101-C41 the analysis of *PKP2* expression in this line was limited to iPSCs. In this analysis *PKP2* transcripts were not significantly less abundant than in other iPSC lines. This would be consistent with the formation of an alternatively spliced mutant transcript that is not degraded by mechanisms such as nonsense mediated decay and may be translated to a mutant protein. Further work is needed to investigate these possibilities. RT-PCR combined with sequencing of the region encoded by exons 10 to 12 region would be useful to assess its effect on exon 11. If a significant level of mutant transcripts could be demonstrated to be present further studies to look for the expression of mutant proteins could be pursued.

The *DSG2* mutation carried by 0202-C13 was demonstrated by clinical testing to result in transcripts missing exon 7 and the insertion of CAG between exons 6 and 8. The primer set used to assess *DSG2* expression was designed to amplify a region between the exon 13-14 junction and part of exon 14 and would therefore detect both normal and abnormal length transcripts. No significant difference was observed in the abundance of *DSG2* transcripts between 0202-C13 and other cell lines in both iPSCs and iPSC-CMs. RT-PCR and sequencing of the *DSG2* transcripts resulting from this mutation had been assessed as part of the subject's clinical assessment. The work in this study suggests that the abnormal transcript produced is not degraded and may result in synthesis of a mutant protein.

^o Created by alternative splicing that excludes exon 6.

The *DSP* mutation carried by 0203-C8 was predicted to result in transcripts containing a premature stop codon in exon 23 that would be predicted to affect both DSP I and II. The primer set used to assess *DSP* was designed to amplify a region between exon 1 and 2 and therefore both normal and abnormal transcripts. A trend towards reduced *DSP* expression was observed in iPSCs and iPSC-CMs but *DSP* expression was only significantly different between cell lines in iPSC-CMs and expression was only lower in 0203-C8 in the pairwise post hoc comparison with 0202-C13. The trend to reduced *DSP* expression in 0203-C8 could be better characterised with samples from a greater number of experimental repeats and by comparison of the expression of a group of PBMC derived control lines from multiple individuals.

Both Ma *et al.* and Caspi *et al.* studied ARVC/D iPSC-CMs bearing *PKP2* mutations and reported an associated reduction in *PKP2* expression. In addition Ma *et al.* reported a reduction in *JUP* expression, the mechanism for which was not elucidated. Neither study quantified the proportion of cells in the samples used for the RT-qPCR analysis. As a result of this, and the fact that non-cardiomyocytes also express desmosomal genes any conclusions regarding desmosomal gene expression in iPSC-CMs that might be drawn from their data are weak.^p In the present study the proportion of cardiomyocytes in samples used for RNA was quantified and was $\geq 75\%$ in all sample used in the analyses of desmosomal genes. In this respect the conclusions of this study, that the expression of desmosomal genes in iPSC-CMs were not affected by an ARVC/D mutation studied, may be considered to have greater validity than those of previous reports.

It could be argued that the use of unrelated iPSC lines as a standard against which changes in expression in mutation bearing lines were compared limited the power of this experiment to detect such changes. Considerable inter-line variations in gene expression was noted e.g. the expression of *DSG2* and *PKP2* in AD3-C1 was significantly greater than other control cell lines. It is conceivable that the effect of the mutation in 0101-C41 was to reduce the expression of *PKP2* from a level similar to that of AD3-C1 to the level observed in this study. Alternative controls could be generated by the correction of ARVC/D mutations using gene editing.

^p Ma *et al.* attempted to control for a variable proportion of cardiomyocytes in the samples by normalising desmosomal gene expression to sarcomeric gene expression (*MYH7* and *ACTN2*). This is based the assumption that sarcomeric gene expression is proportional to the proportion of iPSC-CMs in a sample. It is therefore possible that the difference in *JUP* and *PKP2* expression reported by Ma *et al.* resulted from the control samples containing fewer iPSC-CMs than the ARVC/D samples (and therefore lower *MYH7* expression) combined with containing a non-cardiomyocyte population that expresses desmosomal genes.

6.4.4 Desmosomal gene expression in iPSC-CMs relative to iPSCs and RAA

This study has identified differences between iPSCs, iPSC-CMs and RAA myocardium in the expression of desmosomal genes.

The difference in *DSC1* expression between iPSC-CMs, where it was effectively absent, and RAA, in which mean expression was 6.0 fold reference gene expression (SEM 2.1) is striking. The expression of *DSC1* and its protein by myocardium *in vivo* had been reported by the Human Protein Atlas and the genotype-tissue expression (GTEx) project (Uhlén *et al.*, 2015) (GTEx Consortium, 2013). Data from the GTEx project is of particular interest since it assessed gene expression in atrial appendage samples and left ventricular samples by mRNA sequencing assays. The median level of *DSC1* expression was below the project's detection threshold of 1 transcript per million (TPM) in the left ventricular samples but was detectable in the RAA samples (median expression 9.1 TPM). Since myocardium consists of a mixture of cell types including cardiomyocytes, fibroblasts and endothelial cells, it is possible that these differences in expression reflect differences in the cellular composition of ventricular and atrial myocardium. Immunohistochemistry data from the HPA indicates that the *DSC1* protein is localised to the intercalated discs of cardiomyocytes ("HPA *DSC1* heart immuno," 2018). This raises the possibility that there are regional variations in *DSC1* expression by cardiomyocytes within the heart. In this context the absence of *DSC1* expression iPSC-CMs is difficult to interpret. Further work could be directed at investigating the hypothesis that *DSC1* is a chamber specific cardiomyocyte marker.

The gene expression data in this study also suggested that despite differentiation from pluripotency to a cardiomyocyte cell type the expression of *DSC3* in iPSC-CMs remains similar to that seen in iPSCs and greater than seen in RAA samples. The mean expression of *DSC3* was lower than *DSC2* in iPSCs 0.66 (SEM 0.05) vs 1.80 (SEM 0.20) (2 tailed T-test, $p=0.0001$). These data conflict with that of the Primary Cell Atlas which suggested that *DSC3* expression was low or absent in hESCs and iPSCs (Mabbott *et al.*, 2013). The low levels of *DSC3* in RAA are consistent with data from the HPA which found no evidence of either gene or protein expression in myocardium ("HPA heart *DSC3*," 2018). Further work is needed to confirm the expression of *DSC3* in iPSCs and iPSC-CMs. Sequencing of RT-PCR amplicons from *DSC3* targeted primer sets could be used to provide additional evidence of gene expression. Immunofluorescence and immunoblotting studies with *DSC3* specific antibodies would provide additional evidence of the presence and localisation of the

protein in these cells. If the expression of *DSC3* and its protein were confirmed in iPSCs and iPSC-CMs it would suggest that, despite differentiation, iPSC-CM retain some aspects of the cadherin expression pattern seen in iPSCs. This point is broadly supported by previously reports that the transcriptomic and proteomic profile of hESC-CMs is similar to but distinct from both fetal and adult cardiomyocytes (Cao *et al.*, 2008) (Xu *et al.*, 2009) (Poon *et al.*, 2015).

6.4.5 Desmosomal protein localisation in control an ARVC/D iPSCs and iPSC-CMs

The cellular distribution of desmosomal proteins in undifferentiated ARVC/D iPSCs has not been described in previous reports. Previous reports of cellular manifestations of ARVC/D in tissues other than myocardium (see Chapter 1) provide a precedent for the study of ARVC/D in un-differentiated iPSCs.

No difference was identified between control and ARVC/D iPSCs in terms of protein localisation. In this study the DSC2, DSG2 and DSP signal in ARVC/D iPSCs had the same puncti-linear pattern in the control iPSC line (2-C6). The JUP and PKP2 signal in ARVC/D iPSCs also showed the same pattern as control lines, with the exception of occasional nuclear punctate signals that were not observed in control samples. In iPSC-CMs these punctate nuclear signals were observed in control and ARVC/D samples. Kim *et al.* found a similar JUP signal in ARVC/D iPSC-CMs but not in controls and concluded that this was evidence of the redistribution of JUP from the plasma membrane to the nucleus (Kim *et al.*, 2013). As discussed in chapter 1 JUP and PKP2 have roles in intracellular signalling pathways (such as Wnt and Hippo signalling) which have the potential to produce the cellular pathophysiology characteristic of ARVC/D.

The modulation of Wnt signalling by changes in desmosomal protein expression was demonstrated by Garcia-Gras *et al.* (Garcia-Gras, 2006). They reported that the suppression of DSP (by siRNA in HL-1 cells and in a cardiac restricted DSP knock-out mouse model) resulted in a shift of plakoglobin from the cytoplasm to the nucleus and a suppression of Wnt signalling. Evidence supporting this was mainly in the form of immune-blotting of cytosolic and nuclear fractions. The nuclear JUP immunofluorescence pattern of HL-1 cells manifesting these changes was diffuse and homogenous rather than a punctate signal. This would be consistent with the activity of non-membrane bound JUP which regulates TCF/LEF1 transcription factors and would not therefore be expected to be concentrated at a specific location.

Taken together the evidence that the punctate signal reported by Kim *et al.* and observed in this study represents nuclear redistribution of plakoglobin in weak, and it is suggested that such signals should be regarded as artefact.

There have been two reports of a reduction in the intensity of JUP and PKP2 immunofluorescence signal in ARVC/D iPSC-CMs carrying *PKP2* mutations. Ma *et al.* reported that the average intensity of PKP2 and JUP immunofluorescence signal in images of ARVC/D iPSC-CMs carrying a PKP2 mutation was lower than in a control iPSC-CM (Ma *et al.*, 2012). Caspi *et al.* reported a similar finding but normalised this average signal intensity to the area of cTnT signal with which it was associated (Caspi *et al.*, 2013). The approach of Caspi *et al.* complicates the interpretation of their results since they could result from the ARVC/D iPSC-CMs being larger and flatter rather than containing less PKP2. In addition, neither Ma *et al.* or Caspi *et al.* described whether the investigators were blinded to the sample identity whilst acquiring the images in their studies, raising the possibility that the lower JUP and PKP2 signal they reported in ARVC/D iPSC-CMs was due to observer bias. Neither report stated the number of experimental repeats from which their images were obtained, raising the possibility that the differences they reported were due to experimental variation.

In the present study substantial variation was noted within individual samples in the intensity of desmosomal signal. For the purposes of assessing desmosomal protein distribution cells with the strongest signal were imaged. Quantification of signal intensity in this study would have required a strategy for selecting multiple regions of the sample at random followed by high magnification Z-stack imaging, and repeating this strategy across multiple samples. None of the ARVC/D samples consistently appeared to have less signal intensity or abundance than the control across multiple experiments. Given the wide range of signal intensities observed in all samples the probability that such an approach would detect a statistically significant quantitative difference between cell lines was felt to be too small to justify the resources needed to make this assessment.

6.5 Limitations

Several aspects of the study methodology limit the conclusions that may be drawn from this work. Co-localisation of immunofluorescence signals for desmosomal antibodies would have provided a stronger argument that the proteins present were combining to constitute the desmosomes seen by TEM. This was not possible with

the antibodies used in the work present here since they were all mouse monoclonal antibodies of the IgG1k isotype. Monoclonal antibodies were chosen for this work to provide optimal specificity of the signal. Future work could aim to demonstrate co-localisation using a different selection of anti-desmosomal antibodies.

In addition to the specific limitations already discussed a more general issue with this study is the number and quality of control lines. All PBMC derived control lines in this study came from a single subject that did not provide a match of both age and sex for any of the ARVC/D subjects. Although an additional control line was used (AD3-C1) this had a different cellular origin (fibroblast) to the disease lines, and this may also have an effect on its behaviour. In addition only a single clone from each of the ARVC/D subject was assessed raising the possibility that clonal variation may have masked more subtle ARVC/D changes.

6.6 Conclusions

The work presented in this chapter is consistent with the hypothesis that the generation iPSCs from PBMCs is associated with an upregulation of six desmosomal genes: *DSC2*, *DSC3*, *DSG2*, *PKP2* and *JUP*. The data presented in this chapter also supports the idea that the expression of desmosomal proteins and their incorporation into adhesion junctions (some of which have the typical appearance of desmosomes) is a feature of pluripotent cells in culture in general. It is hypothesised that these intercellular adhesion junctions have a function in regulating colony morphology and pluripotency as part of a more general system of cytoskeletal organisation at the edges of colonies of PSCs *in vitro*.

The differentiation of iPSCs to iPSC-CMs involves further changes in the pattern of desmosomal gene expression, specifically a decrease in the expression levels of the two main desmosomal cadherins (*DSC2* and *DSG2*) and an increase in the expression of the main plakophilin (*PKP2*) and of *JUP*. Despite these changes, the same puncti-linear immunofluorescence pattern of these proteins is seen in both cells types. Further work is needed to assess the co-localisation of these proteins and thus the composition of adhesion junctions identified by TEM.

No changes in the abundance of desmosomal gene transcripts were detected in ARVC/D iPSCs and iPSC-CM relative to controls in genes affected by ARVC/D associated mutations. Suggesting that mutant transcripts were not degraded by mechanisms such as nonsense mediated decay. It is unclear whether this is

representative of the effects of these mutations *in vivo* or whether biological and experimental variability in the iPSC and iPSC-CM models used in this study were sufficiently large to obscure the effects of the mutation. Further work is needed to investigate this possibility and whether these mutations result in the synthesis of abnormal proteins.

There was no evidence of a redistribution of desmosomal proteins (specifically JUP) from the plasma membrane to the nucleus in ARVC/D iPSC-CMs. Furthermore is argued that evidence for this being observed in any previously reported iPSC-CM model of ARVC/D was weak.

The intensity of immunofluorescence signal for all desmosomal proteins was highly variable in this study and therefore the quantification of desmosomal proteins by immunofluorescence was not attempted. Although previous reports have described using this technique for quantification of desmosomal proteins a critical appraisal of their methodology suggests that their reports of a reduction in signal intensity of desmosomal protein should be treated with caution. Other methods of quantification of these proteins such as by immunoblotting may be more robust than quantified cellular immunofluorescence. This approach was not possible in the present study due to the difficulty in consistently generating cultures containing a high proportion of iPSC-CMs. Optimisation of the differentiation protocol and further innovations in iPSC-CM generation and purification may allow this type of analysis in future work.

Chapter 7. A Comparison Of Desmosomal Ultrastructure In Control And ARVC/D iPSC-CMs.

7.1 Introduction

This chapter will discuss the ultrastructural morphology of desmosomes in control and ARVC/D iPSC-CMs. An outline of desmosomal ultrastructure and reports that the morphology of desmosomes differs between control and ARVC/D cardiomyocytes are given in Chapter 1. A description of the methodology of sample collection, processing, imaging and analysis are given Chapter 2.

7.2 Aims and hypotheses

The main aim of this work is to determine whether desmosomes of iPSC-CMs carrying an ARVC/D associated mutation were different to those of control iPSC lines. It was hypothesised that:

- Morphologically abnormal or hazy desmosomes would be present in ARVC/D lines but not in controls.
- Asymmetrical desmosomes are more frequent in ARVC/D lines compared with controls and the total length of asymmetrical segments per desmosome is longer in ARVC/D lines compared with controls.
- The average length of desmosomes is greater in ARVC/D lines compared with controls
- The intermembranous gap and inter-ODP widths would be increased in ARVC/D lines compared with controls.

7.3 Results

7.3.1 Sampling and data structure

All quantitative analyses of iPSC-CMs in this chapter are based on the same sample of 151 desmosome images from control cell lines and 93 desmosome images from ARVC/D iPSC-CMs. The control desmosome images were from four control cell lines (2-C3, 2-C7, 2-C4 and 2-C6) and the ARVC/D desmosomes images were from three ARVC/D cell lines (0101-C41, 0202-C13 and 0203-C8). Desmosome images for each cell line were from three differentiation experiments with each experiment using cells of a different passage, with the exception of 2-C6 which was assessed in six experiments. At least 10 desmosomes were assessed from each experiment.

Averaged values for each cell line were used for comparisons of ARVC/D with control iPSC-CMs. These averaged values were calculated as follows. An average of the parameter across the 10 (or more) desmosomes in each experimental repeat was calculated. If the data in all experiments were normally distributed (Shapiro-Wilk test $p > 0.05$) this average used was the mean, otherwise the median was used. The mean of these experimental averages was then calculated across the three (or more) experimental repeats for each cell line.

A total of 32 desmosome images from three RAA samples, with at least 10 desmosomes per sample, were also assessed and averaged depending on the normality of data distribution as described above.

7.3.2 Hazy desmosomes

Adhesion junctions^a with a hazy appearance were seen in RAA samples, immortalised keratinocytes (HaCaT cells), control iPSC-CMs and ARVC/D iPSC-CMs. In some cases the tilting of samples within the electron beam during imaging changed the appearance of these hazy junctions such that laminated plaques were observed indicating that these junctions were desmosomes (Figure 69).

^a This will be used as a general term to encompass desmosomes, adherens junction and adhesion junctions of an indeterminate type.

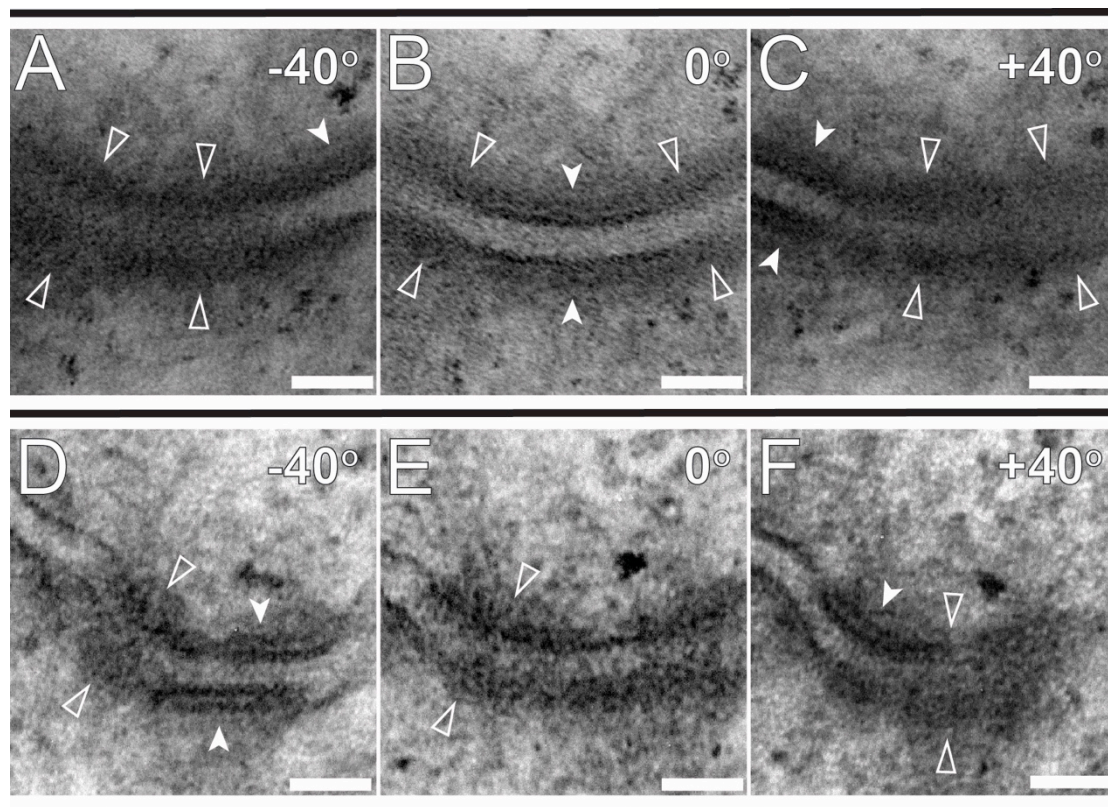


Figure 69 The effect of tilting a sample within the electron beam upon the appearance of desmosomes images by TEM.

Representative example of the effect observed with desmosomes from all tissues. Panels A to C and D to F show images of two desmosomes from different samples of RAA. The electron beam was oriented perpendicular to the TEM level in images B and E. The sample was tilted by 40° anti-clockwise from this starting position to obtain images A and D and by 40° clockwise from this starting position to obtain images C and F. Regions of the image in which typical laminated plaques are seen identifying the structure as a desmosome (solid arrowheads) and those in which it appears hazy (hollow arrowheads) and are indicated in each panel. Scale bars represent 50nm.

7.3.3 Desmosomal asymmetry

Asymmetrical desmosomes were identified within samples from control iPSC-CMs, ARVC/D iPSC-CMs, RAA cardiomyocytes and immortalized keratinocytes (HaCaT) (Figure 70). Short regions of discontinuity in desmosomal plaques were observed. It was also noted that curved desmosomes typically have plaques of slightly different lengths. No definition of desmosomal asymmetry has been published in previous literature. For the purposes of assessing the frequency of asymmetrical desmosomes and their characteristics desmosomes were classified as asymmetrical if the total length of its asymmetrical segments was >20nm. The frequency of greater degrees of asymmetry was also assessed using cut-off values of a total asymmetrical length >50nm and >100nm.

The distribution of total length of asymmetrical segments across all 244 desmosome images had a strong positive skew (skewness 3.4). This pattern was similar in both the control desmosomes and ARVC/D desmosomes (Figure 71 A). If only the 112 asymmetrical desmosomes are considered, the median (Q1-Q3) proportion of total length taken up by asymmetrical segments was 34% (24-49) for control iPSC-CMs and 28% (22-48) for ARVC/D iPSC-CMs (Figure 71 B).

After averaging the mean proportion of desmosomes classified as asymmetrical was 44% (SD 7) for control desmosomes and 48% (SD 5) of ARVC/D desmosomes (two tailed T-test, $p > 0.05$). The mean proportion of desmosomes with asymmetrical segments $> 50\text{nm}$ was 26% (SD 6) for control desmosomes and 28% (SD 4) of ARVC/D desmosomes (two tailed T-test, $p > 0.05$). The mean proportion of desmosomes with asymmetrical segments $> 100\text{nm}$ was 12% (SD 4) for control desmosomes and 10% (SD 4) of ARVC/D desmosomes (two tailed T-test, $p > 0.05$).

Differences at the level of individual lines were also assessed. There was no significant difference between any of the control or ARVC/D cell lines in the degree of asymmetry (Figure 72 A-B) or the frequency of asymmetrical desmosomes using any of the three cut off values ($> 20\text{nm}$, $> 50\text{nm}$ or $> 100\text{nm}$ (Figure 72 C-E) (one way ANOVA, $p > 0.05$).

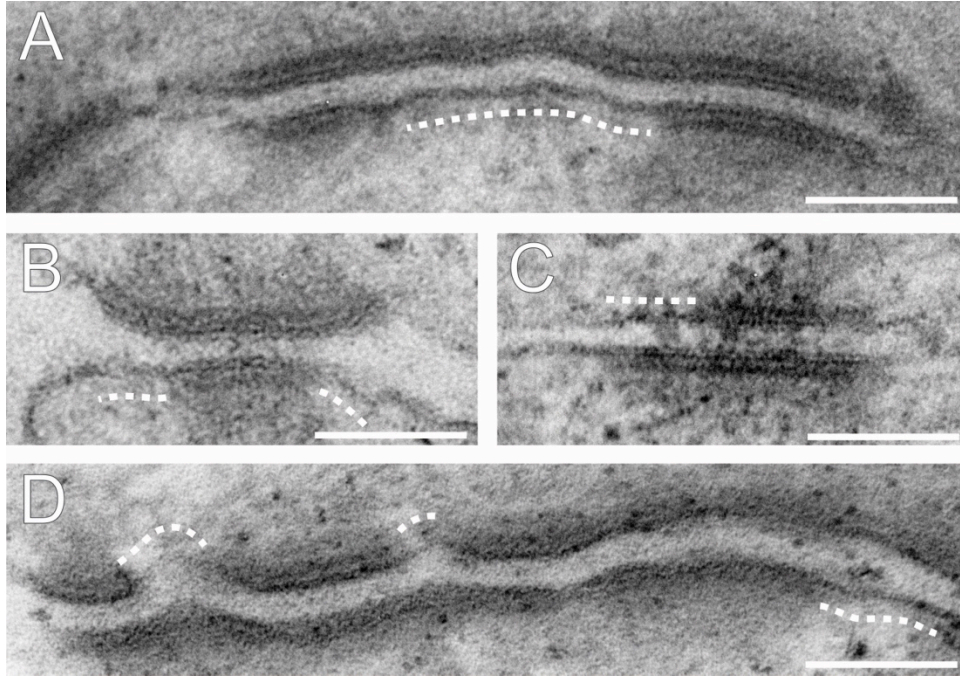


Figure 70 Examples of asymmetrical desmosomes

Representative desmosomes from differentiated iPSCs (2-C6) (Panels A and B), immortalised keratinocytes (HaCaT) (Panel C), and myocardium (RAA) (Panel D). Regions in which a desmosomal plaque is only present on one side of the intermembrane gap are indicated by a dashed line. Scale bars represent 100nm.

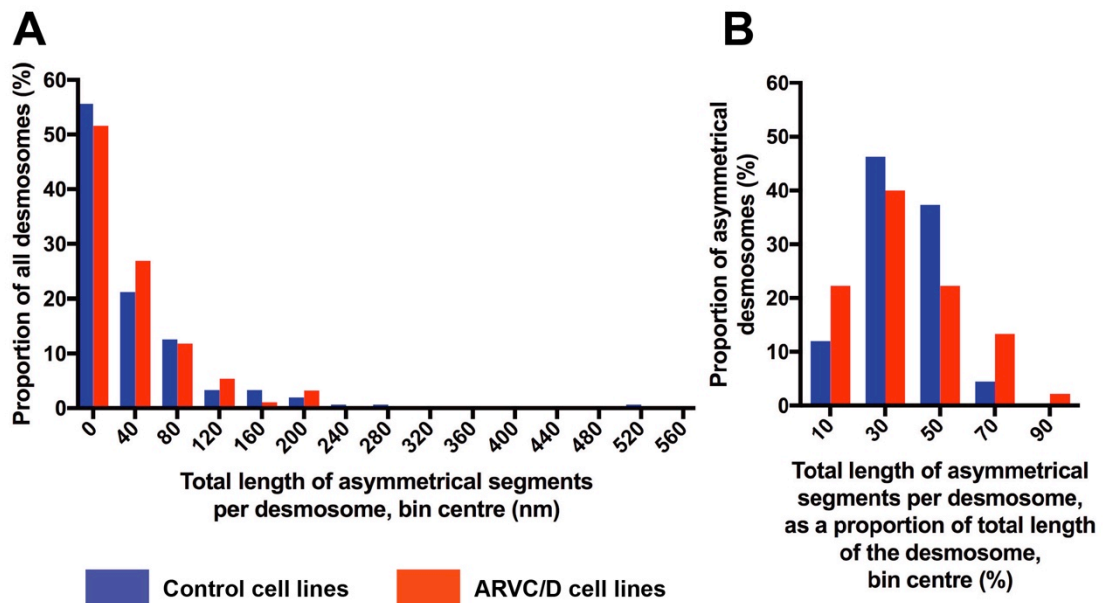


Figure 71 Total length of asymmetrical segments of desmosomes in control and ARVC/D iPSC-CMs

The histogram in panel A summarises the length of asymmetrical segments in all 151 desmosomes assessed across the four control lines (2-C3, 2-C7, 2-C4 and 2-C6) and the 93 desmosomes across the three ARVC/D lines (0101-C41, 0202-C13, 0203-C8). Each bin contains values that are within 20nm of the bin centre value. The histogram in panel B summarises length of asymmetrical segments as a proportion of the total desmosomal length in those desmosome classified as

asymmetrical i.e. with a total of >20nm length of asymmetrical segments. Data from 67 control desmosomes and 45 ARVC/D desmosomes across multiple cell lines is summarised.

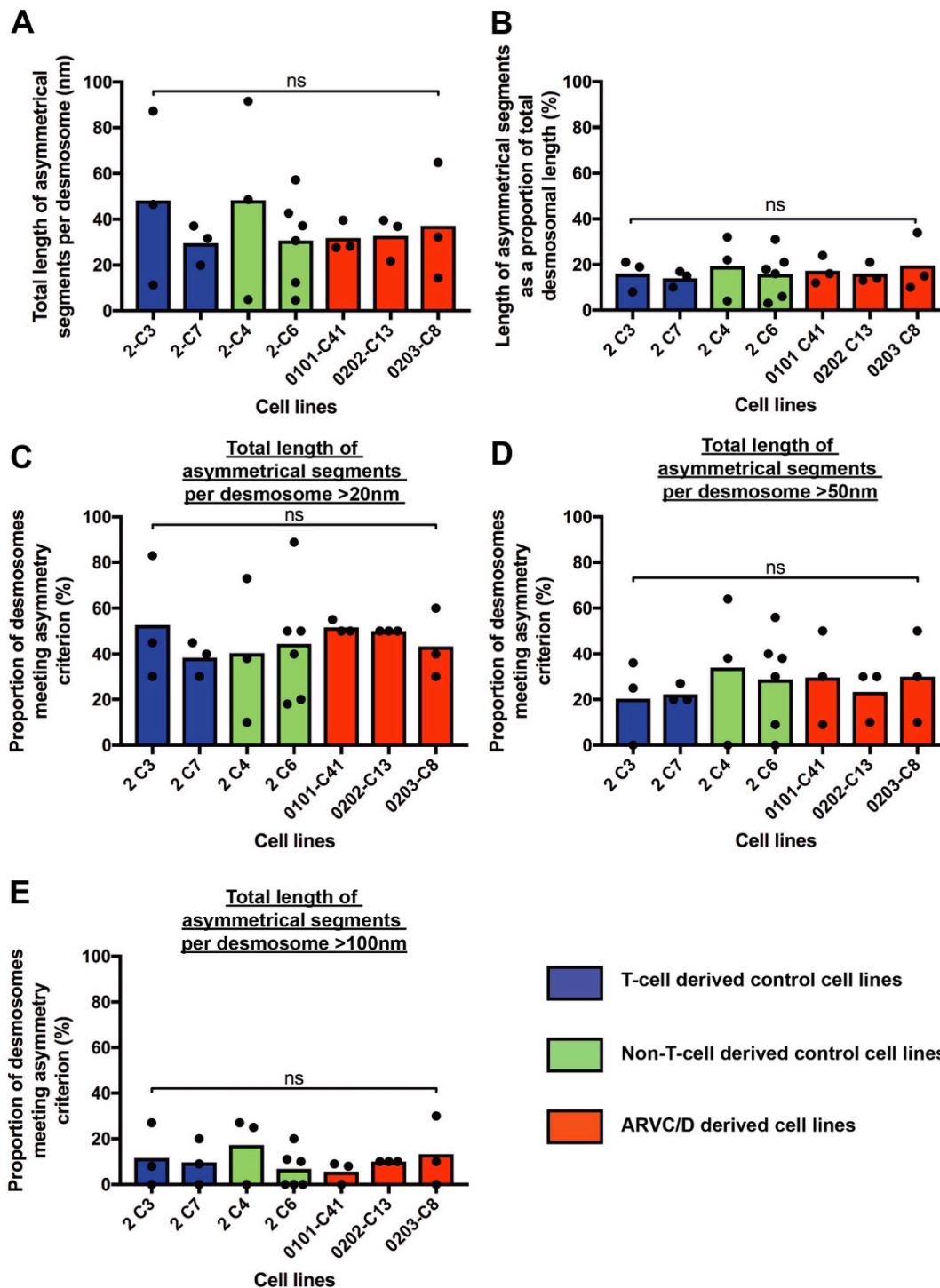


Figure 72 The length and frequency of asymmetrical desmosomes in iPSC-CMs from control and ARVC/D lines.

Bars in all panels represent the mean of the data points in panels A and B represent the means of the 10 desmosomes measured in experimental repeats. Data points in panels C to E represent the proportions of desmosomes meeting the asymmetry criterion in single experimental repeats. Cell lines were compared using one way ANOVA tests, no significant differences were identified in any parameter, $p > 0.05$.

7.3.4 Desmosomal length

Analysis of individual desmosomal length measurements (i.e. not average across experiments and cell lines) confirmed a positively skewed uni-modal distribution in both control and ARVC/D lines (Figure 73). The median (Q1-Q3) length was 156nm (123-233) for control iPSC-CMs (skewness 2.3) and 155nm (117-223) for ARVC/D iPSC-CMs (skewness 1.5). After averaging, the mean desmosomal lengths were 124nm (SD 14) for control iPSC-CMs and 118nm (SD 17) for ARVC/D iPSC-CMs (two tailed T-test, $p>0.05$).

In order to detect whether a greater range of desmosomal sizes were present in ARVC/D iPSC-CMs compared with control iPSC-CMs the spread of lengths within individual experiments (i.e. without averaging according to cell line) was assessed. The mean interquartile range of lengths per experiment was 93nm (SD 29) in control iPSC-CMs and 110nm (SD 7) in ARVC/D iPSC-CMs (two tailed T-test, $p>0.05$).

Differences between individual cell lines were also investigated. No differences were observed between four control lines or the three ARVC/D lines in terms of total desmosomal length or the interquartile range of the lengths per experiment (one way ANOVA, exact $p>0.05$) (Figure 74).

A total of 32 desmosomes in three samples of RAA myocardium were also studied. When length measurements for individual desmosomes were considered the median (Q1-Q3) total length was 205nm (118-300). After averaging within samples the mean total length was 224nm (SD 74), this was not significantly different from the values obtained for the control iPSC-CMs (two tailed T-test, $p>0.05$).

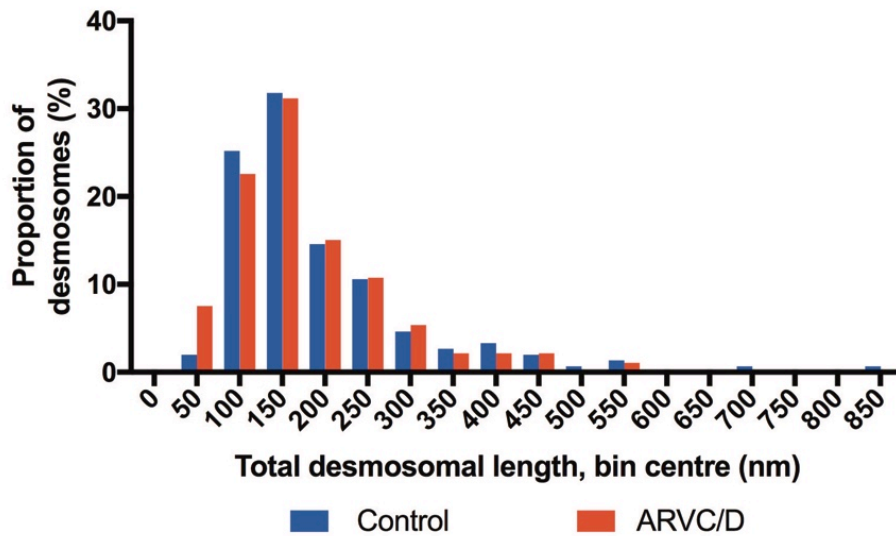


Figure 73 Histogram of individual desmosomal length measurements.

The histogram summarises the total length in all 151 desmosomes assessed across the four control lines (2-C3, 2-C7, 2-C4 and 2-C6) and the 93 desmosomes across the three ARVC/D lines (0101-C41, 0202-C13, 0203-C8). Each bin contains values that are within 25nm of the bin centre value.

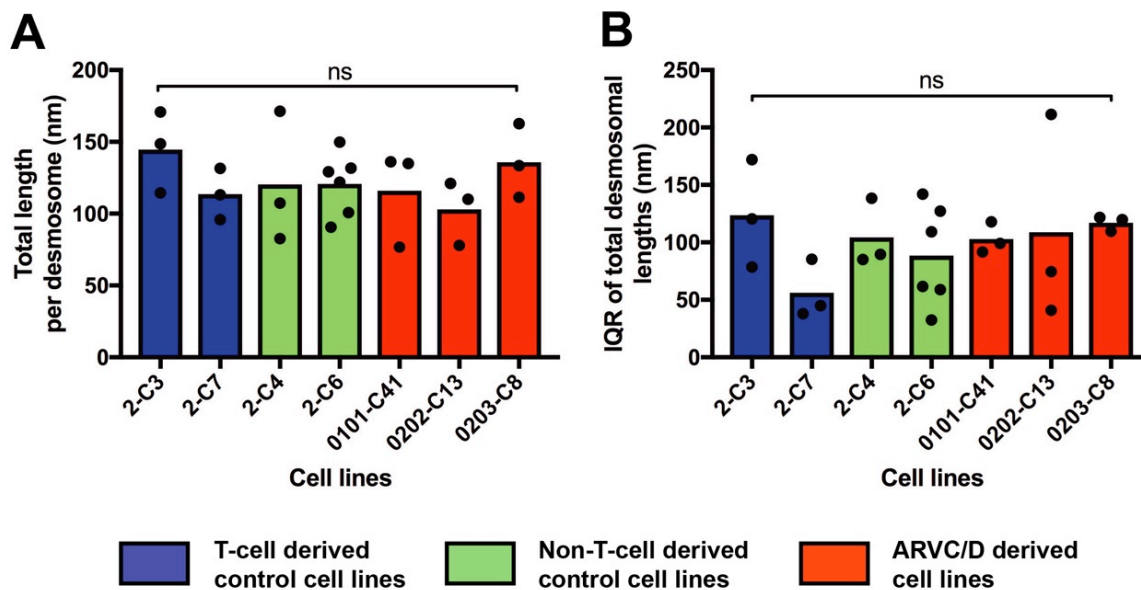


Figure 74 Total desmosomal length and interquartile range of total lengths in control and ARVC/D iPSC-CMs

Bars in all panels represent the median of the data. Data points represent the means of the 10 desmosomes measured in experimental repeats. Cell lines were compared using the one way ANOVA, no significant differences were identified in either parameter, $p > 0.05$.

7.3.5 Desmosomal width

Of the 244 iPSC-CM desmosomes images assessed, IMW1 measurements were possible in 243 images (99.6%), IMW2 measurements were possible in 224 images (91.8%) and IOW measurements were possible in 241 images (98.8%).

When width measurements for individual desmosomes are considered (i.e. without averaging) the mean values for IMW1 was 12.4 nm (SD 1.6) for control iPSC-CMs and 12.6nm (SD 1.6) for ARVC/D iPSC-CMs, for IMW2 the mean was 22.0nm (SD 2.3) for control iPSC-CMs and 21.3nm (SD 2.3) for ARVC/D iPSC-CMs, and for IOW the mean was 49.5nm (SD 4.1) for control iPSC-CMs and 50.9nm (SD 4.1) for ARVC/D iPSC-CMs.

After averaging within experiments, across repeats and cell lines the mean IMW1 was 12.39nm (SD 0.25) in the control lines and 12.66 (SD 0.07) in the ARVC/D lines, the mean IMW2 was 21.83nm (SD 0.42) in the control lines and 21.32 (SD 0.03) in the ARVC/D lines and the mean IOW was 49.33nm (SD 1.61) in the control lines and 50.96 (SD 1.03) in the ARVC/D lines. None of the differences in means between control and ARVC/D lines were statistically significant (two tailed T-test, $p>0.05$).

Differences between individual cell lines were also investigated (Figure 75). There was no significant difference detected between four clones from the same control iPSC line in terms of three of the desmosomal width parameters i.e. IMW1, IMW2 and IOW (one way ANOVA, $p>0.05$).

The widths of desmosomes in the RAA myocardium samples were also studied. When width measurements for individual desmosomes are considered (i.e. without averaging between samples) the mean IMW1 was 13.4nm (SD 1.3), the mean IMW2 was 21.5nm (SD 1.6) and mean IOW was 52.1nm (SD 2.7). After averaging between samples the mean IMW1 was 13.3nm (SD 0.7), the mean IMW2 was 21.53nm (SD 0.7) and mean IOW was 52.0nm (SD 1.1). There was no significant difference between these values and those of the control iPSC-CMs (two tailed T-test, $p>0.05$).

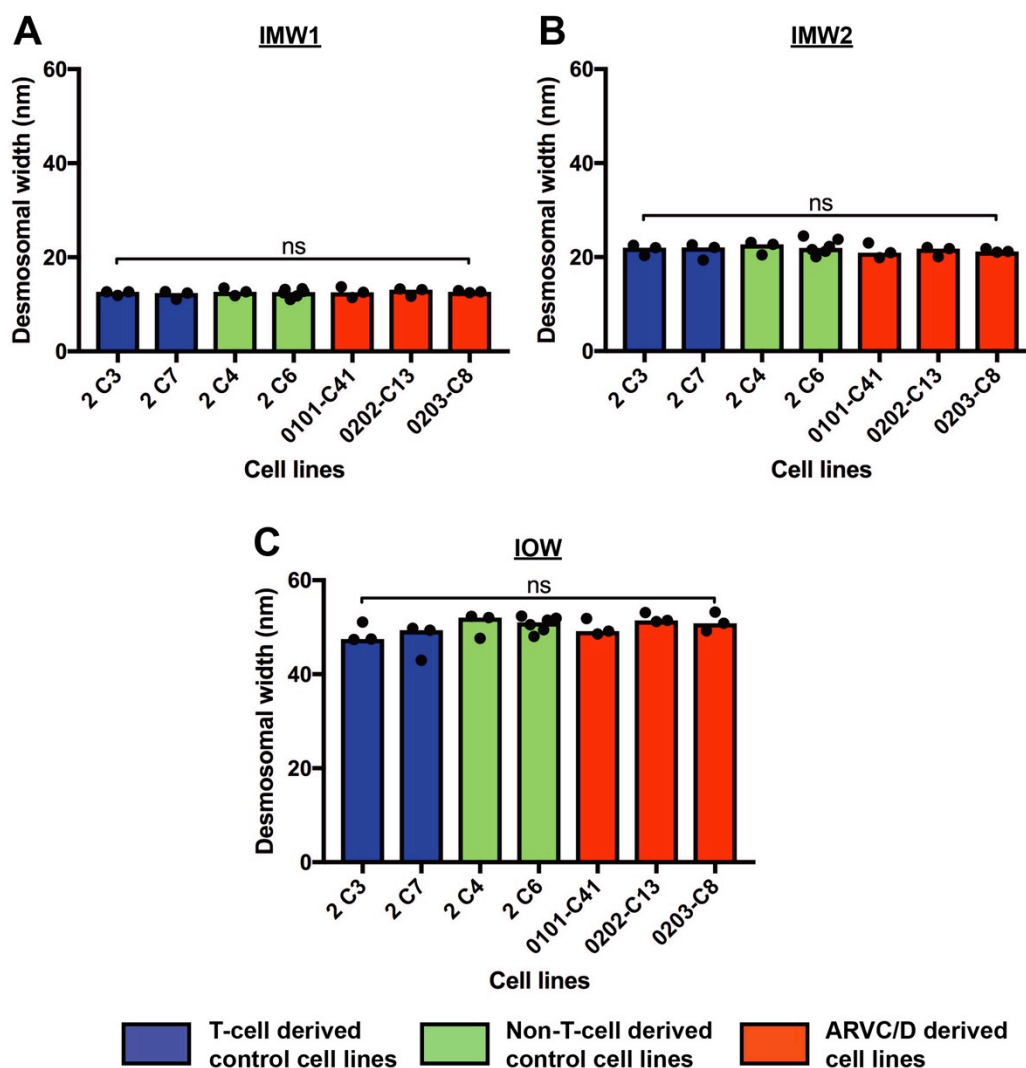


Figure 75 Desmosomal width in control and ARVC/D lines

Bars in all panels illustrate the mean of the data. Data points represent the means of the 10 desmosomes measured in experimental repeats. Cell lines were compared using the one way ANOVA test, no significant differences were identified in any of the three parameters, $p > 0.05$.

7.4 Discussion

This study found no significant difference between control and ARVC/D iPSC-CMs in any of the measures of desmosomal morphology that have been described as abnormal in ARVC/D in previous reports.

The choice of parameters to be investigated in this study was based on two previous reports of ultrastructural abnormalities in ARVC/D. The only study of ARVC/D iPSC-CMs in which desmosomal morphology was quantified was by Caspi *et al.* (Caspi *et al.*, 2013). There have been multiple reports of the ultrastructure of desmosomes in the myocardium from subjects with ARVC/D, but only the study by Basso *et al.* performed systematic quantitative analysis comparing cohorts of

ARVC/D cases and controls (Basso, 2006). The following sections will discuss the findings of this study with respect to these previous reports, with particular focus on differences in methodology between this study and these reports.

7.4.1 Hazy desmosomes

Hazy desmosomes were observed in all the samples in this study (including control iPSC-CMs, adult cardiomyocytes and immortalized keratinocytes). For some of these hazy desmosomes, tilting the sample within the electron beam during imaging changed their appearance to that of a typical (non-hazy) desmosome with the characteristic laminated plaques.

This phenomenon may be explained by consideration of the spatial orientation of desmosomes within a TEM level. Desmosomes are thought to consist of two disc-like plaques oriented in parallel and separated by an intermembranous gap (Figure 76 A and B). When captured within a TEM level (Figure 76 C and F) such a structure will only produce an image that is typical of desmosome (two parallel oriented linear structures separated by a gap) when the electron beam used to image the sample is oriented along the same plane as the intermembranous gap (Figure 76 D and H).

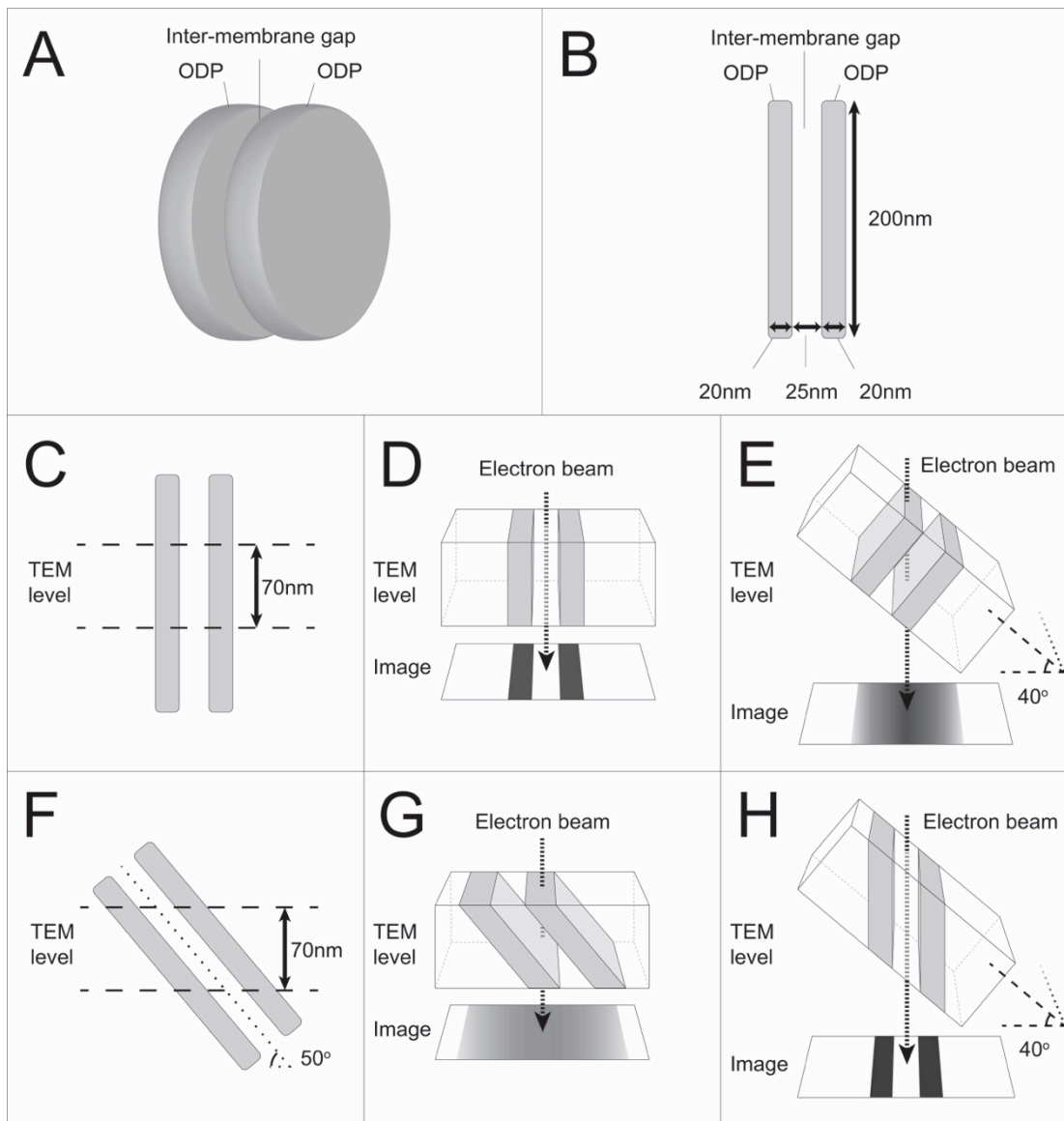


Figure 76 Schematic representing a simplified desmosome; its possible orientations within a TEM level; and the effect of tilting a level within the electron beam of a TEM on the resultant image.

Panels A and B show a simplified representation of a desmosome consisting of two cylindrical outer dense plaques whose circular surfaces are separated by and oriented parallel to the plane of an intermembrane gap. Panel A shows illustrates this arrangement in three dimensions. Panel B illustrates the structure when viewed along the same plane as the intermembrane gap. The dimensions are provided to give an approximate indication of scale, the normal range of values for ODP width and desmosomal plaque length are discussed in the text. Panels C and F illustrates the part of a desmosome that may be contained within a given TEM level depending on its orientation in relation to the level. Panel C illustrates the region contained within a desmosome whose intermembrane plane is oriented perpendicular to the plane of the TEM level. Panel F illustrates the region contained within a desmosome whose intermembrane plane is oriented at 50° to the plane of the TEM level. Panels D and G illustrate how these different orientations will affect the resultant TEM image if the level is studied with the electron beam perpendicular to the TEM level. Panels E and H illustrate the effect of tilting the TEM level within the electron beam upon the resultant TEM image.

This study has demonstrated that a proportion of hazy desmosomes are the result of sectioning and imaging artefact. The appearance of a proportion of hazy desmosomes could not be normalised by tilting. The suggestion that such desmosomes may genuinely have a structural abnormality is speculative.

The idea that hazy desmosomes result from ARVC/D could be investigated by determining the frequency with which they are found in ARVC/D samples compared with controls. This could be considered in future work.

Caspi *et al.* reported that abnormal and “hazy” desmosomes were found in ARVC/D iPSC-CMs and not in control iPSC-CMs (Caspi *et al.*, 2013). The identity of many of the structures presented by Caspi *et al.* as examples of abnormal desmosomes (Figure 77) is questionable. One such structure (Figure 77, panel D) does not appear to be associated with a plasma membrane and has a very high electron density with no obvious linear plaques, on these grounds it could be argued that it is more likely to be staining artefact than a desmosome. Other structures presented as desmosomes (Figure 77, panels E and F) are membrane associated collections of electron dense materials but without any apparent laminated plaques. Desmosomes are defined morphologically by this laminated electron dense structure. In order for a structure to be an abnormal desmosome it must have some features to identify it as a desmosome as opposed to any other type of adhesion junction. The argument in favour of these structures being desmosomes is therefore weak.

Some of the abnormal structures desmosomes presented by Caspi *et al.* do have a resemblance to desmosomes (Figure 77, panels A and B). These structures have an appearance that is very similar to the desmosomes from this study that had a normal appearance after tilting (Figure 69). No mention is made of tilting samples to correct artefactual haziness in Caspi’s methodology.

Overall the evidence present by Caspi that desmosomal morphology was abnormal in ARVC/D iPSC-CMs is weak. Despite these criticisms it remains unclear why hazy desmosomes were not noted in the control iPSC-CMs in their study. Caspi *et al.* stated that the investigator performing the analysis was blinded to the sample identity and therefore observer bias should not be the cause. The differentiation protocol used in this study was different to that of Caspi *et al.*^a. If it is assumed that hazy desmosomes genuinely represent abnormal junctions it may be that the differentiation protocol used in this study induced structural abnormalities in the

^a Caspi *et al.* used iPSCs maintained in MEF co-culture and a non-directed EB based cardiac differentiation protocol.

desmosomes of all cell lines (including control iPSC-CMs) whereas Caspi's protocol did not.

An additional argument in favour of hazy desmosomes being artefact is that they have not been reported as a feature of ARVC/D *in vivo*, particularly by Basso *et al.*

In summary the data from this study suggests that hazy desmosomes are not specific to ARVC/D and there is a strong argument that they represent artefact rather than abnormal desmosomal ultrastructure.

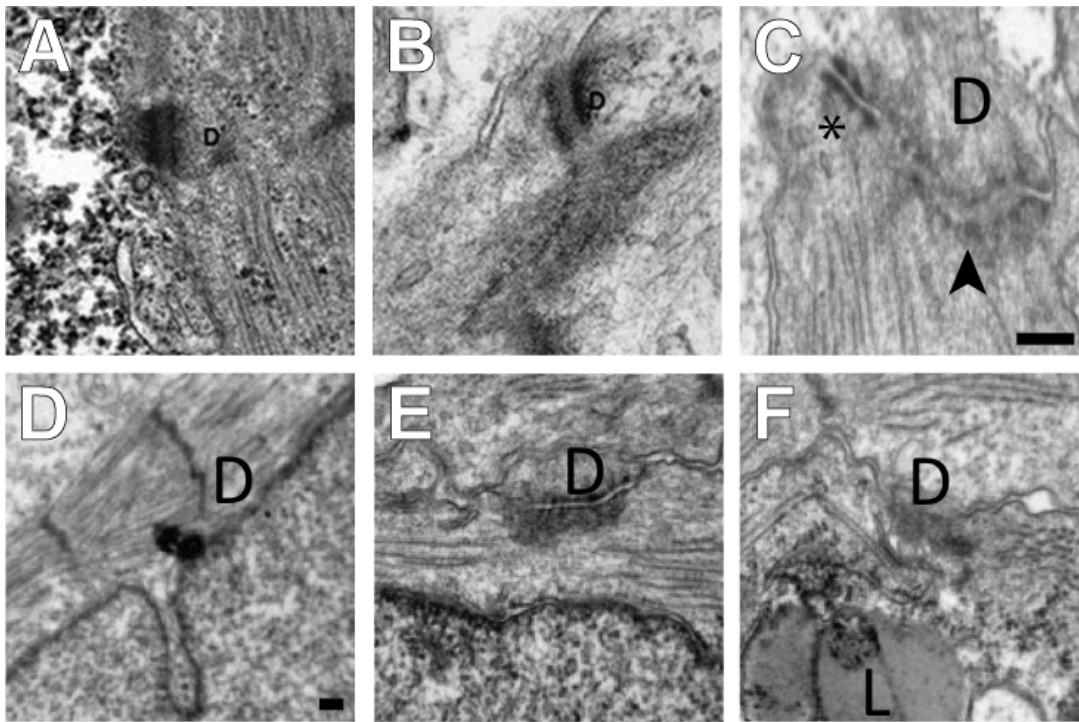


Figure 77 Images provided in Caspi *et al.* of hazy and abnormal desmosomes.

Images contain the original annotations of Caspi *et al.* who labelled structures considered to be desmosomes (D). Panels A and B show structures with parallel electron dense plaques typical of desmosomes. The hazy appearance of the intercellular gaps and plaques are similar to those shown in Figure 69 and Figure 76 and are considered to be an artefact of sample orientation within the electron beam. Panel C illustrates an asymmetrical but not hazy desmosome (*). Panel E, panel F and the region in panel C indicated by an arrowhead contain ill defined electron dense regions in proximity to the intermembranous gap. Whilst it is possible that these represent inter-cellular adhesion junctions, in the absence of a distinct electron dense plaque it is speculative to refer to them as desmosomes. The structure labelled in panel D is not associated with a plasma membrane and its high electron density is suggestive of artefact. Scale bars in panels C and D indicate 200nm, scale bars are unavailable for the other panels.

7.4.2 Asymmetrical desmosomes

The identification of asymmetrical desmosomes in all iPSC-CMs tested suggests that their presence or absence is not a useful indicator of an ARVC/D associated mutations in a cell line. This is in contrast to the findings of Caspi *et al.* who reported that asymmetrical desmosomes were only present in ARVC/D iPSC-CMs (Caspi *et al.*, 2013).

This might be explained if the differences in differentiation protocol (as described above) induced desmosomal asymmetry in control iPSC-CMs in this study. Also Caspi *et al.* examined iPSC-CMs after 40 days of differentiation, whereas in this study samples were examined after 30 days. It is possible that the presence of asymmetrical desmosomes in the control iPSC-CMs reflects their relative immaturity.

The possibility that ARVC/D lines had a greater tendency to contain asymmetrical desmosomes than control iPSC-CMs was considered in this study through assessments of the frequency of different degrees of asymmetry and the total length of asymmetrical segments. This analysis found no difference between ARVC/D and controls.

The identification of asymmetrical desmosomes in non ARVC/D myocardium and immortalised keratinocytes suggests that this is not a feature that is unique to iPSC-CMs. Reports of myocardial tissue from subjects with ARVC/D (including Basso *et al.* (Basso, 2006)) did not describe asymmetrical desmosomes as a feature of the disease.

In summary the data from this study taken in the context of previous reports suggest that desmosomal asymmetry is a common feature of desmosomes in iPSC-CMs and that asymmetry is not more frequent of more in iPSC-CMs containing ARVC/D associated mutations.

7.4.3 Desmosomal length

No differences in length parameters were identified between control and ARVC/D iPSC-CMs. Desmosomal length parameters were not reported in Caspi's study. Basso *et al.* reported that the desmosomes in ARVC/D myocardial tissue had a mean length of 310nm (SD 80) compared with a mean length of 160nm (SD 80) in controls ($p < 0.001$) (Basso, 2006). They also reported that overall desmosomes constituted a greater proportion of the total length of the intercalated discs in ARVC/D myocardium than in controls. Other reports of ARVC/D myocardium did not describe an increase in desmosomal length (Pilichou, 2006) (Lahtinen *et al.*, 2008). In this study the mean total length of desmosomes was (224nm, SD 74) in RAA and (193nm, SD 120) in

control iPSC-CMs, these values are similar to those reported by Basso *et al.*. There was no significant difference between the length of ARVC/D iPSC-CM desmosomes (177nm, SD 93) and control iPSC-CMs. This may indicate that the processes resulting in longer desmosomes in ARVC/D develop in response to electromechanical and neurohumoral stimuli that are present *in vivo* but absent in the *in vitro* system used in this study.

Several reports of ARVC/D myocardium have described chains of multiple desmosomes or desmosome like junctions that are not localised to the intercalated discs (Pilichou, 2006) (Lahtinen *et al.*, 2008) (Basso, 2006). In this study the absence of a bimodal distribution in desmosomal lengths in ARVC/D iPSC-CMs and the lack of a difference in the interquartile range of desmosomal lengths between ARVC/D and control iPSC-CMs suggests that ARVC/D iPSC-CMs did not contain a combination of larger and smaller than normal desmosomes, as had been described in myocardial tissue.

7.4.4 Desmosomal gap width

In this study the regions of desmosomal plaque that define the inter-cellular/intermembranous gap had a complex laminated appearance. This appearance has been reported by previous authors and is due to protein dense regions either side of the central (electron-lucent) lipid bilayer of the plasma membrane (Kelly, 1966) (North *et al.*, 1999). On this basis, IMW1 was considered to measure the distance between the outer (extracellular) surfaces of the plasma membranes of adjacent cells and IMW2 was thought to measure the distance between the intracellular surfaces.

The similarity of the mean IMW1 and mean IMW2 values for RAA and control iPSC-CM supports the idea that this aspect of desmosomal morphology is preserved between tissue types.

In this study no significant difference was observed in IMW1 and IMW2 between control and ARVC/D iPSC-CMs. This result is in contrast to the findings of Caspi *et al.* who reported that the mean desmosomal gap width of control iPSC-CMs was 24nm (SEM 1) compared with 32nm (SEM 2) in ARVC/D iPSC-CMs ($p < 0.05$) (Caspi *et al.*, 2013). Basso *et al.* reported that the mean desmosomal gap width was 22nm (SD 3) in control myocardium and 29nm (SD 9) in ARVC/D myocardium ($p = 0.004$) (Basso, 2006).

Many of the points discussed in 7.4.2 are equally relevant in explaining the conflict between the results of this study and that of Caspi *et al.* with respect to desmosomal

gap width. The EB differentiation protocol use by Caspi *et al.* may have had a greater potential to precipitate desmosomal structural changes than the monolayer protocol and the later time-point of analysis may have allowed more time for this to be manifest. Similarly the development of increased desmosomal gap width in the myocardial tissues studies by Basso *et al.* may be precipitated by factors that are absent in the *in vitro* model used in this study.

Another explanation for the difference in results compared with both Caspi *et al.* and Basso *et al.* could be that the development of an increased desmosomal gap width in an iPSC-CMs model is dependent on the specific mutation present. The mutations present in ARVC/D iPSC-CMs in this study were different to those studied by both Caspi *et al.* and Basso *et al.* ^a (Caspi *et al.*, 2013) (Basso, 2006).

Both Caspi *et al.* and Basso *et al.* reported using investigators that were blinded to the sample identity during desmosomal analysis therefore it must be assumed that observer bias is not responsible for the differences they described between cells with ARVC/D mutations and controls.

Caspi *et al.* did not describe the number of independent differentiation experiments from which their TEM samples originated. The possibility that the data for this cell line came from a single experiment and possibly from a single TEM section cannot be excluded. In this situation the apparent difference in desmosomal width between control and ARVC/D may be due to variation resulting from the differentiation protocol and/or the collection and processing of samples rather than a property of the cell lines. In this study the greatest difference in mean desmosomal widths for experimental repeats was 2.7nm for IMW1 and 5.2nm for IMW2. This is less than the 8nm difference in desmosomal gap they reported between the ARVC/D and control line. This makes the argument that their results may be due to a lack of experimental repeats weaker, but does not refute it since the degree of inter-experimental variability was not quantified in their study and may therefore be greater than in this study.

7.4.5 Desmosomal plaque width

In this study the distance between the cytoplasmic edges of the ODPs (IOW) was measured as an indirect assessment of the width of the ODPs. Caspi *et al.* reported that a parameter referred to as total desmosomal width (TDW) was 171nm (SEM 12) in ARVC/D iPSC-CMs and 101nm (SEM 5) in control iPSC-CMs. The illustration

^a The mutation studied by Caspi *et al.* produced a premature stop codon in exon 3 of *PKP2*. The *PKP2* mutation carried by 0101-C41 is predicted to result in aberrant splicing of exon 11.

provided by Caspi *et al.* to define this parameter suggests that it describes the sum of the desmosomal gap width, the width of the ODPs and the width of electron dense material in the region of the IDP and its junction with the intermediate filaments (IFs) (Figure 78). Caspi *et al.* did not describe which of these desmosomal components had an increased width leading to this result. Since the difference in mean desmosomal gap they reported was only 8nm it may be inferred that some increase in the width of the plaque components was present, but Caspi *et al.* offer no suggestion as to whether this is due to a change in ODP structure, IDP structure or a more prominent appearance of the IFs at the IDP boundary. IOW was measured in this study to provide a more detailed assessment of the width of desmosomal plaque components than TDW. In this study the appearance of the IDP was found to be highly variable and the point of transition between the IDP and intermediate filaments indistinct such that a clear line of transition from IDP to cytoplasm running parallel to the ODPs was rarely seen. The gradual reduction in electron density at the junction of the IDP and intermediate filaments meant that the apparent width of the IDP was very sensitive to changes in brightness and contrast of the image. Consequently it was decided that accurate and reproducible measurements of the IDP width were not possible in this study and no equivalent to TDW was measured.

The mean IOW in control iPSC-CMs was 49nm in this study. This is consistent with previous reports describing the width of the ODPs in other tissues (North *et al.*, 1999) (Karrer, 1960) (Kelly, 1966). The lack of difference between mean IOW in ARVC/D and control iPSC-CMs suggests that the structure of the ODP was not affected by the ARVC/D mutations present in the cell lines.

Taken together these data suggest that the ODP width of iPSC-CMs was not affected by the ARVC/D mutations tested in this study. It is also suggested that the parameter TDW as measured by Caspi *et al.* is highly un-informative with respect to understanding the ultrastructural effects of ARVC/D mutations.

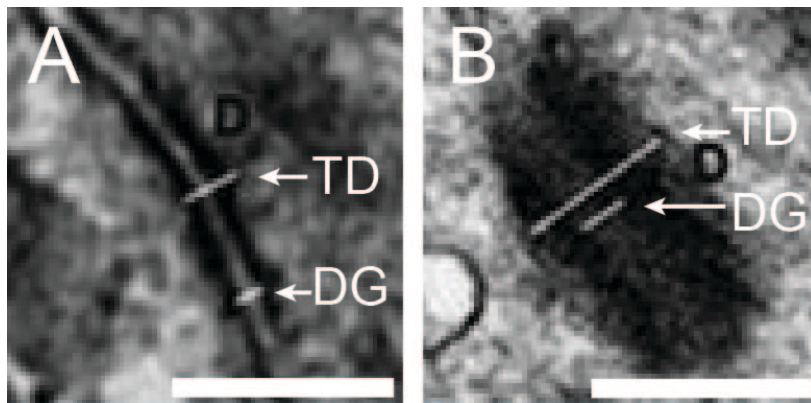


Figure 78 Image from Caspi *et al.* illustrating the desmosomal width parameters measured in that study.

Image A shows a desmosome from a control iPSC-CM. Image B shows ARVC/D iPSC-CMs. Desmosomal gap width (DG) and total desmosomal width (TD) measurements are indicated. Scale bars illustrate 200nm.

7.4.6 Limitations

The limitations resulting from having control iPSCs from only a single subject have been discussed in Chapter 3. The highly conserved desmosomal width parameters in all iPSC-CM lines suggest that assessment of additional control lines would be unlikely to reveal a difference between ARVC/D and control lines.

The methodology of this study only allowed the morphometric assessment of junctions that could be positively identified as desmosomes by the presence of laminated plaques. It could be argued that this introduced a selection bias whereby abnormal desmosomes in which the plaque structure was disorganised and lacked this laminated structure were systematically excluded from the analysis. In this way the disease phenotype may not have been captured by the study methodology. The problem with this criticism is that the presence of laminated plaques are the only consistent feature allowing desmosomes to be distinguished from features such as small adherens junctions or junctions that appear disorganised due to sectioning artefact.

7.5 Conclusions

The data from this study found no difference in the ultrastructural appearance of desmosomes between control iPSC-CMs and those from subjects with ARVC/D.

Critical appraisal of the only previous report describing desmosomal ultrastructural abnormalities in iPSC-CMs has identified numerous methodological issues which

weaken its conclusions. The methodology of this study was intended to be transparent, objective and robust providing a high degree of confidence in the veracity of these conclusions.

Further work is needed to determine whether the changes in desmosomal ultrastructure previously reported in ARVC/D iPSC-CMs: (1) are mutation specific, (2) only occur in the context of specific culture conditions (3) are an artefact of the experimental design and methodology used to analyse desmosomal ultrastructure.

The approach to quantitative assessment of iPSC-CM desmosomal ultrastructure described in this study may be useful for the design any future studies in this area.

Chapter 8. Conclusion And Future Perspectives

The main aim of this work was to determine whether iPSC-CMs carrying ARVC/D associated desmosomal mutations that have not previously been studied by *in vitro* modelling recapitulate features of ARVC/D. This study specifically focused on abnormalities of desmosomal ultrastructure and the reduced abundance and/or redistribution of desmosomal proteins since both have been proposed as components of a common pathway of pathogenesis for the disease.

8.1 Major findings

Expandable cell lines were successfully derived from the PBMCs of three subjects with clinical diagnosis of ARVC/D that each carried different ARVC/D associated desmosomal mutations and from the PBMCs of a single control subject. Seven of the expandable cell lines (four control lines and three ARVC/D lines) were fully characterised. These cell lines met the study criteria for pluripotency and were therefore classified as iPSCs.

Spontaneously contracting cultures were generated from all seven iPSC lines using a monolayer differentiation protocol which involved the transient manipulation of Wnt signalling by small molecule inhibitors. Differentiated cultures contained cells with the characteristics of functional cardiomyocytes including the presence of cardiac isoforms of sarcomeric proteins organised into striated myofibrils, confirming the generation of iPSC-CMs.

Pluripotent cells were found to express desmosomal genes at a level comparable to that of desmosome bearing tissues. Desmosomal proteins were expressed in a pattern consistent with their participation in intercellular adhesion. These cultures also contained junctions that were morphologically typical of desmosomes when assessed by TEM.

The differentiation of iPSCs to iPSC-CMs was associated with a relative reduction in the expression of the genes encoding desmosomal cadherins and an increase in expression of genes encoding arm-repeat proteins. The cellular distribution of desmosomal protein signal by immunofluorescence changed from being exclusively punctate to one in which the signal was distributed in a continuous linear pattern. It was argued that this was consistent with the formation of area composite that have been described in cardiac ICDs.

No differences were detected in the abundance of transcripts of desmosomal genes when comparing ARVC/D iPSC-CMs (and iPSCs) with controls. This included genes

affect by ARVC/D associated variants that might have been affected by nonsense-mediated decay.

There was no evidence of the cellular redistribution of desmosomal proteins, particularly plakoglobin and plakophilin 2 from the plasma membrane to the cytoplasm or nucleus in ARVC/D or control iPSC-CMs.

There was also no difference between ARVC/D and control iPSC-CMs in terms of the ultrastructural parameters: intermembrane gap width, plaque width, length and asymmetry.

Several of the features reported in previous publications as evidence of an ARVC/D phenotype in iPSC-CMs were seen in both control and ARVC/D lines. These features include hazy and asymmetrical desmosomes assessed by TEM and the presence of punctate high intensity immunofluorescence signal localised to the nucleus of cells. It is argued that many of these features should be considered to be either artefact or a normal feature of the iPSC-CMs, and the evidence that these same features represented an ARVC/D phenotype in other studies is weak.

8.2 Limitations

As discussed in chapter 3 the use of PBMC derived iPSC and iPSC-CM control lines from a single subject for comparison with ARVC/D lines limits the generalizability of this study's conclusions. Although no significant differences in desmosomal morphology were noted between the control line clones and ARVC/D lines it remains possible that the control lines from this subject are unrepresentative of control iPSC-CMs in general. As such the possibility that there are differences between iPSC-CMs from a population of ARVC/D subjects and iPSC-CMs from a population of controls cannot be excluded.

An important limitation to this study was the inability to quantify desmosomal protein abundance in iPSC-CMs. This was the result of difficulty in generating samples in which >70% of cells were iPSC-CMs. A sufficient number of such samples were generated for gene expression analysis but not for western blotting and resources and time were not available to conduct further differentiation experiments to generate such samples. Quantitative immunofluorescence was not attempted as an alternative since the range of fluorescence intensities within all samples was so large that it was judged to be futile.

8.3 Suggestions for future work

As discussed in chapter 6, the role of desmosomal proteins and adhesion junctions containing them in pluripotent cells could be the subject of further investigation. The following questions could be addressed:

- Are desmosomal proteins co-localised to the same junctions?
- Are there regional differences in the abundance of desmosomal proteins in colonies of pluripotent cells?
- Do cells with adhesion junctions and punctate desmosomal protein signal at the peripheries of colonies differ in terms of pluripotency markers to those without these features at the centre of colonies?
- Are the adhesion junctions associated with organised intermediate filaments?
- Do desmosomal proteins and the junctions in which they participate have a role in the maintenance of pluripotency and regulation of colony expansion *in vitro*?

Further investigation of ARVC/D using iPSC-CMs could address the following questions:

- Are mutant ARVC/D transcripts and proteins expressed in iPSCs and iPSC-CMs in this study? This could be assessed by a combination of RNA sequencing and immunoblotting of cell lysate.
- Is there evidence of altered Wnt or Hippo signalling in ARVC/D lines compared to controls? The mutations studied in this work may be such that the mutant proteins do not affect the assembly of desmosomes but are pathological by virtue of their effect on intracellular signalling pathways.
- Were the differences in differentiation protocols between this study and previous reports of ARVC/D iPSC-CMs responsible for the absence of a detected disease phenotype in this work? This could be investigated by generating iPSC-CMs using this study's protocol from one or more of the iPSCs lines described in previous publications.
- How is iPSC-CM desmosomal ultrastructure and protein expression influenced by the duration and conditions of maturation? Could modified maturation conditions precipitate a disease phenotype?

This final question is of particular relevance since ARVC/D is an adult onset disease and physical training has been associated with the precipitation and exacerbation the disease phenotype (James *et al.*, 2013) (Saberniak *et al.*, 2014). The absence of a

disease phenotype in iPSC-CMs in this study could be a reflection of their relative immaturity and aspects of their exposure to the forces of contractile activity. The idea that the appearance of a disease phenotype in ARVC/D models is dependent on exposure to mechanical forces and/or contractile activity is supported by several studies. Cruz *et al.* reported that a mouse model of an ARVC/D associated *PKP2* mutation only manifested a disease phenotype after exercise training (Cruz *et al.*, 2015). Similarly, Hariharan *et al.* reported that neonatal rat ventricular myocytes (NRVMs) expressing mutant JUP or *PKP2* only displayed a disease phenotype^a after exposure to shear stress (Hariharan *et al.*, 2014). Hariharan *et al.* applied shear stress by oscillation of culture medium of cultures within a flow chamber. The same approach could be applied to iPSC-CMs in future work. An alternative to fluid shear stress are the mechanical forces to which iPSC-CMs are already exposed through their intrinsic contractility. Factors that have been reported to be important in regulating the contractility of iPSC-CMs include: (1) duration in culture, (2) mechanical properties of their culture substrate, (3) frequency of contractions and (4) loading conditions. A study of iPSC-CMs reported a significant increase in force generation during the first 30 days of maturation (Wheelwright *et al.*, 2018). The same study also reported that force generation was enhanced by culture on a substrate with a low elastic modulus (Wheelwright *et al.*, 2018). Cardiac tissue constructs with a low elastic modulus may be generated by combining iPSC-CMs with hydrogels of extracellular matrix proteins and in some cases fibroblasts to mimic the mixture of cell populations seen in myocardium (Nunes *et al.*, 2013) (Breckwoldt *et al.*, 2017) (Tiburcy *et al.*, 2017) (Ronaldson-Bouchard *et al.*, 2018). The maturation of iPSC-CMs in these constructs reported to be enhanced compared with adherent monolayers, particularly when these constructs are exposed to static loading and the stimulation of frequent contractions through electrical pacing (Jackman *et al.*, 2016) (Ronaldson-Bouchard *et al.*, 2018) (Nunes *et al.*, 2013). iPSC-CMs in these culture have been reported to show a reversal of the negative force-frequency relationship typically observed in iPSC-CMs to the positive relationship seen in adult myocardium (Germanguz *et al.*, 2011) (Ruan *et al.*, 2016). This is accompanied by a greater alignment of sarcomeres and changes in calcium handling apparatus. There is also evidence that intercellular adhesion is affected by these culture conditions. Nunes *et al.* reported an increase in the number of desmosomes

^a The disease phenotype was a failure of junctional plakoglobin immunofluorescence signal intensity to increase following shear stress.

in tissue constructs continuously paced at higher frequencies (Nunes *et al.*, 2013). The characteristics of desmosomal gene and protein expression have yet to be reported in these paced tissue constructs. In summary there is evidence supporting the idea that cardiac tissue constructs may be superior to monolayer iPSC-CM cultures in modelling ARVC/D by (1) promoting a cardiac phenotype that is closer to that of the adult cardiomyocytes in which the disease is manifest *in vivo* and (2) by enhancing the exposure of iPSC-CMs to the mechanical forces that have been associated with manifestation of a disease phenotype in other cellular and animal models of the disease.

iPSC-CMs have the potential to provide valuable insights into the pathogenesis of ARVC/D within cardiomyocytes. This is of particular importance since the most clinically important features of ARVC/D are cardiac. However many of the questions relating to the pathogenesis of ARVC/D variant could be addressed using less resource intensive cellular modelling techniques. These may be grouped into: (1) techniques involving the generation of expandable cell line directly from ARVC/D subjects bearing variants of interest i.e. patient specific cell lines and (2) techniques involving the expression of ARVC/D variants in established cell lines by genetic modification.

Expandable keratinocyte lines have been generated from skin biopsy samples of subjects with ARVC/D carrying pathogenic *DSP*, *DSG2* and *PKP2* variants (T B Rasmussen *et al.*, 2013) (Torsten B Rasmussen *et al.*, 2013) (Rasmussen *et al.*, 2014). These keratinocytes cell lines were used to demonstrate changes in gene transcription, protein quantity and protein localisation resulting from the ARVC/D associated variants. In cases where myocardial tissue was also available the investigators were able to demonstrate that the findings in keratinocytes mirrored the patterns seen in the patient myocardium. Cells from the non-keratinised stratified squamous epithelium of the buccal mucosa have also been investigated as for patient specific patterns of desmosomal protein expression resulting from ARVC/D variants (Asimaki *et al.*, 2016). Immunofluorescence microscopy of these cells has been reported to show the expression of desmosomal proteins and changes in the cellular distribution of plakoglobin similar to those reported in myocardium (Asimaki *et al.*, 2016). To date expandable cell lines have not been generated from this cell type and further work is needed to establish the value of this cell source for modelling ARVC/D.

The expression of ARVC/D mutant transcripts has been induced in a variety of desmosome bearing cell lines (e.g. HEK, COS-1, neonatal rat ventricular myocytes and HL-1 see Table 20 for references) by either site directed mutagenesis of DNA or transduction with mRNA encoding the mutant variant. The culture of these cell types is generally less resource intensive than iPSCs and iPSC-CM differentiation, making it easier to conduct on a larger scale, allowing a greater number of experimental repeats and ensuring that there is enough culture material for testing with a wide range of modalities. Avoiding attempts at transforming cells from only type to another (e.g. by cardiac differentiation) also makes it easier to obtain samples of a single cell type for analysis and avoids transitions in culture conditions which may introduced experimental variation and bias.

Preliminary work studying ARVC/D associated variants with a non-iPSC-CM model could have been valuable in this study. If such work had demonstrated that the ARVC/D variants under investigation produced a disease phenotype in a non-iPSC-CM model it would make the lack of phenotype in iPSC-CMs more likely to be due to problems with iPSC-CM maturity and culture conditions.

8.4 Significance of the findings

ARVC/D is a relatively common inherited cardiac disease for which there is no proven disease modifying therapy. The development of such therapies requires an understanding of the mechanisms by which a wide range of mutations result in a similar clinical phenotype. Patient specific iPSC-CMs have the potential to be a valuable tool in developing this knowledge. However, iPSC-CMs have a greater similarity to fetal cardiomyocytes and ARVC/D typically manifests in adulthood. It is therefore important to verify that this immaturity does not limit or modify the phenotype of iPSC-CM based models of ARVC/D. Prior to this study the only mutations in *PKP2* had been modelled with iPSC-CMs and were reported to show features consistent with the clinical disease. The finding of this study suggests that iPSC-CM models of at least one *PKP2* mutation and of mutations in *DSP* and *DSG2* may either require specific culture conditions to manifest features of ARVC/D in iPSC-CMs, or may not do so at all. Future work should take advantages of non-iPSC-CM cellular models of ARVC/D to assess the mechanisms of pathogenicity of ARVC/D associated variants. The use of iPSC-CMs to investigate pathogenic mechanisms in cardiomyocytes should take account of the advances in understanding of the maturation of iPSC-CMs and innovations in *in vitro* culture

environments to maximise the potential that a clinically relevant disease phenotype will develop.

References

- Ackerman, M.J., Priori, S.G., Willems, S., Berul, C., Brugada, R., Calkins, H., Camm, A.J., Ellinor, P.T., Gollob, M., Hamilton, R., Hershberger, R.E., Judge, D.P., Le Marec, H., McKenna, W.J., Schulze-Bahr, E., Semsarian, C., Towbin, J.A., Watkins, H., Wilde, A., Wolpert, C., Zipes, D.P., 2011. HRS/EHRA Expert Consensus Statement on the State of Genetic Testing for the Channelopathies and Cardiomyopathies: This document was developed as a partnership between the Heart Rhythm Society (HRS) and the European Heart Rhythm Association (EHRA). *Europace* 13, 1077–1109.
<https://doi.org/10.1093/europace/eur245>
- Akiyama, T., 2000. Wnt/beta-catenin signaling. *Cytokine Growth Factor Rev.* 11, 273–282.
- Al-Amoudi, A., Castaño-Diez, D., Devos, D.P., Russell, R.B., Johnson, G.T., Frangakis, A.S., 2011. The three-dimensional molecular structure of the desmosomal plaque. *Proc. Natl. Acad. Sci. U. S. A.* 108, 6480–6485.
<https://doi.org/10.1073/pnas.1019469108>
- Alcalai, R., Metzger, S., Rosenheck, S., Meiner, V., Chajek-Shaul, T., 2003. A recessive mutation in desmoplakin causes arrhythmogenic right ventricular dysplasia, skin disorder, and woolly hair. *J. Am. Coll. Cardiol.* 42, 319–327.
- Amersham Biosciences, 2001. Ficoll-Paque PLUS, for in vitro isolation of lymphocytes.
- Angst, B.D., Nilles, L.A., Green, K.J., 1990. Desmoplakin II expression is not restricted to stratified epithelia. *J. Cell Sci.* 97 (Pt 2), 247–257.
- ARVC database [WWW Document], n.d. URL <http://www.arvcdatabase.info>
- Asimaki, A., Kapoor, S., Plovie, E., Karin Arndt, A., Adams, E., Liu, Z., James, C.A., Judge, D.P., Calkins, H., Churko, J., Wu, J.C., MacRae, C.A., Kléber, A.G., Saffitz, J.E., 2014. Identification of a new modulator of the intercalated disc in a zebrafish model of arrhythmogenic cardiomyopathy. *Sci. Transl. Med.* 6, 240ra74. <https://doi.org/10.1126/scitranslmed.3008008>
- Asimaki, A., Protonotarios, A., James, C.A., Chelko, S.P., Tichnell, C., Murray, B., Tsatsopoulou, A., Anastasakis, A., te Riele, A., Kléber, A.G., Judge, D.P., Calkins, H., Saffitz, J.E., 2016. Characterizing the Molecular Pathology of Arrhythmogenic Cardiomyopathy in Patient Buccal Mucosa Cells. *Circ. Arrhythm. Electrophysiol.* 9, e003688.
<https://doi.org/10.1161/CIRCEP.115.003688>

- Asimaki, A., Syrris, P., Wichter, T., Matthias, P., Saffitz, J.E., McKenna, W.J., 2007. A Novel Dominant Mutation in Plakoglobin Causes Arrhythmogenic Right Ventricular Cardiomyopathy. *Am. J. Hum. Genet.* 81, 964–973. <https://doi.org/10.1086/521633>
- Asimaki, A., Tandri, H., Huang, H., Halushka, M.K., Gautam, S., Basso, C., Thiene, G., Tsatsopoulou, A., Protonotarios, N., McKenna, W.J., Calkins, H., Saffitz, J.E., 2009. A new diagnostic test for arrhythmogenic right ventricular cardiomyopathy. *N. Engl. J. Med.* 360, 1075–1084. <https://doi.org/10.1056/NEJMoa0808138>
- Avery, S., Hirst, A.J., Baker, D., Lim, C.Y., Alagaratnam, S., Skotheim, R.I., Lothe, R.A., Pera, M.F., Colman, A., Robson, P., Andrews, P.W., Knowles, B.B., 2013. BCL-XL mediates the strong selective advantage of a 20q11.21 amplification commonly found in human embryonic stem cell cultures. *Stem Cell Rep.* 1, 379–386. <https://doi.org/10.1016/j.stemcr.2013.10.005>
- Avila, M., Kirchhoff, M., Marle, N., Hove, H.D., Chouchane, M., Thauvin-Robinet, C., Masurel, A., Mosca-Boidron, A.-L., Callier, P., Mugneret, F., Kjaergaard, S., Faivre, L., 2013. Delineation of a new chromosome 20q11.2 duplication syndrome including the ASXL1 gene. *Am. J. Med. Genet. A.* 161A, 1594–1598. <https://doi.org/10.1002/ajmg.a.35970>
- Avilion, A.A., Nicolis, S.K., Pevny, L.H., Perez, L., Vivian, N., Lovell-Badge, R., 2003. Multipotent cell lineages in early mouse development depend on SOX2 function. *Genes Dev.* 17, 126–140. <https://doi.org/10.1101/gad.224503>
- Avior, Y., Biancotti, J.C., Benvenisty, N., 2015. TeratoScore: Assessing the Differentiation Potential of Human Pluripotent Stem Cells by Quantitative Expression Analysis of Teratomas. *Stem Cell Rep.* 4, 967–974. <https://doi.org/10.1016/j.stemcr.2015.05.006>
- Awad, M.M., Dalal, D., Tichnell, C., James, C., Tucker, A., Abraham, T., Spevak, P.J., Calkins, H., Judge, D.P., 2006. Recessive arrhythmogenic right ventricular dysplasia due to novel cryptic splice mutation in PKP2. *Hum. Mutat.* 27, 1157–1157. <https://doi.org/10.1002/humu.9461>
- Bain, B.J., 1996. Ethnic and sex differences in the total and differential white cell count and platelet count. *J. Clin. Pathol.* 49, 664–666.
- Basic Local Alignment Search Tool (BLAST) [WWW Document], n.d. URL <https://blast.ncbi.nlm.nih.gov/Blast.cgi>

- Baskin, B., Skinner, J.R., Sanatani, S., Terespolsky, D., Krahn, A.D., Ray, P.N., Scherer, S.W., Hamilton, R.M., 2013. TMEM43 mutations associated with arrhythmogenic right ventricular cardiomyopathy in non-Newfoundland populations. *Hum. Genet.* 132, 1245–1252. <https://doi.org/10.1007/s00439-013-1323-2>
- Basso, C., 2006. Ultrastructural evidence of intercalated disc remodelling in arrhythmogenic right ventricular cardiomyopathy: an electron microscopy investigation on endomyocardial biopsies. *Eur. Heart J.* 27, 1847–1854. <https://doi.org/10.1093/eurheartj/ehl095>
- Basso, C., Ronco, F., Marcus, F., Abudurehman, A., Rizzo, S., Frigo, A.C., Bauce, B., Maddalena, F., Nava, A., Corrado, D., Grigoletto, F., Thiene, G., 2008. Quantitative assessment of endomyocardial biopsy in arrhythmogenic right ventricular cardiomyopathy/dysplasia: an in vitro validation of diagnostic criteria. *Eur. Heart J.* 29, 2760–2771. <https://doi.org/10.1093/eurheartj/ehn415>
- Basso, C., Thiene, G., 2005. Adipositas cordis, fatty infiltration of the right ventricle, and arrhythmogenic right ventricular cardiomyopathy. Just a matter of fat? *Cardiovasc. Pathol.* 14, 37–41. <https://doi.org/10.1016/j.carpath.2004.12.001>
- Basso, C., Thiene, G., Corrado, D., Angelini, A., Nava, A., Valente, M., 1996. Arrhythmogenic right ventricular cardiomyopathy. Dysplasia, dystrophy, or myocarditis? *Circulation* 94, 983–991.
- Bass-Zubek, A.E., Godsel, L.M., Delmar, M., Green, K.J., 2009. Plakophilins: multifunctional scaffolds for adhesion and signaling. *Curr. Opin. Cell Biol.* 21, 708–716. <https://doi.org/10.1016/j.ceb.2009.07.002>
- Bauce, B., Nava, A., Beffagna, G., Basso, C., Lorenzon, A., Smaniotto, G., De Bortoli, M., Rigato, I., Mazzotti, E., Steriotis, A., Marra, M.P., Towbin, J.A., Thiene, G., Danieli, G.A., Rampazzo, A., 2010. Multiple mutations in desmosomal proteins encoding genes in arrhythmogenic right ventricular cardiomyopathy/dysplasia. *Heart Rhythm* 7, 22–29. <https://doi.org/10.1016/j.hrthm.2009.09.070>
- Bedada, F.B., Chan, S.S.-K., Metzger, S.K., Zhang, L., Zhang, J., Garry, D.J., Kamp, T.J., Kyba, M., Metzger, J.M., 2014. Acquisition of a quantitative, stoichiometrically conserved ratiometric marker of maturation status in stem cell-derived cardiac myocytes. *Stem Cell Rep.* 3, 594–605. <https://doi.org/10.1016/j.stemcr.2014.07.012>

- Bedada, F.B., Wheelwright, M., Metzger, J.M., 2016. Maturation status of sarcomere structure and function in human iPSC-derived cardiac myocytes. *Biochim. Biophys. Acta* 1863, 1829–1838. <https://doi.org/10.1016/j.bbamcr.2015.11.005>
- Beffagna, G., De Bortoli, M., Nava, A., Salamon, M., Lorenzon, A., Zaccolo, M., Mancuso, L., Sigalotti, L., Bauce, B., Occhi, G., Basso, C., Lanfranchi, G., Towbin, J.A., Thiene, G., Danieli, G.A., Rampazzo, A., 2007. Missense mutations in Desmocollin-2 N-terminus, associated with arrhythmogenic right ventricular cardiomyopathy, affect intracellular localization of desmocollin-2 in vitro. *BMC Med. Genet.* 8, 65. <https://doi.org/10.1186/1471-2350-8-65>
- Beffagna, G., Occhi, G., Nava, A., Vitiello, L., Ditadi, A., Basso, C., Bauce, B., Carraro, G., Thiene, G., Towbin, J.A., Danieli, G.A., Rampazzo, A., 2005. Regulatory mutations in transforming growth factor-beta3 gene cause arrhythmogenic right ventricular cardiomyopathy type 1. *Cardiovasc. Res.* 65, 366–373. <https://doi.org/10.1016/j.cardiores.2004.10.005>
- Bennett, R.L., French, K.S., Resta, R.G., Doyle, D.L., 2008. Standardized human pedigree nomenclature: update and assessment of the recommendations of the National Society of Genetic Counselors. *J. Genet. Couns.* 17, 424–433. <https://doi.org/10.1007/s10897-008-9169-9>
- Ben-Ze'ev, A., Geiger, B., 1998. Differential molecular interactions of beta-catenin and plakoglobin in adhesion, signaling and cancer. *Curr. Opin. Cell Biol.* 10, 629–639.
- Beqqali, A., Kloots, J., Ward-van Oostwaard, D., Mummery, C., Passier, R., 2006. Genome-wide transcriptional profiling of human embryonic stem cells differentiating to cardiomyocytes. *Stem Cells Dayt. Ohio* 24, 1956–1967. <https://doi.org/10.1634/stemcells.2006-0054>
- Bhonsale, A., Te Riele, A.S.J.M., Sawant, A.C., Groeneweg, J.A., James, C.A., Murray, B., Tichnell, C., Mast, T.P., van der Pols, M.J., Cramer, M.J.M., Dooijes, D., van der Heijden, J.F., Tandri, H., van Tintelen, J.P., Judge, D.P., Hauer, R.N.W., Calkins, H., 2017. Cardiac phenotype and long-term prognosis of arrhythmogenic right ventricular cardiomyopathy/dysplasia patients with late presentation. *Heart Rhythm* 14, 883–891. <https://doi.org/10.1016/j.hrthm.2017.02.013>
- Bierkamp, C., Mclaughlin, K.J., Schwarz, H., Huber, O., Kemler, R., 1996. Embryonic heart and skin defects in mice lacking plakoglobin. *Dev. Biol.* 180, 780–785. <https://doi.org/10.1006/dbio.1996.0346>

- Bizzozero, G., 1864. Delle cellule cigliate, del reticolo Malpighiano dell' epidermide. *Ann Univ Meal* 190, 110.
- BlueFuse Multi v4.3 Software Guide, 2016.
- Boggon, T.J., Murray, J., Chappuis-Flament, S., Wong, E., Gumbiner, B.M., Shapiro, L., 2002. C-cadherin ectodomain structure and implications for cell adhesion mechanisms. *Science* 296, 1308–1313.
<https://doi.org/10.1126/science.1071559>
- Boheler, K.R., Czyz, J., Tweedie, D., Yang, H.-T., Anisimov, S.V., Wobus, A.M., 2002. Differentiation of pluripotent embryonic stem cells into cardiomyocytes. *Circ. Res.* 91, 189–201.
- Boland, M.J., Hazen, J.L., Nazor, K.L., Rodriguez, A.R., Gifford, W., Martin, G., Kupriyanov, S., Baldwin, K.K., 2009. Adult mice generated from induced pluripotent stem cells. *Nature* 461, 91–94. <https://doi.org/10.1038/nature08310>
- Bonné, S., Gilbert, B., Hatzfeld, M., Chen, X., Green, K.J., van Roy, F., 2003. Defining desmosomal plakophilin-3 interactions. *J. Cell Biol.* 161, 403–416.
<https://doi.org/10.1083/jcb.200303036>
- Bonné, S., van Hengel, J., Nollet, F., Kools, P., van Roy, F., 1999. Plakophilin-3, a novel armadillo-like protein present in nuclei and desmosomes of epithelial cells. *J. Cell Sci.* 112 (Pt 14), 2265–2276.
- Boraas, L.C., Guidry, J.B., Pineda, E.T., Ahsan, T., 2016. Cytoskeletal Expression and Remodeling in Pluripotent Stem Cells. *PLoS One* 11, e0145084.
<https://doi.org/10.1371/journal.pone.0145084>
- Bornslaeger, E.A., Godsel, L.M., Corcoran, C.M., Park, J.K., Hatzfeld, M., Kowalczyk, A.P., Green, K.J., 2001. Plakophilin 1 interferes with plakoglobin binding to desmoplakin, yet together with plakoglobin promotes clustering of desmosomal plaque complexes at cell-cell borders. *J. Cell Sci.* 114, 727–738.
- Borrmann, C.M., Grund, C., Kuhn, C., Hofmann, I., Pieperhoff, S., Franke, W.W., 2006. The area composita of adhering junctions connecting heart muscle cells of vertebrates. II. Colocalizations of desmosomal and fascia adhaerens molecules in the intercalated disk. *Eur. J. Cell Biol.* 85, 469–485.
<https://doi.org/10.1016/j.ejcb.2006.02.009>
- Breckwoldt, K., Letuffe-Brenière, D., Mannhardt, I., Schulze, T., Ulmer, B., Werner, T., Benzin, A., Klampe, B., Reinsch, M.C., Laufer, S., Shibamiya, A., Prondzynski, M., Mearini, G., Schade, D., Fuchs, S., Neuber, C., Krämer, E., Saleem, U., Schulze, M.L., Rodriguez, M.L., Eschenhagen, T., Hansen, A., 2017.

- Differentiation of cardiomyocytes and generation of human engineered heart tissue. *Nat. Protoc.* 12, 1177–1197. <https://doi.org/10.1038/nprot.2017.033>
- Brieher, W.M., Yap, A.S., Gumbiner, B.M., 1996. Lateral dimerization is required for the homophilic binding activity of C-cadherin. *J. Cell Biol.* 135, 487–496.
- Brown, M.E., Rondon, E., Rajesh, D., Mack, A., Lewis, R., Feng, X., Zitur, L.J., Learish, R.D., Nuwaysir, E.F., 2010. Derivation of Induced Pluripotent Stem Cells from Human Peripheral Blood T Lymphocytes. *PLoS ONE* 5, e11373. <https://doi.org/10.1371/journal.pone.0011373>
- Burke, A.P., Farb, A., Tashko, G., Virmani, R., 1998. Arrhythmogenic right ventricular cardiomyopathy and fatty replacement of the right ventricular myocardium: are they different diseases? *Circulation* 97, 1571–1580.
- Burridge, P.W., Matsa, E., Shukla, P., Lin, Z.C., Churko, J.M., Ebert, A.D., Lan, F., Diecke, S., Huber, B., Mordwinkin, N.M., Plews, J.R., Abilez, O.J., Cui, B., Gold, J.D., Wu, J.C., 2014. Chemically defined generation of human cardiomyocytes. *Nat. Methods* 11, 855–860. <https://doi.org/10.1038/nmeth.2999>
- Burridge, P.W., Thompson, S., Millrod, M.A., Weinberg, S., Yuan, X., Peters, A., Mahairaki, V., Koliatsos, V.E., Tung, L., Zambidis, E.T., 2011. A universal system for highly efficient cardiac differentiation of human induced pluripotent stem cells that eliminates interline variability. *PloS One* 6, e18293. <https://doi.org/10.1371/journal.pone.0018293>
- Cao, F., Wagner, R.A., Wilson, K.D., Xie, X., Fu, J.-D., Drukker, M., Lee, A., Li, R.A., Gambhir, S.S., Weissman, I.L., Robbins, R.C., Wu, J.C., 2008. Transcriptional and functional profiling of human embryonic stem cell-derived cardiomyocytes. *PloS One* 3, e3474. <https://doi.org/10.1371/journal.pone.0003474>
- Cao, N., Liu, Z., Chen, Z., Wang, J., Chen, T., Zhao, X., Ma, Y., Qin, L., Kang, J., Wei, B., Wang, L., Jin, Y., Yang, H.-T., 2012. Ascorbic acid enhances the cardiac differentiation of induced pluripotent stem cells through promoting the proliferation of cardiac progenitor cells. *Cell Res.* 22, 219–236. <https://doi.org/10.1038/cr.2011.195>
- Caspi, O., Huber, I., Gepstein, A., Arbel, G., Maizels, L., Boulos, M., Gepstein, L., 2013. Modeling of Arrhythmogenic Right Ventricular Cardiomyopathy with Human Induced Pluripotent Stem Cells. *Circ. Cardiovasc. Genet.* <https://doi.org/10.1161/CIRCGENETICS.113.000188>

- Chambers, I., Colby, D., Robertson, M., Nichols, J., Lee, S., Tweedie, S., Smith, A., 2003. Functional expression cloning of Nanog, a pluripotency sustaining factor in embryonic stem cells. *Cell* 113, 643–655.
- Chelko, S.P., Asimaki, A., Andersen, P., Bedja, D., Amat-Alarcon, N., DeMazumder, D., Jasti, R., MacRae, C.A., Leber, R., Kleber, A.G., Saffitz, J.E., Judge, D.P., 2016. Central role for GSK3 β in the pathogenesis of arrhythmogenic cardiomyopathy. *JCI Insight* 1. <https://doi.org/10.1172/jci.insight.85923>
- Chen, I.-P., Fukuda, K., Fusaki, N., Iida, A., Hasegawa, M., Lichtler, A., Reichenberger, E.J., 2013. Induced Pluripotent Stem Cell Reprogramming by Integration-Free Sendai Virus Vectors from Peripheral Blood of Patients with Craniometaphyseal Dysplasia. *Cell. Reprogramming* 15, 503–513. <https://doi.org/10.1089/cell.2013.0037>
- Chen, S.N., Gurha, P., Lombardi, R., Ruggiero, A., Willerson, J.T.T., Marian, A.J., 2013. The Hippo Pathway is Activated and is a Causal Mechanism for Adipogenesis in Arrhythmogenic Cardiomyopathy. *Circ. Res.* <https://doi.org/10.1161/CIRCRESAHA.114.302810>
- Chen, X., 2002. Protein Binding and Functional Characterization of Plakophilin 2. Evidence for its diverse roles in desmosomes and beta catenin signalling. *J. Biol. Chem.* 277, 10512–10522. <https://doi.org/10.1074/jbc.M108765200>
- Chen, Z., Riggs, A.D., 2011. DNA methylation and demethylation in mammals. *J. Biol. Chem.* 286, 18347–18353. <https://doi.org/10.1074/jbc.R110.205286>
- Chimenti, C., Pieroni, M., Maseri, A., Frustaci, A., 2004. Histologic findings in patients with clinical and instrumental diagnosis of sporadic arrhythmogenic right ventricular dysplasia. *J. Am. Coll. Cardiol.* 43, 2305–2313. <https://doi.org/10.1016/j.jacc.2003.12.056>
- Chitaev, N.A., Averbakh, A.Z., Troyanovsky, R.B., Troyanovsky, S.M., 1998. Molecular organization of the desmoglein-plakoglobin complex. *J. Cell Sci.* 111 (Pt 14), 1941–1949.
- Chitaev, N.A., Leube, R.E., Troyanovsky, R.B., Eshkind, L.G., Franke, W.W., Troyanovsky, S.M., 1996. The binding of plakoglobin to desmosomal cadherins: patterns of binding sites and topogenic potential. *J. Cell Biol.* 133, 359–369.
- Chitaev, N.A., Troyanovsky, S.M., 1997. Direct Ca²⁺-dependent heterophilic interaction between desmosomal cadherins, desmoglein and desmocollin, contributes to cell-cell adhesion. *J. Cell Biol.* 138, 193–201.

- Cho, Y., Park, T., Shin, D., Lee, J.H., Ryu, H.M., Jang, G.-L., Lee, D.-Y., Park, Y., Lee, H., Kim, H., Shin, S.C., Heo, J.-H., Kang, H., Lee, B.-R., Nah, D.-Y., Yang, D.H., Park, H.S., Chae, S.-C., Jun, J.-E., Park, W.-H., 2007. Clinical manifestations of arrhythmogenic right ventricular cardiomyopathy in Korean patients. *Int. J. Cardiol.* 122, 137–142.
<https://doi.org/10.1016/j.ijcard.2006.11.070>
- Choi, H.-J., Weis, W.I., 2005. Structure of the armadillo repeat domain of plakophilin 1. *J. Mol. Biol.* 346, 367–376. <https://doi.org/10.1016/j.jmb.2004.11.048>
- Chou, B.-K., Mali, P., Huang, X., Ye, Z., Dowey, S.N., Resar, L.M., Zou, C., Zhang, Y.A., Tong, J., Cheng, L., 2011. Efficient human iPS cell derivation by a non-integrating plasmid from blood cells with unique epigenetic and gene expression signatures. *Cell Res.* 21, 518–529.
<https://doi.org/10.1038/cr.2011.12>
- Christensen, A., Andersen, C., Tybjaerg-Hansen, A., Haunso, S., Svendsen, J., 2011. Mutation analysis and evaluation of the cardiac localization of TMEM43 in arrhythmogenic right ventricular cardiomyopathy. *Clin. Genet.* 80, 256–264.
<https://doi.org/10.1111/j.1399-0004.2011.01623.x>
- Chun, Y.W., Balikov, D.A., Feaster, T.K., Williams, C.H., Sheng, C.C., Lee, J.-B., Boire, T.C., Neely, M.D., Bellan, L.M., Ess, K.C., Bowman, A.B., Sung, H.-J., Hong, C.C., 2015. Combinatorial polymer matrices enhance in vitro maturation of human induced pluripotent stem cell-derived cardiomyocytes. *Biomaterials* 67, 52–64. <https://doi.org/10.1016/j.biomaterials.2015.07.004>
- Churko, J.M., Burridge, P.W., Wu, J.C., 2013. Generation of human iPSCs from human peripheral blood mononuclear cells using non-integrative Sendai virus in chemically defined conditions. *Methods Mol. Biol. Clifton NJ* 1036, 81–88.
https://doi.org/10.1007/978-1-62703-511-8_7
- Claycomb, W.C., Lanson, N.A., Jr, Stallworth, B.S., Egeland, D.B., Delcarpio, J.B., Bahinski, A., Izzo, N.J., Jr, 1998. HL-1 cells: a cardiac muscle cell line that contracts and retains phenotypic characteristics of the adult cardiomyocyte. *Proc. Natl. Acad. Sci. U. S. A.* 95, 2979–2984.
- Corrado, D., Basso, C., Thiene, G., McKenna, W.J., Davies, M.J., Fontaliran, F., Nava, A., Silvestri, F., Blomstrom-Lundqvist, C., Wlodarska, E.K., Fontaine, G., Camerini, F., 1997. Spectrum of clinicopathologic manifestations of arrhythmogenic right ventricular cardiomyopathy/dysplasia: a multicenter study. *J. Am. Coll. Cardiol.* 30, 1512–1520.

- Corrado, D., Link, M.S., Calkins, H., 2017. Arrhythmogenic Right Ventricular Cardiomyopathy. *N. Engl. J. Med.* 376, 61–72.
<https://doi.org/10.1056/NEJMra1509267>
- Cowin, P., Kapprell, H.P., Franke, W.W., Tamkun, J., Hynes, R.O., 1986. Plakoglobin: a protein common to different kinds of intercellular adhering junctions. *Cell* 46, 1063–1073.
- Cox, M.G.P.J., van der Zwaag, P.A., van der Werf, C., van der Smagt, J.J., Noorman, M., Bhuiyan, Z.A., Wiesfeld, A.C.P., Volders, P.G.A., van Langen, I.M., Atsma, D.E., Dooijes, D., van den Wijngaard, A., Houweling, A.C., Jongbloed, J.D.H., Jordaens, L., Cramer, M.J., Doevendans, P.A., de Bakker, J.M.T., Wilde, A.A.M., van Tintelen, J.P., Hauer, R.N.W., 2011. Arrhythmogenic Right Ventricular Dysplasia/Cardiomyopathy: Pathogenic Desmosome Mutations in Index-Patients Predict Outcome of Family Screening: Dutch Arrhythmogenic Right Ventricular Dysplasia/Cardiomyopathy Genotype-Phenotype Follow-Up Study. *Circulation* 123, 2690–2700.
<https://doi.org/10.1161/CIRCULATIONAHA.110.988287>
- Cruz, F.M., Sanz-Rosa, D., Roche-Molina, M., García-Prieto, J., García-Ruiz, J.M., Pizarro, G., Jiménez-Borreguero, L.J., Torres, M., Bernad, A., Ruíz-Cabello, J., Fuster, V., Ibáñez, B., Bernal, J.A., 2015. Exercise triggers ARVC phenotype in mice expressing a disease-causing mutated version of human plakophilin-2. *J. Am. Coll. Cardiol.* 65, 1438–1450. <https://doi.org/10.1016/j.jacc.2015.01.045>
- Dalal, D., 2006. Clinical Features of Arrhythmogenic Right Ventricular Dysplasia/Cardiomyopathy Associated With Mutations in Plakophilin-2. *Circulation* 113, 1641–1649.
<https://doi.org/10.1161/CIRCULATIONAHA.105.568642>
- Dalal, D., 2005. Arrhythmogenic Right Ventricular Dysplasia: A United States Experience. *Circulation* 112, 3823–3832.
<https://doi.org/10.1161/CIRCULATIONAHA.105.542266>
- Daley, G.Q., Lensch, M.W., Jaenisch, R., Meissner, A., Plath, K., Yamanaka, S., 2009. Broader implications of defining standards for the pluripotency of iPSCs. *Cell Stem Cell* 4, 200–201; author reply 202.
<https://doi.org/10.1016/j.stem.2009.02.009>
- Davis, A.C., Wims, M., Spotts, G.D., Hann, S.R., Bradley, A., 1993. A null c-myc mutation causes lethality before 10.5 days of gestation in homozygotes and reduced fertility in heterozygous female mice. *Genes Dev.* 7, 671–682.

- De Bortoli, M., Beffagna, G., Bauce, B., Lorenzon, A., Smaniotto, G., Rigato, I., Calore, M., Li Mura, I.E.A., Basso, C., Thiene, G., Lanfranchi, G., Danieli, G.A., Nava, A., Rampazzo, A., 2010. The p.A897KfsX4 frameshift variation in desmocollin-2 is not a causative mutation in arrhythmogenic right ventricular cardiomyopathy. *Eur. J. Hum. Genet.* 18, 776–782.
<https://doi.org/10.1038/ejhg.2010.19>
- Delva, E., Tucker, D.K., Kowalczyk, A.P., 2009. The Desmosome. *Cold Spring Harb. Perspect. Biol.* 1, a002543–a002543.
<https://doi.org/10.1101/cshperspect.a002543>
- den Haan, A.D., Tan, B.Y., Zikusoka, M.N., Llado, L.I., Jain, R., Daly, A., Tichnell, C., James, C., Amat-Alarcon, N., Abraham, T., Russell, S.D., Bluemke, D.A., Calkins, H., Dalal, D., Judge, D.P., 2009. Comprehensive Desmosome Mutation Analysis in North Americans With Arrhythmogenic Right Ventricular Dysplasia/Cardiomyopathy. *Circ. Cardiovasc. Genet.* 2, 428–435.
<https://doi.org/10.1161/CIRCGENETICS.109.858217>
- Den, Z., Cheng, X., Merched-Sauvage, M., Koch, P.J., 2006. Desmocollin 3 is required for pre-implantation development of the mouse embryo. *J. Cell Sci.* 119, 482–489. <https://doi.org/10.1242/jcs.02769>
- Dowey, S.N., Huang, X., Chou, B.-K., Ye, Z., Cheng, L., 2012. Generation of integration-free human induced pluripotent stem cells from postnatal blood mononuclear cells by plasmid vector expression. *Nat. Protoc.* 7, 2013–2021.
<https://doi.org/10.1038/nprot.2012.121>
- Draper, J.S., Pigott, C., Thomson, J.A., Andrews, P.W., 2002. Surface antigens of human embryonic stem cells: changes upon differentiation in culture. *J. Anat.* 200, 249–258.
- DSC1 expression in myocardium [WWW Document], 2018. . Hum. Protein Atlas.
URL <https://www.proteinatlas.org/ENSG00000134765-DSC1/tissue>
- DSC1 heart immuno HPA [WWW Document], 2018. URL
<https://www.proteinatlas.org/ENSG00000134765-DSC1/tissue/heart+muscle>
- DSC2 expression in HaCaT cells [WWW Document], 2018. . Hum. Protein Atlas.
URL <https://www.proteinatlas.org/ENSG00000134755-DSC2/cell>
- DSC3 expression in HaCaT cells [WWW Document], 2018. . Hum. Protein Atlas.
URL <https://www.proteinatlas.org/ENSG00000134762-DSC3/cell>
- DSC3 expression in myocardium [WWW Document], 2018. URL
<https://www.proteinatlas.org/ENSG00000134762-DSC3/tissue/heart+muscle>

- DSG1 expression in HaCaT cells [WWW Document], 2018. . Hum. Protein Atlas.
URL <https://www.proteinatlas.org/ENSG00000134760-DSG1/cell>
- DSG2 expression in HaCaT cells [WWW Document], 2018. . Hum. Protein Atlas.
URL <https://www.proteinatlas.org/ENSG00000046604-DSG2/cell>
- DSG3 expression in HaCaT cells [WWW Document], 2018. . Hum. Protein Atlas.
URL <https://www.proteinatlas.org/ENSG00000134757-DSG3/cell>
- DSG4 expression in HaCaT cells [WWW Document], 2018. . Hum. Protein Atlas.
URL <https://www.proteinatlas.org/ENSG00000175065-DSG4/cell>
- DSP expression in HaCaT cells [WWW Document], 2018. . Hum. Protein Atlas. URL
<https://www.proteinatlas.org/ENSG00000096696-DSP/cell>
- Dubois, N.C., Craft, A.M., Sharma, P., Elliott, D.A., Stanley, E.G., Elefanty, A.G., Gramolini, A., Keller, G., 2011. SIRPA is a specific cell-surface marker for isolating cardiomyocytes derived from human pluripotent stem cells. *Nat. Biotechnol.* 29, 1011–1018. <https://doi.org/10.1038/nbt.2005>
- Ducibella, T., Albertini, D.F., Anderson, E., Biggers, J.D., 1975. The preimplantation mammalian embryo: characterization of intercellular junctions and their appearance during development. *Dev. Biol.* 45, 231–250.
- Eberl, M., Hintz, M., Reichenberg, A., Kollas, A.-K., Wiesner, J., Jomaa, H., 2003. Microbial isoprenoid biosynthesis and human gammadelta T cell activation. *FEBS Lett.* 544, 4–10.
- Egli, D., Birkhoff, G., Eggan, K., 2008. Mediators of reprogramming: transcription factors and transitions through mitosis. *Nat. Rev. Mol. Cell Biol.* 9, 505–516. <https://doi.org/10.1038/nrm2439>
- Ermakov, S., Ursell, P.C., Johnson, C.J., Meadows, A., Zhao, S., Marcus, G.M., Scheinman, M., 2014. Plakoglobin immunolocalization as a diagnostic test for arrhythmogenic right ventricular cardiomyopathy. *Pacing Clin. Electrophysiol. PACE* 37, 1708–1716. <https://doi.org/10.1111/pace.12492>
- Eshkind, L., Tian, Q., Schmidt, A., Franke, W.W., Windoffer, R., Leube, R.E., 2002. Loss of desmoglein 2 suggests essential functions for early embryonic development and proliferation of embryonal stem cells. *Eur. J. Cell Biol.* 81, 592–598. <https://doi.org/10.1078/0171-9335-00278>
- Fidler, L.M., Wilson, G.J., Liu, F., Cui, X., Scherer, S.W., Taylor, G.P., Hamilton, R.M., 2009. Abnormal connexin43 in arrhythmogenic right ventricular cardiomyopathy caused by plakophilin-2 mutations. *J. Cell. Mol. Med.* 13, 4219–4228. <https://doi.org/10.1111/j.1582-4934.2008.00438.x>

- Fong, A.H., Romero-López, M., Heylman, C.M., Keating, M., Tran, D., Sobrino, A., Tran, A.Q., Pham, H.H., Fimbres, C., Gershon, P.D., Botvinick, E.L., George, S.C., Hughes, C.C.W., 2016. Three-Dimensional Adult Cardiac Extracellular Matrix Promotes Maturation of Human Induced Pluripotent Stem Cell-Derived Cardiomyocytes. *Tissue Eng. Part A* 22, 1016–1025.
<https://doi.org/10.1089/ten.TEA.2016.0027>
- Fong, H., Hohenstein, K.A., Donovan, P.J., 2008. Regulation of self-renewal and pluripotency by Sox2 in human embryonic stem cells. *Stem Cells Dayt. Ohio* 26, 1931–1938. <https://doi.org/10.1634/stemcells.2007-1002>
- Fontaliran, F., Fontaine, G., Fillette, F., Aouate, P., Chomette, G., Grosogoeat, Y., 1991. [Nosologic frontiers of arrhythmogenic dysplasia. Quantitative variations of normal adipose tissue of the right heart ventricle]. *Arch. Mal. Coeur Vaiss.* 84, 33–38.
- Fontao, L., Favre, B., Riou, S., Geerts, D., Jaunin, F., Saurat, J.-H., Green, K.J., Sonnenberg, A., Borradori, L., 2003. Interaction of the bullous pemphigoid antigen 1 (BP230) and desmoplakin with intermediate filaments is mediated by distinct sequences within their COOH terminus. *Mol. Biol. Cell* 14, 1978–1992.
<https://doi.org/10.1091/mbc.E02-08-0548>
- Forbes, M.S., Sperelakis, N., 1985. Intercalated discs of mammalian heart: a review of structure and function. *Tissue Cell* 17, 605–648.
- Fornes, P., Ratel, S., Lecomte, D., 1998. Pathology of arrhythmogenic right ventricular cardiomyopathy/dysplasia--an autopsy study of 20 forensic cases. *J. Forensic Sci.* 43, 777–783.
- Franke, W.W., Borrmann, C.M., Grund, C., Pieperhoff, S., 2006. The area composita of adhering junctions connecting heart muscle cells of vertebrates. I. Molecular definition in intercalated disks of cardiomyocytes by immunoelectron microscopy of desmosomal proteins. *Eur. J. Cell Biol.* 85, 69–82.
<https://doi.org/10.1016/j.ejcb.2005.11.003>
- Fressart, V., Duthoit, G., Donal, E., Probst, V., Deharo, J.C., Chevalier, P., Klug, D., Dubourg, O., Delacretaz, E., Cosnay, P., Scanu, P., Extramiana, F., Keller, D., Hidden-Lucet, F., Simon, F., Bessirard, V., Roux-Buisson, N., Hebert, J.L., Azarine, A., Casset-Senon, D., Rouzet, F., Lecarpentier, Y., Fontaine, G., Coirault, C., Frank, R., Hainque, B., Charron, P., 2010. Desmosomal gene analysis in arrhythmogenic right ventricular dysplasia/cardiomyopathy:

- spectrum of mutations and clinical impact in practice. *Europace* 12, 861–868. <https://doi.org/10.1093/europace/euq104>
- Freund, C., Ward-van Oostwaard, D., Monshouwer-Kloots, J., van den Brink, S., van Rooijen, M., Xu, X., Zweigerdt, R., Mummery, C., Passier, R., 2008. Insulin redirects differentiation from cardiogenic mesoderm and endoderm to neuroectoderm in differentiating human embryonic stem cells. *Stem Cells Dayt. Ohio* 26, 724–733. <https://doi.org/10.1634/stemcells.2007-0617>
- Fusaki, N., Ban, H., Nishiyama, A., Saeki, K., Hasegawa, M., 2009. Efficient induction of transgene-free human pluripotent stem cells using a vector based on Sendai virus, an RNA virus that does not integrate into the host genome. *Proc. Jpn. Acad. Ser. B* 85, 348–362. <https://doi.org/10.2183/pjab.85.348>
- Gadue, P., Huber, T.L., Paddison, P.J., Keller, G.M., 2006. Wnt and TGF-beta signaling are required for the induction of an in vitro model of primitive streak formation using embryonic stem cells. *Proc. Natl. Acad. Sci. U. S. A.* 103, 16806–16811. <https://doi.org/10.1073/pnas.0603916103>
- Gallicano, G.I., Bauer, C., Fuchs, E., 2001. Rescuing desmoplakin function in extra-embryonic ectoderm reveals the importance of this protein in embryonic heart, neuroepithelium, skin and vasculature. *Dev. Camb. Engl.* 128, 929–941.
- Gallicano, G.I., Kouklis, P., Bauer, C., Yin, M., Vasioukhin, V., Degenstein, L., Fuchs, E., 1998. Desmoplakin is required early in development for assembly of desmosomes and cytoskeletal linkage. *J. Cell Biol.* 143, 2009–2022.
- Gandjbakhch, E., Charron, P., Fressart, V., Lorin de la Grandmaison, G., Simon, F., Gary, F., Vite, A., Hainque, B., Hidden-Lucet, F., Komajda, M., Villard, E., 2011. Plakophilin 2A is the dominant isoform in human heart tissue: consequences for the genetic screening of arrhythmogenic right ventricular cardiomyopathy. *Heart* 97, 844–849. <https://doi.org/10.1136/hrt.2010.205880>
- Gandjbakhch, E., Vite, A., Gary, F., Fressart, V., Donal, E., Simon, F., Hidden-Lucet, F., Komajda, M., Charron, P., Villard, E., 2013. Screening of genes encoding junctional candidates in arrhythmogenic right ventricular cardiomyopathy/dysplasia. *Eur. Eur. Pacing Arrhythm. Card. Electrophysiol. J. Work. Groups Card. Pacing Arrhythm. Card. Cell. Electrophysiol. Eur. Soc. Cardiol.* 15, 1522–1525. <https://doi.org/10.1093/europace/eut224>
- Garcia-Gras, E., 2006. Suppression of canonical Wnt/ -catenin signaling by nuclear plakoglobin recapitulates phenotype of arrhythmogenic right ventricular

- cardiomyopathy. *J. Clin. Invest.* 116, 2012–2021.
<https://doi.org/10.1172/JCI27751>
- Garrod, D., Chidgey, M., 2008. Desmosome structure, composition and function. *Biochim. Biophys. Acta* 1778, 572–587.
<https://doi.org/10.1016/j.bbamem.2007.07.014>
- Garrod, D.R., Berika, M.Y., Bardsley, W.F., Holmes, D., Taberner, L., 2005. Hyperadhesion in desmosomes: its regulation in wound healing and possible relationship to cadherin crystal structure. *J. Cell Sci.* 118, 5743–5754.
<https://doi.org/10.1242/jcs.02700>
- GE Healthcare Life Sciences, 2005. Instructions 28-4039-56 AD for Ficoll-Paque PREMIUM, Ficoll-Paque PREMIUM 1.084 and Ficoll-Paque PREMIUM 1.073.
- Gehmlich, Katja, Asimaki, A., Cahill, T.J., Ehler, E., Syrris, P., Zachara, E., Re, F., Avella, A., Monserrat, L., Saffitz, J.E., McKenna, W.J., 2010. Novel missense mutations in exon 15 of desmoglein-2: role of the intracellular cadherin segment in arrhythmogenic right ventricular cardiomyopathy? *Heart Rhythm Off. J. Heart Rhythm Soc.* 7, 1446–1453.
<https://doi.org/10.1016/j.hrthm.2010.08.007>
- Gehmlich, K., Lambiase, P.D., Asimaki, A., Ciaccio, E.J., Ehler, E., Syrris, P., Saffitz, J.E., McKenna, W.J., 2011. A novel desmocollin-2 mutation reveals insights into the molecular link between desmosomes and gap junctions. *Heart Rhythm Off. J. Heart Rhythm Soc.* 8, 711–718.
<https://doi.org/10.1016/j.hrthm.2011.01.010>
- Gehmlich, K., Syrris, P., Peskett, E., Evans, A., Ehler, E., Asimaki, A., Anastasakis, A., Tsatsopoulou, A., Vouliotis, A.-I., Stefanadis, C., Saffitz, J.E., Protonotarios, N., McKenna, W.J., 2010. Mechanistic insights into arrhythmogenic right ventricular cardiomyopathy caused by desmocollin-2 mutations. *Cardiovasc. Res.* 90, 77–87. <https://doi.org/10.1093/cvr/cvq353>
- Gehmlich, K., Syrris, P., Reimann, M., Asimaki, A., Ehler, E., Evans, A., Quarta, G., Pantazis, A., Saffitz, J.E., McKenna, W.J., 2012. Molecular changes in the heart of a severe case of arrhythmogenic right ventricular cardiomyopathy caused by a desmoglein-2 null allele. *Cardiovasc. Pathol.* 21, 275–282.
<https://doi.org/10.1016/j.carpath.2011.09.005>
- Gemayel, C., Pelliccia, A., Thompson, P.D., 2001. Arrhythmogenic right ventricular cardiomyopathy. *J. Am. Coll. Cardiol.* 38, 1773–1781.

- Germanguz, I., Sedan, O., Zeevi-Levin, N., Shtrichman, R., Barak, E., Ziskind, A., Eliyahu, S., Meiry, G., Amit, M., Itskovitz-Eldor, J., Binah, O., 2011. Molecular characterization and functional properties of cardiomyocytes derived from human inducible pluripotent stem cells. *J. Cell. Mol. Med.* 15, 38–51.
<https://doi.org/10.1111/j.1582-4934.2009.00996.x>
- Gerull, B., Heuser, A., Wichter, T., Paul, M., Basson, C.T., McDermott, D.A., Lerman, B.B., Markowitz, S.M., Ellinor, P.T., MacRae, C.A., Peters, S., Grossmann, K.S., Drenckhahn, J., Michely, B., Sasse-Klaassen, S., Birchmeier, W., Dietz, R., Breithardt, G., Schulze-Bahr, E., Thierfelder, L., 2004. Mutations in the desmosomal protein plakophilin-2 are common in arrhythmogenic right ventricular cardiomyopathy. *Nat. Genet.* 36, 1162–1164.
<https://doi.org/10.1038/ng1461>
- Gomes, J., Finlay, M., Ahmed, A.K., Ciaccio, E.J., Asimaki, A., Saffitz, J.E., Quarta, G., Nobles, M., Syrris, P., Chaubey, S., McKenna, W.J., Tinker, A., Lambiase, P.D., 2012. Electrophysiological abnormalities precede overt structural changes in arrhythmogenic right ventricular cardiomyopathy due to mutations in desmoplakin-A combined murine and human study. *Eur. Heart J.* 33, 1942–1953. <https://doi.org/10.1093/eurheartj/ehr472>
- Graichen, R., Xu, X., Braam, S.R., Balakrishnan, T., Norfiza, S., Sieh, S., Soo, S.Y., Tham, S.C., Mummery, C., Colman, A., Zweigerdt, R., Davidson, B.P., 2008. Enhanced cardiomyogenesis of human embryonic stem cells by a small molecular inhibitor of p38 MAPK. *Differ. Res. Biol. Divers.* 76, 357–370.
<https://doi.org/10.1111/j.1432-0436.2007.00236.x>
- Green, K.J., Parry, D.A., Steinert, P.M., Virata, M.L., Wagner, R.M., Angst, B.D., Nilles, L.A., 1990. Structure of the human desmoplakins. Implications for function in the desmosomal plaque. *J. Biol. Chem.* 265, 2603–2612.
- Groeneweg, J.A., van der Zwaag, P.A., Olde Nordkamp, L.R.A., Bikker, H., Jongbloed, J.D.H., Jongbloed, R., Wiesfeld, A.C.P., Cox, M.G.P.J., van der Heijden, J.F., Atsma, D.E., de Boer, K., Doevendans, P.A., Vink, A., van Veen, T.A.B., Dooijes, D., van den Berg, M.P., Wilde, A.A.M., van Tintelen, J.P., Hauer, R.N., 2013. Arrhythmogenic right ventricular dysplasia/cardiomyopathy according to revised 2010 task force criteria with inclusion of non-desmosomal phospholamban mutation carriers. *Am. J. Cardiol.* 112, 1197–1206.
<https://doi.org/10.1016/j.amjcard.2013.06.017>

- Gropp, M., Shilo, V., Vainer, G., Gov, M., Gil, Y., Khaner, H., Matzrafi, L., Idelson, M., Kopolovic, J., Zak, N.B., Reubinoff, B.E., 2012. Standardization of the teratoma assay for analysis of pluripotency of human ES cells and biosafety of their differentiated progeny. *PLoS One* 7, e45532.
<https://doi.org/10.1371/journal.pone.0045532>
- Grossmann, K.S., Grund, C., Huelsken, J., Behrend, M., Erdmann, B., Franke, W.W., Birchmeier, W., 2004. Requirement of plakophilin 2 for heart morphogenesis and cardiac junction formation. *J. Cell Biol.* 167, 149–160.
<https://doi.org/10.1083/jcb.200402096>
- GTEX Consortium, 2013. The Genotype-Tissue Expression (GTEx) project. *Nat. Genet.* 45, 580–585. <https://doi.org/10.1038/ng.2653>
- Guyette, J.P., Charest, J.M., Mills, R.W., Jank, B.J., Moser, P.T., Gilpin, S.E., Gershlak, J.R., Okamoto, T., Gonzalez, G., Milan, D.J., Gaudette, G.R., Ott, H.C., 2016. Bioengineering Human Myocardium on Native Extracellular Matrix. *Circ. Res.* 118, 56–72. <https://doi.org/10.1161/CIRCRESAHA.115.306874>
- Haegel, H., Larue, L., Ohsugi, M., Fedorov, L., Herrenknecht, K., Kemler, R., 1995. Lack of beta-catenin affects mouse development at gastrulation. *Dev. Camb. Engl.* 121, 3529–3537.
- Hanna, J.H., Saha, K., Jaenisch, R., 2010. Pluripotency and cellular reprogramming: facts, hypotheses, unresolved issues. *Cell* 143, 508–525.
<https://doi.org/10.1016/j.cell.2010.10.008>
- Hariharan, V., Asimaki, A., Michaelson, J.E., Plovie, E., MacRae, C.A., Saffitz, J.E., Huang, H., 2014. Arrhythmogenic right ventricular cardiomyopathy mutations alter shear response without changes in cell-cell adhesion. *Cardiovasc. Res.* 104, 280–289. <https://doi.org/10.1093/cvr/cvu212>
- Hatzfeld, M., 2007. Plakophilins: Multifunctional proteins or just regulators of desmosomal adhesion? *Biochim. Biophys. Acta* 1773, 69–77.
<https://doi.org/10.1016/j.bbamcr.2006.04.009>
- Hatzfeld, M., Green, K.J., Sauter, H., 2003. Targeting of p0071 to desmosomes and adherens junctions is mediated by different protein domains. *J. Cell Sci.* 116, 1219–1233.
- Hatzfeld, M., Haffner, C., Schulze, K., Vinzens, U., 2000. The function of plakophilin 1 in desmosome assembly and actin filament organization. *J. Cell Biol.* 149, 209–222.

- Haywood, A.F.M., Merner, N.D., Hodgkinson, K.A., Houston, J., Syrris, P., Booth, V., Connors, S., Pantazis, A., Quarta, G., Elliott, P., McKenna, W., Young, T.-L., 2013. Recurrent missense mutations in TMEM43 (ARVD5) due to founder effects cause arrhythmogenic cardiomyopathies in the UK and Canada. *Eur. Heart J.* 34, 1002–1011. <https://doi.org/10.1093/eurheartj/ehs383>
- He, J.-Q., Ma, Y., Lee, Y., Thomson, J.A., Kamp, T.J., 2003. Human embryonic stem cells develop into multiple types of cardiac myocytes: action potential characterization. *Circ. Res.* 93, 32–39. <https://doi.org/10.1161/01.RES.0000080317.92718.99>
- Heallen, T., Zhang, M., Wang, J., Bonilla-Claudio, M., Klysik, E., Johnson, R.L., Martin, J.F., 2011. Hippo pathway inhibits Wnt signaling to restrain cardiomyocyte proliferation and heart size. *Science* 332, 458–461. <https://doi.org/10.1126/science.1199010>
- Heid, H.W., Schmidt, A., Zimbelmann, R., Schäfer, S., Winter-Simanowski, S., Stumpp, S., Keith, M., Figge, U., Schnölzer, M., Franke, W.W., 1994. Cell type-specific desmosomal plaque proteins of the plakoglobin family: plakophilin 1 (band 6 protein). *Differ. Res. Biol. Divers.* 58, 113–131.
- Hellemans, J., Mortier, G., De Paepe, A., Speleman, F., Vandesompele, J., 2007. qBase relative quantification framework and software for management and automated analysis of real-time quantitative PCR data. *Genome Biol.* 8, R19. <https://doi.org/10.1186/gb-2007-8-2-r19>
- Henderson, J.K., Draper, J.S., Baillie, H.S., Fishel, S., Thomson, J.A., Moore, H., Andrews, P.W., 2002. Preimplantation human embryos and embryonic stem cells show comparable expression of stage-specific embryonic antigens. *Stem Cells Dayt. Ohio* 20, 329–337. <https://doi.org/10.1634/stemcells.20-4-329>
- Hentze, H., Soong, P.L., Wang, S.T., Phillips, B.W., Putti, T.C., Dunn, N.R., 2009. Teratoma formation by human embryonic stem cells: evaluation of essential parameters for future safety studies. *Stem Cell Res.* 2, 198–210. <https://doi.org/10.1016/j.scr.2009.02.002>
- Heuser, A., Plovie, E.R., Ellinor, P.T., Grossmann, K.S., Shin, J.T., Wichter, T., Basson, C.T., Lerman, B.B., Sasse-Klaassen, S., Thierfelder, L., MacRae, C.A., Gerull, B., 2006. Mutant desmocollin-2 causes arrhythmogenic right ventricular cardiomyopathy. *Am. J. Hum. Genet.* 79, 1081–1088. <https://doi.org/10.1086/509044>

- Holthöfer, B., Windoffer, R., Troyanovsky, S., Leube, R.E., 2007. Structure and Function of Desmosomes, in: *International Review of Cytology*. Elsevier, pp. 65–163.
- Hu, B.-Y., Weick, J.P., Yu, J., Ma, L.-X., Zhang, X.-Q., Thomson, J.A., Zhang, S.-C., 2010. Neural differentiation of human induced pluripotent stem cells follows developmental principles but with variable potency. *Proc. Natl. Acad. Sci. U. S. A.* 107, 4335–4340. <https://doi.org/10.1073/pnas.0910012107>
- Huang, H., Asimaki, A., Lo, D., McKenna, W., Saffitz, J., 2008. Disparate effects of different mutations in plakoglobin on cell mechanical behavior. *Cell Motil. Cytoskeleton* 65, 964–978. <https://doi.org/10.1002/cm.20319>
- Hulot, J.-S., 2004. Natural History and Risk Stratification of Arrhythmogenic Right Ventricular Dysplasia/Cardiomyopathy. *Circulation* 110, 1879–1884. <https://doi.org/10.1161/01.CIR.0000143375.93288.82>
- Illumina, 2017. BlueFuse Multi v4.4 Software Guide.
- Illumina, 2016. HumanCytoSNP-12 v2.1 BeadChip Datasheet.
- Illumina, 2009. Infinium® HD Assay Ultra Protocol Guide.
- Inoue, M., Tokusumi, Y., Ban, H., Kanaya, T., Tokusumi, T., Nagai, Y., Iida, A., Hasegawa, M., 2003. Nontransmissible virus-like particle formation by F-deficient sendai virus is temperature sensitive and reduced by mutations in M and HN proteins. *J. Virol.* 77, 3238–3246.
- International Stem Cell Initiative, Amps, K., Andrews, P.W., Anyfantis, G., Armstrong, L., Avery, S., Baharvand, H., Baker, J., Baker, D., Munoz, M.B., Beil, S., Benvenisty, N., Ben-Yosef, D., Biancotti, J.-C., Bosman, A., Brena, R.M., Brison, D., Caisander, G., Camarasa, M.V., Chen, J., Chiao, E., Choi, Y.M., Choo, A.B.H., Collins, D., Colman, A., Crook, J.M., Daley, G.Q., Dalton, A., De Sousa, P.A., Denning, C., Downie, J., Dvorak, P., Montgomery, K.D., Feki, A., Ford, A., Fox, V., Fraga, A.M., Frumkin, T., Ge, L., Gokhale, P.J., Golan-Lev, T., Gourabi, H., Gropp, M., Lu, G., Hampl, A., Harron, K., Healy, L., Herath, W., Holm, F., Hovatta, O., Hyllner, J., Inamdar, M.S., Irwanto, A.K., Ishii, T., Jaconi, M., Jin, Y., Kimber, S., Kiselev, S., Knowles, B.B., Kopper, O., Kukhareenko, V., Kuliev, A., Lagarkova, M.A., Laird, P.W., Lako, M., Laslett, A.L., Lavon, N., Lee, D.R., Lee, J.E., Li, C., Lim, L.S., Ludwig, T.E., Ma, Y., Maltby, E., Mateizel, I., Mayshar, Y., Mileikovsky, M., Minger, S.L., Miyazaki, T., Moon, S.Y., Moore, H., Mummery, C., Nagy, A., Nakatsuji, N., Narwani, K., Oh, S.K.W., Oh, S.K., Olson, C., Otonkoski, T., Pan, F., Park, I.-H., Pells, S., Pera,

- M.F., Pereira, L.V., Qi, O., Raj, G.S., Reubinoff, B., Robins, A., Robson, P., Rossant, J., Salekdeh, G.H., Schulz, T.C., Sermon, K., Sheik Mohamed, J., Shen, H., Sherrer, E., Sidhu, K., Sivarajah, S., Skottman, H., Spits, C., Stacey, G.N., Strehl, R., Strelchenko, N., Suemori, H., Sun, B., Suuronen, R., Takahashi, K., Tuuri, T., Venu, P., Verlinsky, Y., Ward-van Oostwaard, D., Weisenberger, D.J., Wu, Y., Yamanaka, S., Young, L., Zhou, Q., 2011. Screening ethnically diverse human embryonic stem cells identifies a chromosome 20 minimal amplicon conferring growth advantage. *Nat. Biotechnol.* 29, 1132–1144. <https://doi.org/10.1038/nbt.2051>
- Jackman, C.P., Carlson, A.L., Bursac, N., 2016. Dynamic culture yields engineered myocardium with near-adult functional output. *Biomaterials* 111, 66–79. <https://doi.org/10.1016/j.biomaterials.2016.09.024>
- Jackson, B.W., Grund, C., Winter, S., Franke, W.W., Illmensee, K., 1981. Formation of cytoskeletal elements during mouse embryogenesis. II. Epithelial differentiation and intermediate-sized filaments in early postimplantation embryos. *Differ. Res. Biol. Divers.* 20, 203–216.
- Jaenisch, R., Young, R., 2008. Stem cells, the molecular circuitry of pluripotency and nuclear reprogramming. *Cell* 132, 567–582. <https://doi.org/10.1016/j.cell.2008.01.015>
- James, C.A., Bhonsale, A., Tichnell, C., Murray, B., Russell, S.D., Tandri, H., Tedford, R.J., Judge, D.P., Calkins, H., 2013. Exercise increases age-related penetrance and arrhythmic risk in arrhythmogenic right ventricular dysplasia/cardiomyopathy-associated desmosomal mutation carriers. *J. Am. Coll. Cardiol.* 62, 1290–1297. <https://doi.org/10.1016/j.jacc.2013.06.033>
- Jefferson, J.J., Ciatto, C., Shapiro, L., Liem, R.K.H., 2007. Structural analysis of the plakin domain of bullous pemphigoid antigen1 (BPAG1) suggests that plakins are members of the spectrin superfamily. *J. Mol. Biol.* 366, 244–257. <https://doi.org/10.1016/j.jmb.2006.11.036>
- Jiang, J., Chan, Y.-S., Loh, Y.-H., Cai, J., Tong, G.-Q., Lim, C.-A., Robson, P., Zhong, S., Ng, H.-H., 2008. A core Klf circuitry regulates self-renewal of embryonic stem cells. *Nat. Cell Biol.* 10, 353–360. <https://doi.org/10.1038/ncb1698>
- Joachims, M.L., Chain, J.L., Hooker, S.W., Knott-Craig, C.J., Thompson, L.F., 2006. Human alpha beta and gamma delta thymocyte development: TCR gene rearrangements, intracellular TCR beta expression, and gamma delta

- developmental potential--differences between men and mice. *J. Immunol.* Baltim. Md 1950 176, 1543–1552.
- Josephson, R., Ording, C.J., Liu, Y., Shin, S., Lakshmiathy, U., Toumadje, A., Love, B., Chesnut, J.D., Andrews, P.W., Rao, M.S., Auerbach, J.M., 2007. Qualification of embryonal carcinoma 2102Ep as a reference for human embryonic stem cell research. *Stem Cells Dayt. Ohio* 25, 437–446.
<https://doi.org/10.1634/stemcells.2006-0236>
- Joshi-Mukherjee, R., Coombs, W., Musa, H., Oxford, E., Taffet, S., Delmar, M., 2008. Characterization of the molecular phenotype of two arrhythmogenic right ventricular cardiomyopathy (ARVC)-related plakophilin-2 (PKP2) mutations. *Heart Rhythm* 5, 1715–1723. <https://doi.org/10.1016/j.hrthm.2008.09.009>
- JUP expression in HaCaT cells [WWW Document], 2018. . *Hum. Protein Atlas*. URL <https://www.proteinatlas.org/ENSG00000173801-JUP/cell>
- Kamakura, T., Makiyama, T., Sasaki, K., Yoshida, Y., Wuriyanghai, Y., Chen, J., Hattori, T., Ohno, S., Kita, T., Horie, M., Yamanaka, S., Kimura, T., 2013. Ultrastructural maturation of human-induced pluripotent stem cell-derived cardiomyocytes in a long-term culture. *Circ. J. Off. J. Jpn. Circ. Soc.* 77, 1307–1314.
- Kaminsky, E.B., Kaul, V., Paschall, J., Church, D.M., Bunke, B., Kunig, D., Moreno-De-Luca, D., Moreno-De-Luca, A., Mulle, J.G., Warren, S.T., Richard, G., Compton, J.G., Fuller, A.E., Gliem, T.J., Huang, S., Collinson, M.N., Beal, S.J., Ackley, T., Pickering, D.L., Golden, D.M., Aston, E., Whitby, H., Shetty, S., Rossi, M.R., Rudd, M.K., South, S.T., Brothman, A.R., Sanger, W.G., Iyer, R.K., Crolla, J.A., Thorland, E.C., Aradhya, S., Ledbetter, D.H., Martin, C.L., 2011. An evidence-based approach to establish the functional and clinical significance of copy number variants in intellectual and developmental disabilities. *Genet. Med. Off. J. Am. Coll. Med. Genet.* 13, 777–784.
<https://doi.org/10.1097/GIM.0b013e31822c79f9>
- Kang, L., Wang, J., Zhang, Y., Kou, Z., Gao, S., 2009. iPS cells can support full-term development of tetraploid blastocyst-complemented embryos. *Cell Stem Cell* 5, 135–138. <https://doi.org/10.1016/j.stem.2009.07.001>
- Kannagi, R., Cochran, N.A., Ishigami, F., Hakomori, S., Andrews, P.W., Knowles, B.B., Solter, D., 1983. Stage-specific embryonic antigens (SSEA-3 and -4) are epitopes of a unique globo-series ganglioside isolated from human teratocarcinoma cells. *EMBO J.* 2, 2355–2361.

- Kant, S., Krusche, C.A., Gaertner, A., Milting, H., Leube, R.E., 2016. Loss of plakoglobin immunoreactivity in intercalated discs in arrhythmogenic right ventricular cardiomyopathy: protein mislocalization versus epitope masking. *Cardiovasc. Res.* 109, 260–271. <https://doi.org/10.1093/cvr/cvv270>
- Kaplan, S.R., Gard, J.J., Protonotarios, N., Tsatsopoulou, A., Spiliopoulou, C., Anastasakis, A., Squarcioni, C.P., McKenna, W.J., Thiene, G., Basso, C., Brousse, N., Fontaine, G., Saffitz, J.E., 2004. Remodeling of myocyte gap junctions in arrhythmogenic right ventricular cardiomyopathy due to a deletion in plakoglobin (Naxos disease). *Heart Rhythm Off. J. Heart Rhythm Soc.* 1, 3–11. <https://doi.org/10.1016/j.hrthm.2004.01.001>
- Karrer, H.E., 1960. Cell interconnections in normal human cervical epithelium. *J. Biophys. Biochem. Cytol.* 7, 181–184.
- Kattman, S.J., Witty, A.D., Gagliardi, M., Dubois, N.C., Niapour, M., Hotta, A., Ellis, J., Keller, G., 2011. Stage-specific optimization of activin/nodal and BMP signaling promotes cardiac differentiation of mouse and human pluripotent stem cell lines. *Cell Stem Cell* 8, 228–240. <https://doi.org/10.1016/j.stem.2010.12.008>
- Kehat, I., Kenyagin-Karsenti, D., Snir, M., Segev, H., Amit, M., Gepstein, A., Livne, E., Binah, O., Itskovitz-Eldor, J., Gepstein, L., 2001. Human embryonic stem cells can differentiate into myocytes with structural and functional properties of cardiomyocytes. *J. Clin. Invest.* 108, 407–414. <https://doi.org/10.1172/JCI12131>
- Kelly, D.E., 1966. Fine structure of desmosomes, hemidesmosomes, and an adepidermal globular layer in developing newt epidermis. *J. Cell Biol.* 28, 51–72.
- Kim, C., Wong, J., Wen, J., Wang, S., Wang, C., Spiering, S., Kan, N.G., Forcales, S., Puri, P.L., Leone, T.C., Marine, J.E., Calkins, H., Kelly, D.P., Judge, D.P., Chen, H.-S.V., 2013. Studying arrhythmogenic right ventricular dysplasia with patient-specific iPSCs. *Nature* 494, 105–110. <https://doi.org/10.1038/nature11799>
- Kimura, T.E., Merritt, A.J., Garrod, D.R., 2007. Calcium-independent desmosomes of keratinocytes are hyper-adhesive. *J. Invest. Dermatol.* 127, 775–781. <https://doi.org/10.1038/sj.jid.5700643>
- Kirchner, F., Schuetz, A., Boldt, L.-H., Martens, K., Dittmar, G., Haverkamp, W., Thierfelder, L., Heinemann, U., Gerull, B., 2012. Molecular insights into

- arrhythmogenic right ventricular cardiomyopathy caused by plakophilin-2 missense mutations. *Circ. Cardiovasc. Genet.* 5, 400–411.
<https://doi.org/10.1161/CIRCGENETICS.111.961854>
- Kitamura, R., Takahashi, T., Nakajima, N., Isodono, K., Asada, S., Ueno, H., Ueyama, T., Yoshikawa, T., Matsubara, H., Oh, H., 2007. Stage-specific role of endogenous Smad2 activation in cardiomyogenesis of embryonic stem cells. *Circ. Res.* 101, 78–87. <https://doi.org/10.1161/CIRCRESAHA.106.147264>
- Klauke, B., Kossmann, S., Gaertner, A., Brand, K., Stork, I., Brodehl, A., Dieding, M., Walhorn, V., Anselmetti, D., Gerdes, D., Bohms, B., Schulz, U., zu Knyphausen, E., Vorgerd, M., Gummert, J., Milting, H., 2010. De novo desmin-mutation N116S is associated with arrhythmogenic right ventricular cardiomyopathy. *Hum. Mol. Genet.* 19, 4595–4607.
<https://doi.org/10.1093/hmg/ddq387>
- Kleinman, H.K., McGarvey, M.L., Hassell, J.R., Star, V.L., Cannon, F.B., Laurie, G.W., Martin, G.R., 1986. Basement membrane complexes with biological activity. *Biochemistry* 25, 312–318.
- Kleinman, H.K., McGarvey, M.L., Liotta, L.A., Robey, P.G., Tryggvason, K., Martin, G.R., 1982. Isolation and characterization of type IV procollagen, laminin, and heparan sulfate proteoglycan from the EHS sarcoma. *Biochemistry* 21, 6188–6193.
- Kodama, S., Ikeda, S., Asahara, T., Kishida, M., Kikuchi, A., 1999. Axin directly interacts with plakoglobin and regulates its stability. *J. Biol. Chem.* 274, 27682–27688.
- Kouzarides, T., 2007. Chromatin modifications and their function. *Cell* 128, 693–705.
<https://doi.org/10.1016/j.cell.2007.02.005>
- Kowalczyk, A.P., Bornslaeger, E.A., Borgwardt, J.E., Palka, H.L., Dhaliwal, A.S., Corcoran, C.M., Denning, M.F., Green, K.J., 1997. The amino-terminal domain of desmoplakin binds to plakoglobin and clusters desmosomal cadherin-plakoglobin complexes. *J. Cell Biol.* 139, 773–784.
- Kowalczyk, A.P., Hatzfeld, M., Bornslaeger, E.A., Kopp, D.S., Borgwardt, J.E., Corcoran, C.M., Settler, A., Green, K.J., 1999. The head domain of plakophilin-1 binds to desmoplakin and enhances its recruitment to desmosomes. Implications for cutaneous disease. *J. Biol. Chem.* 274, 18145–18148.

- Krusche, C.A., Holthöfer, B., Hofe, V., Sandt, A.M., Eshkind, L., Bockamp, E., Merx, M.W., Kant, S., Windoffer, R., Leube, R.E., 2011. Desmoglein 2 mutant mice develop cardiac fibrosis and dilation. *Basic Res. Cardiol.* 106, 617–633. <https://doi.org/10.1007/s00395-011-0175-y>
- Kubo, A., Shinozaki, K., Shannon, J.M., Kouskoff, V., Kennedy, M., Woo, S., Fehling, H.J., Keller, G., 2004. Development of definitive endoderm from embryonic stem cells in culture. *Dev. Camb. Engl.* 131, 1651–1662. <https://doi.org/10.1242/dev.01044>
- Kunisato, A., Wakatsuki, M., Shinba, H., Ota, T., Ishida, I., Nagao, K., 2011. Direct generation of induced pluripotent stem cells from human nonmobilized blood. *Stem Cells Dev.* 20, 159–168. <https://doi.org/10.1089/scd.2010.0063>
- Kwon, Y.-S., Park, T.I., Cho, Y., Bae, M.H., Kim, S., 2013. Clinical usefulness of immunohistochemistry for plakoglobin, N-cadherin, and connexin-43 in the diagnosis of arrhythmogenic right ventricular cardiomyopathy. *Int. J. Clin. Exp. Pathol.* 6, 2928–2935.
- Lahtinen, A.M., Lehtonen, A., Kaartinen, M., Toivonen, L., Swan, H., Widén, E., Lehtonen, E., Lehto, V.-P., Kontula, K., 2008. Plakophilin-2 missense mutations in arrhythmogenic right ventricular cardiomyopathy. *Int. J. Cardiol.* 126, 92–100. <https://doi.org/10.1016/j.ijcard.2007.03.137>
- Lahtinen, A.M., Lehtonen, E., Marjamaa, A., Kaartinen, M., Heliö, T., Porthan, K., Oikarinen, L., Toivonen, L., Swan, H., Jula, A., Peltonen, L., Palotie, A., Salomaa, V., Kontula, K., 2011. Population-prevalent desmosomal mutations predisposing to arrhythmogenic right ventricular cardiomyopathy. *Heart Rhythm* 8, 1214–1221. <https://doi.org/10.1016/j.hrthm.2011.03.015>
- Laurent, L.C., Ulitsky, I., Slavin, I., Tran, H., Schork, A., Morey, R., Lynch, C., Harness, J.V., Lee, S., Barrero, M.J., Ku, S., Martynova, M., Semechkin, R., Galat, V., Gottesfeld, J., Izpisua Belmonte, J.C., Murry, C., Keirstead, H.S., Park, H.-S., Schmidt, U., Laslett, A.L., Muller, F.-J., Nievergelt, C.M., Shamir, R., Loring, J.F., 2011. Dynamic changes in the copy number of pluripotency and cell proliferation genes in human ESCs and iPSCs during reprogramming and time in culture. *Cell Stem Cell* 8, 106–118. <https://doi.org/10.1016/j.stem.2010.12.003>
- Lefort, N., Feyeux, M., Bas, C., Féraud, O., Bennaceur-Griscelli, A., Tachdjian, G., Peschanski, M., Perrier, A.L., 2008. Human embryonic stem cells reveal

- recurrent genomic instability at 20q11.21. *Nat. Biotechnol.* 26, 1364–1366.
<https://doi.org/10.1038/nbt.1509>
- Li, D., Liu, Y., Maruyama, M., Zhu, W., Chen, H., Zhang, W., Reuter, S., Lin, S.-F., Haneline, L.S., Field, L.J., Chen, P.-S., Shou, W., 2011. Restrictive loss of plakoglobin in cardiomyocytes leads to arrhythmogenic cardiomyopathy. *Hum. Mol. Genet.* 20, 4582–4596. <https://doi.org/10.1093/hmg/ddr392>
- Li, H.O., Zhu, Y.F., Asakawa, M., Kuma, H., Hirata, T., Ueda, Y., Lee, Y.S., Fukumura, M., Iida, A., Kato, A., Nagai, Y., Hasegawa, M., 2000. A cytoplasmic RNA vector derived from nontransmissible Sendai virus with efficient gene transfer and expression. *J. Virol.* 74, 6564–6569.
- Li, J., Swope, D., Raess, N., Cheng, L., Muller, E.J., Radice, G.L., 2011. Cardiac Tissue-Restricted Deletion of Plakoglobin Results in Progressive Cardiomyopathy and Activation of β -Catenin Signaling. *Mol. Cell. Biol.* 31, 1134–1144. <https://doi.org/10.1128/MCB.01025-10>
- Lian, X., Zhang, J., Azarin, S.M., Zhu, K., Hazeltine, L.B., Bao, X., Hsiao, C., Kamp, T.J., Palecek, S.P., 2013a. Directed cardiomyocyte differentiation from human pluripotent stem cells by modulating Wnt/ β -catenin signaling under fully defined conditions. *Nat. Protoc.* 8, 162–175.
<https://doi.org/10.1038/nprot.2012.150>
- Lian, X., Zhang, J., Zhu, K., Kamp, T.J., Palecek, S.P., 2013b. Insulin inhibits cardiac mesoderm, not mesendoderm, formation during cardiac differentiation of human pluripotent stem cells and modulation of canonical Wnt signaling can rescue this inhibition. *Stem Cells Dayt. Ohio* 31, 447–457.
<https://doi.org/10.1002/stem.1289>
- Lieu, D.K., Fu, J.-D., Chiamvimonvat, N., Tung, K.C., McNERney, G.P., Huser, T., Keller, G., Kong, C.-W., Li, R.A., 2013. Mechanism-based facilitated maturation of human pluripotent stem cell-derived cardiomyocytes. *Circ. Arrhythm. Electrophysiol.* 6, 191–201.
<https://doi.org/10.1161/CIRCEP.111.973420>
- Life Technologies, 2013. CytoTune®-iPS 2.0 Sendai Reprogramming Kit For efficient, integration-free reprogramming of somatic cells into induced pluripotent stem cells (iPSC).
- Life Technologies, 2012. Reprogramming Peripheral Blood Mononuclear Cells (PBMCs) with the CytoTune™-iPS Reprogramming Kit.

- Lobo, F.V., Heggtveit, H.A., Butany, J., Silver, M.D., Edwards, J.E., 1992. Right ventricular dysplasia: morphological findings in 13 cases. *Can. J. Cardiol.* 8, 261–268.
- Loh, Y.-H., Agarwal, S., Park, I.-H., Urbach, A., Huo, H., Heffner, G.C., Kim, K., Miller, J.D., Ng, K., Daley, G.Q., 2009. Generation of induced pluripotent stem cells from human blood. *Blood* 113, 5476–5479. <https://doi.org/10.1182/blood-2009-02-204800>
- Loh, Y.-H., Hartung, O., Li, H., Guo, C., Sahalie, J.M., Manos, P.D., Urbach, A., Heffner, G.C., Grskovic, M., Vigneault, F., Lensch, M.W., Park, I.-H., Agarwal, S., Church, G.M., Collins, J.J., Irion, S., Daley, G.Q., 2010. Reprogramming of T Cells from Human Peripheral Blood. *Cell Stem Cell* 7, 15–19. <https://doi.org/10.1016/j.stem.2010.06.004>
- Loh, Y.-H., Wu, Q., Chew, J.-L., Vega, V.B., Zhang, W., Chen, X., Bourque, G., George, J., Leong, B., Liu, J., Wong, K.-Y., Sung, K.W., Lee, C.W.H., Zhao, X.-D., Chiu, K.-P., Lipovich, L., Kuznetsov, V.A., Robson, P., Stanton, L.W., Wei, C.-L., Ruan, Y., Lim, B., Ng, H.-H., 2006. The Oct4 and Nanog transcription network regulates pluripotency in mouse embryonic stem cells. *Nat. Genet.* 38, 431–440. <https://doi.org/10.1038/ng1760>
- Lombardi, R., da Graca Cabreira-Hansen, M., Bell, A., Fromm, R.R., Willerson, J.T., Marian, A.J., 2011. Nuclear Plakoglobin Is Essential for Differentiation of Cardiac Progenitor Cells to Adipocytes in Arrhythmogenic Right Ventricular Cardiomyopathy. *Circ. Res.* 109, 1342–1353. <https://doi.org/10.1161/CIRCRESAHA.111.255075>
- Longo, K.A., 2002. Wnt Signaling Protects 3T3-L1 Preadipocytes from Apoptosis through Induction of Insulin-like Growth Factors. *J. Biol. Chem.* 277, 38239–38244. <https://doi.org/10.1074/jbc.M206402200>
- Lorenzon, A., Beffagna, G., Bauce, B., De Bortoli, M., Li Mura, I.E.A., Calore, M., Dazzo, E., Basso, C., Nava, A., Thiene, G., Rampazzo, A., 2013. Desmin mutations and arrhythmogenic right ventricular cardiomyopathy. *Am. J. Cardiol.* 111, 400–405. <https://doi.org/10.1016/j.amjcard.2012.10.017>
- Ludwig, T.E., Levenstein, M.E., Jones, J.M., Berggren, W.T., Mitchen, E.R., Frane, J.L., Crandall, L.J., Daigh, C.A., Conard, K.R., Piekarczyk, M.S., Llanas, R.A., Thomson, J.A., 2006. Derivation of human embryonic stem cells in defined conditions. *Nat. Biotechnol.* 24, 185–187. <https://doi.org/10.1038/nbt1177>

- Lundy, S.D., Zhu, W.-Z., Regnier, M., Laflamme, M.A., 2013. Structural and functional maturation of cardiomyocytes derived from human pluripotent stem cells. *Stem Cells Dev.* 22, 1991–2002. <https://doi.org/10.1089/scd.2012.0490>
- Ma, D., Wei, H., Lu, J., Ho, S., Zhang, G., Sun, X., Oh, Y., Tan, S.H., Ng, M.L., Shim, W., Wong, P., Liew, R., 2012. Generation of patient-specific induced pluripotent stem cell-derived cardiomyocytes as a cellular model of arrhythmogenic right ventricular cardiomyopathy. *Eur. Heart J.* <https://doi.org/10.1093/eurheartj/ehs226>
- Mabbott, N.A., Baillie, J.K., Brown, H., Freeman, T.C., Hume, D.A., 2013. An expression atlas of human primary cells: inference of gene function from coexpression networks. *BMC Genomics* 14, 632. <https://doi.org/10.1186/1471-2164-14-632>
- MacDonald, J.R., Ziman, R., Yuen, R.K.C., Feuk, L., Scherer, S.W., 2014. The Database of Genomic Variants: a curated collection of structural variation in the human genome. *Nucleic Acids Res.* 42, D986-992. <https://doi.org/10.1093/nar/gkt958>
- Mack, A.A., Kroboth, S., Rajesh, D., Wang, W.B., 2011. Generation of induced pluripotent stem cells from CD34+ cells across blood drawn from multiple donors with non-integrating episomal vectors. *PloS One* 6, e27956. <https://doi.org/10.1371/journal.pone.0027956>
- Maeda, O., Usami, N., Kondo, M., Takahashi, M., Goto, H., Shimokata, K., Kusugami, K., Sekido, Y., 2004. Plakoglobin (gamma-catenin) has TCF/LEF family-dependent transcriptional activity in beta-catenin-deficient cell line. *Oncogene* 23, 964–972. <https://doi.org/10.1038/sj.onc.1207254>
- Mahe, E., Pugh, T., Kamel-Reid, S., 2017. T cell clonality assessment: past, present and future. *J. Clin. Pathol.* <https://doi.org/10.1136/jclinpath-2017-204761>
- Malynn, B.A., de Alboran, I.M., O'Hagan, R.C., Bronson, R., Davidson, L., DePinho, R.A., Alt, F.W., 2000. N-myc can functionally replace c-myc in murine development, cellular growth, and differentiation. *Genes Dev.* 14, 1390–1399.
- Marcozzi, C., Burdett, I.D., Buxton, R.S., Magee, A.I., 1998. Coexpression of both types of desmosomal cadherin and plakoglobin confers strong intercellular adhesion. *J. Cell Sci.* 111 (Pt 4), 495–509.
- Marcus, F.I., Fontaine, G.H., Guiraudon, G., Frank, R., Laurenceau, J.L., Malergue, C., Grosogeat, Y., 1982. Right ventricular dysplasia: a report of 24 adult cases. *Circulation* 65, 384–398. <https://doi.org/10.1161/01.CIR.65.2.384>

- Marcus, F.I., McKenna, W.J., Sherrill, D., Basso, C., Bauce, B., Bluemke, D.A., Calkins, H., Corrado, D., Cox, M.G.P.J., Daubert, J.P., Fontaine, G., Gear, K., Hauer, R., Nava, A., Picard, M.H., Protonotarios, N., Saffitz, J.E., Sanborn, D.M.Y., Steinberg, J.S., Tandri, H., Thiene, G., Towbin, J.A., Tsatsopoulou, A., Wichter, T., Zareba, W., 2010. Diagnosis of arrhythmogenic right ventricular cardiomyopathy/dysplasia: Proposed Modification of the Task Force Criteria. *Eur. Heart J.* 31, 806–814. <https://doi.org/10.1093/eurheartj/ehq025>
- Marcus, F.I., Zareba, W., Calkins, H., Towbin, J.A., Basso, C., Bluemke, D.A., Estes, N.A.M., Picard, M.H., Sanborn, D., Thiene, G., Wichter, T., Cannom, D., Wilber, D.J., Scheinman, M., Duff, H., Daubert, J., Talajic, M., Krahn, A., Sweeney, M., Garan, H., Sakaguchi, S., Lerman, B.B., Kerr, C., Kron, J., Steinberg, J.S., Sherrill, D., Gear, K., Brown, M., Severski, P., Polonsky, S., McNitt, S., 2009. Arrhythmogenic right ventricular cardiomyopathy/dysplasia clinical presentation and diagnostic evaluation: Results from the North American Multidisciplinary Study. *Heart Rhythm* 6, 984–992. <https://doi.org/10.1016/j.hrthm.2009.03.013>
- Martins-Taylor, K., Nisler, B.S., Taapken, S.M., Compton, T., Crandall, L., Montgomery, K.D., Lalande, M., Xu, R.-H., 2011. Recurrent copy number variations in human induced pluripotent stem cells. *Nat. Biotechnol.* 29, 488–491. <https://doi.org/10.1038/nbt.1890>
- Mathur, M., Goodwin, L., Cowin, P., 1994. Interactions of the cytoplasmic domain of the desmosomal cadherin Dsg1 with plakoglobin. *J. Biol. Chem.* 269, 14075–14080.
- Matin, M.M., Walsh, J.R., Gokhale, P.J., Draper, J.S., Bahrami, A.R., Morton, I., Moore, H.D., Andrews, P.W., 2004. Specific knockdown of Oct4 and beta2-microglobulin expression by RNA interference in human embryonic stem cells and embryonic carcinoma cells. *Stem Cells Dayt. Ohio* 22, 659–668. <https://doi.org/10.1634/stemcells.22-5-659>
- Mayosi, B.M., Fish, M., Shaboodien, G., Mastantuono, E., Kraus, S., Wieland, T., Kotta, M.-C., Chin, A., Laing, N., Ntusi, N.B.A., Chong, M., Horsfall, C., Pimstone, S.N., Gentilini, D., Parati, G., Strom, T.-M., Meitinger, T., Pare, G., Schwartz, P.J., Crotti, L., 2017. Identification of Cadherin 2 (CDH2) Mutations in Arrhythmogenic Right Ventricular Cardiomyopathy. *Circ. Cardiovasc. Genet.* 10. <https://doi.org/10.1161/CIRCGENETICS.116.001605>

- McKoy, G., Protonotarios, N., Crosby, A., Tsatsopoulou, A., Anastasakis, A., Coonar, A., Norman, M., Baboonian, C., Jeffery, S., McKenna, W.J., 2000. Identification of a deletion in plakoglobin in arrhythmogenic right ventricular cardiomyopathy with palmoplantar keratoderma and woolly hair (Naxos disease). *Lancet* 355, 2119–2124. [https://doi.org/10.1016/S0140-6736\(00\)02379-5](https://doi.org/10.1016/S0140-6736(00)02379-5)
- McNutt, N.S., 1970. Ultrastructure of intercellular junctions in adult and developing cardiac muscle. *Am. J. Cardiol.* 25, 169–183.
- Meissner, A., Mikkelsen, T.S., Gu, H., Wernig, M., Hanna, J., Sivachenko, A., Zhang, X., Bernstein, B.E., Nusbaum, C., Jaffe, D.B., Gnirke, A., Jaenisch, R., Lander, E.S., 2008. Genome-scale DNA methylation maps of pluripotent and differentiated cells. *Nature* 454, 766–770. <https://doi.org/10.1038/nature07107>
- Merling, R.K., Sweeney, C.L., Choi, U., De Ravin, S.S., Myers, T.G., Otaizo-Carrasquero, F., Pan, J., Linton, G., Chen, L., Koontz, S., Theobald, N.L., Malech, H.L., 2013. Transgene-free iPSCs generated from small volume peripheral blood nonmobilized CD34+ cells. *Blood* 121, e98–e107. <https://doi.org/10.1182/blood-2012-03-420273>
- Merner, N.D., Hodgkinson, K.A., Haywood, A.F.M., Connors, S., French, V.M., Drenckhahn, J.-D., Kupprion, C., Ramadanova, K., Thierfelder, L., McKenna, W., Gallagher, B., Morris-Larkin, L., Bassett, A.S., Parfrey, P.S., Young, T.-L., 2008. Arrhythmogenic Right Ventricular Cardiomyopathy Type 5 Is a Fully Penetrant, Lethal Arrhythmic Disorder Caused by a Missense Mutation in the TMEM43 Gene. *Am. J. Hum. Genet.* 82, 809–821. <https://doi.org/10.1016/j.ajhg.2008.01.010>
- Merriam, J.M., Rubenstein, A.B., Klymkowsky, M.W., 1997. Cytoplasmically anchored plakoglobin induces a WNT-like phenotype in *Xenopus*. *Dev. Biol.* 185, 67–81. <https://doi.org/10.1006/dbio.1997.8550>
- Mertens, C., Hofmann, I., Wang, Z., Teichmann, M., Sepehri Chong, S., Schnölzer, M., Franke, W.W., 2001. Nuclear particles containing RNA polymerase III complexes associated with the junctional plaque protein plakophilin 2. *Proc. Natl. Acad. Sci. U. S. A.* 98, 7795–7800. <https://doi.org/10.1073/pnas.141219498>
- Mertens, C., Kuhn, C., Franke, W.W., 1996. Plakophilins 2a and 2b: constitutive proteins of dual location in the karyoplasm and the desmosomal plaque. *J. Cell Biol.* 135, 1009–1025.

- Miller, J.R., Moon, R.T., 1997. Analysis of the signaling activities of localization mutants of beta-catenin during axis specification in *Xenopus*. *J. Cell Biol.* 139, 229–243.
- Miravet, S., 2001. The Transcriptional Factor Tcf-4 Contains Different Binding Sites for beta -Catenin and Plakoglobin. *J. Biol. Chem.* 277, 1884–1891.
<https://doi.org/10.1074/jbc.M110248200>
- Mitogawa, T., Nishiya, K., Ota, Z., 1992. Frequency of gamma delta T cells in peripheral blood, synovial fluid, synovial membrane and lungs from patients with rheumatoid arthritis. *Acta Med. Okayama* 46, 371–379.
<https://doi.org/10.18926/AMO/32664>
- Mitsui, K., Tokuzawa, Y., Itoh, H., Segawa, K., Murakami, M., Takahashi, K., Maruyama, M., Maeda, M., Yamanaka, S., 2003. The homeoprotein Nanog is required for maintenance of pluripotency in mouse epiblast and ES cells. *Cell* 113, 631–642.
- Muir, A.R., 1965. Further Observations On The Cellular Structure Of Cardiac Muscle. *J. Anat.* 99, 27–46.
- Müller, F.-J., Schuldt, B.M., Williams, R., Mason, D., Altun, G., Papapetrou, E.P., Danner, S., Goldmann, J.E., Herbst, A., Schmidt, N.O., Aldenhoff, J.B., Laurent, L.C., Loring, J.F., 2011. A bioinformatic assay for pluripotency in human cells. *Nat. Methods* 8, 315–317. <https://doi.org/10.1038/nmeth.1580>
- Mummery, C.L., Zhang, J., Ng, E.S., Elliott, D.A., Elefanty, A.G., Kamp, T.J., 2012. Differentiation of human embryonic stem cells and induced pluripotent stem cells to cardiomyocytes: a methods overview. *Circ. Res.* 111, 344–358.
<https://doi.org/10.1161/CIRCRESAHA.110.227512>
- Munkholm, J., Christensen, A.H., Svendsen, J.H., Andersen, C.B., 2012. Usefulness of Immunostaining for Plakoglobin as a Diagnostic Marker of Arrhythmogenic Right Ventricular Cardiomyopathy. *Am. J. Cardiol.* 109, 272–275.
<https://doi.org/10.1016/j.amjcard.2011.08.044>
- Nagy, A., Góczy, E., Diaz, E.M., Prideaux, V.R., Iványi, E., Markkula, M., Rossant, J., 1990. Embryonic stem cells alone are able to support fetal development in the mouse. *Dev. Camb. Engl.* 110, 815–821.
- Nagy, A., Rossant, J., Nagy, R., Abramow-Newerly, W., Roder, J.C., 1993. Derivation of completely cell culture-derived mice from early-passage embryonic stem cells. *Proc. Natl. Acad. Sci. U. S. A.* 90, 8424–8428.

- Nakatake, Y., Fukui, N., Iwamatsu, Y., Masui, S., Takahashi, K., Yagi, R., Yagi, K., Miyazaki, J.-I., Matoba, R., Ko, M.S.H., Niwa, H., 2006. Klf4 cooperates with Oct3/4 and Sox2 to activate the Lefty1 core promoter in embryonic stem cells. *Mol. Cell. Biol.* 26, 7772–7782. <https://doi.org/10.1128/MCB.00468-06>
- Närvä, E., Stubb, A., Guzmán, C., Blomqvist, M., Balboa, D., Lerche, M., Saari, M., Otonkoski, T., Ivaska, J., 2017. A Strong Contractile Actin Fence and Large Adhesions Direct Human Pluripotent Colony Morphology and Adhesion. *Stem Cell Rep.* 9, 67–76. <https://doi.org/10.1016/j.stemcr.2017.05.021>
- Nichols, J., Zevnik, B., Anastassiadis, K., Niwa, H., Klewe-Nebenius, D., Chambers, I., Schöler, H., Smith, A., 1998. Formation of pluripotent stem cells in the mammalian embryo depends on the POU transcription factor Oct4. *Cell* 95, 379–391.
- Nie, Z., Merritt, A., Rouhi-Parkouhi, M., Tabernero, L., Garrod, D., 2011. Membrane-impermeable cross-linking provides evidence for homophilic, isoform-specific binding of desmosomal cadherins in epithelial cells. *J. Biol. Chem.* 286, 2143–2154. <https://doi.org/10.1074/jbc.M110.192245>
- Nishimura, K., Sano, M., Ohtaka, M., Furuta, B., Umemura, Y., Nakajima, Y., Ikehara, Y., Kobayashi, T., Segawa, H., Takayasu, S., Sato, H., Motomura, K., Uchida, E., Kanayasu-Toyoda, T., Asashima, M., Nakauchi, H., Yamaguchi, T., Nakanishi, M., 2011. Development of defective and persistent Sendai virus vector: a unique gene delivery/expression system ideal for cell reprogramming. *J. Biol. Chem.* 286, 4760–4771. <https://doi.org/10.1074/jbc.M110.183780>
- Noorman, M., Hakim, S., Kessler, E., Groeneweg, J.A., Cox, M.G.P.J., Asimaki, A., van Rijen, H.V.M., van Stuijvenberg, L., Chkourko, H., van der Heyden, M.A.G., Vos, M.A., de Jonge, N., van der Smagt, J.J., Dooijes, D., Vink, A., de Weger, R.A., Varro, A., de Bakker, J.M.T., Saffitz, J.E., Hund, T.J., Mohler, P.J., Delmar, M., Hauer, R.N.W., van Veen, T.A.B., 2013. Remodeling of the cardiac sodium channel, connexin43, and plakoglobin at the intercalated disk in patients with arrhythmogenic cardiomyopathy. *Heart Rhythm Off. J. Heart Rhythm Soc.* 10, 412–419. <https://doi.org/10.1016/j.hrthm.2012.11.018>
- North, A.J., Bardsley, W.G., Hyam, J., Bornslaeger, E.A., Cordingley, H.C., Trinnaman, B., Hatzfeld, M., Green, K.J., Magee, A.I., Garrod, D.R., 1999. Molecular map of the desmosomal plaque. *J. Cell Sci.* 112 (Pt 23), 4325–4336.

- Nunes, S.S., Miklas, J.W., Liu, J., Aschar-Sobbi, R., Xiao, Y., Zhang, B., Jiang, J., Massé, S., Gagliardi, M., Hsieh, A., Thavandiran, N., Laflamme, M.A., Nanthakumar, K., Gross, G.J., Backx, P.H., Keller, G., Radisic, M., 2013. Biowire: a platform for maturation of human pluripotent stem cell-derived cardiomyocytes. *Nat. Methods* 10, 781–787.
<https://doi.org/10.1038/nmeth.2524>
- Ohmine, S., Dietz, A.B., Deeds, M.C., Hartjes, K.A., Miller, D.R., Thatava, T., Sakuma, T., Kudva, Y.C., Ikeda, Y., 2011. Induced pluripotent stem cells from GMP-grade hematopoietic progenitor cells and mononuclear myeloid cells. *Stem Cell Res. Ther.* 2, 46. <https://doi.org/10.1186/scrt87>
- Okita, K., Ichisaka, T., Yamanaka, S., 2007. Generation of germline-competent induced pluripotent stem cells. *Nature* 448, 313–317.
<https://doi.org/10.1038/nature05934>
- Osafune, K., Caron, L., Borowiak, M., Martinez, R.J., Fitz-Gerald, C.S., Sato, Y., Cowan, C.A., Chien, K.R., Melton, D.A., 2008. Marked differences in differentiation propensity among human embryonic stem cell lines. *Nat. Biotechnol.* 26, 313–315. <https://doi.org/10.1038/nbt1383>
- Otten, E., Asimaki, A., Maass, A., van Langen, I.M., van der Wal, A., de Jonge, N., van den Berg, M.P., Saffitz, J.E., Wilde, A.A.M., Jongbloed, J.D.H., van Tintelen, J.P., 2010. Desmin mutations as a cause of right ventricular heart failure affect the intercalated disks. *Heart Rhythm* 7, 1058–1064.
<https://doi.org/10.1016/j.hrthm.2010.04.023>
- Overduin, M., Harvey, T.S., Bagby, S., Tong, K.I., Yau, P., Takeichi, M., Ikura, M., 1995. Solution structure of the epithelial cadherin domain responsible for selective cell adhesion. *Science* 267, 386–389.
- Paige, S.L., Osugi, T., Afanasiev, O.K., Pabon, L., Reinecke, H., Murry, C.E., 2010. Endogenous Wnt/beta-catenin signaling is required for cardiac differentiation in human embryonic stem cells. *PLoS One* 5, e11134.
<https://doi.org/10.1371/journal.pone.0011134>
- Papp, B., Plath, K., 2013. Epigenetics of reprogramming to induced pluripotency. *Cell* 152, 1324–1343. <https://doi.org/10.1016/j.cell.2013.02.043>
- Park, Y.B., Kim, Y.Y., Oh, S.K., Chung, S.G., Ku, S.Y., Kim, S.H., Choi, Y.M., Moon, S.Y., 2008. Alterations of proliferative and differentiation potentials of human embryonic stem cells during long-term culture. *Exp. Mol. Med.* 40, 98–108.
<https://doi.org/10.3858/emm.2008.40.1.98>

- Pasqualini, F.S., Sheehy, S.P., Agarwal, A., Aratyn-Schaus, Y., Parker, K.K., 2015. Structural Phenotyping of Stem Cell-Derived Cardiomyocytes. *Stem Cell Rep.* <https://doi.org/10.1016/j.stemcr.2015.01.020>
- Patel, D.M., Dubash, A.D., Kreitzer, G., Green, K.J., 2014. Disease mutations in desmoplakin inhibit Cx43 membrane targeting mediated by desmoplakin-EB1 interactions. *J. Cell Biol.* 206, 779–797. <https://doi.org/10.1083/jcb.201312110>
- Pećina-Slaus, N., 2010. Wnt signal transduction pathway and apoptosis: a review. *Cancer Cell Int.* 10, 22. <https://doi.org/10.1186/1475-2867-10-22>
- Peiffer, D.A., Le, J.M., Steemers, F.J., Chang, W., Jenniges, T., Garcia, F., Haden, K., Li, J., Shaw, C.A., Belmont, J., Cheung, S.W., Shen, R.M., Barker, D.L., Gunderson, K.L., 2006. High-resolution genomic profiling of chromosomal aberrations using Infinium whole-genome genotyping. *Genome Res.* 16, 1136–1148. <https://doi.org/10.1101/gr.5402306>
- Pesl, M., Acimovic, I., Pribyl, J., Hezova, R., Vilotic, A., Fauconnier, J., Vrbsky, J., Kruzliak, P., Skladal, P., Kara, T., Rotrekl, V., Lacampagne, A., Dvorak, P., Meli, A.C., 2014. Forced aggregation and defined factors allow highly uniform-sized embryoid bodies and functional cardiomyocytes from human embryonic and induced pluripotent stem cells. *Heart Vessels* 29, 834–846. <https://doi.org/10.1007/s00380-013-0436-9>
- Peters, S., Trümmel, M., Meyners, W., 2004. Prevalence of right ventricular dysplasia-cardiomyopathy in a non-referral hospital. *Int. J. Cardiol.* 97, 499–501. <https://doi.org/10.1016/j.ijcard.2003.10.037>
- Philips, B., Madhavan, S., James, C.A., te Riele, A.S.J.M., Murray, B., Tichnell, C., Bhonsale, A., Nazarian, S., Judge, D.P., Calkins, H., Tandri, H., Cheng, A., 2014. Arrhythmogenic right ventricular dysplasia/cardiomyopathy and cardiac sarcoidosis: distinguishing features when the diagnosis is unclear. *Circ. Arrhythm. Electrophysiol.* 7, 230–236. <https://doi.org/10.1161/CIRCEP.113.000932>
- Pieperhoff, S., Franke, W.W., 2007. The area composita of adhering junctions connecting heart muscle cells of vertebrates - IV: coalescence and amalgamation of desmosomal and adhaerens junction components - late processes in mammalian heart development. *Eur. J. Cell Biol.* 86, 377–391. <https://doi.org/10.1016/j.ejcb.2007.04.001>

- Pilichou, K., 2006. Mutations in Desmoglein-2 Gene Are Associated With Arrhythmogenic Right Ventricular Cardiomyopathy. *Circulation* 113, 1171–1179. <https://doi.org/10.1161/CIRCULATIONAHA.105.583674>
- Pilichou, K., Remme, C.A., Basso, C., Campian, M.E., Rizzo, S., Barnett, P., Scicluna, B.P., Bauce, B., van den Hoff, M.J.B., de Bakker, J.M.T., Tan, H.L., Valente, M., Nava, A., Wilde, A.A.M., Moorman, A.F.M., Thiene, G., Bezzina, C.R., 2009. Myocyte necrosis underlies progressive myocardial dystrophy in mouse *dsg2*-related arrhythmogenic right ventricular cardiomyopathy. *J. Exp. Med.* 206, 1787–1802. <https://doi.org/10.1084/jem.20090641>
- Pilichou, K., Thiene, G., Bauce, B., Rigato, I., Lazzarini, E., Migliore, F., Perazzolo Marra, M., Rizzo, S., Zorzi, A., Daliento, L., Corrado, D., Basso, C., 2016. Arrhythmogenic cardiomyopathy. *Orphanet J. Rare Dis.* 11, 33. <https://doi.org/10.1186/s13023-016-0407-1>
- Pinamonti, B., Dragos, A.M., Pyxaras, S.A., Merlo, M., Pivetta, A., Barbati, G., Di Lenarda, A., Morgera, T., Mestroni, L., Sinagra, G., 2011. Prognostic predictors in arrhythmogenic right ventricular cardiomyopathy: results from a 10-year registry. *Eur. Heart J.* 32, 1105–1113. <https://doi.org/10.1093/eurheartj/ehr040>
- PKP1 expression in HaCaT cells [WWW Document], 2018. . Hum. Protein Atlas. URL <https://www.proteinatlas.org/ENSG00000081277-PKP1/cell>
- PKP2 expression in HaCaT cells [WWW Document], 2018. . Hum. Protein Atlas. URL <https://www.proteinatlas.org/ENSG00000057294-PKP2/cell>
- PKP3 expression in HaCaT cells [WWW Document], 2018. . Hum. Protein Atlas. URL <https://www.proteinatlas.org/ENSG00000184363-PKP3/cell>
- Poon, E., Keung, W., Liang, Y., Ramalingam, R., Yan, B., Zhang, S., Chopra, A., Moore, J., Herren, A., Lieu, D.K., Wong, H.S., Weng, Z., Wong, O.T., Lam, Y.W., Tomaselli, G.F., Chen, C., Boheler, K.R., Li, R.A., 2015. Proteomic Analysis of Human Pluripotent Stem Cell-Derived, Fetal, and Adult Ventricular Cardiomyocytes Reveals Pathways Crucial for Cardiac Metabolism and Maturation. *Circ. Cardiovasc. Genet.* 8, 427–436. <https://doi.org/10.1161/CIRCGENETICS.114.000918>
- Prokhorova, T.A., Harkness, L.M., Frandsen, U., Ditzel, N., Schröder, H.D., Burns, J.S., Kassem, M., 2009. Teratoma formation by human embryonic stem cells is site dependent and enhanced by the presence of Matrigel. *Stem Cells Dev.* 18, 47–54. <https://doi.org/10.1089/scd.2007.0266>

- Promega, 2012. ReliaPrep™ RNA Cell Miniprep System Technical Manual.
Instructions for use of products Z6010, Z6011 and Z6012.
- Quarta, G., Muir, A., Pantazis, A., Syrris, P., Gehmlich, K., Garcia-Pavia, P., Ward, D., Sen-Chowdhry, S., Elliott, P.M., McKenna, W.J., 2011a. Familial Evaluation in Arrhythmogenic Right Ventricular Cardiomyopathy: Impact of Genetics and Revised Task Force Criteria. *Circulation* 123, 2701–2709.
<https://doi.org/10.1161/CIRCULATIONAHA.110.976936>
- Quarta, G., Syrris, P., Ashworth, M., Jenkins, S., Zuborne Alapi, K., Morgan, J., Muir, A., Pantazis, A., McKenna, W.J., Elliott, P.M., 2011b. Mutations in the Lamin A/C gene mimic arrhythmogenic right ventricular cardiomyopathy. *Eur. Heart J.* 33, 1128–1136. <https://doi.org/10.1093/eurheartj/ehr451>
- Rampazzo, A., Nava, A., Danieli, G.A., Buja, G., Daliento, L., Fasoli, G., Scognamiglio, R., Corrado, D., Thiene, G., 1994. The gene for arrhythmogenic right ventricular cardiomyopathy maps to chromosome 14q23-q24. *Hum. Mol. Genet.* 3, 959–962.
- Rampazzo, A., Nava, A., Malacrida, S., Beffagna, G., Bauce, B., Rossi, V., Zimbello, R., Simionati, B., Basso, C., Thiene, G., Towbin, J.A., Danieli, G.A., 2002. Mutation in human desmoplakin domain binding to plakoglobin causes a dominant form of arrhythmogenic right ventricular cardiomyopathy. *Am. J. Hum. Genet.* 71, 1200–1206. <https://doi.org/10.1086/344208>
- Rao, T.P., Kuhl, M., 2010. An Updated Overview on Wnt Signaling Pathways: A Prelude for More. *Circ. Res.* 106, 1798–1806.
<https://doi.org/10.1161/CIRCRESAHA.110.219840>
- Rasmussen, T B, Hansen, J., Nissen, P.H., Palmfeldt, J., Dalager, S., Jensen, U.B., Kim, W.Y., Heickendorff, L., Mølgaard, H., Jensen, H.K., Sørensen, K.E., Baandrup, U.T., Bross, P., Mogensen, J., 2013. Protein expression studies of desmoplakin mutations in cardiomyopathy patients reveal different molecular disease mechanisms. *Clin. Genet.* 84, 20–30.
<https://doi.org/10.1111/cge.12056>
- Rasmussen, T.B., Nissen, P.H., Palmfeldt, J., Gehmlich, K., Dalager, S., Jensen, U.B., Kim, W.Y., Heickendorff, L., Mølgaard, H., Jensen, H.K., Baandrup, U.T., Bross, P., Mogensen, J., 2014. Truncating Plakophilin-2 Mutations in Arrhythmogenic Cardiomyopathy Are Associated with Protein Haploinsufficiency in Both Myocardium and Epidermis. *Circ. Cardiovasc. Genet.* <https://doi.org/10.1161/CIRCGENETICS.113.000338>

- Rasmussen, Torsten B, Palmfeldt, J., Nissen, P.H., Magnoni, R., Dalager, S., Jensen, U.B., Kim, W.Y., Heickendorff, L., Mølgaard, H., Jensen, H.K., Baandrup, U.T., Bross, P., Mogensen, J., 2013. Mutated desmoglein-2 proteins are incorporated into desmosomes and exhibit dominant-negative effects in arrhythmogenic right ventricular cardiomyopathy. *Hum. Mutat.* 34, 697–705. <https://doi.org/10.1002/humu.22289>
- Reichert, T., DeBruyère, M., Deneys, V., Tötterman, T., Lydyard, P., Yuksel, F., Chapel, H., Jewell, D., Van Hove, L., Linden, J., 1991. Lymphocyte subset reference ranges in adult Caucasians. *Clin. Immunol. Immunopathol.* 60, 190–208.
- Reik, W., Dean, W., Walter, J., 2001. Epigenetic reprogramming in mammalian development. *Science* 293, 1089–1093. <https://doi.org/10.1126/science.1063443>
- Reubinoff, B.E., Pera, M.F., Fong, C.Y., Trounson, A., Bongso, A., 2000. Embryonic stem cell lines from human blastocysts: somatic differentiation in vitro. *Nat. Biotechnol.* 18, 399–404. <https://doi.org/10.1038/74447>
- Roh, J.Y., Stanley, J.R., 1995. Plakoglobin binding by human Dsg3 (pemphigus vulgaris antigen) in keratinocytes requires the cadherin-like intracytoplasmic segment. *J. Invest. Dermatol.* 104, 720–724.
- Ronaldson-Bouchard, K., Ma, S.P., Yeager, K., Chen, T., Song, L., Sirabella, D., Morikawa, K., Teles, D., Yazawa, M., Vunjak-Novakovic, G., 2018. Advanced maturation of human cardiac tissue grown from pluripotent stem cells. *Nature* 556, 239–243. <https://doi.org/10.1038/s41586-018-0016-3>
- Rosowski, K.A., Mertz, A.F., Norcross, S., Dufresne, E.R., Horsley, V., 2015. Edges of human embryonic stem cell colonies display distinct mechanical properties and differentiation potential. *Sci. Rep.* 5, 14218. <https://doi.org/10.1038/srep14218>
- Ross, S.E., 2000. Inhibition of Adipogenesis by Wnt Signaling. *Science* 289, 950–953. <https://doi.org/10.1126/science.289.5481.950>
- Ruan, J.-L., Tulloch, N.L., Razumova, M.V., Saiget, M., Muskheli, V., Pabon, L., Reinecke, H., Regnier, M., Murry, C.E., 2016. Mechanical Stress Conditioning and Electrical Stimulation Promote Contractility and Force Maturation of Induced Pluripotent Stem Cell-Derived Human Cardiac Tissue. *Circulation* 134, 1557–1567. <https://doi.org/10.1161/CIRCULATIONAHA.114.014998>

- Ruiz, P., Brinkmann, V., Ledermann, B., Behrend, M., Grund, C., Thalhammer, C., Vogel, F., Birchmeier, C., Günthert, U., Franke, W.W., Birchmeier, W., 1996. Targeted mutation of plakoglobin in mice reveals essential functions of desmosomes in the embryonic heart. *J. Cell Biol.* 135, 215–225.
- Runswick, S.K., O'Hare, M.J., Jones, L., Streuli, C.H., Garrod, D.R., 2001. Desmosomal adhesion regulates epithelial morphogenesis and cell positioning. *Nat. Cell Biol.* 3, 823–830. <https://doi.org/10.1038/ncb0901-823>
- Saberniak, J., Hasselberg, N.E., Borgquist, R., Platonov, P.G., Sarvari, S.I., Smith, H.-J., Ribe, M., Holst, A.G., Edvardsen, T., Haugaa, K.H., 2014. Vigorous physical activity impairs myocardial function in patients with arrhythmogenic right ventricular cardiomyopathy and in mutation positive family members. *Eur. J. Heart Fail.* 16, 1337–1344. <https://doi.org/10.1002/ejhf.181>
- Salick, M.R., Napiwocki, B.N., Sha, J., Knight, G.T., Chindhy, S.A., Kamp, T.J., Ashton, R.S., Crone, W.C., 2014. Micropattern width dependent sarcomere development in human ESC-derived cardiomyocytes. *Biomaterials* 35, 4454–4464. <https://doi.org/10.1016/j.biomaterials.2014.02.001>
- Sallam, K., Kodo, K., Wu, J.C., 2014. Modeling inherited cardiac disorders. *Circ. J. Off. J. Jpn. Circ. Soc.* 78, 784–794.
- Salomon, D., Sacco, P.A., Roy, S.G., Simcha, I., Johnson, K.R., Wheelock, M.J., Ben-Ze'ev, A., 1997. Regulation of beta-catenin levels and localization by overexpression of plakoglobin and inhibition of the ubiquitin-proteasome system. *J. Cell Biol.* 139, 1325–1335.
- Sandberg, Y., van Gastel-Mol, E.J., Verhaaf, B., Lam, K.H., van Dongen, J.J.M., Langerak, A.W., 2005. BIOMED-2 multiplex immunoglobulin/T-cell receptor polymerase chain reaction protocols can reliably replace Southern blot analysis in routine clonality diagnostics. *J. Mol. Diagn. JMD* 7, 495–503. [https://doi.org/10.1016/S1525-1578\(10\)60580-6](https://doi.org/10.1016/S1525-1578(10)60580-6)
- Santos, F., Hendrich, B., Reik, W., Dean, W., 2002. Dynamic reprogramming of DNA methylation in the early mouse embryo. *Dev. Biol.* 241, 172–182. <https://doi.org/10.1006/dbio.2001.0501>
- Sathananthan, H., Pera, M., Trounson, A., 2002. The fine structure of human embryonic stem cells. *Reprod. Biomed. Online* 4, 56–61.
- Sato, P.Y., Coombs, W., Lin, X., Nekrasova, O., Green, K.J., Isom, L.L., Taffet, S.M., Delmar, M., 2011. Interactions Between Ankyrin-G, Plakophilin-2, and

Connexin43 at the Cardiac Intercalated Disc. *Circ. Res.* 109, 193–201.

<https://doi.org/10.1161/CIRCRESAHA.111.247023>

Schinzel, A., Schmid, W., Fraccaro, M., Tiepolo, L., Zuffardi, O., Opitz, J.M., Lindsten, J., Zetterqvist, P., Enell, H., Baccichetti, C., Tenconi, R., Pagon, R.A., 1981.

The “cat eye syndrome”: dicentric small marker chromosome probably derived from a no.22 (tetrasomy 22pter to q11) associated with a characteristic phenotype. Report of 11 patients and delineation of the clinical picture. *Hum. Genet.* 57, 148–158.

Schmidt, A., Langbein, L., Rode, M., Prätzel, S., Zimbelmann, R., Franke, W.W., 1997. Plakophilins 1a and 1b: widespread nuclear proteins recruited in specific epithelial cells as desmosomal plaque components. *Cell Tissue Res.* 290, 481–499.

Schopperle, W.M., DeWolf, W.C., 2007. The TRA-1-60 and TRA-1-81 human pluripotent stem cell markers are expressed on podocalyxin in embryonal carcinoma. *Stem Cells Dayt. Ohio* 25, 723–730.

<https://doi.org/10.1634/stemcells.2005-0597>

Schrön, 1863. *Untersuch. z. Naturlehre.* Moleschott.

Schultze, M., 1864. Die Stachel- und Riffzellen der tieferen Schichten der Epidermis, dicker Pflasterepithelien und der Epithelialkrebse. *Virchows Arch Path Anat* 30, 260.

Sekhsaria, S., Fleisher, T.A., Vowells, S., Brown, M., Miller, J., Gordon, I., Blaese, R.M., Dunbar, C.E., Leitman, S., Malech, H.L., 1996. Granulocyte colony-stimulating factor recruitment of CD34+ progenitors to peripheral blood: impaired mobilization in chronic granulomatous disease and adenosine deaminase--deficient severe combined immunodeficiency disease patients. *Blood* 88, 1104–1112.

Seki, T., Yuasa, S., Fukuda, K., 2012. Generation of induced pluripotent stem cells from a small amount of human peripheral blood using a combination of activated T cells and Sendai virus. *Nat. Protoc.* 7, 718–728.

<https://doi.org/10.1038/nprot.2012.015>

Seki, T., Yuasa, S., Fukuda, K., 2011. Derivation of Induced Pluripotent Stem Cells from Human Peripheral Circulating T Cells. *Curr. Protoc. Stem Cell Biol.*

Seki, T., Yuasa, S., Oda, M., Egashira, T., Yae, K., Kusumoto, D., Nakata, H., Tohyama, S., Hashimoto, H., Kodaira, M., Okada, Y., Seimiya, H., Fusaki, N., Hasegawa, M., Fukuda, K., 2010. Generation of Induced Pluripotent Stem

- Cells from Human Terminally Differentiated Circulating T Cells. *Cell Stem Cell* 7, 11–14. <https://doi.org/10.1016/j.stem.2010.06.003>
- Sen-Chowdhry, S., Syrris, P., Ward, D., Asimaki, A., Sevdalis, E., McKenna, W.J., 2007. Clinical and Genetic Characterization of Families With Arrhythmogenic Right Ventricular Dysplasia/Cardiomyopathy Provides Novel Insights Into Patterns of Disease Expression. *Circulation* 115, 1710–1720. <https://doi.org/10.1161/CIRCULATIONAHA.106.660241>
- Shapiro, L., Fannon, A.M., Kwong, P.D., Thompson, A., Lehmann, M.S., Grübel, G., Legrand, J.F., Als-Nielsen, J., Colman, D.R., Hendrickson, W.A., 1995. Structural basis of cell-cell adhesion by cadherins. *Nature* 374, 327–337. <https://doi.org/10.1038/374327a0>
- Sharma, D., Murki, S., Pratap, T., Vasikarla, M., 2014. Cat eye syndrome. *BMJ Case Rep.* 2014. <https://doi.org/10.1136/bcr-2014-203923>
- Shelton, M., Kocharyan, A., Liu, J., Skerjanc, I.S., Stanford, W.L., 2016. Robust generation and expansion of skeletal muscle progenitors and myocytes from human pluripotent stem cells. *Methods San Diego Calif* 101, 73–84. <https://doi.org/10.1016/j.ymeth.2015.09.019>
- Shelton, M., Metz, J., Liu, J., Carpenedo, R.L., Demers, S.-P., Stanford, W.L., Skerjanc, I.S., 2014. Derivation and expansion of PAX7-positive muscle progenitors from human and mouse embryonic stem cells. *Stem Cell Rep.* 3, 516–529. <https://doi.org/10.1016/j.stemcr.2014.07.001>
- Simcha, I., Shtutman, M., Salomon, D., Zhurinsky, J., Sadot, E., Geiger, B., Ben-Ze'ev, A., 1998. Differential nuclear translocation and transactivation potential of beta-catenin and plakoglobin. *J. Cell Biol.* 141, 1433–1448.
- Simpson, M.A., Mansour, S., Ahnood, D., Kalidas, K., Patton, M.A., McKenna, W.J., Behr, E.R., Crosby, A.H., 2009. Homozygous Mutation of Desmocollin-2 in Arrhythmogenic Right Ventricular Cardiomyopathy with Mild Palmoplantar Keratoderma and Woolly Hair. *Cardiology* 113, 28–34. <https://doi.org/10.1159/000165696>
- Singh, V.K., Saini, A., Kalsan, M., Kumar, N., Chandra, R., 2016. Describing the Stem Cell Potency: The Various Methods of Functional Assessment and In silico Diagnostics. *Front. Cell Dev. Biol.* 4, 134. <https://doi.org/10.3389/fcell.2016.00134>
- Smith, E.A., Fuchs, E., 1998. Defining the interactions between intermediate filaments and desmosomes. *J. Cell Biol.* 141, 1229–1241.

- Sonnenblick, E.H., 1968. Correlation of myocardial ultrastructure and function. *Circulation* 38, 29–44.
- Staerk, J., Dawlaty, M.M., Gao, Q., Maetzel, D., Hanna, J., Sommer, C.A., Mostoslavsky, G., Jaenisch, R., 2010. Reprogramming of Human Peripheral Blood Cells to Induced Pluripotent Stem Cells. *Cell Stem Cell* 7, 20–24. <https://doi.org/10.1016/j.stem.2010.06.002>
- Stappenbeck, T.S., Green, K.J., 1992. The desmoplakin carboxyl terminus coaligns with and specifically disrupts intermediate filament networks when expressed in cultured cells. *J. Cell Biol.* 116, 1197–1209.
- Stewart, M.H., Bendall, S.C., Levadoux-Martin, M., Bhatia, M., 2010. Clonal tracking of hESCs reveals differential contribution to functional assays. *Nat. Methods* 7, 917–922. <https://doi.org/10.1038/nmeth.1519>
- Su, R.-J., Baylink, D.J., Neises, A., Kiroyan, J.B., Meng, X., Payne, K.J., Tschudy-Seney, B., Duan, Y., Appleby, N., Kearns-Jonker, M., Gridley, D.S., Wang, J., Lau, K.-H.W., Zhang, X.-B., 2013. Efficient generation of integration-free ips cells from human adult peripheral blood using BCL-XL together with Yamanaka factors. *PloS One* 8, e64496. <https://doi.org/10.1371/journal.pone.0064496>
- Sun, H., Wang, X., Liu, K., Guo, M., Zhang, Y., Ying, Q.-L., Ye, S., 2017. β -catenin coordinates with Jup and the TCF1/GATA6 axis to regulate human embryonic stem cell fate. *Dev. Biol.* 431, 272–281. <https://doi.org/10.1016/j.ydbio.2017.09.004>
- Svensson, A., Åström-Aneq, M., Widlund, K.F., Fluor, C., Green, A., Rehnberg, M., Gunnarsson, C., 2016. Arrhythmogenic Right Ventricular Cardiomyopathy - 4 Swedish families with an associated PKP2 c.2146-1G>C variant. *Am. J. Cardiovasc. Dis.* 6, 55–65.
- Swope, D., Cheng, L., Gao, E., Li, J., Radice, G.L., 2012. Loss of cadherin-binding proteins β -catenin and plakoglobin in the heart leads to gap junction remodeling and arrhythmogenesis. *Mol. Cell. Biol.* 32, 1056–1067. <https://doi.org/10.1128/MCB.06188-11>
- Syed, S.-H., Trinnaman, B., Martin, S., Major, S., Hutchinson, J., Magee, A.I., 2002. Molecular interactions between desmosomal cadherins. *Biochem. J.* 362, 317–327.

- Syrris, P., 2006. Clinical Expression of Plakophilin-2 Mutations in Familial Arrhythmogenic Right Ventricular Cardiomyopathy. *Circulation* 113, 356–364. <https://doi.org/10.1161/CIRCULATIONAHA.105.561654>
- Syrris, P., Ward, D., Evans, A., Asimaki, A., Gandjbakhch, E., Sen-Chowdhry, S., McKenna, W.J., 2006. Arrhythmogenic right ventricular dysplasia/cardiomyopathy associated with mutations in the desmosomal gene desmocollin-2. *Am. J. Hum. Genet.* 79, 978–984. <https://doi.org/10.1086/509122>
- Taapken, S.M., Nisler, B.S., Newton, M.A., Sampsell-Barron, T.L., Leonhard, K.A., McIntire, E.M., Montgomery, K.D., 2011. Karyotypic abnormalities in human induced pluripotent stem cells and embryonic stem cells. *Nat. Biotechnol.* 29, 313–314. <https://doi.org/10.1038/nbt.1835>
- Tabib, A., 2003. Circumstances of Death and Gross and Microscopic Observations in a Series of 200 Cases of Sudden Death Associated With Arrhythmogenic Right Ventricular Cardiomyopathy and/or Dysplasia. *Circulation* 108, 3000–3005. <https://doi.org/10.1161/01.CIR.0000108396.65446.21>
- Takahashi, K., Tanabe, K., Ohnuki, M., Narita, M., Ichisaka, T., Tomoda, K., Yamanaka, S., 2007. Induction of Pluripotent Stem Cells from Adult Human Fibroblasts by Defined Factors. *Cell* 131, 861–872. <https://doi.org/10.1016/j.cell.2007.11.019>
- Tandri, H., Asimaki, A., Dalal, D., Saffitz, J.E., Halushka, M.K., Calkins, H., 2008. Gap Junction Remodeling in a Case of Arrhythmogenic Right Ventricular Dysplasia Due to Plakophilin-2 Mutation. *J. Cardiovasc. Electrophysiol.* 19, 1212–1214. <https://doi.org/10.1111/j.1540-8167.2008.01207.x>
- Tavora, F., Zhang, M., Cresswell, N., Li, L., Fowler, D., Franco, M., Burke, A., 2013. Quantitative Immunohistochemistry of Desmosomal Proteins (Plakoglobin, Desmoplakin and Plakophilin), Connexin-43, and N-cadherin in Arrhythmogenic Cardiomyopathy: An Autopsy Study. *Open Cardiovasc. Med. J.* 7, 28–35. <https://doi.org/10.2174/1874192401307010028>
- Taylor, M., Graw, S., Sinagra, G., Barnes, C., Slavov, D., Brun, F., Pinamonti, B., Salcedo, E.E., Sauer, W., Pyxaras, S., Anderson, B., Simon, B., Bogomolovas, J., Labeit, S., Granzier, H., Mestroni, L., 2011. Genetic Variation in Titin in Arrhythmogenic Right Ventricular Cardiomyopathy-Overlap Syndromes. *Circulation* 124, 876–885. <https://doi.org/10.1161/CIRCULATIONAHA.110.005405>

- Thiene, G., Corrado, D., Basso, C., 2007. Arrhythmogenic right ventricular cardiomyopathy/dysplasia. *Orphanet J. Rare Dis.* 2, 45.
<https://doi.org/10.1186/1750-1172-2-45>
- Thiene, G., Nava, A., Corrado, D., Rossi, L., Pennelli, N., 1988. Right ventricular cardiomyopathy and sudden death in young people. *N. Engl. J. Med.* 318, 129–133. <https://doi.org/10.1056/NEJM198801213180301>
- Thomson, J.A., Itskovitz-Eldor, J., Shapiro, S.S., Waknitz, M.A., Swiergiel, J.J., Marshall, V.S., Jones, J.M., 1998. Embryonic stem cell lines derived from human blastocysts. *Science* 282, 1145–1147.
- Tiburcy, M., Hudson, J.E., Balfanz, P., Schlick, S., Meyer, T., Chang Liao, M.-L., Levent, E., Raad, F., Zeidler, S., Wingender, E., Riegler, J., Wang, M., Gold, J.D., Kehat, I., Wettwer, E., Ravens, U., Dierickx, P., van Laake, L.W., Goumans, M.J., Khadjeh, S., Toischer, K., Hasenfuss, G., Couture, L.A., Unger, A., Linke, W.A., Araki, T., Neel, B., Keller, G., Gepstein, L., Wu, J.C., Zimmermann, W.-H., 2017. Defined Engineered Human Myocardium With Advanced Maturation for Applications in Heart Failure Modeling and Repair. *Circulation* 135, 1832–1847.
<https://doi.org/10.1161/CIRCULATIONAHA.116.024145>
- Tiso, N., Stephan, D.A., Nava, A., Bagattin, A., Devaney, J.M., Stanchi, F., Larderet, G., Brahmbhatt, B., Brown, K., Bauce, B., Muriago, M., Basso, C., Thiene, G., Danieli, G.A., Rampazzo, A., 2001. Identification of mutations in the cardiac ryanodine receptor gene in families affected with arrhythmogenic right ventricular cardiomyopathy type 2 (ARVD2). *Hum. Mol. Genet.* 10, 189–194.
- Tohyama, S., Hattori, F., Sano, M., Hishiki, T., Nagahata, Y., Matsuura, T., Hashimoto, H., Suzuki, T., Yamashita, H., Satoh, Y., Egashira, T., Seki, T., Muraoka, N., Yamakawa, H., Ohgino, Y., Tanaka, T., Yoichi, M., Yuasa, S., Murata, M., Suematsu, M., Fukuda, K., 2013. Distinct metabolic flow enables large-scale purification of mouse and human pluripotent stem cell-derived cardiomyocytes. *Cell Stem Cell* 12, 127–137.
<https://doi.org/10.1016/j.stem.2012.09.013>
- Troyanovsky, R.B., Klingelhöfer, J., Troyanovsky, S., 1999. Removal of calcium ions triggers a novel type of intercadherin interaction. *J. Cell Sci.* 112 (Pt 23), 4379–4387.
- Troyanovsky, S.M., Troyanovsky, R.B., Eshkind, L.G., Krutovskikh, V.A., Leube, R.E., Franke, W.W., 1994a. Identification of the plakoglobin-binding domain in

- desmoglein and its role in plaque assembly and intermediate filament anchorage. *J. Cell Biol.* 127, 151–160.
- Troyanovsky, S.M., Troyanovsky, R.B., Eshkind, L.G., Leube, R.E., Franke, W.W., 1994b. Identification of amino acid sequence motifs in desmocollin, a desmosomal glycoprotein, that are required for plakoglobin binding and plaque formation. *Proc. Natl. Acad. Sci. U. S. A.* 91, 10790–10794.
- Tsankov, A.M., Akopian, V., Pop, R., Chetty, S., Gifford, C.A., Daheron, L., Tsankova, N.M., Meissner, A., 2015. A qPCR ScoreCard quantifies the differentiation potential of human pluripotent stem cells. *Nat. Biotechnol.* 33, 1182–1192. <https://doi.org/10.1038/nbt.3387>
- Ueno, S., Weidinger, G., Osugi, T., Kohn, A.D., Golob, J.L., Pabon, L., Reinecke, H., Moon, R.T., Murry, C.E., 2007. Biphasic role for Wnt/beta-catenin signaling in cardiac specification in zebrafish and embryonic stem cells. *Proc. Natl. Acad. Sci. U. S. A.* 104, 9685–9690. <https://doi.org/10.1073/pnas.0702859104>
- Uhlén, M., Fagerberg, L., Hallström, B.M., Lindskog, C., Oksvold, P., Mardinoglu, A., Sivertsson, Å., Kampf, C., Sjöstedt, E., Asplund, A., Olsson, I., Edlund, K., Lundberg, E., Navani, S., Szigartyo, C.A.-K., Odeberg, J., Djureinovic, D., Takanen, J.O., Hober, S., Alm, T., Edqvist, P.-H., Berling, H., Tegel, H., Mulder, J., Rockberg, J., Nilsson, P., Schwenk, J.M., Hamsten, M., von Feilitzen, K., Forsberg, M., Persson, L., Johansson, F., Zwahlen, M., von Heijne, G., Nielsen, J., Pontén, F., 2015. Proteomics. Tissue-based map of the human proteome. *Science* 347, 1260419. <https://doi.org/10.1126/science.1260419>
- Uosaki, H., Cahan, P., Lee, D.I., Wang, S., Miyamoto, M., Fernandez, L., Kass, D.A., Kwon, C., 2015. Transcriptional Landscape of Cardiomyocyte Maturation. *Cell Rep.* 13, 1705–1716. <https://doi.org/10.1016/j.celrep.2015.10.032>
- Uosaki, H., Taguchi, Y.-H., 2016. Comparative Gene Expression Analysis of Mouse and Human Cardiac Maturation. *Genomics Proteomics Bioinformatics* 14, 207–215. <https://doi.org/10.1016/j.gpb.2016.04.004>
- van den Berg, C.W., Okawa, S., Chuva de Sousa Lopes, S.M., van Iperen, L., Passier, R., Braam, S.R., Tertoolen, L.G., del Sol, A., Davis, R.P., Mummery, C.L., 2015. Transcriptome of human foetal heart compared with cardiomyocytes from pluripotent stem cells. *Dev. Camb. Engl.* 142, 3231–3238. <https://doi.org/10.1242/dev.123810>

- van der Zwaag, P.A., Jongbloed, J.D.H., Van Tintelen, P., 2018. ARVD/C Genetic Variants Database, University Medical Centre Groningen Department of Genetic, Cardiogenetics Research Group [WWW Document]. ARVDC Genet. Var. Database. URL <https://molgenis07.gcc.rug.nl> (accessed 11.11.18).
- van der Zwaag, P.A., van Rijsingen, I.A.W., Asimaki, A., Jongbloed, J.D.H., van Veldhuisen, D.J., Wiesfeld, A.C.P., Cox, M.G.P.J., van Lochem, L.T., de Boer, R.A., Hofstra, R.M.W., Christiaans, I., van Spaendonck-Zwarts, K.Y., Lekanne dit Deprez, R.H., Judge, D.P., Calkins, H., Suurmeijer, A.J.H., Hauer, R.N.W., Saffitz, J.E., Wilde, A.A.M., van den Berg, M.P., van Tintelen, J.P., 2012. Phospholamban R14del mutation in patients diagnosed with dilated cardiomyopathy or arrhythmogenic right ventricular cardiomyopathy: evidence supporting the concept of arrhythmogenic cardiomyopathy. *Eur. J. Heart Fail.* 14, 1199–1207. <https://doi.org/10.1093/eurjhf/hfs119>
- van Hengel, J., Calore, M., Bauce, B., Dazzo, E., Mazzotti, E., De Bortoli, M., Lorenzon, A., Li Mura, I.E.A., Boffagna, G., Rigato, I., Vleeschouwers, M., Tyberghein, K., Hulpiau, P., van Hamme, E., Zaglia, T., Corrado, D., Basso, C., Thiene, G., Daliento, L., Nava, A., van Roy, F., Rampazzo, A., 2013. Mutations in the area composita protein α T-catenin are associated with arrhythmogenic right ventricular cardiomyopathy. *Eur. Heart J.* 34, 201–210. <https://doi.org/10.1093/eurheartj/ehs373>
- van Tintelen, J.P., Hofstra, R.M., Wiesfeld, A.C., van den Berg, M.P., Hauer, R.N., Jongbloed, J.D., 2007. Molecular genetics of arrhythmogenic right ventricular cardiomyopathy: emerging horizon? *Curr. Opin. Cardiol.* 22, 185–192. <https://doi.org/10.1097/HCO.0b013e3280d942c4>
- van Tintelen, J.P., Van Gelder, I.C., Asimaki, A., Suurmeijer, A.J.H., Wiesfeld, A.C.P., Jongbloed, J.D.H., van den Wijngaard, A., Kuks, J.B.M., van Spaendonck-Zwarts, K.Y., Notermans, N., Boven, L., van den Heuvel, F., Veenstra-Knol, H.E., Saffitz, J.E., Hofstra, R.M.W., van den Berg, M.P., 2009. Severe cardiac phenotype with right ventricular predominance in a large cohort of patients with a single missense mutation in the DES gene. *Heart Rhythm* 6, 1574–1583. <https://doi.org/10.1016/j.hrthm.2009.07.041>
- Vandesompele, J., De Preter, K., Pattyn, F., Poppe, B., Van Roy, N., De Paepe, A., Speleman, F., 2002. Accurate normalization of real-time quantitative RT-PCR data by geometric averaging of multiple internal control genes. *Genome Biol.* 3, RESEARCH0034.

- Varlakhanova, N.V., Cotterman, R.F., deVries, W.N., Morgan, J., Donahue, L.R., Murray, S., Knowles, B.B., Knoepfler, P.S., 2010. myc maintains embryonic stem cell pluripotency and self-renewal. *Differ. Res. Biol. Divers.* 80, 9–19. <https://doi.org/10.1016/j.diff.2010.05.001>
- Vite, A., Gandjbakhch, E., Prost, C., Fressart, V., Fouret, P., Neyroud, N., Gary, F., Donal, E., Varnous, S., Fontaine, G., Fornes, P., Hidden-Lucet, F., Komajda, M., Charron, P., Villard, E., 2013. Desmosomal cadherins are decreased in explanted arrhythmogenic right ventricular dysplasia/cardiomyopathy patient hearts. *PloS One* 8, e75082. <https://doi.org/10.1371/journal.pone.0075082>
- Vizcardo, R., Masuda, K., Yamada, D., Ikawa, T., Shimizu, K., Fujii, S., Koseki, H., Kawamoto, H., 2013. Regeneration of Human Tumor Antigen-Specific T Cells from iPSCs Derived from Mature CD8+ T Cells. *Cell Stem Cell* 12, 31–36. <https://doi.org/10.1016/j.stem.2012.12.006>
- Wallis, S., Lloyd, S., Wise, I., Ireland, G., Fleming, T.P., Garrod, D., 2000. The alpha isoform of protein kinase C is involved in signaling the response of desmosomes to wounding in cultured epithelial cells. *Mol. Biol. Cell* 11, 1077–1092.
- Watkins, D.A., Hendricks, N., Shaboodien, G., Mbele, M., Parker, M., Vezi, B.Z., Latib, A., Chin, A., Little, F., Badri, M., Moolman-Smook, J.C., Okreglicki, A., Mayosi, B.M., 2009. Clinical features, survival experience, and profile of plakophylin-2 gene mutations in participants of the Arrhythmogenic Right Ventricular Cardiomyopathy Registry of South Africa. *Heart Rhythm* 6, S10–S17. <https://doi.org/10.1016/j.hrthm.2009.08.018>
- Wesselschmidt, R.L., 2011. The teratoma assay: an in vivo assessment of pluripotency. *Methods Mol. Biol. Clifton NJ* 767, 231–241. https://doi.org/10.1007/978-1-61779-201-4_17
- Wheelwright, M., Win, Z., Mikkila, J.L., Amen, K.Y., Alford, P.W., Metzger, J.M., 2018. Investigation of human iPSC-derived cardiac myocyte functional maturation by single cell traction force microscopy. *PloS One* 13, e0194909. <https://doi.org/10.1371/journal.pone.0194909>
- Whittock, N.V., Bower, C., 2003. Genetic evidence for a novel human desmosomal cadherin, desmoglein 4. *J. Invest. Dermatol.* 120, 523–530. <https://doi.org/10.1046/j.1523-1747.2003.12113.x>
- Willems, E., Spiering, S., Davidovics, H., Lanier, M., Xia, Z., Dawson, M., Cashman, J., Mercola, M., 2011. Small-molecule inhibitors of the Wnt pathway potently

- promote cardiomyocytes from human embryonic stem cell-derived mesoderm. *Circ. Res.* 109, 360–364. <https://doi.org/10.1161/CIRCRESAHA.111.249540>
- Witcher, L.L., Collins, R., Puttagunta, S., Mechanic, S.E., Munson, M., Gumbiner, B., Cowin, P., 1996. Desmosomal cadherin binding domains of plakoglobin. *J. Biol. Chem.* 271, 10904–10909.
- Wobus, A.M., Holzhausen, H., Jäkel, P., Schöneich, J., 1984. Characterization of a pluripotent stem cell line derived from a mouse embryo. *Exp. Cell Res.* 152, 212–219.
- Workman, P., Aboagye, E.O., Balkwill, F., Balmain, A., Bruder, G., Chaplin, D.J., Double, J.A., Everitt, J., Farningham, D. a. H., Glennie, M.J., Kelland, L.R., Robinson, V., Stratford, I.J., Tozer, G.M., Watson, S., Wedge, S.R., Eccles, S.A., Committee of the National Cancer Research Institute, 2010. Guidelines for the welfare and use of animals in cancer research. *Br. J. Cancer* 102, 1555–1577. <https://doi.org/10.1038/sj.bjc.6605642>
- Workman, P., Twentyman, P., Balkwill, F., Balmain, A., Chaplin, D., Double, J., Embleton, J., Newell, D., Raymond, R., Stables, J., Stephens, T., Wallace, J., 1998. United Kingdom Co-ordinating Committee on Cancer Research (UKCCCR) Guidelines for the Welfare of Animals in Experimental Neoplasia (Second Edition). *Br. J. Cancer* 77, 1–10.
- Xu, C., Inokuma, M.S., Denham, J., Golds, K., Kundu, P., Gold, J.D., Carpenter, M.K., 2001. Feeder-free growth of undifferentiated human embryonic stem cells. *Nat. Biotechnol.* 19, 971–974. <https://doi.org/10.1038/nbt1001-971>
- Xu, C., Police, S., Rao, N., Carpenter, M.K., 2002. Characterization and enrichment of cardiomyocytes derived from human embryonic stem cells. *Circ. Res.* 91, 501–508.
- Xu, T., Yang, Z., Vatta, M., Rampazzo, A., Boffagna, G., Pillichou, K., Scherer, S.E., Saffitz, J., Kravitz, J., Zareba, W., Danieli, G.A., Lorenzon, A., Nava, A., Bauce, B., Thiene, G., Basso, C., Calkins, H., Gear, K., Marcus, F., Towbin, J.A., 2010. Compound and Digenic Heterozygosity Contributes to Arrhythmogenic Right Ventricular Cardiomyopathy. *J. Am. Coll. Cardiol.* 55, 587–597. <https://doi.org/10.1016/j.jacc.2009.11.020>
- Xu, X.Q., Soo, S.Y., Sun, W., Zweigerdt, R., 2009. Global expression profile of highly enriched cardiomyocytes derived from human embryonic stem cells. *Stem Cells Dayt. Ohio* 27, 2163–2174. <https://doi.org/10.1002/stem.166>

- Yang, C., Xu, Y., Yu, M., Lee, D., Alharti, S., Hellen, N., Ahmad Shaik, N., Banaganapalli, B., Sheikh, H.A.M., Ramu, E., Przyborski, S., Tenin, G., Williams, S., O'Sullivan, J., Al-Radi, O.O., Atta, J., Harding, S.E., Keavney, B., Lako, M., Armstrong, L., 2017. Induced pluripotent stem cell modelling of HLHS underlines the contribution of dysfunctional NOTCH signalling to impaired cardiogenesis. *Hum. Mol. Genet.* <https://doi.org/10.1093/hmg/ddx140>
- Yang, L., Soonpaa, M.H., Adler, E.D., Roepke, T.K., Kattman, S.J., Kennedy, M., Henckaerts, E., Bonham, K., Abbott, G.W., Linden, R.M., Field, L.J., Keller, G.M., 2008. Human cardiovascular progenitor cells develop from a KDR+ embryonic-stem-cell-derived population. *Nature* 453, 524–528. <https://doi.org/10.1038/nature06894>
- Yang, X., Rodriguez, M., Pabon, L., Fischer, K.A., Reinecke, H., Regnier, M., Sniadecki, N.J., Ruohola-Baker, H., Murry, C.E., 2014. Tri-iodo-L-thyronine promotes the maturation of human cardiomyocytes-derived from induced pluripotent stem cells. *J. Mol. Cell. Cardiol.* 72, 296–304. <https://doi.org/10.1016/j.yjmcc.2014.04.005>
- Yang, Z., 2006. Desmosomal Dysfunction due to Mutations in Desmoplakin Causes Arrhythmogenic Right Ventricular Dysplasia/Cardiomyopathy. *Circ. Res.* 99, 646–655. <https://doi.org/10.1161/01.RES.0000241482.19382.c6>
- Ye, J., Coulouris, G., Zaretskaya, I., Cutcutache, I., Rozen, S., Madden, T.L., 2012. Primer-BLAST: a tool to design target-specific primers for polymerase chain reaction. *BMC Bioinformatics* 13, 134. <https://doi.org/10.1186/1471-2105-13-134>
- Ye, Lin, Muench, M.O., Fusaki, N., Beyer, A.I., Wang, J., Qi, Z., Yu, J., Kan, Y.W., 2013. Blood cell-derived induced pluripotent stem cells free of reprogramming factors generated by Sendai viral vectors. *Stem Cells Transl. Med.* 2, 558–566. <https://doi.org/10.5966/sctm.2013-0006>
- Ye, Lei, Zhang, S., Greder, L., Dutton, J., Keirstead, S.A., Lepley, M., Zhang, L., Kaufman, D., Zhang, J., 2013. Effective cardiac myocyte differentiation of human induced pluripotent stem cells requires VEGF. *PLoS One* 8, e53764. <https://doi.org/10.1371/journal.pone.0053764>
- Ye, Z., Zhan, H., Mali, P., Dowey, S., Williams, D.M., Jang, Y.-Y., Dang, C.V., Spivak, J.L., Moliterno, A.R., Cheng, L., 2009. Human-induced pluripotent stem cells from blood cells of healthy donors and patients with acquired blood disorders. *Blood* 114, 5473–5480. <https://doi.org/10.1182/blood-2009-04-217406>

- Young, B., Stewart, W., O'Dowd, G., 2009. Wheater's basic pathology a text, atlas and review of histopathology.
- Zhang, P., Li, J., Tan, Z., Wang, C., Liu, T., Chen, L., Yong, J., Jiang, W., Sun, X., Du, L., Ding, M., Deng, H., 2008. Short-term BMP-4 treatment initiates mesoderm induction in human embryonic stem cells. *Blood* 111, 1933–1941. <https://doi.org/10.1182/blood-2007-02-074120>
- Zhang, Q., Deng, C., Rao, F., Modi, R.M., Zhu, J., Liu, X., Mai, L., Tan, H., Yu, X., Lin, Q., Xiao, D., Kuang, S., Wu, S., 2013. Silencing of desmoplakin decreases connexin43/Nav1.5 expression and sodium current in HL-1 cardiomyocytes. *Mol. Med. Rep.* 8, 780–786. <https://doi.org/10.3892/mmr.2013.1594>
- Zhao, W., Ji, X., Zhang, F., Li, L., Ma, L., 2012. Embryonic stem cell markers. *Mol. Basel Switz.* 17, 6196–6236. <https://doi.org/10.3390/molecules17066196>
- Zhao, X., Li, W., Lv, Z., Liu, L., Tong, M., Hai, T., Hao, J., Guo, C., Ma, Q., Wang, L., Zeng, F., Zhou, Q., 2009. iPS cells produce viable mice through tetraploid complementation. *Nature* 461, 86–90. <https://doi.org/10.1038/nature08267>

Appendix

Summary of pre-transduction culture media from reports of the reprogramming of PBMCs to iPSCs.

References	Medium	Cytokines	Culture duration	Notes
(Merling <i>et al.</i> , 2013)	X-VIVO 10 (Lonza) Human serum albumin 1%	SCF 50ng/ml FLT3L 50ng/ml TPO 50ng/ml	IL3 5ng/ml or 50ng/ml 2-4 days	Reprogramming started once 50,000 cells available.
(Ye <i>et al.</i> , 2009)	Not described	SCF 100ng/ml FLT3L 100ng/ml TPO 20ng/ml	2-4 days	
(Mack <i>et al.</i> , 2011)	Stemspan SFEM (StemCell Technologies)	SCF 300ng/ml FLT3L 300ng/ml TPO 300ng/ml	IL6 100ng/ml IL3 10ng/ml 3-13 days	

Table 61. Pre-transduction culture conditions used for the reprogramming of CD34+ populations isolated from PBMCs

Reference	Selection prior to culture	Medium	Cytokines used expand/activate target population	Duration of pre-transduction culture	Notes
(Vizcardo <i>et al.</i> , 2013)	CD3+ cells selected using antibody coated magnetic beads	RPMI 1640 FBS 10% L-glutamine 2mM Sodium pyruvate 1mM Sodium bicarbonate 2mg/ml Non-essential amino acid 0.2mM 2-Mercaptoethanol Streptomycin 100mg/ml Penicillin 100U/ml	Anti CD3/CD28 Dynabeads (Life Technologies)	1 day	-
	CD3+ cells selected using antibody coated magnetic beads <i>then</i> CD3+CD4-CD8+ cells selected by FACS				
(Seki <i>et al.</i> , 2010)	CD3+ cells selected by FACS	GT-T502 (Kohjin Bio)	IL2 175 JRU/ml* Plate bound anti CD3	6 days	IL2 is a component of GT502
	No				
(Seki <i>et al.</i> , 2012)	No	GT-T502 (Kohjin Bio)	IL2 175 JRU/ml Plate bound anti CD3	5 days	IL2 is a component of GT502
Brown 2010 ⁴⁸	No	AIM-V (Life Technologies) Penicillin* Streptomycin* Glutamine*	IL2 300 IU/ml Soluble anti CD3 10ng/ml	3 days	Doses of these components were not specified
(Loh <i>et al.</i> , 2010)	No	Stemline dendritic cell medium	SCF* GM-CSF*	2 days	Doses of these components were not specified
		IMDM FBS 15%	SCF 100ng/ml FLT3L 100ng/ml IL3 20ng/ml		

Table 62 Pre-transduction culture medium compositions used in publications describing the generation of T-cell derived iPSCs

* Concentrations not specified in methods

Reference	Medium	Cytokines / antibodies / drugs	Duration of pre-transduction culture	Notes
(Loh <i>et al.</i> , 2010)	Stemline dendritic cell medium	SCF* GM-CSF*	2 days	Doses of these components were not specified
	IMDM FBS 15%	SCF 100ng/ml FLT3L 100ng/ml IL3 20ng/ml		
(Mack <i>et al.</i> , 2011)	Stemspan SFEM (StemCell Technologies) ExCyte Medium supplement (Millipore) Glutamax*	SCF 250ng/ml IL3 20ng/ml EPO 2U/ml IGF-1 40ng/ml Dexamethasone 1µM	Not described	
(Chou <i>et al.</i> , 2011)	IMDM/Ham's F12, 1:1 Lipid concentrate* L-ascorbic acid 0.28mM Glutamine 2mM	Insulin* Transferrin* Selenium* Bovine serum albumin 5mg/ml	SCF 50ng/ml IL3 10ng/ml EPO 2U/ml IGF-1 40ng/ml Dexamethasone 1µM	8-9 days * Concentrations not specified in methods
(Dowey <i>et al.</i> , 2012)	IMDM/Ham's F12, 1:1 Lipid concentrate 1% L-ascorbic acid 2-phosphate 0.17mM L-Glutamine 2mM 1-Thioglycerol 200µM Ethanolamide 33 nM	Insulin 1.7µM Transferrin 0.069 µM Holo-transferrin 1.25 µM Sodium selenite 39 nM Bovine serum albumin 5mg/ml	SCF 50ng/ml IL3 10ng/ml EPO 2U/ml IGF-1 40ng/ml Dexamethasone 1µM	14 days
(Churko <i>et al.</i> , 2013)	IMDM/Ham's F12, 1:1 Lipid concentrate 1% L-ascorbic acid 2-phosphate 0.17mM Glutamine 2mM 1-Thioglycerol 450µM	Insulin 1.7µM Transferrin 1.25 µM Sodium selenite 81nM Bovine serum albumin 5mg/ml	SCF 50ng/ml IL3 10ng/ml EPO 2U/ml IGF-1 40ng/ml Dexamethasone 1µM	6-8 days
(Lin Ye <i>et al.</i> , 2013)	IMDM/Ham's F12, 1:1 Lipid concentrate 1% L-ascorbic acid 0.28mM Glutamine 2mM	Insulin 1.7µM Transferrin 0.069 µM Sodium selenite 29 nM Bovine serum albumin 5mg/ml	SCF 50ng/ml IL3 10ng/ml EPO 2U/ml IGF-1 40ng/ml Dexamethasone 1µM	5-8 days Medium changes on days 3 and 6

Table 63 Pre-transduction culture medium composition used in publications describing the generation of iPSCs from mixed PBMC samples
(Continued)

(Kunisato <i>et al.</i> , 2011)	DMEM FBS 10%	SCF 100ng/ml TPO 100ng/ml IL3 100ng/ml IL6/IL6 receptor fusion protein 20ng/ml		2 days	
		SCF 100ng/ml TPO 100ng/ml IL3 100ng/ml IL6/IL6 receptor fusion protein 20ng/ml	GM-CSF 100ng/ml M-CSF 50ng/ml FLT3L 100ng/ml		
		SCF 100ng/ml TPO 100ng/ml IL3 100ng/ml IL6/IL6 receptor fusion protein 20ng/ml	Anti-CD3 antibody Anti-CD28 antibody Anti-CD40 antibody Lipopolysaccharide		
(Su <i>et al.</i> , 2013)	IMDM FBS 10%	SCF 100ng/ml TPO 100ng/ml IL3 10ng/ml	G-CSF 100ng/ml FLT3-l 100ng/ml StemRegenin1 1 μ M	6-8 days	
(I.-P. Chen <i>et al.</i> , 2013)	DMEM FBS 10%	SCF 20ng/ml TPO 20ng/ml IL3 20ng/ml IL6 20ng/ml	IL6 receptor α 20ng/ml GM-CSF 20ng/ml M-CSF 50ng/ml FLT3L 20ng/ml	5 days	
(Staerk <i>et al.</i> , 2010)	α MEM FBS 10%	IL7 10ng/ml		5 days	
		IL6 10ng/ml IL3 10ng/ml	G-CSF 10ng/ml GM-CSF 10ng/ml		
(Life Technologies, 2012)	StemPro-34 L-Glutamine 2mM	SCF 100ng/ml FLT3L 100ng/ml	TPO 20ng/ml IL6 10ng/ml	4 days	
(Life Technologies, 2013)	StemPro-34 L-Glutamine 2mM	SCF 100ng/ml FLT3L 100ng/ml	IL3 20ng/ml IL6 20ng/ml	4 days	

Summary of directed cardiac differentiation protocols

Publication	hPSC maintenance		Pre-differentiation culture			EB formation	Differentiation								Cardiomyocyte maintenance Medium	
	Substrate	Medium	Substrate	Medium	Protocol		Base medium	Cytokines / small molecules / additives								
								Day 0	Day 1	Day 2	Day 3	Day 4	Day 5	Day 6		Day 7
Yang 2008	MEF	DMEM/F12 KSR 20% NEAA 0.1mM Glutamine 2mM BME 0.1mM 50 U/ml penicillin 50 u/ml streptomycin bFGF 20ng/ml	Matrigel	DMEM/F12 KSR 20% NEAA 0.1mM Glutamine 2mM BME 0.1mM 50 U/ml penicillin 50 u/ml streptomycin bFGF 20ng/ml	Cultured for 24 to 48 hours to deplete MEFs	Formation of clusters of 10-20 cells with: Collagenase B 1mg/ml for 20min Then Trypsin-EDTA (0.05%) for 2min	StemPro34 Glutamine 2mM Monothioglycerol 0.4mM Ascorbic acid 50 µg/ml	BMP4 0.5ng/ml	Activin A 3ng/ml BMP4 10ng/ml bFGF 5ng/ml		VEGF 10ng/ml DKK-1 150ng/ml					StemPro34 Glutamine 2mM Monothioglycerol 0.4mM Ascorbic acid 50 µg/ml VEGF 10ng/ml DKK-1 150ng/ml bFGF 5ng/ml
Kattman 2011	MEF	DMEM/F12 KSR 20% NEAA 0.1mM Glutamine 2mM BME 0.1mM 50 U/ml penicillin 50 u/ml streptomycin bFGF 20ng/ml	Matrigel	DMEM/F12 KSR 20% NEAA 0.1mM Glutamine 2mM BME 0.1mM 50 U/ml penicillin 50 u/ml streptomycin bFGF 20ng/ml	Cultured for 24 to 48 hours to deplete MEFs	Formation of clusters of 10-20 cells with: Collagenase B 1mg/ml for 20min Then Trypsin-EDTA (0.05%) for 2min	StemPro34 Glutamine 2mM Monothioglycerol 0.4mM Ascorbic acid 50 µg/ml	BMP4 0.5 – 5 ng/ml	Activin A 0-6ng/ml BMP4 2-10ng/ml bFGF 5ng/ml		VEGF 10ng/ml DKK-1 150ng/ml SB 5.4µM +/- DM 0.25-0.6 µM		VEGF 10ng/ml DKK-1 150ng/ml			StemPro34 Glutamine 2mM Monothioglycerol 0.4mM Ascorbic acid 50 µg/ml VEGF 10ng/ml bFGF 5ng/ml
Burridge 2011	As for pre-differentiation culture		Geltrex	MEF conditioned DMEM/F12 KSR 15% NEAA 0.1mM L-Glutamine 1mM BME 0.1mM bFGF 4 ng/ml With a further bFGF 4ng/ml added after MEF conditioning	Passaging with TrypLE select every 3 days in T25 flasks, plated at 2.5x10 ⁶ cells/flask	Cell suspension with TrypLE select. Forced aggregation of in 96 well V bottom plates, 5000 cells per well in day 0 differentiation medium.	RPMI 1640 Monothioglycerol 0.4mM	BMP4 25ng/ml bFGF 5ng/ml Insulin 10µg/ml Rcklnh 1µM PVA 4mg/ml CD Lipids 1% 5% O ₂		FBS 20% or L-ascorbic acid 280 µM HAS 5mg/ml CD Lipids 1%						RPMI 1640 Monothioglycerol 0.4mM CD Lipids 1% Insulin 10µg/ml
Burridge 2007	As for pre-differentiation culture		Matrigel	MEF conditioned DMEM/F12 KSR 15% NEAA 0.1mM L-Glutamine 1mM BME 0.1mM bFGF 4 ng/ml With a further bFGF 4ng/ml added after MEF conditioning	Passaging with TrypLE select	Cell suspension with TrypLE select. Forced aggregation of in 96 well V bottom plates, 10,000 cells per well in day 0 differentiation medium.	IMDM/F12 CD Lipids 1% Monothioglycerol 0.45mM Insulin 7µg/ml Transferrin 15µg/ml PVA 1mg/ml	Activin A 10ng/ml bFGF 12ng/ml								DMEM FBS 20%
Elliot 2011	As for pre-differentiation culture		MEF	NA	Passaging with TrypLE select	Cell suspension with TrypLE select. Forced aggregation of in 96 well V bottom, 3,000 cells per well In day 0 differentiation medium.	Low insulin-APEL (1µg/ml)	BMP4 20-40ng/ml Activin A 20ng/ml VEGF 30ng/ml SCF 40ng/ml Wnt3A 50-80ng/ml								Low insulin BEL

279

Table 64 Protocols for directed embryoid body differentiation of hPSCs to cardiomyocytes
(Continued over)

KSR = knock-out serum replacement, DMEM = Dulbecco's modified eagle medium, F12 = Ham's F12 nutrient mix, NEAA = non-essential amino acids, bFGF = basic fibroblast growth factor, BMP4 = bone morphogenetic protein 4, VEGF = vascular endothelial growth factor, SB = SB-431542, BME = β -mercaptoethanol, DM = dorsomorphin MEF = inactivated mouse embryonic fibroblasts, DKK-1 = Dickkopf related protein 1, RckInh = Y-27632, HAS = human serum albumin, CD lipids = chemically defined lipids, SCF = stem cell factor

Publication	hPSC maintenance		Pre-differentiation culture				Differentiation							Cardiomyocyte maintenance Medium
	Substrate	Medium	Substrate	Medium	Cytokines / small molecules / media additives	Protocol	Base medium	Cytokines / small molecules / additives						
								Day 0	Day 1	Day 2	Day 3	Day 4	Day 5	
Lafamme 2007	Matrigel	MEF conditioned KO DMEM KSR 20% NEAA 0.1mM L-Glutamine 1mM BME 0.1mM bFGF 4 ng/ml With a further bFGF 4ng/ml added after MEF conditioning	Matrigel, growth factor reduced	MEF conditioned KO DMEM KSR 20% NEAA 0.1mM L-Glutamine 1mM BME 0.1mM bFGF 4 ng/ml With a further bFGF 8ng/ml added after MEF conditioning	None	Passaged with EDTA 0.5mM or collagenase IV 200U/ml to Matrigel. Cultured till confluent.	RPMI 1640 B27 with insulin 2%	Activin A 100ng/ml	BMP4 10ng/ml					RPMI 1640 B27 2%
Zhang 2012	MEF	DMEM/F12 KSR 20% NEAA 0.1mM L-Glutamine 1mM BME 0.1mM bFGF 4 – 100ng/ml	Matrigel, growth factor reduced	mTeSR1	Y27632 10µM on day of single cell suspension. Matrigel, growth factor reduced 0.03 – 0.06mg/ml	Passaged from MEFs to Matrigel and cultured for 5-6 days. Further passage with EDTA to produce a single cell suspension. Matrigel added when 80-90% confluence. Further culture for 1-2 days until 100% confluence	RPMI 1640 B27 without insulin 2%	Activin A 100ng/ml Matrigel	BMP4 5-10ng/ml bFGF 5-10ng/ml					RPMI 1640 B27 with insulin 2%
Ye 2013	MEF	DMEM/F12 85% KSR 15% bFGF 8ng/ml Pen/Strep 0.5% NEAA 0.1mM L-Glutamine 1mM BME 55µM	Matrigel, growth factor reduced	mTeSR1	None	Passaged from MEFs to Matrigel, Plated as single cells and cultured for 4 days or until confluent	RPMI 1640 B27 without insulin 2%	Activin A 50ng/ml BMP4 25ng/ml	VEGF 5 or 10ng/ml					RPMI 1640 B27 with insulin 2%
Hudson 2012	MEF	NA cells passages enzymatically with TrypLE select	Matrigel	mTeSR1	None	Passaged from MEFs to Matrigel, Plated as single cells and cultured for 4 days or until confluent	RPMI 1640 B27 with insulin 2%	Activin A 6ng/ml BMP4 20ng/ml	IMP4 5 µM Or IWR1 10µM (continued until day 15)					RPMI 1640 B27 with insulin 2% (from day 15)
Lian 2013 Protocol B	Matrigel, hESC certified	mTeSR1	Matrigel, hESC certified	mTeSR1	RckInh 5µM on day of single cell suspension.	Single cells plated and cultured for 4 days or until confluent	RPMI 1640 B27 without insulin 2%	CHIR99021 12µM	None	IWP2 5µM		None		RPMI 1640 B27 with insulin 2%
Lian 2013 Protocol C	Matrigel, hESC certified	mTeSR1	Matrigel, hESC certified	mTeSR1	RckInh 5 µM on day of single cell suspension. CHIR99021 1µM from day after plating until day 0.	Single cells plated and cultured for 4 days or until confluent	RPMI 1640 B27 without insulin 2%	Activin A 100ng/ml bFGF 10ng/ml	BMP4 5ng/ml bFGF 5ng/ml			None		RPMI 1640 B27 with insulin 2%

Table 65 Protocols for directed monolayer differentiation of hPSCs to cardiomyocytes
(Continued over)

KSR = knock-out serum replacement, DMEM = Dulbecco's modified eagle medium, F12 = Ham's F12 nutrient mix, NEAA = non-essential amino acids, bFGF = basic fibroblast growth factor, BMP4 = bone morphogenetic protein 4, VEGF = vascular endothelial growth factor, SB = SB-431542, BME = β -mercaptoethanol, DM = dorsomorphin MEF = inactivated mouse embryonic fibroblasts, DKK-1 = Dickkopf related protein 1, RckInh = Y-27632, HAS = human serum albumin, CD lipids = chemically defined lipids, SCF = stem cell factor

SNP array quality control indices

Sample	Median Log R Deviation	Median Call Rate
2-PBMC	0.19	0.98
2-C7	0.22	0.97
2-C6	0.22	0.98
2-C4	0.19	0.98
2-C3	0.21	0.97
2-C2	0.19	0.97
2-C1	0.18	0.98
0101 PBMC	0.22	0.98
0101-C41	0.21	0.97
0202 PBMC	0.22	0.98
0202-C13	0.21	0.97
0203 PBMC	0.23	0.98
0203-C8	0.21	0.97

Table 66 SNP microarray quality control indices for PBMC and iPSC lines

The array manufacturer considers median log R deviations <0.20 and median call rates >0.98 to indicate high quality data.

Copy number variations in iPSCs

Classification of CNV		Sample	Predicted location of CNV		Size of CNV (bp)	Mean Log R ratio of CNV	Additional comments
			Cytogenetic	GRCh37/h19			
Pathogenic	Present before and after reprogramming	None					
	Acquired during reprogramming	2-C1	4q34.3 - 4q35.1	4:181,008,167-183,628,586	2,620,420	0.22	BAF pattern present, no obvious anti/proapoptotic genes
			7q36.1	7:150,327,024-151,893,675	1,566,652	0.16	BAF pattern present, KCNH2, PRKAG2,
			22q11.1 - 22q11.21	22:16,079,545-18,908,641	2,829,097	0.15	BCL2L and BID both of which are pro-apoptotic
	2-C4	20p11.1 - 20q11.21	20:26,158,741-31,042,348	4,883,608	0.09	adjacent to centromere mainly in 20q BCL2-L1	
Unknown pathogenicity	Present before and after reprogramming	None					
	Acquired during reprogramming	None					
Benign	Present before and after reprogramming	0203 PBMC	10q11.22	10:47,596,804-47,694,722	97,919	0.17	
		2 PBMC	16p13.3	16: 6,299,235- 6,387,348	88,113	-0.27	
		2 PBMC	21q21.1	21:23,624,026-23,759,395	135,370	-0.41	
		0101 PBMC	14q11.2	14:20213937-20386397	172461	-0.21	
	Acquired during reprogramming	None					
T-cell receptor genes	CNVs of T-cell receptor genes	2-C2	14q11.2	14:22,590,996-23,015,874	424,879	-3.31	This CNV includes <i>TRD</i> and the variable region of <i>TRA</i> .
		2-C3		14:22,351,008-22,957,900	606,893	-2.96	
		2-C7		14:22,260,045-22,984,586	724,542	-3.88	
		0203 PBMC		14:22,536,874-22,983,223	446,350	-0.39	
		0202 PBMC		14:22,562,099-22,993,720	431,621	-0.23	
		2-C3	7p14.1	7:38,298,285-38,418,891	120,607	-1.14	This CNV includes part of <i>TRG</i>
		C2	7q34	7:142,122,115-142,418,236	296,122	-0.33	This CNV includes part of <i>TRB</i>

Table 67 Summary of CNVs detected by SNP microarray in all samples tested

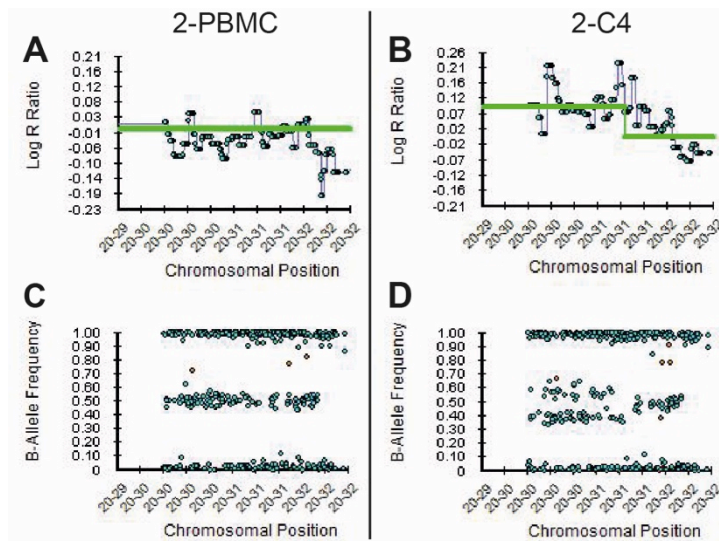


Figure 79 Characterisation of CNV predicted to be at 20p11.1-20q11.21 in the iPSC line 2-C4.

X-axis ticks indicate approximate positions within GRCh37/h19 e.g. “20-30” indicates the approximate position 30,000,000 in chromosome 20. Data from valid SNP calls are displayed as blue dots, no-calls are displayed as orange dots. The average Log R ratio is indicated by a green line, this is at zero in regions the BlueFuse Multi algorithm considers structurally normal. CNVs are indicated by a step change in this line, with the degree of deviation indicating the median Log R ratio across the CNV. The localised increase in log R ratio (B) and pattern of BAF values (D) in the same region suggest an increase in copy number of this region in 2-C4. This pattern is absent in 2-PBMCs (B and D).

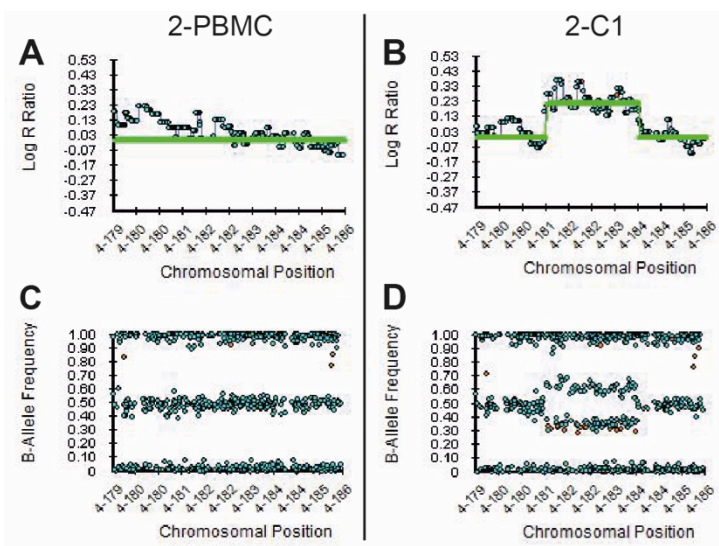


Figure 80 Characterisation of CNV predicted to be at 4q34.3 - 4q35.1 in the iPSC line 2-C1.

The localised increase in log R ratio (B) and pattern of BAF values (D) suggest an increase in copy number in 4q34.3 - 4q35 in 2-C1. This pattern is absent in 2-PBMCs (B and D).

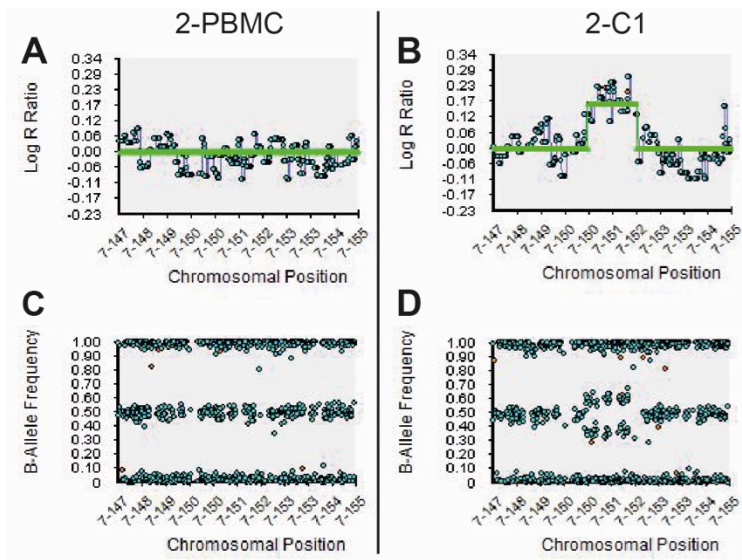


Figure 81 Characterisation of CNV predicted to be at 7q36.1 in the iPSC line 2-C1.

The localised increase in log R ratio (B) and pattern of BAF values (D) in 7q36.1 of 2-C2 suggest an increase in copy number of this region. This pattern is absent in 2-PBMCs (B and D).

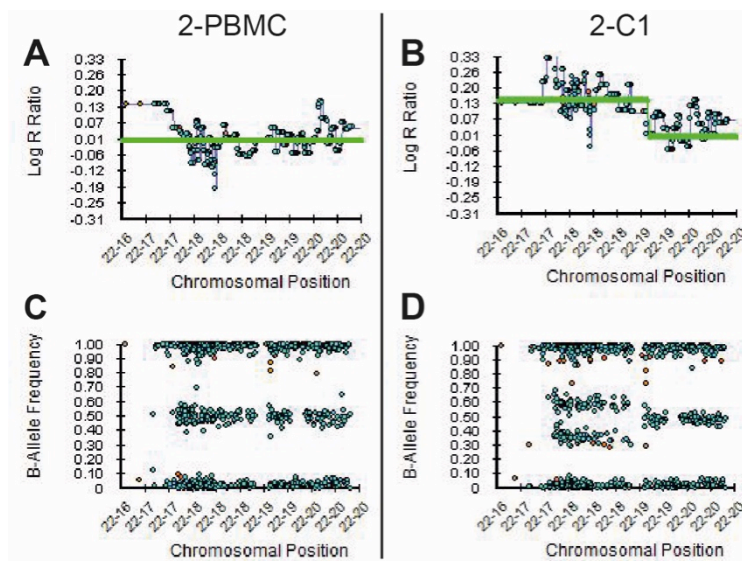


Figure 82 Characterisation of CNV predicted to be at 22q11.1 - 22q11.21 in the iPSC line 2-C1.

The localised increase in log R ratio (B) and pattern of BAF values (D) in 22q11.1 - 22q11.21 in 2-C1 suggest an increase in copy number of this region. This pattern is absent in 2-PBMCs (B and D).

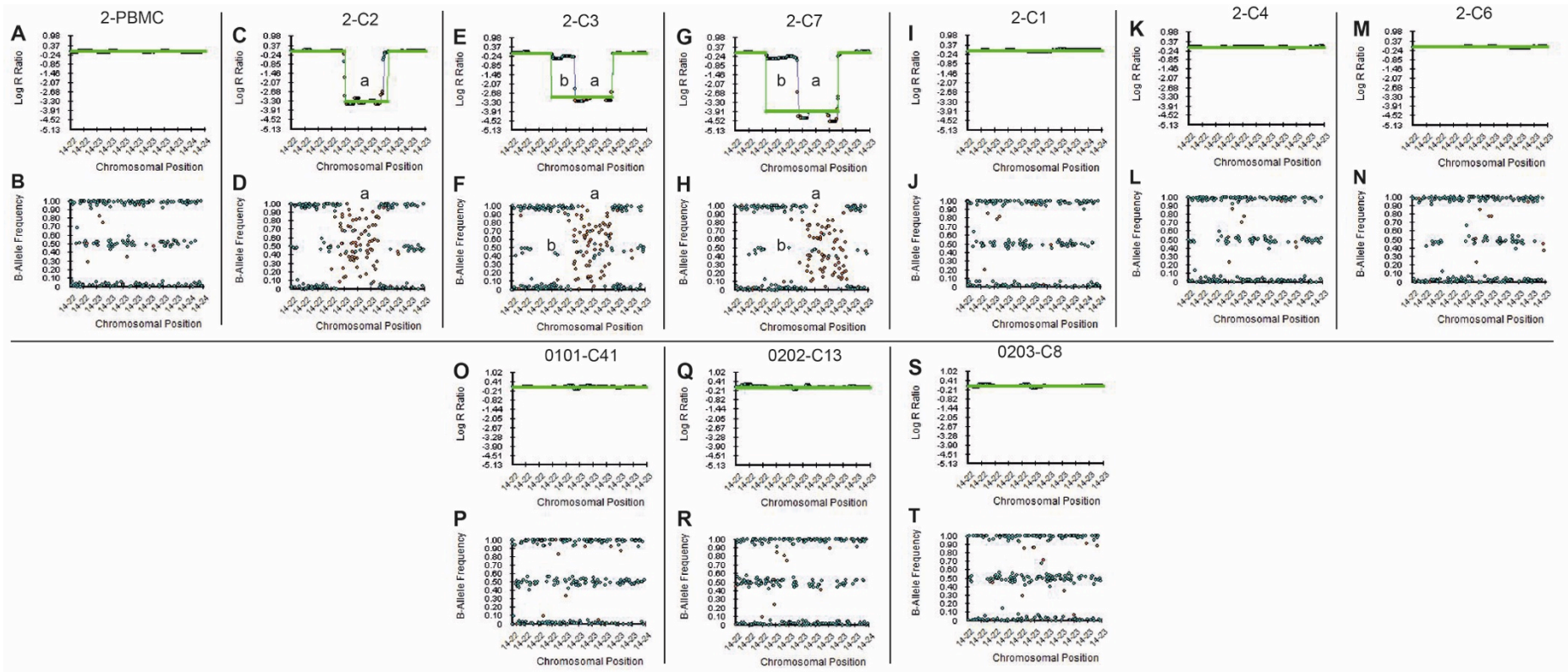


Figure 83 Characterisation of CNVs predicted to be at 14q11.2 in the multiple iPSC lines.

A localised reduction in Log R ratio and large number of failed SNP calls at 14q11.2 in three iPSC clones derived from 2-PBMCs suggests a loss of all copies of this region of the genome in these clones (region a in panels C – H). In two of these clones (2-C3 and 2-C7) there is an adjacent region with a reduced log R ratio and a BAF pattern consistent with a loss in copy number (region b in panels E - H). This CNV was not detected in the PBMCs from which the clones were derived or from three other clones derived from this individual.

Clone	Location	Direction of change	HGNC genes affected			OMIM genes affected		OMIM associated diseases	Reference to description of clinical phenotype associated with the CNV identified
2-C1(NT)	4q34	Gain	LINC00290 MIR1305	RN7SKP13 RN7SKP67	RNU2-34P TENM3	ODZ3 (*610083)		MCOPCB9 (#615145)	No published reports of the clinical phenotype of duplication of this region
	7q36	Gain	ABCB8 ABCF2 AGAP3 AOC1 ASB10 ASIC3 ATG9B CDK5 CHPF2 CRYGN GBX1 ETF1P2 FASTK	GALNT11 GALNTL5 GIMAP1 GIMAP2 GIMAP5 GIMAP6 IQCA1P1 NOS3 NUB1 PRKAG2 PRKAG2-AS1 RHEB RN7SL76P	KCNH2 KMT2C MIR3907 MIR671 RNU6-604P SLC4A2 SMARCD3 TMEM176A TMEM176B TMUB1 WDR86 WDR86-AS1 YBX1P4	ABCB8 (*605464) ABCF2 (*612510) ABP1 (*104610) ACCN3 (*611741) ASB10 (*615054) ATG9B (*612205) CDK5 (*123831) CHPF2 (*608037) CRYGN (*609603) FASTK (*606965) GALNT11 (*615130) GALNTL5 (*615133) GBX1 (*603354)	GIMAP1 (*608084) GIMAP2 (*608085) GIMAP5 (*608086) HCA112 (*610334) KCNH2 (*152427) LR8 (*610385) MIR671 (*615245) MLL3 (*606833) NOS3 (+163729) NUB1 (*607981) PRKAG2 (*602743) RHEB (*601293) SLC4A2 (*109280)	Familial hypertrophic cardiomyopathy type 6 (#600858) LQT2 (#613688) NOS3 (+163729) Phosphorylase kinase deficiency - glycogen storage disease of heart (#261740) SQT1 (#609620) Wolf-Parkinson-White syndrome (#194200)	No published reports of the clinical phenotype of duplication of this region
	22q11	Gain	ABCD1P4 ACTR3BP6 ANKRD62P1 ANKRD62P1 ARHGAP42P3 ARL2BPP10 ATP6V1E1 BCL2L13 BCRP7 BID BNIP3P2 CCT8L2 CECR1 CECR2 CECR3 CECR5 CECR5-AS1 CECR6 CECR7 CECR9 CHEK2P4 CLCP1 DGCR6	DNAJA1P6 DUXAP8 FABP5P11 FAM32B GAB4 GGT3P GPM6BP3 GRAMD4P2 HSFY1P1 IGKV1OR22-1 IGKV1OR22-5 IGKV2OR22-3 IGKV2OR22-4 IGKV3OR22-2 IL17RA KCNMB3P1 LINC00528 MED15P7 MICAL3 MIR3198-1 MIR648 MTND1P17 NBEAP3	NEK2P2 NF1P6 OR11H1 PABPC1P9 PARP4P3 PEX26 POTEH POTEH-AS1 PRODH RHEBP3 RN7SL843P RNU6-816P SLC25A15P5 SLC25A18 SLC9B1P4 TPTEP1 TUBA8 USP18 VWFP1 XKR3 YME1L1P1 ZNF402P ZNF72P	ATP6V1E (+108746) BID (*601997) CECR1 (*607575) CECR2 (*607576) DGCR6 (*601279) IL17RA (*605461) MICAL3 (*608882) PEX26 (*608666) POTEH (*608913) PRODH (*606810) SLC25A18 (*609303) TUBA8 (*605742) USP18 (*607057) XKR3 (*611674)	CANDF5 (#613953) Cat eye syndrome (115470) Chromosome 22q11.2 deletion syndrome (611867) HPI (#239500) PBD7A (#614872) PBD7B (#614873) Polymicrogyria with optic nerve hypoplasia (#613180) SCZD (#181500) SCZD4 (#600850)	Cat eye syndrome (115470) (Schinzel <i>et al.</i> , 1981) (Sharma <i>et al.</i> , 2014)	
2-C4(NT)	20p11	Gain	ASXL1 BCL2L1 C20orf112 CCM2L COX4I2 DEFB115 DEFB116 DEFB117 DEFB118 DEFB119 DEFB121 DEFB122 DEFB123 DEFB124 DKKL1P1 DUSP15	FOXS1 FRG1B HAUS6P2 HCK HM13 HM13-AS1 HM13-IT1 ID1 KIF3B LINC00028 MIR1825 MIR3193 MIR663A MLLT10P1 MYLK2 PDRG1	PLAGL2 POFUT1 REM1 RNA5SP480 RNA5SP481 RNA5SP482 RNU1-94P RNU6-384P RPL31P3 RSL24D1P6 TM9SF4 TPX2 TSPY26P TTLL9 XKR7	DEFB118 (*607650) REM1 (*610388) HM13 (*607106) ID1 (*600349) COX4I2 (*607976) BCL2L1 (*600039) C20ORF1 (*605917) MYLK2 (*606566) FOXS1 (*602939) PDRG1 (*610789) HCK (*142370) PLAGL2 (*604866) POFUT1 (*607491) KIF3B (*603754) ASXL1 (*612990)	Exocrine pancreatic insufficiency, dyserythropoietic anemia, and calvarial hyperostosis (#612714) Familial hypertrophic cardiomyopathy type 1 (#192600) Bohring-opitz syndrome (#605039) Myelodysplastic syndrome (#614286)	20q11.2 duplication syndrome (Avila <i>et al.</i> , 2013)	

Table 68 Summary of genes affected by those CNVs classified as pathogenic

T-cell receptor gene rearrangements

Signals from the 6FAM and HEX fluorophores which label the PCR products of this assay are referred to as blue and green respectively

Clone	Evidence of T-cell receptor gene re-arrangement	Name of PCR reaction yielding a product
2-C1	No	No product
2-C4	No	No product
2-C6	No	No product
2-C2	Yes <i>TRB</i> and <i>TRG</i>	TCRB Tube B: 266bp and 278bp 6FAM labelled products indicating V β - J β 2 re-arrangement in <i>TRB</i>
		TCRG Tube A: 164bp and 217 HEX labelled products indicating V γ 10 - J γ 1.3/2.3 and V γ 1-8 - J γ 1.3/2.3 re-arrangement in <i>TRG</i>
2-C3	Yes <i>TRB</i> and <i>TRG</i>	TCRB Tube A: 255bp 6FAM labelled product indicating V β - J β 2 re-arrangement in <i>TRB</i>
		TCRG Tube A 217bp HEX labelled product indicating V γ 10 - J γ 1.3/2.3 re-arrangement in <i>TRG</i>
		TCRG Tube B 180bp HEX labelled product indicating V γ 9 - J γ 1.3/2.3 re-arrangement in <i>TRG</i>
2-C7	Yes <i>TRB</i> and <i>TRG</i>	TCRB Tube A 255bp 6FAM labelled product indicating V β - J β 2 re-arrangement in <i>TRB</i>
		TCRG Tube A 164bp and 217bp HEX labelled product indicating V γ 10 - J γ 1.3/2.3 and V γ 1-8 - J γ 1.3/2.3 re-arrangements in <i>TRG</i>

Table 69 Results of T-cell receptor rearrangement assay

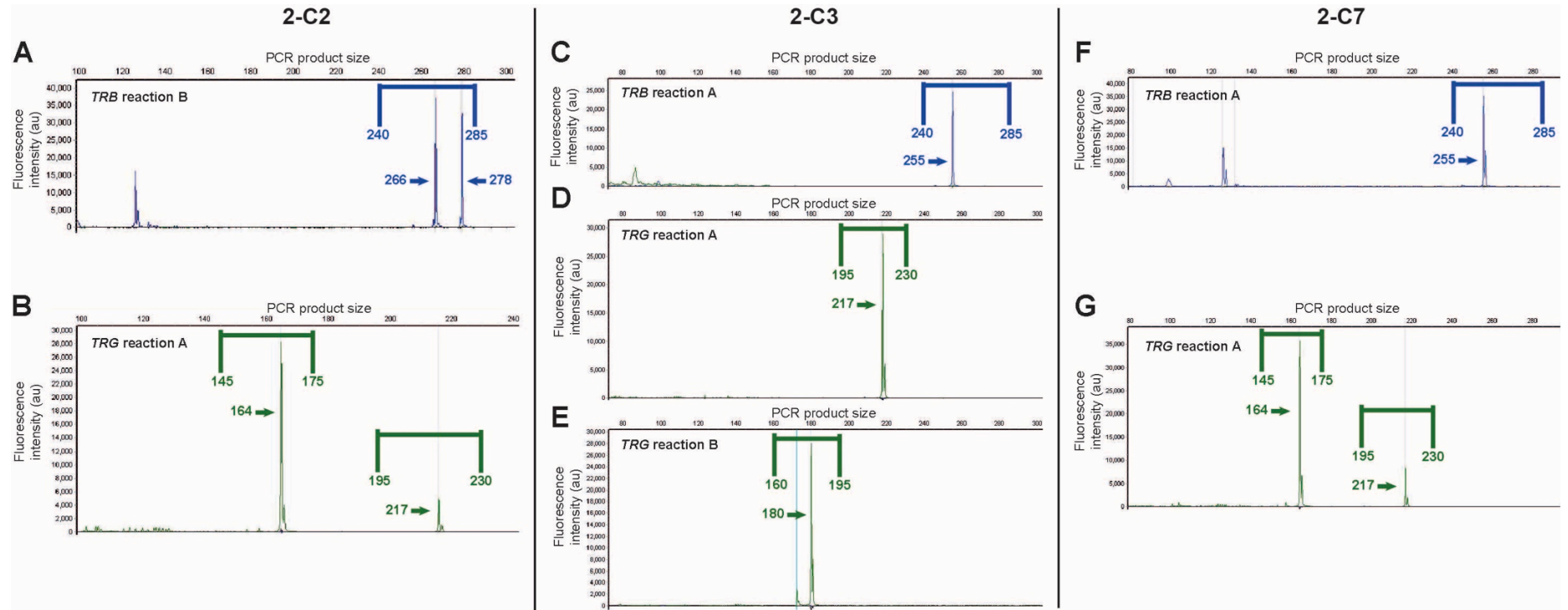


Figure 84. Data plots of the T-cell receptor rearrangement assays which yielded positive results.

Plots of data from TRB and TRG rearrangement PCR assay for 2-C2 (A and B), 2-C3 (C, D and E) and 2-C7 (F and G). Each graph represents data from one multiplex reaction. Products labelled with 6FAM and HEX fluorophores are shown as blue and green peaks respectively. The expected size ranges used to identify peaks as valid positive results are illustrated. Abbreviations: arbitrary units (au), base pairs (bp).

Selection of reference genes for RT-qPCR experiments

Reference genes were selected using the geNorm algorithm accessed via QBase+ as described in the methods chapter. The M-values and coefficients of variance of the 11 candidate reference genes as calculated by the geNorm algorithm are listed in Table 70. These results identified seven candidate genes indicated by M values of <1.0 and a CV values of <50% (Hellemans *et al.*, 2007).

Results of the ranking of the reference genes using the serial exclusion method are shown in Table 71. The geNorm algorithm recommends that at least two reference genes should be used in all cases. In this analysis these genes *PRDM4* and *VIPAS39*. The GeNormV value associated with adding *UBE4A* to *VIPAS39* and *PRDM4* was 0.093. This value is <0.15 indicating that there was little value in this addition and therefore the mean Ct of *VIPAS39* and *PRDM4* were used as a reference value for RT-qPCR analyses across all cell and tissue types in this study (Vandesompele *et al.*, 2002).

Gene	M-value	Coefficient of variance (%)
<i>ACTB</i>	1.371	84.3
<i>GAPDH</i>	1.356	51.0
<i>SCLY</i>	1.198	71.1
<i>ERCC6</i>	1.143	49.7
<i>SDHA</i>	0.966	48.6
<i>ENOX2</i>	0.962	44.7
<i>RPL7</i>	0.956	43.5
<i>RNF20</i>	0.795	26.1
<i>UBE4A</i>	0.769	23.0
<i>PRDM4</i>	0.753	21.1
<i>VIPAS39</i>	0.732	16.1
Mean (all genes)	1.000	43.6

Table 70 Reference genes ranked by M value

Stability	Gene
Least stable	<i>ACTB</i>
	<i>GAPDH</i>
	<i>SCLY</i>
	<i>ERCC6</i>
	<i>RPL7</i>
	<i>ENOX2</i>
	<i>SDHA</i>
	<i>RNF20</i>
	<i>UBE4A</i>
Most stable	<i>PRDM4</i>
	<i>VIPAS39</i>

Table 71 Reference genes ranked by the GeNorm algorithm.

Flow cytometry for pluripotency markers

Marker	Fold difference in median fluorescence of labelled single cell events relative to unlabelled single cell events, mean±SD, x10 ³ au				
	Single labelled experiments		Multi-colour experiments		
	H9, n=1	iPSCs, n=6	HDF, n=1	H9, n=1	iPSC, n=9
NANOG	3.0	3.2±0.6	0.42	3.1	4.5±1.3
OCT4	4.8	4.7±0.9	0.08	3.9	4.6±1.4
TRA-1-60	6.2	23.7±5.0	0.03	1.7	2.3±0.5
SSEA4	25.8	20.8±6.0	0.30	33.0	18.5±7.1

Table 72 Expression of pluripotency associated proteins assessed by flow cytometry, fluorescence of labelled sample relative to unlabelled sample.

Arbitrary units = au

Marker	Percentage of labelled single cell events classified as positive for the marker*, median(Q1,Q3) %			
	Single labelled experiments		Multi-colour experiments	
	hESC, n=1	iPSCs, n=6	hESC n=1	iPSC n=9
NANOG	98.2	97.3 (96.1-97.5)	99.2	98.5 (97.3-98.7)
OCT4	98.9	96.7 (94.4-98.5)	99.6	98.0 (97.5-98.7)
TRA-1-60	96.1	98.2 (97.6-99.4)	99.7	99.3 (98.4-99.4)
SSEA4	100.0	99.8 (99.4-99.9)	99.9	99.6 (99.4-99.8)

Table 73 Expression of pluripotency associated proteins by iPSCs assessed by flow cytometry, proportion of labelled sample classified as positive.

* defined as a fluorescence value greater than the 99th centile fluorescence value of the single cell events in the paired unlabelled sample.

Marker	Reduction in percentage of single cell events in labelled sample classified as positive, mean (min-max), %, n=3
NANOG	7.3 (1.6-12.9)
OCT4	0.4 (0.1-0.6)
TRA-1-60	0.8 (0.1-1.7)
SSEA4	0.1 (0.0-0.1)

Table 74 Reduction in percentage of single cell events in labelled sample classified as positive when FMO isotype control sample was used to define threshold rather than the unlabelled sample

Immunofluorescence microscopy for pluripotency associated proteins

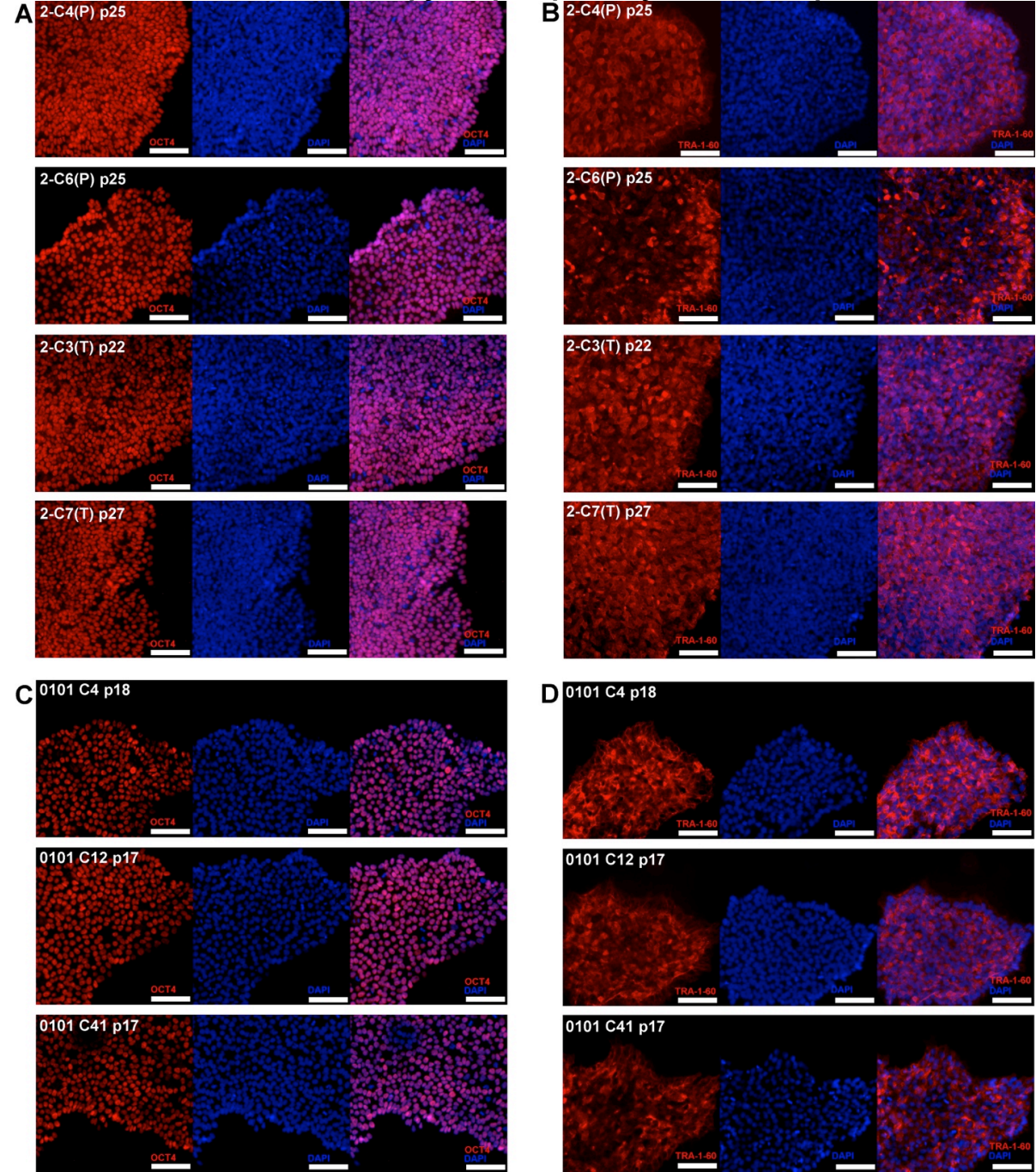
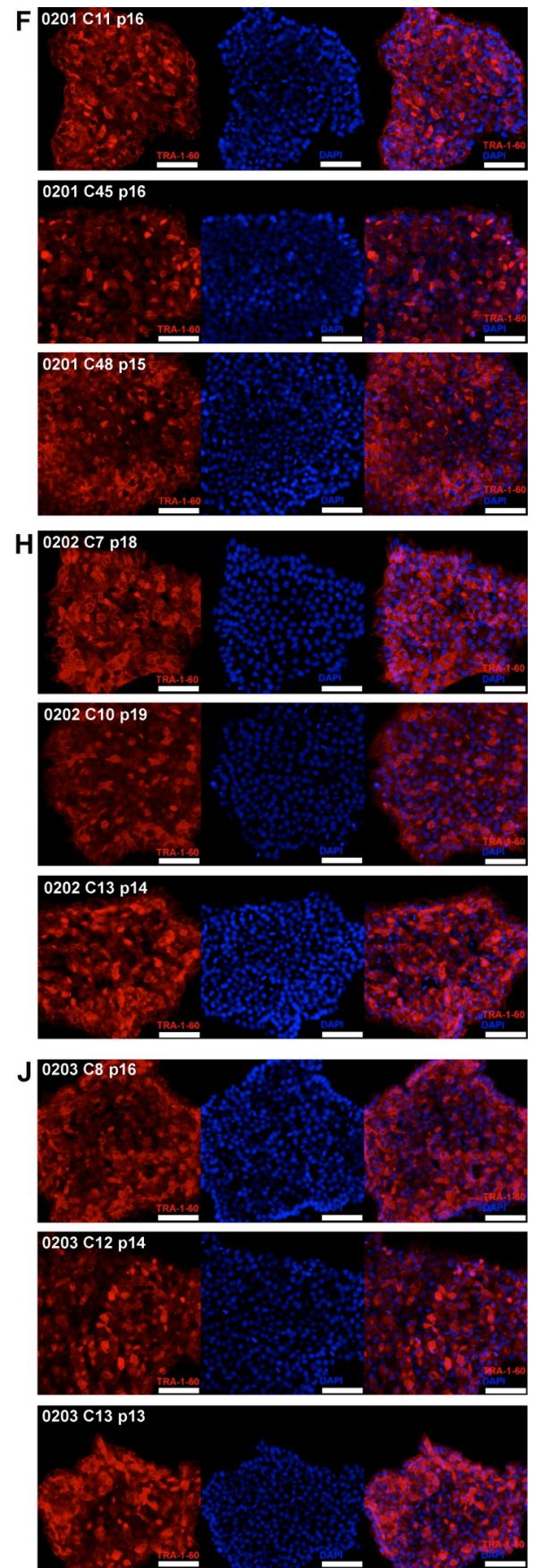
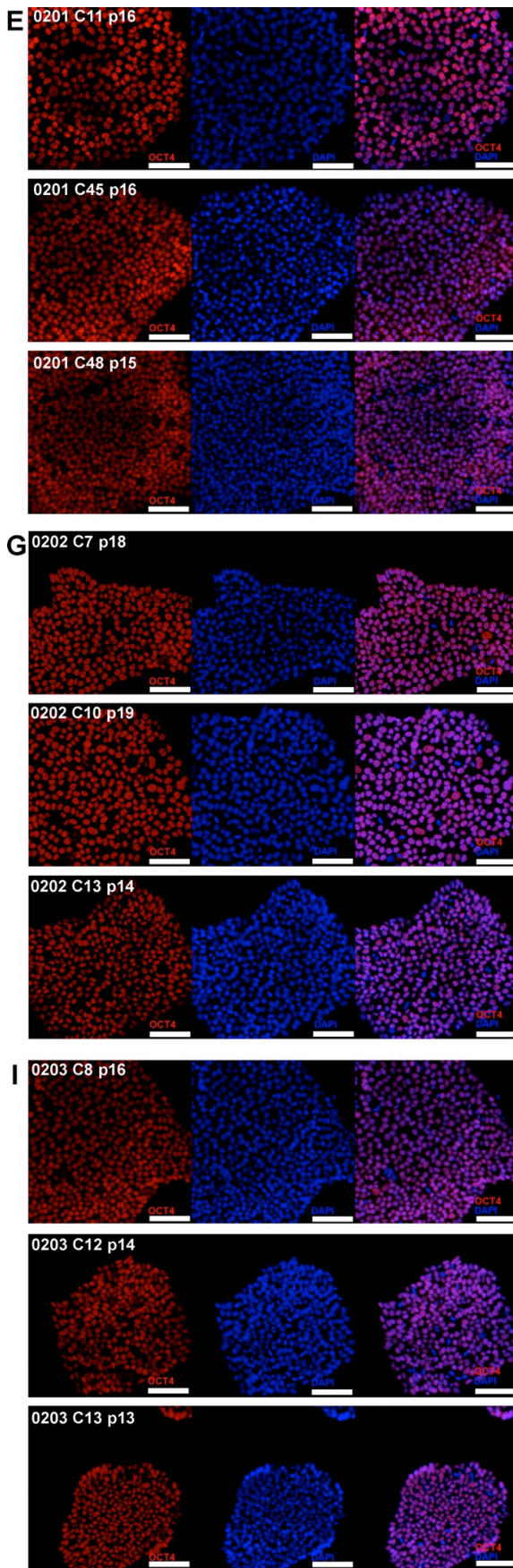
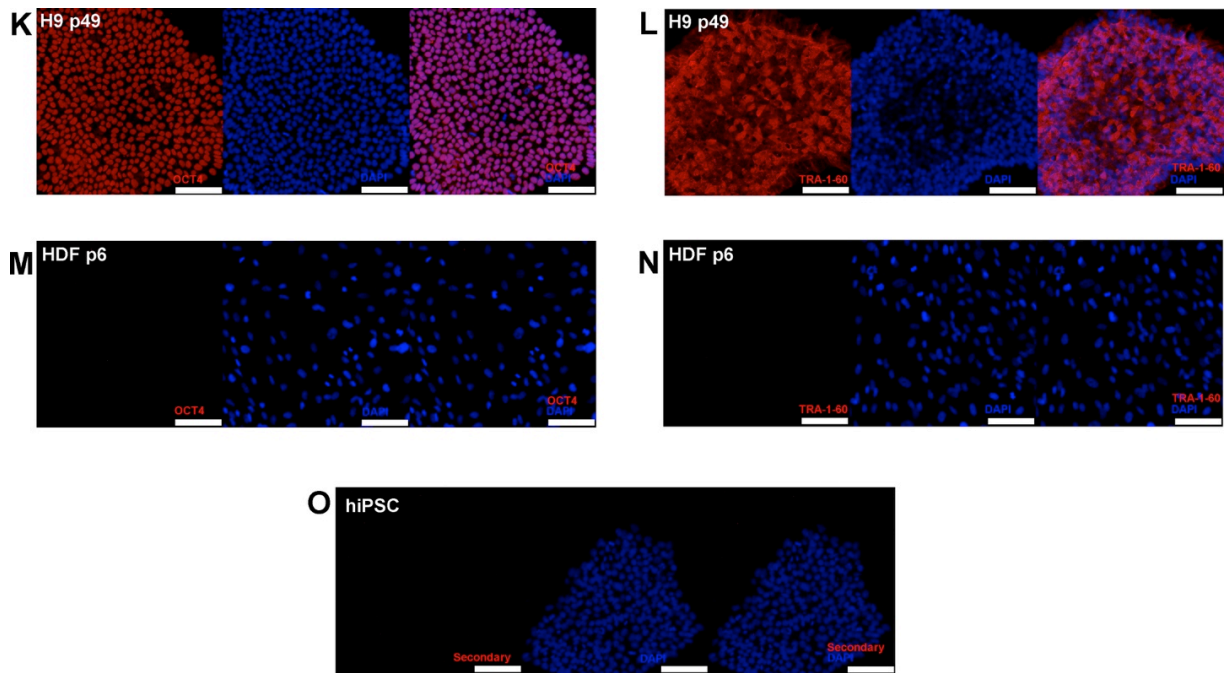


Figure 85 Immunofluorescent microscopy for pluripotency markers.
(continued over)



(continued over)



(continued)

The images show OCT4 signal co-localised with DAPI and a more diffuse TRA-1-60 signal consistent with a cell surface protein in iPSC clones and derived from: Subject 2 (A – B), Subject 0101 (C – D), Subject 0201 (E – F), Subject 0202 (G – H), Subject 0203 (I – J). The pattern of signal was identical to that observed in H9 hESCs (K – L) which acted as a positive control. No evidence of either marker was identified in HDFs (M – N) and no signal was detected in the absence of the primary antibodies (O). Scale bars: 100µm.

Expression of proteins indicating differentiation to the three primitive germ cell layers

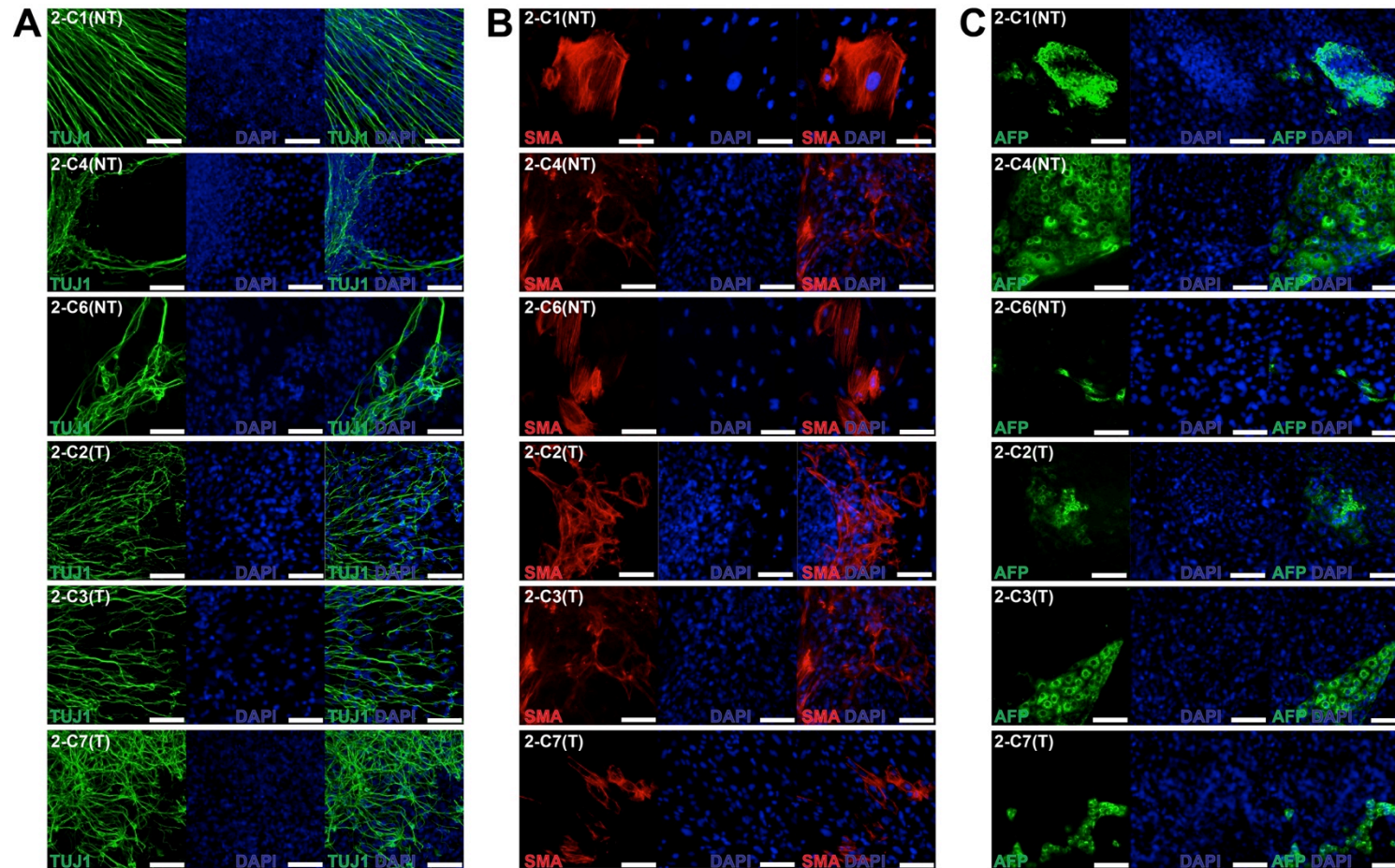
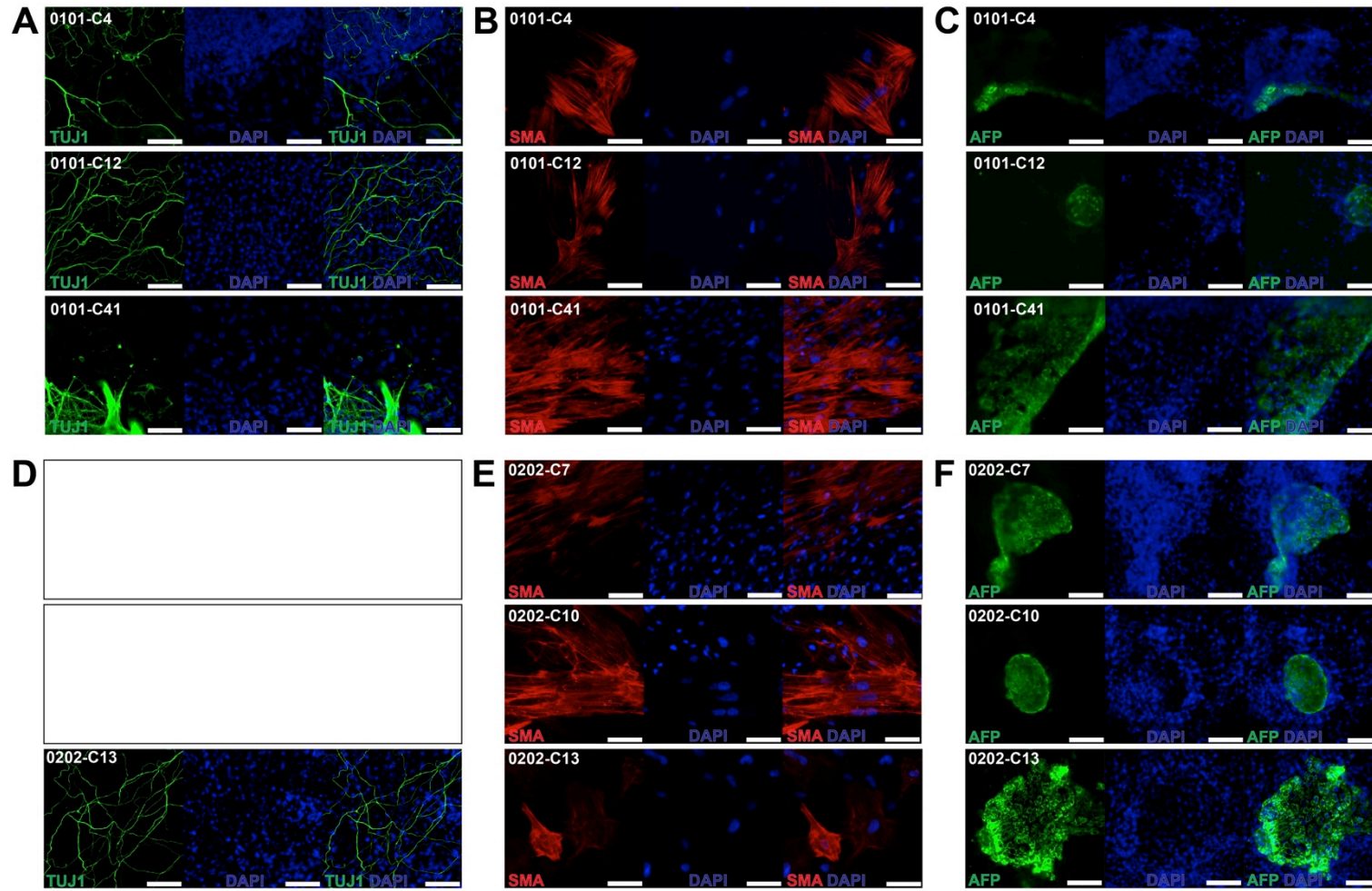


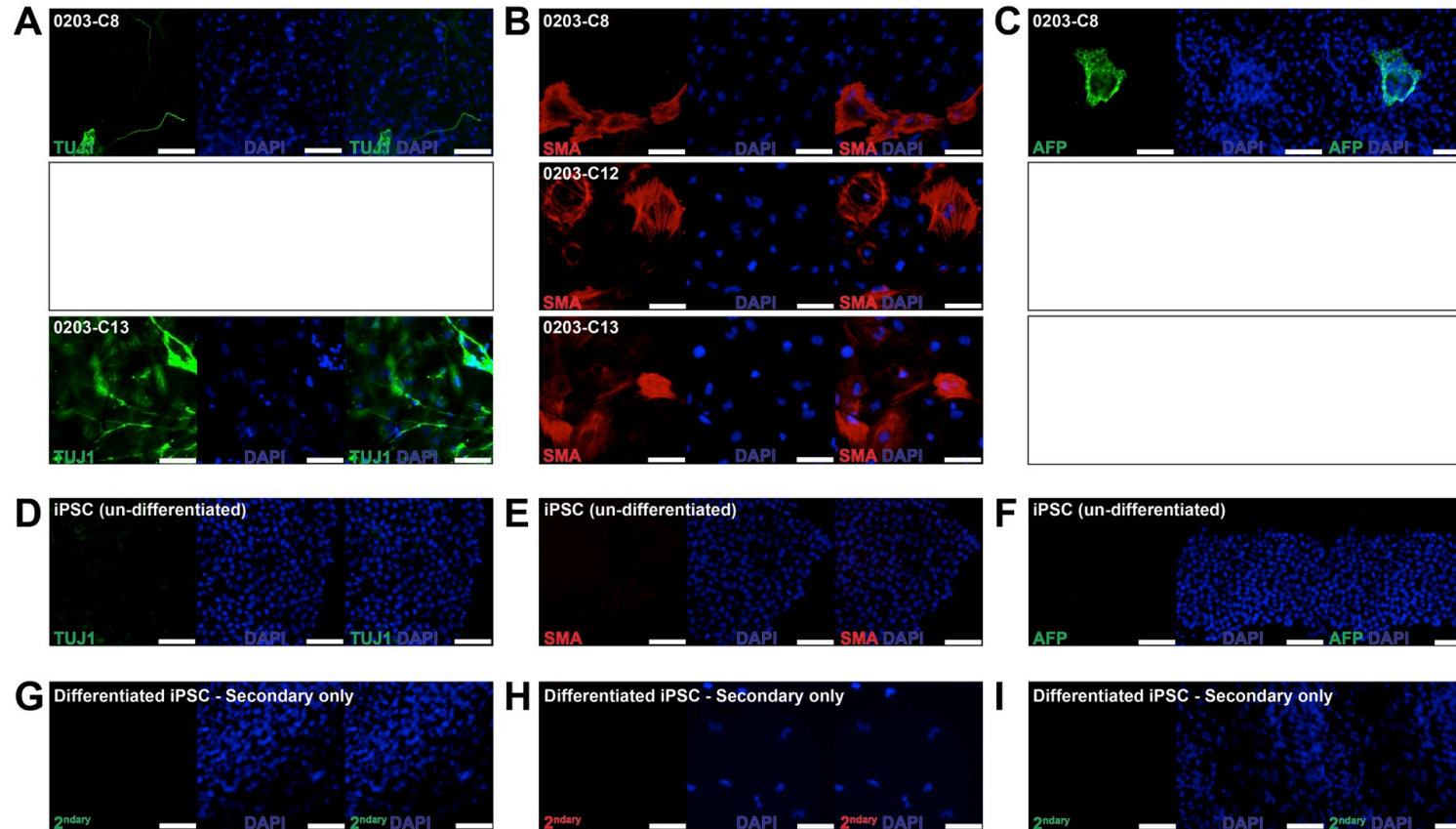
Figure 86 Immunofluorescence microscopy assessment of TUJ1, SMA and AFP expression in cultures generated from iPSCs that underwent differentiation in the presence of serum.

(continued over)

298



(continued over)



Immunofluorescence microscopy images of differentiated hiPSCs from subject 2 (A - C), 0101 (D - F), 0201 (G - I), 0202 (J - K) and 0203 (L - M) labelled for TUJ1 (left hand panels), SMA (middle panels) and AFP (right hand panels) indicative of differentiation to neuroectoderm, mesoderm and endoderm respectively. Undifferentiated hiPSCs (N - P) and differentiated hiPSCs labelled with secondary antibodies only (Q - S) were negative controls. Scale bars: 100µm.

The testing of primer sets using in RT-qPCR experiments to assess desmosomal gene expression

The primer sets used for these assessments were tested using sample from HaCaT cells. RNA array data from the Human Protein Atlas suggested that most of the desmosomal genes targeted in this study would be expressed at relatively high levels in HaCaT cells. The exceptions were *DSG4* which was expected to have an intermediate expression level and *DSC1* and *DSG1* which were present at very low levels or were absent (Uhlén *et al.*, 2015) (“HPA heart *DSC1*,” 2018) (“HPA HaCaT *DSC2*,” 2018) (“HPA HaCaT *DSC3*,” 2018) (“HPA HaCaT *DSG1*,” 2018) (“HPA HaCaT *DSG2*,” 2018) (“HPA HaCaT *DSG3*,” 2018) (“HPA HaCaT *DSG4*,” 2018) (“HPA HaCaT *PKP1*,” 2018) (“HPA HaCaT *PKP2*,” 2018) (“HPA HaCaT *PKP3*,” 2018) (“HPA HaCaT *JUP*,” 2018) (“HPA HaCaT *DSP*,” 2018).

All primer sets were tested with HaCaT samples by RT-PCR and gel electrophoresis. In all cases a single product in the predicted size range was identified (including for the primer sets targeting *DSG1* and *DSC1* transcripts). Gene expression was then assessed by RT-qPCR and confirmed the expected pattern of gene expression reported by the Human Protein Atlas (Figure 87). All reactions generate a melt curve with a single peak. The results of standard curve experiments use to predict reaction efficiencies have already been described in the methods chapter. Gene expression was normalised to the mean expression of the reference genes selected by the Genom pilot experiment to be optimal for comparing samples from PBMCs, iPSCs, hESCs, iPSC-CMs and RAA.

The HPA reported that heart tissue expressed *DSC1* and therefore RAA samples were used to confirm the efficacy of the *DSC1* primer set (“HPA heart *DSC1*,” 2018). No alternative positive control was obtained to test the *DSG1* primer set.

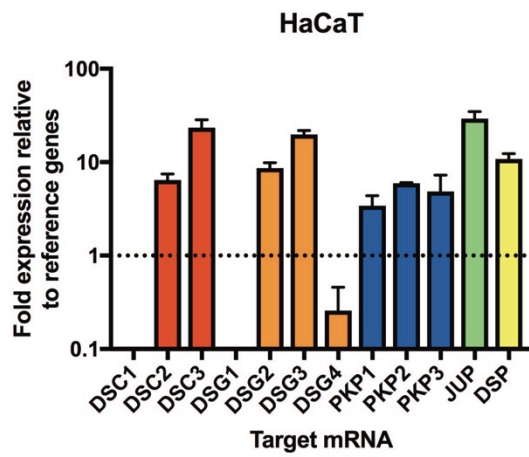


Figure 87 Expression of desmosomal genes in HaCaT cells

Bars indicate mean expression. Whiskers indicate the SEM. Each gene was assessed in samples from three different passages of HaCaT cells. Genes expressed at a level more than ten fold less than the reference genes were considered to be absent and are not shown.